目　　次

Ⅰ．総括研究報告

悪性中皮腫に対するヒト化抗 CD26 抗体を基盤とする安全かつ有効な新規併用療法の確立・・・・・1
研究代表者　森本　幾夫 順天堂大学大学院医学研究科　免疫病・がん先端治療学講座 客員教授

Ⅱ．分担研究報告

１．ヒト化 CD26 抗体と YB-1 阻害アンチセンスとの in vitro 及び in vivo での併用効果について
・・・・・11

研究代表者　森本　幾夫
順天堂大学大学院医学研究科免疫病・がん先端治療学講座 客員教授
共同研究者　岡本　俊博
順天堂大学大学院医学研究科免疫病・がん先端治療学講座 研究補助員
共同研究者　波多野　良
順天堂大学大学院医学研究科免疫病・がん先端治療学講座 博士研究員
共同研究者　中野　賢二
九州大学 先端融合医療ﾚﾄﾞｯｸｽﾅﾋﾞ研究拠点 教授

２．中皮腫における CD26 および YB-1 発現について・・・・・・・・・・・・・・・・・・・・・・・・21
研究分担者　山田　健人
埼玉医科大学 病理学 教授

３．CD26 抗体の抗腫瘍作用メカニズムの解明：免疫チェックポイント阻害薬としての新たな可能性・・・27

研究代表者　森本　幾夫
順天堂大学大学院医学研究科免疫病・がん先端治療学講座 客員教授
研究分担者　山田　健人
埼玉医科大学病理学 教授
共同研究者　波多野　良
順天堂大学大学院医学研究科免疫病・がん先端治療学講座 博士研究員
共同研究者　大沼　圭
順天堂大学大学院医学研究科免疫病・がん先端治療学講座 准教授

Ⅲ．研究成果の刊行に関する一覧表・・・・・・・・・・・・・・・・・・・

Ⅰ．　総括研究報告

厚生労働科学研究費補助金（労災疾病臨床研究事業）
総括研究報告書

悪性中皮腫に対するヒト化抗 CD26 抗体を基盤とする安全かつ有効な新規併用療法の確立

研究代表者　　森本　幾夫　順天堂大学大学院医学研究科
免疫病・がん先端治療学講座客員教授

研究要旨

悪性胸膜中皮腫はアスベストばく露によって起こる胸膜中皮由来の難治性悪性腫瘍であり、現時点で満足できる治療法はなく、新たな治療法の確立が望まれる。われわれは、新規治療標的分子として悪性胸膜中皮腫細胞に発現する CD26 に着目し、ヒト化 CD26 抗体を開発しフランスにて第 I 相臨床試験を行った。安全性が確認されるとともにその有効性を示唆する結果も得られ､平成 28 年 10 月から国内での第 I/II 相臨床試験を予定している。しかしながら、CD26 抗体単剤投与を行ったフランスでの臨床試験では、Stable Disease が認められるも完全寛解までは得られず、悪性胸膜中皮腫患者に完全寛解と肺機能改善をもたらす安全かつ有効な CD26 抗体との革新的な併用療法の開発が望まれる。Y-box binding protein (YB1)はがんの浸潤・転移促進に関与することから、有用な治療標的として着目されている分子であり、近年、共同研究者の中野賢二博士により良質な YB1 antisense oligonucleotide (YB1-ASO)が開発された。そこで本研究の初年度の取り組みとして、まず悪性胸膜中皮腫の浸潤及び増殖に対してヒト化 CD26 抗体と YB1-ASO の併用が相加的・相乗的な抑制効果を示すか検討した。in vitro 及び in vivo の結果から両者の併用の有用性を示唆する結果が得られ、今後 CD26 抗体と YB1-ASO を併用した際の抗腫瘍作用メカニズムの詳細を明らかにする。

悪性中皮腫の新規治療法として期待されるヒト化 CD26 抗体療法および YB-1 アンチセンス療法においては、腫瘍組織における CD26 および YB-1 分子の発現の適確な評価が重要である。本研究では、すでに確立された CD26 発現評価方法とともに、新たに YB-1 発現評価方法の確立を通じて、臨床検体における本分子群の免疫染色での発現評価法の確立を行い検討した。初年度は、抗 YB-1 抗体について抗原賦活化やシグナル増幅等の至適化を行い染色法を確立した。その結果、CD26 および YB-1 発現は、悪性中皮腫 61 症例において、それぞれ 53、58 症例で陽性であり、YB-1 は肉腫型にも高率に発現していることを見出した。また YB-1 は腫瘍血管内皮細胞においても発現が認められ、その局在は腫瘍および内皮ともに細胞質であった。

有効かつ安全な CD26 抗体との併用療法の開発とともに、CD26 抗体の抗腫瘍作用メカニ

ズムの更なる解明は極めて重要である。CD26 は T 細胞に活性化シグナルを伝達する共刺激分子としても機能するため、CD26 抗体は免疫系にも影響する可能性が考えられる。そこで、強い CD26 シグナルが入ることで発現が誘導される免疫チェックポイント分子及び抑制性サイトカインの解析を行った結果、CD26 共刺激特異的に LAG3 と BTLA の高発現、IL-10 の高産生が誘導されることを明らかにした。このことから、CD26 抗体は T 細胞への CD26 シグナルの伝達をブロックし、それらの抑制性分子の発現誘導を阻害する免疫チェックポイント阻害薬としても作用する可能性が示唆された。

研究分担者

岸本　卓巳：岡山労災病院・副院長

山田　健人：埼玉医科大学医学部
病理学 教授

共同研究者

青江　啓介：山口宇部医療センター
内科系診療部長

藤本　伸一：岡山労災病院
第二呼吸器内科部長

大沼　　圭：順天堂大学大学院医学研究科
免疫病・がん先端治療学講座准教授

波多野　良：順天堂大学大学院医学研究科
免疫病・がん先端治療学講座博士研究員

中野　賢二：九州大学先端融合医療レドックスナビ研究拠点教授

A 研究目的

悪性中皮腫は、アスベストばく露により発生する難治性悪性腫瘍である。アスベストばく露から悪性中皮腫発生までの潜伏期間は約 30～50 年とされ本邦においても患者数は今後ますます増加すると予想されている。悪性胸膜中皮腫に対する治療法としては手術療法、放射線療法、化学療法などが施行されているが、いずれも満足できる治療成績ではない。更に化学療法の標準治療とされているアリムタ、シスプラチンなどの抗がん剤治療では日本人では副作用が強く、その治療を完遂できる患者は約半数に満たず、生存期間は約 1 年と極めて予後不良である。また悪性中皮腫はアスベストばく露により発症するため労災疾病行政上も病態解明と安全で有効な新規治療法開発が急務とされている。

CD26 分子は T 細胞共刺激分子で DPPIV 酵素活性を有し、研究代表者の森本らは CD26cDNA の単離から CD26 抗体の開発を世界に先駆けて行い当分野では最先端に位置している。CD26 は正常中皮には発現しないが上皮型悪性中皮腫では約 8 割に発現しており、中皮腫細胞の増殖・浸潤に重要な役割を果たすことから、抗腫瘍作用を有する良質なヒト化 CD26 抗体を開発し、悪性中皮腫の新規治療法として有効な可能性が示唆された。(Clin Cancer.Res.2007)

アリスタ、シスプラチンなど抗がん剤治療抵抗性の悪性中皮腫及びその他 CD26 陽性悪性腫瘍を対象に、フランスで本抗体の第 1 相臨床試験を施行し、その安全性が確認され、悪性中皮腫 19 例中 10 例が Stable Disease(SD)となり、その内 6 例で 3 ヶ月

以上(5 例は 6 ヶ月以上)SD が継続し、その有効性が示唆され本邦でも本年 10 月から第 1 相臨床試験がスタートする。本臨床試験ではヒト化 CD26 抗体の単独投与のため完全寛解は得られず、症状緩和、肺の機能改善、治癒を目指す安全かつ有効な新規治療薬との併用療法の確立が望まれる。

Y-box binding protein-1(YB-1)は癌細胞の増殖、浸潤に関与する転与因子で悪性中皮腫でも高発現している(Oncology2014)。研究協力者九州大学中野賢二博士らは YB-1 発現を阻害する架橋型核酸アンチセンスを開発し、膵癌モデルの系で有効かつ毒性も低いことを報告した(特願 2012-89772)。更に中皮腫組織での CD26 陽性度評価がアリムタを含む化学療法剤の効果予測として有用なことを我々はすでに報告している(Clin Cancer Res 2012)。

本研究では(1)ヒト化 CD26 抗体と YB-1 アンチセンスとの併用による副作用の少ない安全で有効な悪性中皮腫の焦学的治療法の確立を目指すと伴に(2)悪性中皮腫における CD26 と YB-1 発現と治療反応性や予後を含む臨床パラメーターとの相関を明らかにする。また最近 CTLA-4 抗体や PD-1/PD-L1 抗体が免疫チェックポイント阻害薬として悪性黒色腫や肺癌治療薬として注目されつつあるが、CD26 抗体も免疫チェックポイント阻害薬として作用する可能性を示唆するデータも得られ(J.Immnnol.2015),(3)CD26 シグナルによる免疫チェックポイント分子の発現誘導メカニズムを明らかにすることを目的として研究を行った。

B 研究方法

各分担研究報告書に著述

(倫理面への配慮)

ヒト化 CD26 抗体及び YB1-ASO の抗腫瘍効果を評価するためのマウスを用いた動物実験は、順天堂大学医学部実験動物委員会の審査を受け承認されている(承認番号 270138)。

患者検体などについては研究対象者に対する人権擁護上の配慮及び研究により研究対象者が受ける不利益、利益等の説明を患者及び遺族に対して行い、書面でのインフォームド・コンセントを得ている。また病理組織について免疫染色して CD26 発現を解析する研究については、慶應義塾大学医学部および埼玉医科大学の倫理委員会の審査にて承認されている（承認番号 20120100 および 734）。

成人健常者の末梢血を用いた研究については、順天堂大学医学部研究等倫理委員会の審査を受け承認されている(承認番号 2015008)。末梢血の提供を受ける際には、研究対象者に対する人的擁護上の配慮及び研究により研究対象者が受ける不利益、利益等の説明を行い、書面でのインフォームド・コンセントを得ている。

C 研究結果

1.ヒト化 CD26 抗体と YB1 阻害アンチセンスとの in vitro 及び in vivo での併用効果について

Y-box binding protein (YB1)はがんの浸潤・転移促進に関与することから、有用な治療標的として着目されている分子であり、近年、共同研究者の中野賢二博士により良質な YB1 antisense oligonucleotide (YB1-ASO)が開発された。そこで本研究の

初年度の取り組みとして、まず悪性胸膜中皮腫の浸潤及び増殖に対してヒト化 CD26 抗体と YB1-ASO の併用が相加的・相乗的な抑制効果を示すか検討した。in vitro 及び in vivo の結果から両者の併用の有用性を示唆する結果が得られ、今後 CD26 抗体と YB1-ASO を併用した際の抗腫瘍作用メカニズムの詳細を明らかにする。

更に、増殖に対する抑制効果の経時的変化を観察する目的で in vivo imaging system の実験系の確立を試みた。研究方法に記載した方法により Luciferase 発現 H226 細胞株及び JMN 細胞株を樹立した。この細胞株を SCID マウスに腹腔内移植(1 x 10^5 cells/mouse)し、ヒト化 CD26 抗体の効果を検討したところ CD26 抗体の増殖抑制効果が確認できた。今後この系を用いて YB1-ASO とヒト化 CD26 抗体の併用効果を検討する。

2.中皮腫における CD26 および YB-1 の発現について

悪性中皮腫の新規治療法として期待されるヒト化 CD26 抗体療法および YB-1 アンチセンス療法においては、腫瘍組織における CD26 および YB-1 分子の発現の適確な評価が重要である。本研究では、すでに確立された CD26 発現評価方法とともに、新たに YB-1 発現評価方法の確立を通じて、臨床検体における本分子群の免疫染色での発現評価法の確立を行い検討した。初年度は、抗 YB-1 抗体について抗原賦活化やシグナル増幅等の至適化を行い染色法を確立した。その結果、CD26 および YB-1 発現は、悪性中皮腫 61 症例において、それぞれ 53、58 症例で陽性であり、YB-1 は肉腫型にも高率に発現していることを見出した。また YB-1 は腫瘍血管内皮細胞においても発現が認められ、その局在は腫瘍および内皮ともに細胞質であった

3.ヒト化 CD26 抗体の抗腫瘍作用メカニズムの解明：

免疫チェックポイント阻害薬としての新たな可能性

近年、がんの新たな治療法として免疫系に抑制シグナルを伝達するチェックポイント分子をブロックすることで腫瘍免疫を活性化させる免疫チェックポイント阻害薬が非常に注目されており、CTLA4 抗体や PD-1/PD-L1 抗体はすでに臨床現場で用いられ始めている。

CD26 抗体は免疫系にも影響する可能性が考えられる。そこで、強い CD26 シグナルが入ることで発現が誘導される免疫チェックポイント分子及び抑制性サイトカインの解析を行った結果、CD26 共刺激特異的に LAG3 と BTLA の高発現、IL-10 の高産生が誘導されることを明らかにした。このことから、CD26 抗体は T 細胞への CD26 シグナルの伝達をブロックし、それらの抑制性分子の発現誘導を阻害する免疫チェックポイント阻害薬としても作用する可能性が示唆された。

D 考察

In vitro 浸潤アッセイにおいて YB1-ASO とヒト化 CD26 抗体の併用により浸潤の抑制作用が増強され、相乗効果が認められた。一方、in vitro 増殖アッセイでは併用により増殖の抑制において相加効果が確認された。悪性中皮腫は腫瘍の促進に胸膜への浸潤が大きく関与しているため、YB1-ASO とヒト化 CD26 抗体の併用は期待される治療

法であると考えられる。
併用効果のメカニズムに対する考察として、CD26 と YB1 が特に細胞質で複合体を形成していることが示され、CD26 と YB1 が何らかの相互作用をしていると予想される。YB1-ASO の導入により CD26 mRNA 発現が抑制された一方で、細胞質画分、核画分における CD26 タンパクの発現は増強された。YB1 は mRNA の安定化に関与することが報告されているため、CD26 mRNA を安定化させていた YB1 が YB1-ASO により減少することで CD26 mRNA も減少した可能性が考えられる。一方で YB1 は翻訳を制御することも報告されており、結果的に YB1-ASO は CD26 の翻訳を増強させることにより CD26 発現を上昇させると考えられ、この発現上昇した CD26 に対してヒト化 CD26 抗体が作用することで併用効果が認められた可能性が考えられる。

また、in vivo 浸潤アッセイ系における YB1-ASO と抗 CD26 抗体の併用効果、YB1-ASO による CD26 の発現誘導メカニズム、発現誘導された CD26 によりどのような分子が.誘発されるのかの検討も必要であると考えられる。
CD26 は、細胞膜貫通型の細胞表面に局在する糖蛋白質であるが、細胞内での局在は、細胞膜のみならず細胞質でのライソゾームや核内と広範囲である。一方、YB-1 は、転写・翻訳に関わる分子であるが、免疫染色での観察では、主たる局在は細胞質であり、核の陽性像はほとんど得られていない。これらの分子の腫瘍細胞における局在は重要な意味を持つ可能性があるが、免疫染色での光学顕微鏡での観察では、CD26 と YB-1 が中皮腫細胞の細胞質において、類似した瀰漫性の局在を示すことは、これらの分子の相互作用の可能性も考慮する必要があると考える。
今後、悪性中皮腫における CD26 および YB-1 発現について細胞局在、陽性率、陽性強度などの各種パラメーターで詳細に定量評価することで、抗体療法の効果や予後などとの関連性あるいは臨床パラメーターを検証する基礎を構築していくことが重要と考える。

ヒト化 CD26 抗体の抗腫瘍作用メカニズムの更なる解明を目的として、CD26 抗体の免疫系への影響、特に新たながん治療法として近年非常に着目されている免疫チェックポイント阻害薬として機能する可能性について検討した。
免疫チェックポイント分子の多くが、その細胞内ドメインに SHP-1/2 をはじめとしたフォスファターゼが会合し、T 細胞受容体からのシグナル伝達(キナーゼカスケード)を阻害することで T 細胞の活性化を負に制御する。CD26 の細胞内ドメインはわずか 6 アミノ酸で構成されており、フォスファターゼが会合することが知られている ITIM や ITSM と呼ばれる既存の配列は存在しない。このことから、CD26 分子の細胞内ドメインを介して直接抑制性のシグナルが伝達する可能性は低いと考えられる。そのため、CD26 分子を介して直接抑制性シグナルが伝達するのではなく、CD26 シグナルによって抑制機能を有する免疫チェックポイント分子を誘導し、それらを介して免疫応答を負に制御する、すなわち免疫チェックポイント分子として機能する可能性を検討した。本年度の結果から、CD26 共刺激は CD4 T 細胞に対して LAG3 と BTLA の

高発現、IL-10 の高産生を誘導し、CD8 T 細胞に対しても CD28 共刺激と比較して BTLA の発現を顕著に誘導することから、CD26 はがん細胞周囲に浸潤した T 細胞にそれらの抑制性分子を誘導する免疫チェックポイント分子としても機能する可能性が示唆された。

E.結論

In vitro 及び in vivo study の解析の結果からヒト化 CD26 抗体と YB-1－ASO との併用はその有用性を示唆する結果が得られ、更に詳しい併用効果及びその抗腫瘍メカニズムを明らかにする予定である。

臨床検体における YB-1 の発現評価方法を確立した。中皮腫症例における CD26 と YB-1 の発現を明らかにし、いずれも高い比率で発現しており、共発現している症例がほとんどであることが明らかとなった。

健常者の末梢血 CD4 T 細胞、CD8 T 細胞に発現する免疫チェックポイント分子を解析した結果、両 T 細胞に PD1、TIGIT、2B4 (CD244)、CD39 と少量の CD160 が発現していることが示された。CD26 共刺激は CD4 T 細胞に対して LAG3 と BTLA の高発現、IL-10 の高産生を誘導し、CD8 T 細胞に対しても CD28 共刺激と比較して BTLA の発現を顕著に誘導することから、CD26 はがん細胞周囲に浸潤した T 細胞にそれらの抑制性分子を誘導する免疫チェックポイント分子としても機能する可能性が示唆された。

F.健康危険情報

現時点では、特記すべき健康危険情報はない。

G.次年度以降の計画

Luciferase 発現 H226 、JMN 株を用いて免疫不全マウスへ移植して in vivo モニタリング系にて至適量・投与間隔を定めて CD26 抗体、YB-1－ASO の併用に寄る詳しい抗腫瘍効果を検討する。また CD26 処理後の CD26･YB-1 の変化やその会合分子及びシグナル系の分子生物学解析を行いクロストーク及び併用療法と基礎となる評価を行う予定である。

初年度に引き続き、中皮腫組織（岡山労災病院 24 例、山口宇部医療センター35 例、慶應義塾大学病院 2 症例）について YB-1 と CD26 の発現を検討し、YB-1 と CD26 の発現レベルと臨床病理学的指標である、１）特異な浸潤増殖態度、２）遠隔転移、３）治療反応性、４）病期・生存期間、との関連を解析する。また森本博士らが見出しつつある CD26 シグナル系と YB-1 シグナル系の標的遺伝子やシグナルのクロストークする中でバイオマーカーとなりうる分子について免疫染色にて発現を検討して、中皮腫の臨床病理学的指標との関連を解析する

IL-10 産生や LAG3 発現の誘導に関わるシグナル伝達経路の更なる解明とともに、今回新たに見出された BTLA の発現を誘導するシグナル伝達経路、及び転写因子についての解析が必要となる。また、本年度は健常者の末梢血 T 細胞における免疫チェックポイント分子の発現パターンについて解析を行ったが、次年度は、悪性中皮腫患者におけるそれらの分子の発現パターンを末梢血 T 細胞、胸水 T 細胞、悪性中皮腫周囲に浸潤した T 細胞を用いて解析する。また、

悪性中皮腫自身やその周囲の細胞に LAG3、BTLA のリガンドである MHC class II や HVEM が発現しているかも免疫組織染色で検討していく予定である。

H.研究発表

1. 論文

1) Ohnuma K, Hatano R, MorimotoC. DPP4 in anti-tumor immunity: going beyond the enzyme. Nat Immunol.2015; 16:791-2.

2) Ohnuma K, Hatano R, Aune TM,Otsuka H, Iwata S, Dang NH, Yamada T, Morimoto C. Regulation of pulmonary GVHD by IL-26+CD4 T lymphocytes through CD26/caveolin-1 interaction. J Immunol. 2015; 194:3697-3712.

3) Katayose T, Iwata S, Oyaizu N, Hosono O, Yamada T, Dang NH, Hatano R, Tanaka H, Ohnuma K, Morimoto C. The role of Cas-L/NEDD9 as a regulator of collagen-induced arthritis in a murine model.Biochem Biophys Res Commun. 2015; 460:1069-75.

4) Otsuki N, Iwata S, Yamada T, Hosono O, Dang NH, Hatano R,Ohnuma K, Morimoto C. Modulation of immunological responses andamelioration of collagen-induced arthritis by the novel roxithromycin derivative 5-I. Mod Rheumatol. 2015; 25:562-70.

5) Ohnuma K, Saito T, Hatano R, Hosono O, Iwata S, Dang NH, Ninomiya H, Morimoto C. Comparison of two commercial ELISAs against an in-house ELISA for measuring soluble CD26 in human serum. J Clin Lab Anal. 2015; 29:106-11.

6) Hatano R, Ohnuma K, Otsuka H, Komiya E, Taki I, Iwata S, Dang NH, Okumura K, Morimoto C. CD26-mediated induction ofEGR2 and IL-10 as potential regulatory mechanism for CD26 costimulatory pathway. J Immunol. 2015; 194:960-972.

7) Adachi T, Kobayashi T, Sugihara E, Yamada T, Ikuta K, Pittaluga S, Saya H, Amagai M, Nagao K. Hair follicle-derived IL-7 and IL-15 mediate skin-resident memory T cell homeostasis and lymphoma. Nature Medicine 2015; 21:1272-9.

8) Sakiyama T, Kubo A, Sasaki T, Yamada T, Yabe N, Matsumoto K, Futei Y. Recurrent gastrointestinal perforation in a patient with Ehlers-Danlos syndrome due to tenascin-X deficiency. J. Dermatol.2015; 42:511-514.

9) Matsushita M, Ozaki Y,

Hasegawa Y, Terada F, Tabata N, Shiheido H, Yanagawa H, Oikawa T, Matsuso K, Du W, Yamada T, Ichikawa D, Hattori Y A novel phthalimide derivative, TC11, has preclinical effects on high-risk myeloma cells and osteoclasts. PLoS One. 2015;10:e0116135.

10) Nojima D, Fujimoto N, Kato K, Fuchimoto Y, Kiura K, Kishimoto T, Tanimoto M. Pilot analysis of asbestos-induced diffuse pleural thickening with respiratory compromise. Acta Med Okayama 2015;69:261-6.

11) Yamagishi T, Fujimoto N, Nishi H, Miyamoto Y, Hara N, Asano M, Fuchimoto Y, Wada S, Kitamura K, Ozaki S, Kishimoto T. Prognostic significance of the lymphocyte-to-monocyte ratio in patients with malignant pleural mesothelioma. Lung Cancer 2015 Oct;90:111-7. doi: 10.1016/j.lungcan.2015.07.014. Epub 2015 Jul 30.

12) Furukawa M, Toyooka S, Hayashi T, Yamamoto H, Fujimoto N, Soh J, Hashida S, Shien K, Asano H, Aoe K, Okabe K, Pass HI, Tsukuda K, Kishimoto T, Miyoshi S. DNA copy number gains in malignant pleural mesothelioma. Oncol Letter (in press)

13) Fujimoto N, Gemba K, Aoe K, Kato K, Yokoyama T, Usami I, Onishi K, Mizuhashi K, Yusa T, Kishimoto T. Clinical investigation of benign asbestos pleural effusion. Pulm Med. 2015;2015:416179. doi: 10.1155/2015/416179.

14) Yamagishi T, Fujimoto N, Miyamoto Y, Asano M, Fuchimoto Y, Wada S, Kitamura K, Ozaki S, Nishi H, Kishimoto T. Brain Metastases in Malignant Pleural Mesothelioma. Clin Exp Metastasis (in press)

15) Miyamoto Y, Fujimoto N, Asano M, Nakasuka T, Hara N, Yamagishi T, Fuchimoto Y, Wada S, Kitamura K, Ozaki S, Kishimoto T. Lymphohistiocytoid mesothelioma with a response to cisplatin plus pemetrexed: a case report. Cancer Treatment Communications 2015;4:1-5. DOI information: 10.1016/j.ctrc.2015.02.003

16) Matsumoto S, Fujimoto N, Fuchimoto Y, Asano M, Yano T, Kishimoto T. Endobronchial T-cell lymphoma in a patient with chronic pyothorax. Respirol Case Rep 2015;3:44-7. doi: 10.1002/rcr2.103. Epub 2015 Apr 30.

17) Nakasuka T, Fujimoto N, Hara N, Miyamoto Y, Yamagishi T, Asano M, Nishi H, Kishimoto T. Foreign body granuloma mimicking recurrence of malignant pleural mesothelioma. Res Med Case Rep 16(2015)95-96.

18) Yamagishi T, Fujimoto N, Miyamoto Y, Hara N, Asano M, Fuchimoto Y, Wada S, Kitamura K, Ozaki S, Nishi H, Kishimoto T. The Rapid Appearance and Disappearance of Dendriform Pulmonary Ossification Following Diffuse Alveolar Hemorrhage. Am J Res Crit Care Med (in press)

19) Hara N, Fujimoto N, Miyamoto Y, Yamagishi T, Asano M, Fuchimoto Y, Wada S, Ozaki S, Kishimoto T. Lymphoproliferative disorder in pleural effusion in a subject with past asbestos exposure. Respiratory Medicine Case Reports.2015,16:169-71.doi.10.1016/j.rmcr.2015.11.002

2. 著書

山田健人　石綿の暴露はヒト体内で何を起こすのか:培養細胞を用いたモデル実験　石綿関連疾患の病理とそのリスクコミュニケーション　井内康輝編著　篠原出版新社　2015年12月25刊行

3.学会発表

1) 森本幾夫. CD26 の機能と治療応用. 中皮腫シンポジウム, 2015 年 12 月 26 日, 兵庫

2) 森本幾夫. CD26 抗体を基盤とするトランスレーショナルリサーチ.第 57 回日本小児血液・がん学会,2015 年 11 月 27 日, 山梨

3) Nishida H, Morimoto C, Sakamoto M, Yamada T. CD26 Is a Novel Target of Treatment for Tumor Progression and Its Related Bone Disease in Multiple Myeloma. The 57th ASH Annual Meeting and Exposition December 5-8, 2015, Orlando, FL, USA

4) Ryo Hatano, Taketo Yamada, Haruna Otsuka, Eriko Komiya, Noriaki Iwao, Ko Okumura, Chikao Morimoto, Kei Ohnuma. Anti-interleukin-26 therapy for lung fibrosis of GVHD. 第 77 回日本血液学会学術集会, 2015 年 10 月 16－18 日, 金沢

5) 古宮栄利子, 山崎裕人, 山田健人, 森本幾夫. CD26 promotes invasiveness of malignant pleural mesothelioma cell via upregulation of periostin. 第 74 回日本癌学会学術総会, 2015 年 10 月 8-10 日, 名古屋

6) 林睦, 間所裕子, 山田幸司, 西田浩子, 坂元亨宇, 森本幾夫, 山田健人. Antitumor activity of anti-CD26 humanized monoclonal antibody conjugated with triptolide via intranulear transportation. 第 74 回日本癌学会学術総会, 2015 年 10 月 8-10 日, 名古屋

7) Angevin E, Isambert N,Trillet-Lenoir VN, You V, Alxandre J, Zalcman G, Viel P, Farace F, Valleix F, Podoll T, Kuramochi Y, Miyashita I, HosonoO, Dang NH, Ohnuma K, Yamada T, Kaneko Y, Morimoto C. First -in-human phase I administration of YS110, a monoclonal antibody directed against the CD26 immunostimulatory molecule in advanced cancer patients. The 2015 ASCO, May 29-June 2, 2015, Chicago, USA
8) 波多野良, 大沼圭, 石井智徳, 岩田哲史, 奥村康, 関川巖, 森本幾夫. T 細胞共刺激分子 CD26 に基づく全身性エリテマトーデスの病態および疾患活動性の新規バイオマーカーの探索. 第 59 回日本リウマチ学会学術集会, 2015 年 4 月 23－25 日, 名古屋
9) Fujimoto N, Ohnuma K, Aoe K, Hosono O, Yamada T, Kishimoto T, Morimoto C. Clinical significance of soluble CD26 in malignant pleural mesothelioma. The 103th Annual Meeting of American Association of Cancer Research. April 18-22, 2015, Philadelphia, USA.
10) Fujimoto N, Ohnuma K, Aoe K, Hosono O, Yamada T, Kishimoto T, Morimoto C. Clinical significance of soluble CD26 in malignant pleural mesothelioma. 16th World Conference of Lung Cancer. Sep 6-9,2015, Denver, USA.
11) 藤本伸一、岸本卓己、青江啓介、加藤勝也、堀田勝幸、尾瀬功、長松康子。胸膜中皮腫に対する新規治療法の臨床導入に関する研究.第 63 回日本職業・災害医学会学術大会.平成 27 年 11 月 22 日,東京
12) 藤本伸一、宮本洋輔、山岸智子、浅野美智子、渕本康子、和田佐恵、北村賢一、小崎晋司、岸本卓己。悪性胸膜中皮腫診断における胸水中の secretory leukocyte pepitidase inhibitor (SLPI) の有用性について.第 56 回日本肺癌学会学術集会.平成 27 年 11 月 28 日,横浜

I. 知的財産権の出願・登録状況（予定を含む）

1. 特許取得

なし

2. 実用新案登録

なし

3.その他

【特許出願状況】

名称	:抗 CD26 抗体と他の抗がん剤とを組み合わせた癌治療用組成物
出願人(権利者)	:ワイズ・エー・シー株式会社
発明人	:山田健人，林睦、山田幸司、森本幾夫、岡本俊博、金子有太郎
出願日	:2015 年 9 月 11 日
出願番号	:特願 2015-179672
出願国	:日本及び PCT 加盟国

Ⅱ．　分担研究報告

厚生労働科学研究費補助金（労災疾病臨床研究事業）

分 担 研 究 報 告 書

【ヒト化 CD26 抗体と YB1 阻害アンチセンスとの in vitro 及び in vivo での併用効果について】

研究代表者　森本　幾夫　順天堂大学大学院医学研究科
免疫病・がん先端治療学講座 客員教授

共同研究者　岡本　俊博　免疫病・がん先端治療学講座 研究補助員

共同研究者　波多野　良　免疫病・がん先端治療学講座 博士研究員

共同研究者　中野　賢二　九州大学 先端融合医療ﾚﾄﾞｯｸｽﾅﾋﾞ研究拠点 教授

研究要旨

悪性胸膜中皮腫はアスベストばく露によって起こる胸膜中皮由来の難治性悪性腫瘍であり、現時点で満足できる治療法はなく、新たな治療法の確立が望まれる。われわれは、新規治療標的分子として悪性胸膜中皮腫細胞に発現する CD26 に着目し、ヒト化 CD26 抗体を開発しフランスにて第 I 相臨床試験を行った。安全性が確認されるとともに治療薬としての有効性を示唆する結果も得られ、平成 28 年 10 月から国内での第 I/II 相臨床試験を予定している。しかしながら、CD26 抗体単剤投与を行ったフランスでの臨床試験では、Stable Disease が認められるも完全寛解までは得られず、悪性胸膜中皮腫患者に完全寛解と肺機能改善をもたらす安全かつ有効な CD26 抗体との革新的な併用療法の開発が望まれる。Y-box binding protein (YB1)はがんの浸潤・転移促進に関与することから、有用な治療標的として着目されている分子であり、近年、共同研究者の中野賢二博士により良質な YB1 antisense oligonucleotide (YB1-ASO)が開発された。そこで本研究の初年度の取り組みとして、まず悪性胸膜中皮腫の浸潤及び増殖に対してヒト化 CD26 抗体と YB1-ASO の併用が相加的・相乗的な抑制効果を示すか検討した。in vitro 及び in vivo の結果から両者の併用の有用性を示唆する結果が得られ、今後 CD26 抗体と YB1-ASO を併用した際の抗腫瘍作用メカニズムの詳細を明らかにする。

A.研究目的

悪性胸膜中皮腫はアスベストばく露によって起こる胸膜中皮由来の難治性悪性腫瘍である。アスベストばく露から発症までの潜伏期間は 30-50 年とされ、日本を含めアジアやヨーロッパなど世界規模で胸膜中皮腫患者数は今後ますます増加すると考えられている。悪性胸膜中皮腫に対しては手術療法、化学療法、放射線療法などが行われるが、いずれも満足できる治療成績ではなく、化学療

法の標準治療法とされているアリムタ・シスプラチンの併用投与でも生存期間中央値は約 1 年と非常に短い。このことから、新たな治療法の確立が切望されている。われわれは、新規治療標的分子として悪性胸膜中皮腫細胞に発現する CD26 に着目し、ヒト化 CD26 抗体を開発しフランスにて悪性胸膜中皮腫を中心とした CD26 陽性腫瘍に対する第 I 相臨床試験を行った。特記すべき副作用もなく安全性が確認されるとともに、抗がん剤抵抗性の悪性胸膜中皮腫患者 19 例中 10 例が Stable Disease (SD)となり治療薬としての有効性を示唆する結果も得られ、平成 28 年 10 月から国内での第 I/II 相臨床試験を予定している。しかしながら、ヒト化 CD26 抗体単剤投与を行った上記の臨床試験では、SD が認められるも完全寛解までは得られず、副作用の少ない安全かつ有効な CD26 抗体との併用療法の開発が望まれる。

Y-box binding protein (YB-1)はコールドショック蛋白族に属するメンバーに属し、RNA の転写・翻訳の制御に関係するタンパク質でヒト癌細胞の核内と細胞質に局在する。P-糖蛋白質（MDR1,ABCB1）などの ABC トランスポーターや DNA 修復関連酵素の発現を上昇させ、広く薬剤耐性の獲得について重要な鍵を握るとされている。またさまざまな癌種において、YB-1 の核内局在や発現レベルはがんにおける薬剤耐性や予後の有用な予測因子ともいわれている。更にがん細胞の上皮間葉転換（EMT）を誘発し、浸潤、転移の促進にも関与することから、がんの有用な治療標的として注目されている。近年、共同研究者の九州大学中野賢二博士により生物活性や安定性に優れた良質な YB-1antisence oligonucleotide(YB-1ASO)が開発され、膵がんに対して増殖抑制効果、浸潤・転移抑制効果を示すことが報告された(特願　2012-89772)。

そこで、悪性胸膜中皮腫患者に完全寛解、及び肺機能改善をもたらす革新的な CD26 抗体との併用療法の確立を目指し、まず悪性胸膜中皮腫細胞株の浸潤及び増殖に対してヒト化 CD26 抗体と YB1-ASO の併用が相加的・相乗的な抑制効果を示すか検討した。効果を示すか検討した。

B. 研究方法

1) 細胞

本研究には、CD26 陽性ヒト悪性胸膜中皮腫細胞株 H226 及び JMN、CD26 陰性ヒト悪性胸膜中皮腫細胞株 MSTO-211H (MSTO-parent)に完全長のヒト CD26 を強制発現させた MSTO-CD26 を用いた。

2) 抗体及び試薬

ヒト化 CD26 抗体 YS110(Human IgG1 isotype)は Y's therapeutics により開発された。Goat anti-Human CD26 pAb (AF1180)は R&D Systems より購入した。Rabbit anti-Human YB1 mAb (clone ab74182)は abcam より購入した。YB1 antisense oligonucleotide (ASO)は九州大学 中野賢二博士によって開発されたものをいただいた。Control siRNA は Qiagen より購入した。Lipofectamine RNAiMAX Reagent (Thermo Fisher Scientific) を用いて YB1-ASO、control siRNA をどちらも終濃度 50-150 nM で細胞に添加し、transfection を行った。

3) in vitro 浸潤アッセイ及び増殖アッセイ

In vitro の浸潤測定には Boyden chamber アッセイを使用した。マトリゲルでコーティングされたインサートウェルに 2.5-3.5 x 10^4 個/ウェルで細胞を播種し、10%ウシ胎児血清(FCS)を誘引物質として用いた。浸潤した細胞はディフ・クィック(シスメックス)を用いて染色し、24 時間、48 時間後における細胞の浸潤を測定した。

In vitro 増殖アッセイには 96 well プレートを用い、2-4 x 10^3 個/ウェルで細胞を播種して 1 時間後に抗 CD26 抗体を添加した。24-72 時間後に MTT アッセイを行い細胞の増殖を測定した。

4) Luciferase 発現株の作製

H226 及び JMN を 24 well プレートに播種し接着後、CAG promoter 下に firefly Luciferase (Luc)遺伝子と RSV promoter 下に GFP と Puromycin 耐性遺伝子が組み込まれたベクターを含む pre-made のレンチウイルス粒子(GenTarget Inc)を Lnti-X Accelerator (Clontech)を用いて遺伝子導入した。その後、Puromycin を継続的に添加して Luc 発現細胞の selection を行い、さらに MoFlo Astrios (Beckman Coulter)を用いて GFP^+CD26^+ 画分を sorting することで GFP^+≧99%の H226-Luc、JMN-Luc を得た。

5) in vivo での腫瘍増殖評価

ヒト化 CD26 抗体と YB1-ASO の腫瘍増殖抑制効果を in vivo で評価するために、雌の C.B17-scid マウスの dorsal region に JMN 細胞株 1.2 x 10^5 cells を皮下移植し、翌日からヒト化 CD26 抗体を 400μg/dose で週 2 回腹腔内投与、YB1-ASO を 200μg/dose で週 2 回尾静脈注射した。腫瘍移植後 16 日目にマウスを安楽死させて解剖し、腫瘍を摘出して重量を測定した。全身性の腫瘍増殖に対するヒト化 CD26 抗体と YB1-ASO の効果を経時的にモニタリングするために、C.B17-scid マウスに Luciferase 発現 JMN 細胞株 1 x 10^5 cells を腹腔内移植し、翌日からヒト化 CD26 抗体を 200μg/dose で週 2 回腹腔内投与した。in vivo bioluminescence imaging は、マウスをイソフルランガスで麻酔した後、D-luciferin (Wako) を 3 mg/dose で腹腔内に注射し、基質を注射後 3 min, 6 min, 10 min 後に Caliper IVIS Lumina II In Vivo Imaging System (Perkin-Elmer)を用いて撮影した。画像データは Caliper Living Image software (Perkin-Elmer) で解析し、total flux of photons per second で発光強度を示した。

6) Flow cytometry

細胞を trypsin 処理して回収した後、FACS buffer (1%FCS 含有 PBS)で懸濁した。細胞膜上の CD26 の発現は、PE-conjugated Mouse anti-Human CD26 mAb (clone M-A261, BD Biosciences)を用いて染色した。細胞内の YB1 の発現は、BD Cytofix/Cytoperm Plus fixation/ permeabilization kit (BD Biosciences)を用いて細胞膜の固定/膜透過処理を行った後、一次抗体として Rabbit anti-Human YB1 mAb (clone ab12148, abcam)を使用し、二次抗体として FITC-conjugated anti-Rabbit IgG を用いた。Flow cytometry の解析は FACSCalibur (BD Biosciences)を用いて行った。

7) 免疫沈降及び Western Blot

細胞溶解液で細胞を処理後 SDS で denature を行い western blot に用いるサンプルを準備した。細胞質分画、核分画は NE-PER Nuclear and Cytoplasmic extraction Kit (Thermo Scientific)を用いて分取した。5-15μg のタンパクを SDS-PAGE に供し、セミドライ式ブロッテイングにて membrane に transfer した後、LAS 4000 (GE Healthcare)を用いてタンパク質を検出した。免疫沈降では細胞溶解液とヒト化 CD26 抗体(5-10μg)または抗 YB1 抗体(5-10μg)を 4℃で 2-24 時間反応させた。

8) Real-Time RT-PCR

Total RNA は RNeasy Mini kit (Qiagen)を用いて抽出し、PrimeScript II first strand cDNA synthesis kit (TaKaRa Bio)により cDNA を作製した。Human HPRT1 を内因性コントロールとして 7500 Real-Time PCR System と SYBR Select Master Mix (Applied Biosystems)を用いて mRNA の定量を行った。

9) 統計処理

統計解析には t 検定を用い、併用効果の解析には two-way ANOVA を使用した。

(倫理面への配慮)

ヒト化 CD26 抗体及び YB1-ASO の抗腫瘍効果を評価するためのマウスを用いた動物実験は、順天堂大学医学部実験動物委員会の審査を受け承認されている(承認番号 270138)。

C. 研究結果

1) *in vitro* での YB1-ASO による浸潤抑制効果

YB1 は EMT を誘発し、転移や浸潤に関与することが報告されている。そこで最初に YB1-ASO の浸潤に対する効果を CD26 陰性の MSTO-parent、CD26 を強制発現させた MSTO-CD26 を用いて検討した。MSTO-parent、MSTO-CD26 に YB1-ASO、control siRNA を導入し 24 時間後に Boyden chamber アッセイを行った。その結果、MSTO-CD26 では YB1-ASO により浸潤が抑制されたが、MSTO-parent に対して有意な抑制効果は観察できなかった (図 1)。このことから YB1 は特に CD26 陽性細胞において浸潤を促進している可能性が示唆された。

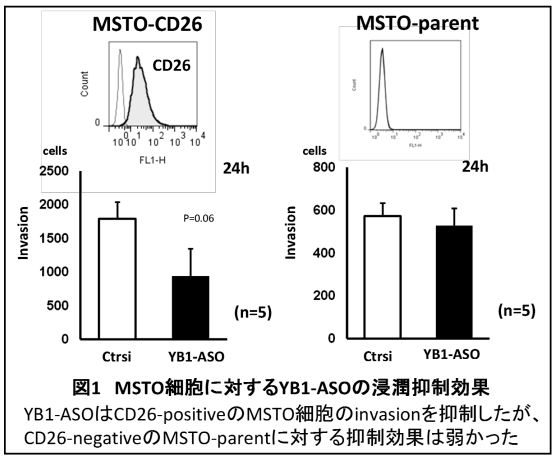

図1 MSTO細胞に対するYB1-ASOの浸潤抑制効果
YB1-ASOはCD26-positiveのMSTO細胞のinvasionを抑制したが、CD26-negativeのMSTO-parentに対する抑制効果は弱かった

2) *in vitro* での浸潤に対するヒト化 CD26 抗体と YB1-ASO の併用効果

そこで次に natural に CD26 を発現している H226, JMN に対する YB1-ASO の浸潤抑制効果、及びヒト化 CD26 抗体との併用効果について検討を行った。H226、JMN に YB1-ASO、control siRNA を導入し 24 時間後に Boyden chamber アッセイを行い、ヒト化 CD26 抗体との併用効果を検討した。その結果、ヒト化 CD26 抗体(終濃度 10,

20μg/ml)、YB1-ASO それぞれ単独で浸潤を抑制したが、YB1-ASO とヒト化 CD26 抗体を併用した場合にはより強く浸潤が抑制され、相乗効果が確認された(図 2)。

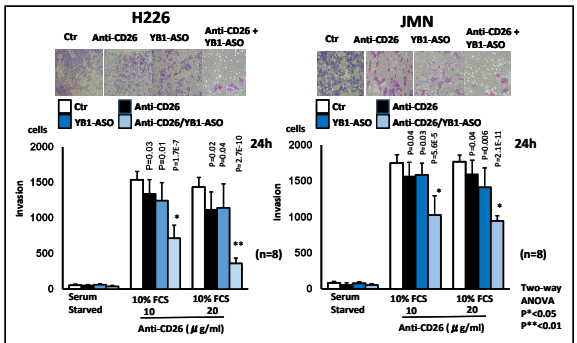

図2 H226細胞、JMN細胞の浸潤に対するヒト化CD26抗体とYB1-ASOの併用効果
YB1-ASOとヒト化CD26抗体の併用はinvasionの抑制を増強し、相乗効果が認められた

3) *in vitro* での増殖に対するヒト化 CD26 抗体と YB1-ASO の併用効果

YB1 は CD26 陽性細胞において浸潤を促進している可能性が考えられ、CD26 陽性細胞において YB1-ASO とヒト化 CD26 抗体との併用により浸潤抑制に相乗効果が認められた。そこで次に YB1-ASO とヒト化 CD26 抗体の増殖に対する併用効果を検討した。CD26 陰性の MSTO-parent に対して YB1-ASO は有意な増殖抑制効果を示さなかったが CD26 を強制発現させた MSTO-CD26 では YB1-ASO は抑制効果を示した(図 3A)。このことから、YB1 は CD26 陽性細胞の増殖も促進している可能性が示唆された。

次に natural に CD26 を発現している H226, JMN の増殖に対する YB1-ASO とヒト化 CD26 抗体との併用効果を検討した。H226、JMN に YB1-ASO、control siRNA を導入し 24 時間後に細胞を 96 well プレートに播種した。細胞を播種して 1 時間後にヒト化 CD26 抗体(終濃度 10μg/ml)を添加し、48 時間後に MTT assay を行った。その結果、ヒト化 CD26 抗体、YB1-ASO それぞれ単独において増殖を抑制し、YB1-ASO とヒト化 CD26 抗体の併用では増殖抑制効果が増強された(相加効果) (図 3B)。

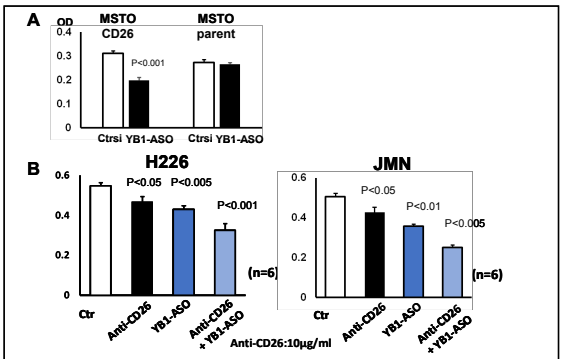

図3 CD26陽性中皮腫株の増殖に対するヒト化CD26抗体とYB1-ASOの併用効果
YB1-ASOとヒト化CD26抗体の併用は増殖の抑制を増強し、相加効果が認められた

4) *in vivo* での腫瘍皮下移植モデルにおけるヒト化 CD26 抗体と YB1-ASO の併用効果

In vitro 増殖アッセイにおいて YB1-ASO とヒト化 CD26 抗体の併用は増殖抑制効果を増強することが示された。そこで次に腫瘍細胞皮下移植モデルを用いて、in vivo での YB1-ASO とヒト化 CD26 抗体の増殖抑制効果を検討した。SCID マウスに JMN を皮下移植(1.2 x 10^5 cells/mouse)し、翌日から YB1-ASO (10 mg/kg, i.v.)とヒト化 CD26 抗体(20 mg/kg, i.p.)を週 2 回ずつ投与した。腫瘍移植後 16 日目に解剖し、腫瘍を摘出して重量を測定した。その結果、ヒト化 CD26 抗体、YB1-ASO それぞれ単独で増殖を抑制し、YB1-ASO とヒト化 CD26 抗体の併用により抑制作用が増強される傾向が観察された(図 4)。

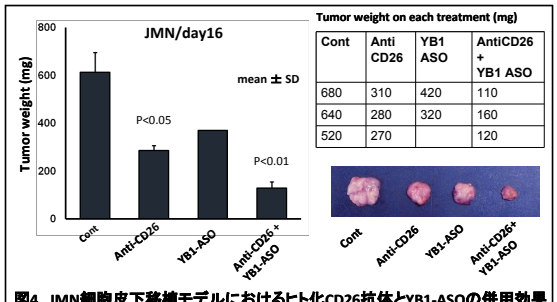

図4 JMN細胞皮下移植モデルにおけるヒト化CD26抗体とYB1-ASOの併用効果
in vivoにおいてもYB1-ASOとヒト化CD26抗体の併用により
腫瘍増殖抑制効果が増強される傾向が見られた

5) in vivo imaging system による経時的抗腫瘍効果の評価方法の確立

腫瘍の皮下移植モデルにおいて YB1-ASO とヒト化 CD26 抗体の併用により増殖抑制効果が増強される傾向が観察されたため、次に増殖に対する抑制効果の経時的変化を観察する目的で in vivo imaging system の実験系の確立を試みた。研究方法に記載した方法により Luciferase 発現 H226 細胞株及び JMN 細胞株を樹立した。この細胞株を SCID マウスに腹腔内移植(1 x 10^5 cells/mouse)し、ヒト化 CD26 抗体の効果を検討したところ CD26 抗体の増殖抑制効果が確認できた(図 5)。今後この系を用いて YB1-ASO とヒト化 CD26 抗体の併用効果を検討する。

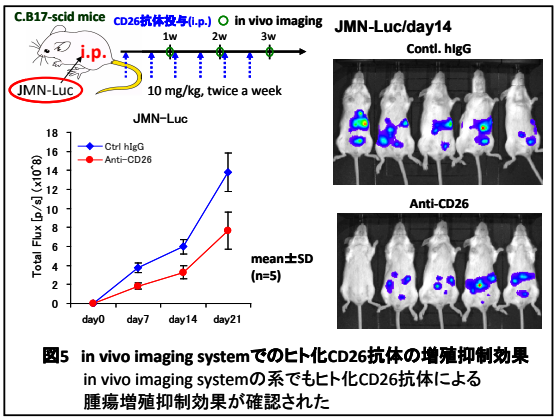

図5 in vivo imaging systemでのヒト化CD26抗体の増殖抑制効果
in vivo imaging systemの系でもヒト化CD26抗体による腫瘍増殖抑制効果が確認された

6) 悪性中皮腫細胞株における CD26 と YB1 の発現

YB1-ASO とヒト化 CD26 抗体の併用は浸潤抑制においては相乗効果を示し、増殖抑制においては相加効果が示された。YB1-ASO による浸潤抑制効果、増殖抑制効果は CD26 陽性細胞株で特に強く認められたことから、これらの併用効果には YB1 と CD26 の相互作用が重要であることが予想される。そこで、悪性中皮腫細胞株 H226、JMN 及び MSTO における CD26 と YB1 の発現をまず Flow cytometry により解析した。膜透過処理を行い、細胞質の YB1 を検出した結果、H226 と JMN 及び MSTO-CD26 においていずれも CD26 を発現している細胞の population に YB1 が発現していることが示された(図.6)。

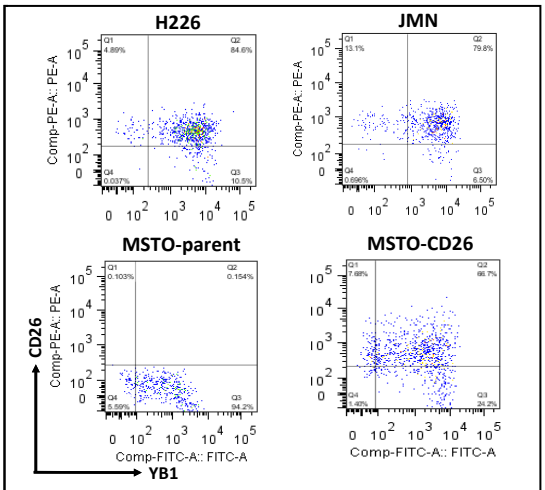

図6 悪性中皮腫細胞株におけるCD26とYB1の発現
CD26陽性populationのほとんどにYB1も発現している

7) YB1-ASO の CD26 mRNA およびタンパク質発現に対する作用

YB1 は CD26 を発現している細胞の population に発現していることが示された。次に YB1-ASO により CD26 発現に影響があるかどうか検討を行った。H226、JMN に YB1-ASO を導入して 48 時間後に Total RNA を抽出した。qPCR により CD26 mRNA 発現を定量した結果、YB1-ASO の導入により CD26 発現は mRNA レベルで減少することが示された(図 7A)。一方で、H226、JMN に YB1-ASO、control siRNA を導入し、48 時間後に細胞質画分、核画分のタンパク質を抽出して Western blot により CD26,と YB1 発現を測定した結果、細胞質画分、核画分ともに CD26 の発現がタン

パクレベルでは増加することが示された(図7B)。したがって YB1-ASO の導入により CD26 mRNA の転写は抑制されるが、翻訳は促進されることが示唆された。

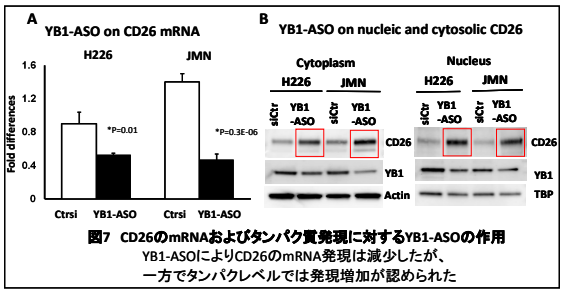

図7 CD26のmRNAおよびタンパク質発現に対するYB1-ASOの作用
YB1-ASOによりCD26のmRNA発現は減少したが、
一方でタンパクレベルでは発現増加が認められた

8) 細胞質及び核における CD26 と YB1 の相互作用

YB1-ASO により CD26 のタンパク質発現が増加することが示された。次に CD26 と YB1 が associate しているかどうかの検討を行った。H226、JMN の細胞質画分、核画分を分取し、それぞれの画分にヒト化 CD26 抗体、抗 YB1 抗体を 24 時間反応させて共沈実験を行った。その結果、CD26 と YB1 は核内よりも細胞質内に多く存在し、特に細胞質内で複合体を形成し、association している可能性が示された(図 8

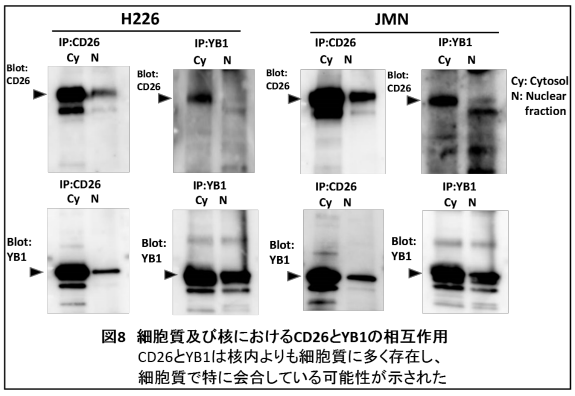

図8 細胞質及び核におけるCD26とYB1の相互作用
CD26とYB1は核内よりも細胞質に多く存在し、
細胞質で特に会合している可能性が示された

D. 考察

YB1-ASO とヒト化 CD26 抗体の併用は浸潤抑制においては相乗効果を示し、増殖抑制においては相加効果が示された。MSTO-parent と MSTO-CD26 transfectant を用いた実験により、YB1 は CD26 存在下でより強く浸潤や増殖を促進する可能性が示された。ヒト化 CD26 抗体と YB1-ASO との併用療法を考えるうえで、今後このメカニズムを解明していくことが重要である。

In vitro 浸潤アッセイにおいて YB1-ASO とヒト化 CD26 抗体の併用により浸潤の抑制作用が増強され、相乗効果が認められた。一方、in vitro 増殖アッセイでは併用により増殖の抑制において相加効果が確認された。悪性中皮腫は腫瘍の促進に胸膜への浸潤が大きく関与しているため、YB1-ASO とヒト化 CD26 抗体の併用は期待される治療法であると考えられる。今後、胸膜内に腫瘍細胞を移植する in vivo の系で胸膜への浸潤に対する併用効果を検討していく必要があると考えられる。

併用効果のメカニズムに対する考察として、CD26 と YB1 が特に細胞質で複合体を形成していることが示され、CD26 と YB1 が何らかの相互作用をしていると予想される。YB1-ASO の導入により CD26 mRNA 発現が抑制された一方で、細胞質画分、核画分における CD26 タンパクの発現は増強された。YB1 は mRNA の安定化に関与することが報告されているため、CD26 mRNA を安定化させていた YB1 が YB1-ASO により減少することで CD26 mRNA も減少した可能性が考えられる。一方で YB1 は翻訳を制御することも報告されており、結果的に YB1-ASO は CD26 の翻訳を増強させることにより CD26 発現を上昇させると考えられ、

この発現上昇した CD26 に対してヒト化 CD26 抗体が作用することで併用効果が認められた可能性が考えられる。CD26 を介していかなる分子が会合し、YB-1 とそれらがどのようなクロストークを行って機能発現に関与しているのか詳しい分子機構の解明が必要である。

また、in vivo 浸潤アッセイ系における YB1-ASO と抗 CD26 抗体の併用効果、YB1-ASO による CD26 の発現誘導メカニズム、発現誘導された CD26 によりどのような分子が誘発されるのかの検討も必要であると考えられる。

E. 結論

In vitro 及び in vivo study の解析の結果からヒト化 CD26 抗体と YB-1－ASO との併用はその有用性を示唆する結果が得られ、更に詳しい併用効果及びその抗腫瘍メカニズムを明らかにする予定である。

F. 次年度以降の計画

Luciferase 発現 H226 、JMN 株を用いて免疫不全マウスへ移植して in vivo モニタリング系にて至適量・投与間隔を定めて CD26 抗体、YB-1－ASO の併用に寄る詳しい抗腫瘍効果を検討する。また CD26 処理後の CD26・YB-1 の変化やその会合分子及びシグナル系の分子生物学解析を行いクロストーク及び併用療法と基礎となる評価を行う予定である。

G. 研究発表

1. 論文発表

1) Onuma K, Hatano R, MorimotoC. DPP4 in anti-tumor immunity: going beyond the enzyme. Nat Immunol.2015; 16:791-2.

2) Ohnuma K, Hatano R, Aune TM,Otsuka H, Iwata S, Dang NH, Yamada T, Morimoto C. Regulation of pulmonary GVHD by IL-26+CD4 T lymphocytes through CD26/caveolin-1 interaction. J Immunol. 2015; 194:3697-3712.

3) Katayose T, Iwata S, Oyaizu N, Hosono O, Yamada T, Dang NH, Hatano R, Tanaka H, Ohnuma K, Morimoto C. The role of Cas-L/NEDD9 as a regulator of collagen-induced arthritis in a murine model.Biochem Biophys Res Commun. 2015; 460:1069-75.

4) Otsuki N, Iwata S, Yamada T, Hosono O, Dang NH, Hatano R,Ohnuma K, Morimoto C. Modulation of immunological responses andamelioration of collagen-induced arthritis by the novel roxithromycin derivative 5-I. Mod Rheumatol. 2015; 25:562-70.

5) Ohnuma K, Saito T, Hatano R, Hosono O, Iwata S, Dang NH, Ninomiya H, Morimoto C. Comparison of two commercial ELISAs against an in-house ELISA for measuring soluble CD26 in human serum. J Clin Lab Anal. 2015; 29:106-11.

6) Hatano R, Ohnuma K, Otsuka H,

Komiya E, Taki I, Iwata S, Dang NH, Okumura K, Morimoto C. CD26-mediated induction ofEGR2 and IL-10 as potential regulatory mechanism for CD26 costimulatory pathway. J Immunol. 2015; 194:960-972.

2.学会発表

1) 森本幾夫. CD26 の機能と治療応用. 中皮腫シンポジウム, 2015 年 12 月 26 日, 兵庫

2) 森本幾夫. CD26 抗体を基盤とするトランスレーショナルリサーチ.第 57 回日本小児血液・がん学会,2015 年 11 月 27 日, 山梨

3) Nishida H, Morimoto C, Sakamoto M, Yamada T. CD26 Is a Novel Target of Treatment for Tumor Progression and Its Related Bone Disease in Multiple Myeloma. The 57th ASH Annual Meeting and Exposition December 5-8, 2015, Orlando, FL, USA

4) Ryo Hatano, Taketo Yamada, Haruna Otsuka, Eriko Komiya, Noriaki Iwao, Ko Okumura, Chikao Morimoto, Kei Ohnuma. Anti-interleukin-26 therapy for lung fibrosis of GVHD. 第 77 回日本血液学会学術集会, 2015 年 10 月 16－18 日, 金沢

5) 古宮栄利子, 山崎裕人, 山田健人, 森本幾夫. CD26 promotes invasiveness of malignant pleural mesothelioma cell via upregulation of periostin. 第 74 回日本癌学会学術総会, 2015 年 10 月 8-10 日, 名古屋

6) 林睦, 間所裕子, 山田幸司, 西田浩子, 坂元亨宇, 森本幾夫, 山田健人. Antitumor activity of anti-CD26 humanized monoclonal antibody conjugated with triptolide via intranulear transportation. 第 74 回日本癌学会学術総会, 2015 年 10 月 8-10 日, 名古屋

7) Angevin E, Isambert N,Trillet-Lenoir VN, You V, Alxandre J, Zalcman G, Viel P, Farace F, Valleix F, Podoll T, Kuramochi Y, Miyashita I, HosonoO, Dang NH, Ohnuma K, Yamada T, Kaneko Y, Morimoto C. First -in- human phase I administration of YS110, a monoclonal antibody directed against the CD26 immunostimulatory molecule in advanced cancer patients. The 2015 ASCO, May 29-June 2, 2015, Chicago, USA

8) 波多野良, 大沼圭, 石井智徳, 岩田哲史, 奥村康, 関川巖, 森本幾夫. T 細胞共刺激分子 CD26 に基づく全身性エリテマトーデスの病態および疾患活動性の新規バイオマーカーの探索. 第 59 回日本リウマチ学会学術集会, 2015 年 4 月 23－25 日, 名古

屋

9) Fujimoto N, Ohnuma K, Aoe K, Hosono O, Yamada T, Kishimoto T, Morimoto C. Clinical significance of soluble CD26 in malignant pleural mesothelioma. The 103th Annual Meeting of American Association of Cancer Research. April 18-22, 2015, Philadelphia, USA.

10) Fujimoto N, Ohnuma K, Aoe K, Hosono O, Yamada T, Kishimoto T, Morimoto C. Clinical significance of soluble CD26 in malignant pleural mesothelioma. 16th World Conference of Lung Cancer. Sep 6-9, 2015, Denver, USA.

H. 知的財産権の出願・登録状況（予定を含む）

1. 特許取得
   なし
2. 実用新案登録
   なし
3. その他

【特許出願状況】

名称：抗 CD26 抗体と他の抗がん剤とを組み合わせた癌治療用組成物

出願人(権利者)：ワイズ･エー･シー株式会社

発明人：山田健人，林睦、山田幸司、森本幾夫、岡本俊博、金子有太郎

出願日：2015 年 9 月 11 日

出願番号：特願 2015-179672

出願国：日本及び PCT 加盟国

厚生労働科学研究費補助金（労災疾病臨床研究事業）
分 担 研 究 報 告 書

【中皮腫におけるCD26およびYB-1発現について】

研究分担者　　山田　健人　埼玉医科大学 病理学教授

研究要旨

悪性中皮腫の新規治療法として期待されるヒト化 CD26 抗体療法および YB-1 アンチセンス療法においては、腫瘍組織における CD26 および YB-1 分子の発現の適確な評価が重要である。本研究では、すでに確立された CD26 発現評価方法とともに、新たに YB-1 発現評価方法の確立を通じて、臨床検体における本分子群の免疫染色での発現評価法の確立を行い検討した。初年度は、抗 YB-1 抗体について抗原賦活化やシグナル増幅等の至適化を行い染色法を確立した。その結果、CD26 および YB-1 発現は、悪性中皮腫 61 症例において、それぞれ 53、58 症例で陽性であり、YB-1 は肉腫型にも高率に発現していることを見出した。また YB-1 は腫瘍血管内皮細胞においても発現が認められ、その局在は腫瘍および内皮ともに細胞質であった。

A. 研究目的

仏にて施行されたヒト化 CD26 抗体療法の第 I 相臨床試験では、特記すべき有害事象なく、また中皮腫では 19 症例中 10 症例で「安定」(Stable Disease;SD)への導入が可能であり、安全性のみならず、その腫瘍効果も期待される成果が得られた。本研究課題では、この CD26 抗体療法とともに中皮腫細胞の増殖・細胞死を司る他の分子メカニズムを阻害することで、相加相乗効果を狙った新規治療法を目指している。その標的分子が、YB-1 である。YB-1 は、Ybox (CAAT/ATTG)と呼ばれる塩基配列を認識して標的遺伝子に結合する転写因子の一つであり、cold shock domain 蛋白スーパーファミリーに属する。本分子は、細胞周期関連分子や癌抑制分子などの細胞増殖や腫瘍悪性化に関与する転写・翻訳を制御するとともに、DNA-RNA との結合を介して翻訳にも関わる多機能分子である。この YB-1 は、ヒトがんにおける発現解析から、肺癌や乳癌の抗がん剤感受性や予後と相関するとの報告がなされている。また研究協力者・中野賢二博士は、この YB-1 に対するアンチセンス療法の開発にすでに成功している。

そこで本研究においては、まず悪性中皮腫症例における CD26 と YB-1 発現を詳細に明らかにし、CD26 とともに YB-1 が中皮腫における標的分子としてどのような発現パターンを示すのかを明らかにし、CD26 抗体および YB-1 アンチセンスの併用療法にそなえた基礎的検討を行うものである。また CD26 発現は現在用いられているアリムタ、シスプラチンなど化学療法剤の治療効果予測バイオマーカーとして

も有望な結果を得て報告(Clin Cancer Res 18:1447, 2012)してきたが、さらにCD26およびYB−１発現を細胞局在、陽性率、陽性強度など様々な要素で解析し、各種の臨床パラメーターとの相関を明らかにすることで、バイオマーカーとなりうるかどうかを検討することを目的とした。

B. 研究方法

YB-1の発現を臨床検体で検討するために、抗YB-1抗体（Rabbit monoclonal antibody(EP2708Y), ABCAM社ab76149）を用いた。本抗体は、ヒトYB-1のC末端領域を抗原として作成されたものであり、ヒトおよびげっ歯類のYB-1と反応する。YB−１陽性対照標本としては、ヒト癌細胞株（HeLa, SW480, A549, MCF7）を免疫不全マウス（NOD/SCID）皮下に移植して形成された腫瘍をホルマリン固定したものを用いた。またヒト組織としては、ホルマリン固定したパラフィン切片（CD26陽性である正常ヒト腎、肝、前立腺及び悪性中皮腫の組織および肺）を用いた。これらの組織でYB-1が染色可能であるかを検討するために、抗原賦活化として、１）前処置なし、２）0.1%トリプシン　室温、30分、３）0.04%　プロテイナーゼK　室温、15分、４）オートクレーブ処置（120℃、20分、0.01M Citrate Buffer pH8.0）、５）煮沸（10分、0.01M Citrate Buffer pH6.0）、の5つの条件を比較検討した。二次抗体は、Peroxidase付加抗ラビットIgG抗体(ImmPRESS社製)を用い、発色は、DAB液（Simple Stain DAB, Histofine）を用いた。

岡山労災病院および山口宇部医療センターにおける中皮腫61症例の腫瘍の病理組織（生検及び手術材料、10%ホルマリン固定、パラフィン切片）について、免疫染色を行った。抗原賦活化は、オートクレーブ処置（120℃、20分、0.01M　Citrate Buffer　pH8.0）を行った。抗CD26抗体は、仏の臨床試験で用いているR&D社製抗CD26ヤギ・ポリクロナール抗体（Lot.No. JOQ107061）およびマウス・モノクローナル抗体クローン19-32 を用いた。二次抗体は、Peroxidase付加抗ヤギIgG抗体(ImmPRESS社製)あるいはPeroxidase付加抗マウスIgG抗体(ImmPRESS社製)を用い、発色は、DAB液（Simple Stain DAB, Histofine）を用いた。いずれの染色においても、陽性対照には、正常ヒト腎、肝、前立腺及び悪性中皮腫を用い、陰性対照には、これらの正常組織切片内の各種組織（平滑筋、脂肪組織、結合組織など）とCD26陰性肺癌組織を用いた。

（倫理面への配慮）

患者検体などについては研究対象者に対する人権擁護上の配慮及び研究により研究対象者が受ける不利益、利益等の説明を患者及び遺族に対して行い、書面でのインフォームド・コンセントを得ている。また病理組織について免疫染色してCD26発現を解析する研究については、慶應義塾大学医学部および埼玉医科大学の倫理委員会の審査にて承認されている（承認番号20120100および734）。

C. 研究結果

ヒト癌細胞株（HeLa, SW480, A549,

MCF7）により抗原賦活化の方法を検討した。その結果、オートクレーブ処置（120℃、20 分、0.01M Citrate Buffer pH8.0）が最も染色性が強く、またバックグラウンドも低く抑えられることが判明した。そこで CD26 陽性であるヒト腎、肝、前立腺及び悪性中皮腫 1 症例および肺の組織を用いて、この抗原賦活化により YB-1 染色を施行した。その結果、正常肺組織においては、肺気管支上皮細胞や内皮細胞において、細胞質に瀰漫性の陽性所見を認めた。また中皮腫においても、腫瘍細胞の細胞質に瀰漫性で強い陽性像を観察した。そこで、中皮腫組織（上皮型 46 例、二相型 6 例、肉腫型 9 例）について、同様に YB-1 の免疫染色を行った。その結果、中皮腫組織において、YB-1 は腫瘍細胞の細胞質に瀰漫性に強陽性となり、その頻度は 61 例中 58 例が陽性であった（表 1 および図 1）。また腫瘍組織における腫瘍血管の内皮細胞において、細胞質に YB-1 発現を認めた。次にこれらの中皮腫組織における YB－1 陽性所見が真に YB－1 蛋白であるかどうかを確認するために、一次抗体について YB－1 蛋白による吸収実験を行った。ラビット抗ヒト YB-1 モノクローナル抗体と YB-1 蛋白を 4℃で 3 時間反応させた後、同様に免疫染色を施行した。その結果、中皮腫組織および血管内皮細胞における YB－1 陽性像がほぼ完全に消失したことから、この YB-1 の免疫染色は特異的に切片上の YB-1 蛋白発現を認識していると考えられた（図 1）。

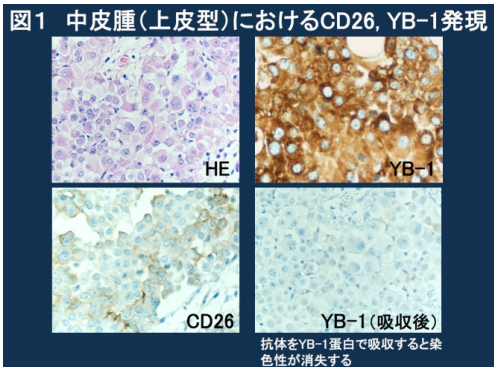

次に上記の中皮腫 61 症例について、ヒツジ抗ヒト CD26 ポリクローナル抗体を用いて同一検体での CD26 染色を行った（表 1）。その結果、CD26 陽性症例は 61 例中 53 例であり、CD26 陰性 8 症例中 2 症例は YB-1 も陰性であった。一方、CD26 陽性 53 例中、YB-1 陰性例は 1 例であった。

表1　中皮腫におけるCD26・YB−1発現
61症例（上皮型46例、二相型6例、肉腫型9例）

CD26	YB−1発現 陽性(58) C/N = 58/0	YB−1発現 陰性(3)
陽性(53) M/M+C/N = 20/29/4	52 / 61	1 / 61
陰性(8)	6 / 61	2 / 61

M:Membrane　C:Cytoplasmic　N:Nuclear

現在、これらの染色標本をデジタル画像とし、imageProPlus プログラムにて詳細に半定量的に発現を解析するための基礎検討を行っており、このデータベースを構築後に臨床パラメーターとの相関について検討する予定である。

悪性中皮腫の中で肉腫型あるいは二相型の肉腫成分において、CD26 陽性率が上皮型よりも低いことが、抗 CD26 ポリクローナル抗体を用いた検討から明らかになっている（上皮型 90%、肉腫型 30%）。ところが、抗 CD26 モノクローナル抗体クローン 19-32 を用いた免疫染色では肉腫型の 70%の症例で陽性となる（図 2）。

この 19-32 を用いた免疫染色での肉腫型における CD26 の陽性率は、肉腫型における YB-1 の陽性率と近いものであり、今後、肉腫型中皮腫ではポリクローナル抗体のみならず、モノクローナル抗体 19-32 と併用して CD26 発現を検討して行く予定である。

D. 考察

CD26 は、細胞膜貫通型の細胞表面に局在する糖蛋白質であるが、細胞内での局在は、細胞膜のみならず細胞質でのライソゾームや核内と広範囲である。一方、YB-1

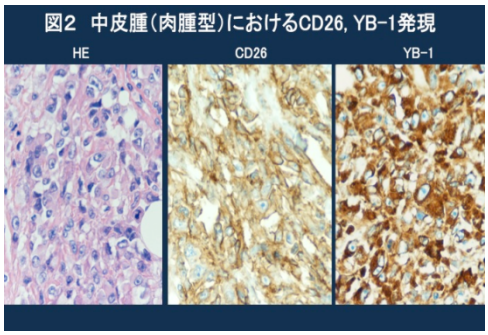

は、転写・翻訳に関わる分子であるが、免疫染色での観察では、主たる局在は細胞質であり、核の陽性像はほとんど得られていない。これらの分子の腫瘍細胞における局在は重要な意味を持つ可能性があるが、免疫染色での光学顕微鏡での観察では、CD26 と YB-1 が中皮腫細胞の細胞質において、類似した瀰漫性の局在を示すことは、これらの分子の相互作用の可能性も考慮する必要があると考える。本研究課題では、CD26 を標的とした抗体療法は、抗体による免疫学的細胞傷害や CD26 機能の抑制が主体であり、腫瘍細胞の細胞表面 CD26 は抗体により細胞質内に内在化される。一方、YB-1 を標的としたアンチセンス療法は、アンチセンスによる YB-1 蛋白発現抑制が主体である。このように併用療法においては、抗体により CD26 は細胞質内での増加とその核内移行が惹起され、一方、YB-1 蛋白はアンチセンスにより減少することが想像されるが、その場合に、中皮腫細胞における細胞増殖や細胞死の変化がどうなるか、さらなる検証が期待される。

また今後、悪性中皮腫における CD26 および YB-1 発現について細胞局在、陽性率、陽性強度などの各種パラメーターで詳細に定量評価することで、抗体療法の効果や予後などとの関連性あるいは臨床パラメーターを検証する基礎を構築していくことが重要と考える。

E. 結論

臨床検体における YB-1 の発現評価方法を確立した。中皮腫症例における CD26 と YB-1 の発現を明らかにし、いずれも高い比率で発現しており、共発現している症例がほとんどであることが明らかとなった。

F. 次年度以降の計画

初年度に引き続き、中皮腫組織（岡山労災病院 24 例、山口宇部医療センター35 例、慶應義塾大学病院 2 症例）について YB-1 と CD26 の発現を検討し、YB-1 と CD26 の発現レベルと臨床病理学的指標である、1）特異な浸潤増殖態度、2）遠隔転移、3）治療反応性、4）病期・生存期間、との関連を解析する。また森本博士らが見出しつつある CD26 シグナル系と YB-1 シグナル系の標的遺伝子やシグナルのクロストークする中でバイオマーカーとなりうる分子について免疫染色にて発現を検討

して、中皮腫の臨床病理学的指標との関連を解析する。

G. 研究発表

1. 論文発表

1) Adachi T, Kobayashi T, Sugihara E,Yamada T, Ikuta K, Pittaluga S, Saya H, Amagai M, Nagao K. Hair follicle-derived IL-7 and IL-15 mediate skin-resident memory T cell homeostasis and lymphoma. Nature Medicine 21:1272-9, 2015

2) Katayose T, Iwata S, Oyaizu N, Hosono O,Yamada T, Dang NH, Hatano R, Tanaka H, Ohnuma K, Morimoto C. The role of Cas-L/NEDD9 as a regulator of collagen-induced arthritis in a murine model. Biochem Biophys Res Commun. 460:1069-75, 2015

3) Ohnuma K, Hatano R, Aune TM, Otsuka H, Iwata S, Dang NH, Yamada T, Morimoto C. Regulation of pulmonary graft-versus-host disease by IL-26+CD26+CD4 T lymphocytes. J. Immunol. 194:3697-712, 2015

4) Sakiyama T, Kubo A, Sasaki T, Yamada T, Yabe N, Matsumoto K, Futei Y. Recurrent gastrointestinal perforation in a patient with Ehlers-Danlos syndrome due to tenascin-X deficiency. J. Dermatol. 42:511-514, 2015

5) Matsushita M, Ozaki Y, Hasegawa Y, Terada F, Tabata N, Shiheido H, Yanagawa H, Oikawa T, Matsuso K, Du W, Yamada T, Ichikawa D, Hattori Y A novel phthalimide derivative, TC11, has preclinical effects on high-risk myeloma cells and osteoclasts. PLoS One. 10:e0116135, 2015

6) Otsuki N, Iwata S, Yamada T, Hosono O, Dang NH, Hatano R, Ohnuma K, Morimoto C. Modulation of immunological responses and amelioration of collagen-induced arthritis by the− novel roxithromycin derivative 5-I. Modern Rheumatology Mod Rheumatol. 25:562-70, 2015

著書

山田健人　石綿の暴露はヒト体内で何を起こすのか：培養細胞を用いたモデル実験　石綿関連疾患の病理とそのリスクコミュニケーション　井内康輝編著篠原出版新社　2015年12月25日

2. 学会発表

1) Angevin E, Isambert N, Trillet-Lenoir V, You B, Alexandre J, Zalcman G, Vielh P, Farace F, Valleix F, Podoll T, Kuramochi Y, Miyashita I, Hosono O, Dang NH, Ohnuma K, Yamada T, Kaneko Y, Morimoto C. Phase I administration of YS110, a monoclonal antibody directed against the CD26 immunostimulatory molecule in advanced cancer patients. 2015,The 2015 ASCO, Chicago, USA, May

29-June 2,

2) 古宮栄利子、山崎裕人、山田健人、森本幾夫 CD26 promotes invasiveness of malignant pleural mesothelioma cell via upregulation of periostin. 第 74 回日本癌学会学術総会,2015 年 10 月 8-10 日,名古屋
3) 林　睦、間所裕子、山田幸司、西田浩子、坂元亨宇、森本幾夫、山田健人 Antitumor activity of anti-CD26 humanized monoclonal antibody conjugated with triptolide via intranulear transportation. 第 74 回日本癌学会学術総会,2015 年 10 月 8-10 日,名古屋
4) Nishida H, Morimoto C, Sakamoto M, Yamada T. CD26 Is a Novel Target of Treatment for Tumor Progression and Its Related Bone Disease in Multiple Myeloma. The 57th ASH Annual Meeting and Exposition (December 5-8, 2015) in Orlando, FL, USA

H.知的財産権の出願・登録状況（予定を含む）

１．特許取得
なし

２．実用新案登録
なし

３．その他
【特許出願状況】
名称：抗 CD26 抗体と他の抗がん剤とを組み合わせた癌治療用組成物
出願人(権利者)　：ワイズ･エー･シー株式会社
発明人：山田健人，林睦、山田幸司、森本幾夫、岡本俊博、金子有太郎
出願日：2015 年 9 月 11 日
出願番号　　：特願 2015-179672
出願国：日本及び PCT 加盟国

厚生労働科学研究費補助金（労災疾病臨床研究事業）

分 担 研 究 報 告 書

【ヒト化 CD26 抗体の抗腫瘍作用メカニズムの解明：免疫チェックポイント阻害薬としての新たな可能性】

研究代表者　森本　幾夫　順天堂大学大学院医学研究科
免疫病・がん先端治療学講座 客員教授

研究分担者　山田　健人　埼玉医科大学医学部 病理学 教授

共同研究者　波多野　良　順天堂大学大学院医学研究科
免疫病・がん先端治療学講座 博士研究員

共同研究者　大沼　圭　順天堂大学大学院医学研究科
免疫病・がん先端治療学講座 准教授

研究要旨

悪性胸膜中皮腫はアスベストばく露によって起こる胸膜中皮由来の難治性悪性腫瘍であり、現時点で満足できる治療法はなく、新たな治療法の確立が望まれる。われわれは、新規治療標的分子として悪性胸膜中皮腫細胞に発現する CD26 に着目し、ヒト化 CD26 抗体を開発しフランスにて第 I 相臨床試験を行った。安全性が確認されるとともに治療薬としての有効性を示唆する結果も得られ、平成 28 年 10 月から国内での第 I/II 相臨床試験を予定している。有効かつ安全な CD26 抗体との併用療法の開発とともに、CD26 抗体の抗腫瘍作用メカニズムの更なる解明は極めて重要である。CD26 は T 細胞に活性化シグナルを伝達する共刺激分子としても機能するため、CD26 抗体は免疫系にも影響する可能性が考えられる。そこで、強い CD26 シグナルが入ることで発現が誘導される免疫チェックポイント分子及び抑制性サイトカインの解析を行った結果、CD26 共刺激特異的に LAG3 と BTLA の高発現、IL-10 の高産生が誘導されることを明らかにした。このことから、CD26 抗体は T 細胞への CD26 シグナルの伝達をブロックし、それらの抑制性分子の発現誘導を阻害する免疫チェックポイント阻害薬としても作用する可能性が示唆された。

A. 研究目的

悪性胸膜中皮腫はアスベストばく露によって起こる胸膜中皮由来の難治性悪性腫瘍である。アスベストばく露から発症までの潜伏期間は 30-50 年とされ、日本を含めアジアやヨーロッパなど世界規模で胸膜中皮腫患者数は今後ますます増加すると考えられている。悪性胸膜中皮腫に対しては手術療法、化学療法、放射線療法などが行われるが、いずれも満足できる治療成績ではなく、新たな治療法の確立が望まれる。われわれは、新規治療標的分子として悪性胸膜中皮腫細胞に

発現する CD26 に着目し、ヒト化 CD26 抗体を開発しフランスにて第 I 相臨床試験を行った。特記すべき副作用もなく安全性が確認されるとともに、抗がん剤抵抗性の悪性中皮腫患者 19 例中 10 例が Stable Disease (SD)となり治療薬としての有効性を示唆する結果も得られた。平成 28 年 10 月から国内での第 I/II 相臨床試験を予定しているが、有効かつ安全な CD26 抗体との併用療法の開発とともに、CD26 抗体の抗腫瘍作用メカニズムの更なる解明は極めて重要である。

われわれはこれまでにヒト化 CD26 抗体の抗腫瘍作用メカニズムとして、抗体医薬特有の抗体依存性細胞傷害(ADCC)活性・補体依存性細胞傷害(CDC)活性に加え、CD26 陽性腫瘍に抗体が結合することによる直接的な作用があることを明らかにしてきた。がん細胞の細胞膜上の CD26 にヒト化 CD26 抗体が結合すると、cyclin dependent kinase inhibitor である p21 や p27 の発現が上昇し cell cycle arrest を起こさせること(Clin Cancer Res. 2001, Immunology. 2002, Clin Cancer Res. 2007)、CD26 抗体と CD26 の複合体が膜から細胞質、さらに核内へと移行し、RNA polymerase である POLR2A 遺伝子の転写領域下流に結合することで POLA2A の転写を抑制し増殖抑制に働くことを明らかにした(PLoS One. 2013)。また、CD26 は collagen や fibronectin との結合タンパクであるが、CD26 抗体が結合することでそれらのタンパクへの接着が阻害され(Clin Cancer Res. 2007)、このことから CD26 抗体が CD26 陽性腫瘍の浸潤・転移の抑制にも働くことが示唆された。

CD26 はヒト T 細胞に活性化シグナルを伝達する T 細胞共刺激分子であり、CD26 抗体は CD26 のリガンドである caveolin-1 の CD26 への結合をブロックする。また、CD26 の機能の一つに dipeptidyl peptidase IV (DPPIV)酵素活性があり、N 末から 2 番目にプロリンまたはアラニンを有するペプチドの 2 アミノ酸を切断する。生体内で様々な生理活性物質がその基質となることが知られているが、いくつかのケモカインも DPPIV による切断を受けその細胞遊走活性が不活性化される。CD26 抗体は DPPIV 酵素活性自体に直接は影響しないが、フランスでの第 I 相臨床試験の結果からヒト化 CD26 抗体の投与により血中の可溶性 CD26 の量が顕著に低下し、DPPIV 酵素活性も同様に低下することが示されている。DPPIV 酵素活性の低下によりケモカインの切断と不活性化が抑えられ、免疫細胞が腫瘍組織に遊走しやすくなる可能性が考えられる(Nat Immunol. 2015)。これらの知見から、CD26 抗体は免疫系にも影響する可能性が強く示唆される。

近年、がんの新たな治療法として免疫系に抑制シグナルを伝達するチェックポイント分子をブロックすることで腫瘍免疫を活性化させる免疫チェックポイント阻害薬が非常に着目されており、CTLA4 抗体や PD1 抗体は既に臨床現場で用いられ始めている。われわれは最近、ヒト CD4 T 細胞に強い CD26 共刺激シグナルが伝達するとチェックポイント分子である LAG3 の発現と代表的な抑制性サイトカインである IL-10 の産生が強く誘導されることを報告した(J Immunol. 2015)。そこで、CD26 抗体が免疫チェックポイント阻害薬としても機能する可能性を考え、CD26 共刺激によって誘導される免疫チェックポイント分子及び抑制

性サイトカインの解析を行った。

B. 研究方法

1) ヒト T 細胞の調製

順天堂大学医学部研究等倫理委員会での承認を得て、インフォームド・コンセントを書面で得られた成人健常者の末梢血から、Ficoll 密度分離法により末梢血単核球(PBMC)を調製した。PBMC から T 細胞への精製には MACS(磁気細胞分離)システム(Miltenyi Biotec)を用いた。ヒト CD4 T 細胞、CD8 T 細胞への精製には、それぞれ human $CD4^+$ T cell isolation kit, human $CD8^+$ T cell isolation kit (Miltenyi Biotec)を使用し、それぞれ $CD3^+CD4^+$ が 97%以上、$CD3^+CD8^+$ $CD56^{nega}$ が 95%以上であることを FACS Calibur (BD Biosciences)にて確認した。

2) 抗体と試薬

ヒト T 細胞の刺激には anti-CD3 mAb (OKT3), anti-CD28 mAb (4B10)及び anti-CD26 mAb (1F7)を用いた。Flow cytometry には下記のヒト抗原特異抗体を用いた。FITC-labeled anti-CD28 mAb (clone CD28.2), PE-labeled anti-CD26 mAb (clone M-A261) 及び APC-labeled anti-CTLA4 mAb (clone BNI3) は BD Biosciences から購入した。FITC-labeled anti-LAG3 mAb (clone 3DS223H) と PE/Cy7-labeled anti-TIGIT mAb (clone MBSA43)は eBioscience から購入した。PerCP/Cy5.5-labeled anti-CD244 (2B4) mAb (clone C1.7), PE/Cy7-labeled anti-Tim3 mAb (clone F38-2E2), PE/Cy7-labeled anti-CD160 mAb (clone BY55), APC-labeled anti-PD1 mAb (clone EH12.2H7), APC-labeled anti-BTLA mAb (clone MIH26), APC-labeled anti-CD39 mAb (clone A1), APC-labeled anti-DNAM1 (CD226) (clone 11A8)は BioLegend から購入した。

3) フローサイトメトリー

精製した末梢血 CD4 T 細胞、CD8 T 細胞を、抗 CD3 抗体 0.5μg/ml と抗 CD28 抗体または抗 CD26 抗体 2, 5, 10, 20, 50μg/ml で固相化した 96 well 平底プレート(Costar)に 1 x 10^5 cells/well で播種し、96 時間後に細胞を回収して細胞膜上の免疫チェックポイント分子の発現を解析した。活性化刺激を入れる前の末梢血から精製した直後の CD4 T 細胞、CD8 T 細胞に関しても同様の解析を行った。FACSCalibur (BD Biosciences)で測定を行い、得られたデータを FlowJo (Tree Star)で解析した。

4) 培養上清の調製とサイトカインの定量

精製した末梢血 CD4 T 細胞、CD8 T 細胞を、抗 CD3 抗体 0.5μg/ml と抗 CD28 抗体または抗 CD26 抗体 2, 5, 10, 20, 50μg/ml で固相化した 96 well 平底プレートに 1 x 10^5 cells/well で播種し、96 時間後に培養上清を回収した。培養上清中の IL-10 濃度の定量には BD OptEIA Human IL-10 ELISA Kit (BD Biosciences)を用いた。450/570 nm の吸光値を microplate reader (Bio-Rad)で測定し、得られたデータを Microplate Manager 6 (Bio-Rad)で解析した。

(倫理面への配慮)

成人健常者の末梢血を用いた研究につい

ては、順天堂大学医学部研究等倫理委員会の審査を受け承認されている（承認番号2015008）。末梢血の提供を受ける際には、研究対象者に対する人的擁護上の配慮及び研究により研究対象者が受ける不利益、利益等の説明を行い、書面でのインフォームド・コンセントを得ている。

C. 研究結果

1）健常者末梢血 CD4 T 細胞、CD8 T 細胞における各種免疫チェックポイントの分子の発現

近年、免疫系に抑制シグナルを伝達するチェックポイント分子をブロックすることで腫瘍免疫を活性化させる免疫チェックポイント阻害薬が新たながん治療法として非常に着目されている。様々ながん種において様々な免疫チェックポイント分子の報告がされているが、いずれも CD8 T 細胞にスポットが当てられている。われわれは腫瘍微小環境において CD8 T 細胞の抑制だけでなく、CD4 T 細胞の抑制も免疫応答の不活性化を起こさせるうえで重要な現象と考え、CD8 T 細胞とともに CD4 T 細胞の解析も行うこととした。まず近年着目されている免疫チェックポイント分子に関して、それぞれのリガンドとの関係を図 1 にまとめた。

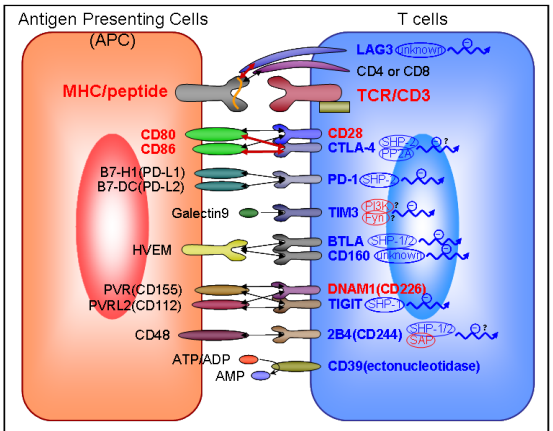

図1 近年着目されているcoinhibitory(immune checkpoint) molecule

メラノーマに対する治療薬として既に承認されている CTLA4 抗体、PD1 抗体に加え、LAG3 抗体も様々がん種に対する臨床試験が行われている。その他にも TIM3、BTLA、CD160、TIGIT なども最近の総説で有望な免疫チェックポイント阻害薬の標的分子として取り上げられている。

そこでまず、健常者の末梢血 CD4 T 細胞、CD8 T 細胞に発現している免疫チェックポイント分子の解析を行った。CD26 は末梢血 CD4 T 細胞、CD8 T 細胞ともに強陽性（$CD26^{high}$）、弱陽性（$CD26^{int}$）、陰性（$CD26^{nega}$）の三相性の発現パターンを示すため、CD26 との発現関係についても解析を行った。健常者 5 名の解析を行った結果、発現している割合に個人差はあるが、いずれの提供者でも PD1、TIGIT、2B4(CD244)、CD39 は CD4 T 細胞の 5%以上に発現していた(図 2)。CD160 も 3%程度ながら発現が認められた。CTLA4、LAG3、TIM3、BTLA に関しては 3%未満の非常に少数の細胞集団にのみ発現していることが示された。CD8 T 細胞に関しても CD4 T 細胞と発現している割合に違いはあるが、発現している分子は共通しており、PD1、TIGIT、2B4(CD244)、

CD39 が CD8 T 細胞の 5%以上に発現していた(図 2)。特に 2B4(CD244)は CD8 T 細胞の $CD26^{high}$ と $CD26^{nega}$ のサブセットに顕著な発現が認められた。CD160 も 3-5%程度の発現が認められ、CTLA4、LAG3、TIM3、BTLA に関しては CD4 T 細胞と同様に極少数の細胞集団にのみ発現していることが示された。

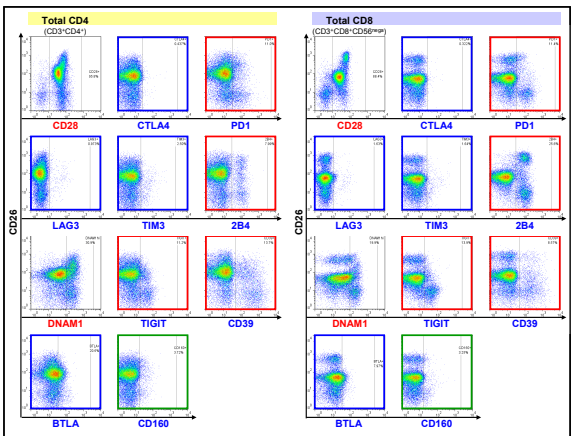

図2 健常者末梢血CD4, CD8 T細胞における免疫チェックポイント分子の発現

CD4 T 細胞、CD8 T 細胞に発現が認められた PD1、TIGIT、2B4(CD244)、CD39、CD160 と CD26 との発現関係に着目すると、それらの分子は $CD26^{nega}$ の画分に多く発現しており、$CD26^{high}$ や $CD26^{int}$ にも少ないながら発現している population が存在することが示された(図 2)。

2) CD26 共刺激によって特徴的に発現が増強する免疫チェックポイント分子の解析

CD26 の細胞内ドメインには ITIM や ITSM のような既存のシグナル伝達タンパク結合配列は存在しない。そのため、CD26 分子を介して直接抑制性シグナルが伝達するのではなく、CD26 シグナルによって抑制機能を有する免疫チェックポイント分子を誘導し、それらを介して免疫応答を負に制御する、すなわち免疫チェックポイント分子として機能する可能性を検討した。そこで、代表的な T 細胞活性化刺激である CD28 共刺激と比較して CD26 共刺激によって特徴的に発現が増強する免疫チェックポイント分子が存在するか解析を行った。健常者 5 名の解析を行った結果、活性化刺激によって誘導される割合に個人差はあるが、いずれの提供者でも CTLA4、PD1、LAG3、TIM3、BTLA の発現上昇が認められた(図 3)。中でも CD4 T 細胞の LAG3 と BTLA、CD8 T 細胞の BTLA は CD28 共刺激と比較して CD26 共刺激によって顕著に発現が増強することが示された(図 3)。CD8 T 細胞の LAG3 の発現に関しては提供者による違いが見られ、まだ検討を行っている。TIGIT は刺激前の T 細胞にも 10%以上発現しており、CD26 や CD28 の刺激強度依存的な発現上昇も見られなかった。2B4(CD244)、CD39、CD160 に関しては共刺激による発現上昇はほとんど認められなかった。

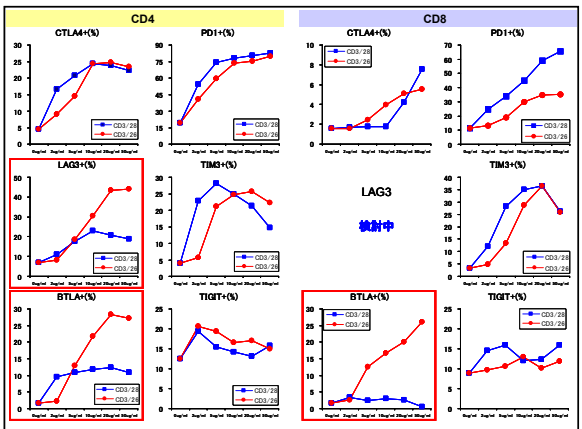

図3 CD26共刺激によってLAG3とBTLAの発現が顕著に亢進される

このことから、強い CD26 シグナルが CD4 T 細胞、CD8 T 細胞に伝達すると免疫チェックポイント分子である LAG3 と BTLA の発現が顕著に増強し、それらの分子を介して T 細胞に抑制シグナルが伝達する可能性が考

えられる。

3) CD26 共刺激による IL-10 産生誘導の解析

われわれは最近、健常者の末梢血 CD4 T 細胞に強い CD26 共刺激シグナルが伝達すると代表的な抑制性サイトカインである IL-10 の産生が強く誘導されることを見出した(J Immunol. 2015)。CD8 T 細胞の解析はまだ行っていなかったため、CD26 共刺激によって CD8 T 細胞にも抑制性サイトカインの産生が誘導されるか検討した。その結果、CD4 T 細胞に対しては CD28 共刺激と比較して CD26 刺激の強度が強いほど IL-10 の高産生が誘導されたのに対し、CD8 T 細胞に対しては CD26 共刺激による顕著な IL-10 産生の誘導は認められなかった(図 4)。IL-10 の産生量自体も CD8 T 細胞による産生は CD4 T 細胞と比較するとかなり低いことが示された(図 4)。また、IL-10 以外の代表的な抑制性サイトカインである TGF-β1、TGF-β3 に関しては、CD4 T 細胞、CD8 T 細胞ともに CD26 共刺激でも CD28 共刺激でも著明な産生は認められなかった(データ未掲載)。

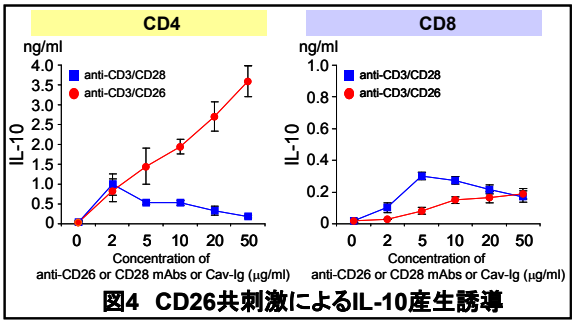

図4 CD26共刺激によるIL-10産生誘導

これらの結果から、CD26 共刺激は CD4 T 細胞に対して免疫チェックポイント分子である LAG3 と BTLA の高発現、抑制性サイトカインである IL-10 の高産生を誘導し、CD8 T 細胞に対しても CD28 共刺激と比較して BTLA の発現を顕著に誘導することから、CD26 はがん細胞周囲に浸潤した T 細胞にそれらの抑制性分子を誘導する免疫チェックポイント分子としても機能する可能性が示唆された。

D. 考察

ヒト化 CD26 抗体の抗腫瘍作用メカニズムの更なる解明を目的として、CD26 抗体の免疫系への影響、特に新たながん治療法として近年非常に着目されている免疫チェックポイント阻害薬として機能する可能性について検討した。

免疫チェックポイント分子の多くが、その細胞内ドメインに SHP-1/2 をはじめとしたフォスファターゼが会合し、T 細胞受容体からのシグナル伝達(キナーゼカスケード)を阻害することで T 細胞の活性化を負に制御する。CD26 の細胞内ドメインはわずか 6 アミノ酸で構成されており、フォスファターゼが会合することが知られている ITIM や ITSM と呼ばれる既存の配列は存在しない。このことから、CD26 分子の細胞内ドメインを介して直接抑制性のシグナルが伝達する可能性は低いと考えられる。そのため、CD26 分子を介して直接抑制性シグナルが伝達するのではなく、CD26 シグナルによって抑制機能を有する免疫チェックポイント分子を誘導し、それらを介して免疫応答を負に制御する、すなわち免疫チェックポイント分子として機能する可能性を検討した。本年度の結果から、CD26 共刺激は CD4 T 細胞に対して LAG3 と BTLA の高発現、IL-10 の高産生を誘導し、CD8 T 細胞に対しても CD28 共刺激と比較して BTLA の発現を顕

著に誘導することから、CD26 はがん細胞周囲に浸潤した T 細胞にそれらの抑制性分子を誘導する免疫チェックポイント分子としても機能する可能性が示唆された。

われわれは強い CD26 共刺激シグナルによって CD4 T 細胞の IL-10 高産生が誘導されるメカニズムの一端として、CD26 共刺激では CD28 共刺激よりも NFAT シグナルが強く、また ERK1/2 シグナルが強度は CD28 刺激よりも弱いながら長時間持続することを示した(J Immunol. 2015)。また、CD26 共刺激により転写因子 EGR2 の発現が強く誘導され、IL-10 産生や LAG3 発現に関与していることが示唆された。今後、IL-10 産生や LAG3 発現の誘導に関わるシグナル伝達経路の更なる解明とともに、今回新たに見出された BTLA の発現を誘導するシグナル伝達経路、及び転写因子についての解析が必要となる。それらの抑制性因子の発現を特異的に制御するシグナル伝達経路を明らかにできれば、そのシグナルを阻害する低分子化合物を抗体に代わる免疫チェックポイント阻害薬として応用できる可能性も期待できる。

本年度は健常者の末梢血 T 細胞における免疫チェックポイント分子の発現パターンについて解析を行ったが、次年度は、悪性中皮腫患者におけるそれらの分子の発現パターンを末梢血 T 細胞、胸水 T 細胞、悪性中皮腫周囲に浸潤した T 細胞を用いて解析する。また、平成 28 年 10 月から予定しているヒト化 CD26 抗体の国内第 I/II 相臨床試験で、実際にヒト化 CD26 抗体を投与した後の末梢血 T 細胞のエフェクター機能、IL-10 産生能、チェックポイント分子の発現変化についても、特に LAG3 と BTLA に着目して解析を行う予定である。これらの研究により、CD26 抗体が免疫チェックポント阻害薬としても機能しているかを明らかにする。

E. 結論

健常者の末梢血 CD4 T 細胞、CD8 T 細胞に発現する免疫チェックポイント分子を解析した結果、両 T 細胞に PD1、TIGIT、2B4 (CD244)、CD39 と少量の CD160 が発現していることが示された。CD26 共刺激は CD4 T 細胞に対して LAG3 と BTLA の高発現、IL-10 の高産生を誘導し、CD8 T 細胞に対しても CD28 共刺激と比較して BTLA の発現を顕著に誘導することから、CD26 はがん細胞周囲に浸潤した T 細胞にそれらの抑制性分子を誘導する免疫チェックポイント分子としても機能する可能性が示唆された。

F. 次年度以降の計画

IL-10 産生や LAG3 発現の誘導に関わるシグナル伝達経路の更なる解明とともに、今回新たに見出された BTLA の発現を誘導するシグナル伝達経路、及び転写因子についての解析が必要となる。また、本年度は健常者の末梢血 T 細胞における免疫チェックポイント分子の発現パターンについて解析を行ったが、次年度は、悪性中皮腫患者におけるそれらの分子の発現パターンを末梢血 T 細胞、胸水 T 細胞、悪性中皮腫周囲に浸潤した T 細胞を用いて解析する。また、悪性中皮腫自身やその周囲の細胞に LAG3、BTLA のリガンドである MHC class II や HVEM が発現しているかも免疫組織染色で検討していく予定である。

G. 研究発表

1. 論文発表

1) Ohnuma K, Hatano R, MorimotoC. DPP4 in anti-tumor immunity: going beyond the enzyme. Nat Immunol.2015; 16:791-2.

2) Ohnuma K, Hatano R, Aune TM,Otsuka H, Iwata S, Dang NH, Yamada T, Morimoto C. Regulation of pulmonary GVHD by IL-26+CD4 T lymphocytes through CD26/caveolin-1 interaction. J Immunol. 2015; 194:3697-3712.

3) Katayose T, Iwata S, Oyaizu N, Hosono O, Yamada T, Dang NH, Hatano R, Tanaka H, Ohnuma K, Morimoto C. The role of Cas-L/NEDD9 as a regulator of collagen-induced arthritis in a murine model.Biochem Biophys Res Commun. 2015; 460:1069-75.

4) Otsuki N, Iwata S, Yamada T, Hosono O, Dang NH, Hatano R,Ohnuma K, Morimoto C. Modulation of immunological responses andamelioration of collagen-induced arthritis by the novel roxithromycin derivative 5-I. Mod Rheumatol. 2015; 25:562-70.

5) Ohnuma K, Saito T, Hatano R, Hosono O, Iwata S, Dang NH, Ninomiya H, Morimoto C. Comparison of two commercial ELISAs against an in-house ELISA for measuring soluble CD26 in human serum. J Clin Lab Anal. 2015; 29:106-11.

6) Hatano R, Ohnuma K, Otsuka H, Komiya E, Taki I, Iwata S, Dang NH, Okumura K, Morimoto C. CD26-mediated induction ofEGR2 and IL-10 as potential regulatory mechanism for CD26 costimulatory pathway. J Immunol. 2015; 194:960-972.

2. 学会発表

1) 森本幾夫. CD26 の機能と治療応用. 中皮腫シンポジウム, 2015 年 12 月 26 日, 兵庫

2) 森本幾夫. CD26 抗体を基盤とするトランスレーショナルリサーチ.第 57 回日本小児血液・がん学会,2015 年 11 月 27 日, 山梨

3) Nishida H, Morimoto C, Sakamoto M, Yamada T. CD26 Is a Novel Target of Treatment for Tumor Progression and Its Related Bone Disease in Multiple Myeloma. The 57th ASH Annual Meeting and Exposition December 5-8, 2015, Orlando, FL, USA

4) Ryo Hatano, Taketo Yamada, Haruna Otsuka, Eriko Komiya, Noriaki Iwao, Ko Okumura, Chikao Morimoto, Kei Ohnuma. Anti-interleukin-26 therapy for lung fibrosis of GVHD. 第 77 回日本血液学会学術集会, 2015 年 10 月 16－18 日, 金沢

5) 古宮栄利子, 山崎裕人, 山田健人, 森本幾夫. CD26 promotes invasiveness of malignant pleural mesothelioma cell via upregulation of periostin. 第 74 回日本癌学会学術総会, 2015 年 10 月 8-10 日, 名古屋

6) 林睦, 間所裕子, 山田幸司, 西田浩子, 坂元亨宇, 森本幾夫, 山田健人. Antitumor activity of anti-CD26 humanized monoclonal antibody conjugated with triptolide via intranulear transportation. 第74回日本癌学会学術総会, 2015 年 10 月 8-10 日, 名古屋

7) Angevin E, Isambert N,Trillet-Lenoir VN, You V, Alxandre J, Zalcman G, Viel P, Farace F, Valleix F, Podoll T, Kuramochi Y, Miyashita I, HosonoO, Dang NH, Ohnuma K, Yamada T, Kaneko Y, Morimoto C. First -in-human phase I administration of YS110, a monoclonal antibody directed against the CD26 immunostimulatory molecule in advanced cancer patients. The 2015 ASCO, May 29-June 2, 2015, Chicago, USA

8) 波多野良, 大沼圭, 石井智徳, 岩田哲史, 奥村康, 関川巖, 森本幾夫. T 細胞共刺激分子 CD26 に基づく全身性エリテマトーデスの病態および疾患活動性の新規バイオマーカーの探索. 第 59 回日本リウマチ学会学術集会, 2015 年 4 月 23－25 日, 名古屋

9) Fujimoto N, Ohnuma K, Aoe K, Hosono O, Yamada T, Kishimoto T, Morimoto C. Clinical significance of soluble CD26 in malignant pleural mesothelioma. The 103th Annual Meeting of American Association of Cancer Research. April 18-22, 2015, Philadelphia, USA.

10) Fujimoto N, Ohnuma K, Aoe K, Hosono O, Yamada T, Kishimoto T, Morimoto C. Clinical significance of soluble CD26 in malignant pleural mesothelioma. 16th World Conference of Lung Cancer. Sep 6-9,2015, Denver, USA.

H. 知的財産権の出願・登録状況（予定を含む）

1. 取得
   なし
2. 実用新案登録
   なし
3. その他

【特許出願状況】

名称：抗 CD26 抗体と他の抗がん剤とを組み合わせた癌治療用組成物
出願人(権利者)：ワイズ· エー· シー株式会社
発明人：山田健人, 林睦、山田幸司、森本幾夫、岡本俊博、金子有太郎
出願日：2015 年 9 月 11 日
出願番号：特願 2015-179672
出願国：日本及び PCT 加盟国

Ⅲ.　研究成果の刊行に関する一覧表

＜研究成果の刊行に関する一覧表＞

【書　籍】

著者氏名	論文タイトル名	書籍全体の編集者名	書　籍　名	出版社名	出版地	ページ	出版年
山田健人	石綿の暴露はヒト体内で何を起こすのか：培養細胞を用いたモデル実験	井内康輝編著	石綿関連疾患の病理とそのリスクコミュニケーション	篠原出版新社	東京	30－38	2015

【雑　誌】

発表者氏名	論文タイトル名	発表誌名	巻号	ページ	出版年
Ohnuma K, Hatano R, MorimotoC	DPP4 in anti-tumor immunity: going beyond the enzyme	Nat Immunol	16	791－2	2015
Ohnuma K, Hatano R, Aune TM,Otsuka H, Iwata S, Dang NH, Yamada T, Morimoto C	Regulation of pulmonary GVHD by IL-26+CD4 T lymphocytes through CD26/caveolin-1 interaction	J Immunol	194	3697－3712	2015
Katayose T, Iwata S, Oyaizu N, Hosono O, Yamada T, Dang NH, Hatano R, Tanaka H, Ohnuma K, Morimoto C	The role of Cas-L/NEDD9 as a regulator of collagen-induced arthritis in a murine model.	Biochem Biophys Res Commun	460	1069－75	2015

発表者氏名	論文タイトル名	発表誌名	巻号	ページ	出版年
Otsuki N, Iwata S, Yamada T, Hosono O, Dang NH, Hatano R,Ohnuma K, Morimoto C	Modulation of immunological responses andamelioration of collagen-induced arthritis by the novel roxithromycin derivative 5-I	Mod Rheumatol	25	562－70	2015
Ohnuma K, Saito T, Hatano R, Hosono O, Iwata S, Dang NH, Ninomiya H, Morimoto C	Comparison of two commercial ELISAs against an in-house ELISA for measuring soluble CD26 in human serum	J Clin Lab Anal	29	106－11	2015
Hatano R, Ohnuma K, Otsuka H, Komiya E, Taki I, Iwata S, Dang NH, Okumura K, Morimoto C	CD26-mediated induction ofEGR2 and IL-10 as potential regulatory mechanism for CD26 costimulatory pathway	J Immunol	194	960－972	2015
Adachi T, Kobayashi T, Sugihara E, Yamada T, Ikuta K, Pittaluga S, Saya H, Amagai M, Nagao K	Hair follicle-derived IL-7 and IL-15 mediate skin-resident memory T cell homeostasis and lymphoma	Nat Med	21	1272-9	2015
Sakiyama T, Kubo A, Sasaki T, Yamada T, Yabe N, Matsumoto K, Futei Y.	Recurrent gastrointestinal perforation in a patient with Ehlers-Danlos syndrome due to tenascin-X deficiency	J. Dermatol	42	511-514	2015

発表者氏名	論文タイトル名	発表誌名	巻号	ページ	出版年
Matsushita M, Ozaki Y, Hasegawa Y, Terada F, Tabata N, Shiheido H, Yanagawa H, Oikawa T, Matsuso K, Du W, Yamada T, Ichikawa D, Hattori Y	A novel phthalimide derivative, TC11, has preclinical effects on high-risk myeloma cells and osteoclasts	PLoS One	10	e0116135	2015
Nojima D, Fujimoto N, Kato K, Fuchimoto Y, Kiura K, Kishimoto T, Tanimoto M	Pilot analysis of asbestos-induced diffuse pleural thickening with respiratory compromise.	Acta Med Okayama	69	261-6	2015
Yamagishi T, Fujimoto N, Nishi H, Miyamoto Y, Hara N, Asano M, Fuchimoto Y, Wada S, Kitamura K, Ozaki S, Kishimoto T.	Prognostic significance of the lymphocyte-to-monocyte ratio in patients with malignant pleural mesothelioma.	Lung Cancer	90	111-7	2015
Furukawa M, Toyooka S, Hayashi T, Yamamoto H, Fujimoto N, Soh J, Hashida S, Shien K, Asano H, Aoe K, Okabe K, Pass HI, Tsukuda K, Kishimoto T, Miyoshi S.	DNA copy number gains in malignant pleural mesothelioma.	Oncol Lett	10	3274-8	2015

発表者氏名	論文タイトル名	発表誌名	巻号	ページ	出版年
Fujimoto N, Gemba K, Aoe K, Kato K, Yokoyama T, Usami I, Onishi K, Mizuhashi K, Yusa T, Kishimoto T	Clinical investigation of benign asbestos pleural effusion	Pulm Med	2015	416179	2015
Yamagishi T, Fujimoto N, Miyamoto Y, Asano M, Fuchimoto Y, Wada S, Kitamura K, Ozaki S, Nishi H, Kishimoto T	Brain Metastases in Malignant Pleural Mesothelioma	Clin Exp Metastasis			In Press
Miyamoto Y, Fujimoto N, Asano M, Nakasuka T, Hara N, Yamagishi T, Fuchimoto Y, Wada S, Kitamura K, Ozaki S, Kishimoto T	Lymphohistiocytoid mesothelioma with a response to cisplatin plus pemetrexed: a case report	Cancer Treatment Communications	4	1-5	2015
Matsumoto S, Fujimoto N, Fuchimoto Y, Asano M, Yano T, Kishimoto T	Endobronchial T-cell lymphoma in a patient with chronic pyothorax	Respirol Case Rep	3	44-7	2015
Nakasuka T, Fujimoto N, Hara N, Miyamoto Y, Yamagishi T, Asano M, Nishi H, Kishimoto T	Foreign body granuloma mimicking recurrence of malignant pleural mesothelioma	Res Med Case Rep	16	95-6	2015

発表者氏名	論文タイトル名	発表誌名	巻号	ページ	出版年
Yamagishi T, Fujimoto N, Miyamoto Y, Hara N, Asano M, Fuchimoto Y, Wada S, Kitamura K, Ozaki S, Nishi H, Kishimoto T	The Rapid Appearance and Disappearance of Dendriform Pulmonary Ossification Following Diffuse Alveolar Hemorrhage	Am J Res Crit Care Med	193	333－4	2016
Hara N, Fujimoto N, Miyamoto Y, Yamagishi T, Asano M, Fuchimoto Y, Wada S, Ozaki S, Kishimoto T	Lymphoproliferative disorder in pleural effusion in a subject with past asbestos exposure	Respir Med Case Rep	16	169－71	2015

Ⅳ.　研究成果の別刷

石綿関連疾患の病理とそのリスクコミュニケーション

井内　康輝　編著

篠原出版新社

執筆者一覧

Amatya V. Jeet（広島大学大学院医歯薬保健学研究院病理学研究室）
石川雄一（がん研究会がん研究所病理部）
井内康輝（広島大学名誉教授／NPO 法人総合遠隔医療支援機構／株式会社病理診断センター）
岡　輝明（関東中央病院病理科）
岡本賢三（北海道中央労災病院病理診断科）
亀井敏昭（現 PCL 福岡 病理・細胞診センター，前 山口県立総合医療センター病理診断科・中央検査部）
河合俊明（現 戸田中央臨床検査研究所，前 防衛医科大学校臨床検査医学）
河原邦光（大阪府立呼吸器・アレルギー医療センター病理診断科）
櫛谷　桂（広島大学大学院医歯薬保健学研究院病理学研究室）
酒井康裕（神戸大学医学部附属病院病理診断科）
佐藤鮎子（兵庫医科大学病理学講座分子病理部門）
清水重喜（兵庫医科大学病理学講座分子病理部門）
関戸好孝（愛知県がんセンター研究所分子腫瘍学部）
高田礼子（聖マリアンナ医科大学予防医学）
武島幸男（広島大学大学院医歯薬保健学研究院病理学研究室）
辻村　亨（兵庫医科大学病理学講座分子病理部門）
外山尚紀（東京労働安全衛生センター）
豊國伸哉（名古屋大学大学院医学系研究科病理病態学講座生体反応病理学・分子病理診断学）
鳥井郁子（兵庫医科大学病理学講座分子病理部門）
鍋島一樹（福岡大学医学部病理学講座）
濵﨑　慎（福岡大学病院病理部）
廣島健三（東京女子医科大学八千代医療センター病理診断科）
古谷杉郎（全国労働安全衛生センター連絡会議／石綿対策全国連絡会議）
松本慎二（福岡大学病院病理部）
山田健人（現 埼玉医科大学医学部病理学，前 慶應義塾大学医学部病理学教室）

（五十音順）

目　次

序文 …… 井内康輝　iii
執筆者一覧 …… iv

第Ⅰ章　石綿関連疾患の病理

石綿の曝露はヒト体内で何を起こすのか
ヒトにおける疾患 …… 井内康輝　3
ヒトにおける遺伝子変異 …… 関戸好孝　15
動物実験を用いた研究 …… 豊國伸哉　23
培養細胞を用いたモデル実験 …… 山田健人　30
中皮腫の病理
通常型中皮腫の病理
…… 武島幸男・櫛谷　桂・Amatya V. Jeet・井内康輝　39
特殊型中皮腫の病理 …… 河合俊明　57
早期中皮腫の病理 …… 廣島健三　68
中皮腫診断における免疫組織化学的所見の有用性 …… 酒井康裕　76
中皮腫の遺伝子異常
…… 清水重喜・鳥井郁子・佐藤鮎子・辻村　亨　91
中皮腫診断での体腔液細胞診の特徴と考え方 …… 亀井敏昭　103
中皮腫診断における FISH 法による *p16* の有用性
…… 鍋島一樹・濵﨑　慎・松本慎二　113
アスベスト肺がんの病理学 …… 石川雄一　121
石綿肺の病理
石綿肺の病理学的特徴 …… 岡本賢三　130
石綿肺と鑑別すべき肺病変の病理 …… 岡　輝明　143
石綿関連疾患の診断の新しいヘルシンキ・クライテリア …… 井内康輝　148
石綿小体の定量と分析－低侵襲・簡便・高精度な新定量法の紹介を含めて－
…… 河原邦光　158
石綿代替製品への曝露の病理 …… 高田礼子　169

第Ⅱ章　リスクコミュニケーション

石綿関連疾患の補償と救済の現状 …… 古谷杉郎　185
石綿関連疾患の予防と対策
石綿と震災 …… 外山尚紀　201
索引 …… 220

石綿の曝露はヒト体内で何を起こすのか
培養細胞を用いたモデル実験

山田　健人

1　石綿のヒトへの影響－培養細胞を用いた研究の現状

石綿が，肺に石綿肺を，胸膜に胸膜プラークや中皮腫を引き起こす．そこで肺や胸膜から取り出した細胞が石綿に対してどのような反応をするかを調べることは，このような病気の発症メカニズムや予防，治療を考える上で重要である．これまでに試験管内で培養される様々な細胞に石綿を加えて起こる現象や細胞内での生化学的，分子生物学的知見が集まってきている．しかし，試験管の中で石綿が培養細胞をただちにがん化することはないため，試験管内で観察される一つ一つの現象・知見を組み合わせることで，体内ではおそらくこのようなことが積み重なって長い年月を経て細胞のがん化が起こるのだろう，と推測することになる．

石綿に暴露している作業者は，肺胞腔内に好中球（白血球の一つ）の浸潤が多いことが知られている[1]．そこでヒトⅡ型肺胞上皮細胞株 A549 およびヒト気管支上皮細胞を石綿で刺激したところ，培養液中にインターロイキン 8（IL-8）という好中球を呼びよせて刺激するサイトカインの分泌を亢進させた[2]．しかし石綿以外の酸化チタンなどの物質では，IL-8 の誘導はみられなかった．また同様に石綿でラット肺上皮細胞および中皮細胞を 20 分間刺激したところ，4～8 時間後に炎症や線維化に関連する転写因子 NF κ B の一部 p65 が誘導され，核内への移行が進み DNA への結合能が高まった[3]．さらに石綿をラットに経気道的に吸引（6 時間／日，5 日／週，5 または 20 日）させたところ，肺における p65 の誘導は，5 日目から認められ，20 日間持続した．このことは石綿による肺や中皮細胞の刺激で惹起される炎症やその後の線維化の進行に必要な期間，炎症を引き起こしうることを示した[3]．またマウス腹腔マクロファージ（白血球のひとつ）を石綿で刺激すると，マクロファージは石綿を貪食するとともに，活性酸素の産生が上昇し，マクロファージは細胞死に陥る[4]．この時に，あらかじめ石綿から鉄イオンを除去しておくと，このマクロファージの細胞死はみられなかった．このことから石綿がマクロファージに貪食されるときに鉄イオンがあると活性酸素の産生が亢進して細胞死を引き起こすと推測される．一方，石綿の刺激は，マウス胸腔中皮細胞の中のグルタチオン（3 つのアミノ酸からなる抗酸化分子で活性酸素から細胞を保護する）を減少させることで，石綿刺激後にがん遺伝子である *c-fos* および *c-jun* を誘導する[5]．この現象は，石綿が細胞内において活性酸素から保護するレドックス（細胞内の酸化・還元状態）を変化させることで，がん化の最初の一歩を踏み出させている可能性を示唆する．正常ヒト中皮細胞を石綿とともに培養すると石綿の濃度依存性に細胞死が誘導される．しかし一定の濃度で石綿処理を行うと正常ヒト中皮細胞は腫瘍壊死因子 TNF- α（サイトカインの一種でがん細胞を殺傷することで発見された）を産生するとともに TNF- α 受容体が誘導される．このように一定量の TNF- α が誘導されると TNF- α 受容体を介して NF κ B が活性化して，その結果として正常ヒト中皮細胞は石綿に対して抵抗性を獲得する．この時，石綿と TNF- α の両方の存在下で正常ヒト中皮細胞を培養していると，頻度は低いながら通常の培養では観察できないような異常な細胞分裂像を認めるようになる[6]．これらの結果は，石綿で傷つけられながらも生き残った中皮細胞は，サイトカインの誘導

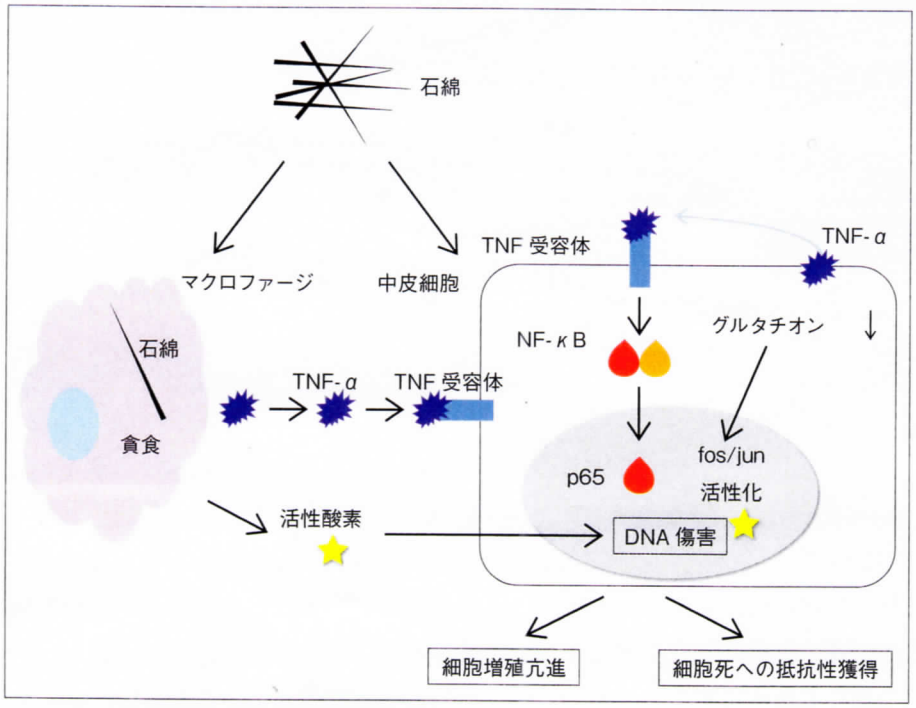

図 1　石綿のヒト培養細胞への影響

を介してさらなる細胞傷害や細胞死に抵抗性を獲得して，長い年月を経る間に悪性化していくことを推測させる．この石綿による中皮細胞の細胞死においては，細胞死の実行分子の一つである poly（ADP-ribose）polymerase の活性化と high mobility group box 1（HMGB1）タンパク質の核から細胞質への移動と細胞外への分泌が観察された[7]．HMGB1 の細胞外への分泌は，マクロファージからの TNF-α 産生を亢進させ，上記のように中皮腫細胞での石綿に対する抵抗性獲得を誘導した．実際に，血清中の HMGB1 濃度は，石綿暴露作業者において有意に高値を示した（**図 1**）．

このように石綿で培養細胞を刺激する試験管内の実験からは，石綿肺や中皮腫などの石綿関連疾患の発症メカニズムに関する多くの基礎的な知見が得られる．この知見をもとに以下に述べるモデル動物を使った研究や実際に石綿関連疾患患者の病態の解析に進み，これらの知見が本当に石綿関連疾患に関与しているかを判明していくことが重要と思われる．

2　中皮腫の培養細胞株

1）培養がん細胞

培養細胞は，最低限の必須な栄養を含む液体（培養液）にウシ血清を加えて，プラスチック製の培養皿の中で無菌的に育てられる．培養皿は，一定の濃度の二酸化炭素ガスの中で一定温度の培養器の中に置かれ，2～3 日に一度，培養液を取り替えることで細胞を増殖させる．細胞が多くなってきたら，細胞を培養皿から剥がすために，酵素液を使い，剥がした細胞の一部を次の培養皿に移して，再び培養することで細胞を増殖させる（継代培養）．ヒト成人の正常な細胞は，通常は一定期間，培養すると死滅してしまう．がん組織から採取されたがん細胞も，大部分の細胞は死滅するが，一部の細胞は培養液に順応して増殖を始める．増殖してきたがん細胞は，継代培養を繰り返せるようになり，冷凍保存が可能となる．このように安定して増殖するとともに凍結保存ができる細胞は細胞株とよばれる．

がん組織は様々な状態（染色体の質・量あるいは特定の遺伝子変異の有無，生化学的状態など）の細胞が集合しているものであることから，細胞株として均質なものを得るために，がん細胞を一つだけ取り出して，その単一の細胞から増殖させることで，クローン（または亜株）を得ることができる．このクローンは，単一細胞由来なので，染色体や遺伝子の状態や栄養要求などの生化学的状態が一定と推測され，より厳密ながん細胞株となる．このように，がん細胞株は，患者のがん組織に由来し，一定の組成の液体の中で増殖性を有し凍結保存に耐えるものである．さらにクローン化した細胞株では培養条件

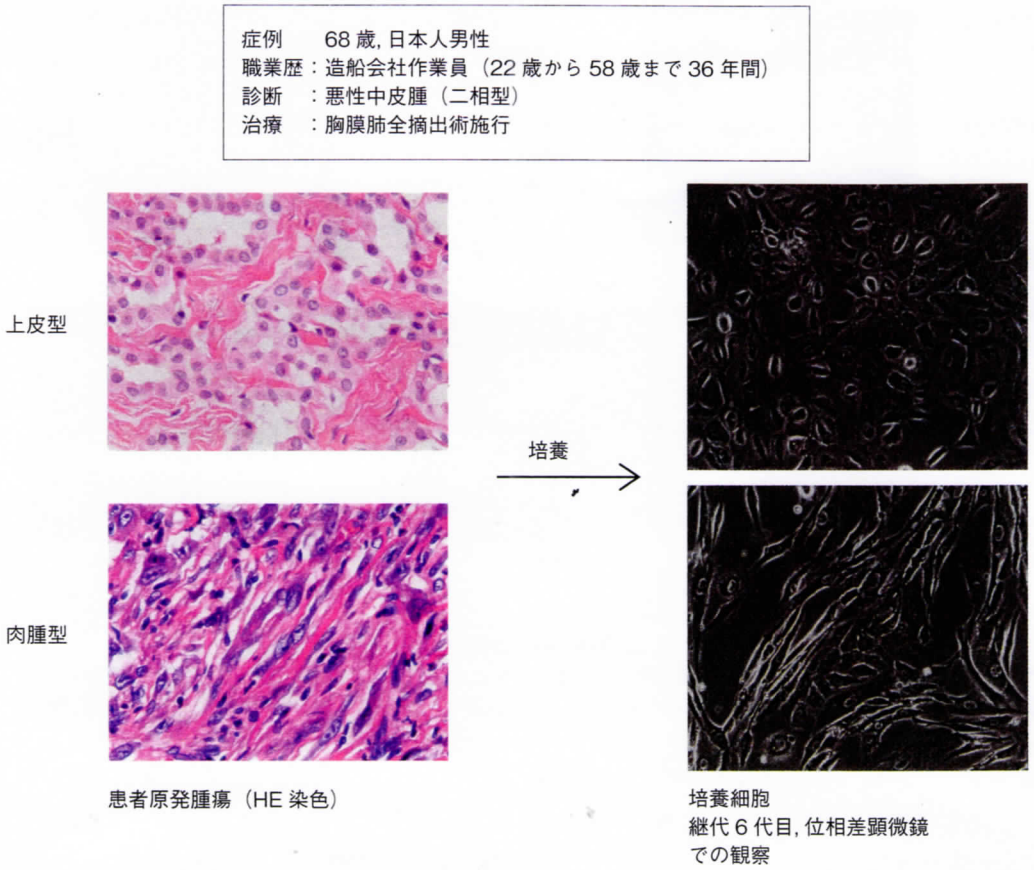

図2　中皮腫からの細胞培養
上皮型（HE染色，対物×20）と肉腫型（HE染色，対物×20）からでは培養細胞の形が異なる．
上皮型からは類円形の細胞，肉腫型からは紡錘形の細胞が増殖してくる．

を同じにすれば世界中のどこでも同様の培養が可能であり，大量の細胞が均一に安定して得られることから，さまざまながん研究に使用できる貴重で便利なものである．

2）中皮腫の培養細胞

中皮腫はきわめて悪性度の高いがんであるが，腫瘍としての進展速度は比較的遅いと考えられている．患者の同意のもとに中皮腫組織を採取して，そこからがん細胞を培養すると，患者の体腔内と同様に培養皿に接着して皿底に広がりながら増殖する．また胸水に浮遊していた中皮腫細胞を培養しても，同様に培養皿に接着して増殖する．患者の中皮腫組織や胸水から，いろいろな培養方法で多くの細胞株がこれまで樹立されてきた[8～11]．中皮腫は，患者の胸腔，腹腔，心嚢腔などの体腔を覆う中皮細胞から発生する腫瘍であり，別項目2で詳細に述べられているように体腔を這うように進展し，もともとあった組織に浸潤していく腫瘍である．

中皮腫は，その組織を顕微鏡で観察すると上皮型，肉腫型とこれらの両者が混在した二相型に分類される．これまで樹立されてきた中皮腫細胞株もこれらの様々な型の腫瘍から由来していて，培養皿の底で増殖する細胞の形は，由来となる型と相関することが多く，たとえば上皮型中皮腫由来の細胞株は，目玉焼きのような円形であったり，下駄のような長方形であったりして，それぞれが畳を並べたように互いの細胞が肩を寄せ合いながら増殖することが多い（**図2**）．

一方，肉腫型は紡錘形の細胞からなることが多く，いろいろな方向を向きながら互いに重なり合いながら秩序に乏しく増殖する（**図2**）．二相型からも細胞株が樹立されているが，前述したように多くの細胞株はクローン化されているため，上皮型か肉腫型かどちらかに類似しているもののみが得られている（両方の型が混じっている細胞株は樹立が難しい）[8, 9]．たとえば，JMN細胞は1982年に樹立し報告された細胞株で，腹膜原発の二相型中皮腫の患

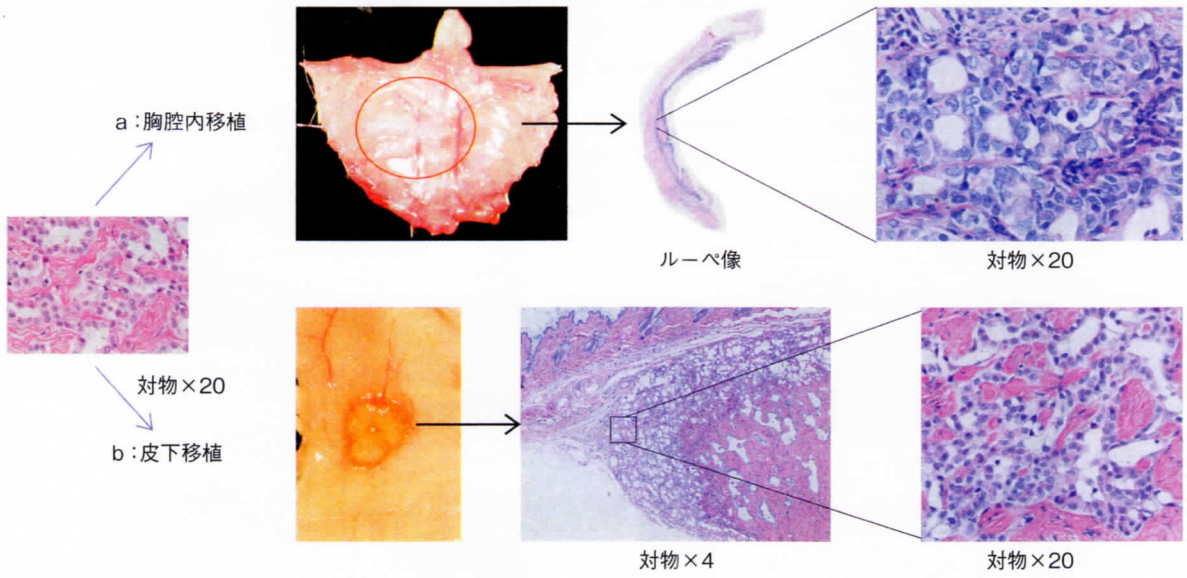

図3　中皮腫手術検体を用いた中皮腫動物モデル
患者（**図2**）の中皮腫組織（上皮型）をマウスへ同所移植（**a**：胸腔内移植）と異所移植（**b**：皮下移植）し，3カ月後にマウス胸腔（**a**）と皮下組織（**b**）に形成された腫瘍（いずれも上皮型）が観察される．胸腔内では，広がりをもった腫瘍が形成されるが（赤丸），皮下組織では，限局した腫瘤の形成にとどまる．染色はいずれもHE染色．

者の腹水から得られたものであり，後述するように新しい動物モデルや治療法の開発に役立っている貴重な細胞である[8]．この報告では，細胞株は培養において紡錘形細胞からなり，継代を重ねると紡錘形細胞はさらに細長くなり，重なり合いが強くなった．また，この細胞を免疫不全マウスの皮下に移植して形成された腫瘍では，上皮型や肉腫型の両方ができたと記載されている．ところが，現在，2015年の時点で入手できるJMN細胞は，紡錘形細胞からなり，免疫不全マウスの皮下や胸腔あるいは腹腔に移植すると肉腫型中皮腫のみが形成され，上皮型は全く認められない．このことは，当初は上皮型の細胞が混在していたものの，継代を続けるうちに，培養状態による選別がかかり，その条件で増殖しやすいものが優勢に増殖していくことで，細胞に様々な変化が加わってきたものと推測される．このように培養細胞株を用いたがん研究においては，最初に樹立されて報告された時とは細胞の性格やふるまい（染色体や遺伝子の構造・状態変化）が異なっている可能性があることを注意し，今，使用している細胞株がどのような状態であるかを確認する必要があることを示している．

3　中皮腫モデル動物の作出

1）同所移植と異所移植

ヒトがん組織を免疫不全マウスに移植することで，ヒトがん組織・細胞を生体内で観察することが可能である．通常，ヒトがんは，外表から観察しやすいマウス皮下組織に移植し，その後，時間とともに大きくなる腫瘍のサイズを計測する．このモデルを使うと，そのがんの増殖や細胞死に関わる遺伝子や機能分子の解析が可能であり，また新しい抗がん療法の効果を調べることも可能である．しかし，マウス皮下組織にヒトがんがある状態は，患者でいえば皮膚に転移した腫瘍をみていることになるが，がんが発生する場所にヒトがんを移植することで，原発腫瘍と似た状態でヒトがんを観察することが可能となる．たとえば，膵がんであればマウス膵臓に，肝がんであればマウス肝臓に移植する訳である．このような移植を同所移植と呼ぶ．

一方，ヒト膵がんや肝がんをマウス皮下組織に移植することを異所移植と呼ぶ．さて中皮腫の場合は，胃がん，肺がんや乳がんなどの一般的ながんとは，発生部位や組織像が異なるだけでなく，その増殖様式が大きく異なる．中皮腫では腫瘍が体腔表面を這うように進展し，さらに周囲の組織に浸潤することで，胸腔であれば胸壁や肺表面での強い痛みを引き

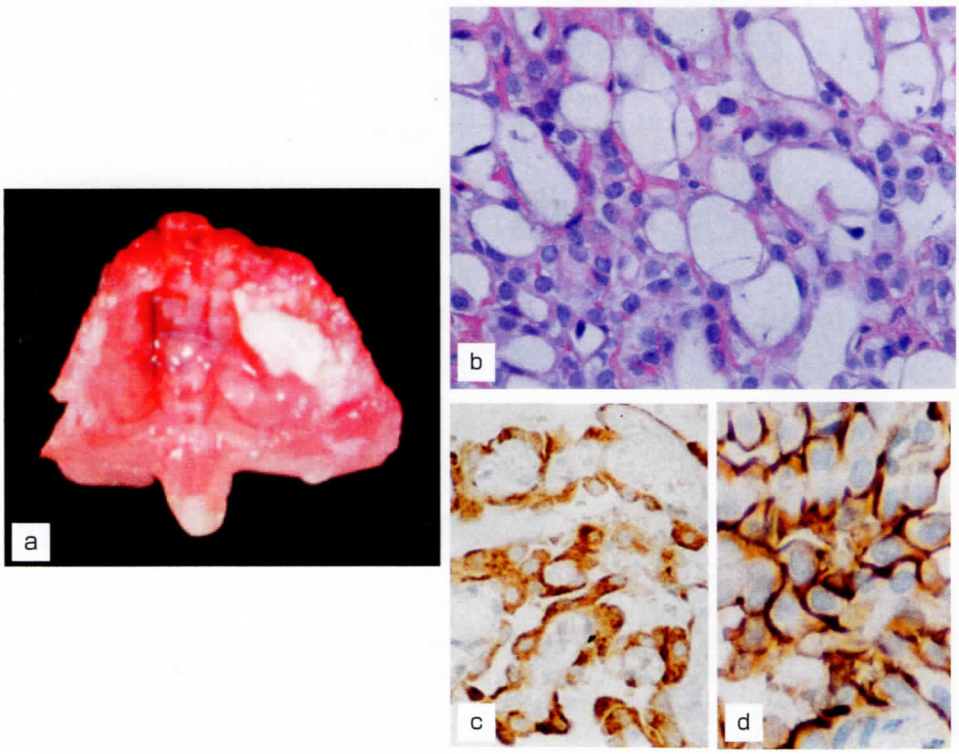

図 4　図 2 の腫瘍から樹立した KMES 細胞株の同所移植による中皮腫モデル
a：マウス胸腔を裏側から観察した．白色から薄いピンク色の腫瘍が胸腔を這うように進展している．
b：上皮型中皮腫の組織像が再現されている（HE 染色，対物× 20）．
c：Calretinin 染色陽性像（褐色．対物× 20）．
d：D2-40 染色陽性像（褐色．対物× 20）．

起こし，さらに進行すると呼吸機能低下を惹起する．このような特徴を持つ中皮腫を研究するには，なるべく患者の状態と近いモデル動物を作ることが重要である[12]．そこで中皮腫患者の同意を得て手術で摘出された腫瘍から小片組織を採取して，免疫不全マウスの胸腔内（同所）と皮下組織（異所）に移植した．移植後 3 カ月の時点でマウスを解剖して，胸腔内と皮下組織を観察した（**図 3**）．このように胸腔内に同所移植すると腫瘍は一カ所に留まらず，広がって増殖する傾向が認められ，患者の病態に近い像を示す．一方，皮下組織に異所移植した場合には腫瘍は一カ所に腫瘤を形成する．このように同じ腫瘍組織でも移植場所によって進展様式が異なることから，なるべく患者の病態に近いモデルを作って行くことが大事と考える．

2）腫瘍組織の移植と培養細胞株の移植

前述したように患者の中皮腫組織をマウスに移植して疾患モデルを作ることは可能であるが，手術をして組織を採取したときにのみ可能なモデルであり，患者によって，あるいは腫瘍ごとに様々な病態がマウスに再現されると考えられる．また，この場合には**図 2** のような腫瘍を形成するのに 3 ～ 6 カ月かかるのが通常である．そこで，どこの研究室でも均一な再現性が高いモデルが素早く可能にするのが，中皮腫培養細胞株を用いたモデル動物である．培養細胞株の 5 万個～ 50 万個の細胞を免疫不全マウスの胸腔内，腹腔内あるいは皮下組織に移植すると，おおむね 3 ～ 6 週間で腫瘍が形成される．培養細胞においても細胞株を選別することで，胸腔内への同所移植により再現性高く胸腔に沿って広がる進展方式を伴う中皮腫モデルができる[10, 13, 14]．

二相型中皮腫由来の細胞株である KMES 細胞 10 万個をマウス右胸腔内に移植して 4 週後にマウスを解剖した（**図 4**）．胸壁を心臓，肺側からみると胸腔内に中皮腫腫瘍組織が広範囲にわたって進展増殖していることがわかる（**図 4a**）．この進展は移植した右胸腔から胸骨の裏側を進み，移植 6 週後には左胸腔へ達して両側胸腔内に血性胸水を大量に貯留させる．またこの腫瘍について顕微鏡的観察を行うと

患者の腫瘍組織で観察された上皮型の成分の中皮腫ときわめて類似した組織像を示すことがわかった（**図 4b**）．さらにこの腫瘍組織について，中皮腫のマーカー（別項「中皮腫診断での体腔液細胞診の特徴と考え方」103 頁参照）である calretinin と D2-40 について免疫染色を行うと両者ともに陽性であることが明らかとなった（**図 4c，d**）．このように培養細胞株を移植することで中皮腫動物モデルを作出することで，世界中の研究室で均質で安定した再現性高い疾患モデルが利用できることことから，多くの培養細胞株がそれぞれの特徴を生かした分子レベルでの中皮腫の研究や新しい治療法の探索に広く利用されている．

4 培養細胞株を用いた中皮腫モデルあるいはモデル動物を用いた診断・治療法の開発

1）培養細胞株を用いた中皮腫の研究と治療法の開発

中皮腫細胞株を用いることで中皮腫の増殖や細胞死の分子機構を解析できることから，多くの研究がなされている．しかし，中皮腫は腫瘍組織も多彩で不均一であり個人差も大きい上，細胞株は樹立する過程でさまざまな要因から選別されることで，もとの腫瘍の一部の細胞（培養に順応できて，増殖能が高いもの）のみが得られると推測される．さらに一つの研究で用いられる細胞株は，数種類に限られてしまうことから，中皮腫全般における基盤となる分子機構を明らかにしていくには困難が多い．

6 種類の中皮腫細胞株（上皮型 1 株，肉腫型 1 株，二相型 4 株）を用いて，抗がん剤である selenite，bortezomib，carboplatin，pemetrexed，doxorubicin と gemcitabine とその様々な組み合わせによる増殖抑制効果を比較した報告がある．その中で，selenite 単独では，4 種類の細胞株（上皮型 1 株，二相型 3 株）では増殖抑制が観察されたが，他の 2 種類の細胞株（肉腫型 1 株，二相型 1 株）では効果がみられなかった．また他の単剤あるいは 2 種類の併用では，全体的に上皮型の方が，肉腫型よりも抗がん剤への感受性が高い傾向が認められた[15]．このように培養細胞株を用いて中皮腫のがんとしての性質を明らかにし，抗がん剤の開発を行うためには，上皮型，肉腫型，二相型の多種類の細胞株を併用して用いて行うことが望ましく，細胞株で得られた知見は，必ず患者の中皮腫組織において，本当にその知見が正しいかどうかを慎重に確かめて行くことが重要である．

二相型中皮腫由来 MSTO-211H 細胞株を用いることで，タンパク質の網羅的解析から中皮腫に多く発現している AHNAK 分子が同定された[16]．この分子は，他の中皮腫細胞株 7 種類すべてにおいて高い発現が確認されたが，正常ヒト中皮細胞では発現がみられなかった．さらに患者の中皮腫組織で調べたところ，上皮型，肉腫型および二相型のいずれの組織型においても発現がみられた．次に試験管の中で細胞が運動するときや細胞外マトリックスに浸潤するときにこの AHNAK 分子が積極的に機能していることが，これらの培養細胞株を用いることで明らかとなった．この研究は，中皮腫細胞株に特異的に多く発現している分子をみつけることで，新しいバイオマーカーの発見を行ったものであり，培養細胞を利用することで，その見い出された分子ががん細胞のどのような機能に関係するか，試験管内で探索することを可能にすることを示している．

ここでは多くの例は示せないが，最近，がん研究の中で発見されたマイクロ RNA（タンパク質にはならない非コード RNA）が中皮細胞において新しく見い出されたり[17]，中皮腫において CD26 という細胞膜表面分子が高い発現を示し，細胞接着や浸潤に関与していること，さらに抗 CD26 ヒト化抗体が中皮腫細胞株に対して抗がん効果を示すこと[18]，あるいは細胞内でタンパク質を分解する巨大な酵素複合体であるプロテアゾームの阻害剤が中皮腫細胞株の増殖を阻止すること[19]など，細胞株を利用した中皮腫の研究が蓄積しつつある．

2）モデル動物を用いた中皮腫の研究と診断・治療法の開発

試験管内で培養細胞を使って研究を行うことは，比較的均一な条件の中で生物学的現象を明らかにすることができることから，前述したような機能分子の同定や中皮腫で多く発現している分子の探索にとても有用である．さらに細胞増殖，接着，運動などの細胞の機能を定量的に解析できるのも培養実験の利点である．こうして見い出された分子が，細胞の機能に関わっていることをさらにヒト病態に近い状

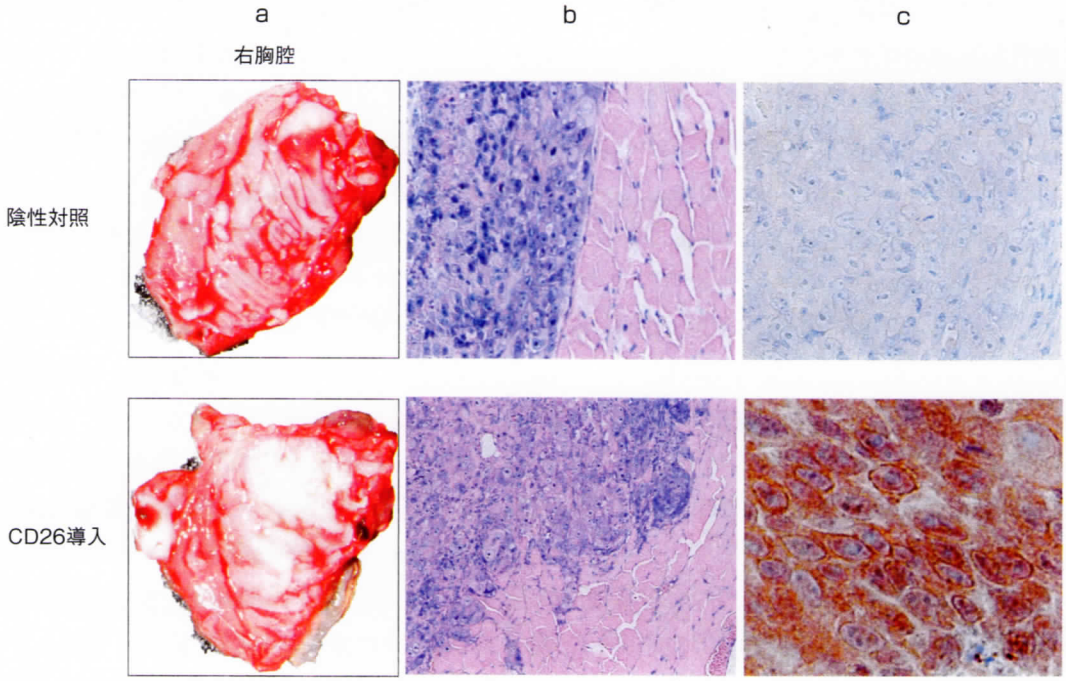

図5　MSTO-211H細胞による中皮腫モデルを用いたCD-26の機能解析

a：CD26発現がない細胞を移植した場合（陰性対照，**上図**）と比較してCD26発現がある場合（**下図**）では腫瘍の増殖が亢進する．

b：胸壁の標本では，陰性対照（**上図**：HE染色，対物×10）では筋組織との境界が明瞭であるのに対して，CD26導入群（**下図**：HE染色，対物×10）では筋組織への浸潤がみられる．

c：CD26発現（褐色）を示す（**上図**：CD26免疫染色，対物×20，**下図**：CD26免疫染色，対物×20）．

態で観察するために，前述したヒト中皮腫モデル動物が有用となる．中でも培養細胞株を免疫不全マウスへ移植して作出するモデルは，がん細胞とがんの環境を形成する周囲の細胞（血管，間質細胞や免疫担当細胞など）と細胞外マトリックス（細胞と細胞の間に存在して，足場や栄養などを提供する）の相互作用を観察することができる．

まずは中皮腫の組織型（上皮型，肉腫型）のモデルについて紹介する．上皮型細胞株STAV-ABと肉腫型細胞株STAV-FCSを免疫不全マウス皮下組織あるいは腹腔内に移植し，8週後にその腫瘍が解析された．その結果，いずれの細胞株も腫瘍の組織型としては上皮型の像を示したが，肉腫型の方が増殖速度が早かった．しかし，第3番染色体のCGHアレイ解析（comparative genomic hybridization，2色の蛍光色素でラベルした検体を競合的にマイクロアレイ上でハイブリダイズさせてコピー数を比較定量する解析技術）からは，培養細胞ではSTAV-AB細胞とSTAV-FCS細胞では，異なるパターンを示したのに対して，マウスに移植した腫瘍では，さらに異なったCGHパターンを示すとともに，2つの細胞株での差異は消失していた[20]．この研究は，培養細胞とモデル動物での細胞を取り巻く環境が異なることが原因で，細胞が増殖とともに腫瘍を形成する過程で，選別される可能性を示唆している．

次に培養細胞株では観察できない研究として，腫瘍とともに増生する血管についての研究を紹介したい．二相型中皮腫患者さんの血性胸水からEHMES-10細胞株を樹立された[10]．この細胞を免疫不全マウスの胸腔内に同所移植すると，5週後には血性胸水の貯留とともに胸腔内に腫瘍が広がっていた．腫瘍を顕微鏡で観察すると，腫瘍の中にはいわゆる腫瘍血管（マウス由来）が多く認められた．そこでEHMES-10細胞における血管内皮細胞の増殖因子であるvascular endothelial growth factor（VEGF）とその受容体VEGFR-2の発現を調べてみると，VEGFとVEGFR-2の両方の発現が高いことが判明した．このことは，この中皮腫細胞では，VEGFがオートクライン機構（みずから産生する増殖因子でみずからを増殖させること）で増殖亢進に寄与していることを示す．その後，同じ研究グループは，このVEGFの中和抗体bevacizumab（VEGFの作用を阻害する抗体）がpemetrexedとの併用により中皮腫の抗がん作用を発揮することを報告している[21]．

Imatinibは，受容体型チロシンキナーゼの阻害剤であり，慢性骨髄性白血病の分子標的薬として開発された分子である．阻害できる受容体型チロシンキナーゼとしては，Bcr-Abl，v-abl，c-abl，PDGF受容体およびc-Kitが知られている．このPDGF受容体が中皮腫において発現が多いことから，PDGF受容体陽性のREN細胞株を用いることで，imatinibがgemcitabineとの併用により抗腫瘍効果を示すことが報告された[22]．この研究でREN細胞株には，ルシフェラーゼ（ホタルが発光するための酵素，レポーター遺伝子とよぶ）の発現ベクターを導入しておき，そのルシフェラーゼ陽性REN細胞を免疫不全マウス腹腔に移植後，4週間経過観察する．マウス体内の腫瘍の様子は，あらかじめルシフェリン（ルシフェラーゼの基質でありルシフェリンがATP存在下にアデニレート化されて発光する）を注射してから，それにより発光した腫瘍をマウス体外から検出できる特別な装置を使って観察する．これにより，マウスを生かしたままで，経時的に腫瘍の増大や縮小を観察することができる（生体バイオイメージング）．この実験により，imatinibは単独では抗がん作用は明らかでないが，gemcitabineとの併用によりマウス体内の腫瘍増殖を抑制すること，そのときに中皮腫組織での細胞分裂は抑えられ，細胞死は増加することが判明した．さらにREN細胞株を移植したマウスをそのまま飼育していくと，gemcitabine単独投与と比較してimatinibとgemcitabineの併用投与により，マウスの生存期間は約20日延長した．この研究は，現在，他の疾患で有用な分子標的薬などの抗がん剤においても，中皮腫における同様の分子機構が解明されれば，中皮腫にも応用が可能であることを示唆している．さらにバイオイメージング技術の発達により，ルシフェラーゼなどのレポーター遺伝子を導入可能な培養細胞株をマウスに移植することで，生きたままで腫瘍の動態が観察できるようになり，がんモデル動物研究はさらに発展することが期待される．

5　中皮腫におけるCD26の機能とヒト化抗体を用いた分子標的療法

最後に中皮腫におけるCD26の機能とヒト化抗体を用いた分子標的療法について紹介する．中皮腫症例においては，上皮型の88％にCD26が高発現しているが，肉腫型での発現頻度は低い[23]．このCD26は，Tリンパ球の一部や血管内皮細胞，腎臓近位尿細管上皮などで発現が知られているが，がんにおける機能は不明であった．そこでまず中皮腫におけるCD26の機能を解析したところ，JMN細胞株を用いた検討から，CD26がファイブロネクチンやⅠ型コラーゲンとの接着に関与すること，抗CD26ヒト化モノクローナル抗体により細胞増殖が抑制されることが明らかとなった[18]．このCD26を発現ベクターにより，CD26陰性中皮腫細胞株MSTO-211Hに遺伝子導入して，CD26陽性MSTO-211H細胞を作製し，免疫不全マウス胸腔内に同所移植した．その結果，CD26陽性MSTO-211H移植マウスでは，CD26陰性細胞移植群と比較して胸腔内腫瘍の増大が促進され，移植6週後において腫瘍はより大きく厚くなっていた（**図5a，c**）．さらに腫瘍を顕微鏡的に観察すると，CD26陰性細胞移植腫瘍では，マウス胸壁筋組織への浸潤は示さず，境界が明瞭であったのに対して，CD26陽性細胞移植腫瘍では，胸壁筋組織に浸潤性の増殖を示した（**図5b**）．このことは，培養細胞を用いた細胞運動，浸潤の研究では限界があった中皮腫の特徴（胸腔に広がりながら胸壁や肺に浸潤性増殖する）をこのモデルでは再現しうることを示す．CD26陽性MSTO-211H細胞を同所移植するモデルにおいて，抗CD26ヒト化モノクローナル抗体を定期的に腹腔内投与すると，CD26陰性細胞移植群では腫瘍抑制効果はないが，CD26陽性細胞移植群では腫瘍径が1/2以下，腫瘍重量では1/3以下となった[14]．

このようにヒト中皮腫細胞株を用いることで，新たな分子を探索し着目して試験管内で分子・細胞レベルの詳細な研究を行い，さらに細胞株をマウスへ移植することでより疾患に類似した病態を再現するモデル動物を作って，そこであらためて分子の生体内での機能を解析できる．ときにはその分子を標的にした新規の治療法を考案して，その効果や安全性を動物モデルで評価する．このように培養細胞と実験動物を行ったり来たりしながら，中皮腫の研究を進めていくことが新しい診断法や治療法に繋がるものと期待している．最後に，これらの細胞培養株は患者の勇気ある決意と寛容な心に基づいて腫瘍組織

を提供していただいたことで初めて存在するものであり，すでに樹立して40年以上経っているもの，最近，樹立されたものを含めて感謝の念を述べたい．

文 献

1) Robinson BW, Rose AH, James A, et al：Alveolitis of pulmonary asbestosis. Bronchoalveolar lavage studies in crocidolite- and chrysotile-exposed individuals. *Chest* **90**：396-402, 1986
2) Rosenthal GJ, Germolec DR, Blazka ME, et al：Asbestos stimulates IL-8 production from human lung epithelial cells. *J Immunol* **153**：3237-3244, 1994
3) Janssen YM, Driscoll KE, Howard B, et al：Asbestos causes translocation of p65 protein and increases NF-κ B DNA binding activity in rat lung epithelial and pleural mesothelial cells. *Am J Pathol* **151**：389-401, 1997
4) Goodglick LA, Kane AB：Role of reactive oxygen metabolites in crocidolite asbestos toxicity to mouse macrophages. *Cancer Res* **46**：5558-5566, 1986
5) Janssen YM, Heintz NH, Mossman BT：Induction of c-fos and c-jun proto-oncogene expression by asbestos is ameliorated by N-acetyl-L-cysteine in mesothelial cells. *Cancer Res* **55**：2085-2089, 1995
6) Yang H, Bocchetta M, Kroczynska B, et al：TNF-alpha inhibits asbestos-induced cytotoxicity via a NF-κ B-dependent pathway, a possible mechanism for asbestos-induced oncogenesis. *Proc Natl Acad Sci USA* **103**：10397-10402, 2006
7) Yang H, Rivera Z, Jube S, et al：Programmed necrosis induced by asbestos in human mesothelial cells causes high-mobility group box 1 protein release and resultant inflammation. *Proc Natl Acad Sci USA* **107**：12611-12616, 2010
8) Behbehani AM, Hunter WJ, Chapman AL, et al：Studies of a human mesothelioma. *Hum Pathol* **13**：862-866, 1982
9) Bepler G, Koehler A, Kiefer P, et al：Characterization of the state of differentiation of six newly established human non-small-cell lung cancer cell lines. *Differentiation* **37**：158-171, 1988
10) Nakataki E, Yano S, Matsumori Y, et al：Novel orthotopic implantation model of human malignant pleural mesothelioma (EHMES-10 cells) highly expressing vascular endothelial growth factor and its receptor. *Cancer Sci* **97**：183-191, 2006
11) Relan V, Morrison L, Parsonson K, et al：Phenotypes and karyotypes of human malignant mesothelioma cell lines. *PLoS One* **8**：e58132, 2013
12) Colt HG, Astoul P, Wang X, et al：Clinical course of human epithelial-type malignant pleural mesothelioma replicated in an orthotopic-transplant nude mouse model. *Anticancer Res* **16**：633-639, 1996
13) Nayak TK, Bernardo M, Milenic DE, et al：Orthotopic pleural mesothelioma in mice：SPECT/CT and MR imaging with HER1- and HER2-targeted radiolabeled antibodies. *Radiology* **267**：173-182, 2013
14) Yamada K, Hayashi M, Madokoro H, et al：Nuclear localization of CD26 induced by a humanized monoclonal antibody inhibits tumor cell growth by modulating of POLR2A transcription. *PLoS One* **8**：e62304, 2013
15) Szulkin A, Nilsonne G, Mundt F, et al：Variation in drug sensitivity of malignant mesothelioma cell lines with substantial effects of selenite and bortezomib, highlights need for individualized therapy. *PLoS One* **8**：e65903, 2013
16) Sudo H, Tsuji AB, Sugyo A, et al：AHNAK is highly expressed and plays a key role in cell migration and invasion in mesothelioma. *Int J Oncol* **44**：530-538, 2014
17) Wright CM, Kirschner MB, Cheng YY, et al：Long non coding RNAs (lncRNAs) are dysregulated in Malignant Pleural Mesothelioma (MPM). *PLoS One* **8**：e70940, 2013
18) Inamoto T, Yamada T, Ohnuma K, et al：Humanized anti-CD26 monoclonal antibody as a treatment for malignant mesothelioma tumors. *Clin Cancer Res* **13**：4191-4200, 2007
19) Gordon GJ, Mani M, Maulik G, et al：Preclinical studies of the proteasome inhibitor bortezomib in malignant pleural mesothelioma. *Cancer Chemother Pharmacol* **61**：549-558, 2008
20) Darai-Ramqvist E, Nilsonne G, Flores-Staino C, et al：Microenvironment-Dependent Phenotypic Changes in a SCID Mouse Model for Malignant Mesothelioma. *Front Oncol* **3**：203, 2013
21) Li Q, Yano S, Ogino H, et al：The therapeutic efficacy of anti vascular endothelial growth factor antibody, bevacizumab, and pemetrexed against orthotopically implanted human pleural mesothelioma cells in severe combined immunodeficient mice. *Clin Cancer Res* **13**：5918-5925, 2007
22) Bertino P, Piccardi F, Porta C, et al：Imatinib mesylate enhances therapeutic effects of gemcitabine in human malignant mesothelioma xenografts. *Clin Cancer Res* **14**：541-548, 2008
23) Amatya VJ, Takeshima Y, Kushitani K, et al：Overexpression of CD26/DPPIV in mesothelioma tissue and mesothelioma cell lines. *Oncol Rep* **26**：1369-1375, 2011

DPP4 in anti-tumor immunity: going beyond the enzyme

Kei Ohnuma, Ryo Hatano & Chikao Morimoto

Effective anti-tumor immune therapy in solid tumors relies on the presence of effector T cells. Inhibition of the dipeptidylpeptidase DPP4 (CD26) enhances chemokine CXCL10–mediated infiltration of lymphocytes into the tumor parenchyma, which results in diminished tumor growth.

The dipeptidylpeptidase DPP4 is a homodimeric type II transmembrane glycoprotein expressed in many cell types and is identical with the leukocyte surface antigen CD26 (ref. 1). It is also present in serum and other body fluids in a truncated form. It preferentially cleaves amino-terminal dipeptides from polypeptides with proline or alanine in the penultimate position and regulates the activities of various cytokines and chemokines. However, direct *in vivo* evidence of a role for DPP4 in tumor biology and its interaction with the tumor microenvironment (TME) has not yet been reported. In this issue of *Nature Immunology*, work by Barreira da Silva *et al.* highlights the interaction between DPP4 and its substrate, the chemokine CXCL10, to demonstrate the function of DPP4-mediated post-translational modification of chemokines in regulating tumor immunity[2].

The TME consists of various cell types, along with the neoplastic cells themselves. Among these are effector lymphocytes that are able to infiltrate the tumor sites and are specifically required for the anti-cancer immune response[3]. Barreira da Silva *et al.* utilize a tumor-transplant model of the mouse melanoma cell line B16F10 to show that tumor growth is significantly delayed in *Dpp4*$^{-/-}$ mice relative to that in their heterozygous littermates. Moreover, their studies of wild type (*Dpp4*$^{+/+}$) mice fed chow formulated to contain the DPP4-specific inhibitor sitagliptin demonstrate that inhibition of DPP4 results in diminished tumor growth (**Fig. 1**). In addition, inhibition of DPP4 significantly reduces the number of lung metastases following intravenous injection of B16F10 cells. Although DPP4 is not expressed by B16F10 cells cultured *in vitro*, the authors detect high activity and expression of DPP4 in tumors resected from wild-type mice. However, they detect only a low level of tumor-associated DPP4 activity when they implant B16F10 cells into *Dpp4*$^{-/-}$ mice. These findings suggest that DPP4 has a role in regulating tumor growth and that the contribution of DPP4 activity *in vivo* is from both tumor-induced effects on the stroma as well as the tumor cells themselves.

CXCL10 is a chemoatractant for cells of the immune system, such as monocytes, T cells and natural killer cells, and is secreted from a variety of cells, including monocytes, neutrophils, eosinophils, epithelial cells, endothelial cells, fibroblasts and keratinocytes, in response to interferon-γ[4]. Cellular analysis of tumor-infiltrating leukocytes shows that large amounts of CXCL10 correlate with a greater number of CD4$^+$ and CD8$^+$ T cells in wild-type mice given implantation of B16F10 cells and fed chow containing sitagliptin. Meanwhile, the authors observe no significant difference between mice fed chow containing sitagliptin and those fed control chow (lacking sitagliptin) in the number of tumor-infiltrating myeloid cells, natural killer cells, B cells or CD25^{hi} regulatory T cells. The authors do not find the beneficial effect of the inhibition of DPP4 on the reduction in tumor growth in B cell– and T cell–deficient *Rag2*$^{-/-}$ mice fed sitagliptin-containing chow or control chow, which suggests that inhibition of DPP4 activates anti-tumor immunity via chemokine-mediated trafficking of T cells. Barreira da Silva *et al.* confirm this hypothesis by showing that mice deficient in the CXCL10 receptor CXCR3, mice deficient in CXCL10 and wild-type mice treated with a blocking antibody to CXCL10 (anti-CXCL10) fail to exhibit diminished melanoma growth following inhibition of DPP4. The authors extend their initial observation to other tumor models by implanting CT26 mouse colon carcinoma cells into BALB/c mice fed sitagliptin-containing chow. Inhibition of DPP4 results in a marked delay of CT26 tumor growth, which correlates with increased infiltration of T cells and natural killer cells. Meanwhile, treatment with blocking anti-CXCR3 abrogates the reduction in CT26 tumor growth mediated by inhibition of DPP4. These findings indicate that DPP4 in the TME acts to negatively regulate CXCR3-mediated anti-tumor immunity and effectively limit the infiltration of T cells into the tumor parenchyma.

Focusing on the anti-tumor response via TME-driven regulation of T cells provides scope for novel anti-cancer therapies; among these, adjuvant therapy, adoptive T cell–transfer therapy, and checkpoint-blockade therapy (with antibodies to the immunomodulatory receptors CTLA-4 (CD152) and PD-1) have led to important clinical advances. Barreira da Silva *et al.* demonstrate the efficacy of an anti-cancer treatment that combines inhibition of DPP4 with the adjuvant oligodeoxynucleotide CpG, which induces the production of bioactive CXCL10 in plasma. Notably, CpG-mediated tumor immunity is dependent on interferon signaling and CXCR3 expression. Inhibition of DPP4 stabilizes the biologically active form of CXCL10, which results in enhanced migration of T cells into the TME as a strategy for enhancing adjuvant-based tumor immunity. The use of ovalbumin-expressing B16F10 melanoma cells that are recognized by CD8$^+$ OT-I T cells (which transgenically express an ovalbumin-specific T cell antigen receptor) demonstrates a synergistic effect on the reduction in tumor size when adoptive transfer of OT-I cells is combined with sitagliptin treatment. The most

Kei Ohnuma, Ryo Hatano and Chikao Morimoto are in the Department of Therapy Development and Innovation for Immune Disorders and Cancers, Graduate School of Medicine, Juntendo University, Tokyo, Japan.
e-mail: morimoto@ims.u-tokyo.ac.jp

striking effects are produced by a combination of inhibition of DPP4 and checkpoint blockade: a triple therapy involving sitagliptin, anti-CTLA-4 and anti-PD-1 results in rejection of CT26 tumors by 100% of mice, whereas double therapy of anti-CTLA-4 plus anti-PD-1 cures only 42% of the mice. Barreira da Silva *et al.* therefore provide direct evidence of DPP4 as an *in vivo* regulator of CXCL10-mediated T cell trafficking, with relevance for tumor immunity and immunotherapy.

CXCL10 seems to have a dual role in tumor growth, with its proliferative or anti-proliferative activity being dependent on the cell type as a result of differences in the subtype of its receptor, CXCR3 (ref. 4). Expression of CXCR3 is rapidly induced on naive T cells following activation, and high CXCR3 expression is retained 'preferentially' on $CD4^+$ cells of the T_H1 subset of helper T cells and on $CD8^+$ cytotoxic T lymphocytes (CTLs), which results in enhancement of T cell migration to facilitate immunological responses to tumors[5]. Although strong T_H1 and CTL responses in the TME are beneficial for tumor suppression, these responses are counterbalanced to prevent unwanted tissue damage and immunopathology by disruption of the proinflammatory loop; indeed, $CXCR3^+$ regulatory T cells have been identified that ameliorate just such harmful inflammation[6]. Such cells are generated by interferon-γ signaling, which upregulates their expression of the T_H1-related transcription factor T-bet and in turn promotes their expression of CXCR3 in the inflammatory sites. Moreover, CXCR3 is also a marker of $CD8^+$ cells that produce interleukin 10 and have suppressive activity in both mice and human[7]. The exact factors that determine whether $CXCR3^+$ effector T cells and $CXCR3^+$ regulatory lymphocytes oppose each other or act cooperatively with each other during the tumor growth process *in vivo* remain to be elucidated.

Direct biological effects of DPP4 on tumor cells are also relevant to the malignant activity of tumors. In several human malignancies, including colorectal cancer, chronic myeloid leukemia and malignant mesothelioma, DPP4 expression is reported to be a marker of cancer stem cells[8]. Interestingly, the enzyme activity of DPP4 is important for regulating the growth of leukemic stem cells in the $CD34^+CD38^-Lin^-$ fraction in chronic myeloid leukemia and is a potential therapeutic target[9]. Although a direct correlation between disease aggressiveness and DPP4 expression has been reported in human T cell malignancies, an inverse correlation between DPP4 expression and the degree of malignant activity has been shown in melanocytes[10]. In addition to differences among cell types, the expression and function of DPP4 in the human immune system appears to differ from that in mice. Although the predicted amino acid sequence of human DPP4 shares approximately 85% homology with mouse DPP4, mouse DPP4 is neither a T cell–activation marker nor an adenosine deaminase–binding protein[1]. The differences between rodent DPP4 and human DPP4 therefore highlight the potentially limited utility of murine models for elucidating the function of human DPP4. Future work specifically focusing on the direct biological effects of DPP4 on human tumor cells will undoubtedly contribute to a more in-depth understanding of its role in various physiological states and as a possible anti-cancer therapeutic target.

Work on DPP4 in T cell immunity has reported that costimulation via the invariant signaling protein CD3 and CD26 (DPP4) induces the development of human type 1 regulatory T cells from $CD4^+$ T cells with substantial production of interleukin 10 and high expression of the coinhibitory receptor LAG-3 (ref. 11). Preclinical models have shown that antibody-mediated blockade of LAG-3 as a potential anti-cancer therapy leads to enhanced activation of antigen-specific T cells at tumor sites and disruption of tumor growth[12]. Moreover, dual-blockade therapy with anti-LAG-3 and anti-PD-1 cured most mice of established tumors that were largely resistant to single antibody treatment[12]. Thus, it is conceivable that DPP4 itself might function as an inhibitory molecule of an immunological-checkpoint system in certain disease conditions, similar to LAG-3 or PD-1.

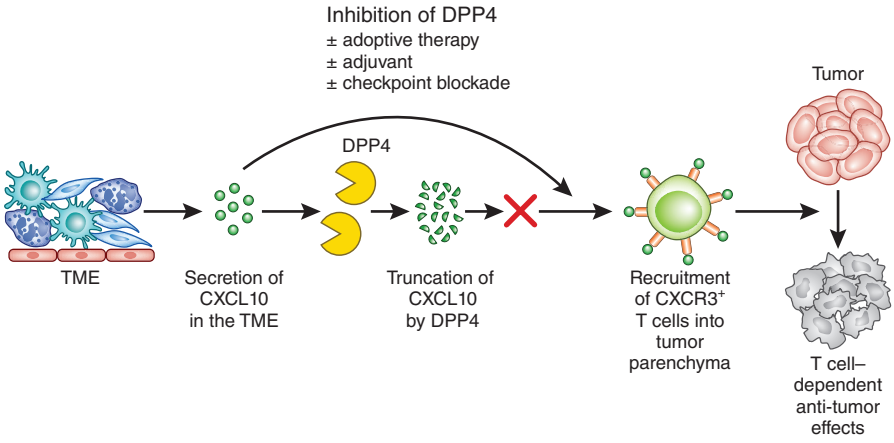

Figure 1 Inhibition of DPP4 suppresses truncation of its ligand CXCL10, which leads to the recruitment of $CXCR3^+$ T cells into tumor parenchyma. Barreira da Silva *et al.* use *in vivo* tumor-transplant models to show that inhibition of DPP4 diminishes tumor growth through the preservation of bioactive CXCL10 in the TME. In the normal physiological state, CXCL10 is rapidly degraded by DPP4, which results in less recruitment and migration of $CXCR3^+$ T cells into the tumor parenchyma. In contrast, inhibition of DPP4 enhances tumor rejection by preserving the full-length biologically active form of CXCL10, which leads to increased trafficking of $CXCR3^+$ T cells into the tumor parenchyma. This anti-tumor response is potentiated in combination with other anti-tumor immunotherapeutic approaches, including CpG adjuvant therapy, adoptive T cell–transfer therapy and checkpoint-blockade therapy (anti-CTLA-4 and anti-PD-1). ±, with or without.

In developing new assays for the intact form of CXCL10, Barreira da Silva *et al.* have also provided the first experimental evidence that amino-terminal truncation of post-translationally modified CXCL10 has an *in vivo* biological importance and that the regulation of this process through DPP4 affects lymphocyte migration and tumor immunity. Although DPP4 and CXCL10 have a plethora of biological functions in human tumor cells and the immune system, further detailed understanding of the role of these molecules in various clinical settings could lead potentially to novel therapeutic approaches. Indeed, DPP4-specific inhibitors already used as anti-diabetic drugs worldwide and could in theory be readily repurposed to enhance existing anti-tumor immunotherapies.

COMPETING FINANCIAL INTERESTS
The authors declare no competing financial interests.

1. Ohnuma, K., Dang, N.H. & Morimoto, C. *Trends Immunol.* **29**, 295–301 (2008).
2. Barreira da Silva, R. *et al. Nat. Immunol.* **16**, 850–858 (2015).
3. van der Bruggen, P. *et al. Science* **254**, 1643–1647 (1991).
4. Liu, M., Guo, S. & Stiles, J.K. *Oncol. Lett.* **2**, 583–589 (2011).
5. Groom, J.R. & Luster, A.D. *Exp. Cell Res.* **317**, 620–631 (2011).
6. Koch, M.A. *et al. Nat. Immunol.* **10**, 595–602 (2009).
7. Shi, Z. *et al. Eur. J. Immunol.* **39**, 2106–2119 (2009).
8. Davies, S., Beckenkamp, A. & Buffon, A. *Biomed. Pharmacother.* **71**, 135–138 (2015).
9. Herrmann, H. *et al. Blood* **123**, 3951–3962 (2014).
10. Havre, P.A. *et al. Front. Biosci.* **13**, 1634–1645 (2008).
11. Hatano, R. *et al. J. Immunol.* **194**, 960–972 (2015).
12. Nguyen, L.T. & Ohashi, P.S. *Nat. Rev. Immunol.* **15**, 45–56 (2015).

Regulation of Pulmonary Graft-versus-Host Disease by IL-26$^+$CD26$^+$CD4 T Lymphocytes

Kei Ohnuma,* Ryo Hatano,* Thomas M. Aune,† Haruna Otsuka,* Satoshi Iwata,* Nam H. Dang,‡ Taketo Yamada,§ and Chikao Morimoto*

Obliterative bronchiolitis is a potentially life-threatening noninfectious pulmonary complication after allogeneic hematopoietic stem cell transplantation and the only pathognomonic manifestation of pulmonary chronic graft-versus-host disease (cGVHD). In the current study, we identified a novel effect of IL-26 on transplant-related obliterative bronchiolitis. Sublethally irradiated NOD/Shi-*scid*IL2rγ^{null} mice transplanted with human umbilical cord blood (HuCB mice) gradually developed clinical signs of graft-versus-host disease (GVHD) such as loss of weight, ruffled fur, and alopecia. Histologically, lung of HuCB mice exhibited obliterative bronchiolitis with increased collagen deposition and predominant infiltration with human IL-26$^+$CD26$^+$CD4 T cells. Concomitantly, skin manifested fat loss and sclerosis of the reticular dermis in the presence of apoptosis of the basilar keratinocytes, whereas the liver exhibited portal fibrosis and cholestasis. Moreover, although IL-26 is absent from rodents, we showed that IL-26 increased collagen synthesis in fibroblasts and promoted lung fibrosis in a murine GVHD model using *IL-26* transgenic mice. In vitro analysis demonstrated a significant increase in IL-26 production by HuCB CD4 T cells following CD26 costimulation, whereas Ig Fc domain fused with the N-terminal of caveolin-1 (Cav-Ig), the ligand for CD26, effectively inhibited production of IL-26. Administration of Cav-Ig before or after onset of GVHD impeded the development of clinical and histologic features of GVHD without interrupting engraftment of donor-derived human cells, with preservation of the graft-versus-leukemia effect. These results therefore provide proof of principle that cGVHD of the lungs is caused in part by IL-26$^+$CD26$^+$CD4 T cells, and that treatment with Cav-Ig could be beneficial for cGVHD prevention and therapy. ***The Journal of Immunology*****, 2015, 194: 3697–3712.**

Allogeneic hematopoietic stem cell transplantation (alloHSCT) is a potentially curative treatment for many diseases arising from hematopoietic cells (1). However, chronic graft-versus-host disease (cGVHD) remains a significant barrier to successful alloHSCT (2). In particular, the lung damage in cGVHD causes potentially life-threatening complications (3). According to the National Institutes of Health consensus criteria, obliterative bronchiolitis (historically named bronchiolitis obliterans by pathologists) is the only pathognomonic manifestation of pulmonary cGVHD (4). It is recognized that obliterative bronchiolitis has been associated with an increased risk of death, and patients diagnosed with obliterative bronchiolitis after alloHSCT have a 5-y survival rate of only 10% (5).

Although many preclinical models mimicking human cGVHD including obliterative bronchiolitis have been established (6), control of obliterative bronchiolitis after alloHSCT has not yet been achieved thoroughly (7). The clinical application of murine data is limited because multiple, yet limited schema have arisen to identify alloimmune reactions in cross-species comparisons. For instance, one extensively used model of cGVHD clearly exhibited immune-complex glomerulonephritis, which is rarely seen in human cGVHD (8). Moreover, transfer of autoantibodies from mice with GVHD to normal mice failed to cause autoimmune pathology (9). These limitations are based on preparative regimens, composition of donor graft, and genetic backgrounds of donor and recipient animals (6). In addition, recent work has demonstrated multiple differences in immunological functions between humans and mice (10, 11). In contrast, because in vivo T cell depletion is the only prophylactic measure that effectively decreases the incidence of cGVHD (2, 12), donor T cells clearly play an important role in the immune pathology of cGVHD. Taken together, to develop novel therapeutic strategies for use in the clinical setting, the establishment of a humanized murine model of cGVHD is urgently needed. We previously analyzed a humanized murine acute GVHD (aGVHD) model involving mice transplanted with human adult PBL, and showed that liver and skin were predominantly involved as target organs in this model of aGVHD, which was clearly impeded by the administration of anti-CD26 mAb (13). Our data suggest that CD26$^+$ T cells play an effector role in this aGVHD model. However, because the mice studied in our previous work succumbed to aGVHD ~4 wk

*Department of Therapy Development and Innovation for Immune Disorders and Cancers, Graduate School of Medicine, Juntendo University, Tokyo 113-8421, Japan; †Department of Medicine, Vanderbilt University School of Medicine, Vanderbilt University Medical Center, Nashville, TN 37232; ‡Division of Hematology and Oncology, University of Florida, Gainesville, FL 32610; and §Department of Pathology, Keio University School of Medicine, Tokyo, 160-8582, Japan

Received for publication November 4, 2014. Accepted for publication February 16, 2015.

This work was supported in part by a grant from the Ministry of Education, Science, Sports, and Culture, Japan (to K.O. and C.M.); a grant from the Ministry of Health, Labour, and Welfare, Japan (to C.M.); a grant-in-aid (S1311011) from the Foundation of Strategic Research Projects in Private Universities from the Ministry of Education, Culture, Sports, Science, and Technology, Japan (to K.O. and C.M.); and National Institutes of Health Grant RO1 AI044924 (to T.M.A.).

Address correspondence and reprint requests to Prof. Chikao Morimoto, Department of Therapy Development and Innovation for Immune Disorders and Cancers, Graduate School of Medicine, Juntendo University, 2-1-1, Hongo, Bunkyo-ku, Tokyo 113-8421, Japan. E-mail address: morimoto@ims.u-tokyo.ac.jp

The online version of this article contains supplemental material.

Abbreviations used in this article: aGVHD, acute GVHD; ALL, acute lymphoblastic leukemia; alloHSCT, allogeneic hematopoietic stem cell transplantation; alloPBSCT, allogeneic peripheral blood-stem cell transplant; B6, C57BL/6; BAC, bacterial artificial chromosome; Cav-Ig, Ig Fc domain fused with the N-terminal of caveolin-1; cGVHD, chronic GVHD; CNS, conserved noncoding sequence; DPP4, dipeptidyl peptidase IV; GVHD, graft-versus-host disease; GVL, graft-versus-leukemia; HPRT1, hypoxanthine phosphoribosyltransferase 1; HSC, hematopoietic stem cell; HuCB, human umbilical cord blood; MNC, mononuclear cell; NHLF, normal human lung fibroblast; pAb, polyclonal Ab; RA, rheumatoid arthritis; RIPA, radioimmunoprecipitation assay; Tg, transgenic.

Copyright © 2015 by The American Association of Immunologists, Inc. 0022-1767/15/$25.00

after transplantation of human adult PBL, this early-onset model of aGVHD does not permit the assessment of longer-term consequences of interventional therapies such as the development of obliterative bronchiolitis, a form of cGVHD of the lung.

CD26 is associated with T cell signal transduction processes as a costimulatory molecule, as well as being a marker of T cell activation in human adult PBL (14–16). In fact, patients with autoimmune diseases such as multiple sclerosis and rheumatoid arthritis (RA) have been found to have increased numbers of $CD26^+CD4$ T cells in both inflamed tissues and the peripheral blood, with enhancement of CD26 expression in these autoimmune diseases correlating with disease severity (17). Previously, we have demonstrated that caveolin-1 is a costimulatory ligand for human CD26, and that CD26 on activated memory T cells interacts with caveolin-1 on recall Ag-primed monocytes (18, 19). More recently, we demonstrated in in vitro experiments that blockade of CD26-mediated T cell costimulation by soluble Fc fusion proteins containing the N-terminal domain of caveolin-1 (Cav-Ig) diminished primary and secondary proliferative responses not only to recall Ag, but also to unrelated allogeneic APC (20). In contrast to adult PBL, the human umbilical cord blood (HuCB) lymphocytes have been reported to be immature, predominantly consisting of $CD45RA^+$ naive cells (21, 22). We previously showed that, although all HuCB CD4 T cells constitutively expressed CD26, CD26-mediated costimulation was considerably attenuated in HuCB CD4 T cells, compared with the robust activation via CD26 costimulation of adult PBL (21). Additionally, HuCB CD4 T cells exhibited only slight activation after long-sustained stimulation of CD26. These findings provided further insights into the cellular mechanisms of immature immune response in HuCB. Furthermore, it has been reported that humanized mice transplanted with human hematopoietic stem cell (HSC) isolated from HuCB exhibited human hematopoiesis reconstitution as well as B cell engraftment with a similar Ab repertoire as observed in B cells in human (23, 24). Based on these findings, we hypothesized that HuCB naive CD4 T cells gradually acquire a xenogeneic response via attenuated stimulatory signaling with indolent inflammation in the target organs, leading eventually to chronic inflammatory changes. We therefore sought to develop a humanized murine pulmonary cGVHD model utilizing HuCB donor cells, and to overcome the limitations seen in the humanized murine aGVHD model such as vigorous activation of all engrafted T cells and extensive loss of B cell maturation and activation (23).

In the current study, we established a xenogeneic pulmonary cGVHD murine model induced by transplantation of HuCB, which exhibited obliterative bronchiolitis as well as sclerodermatous skin and primary biliary cirrhosis-like liver. Moreover, we determined a novel effect of IL-26 produced by donor-derived human CD4 T cells on fibroproliferation of obliterative bronchiolitis, which was also shown in the murine alloHSCT model using human *IL26* transgenic mice. In addition, our findings indicated a decrease of collagen deposition in the lung of xenogeneic pulmonary cGVHD mice treated with anti–IL-26 neutralizing Ab. Our analysis of a patient specimen demonstrated the predominant infiltration of $IL\text{-}26^+CD26^+CD4$ T cells in the lung of obliterative bronchiolitis after alloHSCT. In in vitro experiments, we showed that IL-26 of HuCB CD4 T cells was produced via CD26 costimulation by its ligand caveolin-1, whereas CD28 costimulation did not generally enhance IL-26 production. Furthermore, abrogation of CD26 costimulation by Cav-Ig before or during early onset of GVHD impeded the development of pulmonary cGVHD. These results provide proof of principle that human $IL\text{-}26^+CD26^+CD4$ T cells are involved in the pathophysiology of pulmonary cGVHD, and that blockade of CD26 costimulation by Cav-Ig appears to be a promising novel therapeutic strategy for the clinical control of cGVHD.

Materials and Methods

Abs, reagents, and cells

Mouse mAbs to human CD3 (OKT3, IgG2b), CD26 (1F7, IgG1), and CD28 (4B10, IgG1) for costimulation experiments were developed in our laboratory (25). Anti–IL-26 goat polyclonal Ab (pAb) (AF1375), which is available for neutralizing experiments (26), was obtained from R&D Systems (Minneapolis, MN). Human rIL-26 was purchased from R&D Systems and stocked at 1 $\mu g\ ml^{-1}$ in PBS. Cav-Ig and its control Fc protein were made in our laboratory, with previous references in the literature (27). Normal human lung fibroblast (NHLF) and the culture medium FGF-2 were purchased from LONZA (Walkersville, MD). Mouse fibroblast cell line NIH3T3 and mononuclear cells (MNCs) isolated from HuCB with Ficoll density gradation method were purchased from RIKEN BioResource Center (Tsukuba, Japan). T cell–depleted $CD34^+$ cells were purified from MNCs of HuCB using human CD34 MicroBead Kit (Miltenyi Biotec, Bergisch Gladbach, Germany).

Mice

NOD/SCID/$\gamma_c^{-/-}$ NOD.Cg-Prkdcscid Il2rgtm1Sug/Jic mice (NOG mice) ($H\text{-}2^d$) were purchased from the Central Institute for Experimental Animals (Kawasaki, Japan). C57BL/6 (B6) mice ($H\text{-}2^b$) were obtained from CLEA Japan (Tokyo, Japan). B6 mice carrying a 190-kb bacterial artificial chromosome (BAC) transgene with human *IFNG* and *IL26* gene (190-*IFNG* transgenic [Tg]) and a BAC Tg-deleting conserved noncoding sequence (CNS) positioned upstream of the *IFNG* transcription start site (ΔCNS-77 Tg) were developed in Thomas Aune's laboratory (28). All mice were housed in a specific pathogen-free facility in microisolator cages. Mice were used at 8–12 wk. Animal protocol was approved by the Institutional Animal Care and Use Committee.

Transplantation and assessment of GVHD

On day −1, NOG mice received 200 cGy irradiation. On day 0, mice were injected i.p. with 1×10^7 MNC (whole CB transplant) or 1×10^5 $CD34^+$ cells ($CD34^+$ transplant) purified from HuCB. Mice were assessed for survival daily and weighed thrice weekly. In IL-26 blockade experiments, mice were treated with anti–IL-26 pAb or control goat IgG at 50 μg per dose i.p. thrice per week from day +21 until day +32 (total six doses). In cGVHD prevention experiments, mice were given human Cav-Ig, or control human Fc at 100 μg per dose i.p. thrice per week from day +1 until day +28 (total 12 doses). In cGVHD treatment experiments, at onset of first clinical signs of disease 28 d after HuCB transplantation, mice were given human Cav-Ig, or control human Fc at 100 μg per dose i.p. thrice per week from day +29 until day +56 (total 12 doses) after confirmation of engraftment. Engraftment of HuCB was confirmed by quantification of human $CD45^+$ leukocytes in mouse peripheral blood using flow cytometry. The clinical GVHD score was assessed at least weekly according to the previous reference in the literature (29). For allogeneic bone marrow transplantation experiments using Tg mice, sublethally irradiated (200 cGy) NOG mice were transplanted with 1×10^7 bone marrow and 1×10^6 splenocytes isolated from 190-*IFNG* Tg, ΔCNS-77 Tg or parental B6 (B6 wild-type) mice. Recipients were sacrificed at 4 wk posttransplantation, and the lungs were removed for histopathological evaluation.

Tissue histopathology and immunohistochemistry

Skin from the upper back, the left lung, and liver specimens of recipients were fixed in 10% formalin, embedded in paraffin, sectioned, mounted in slides, and stained with H&E to determine pathology. The lung specimen of a patient undergoing an allogeneic peripheral blood-stem cell transplant (alloPBSCT) for acute lymphoblastic leukemia (ALL) was prepared for histopathologic and immunohistochemical studies by the same method as described above. Images were captured with an Olympus digital camera DP21 attached to an Olympus BX43 microscope using CellSens software (OLYMPUS, Tokyo, Japan). Slides were scored by a pathologist blinded to experimental groups. The GVHD pathology score was assessed according to the previous references in the literature (29–31). For detection of collagen, slides were stained with Azan-Mallory staining. Abs used in immunohistochemistry were anti-human CD4 mAb (4B12, mouse IgG1) and anti-human CD8 mAb (C8/144B, mouse IgG1) from Dako (Tokyo, Japan), anti-human CD26 goat pAb (AF1180) from R&D Systems, anti–IL-26 rabbit pAb (bs-2626R) from Bioss (Wobum, MA), and anti–IL-17A rab-

bit pAb (H-132) from Santa Cruz Biotechnology (Santa Cruz, CA). Immunohistochemical staining for CD4, CD8, CD26, or IL-26 was performed at the Department of Pathology, Keio University School of Medicine (Tokyo, Japan), as described previously (32). Immunohistochemical staining for IL-17A was conducted at the laboratory of MorphoTechnology (Sapporo, Japan).

Real-time quantitative RT-PCR

In experiments assessing expression of mRNA of effector molecules, a single-cell suspension was isolated from the lung of recipient mice using Lung Dissociation Kit (Miltenyi Biotec), followed by purification of human CD4 T cells using human CD4 MicroBeads (Miltenyi Biotec). Isolation and quantification of mRNA were performed, as described previously (33). Expression levels of mRNA were calculated on the basis of standard curves generated for each gene, and hypoxanthine phosphoribosyltransferase 1 (HPRT1) mRNA was used as an invariant control. Sequences of primers used in real-time RT-PCR analysis are as follows: human IL-2, forward 5′-AGAAGGCCACAGAACTGAAAC-3′, reverse 5′-GCTGTCTCATCAGCATATTCAC-3′; human IL-4, forward 5′-CAGTTCTACAGCCACCATGAGA-3′, reverse 5′-CGTCTTTAGCCTTTCCAAGAAG-3′; human IL-6, forward 5′-GCCAGAGCTGTGCAGATGAG-3′, reverse 5′-TCAGCAGGCTGGCATTTG-3′; human IL-10, forward 5′-CTGGGGGAGAACCTGAAGAC-3′, reverse 5′-TGGCTTTGTAGATGCCTTTCTC-3′; human IL-17A, forward 5′-ACATCCATAACCGGAATACCAA-3′, reverse 5′-ACATCCATAACCGGAATACCAA-3′; human IL-21, forward 5′-GACACTGGTCCACAAATCAAGCTC-3′, reverse 5′-TGCTGACTTTAGTTGGGCCTTC-3′; human IL-26, forward 5′-CAATTGCAAGGCTGCAAGAA-3′, reverse 5′-TCTCTAGCTGATGAAGCACAGGAA-3′; human IFN-γ, forward 5′-GTGTGGAGACCATCAAGGAAG-3′, reverse 5′-ATGTATTGCTTTGCGTTGGA-3′; human TNF-α, forward 5′-TCAGCCTCTTCTCCTTCCTG-3′, reverse 5′-TTTGCTACAACATGGGCTACA-3′; human CD26, forward 5′-GTACACAGAACGTTACATGGGTCTC-3′, reverse 5′-TCAGCTCTGCTCATGACTGTTG-3′; and human HPRT1, forward 5′-CAGTCAACAGGGGACATAAAAG-3′, reverse 5′-CCTGACCAAGGAAAGCAAAG-3′.

Flow cytometry

The following Abs were from BD Biosciences (San Jose, CA): anti-human CD3 (UCHT1, mouse IgG1), anti-human CD4 (RPA-Ta, mouse IgG1), anti-human CD8 (HIT8a, mouse IgG1), anti-human CD14 (M5E2, mouse IgG1), anti-human CD19 (HIB19, mouse IgG1), anti-human CD26 (M-A261, mouse IgG1), anti-human CD45 (HI30, mouse IgG1), anti-human CD56 (B159, mouse IgG1), anti-human IFN-γ (B27, mouse IgG1), anti-human IL-17A (N49-653, mouse IgG1) mAbs, and relevant control mAbs of the same Ig isotype. Fluorescent conjugates were FITC, PE, PerCP-Cy5.5, and allophycocyanin. Anti–IL-10RB rabbit pAb (bs-2602R) was purchased from Bioss, and anti–IL-20RA rabbit pAb (06-1073) from Millipore (Billerica, MA). Anti–IL-10RB and anti–IL-20RA pAbs recognize both human and murine Ags. mAb staining of intracellular IL-26 (clone 510414, mouse IgG1) was purchased from R&D Systems, being conjugated with Alexa Fluor 647 using Antibody Labeling Kit (Invitrogen, Carlsbad, CA). RBCs in samples of murine peripheral blood were lysed using BD FACS Lysing Solution (BD Biosciences). For analyzing lymphocytes infiltrated in the lung, a single-cell suspension was prepared using Lung Dissociation Kit, followed by purification with human CD45 MicroBeads (Miltenyi Biotec). For intracellular cytokine analysis, purified human $CD45^+$ cells were restimulated for 4 h with 25 ng ml^{-1} PMA (Sigma-Aldrich, St. Louis, MO) plus 1 μg ml^{-1} ionomycin (Sigma-Aldrich) in the presence of BD GolgiPlug (BD Biosciences). Intracellular flow cytometry was performed according to the manufacturer's instructions using Human Intracellular Cytokine Staining Kit (BD Biosciences). Analysis was performed on two-laser FACSCalibur (BD Biosciences), and files were analyzed in CellQuest software (BD Biosciences).

Western blotting

To analyze expression of IL-20RA or IL-10RB, 10 μg lysates of NHLF and NIH3T3 were prepared using radioimmunoprecipitation assay (RIPA) buffer, being resolved by SDS-PAGE in reducing condition and immunoblotted using anti–IL-20RA (ab25922; Abcam, Cambridge, MA) or anti–IL-10RB (bs-2602R; Bioss) rabbit pAbs recognizing both human and murine Ags. For analysis of phosphorylated STAT3 induced by exogenous IL-26, 1×10^5 cells were seeded in 96-well flat-bottom plate, and the next day IL-26 (10 ng ml^{-1} in PBS) was added to each well. Cells were harvested at each time point, and cell lysates were prepared in RIPA buffer containing Halt Protease and Phosphatase inhibitor mixture (Thermo Fisher Scientific, Waltham, MA). Each 10 μg lysate was resolved by SDS-PAGE in reducing condition and immunoblotted with antiphosphorylated STAT3 (pY-STAT3) (#11045; SAB, Collage Park, MD) recognizing both human and murine Ags, followed by stripping and reprobing with anti-STAT3 pAb (total STAT3) (GTX15523; GeneTex, Irvine, CA) recognizing both human and murine Ags.

Measurement of cytokines and soluble CD26/dipeptidyl peptidase IV

The collected sera were analyzed for inflammatory cytokines other than human IL-26 using Bio-Plex Pro Human Cytokine Assay (Bio-Rad Laboratories, Hercules, CA). IL-26 was assayed using Human IL-26 ELISA Kit (CUSABIO, Hubei, China). Assay for soluble CD26/dipeptidyl peptidase IV (DPP4) was developed in our laboratory (34). All samples were run in triplicates.

In vitro and in vivo collagen assay

NHLF or NIH3T3 cells were seeded in 96-well flat-bottom plate (1×10^5 /well), and the next day IL-26 (0.1, 2.0, 5.0, or 10 ng ml^{-1} in PBS) or PBS alone was added to each well. In neutralizing experiments, neutralizing anti–IL-20RA rabbit pAb (06-1073; R&D Systems) or control rabbit Ig (10 μg ml^{-1} each) was added to each well 1 h before exogenous IL-26 was added. The supernatants were harvested 48 h after IL-26 was added, followed by measuring soluble collagen using Sircol Collagen Assay Kit (Biocolor, County Antrim, U.K.). The total collagen of the left lung was extracted using acid–pepsin solution and measured according to the manufacturer's instructions of Sircol Collagen Assay Kit. All samples were examined in triplicates.

In vitro costimulation assay

For analysis of mRNA expression, CD4 T cells were purified isolated from HuCB MNCs, and 1×10^5 cells/well were seeded in 96-well flat-bottom plate with immobilized anti-CD3 (0.05 μg ml^{-1}) plus anti-CD28 (10 μg ml^{-1}) or anti-CD26 (10 μg ml^{-1}) mAbs. After 7 d of stimulation, cell were harvested, mRNA was prepared, and transcript levels of human *IL2*, *IFNG*, *IL17A*, *IL26*, and *DPP4* were quantified by real-time RT-PCR. For IL-26 production analysis via costimulation, 1×10^5 HuCB CD4 T cells were stimulated with plate-bound anti-CD3, anti-CD28, anti-CD26 mAbs, or Cav-Ig immobilized at the indicated concentration. The supernatants were harvested 7 or 14 d after stimulation. For inhibition assay, 1×10^5 cells/well HuCB CD4 T cells were treated with blocking Cav-Ig or control Ig at the various concentrations (0, 1, 5, 10, 20, or 50 μg ml^{-1}) prior to stimulation. After 1-h blocking period, cells were stimulated with immobilized anti-CD3 (0.05 μg ml^{-1}) plus Cav-Ig (20 μg ml^{-1}), anti-CD28 (20 μg ml^{-1}), or anti-CD26 (20 μg ml^{-1}) mAbs. After 7 d of stimulation, the supernatants were harvested. HuCB CD4 T cells were cultured in AIM V serum-free medium (Invitrogen).

Graft-versus-leukemia and bioluminescence imaging

Firefly luciferase-transfected A20 murine lymphoma cells (A20-luc) of BALB/c background ($H\text{-}2^d$) were provided by X. Chen (Medical College of Wisconsin, Milwaukee, WI) (35). NOG mice were irradiated at sublethal dose (200 cGy), inoculated the next day with 1×10^4 A20-luc cells via tail vein, and then transplanted the following day with 1×10^7 MNCs isolated from HuCB. Cav-Ig or control Ig (100 μg/dose) was administered i.p. thrice per week, beginning at day +1 after transplantation until day +28 (total 12 doses). For other graft-versus-leukemia (GVL) experiments, NOG mice were irradiated at sublethal dose (200 cGy), and the next day were transplanted with 1×10^7 MNCs isolated from HuCB. Cav-Ig or control Ig (100 μg/dose) was administered i.p. thrice per week, beginning at day +1 after transplantation until day +28 (total 12 doses). A total of 1×10^5 A20-luc cells was inoculated via tail vein on day +28 posttransplantation. Tumor dissemination was monitored every week using in vivo bioluminescence imaging, as previously described in the literature (36).

Statistics

Data were analyzed by two-tailed Student *t* test for two-group comparison or by ANOVA test for multiple comparison testing, followed by the Tukey-Kramer posthoc test. The *p* values ≤ 0.05 were considered statistically significant. Survival rates were analyzed by log-rank test using Kaplan–Meier method. Calculations were performed and graphed using GraphPad Prism 6 (GraphPad Software, La Jolla, CA).

Study approval

Human study protocols were approved by the Ethics Committees at Juntendo University (authorization number 2012077), and at Keio University (authorization number 20120206). Informed consent was obtained from a patient. Animal experiments were conducted following protocols approved by

the Animal Care and Use Committees at Juntendo University (authorization number 1082).

Results

Establishment of obliterative bronchiolitis in mice transplanted with HuCB

As described above, the establishment of a humanized murine model of pulmonary cGVHD is needed to better understand and treat this serious and often fatal complication of alloHSCT. To determine whether pulmonary cGVHD is induced by human immune cells in a murine model, we first attempted to establish a humanized murine model utilizing NOG mice as recipients and HuCB as donor cells. To establish a control that did not develop GVHD following hematopoietic reconstitution, we used T cell–depleted $CD34^+$ cells isolated from HuCB (37–39). As shown in Fig. 1A and Supplemental Fig. 1A, $CD34^+$ transplant mice survived for 5 mo without any sign or symptom of GVHD. Meanwhile, whole CB transplant mice exhibited clinical signs/symptoms of GVHD as early as 4 wk posttransplant (Fig. 1A), and demonstrated significantly decreased survival rate (Supplemental Fig. 1A). Human cells were engrafted similarly in both groups, as shown in Supplemental Fig. 1B. Previous work with other humanized murine models showed that reconstituted human $CD45^+$ cells were overcome by $CD3^+$ T cells posttransplantation due to reduced B cell development (23), which may impair the integrity of host immunity. In contrast, we confirmed that NOG mice transplanted with HuCB maintained a stable number of T and B cells (Supplemental Fig. 1C), consistent with previously reported results (24, 38–40). Therefore, the human immune system appeared to be effectively reconstituted in the present murine model involving whole CB as well as $CD34^+$ transplant. We next conducted histological studies of GVHD target organs. The lung of whole CB transplant mice showed perivascular and subepithelial inflammation and fibrotic narrowing of the bronchiole (Fig. 1B), whereas $CD34^+$ transplant control group displayed normal appearance of GVHD target organs such as the lung (Fig. 1C, *left panel*). For the diagnosis of pulmonary cGVHD, it is necessary to show concomitant active GVHD findings in other organs, including skin and liver (4). Skin of whole CB transplant mice manifested fat loss, follicular dropout, and sclerosis of the reticular dermis in the presence of apoptosis of the basilar keratinocytes, whereas the liver exhibited portal fibrosis and cholestasis (Supplemental Fig. 2). These findings indicate that whole CB transplant mice develop pulmonary cGVHD as well as concomitant active GVHD in skin and liver. Because obliterative bronchiolitis can be characterized as a fibroproliferative disease (7), we also performed Mallory staining and lung collagen assays to quantify collagen contents as a measurement of extent of disease. The lung of whole CB transplant mice displayed a significant increase in peribronchiolar and perivascular collagen deposition and in total lung collagen content, compared with $CD34^+$ transplant mice (Fig. 1C, 1D). Taken together, our data demonstrate that the lung of whole CB transplant mice exhibits obliterative bronchiolitis as manifestation of pulmonary GVHD.

To determine the potential cellular mechanisms involved in the pathogenesis of pulmonary GVHD, we next analyzed the composition of human lymphocytes in the GVHD lung. In contrast to data demonstrating that PBL contained human $CD19^+$, $CD33^+$, or $CD56^+$ as well as $CD3^+$ cells (Supplemental Fig. 1C), human $CD3^+$ cells were the predominant cell type observed in the lung of whole CB transplant mice, comprising $>99\%$ of the lymphocyte population (Fig. 1E). Moreover, human CD4 T cell subset was predominantly observed compared with CD8 T cells (Fig. 1F). These findings were also confirmed by immunohistochemistry studies of the lung specimens (Fig. 1G). These data suggest that the development of obliterative bronchiolitis found in whole CB transplant mice involves donor-derived human CD3 lymphocytes, particularly CD4 T cells.

IL-26–producing CD4 T cell infiltration in the lung of mice with obliterative bronchiolitis

We next analyzed the expression profile of mRNAs of various inflammatory cytokines in human CD4 T cells isolated from the lung of whole CB transplant mice. As shown in Fig. 2A, *IFNG*, *IL17A*, *IL21*, and *IL26* were significantly increased over the course of GVHD development following whole CB transplantation, whereas *IL2*, *TNF* (TNF-α), *IL4*, *IL6*, and *IL10* were decreased. In addition, substantial increases were seen in levels of *IFNG* and *IL26*, with *IL17A* and *IL21* remaining at a low level. It has been reported that IFN-γ and IL-26 are produced by Th1 cells (41), whereas IFN-γ, IL-17A, and IL-26 are produced by Th17 cells (42). Because both Th1 and Th17 cells strongly express CD26 (15, 43), we next analyzed the expression level of CD26/DPP4. *DPP4* mRNA expression in human CD4 T cells infiltrating in the lung of mice with obliterative bronchiolitis was significantly increased (Fig. 2A).

To determine whether these cytokines were produced by the infiltrating human $CD26^+CD4$ T cells, we next conducted flow cytometric analysis of lymphocytes isolated from the lung of whole CB or $CD34^+$ transplant control mice. As shown in Fig. 2B, levels of human IFN-γ^+ or IL-26^+CD26^+CD4 T cells were significantly increased in whole CB transplant mice as compared with $CD34^+$ transplant control mice, whereas levels of IL-$17A^+$ $CD26^+CD4$ T cells were similarly very low in both groups. These findings were also confirmed by immunohistochemistry studies of the lung specimens (Fig. 2C). To determine whether $CD26^+CD4$ T cells produced IL-26, IFN-γ, and/or IL-17A, multicolor-staining flow cytometric study was conducted. As shown in Fig. 2Di, $CD26^+$ CD4 T cells in the lung of whole CB transplant mice predominantly produced IL-26 rather than IFN-γ. In addition, whereas $CD26^+$IFN-γ^+CD4 cells exclusively expressed IL-26, $CD26^+$IL-26^+CD4 cells were predominantly IFN-γ–negative cells, and IL-$17A^+$ cells were exclusively IL-26 negative (Fig. 2Dii). These data suggest that $CD26^+CD4$ T cells in the lung of mice with obliterative bronchiolitis express IL-26 as well as IFN-γ, but do not belong to the Th17 cell population.

To further confirm the above findings, we examined protein levels of the relevant cytokines. In addition, because soluble CD26/DPP4 level is correlated with T cell CD26 protein level and hematopoiesis (44, 45), we examined protein levels of human soluble CD26/DPP4 in murine sera. As shown in Fig. 2E, serum levels of human IFN-γ, IL-26, and human soluble CD26/DPP4 were significantly increased in whole CB transplant mice as compared with $CD34^+$ transplant control mice. Meanwhile, serum levels of human IL-2, IL-4, IL-6, IL-10, IL-17A, and TNF-α were undetectable in both groups (data not shown). Taken together, these findings strongly suggest that IFN-γ^+ and/or IL-26^+CD26^+ CD4 T cells play an important role in the pathophysiology of obliterative bronchiolitis after HSCT.

To investigate the role of IL-26^+CD26^+CD4 T cells in humans, we conducted immunohistochemistry studies of a human lung specimen obtained from a patient with cGVHD. A 64-y-old woman underwent an alloPBSCT for ALL after being treated with busulfan, fludarabine, and melphalan as conditioning regimen. Tacrolimus was administered for the prevention of GVHD. The patient developed acute skin GVHD (stage 2 and grade I) on day +33 posttransplant. On day +95, the patient had dyspnea and the chest X-ray revealed ground glass opacity bilaterally. Transbronchial lung biopsy was performed on day +101. Histologic findings of the lung

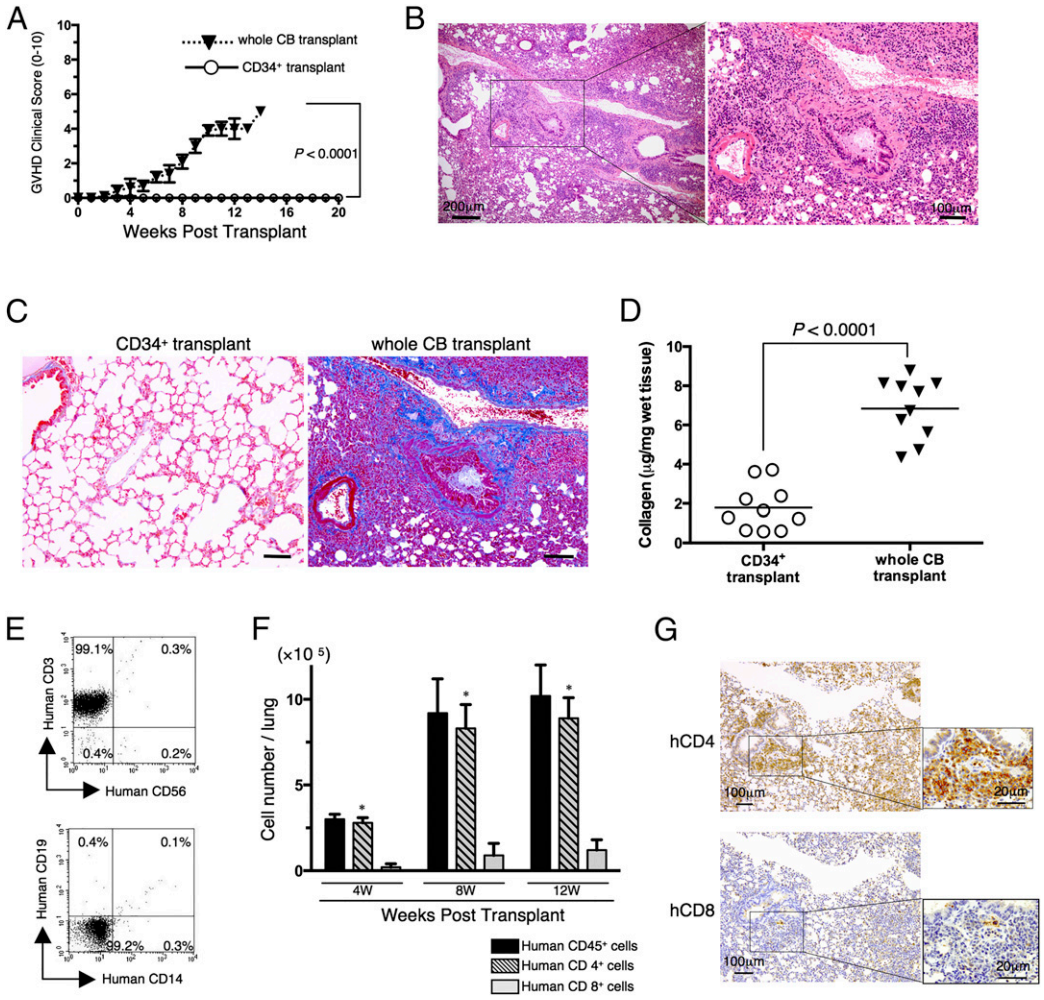

FIGURE 1. Obliterative bronchiolitis in sublethally irradiated NOG mice transplanted with HuCB cells. NOG mice were irradiated at sublethal dose (200 cGy) and the next day were transplanted with 1×10^5 T cell–depleted $CD34^+$ cells purified from HuCB ($CD34^+$ transplant) or with 1×10^7 MNCs isolated from HuCB (whole CB transplant). (**A**) Clinical GVHD score (mean ± SEM). Data are cumulative results from three independent experiments (for each, $n = 10$). The p value was calculated by log-rank test. (**B**) H&E staining of the lung of whole CB transplant (8 wk posttransplantation). The *left panel* shows lower original magnification (×40) and the *right panel* shows higher original magnification (×100). Representative histology is shown from three independent experiments (for each, $n = 10$). (**C**) Collagen deposition was evaluated in the lung tissues of $CD34^+$ or whole CB transplant (8 wk posttransplantation) with an Azan-Mallory staining. The histology shown in whole CB transplant is a sequential section of (B). Dark blue areas indicating collagen deposition are clearly observed in whole CB transplant mice, compared with those in $CD34^+$ transplant mice. Representative histology is shown from three independent experiments (for each, $n = 10$). Original magnification ×100. Scale bars, 100 μm. (**D**) Collagen contents in the lung were quantified by Sircol Collagen Assay. The mean number (±SEM) of total collagen contents (μg) per wet lung tissue weight (mg) was determined from three independent experiments (for each, $n = 10$). Increased collagen contents were clearly observed in whole CB transplant mice, compared with those in $CD34^+$ transplant mice. Each dot indicates individual value, and horizontal bars indicate mean value. (**E**) Representative two-dimensional dot plots of human lymphocyte composition in the lung of whole CB transplant mice (8 wk posttransplantation). Single-suspension cells isolated from the lung of whole CB transplant mice (8 wk posttransplantation) were sorted by human $CD45^+$ cells and then analyzed using flow cytometry. The *upper panel* shows representative human CD3 and/or CD56 staining, and the *lower panel* shows representative human CD19 and/or CD14 staining. Numbers indicate relative percentages per quadrant. Similar results were observed in independent experiments ($n = 8$). (**F**) Absolute cell numbers (mean ± SEM) of human $CD45^+$, $CD4^+$, or $CD8^+$ cells per lung of whole CB transplant mice were quantified by flow cytometry. $CD4^+$ T cells were predominantly observed in the lung of whole CB transplant mice. Data are cumulative results from three independent experiments ($n = 10$ at 4 wk, $n = 8$ at 8 wk, and $n = 3$ at 12 wk). $*p < 0.0001$ versus $CD8^+$ cells. (**G**) Anti-human CD4 or CD8 immunohistochemistry of sequential sections of lung tissue of whole CB transplant mice (8 wk posttransplantation). Predominant infiltration of $CD4^+$ cells was observed, with similar results to those obtained by flow cytrometry, as shown in (F). Representative histology is shown from three independent experiments (for each, $n = 10$). Original magnification ×100 or ×400 (*inset* in each panel).

specimen revealed perivascular and subepithelial inflammation and narrowing of the bronchiole with manifestation of peribronchiolar and perivascular collagen deposition (Fig. 2F). The patient was diagnosed as having pulmonary cGVHD with obliterative bronchiolitis. Immunohistochemistry studies showed predominant infiltration of IL-$26^+$$CD26^+$CD4 T cells. These findings suggest that IL-$26^+$$CD26^+$CD4 T cells play an important role in the pathophysiology of obliterative bronchiolitis after HSCT in human as well as humanized murine model.

Contribution of IL-26 to collagen production in pulmonary GVHD

Because it has been reported that pulmonary GVHD development is independent of IFN-γ (46), we therefore focused on IL-26 as a potential effector cytokine for pulmonary GVHD. As the IL-26 gene is absent in rodents (41, 47), we cannot formally exclude the possibility that human IL-26 activates murine cells. We therefore conducted in vitro assays to determine the effect of human IL-26 on murine cells. In human cells, IL-26 binds initially to IL-20RA to form the binary complex IL-26 plus IL-20RA, followed by

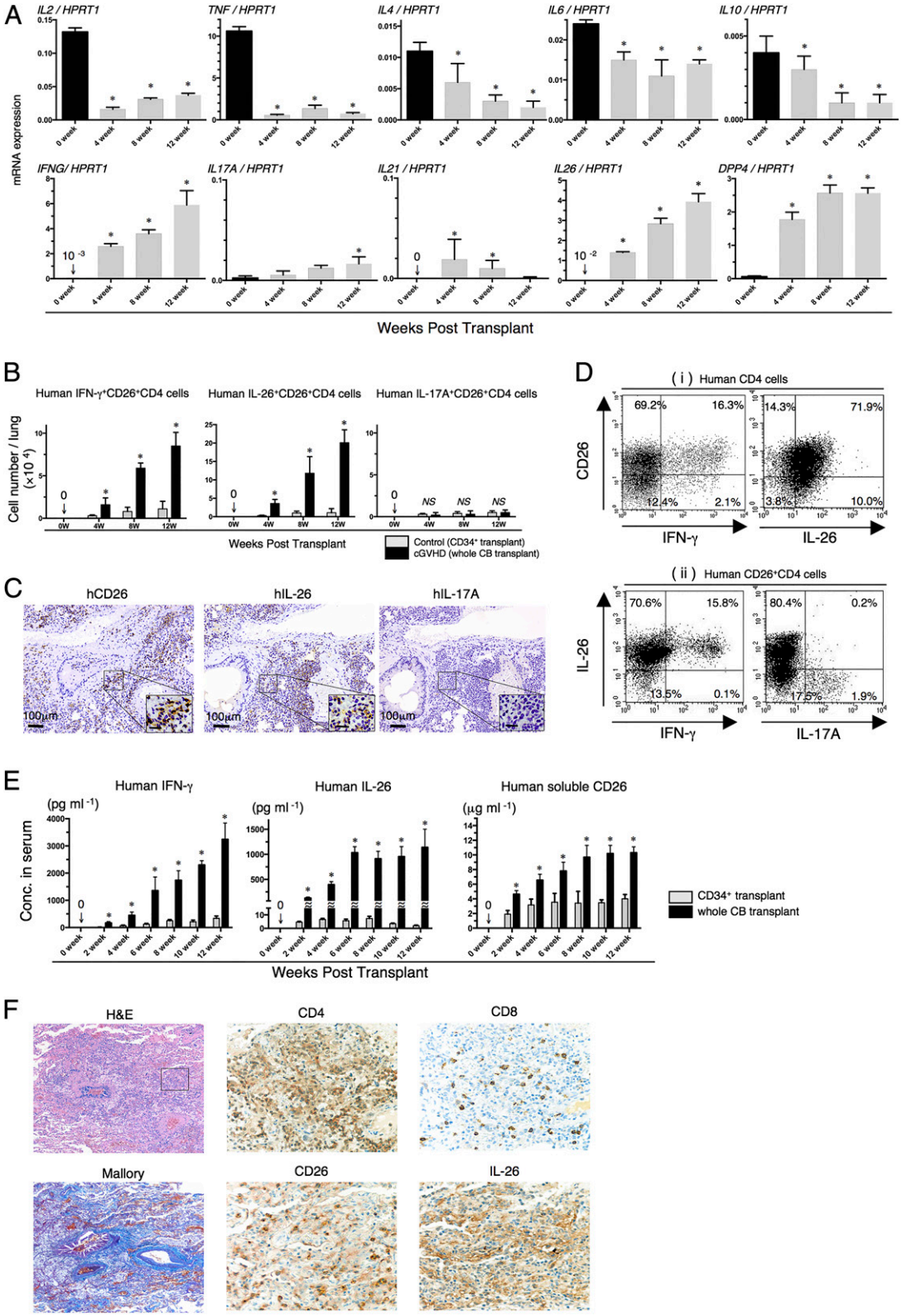

FIGURE 2. Predominant infiltration of IL-26$^+$CD26$^+$CD4 T cells in the lung of obliterative bronchiolitis. (**A**) Whole CB transplant mice were sacrificed at 4, 8, and 12 wk posttransplantation, and the lungs were removed, followed by isolation of human CD4$^+$ cells. mRNA expression of human cytokines or CD26/DPP4 was quantified by real-time RT-PCR. Each expression was normalized to HPRT1. Data at 0 wk were obtained using freshly isolated HuCB CD4 T cells of three different donors. Data are cumulative results from three independent experiments (n = 10 at 4 wk, n = 8 at 8 wk, and n = 3 at 12 wk). *$p < 0.0001$ versus each at 0 wk. (**B**) Absolute cell numbers of human IFN-γ$^+$CD26$^+$CD4, IL-26$^+$CD26$^+$CD4, or IL-17A$^+$CD26$^+$CD4 cells in the lung of CD34$^+$ transplant or whole CB transplant mice were quantified by flow cytometry. Data are cumulative results from three independent experiments (for each, n = 10 in CD34$^+$ transplant group, and n = 10 at 4 wk, n = 8 at 8 wk, and n = 3 at 12 wk in whole CB transplant group). *$p < 0.0001$ versus corresponding CD34$^+$ transplant group. (**C**) Anti-human CD26, IL-26, or IL-17A immunohistochemical staining of sequential sections of the lung from whole CB transplant mice (8 wk posttransplantation). The lung of whole CB transplant mice was clearly infiltrated with human CD26 or IL-26 (brown stained cells), but not with IL-17A–positive cells. Representative histology is shown from three independent experiments (*Figure legend continues*)

recruitment of the IL-10RB chain, leading to STAT3 phosphorylation (26). We thus confirmed that both IL-20RA and IL-10RB were expressed in murine fibroblast cell line NIH3T3 as well as NHLF (Fig. 3A, 3B). In both NHLF and NIH3T3, exogenous human rIL-26 induced phosphorylation of STAT3 (Fig. 3C), indicating that human IL-26 was active not only in NHLF, but also in murine fibroblast. To examine a functional effect of IL-26 on murine fibroblasts, we next conducted an in vitro assay for collagen production. As shown in Fig. 3D, increased levels of collagen production in NIH3T3 as well as in NHLF were observed in a dose-dependent manner following the addition of exogenous IL-26, and collagen production was inhibited by neutralizing anti–IL-20RA pAb. These results strongly suggest that human IL-26 activates both human and murine fibroblasts via IL-20RA, leading to increased collagen production.

To further extend the above in vitro results to an in vivo system, we analyzed the lung of murine alloreactive GVHD using human *IL26* Tg mice. For this purpose, we used mice carrying human *IFNG* and *IL26* transgene (190-*IFNG* Tg mice) or mice carrying human *IFNG* transgene with deleting *IL26* transcription (ΔCNS-77 Tg mice). The 190-*IFNG* Tg mice exhibited production of IL-26 by CD4 T cells under Th1- or Th17-polarizing conditions, whereas expression of IL-26 was completely abrogated in ΔCNS-77 Tg mice (41). In addition, production of IFN-γ by T or NK cells was equivalent in both 190-*IFNG* Tg and ΔCNS-77 Tg mice (28). As shown in Fig. 3E, lung histology of recipient NOG mice deriving from B6 wild-type or ΔCNS-77 Tg mice showed peribronchial infiltration and cuffing denoting GVHD, whereas collagen deposit was not detected by Mallory staining, and IL-26$^+$ cells were not detected. In contrast, histology of recipient NOG mice deriving from 190-*IFNG* Tg mice showed peribronchial infiltration and cuffing denoting GVHD with collagen deposition and IL-26$^+$ cell infiltration. Significant increase in collagen contents of the lung of recipient NOG mice deriving from 190-*IFNG* Tg mice was noted (Fig. 3F). These results suggest that human IL-26, but not human IFN-γ, plays a critical role in the pulmonary fibrosis associated with obliterative bronchiolitis after HSCT.

To further define the role of IL-26 in the pulmonary fibrosis associated with HSCT, we conducted studies to evaluate whether lung collagen contents were reduced by neutralizing IL-26 in whole CB transplant mice. For this purpose, anti–IL-26 pAb or control pAb was administered in sublethally irradiated NOG mice transplanted with whole CB on day +21 until day +32 thrice per week, followed by resection of the lung to measure total collagen content. As shown in Fig. 3G, a significant decrease in collagen contents of the lung of recipient NOG mice treated with anti–IL-26 pAb was noted. Taken together, our data strongly suggest that IL-26 plays a critical role in the pulmonary fibrosis observed following HSCT.

IL-26 production via CD26-mediated T cell costimulation

IL-26 was preferentially expressed in CD26$^+$CD4 T cells in the lung of whole CB transplant mice experiencing obliterative bronchiolitis (Fig. 2D), with increased expression of *DPP4* (Fig. 2A). Although upstream stimulation of IL-26 synthesis has not yet been determined, CD26/DPP4 as well as IFN-γ is preferentially expressed on Th1 cells activated via CD26-mediated costimulation (15). We thus hypothesized that human CD4 T cells produce IL-26 following CD26 costimulation. To test this hypothesis, we conducted in vitro costimulatory experiments using HuCB CD4 T cells and analyzed expression of various inflammatory cytokines. As shown in Fig. 4A, although expression levels of *IL26* and *DPP4* were enhanced by CD28 (*) or CD26 (**) costimulation, significantly greater increase in levels of *IL26* and *DPP4* was observed following CD26 costimulation than CD28 costimulation (***). In contrast, expression levels of *IL2*, *IFNG*, and *IL17A* were not increased following either CD26 costimulation or CD28 costimulation (Fig. 4A), due to the immaturity of HuCB T cells, as was previously reported (21, 48). We next conducted costimulatory experiments evaluating dose effect and time kinetics using the CD26 costimulatory ligand Cav-Ig as well as anti-CD26 or anti-CD28 mAbs, and assayed for secreted IL-26. As shown in Fig. 4B, production of IL-26 was increased following CD26 costimulation with Cav-Ig (*) or anti-CD26 (**) mAb in dose- and time-dependent manners, whereas a slight increase in IL-26 level was observed following CD28 costimulation only at higher doses of mAb and longer stimulation periods (***). Blocking experiments were then performed for further confirmation, showing that IL-26 production induced by Cav-Ig or anti-CD26 mAb was clearly inhibited by treatment with soluble Cav-Ig in a dose-dependent manner (Fig. 4C), whereas no change was observed with CD28 costimulation (Fig. 4C). These findings strongly suggest that production of IL-26 by HuCB CD4 T cells is regulated via CD26-mediated costimulation. Moreover, because the functional sequences of the N-terminal of caveolin-1 are highly conserved between human and mouse (49), allowing for the capability to bind human CD26 as a costimulatory ligand, it is conceivable that donor HuCB T cells transferred into mice were activated via CD26 costimulation triggered by murine caveolin-1. Taken together, CD26-mediated IL-26 production triggered by caveolin-1 is identified as a possible therapeutic target in pulmonary cGVHD through the use of whole CB transplant mice.

($n = 10$). Original magnification ×100 or ×400 (*inset* in each panel). Scale bars in the *inset*, 20 μm. (**D**) Representative two-dimensional dot plots of human CD26 and IFN-γ or IL-26 cells by gating for human CD4$^+$ cells (D**i**), and of human IFN-γ or IL-17A among IL-26$^+$ cells by gating for human CD26$^+$CD4$^+$ cells (D**ii**). Single-suspension cells isolated from the lung of whole CB transplant mice (8 wk posttransplantation) were sorted by human CD45$^+$ cells and then analyzed using flow cytometry. Numbers indicate relative percentages per quadrant. Similar results were observed in independent experiments ($n = 10$). (**E**) Sera of CD34$^+$ transplant or whole CB transplant mice were collected at the indicated week posttransplantation, and serum levels of human IFN-γ, IL-26, and soluble CD26/DPP4 were quantified. Data are cumulative results from three independent experiments (for each, $n = 10$ in CD34$^+$ transplant group, and $n = 10$ at 0–6 wk, $n = 8$ at 8 wk, $n = 7$ at 10 wk, and $n = 3$ at 12 wk in whole CB transplant group). $*p < 0.0001$ versus corresponding CD34$^+$ transplant group. (**F**) H&E, Azan-Mallory, anti-human CD4, CD8, CD26, or IL-26 immunohistochemical staining of sequential sections of the lung from a patient undergoing alloPBSCT for ALL. After having acute skin GVHD on day +33 posttransplant, the patient experienced dyspnea with ground glass opacity detected on the chest X-ray examination on day +95. The lung specimen was obtained by transbronchial lung biopsy on day +101, showing perivascular and subepithelial inflammation and narrowing of the bronchiole (H&E staining). Peribronchiolar and perivascular collagen deposition was detected by Azan-Mallory staining. The lung was clearly infiltrated with CD4-, CD26-, or IL-26–positive cells (brown stained cells), with CD8-positive cells found at a very low level. The histology shown in immunohistochemical staining is focused in the *inset* of the H&E staining panel. Original magnification ×100 (H&E and Azan-Mallory) or ×400 (anti-CD4, CD8, CD26, and IL-26 staining).

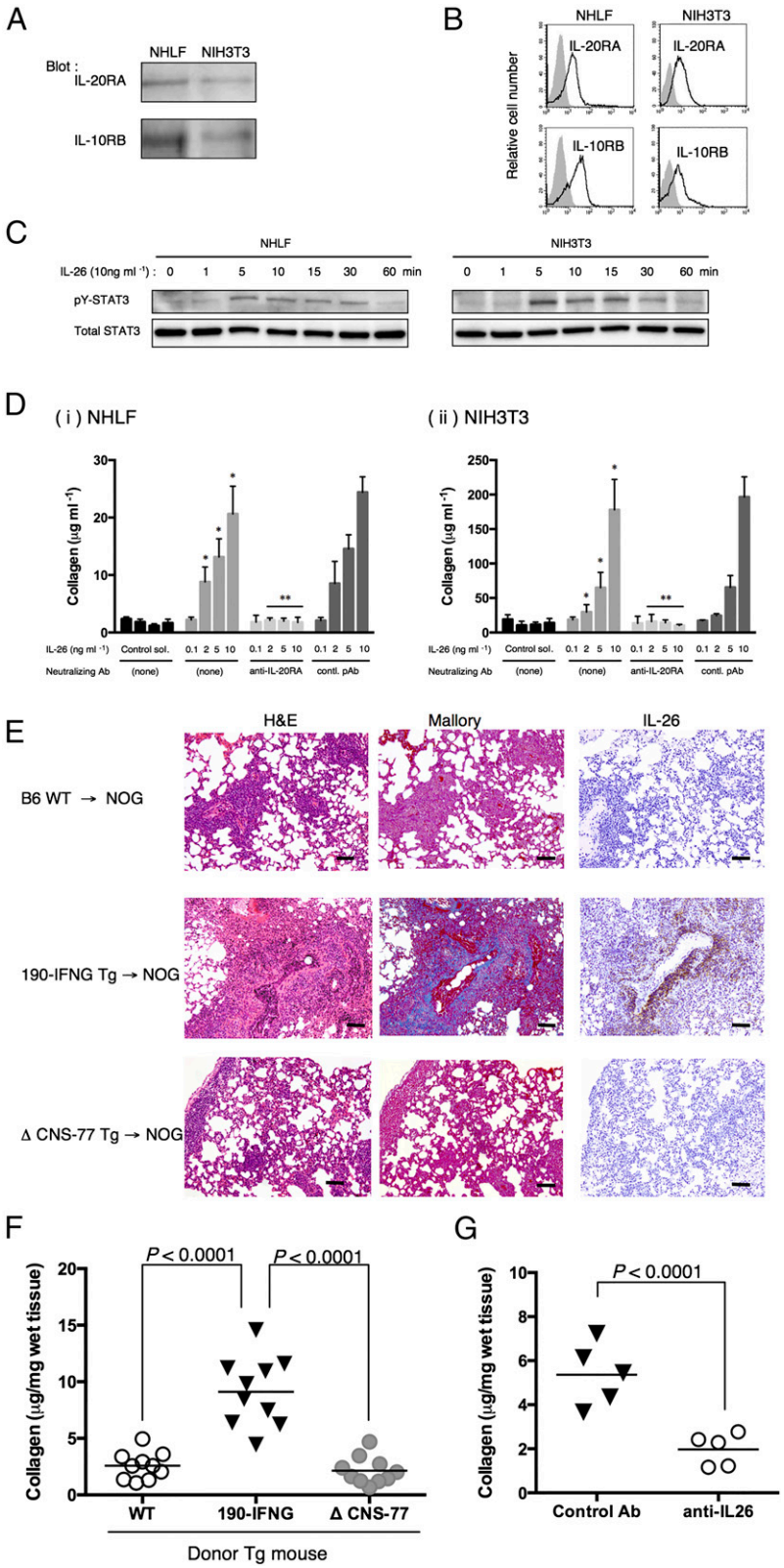

FIGURE 3. IL-26 stimulates fibroblast, and collagen deposition in the lung of obliterative bronchiolitis is induced in NOG mice receiving bone marrow cells and splenocytes of *IL26* Tg mice. (**A**) Western blot analysis of IL-20RA and IL-10RB in NHLF and NIH3T3 cells. Lysates (each, 10 μg) were prepared using RIPA buffer, being resolved by SDS-PAGE in reducing condition and immunoblotted using anti–IL-20RA or anti–IL-10RB pAbs recognizing both human and murine Ags. (**B**) Representative histogram of IL-20RA and IL-10RB of NHLF and NIH3T3 cells. Single-suspension cells were stained with anti–IL-20RA or anti–IL-10RB pAbs recognizing both human and murine Ags, and analyzed using flow cytometry (bold line). Gray histograms indicate isotype control (rabbit polyclonal IgG and anti-rabbit IgG-PE). (**C**) A total of 1×10^5 cells of NHLF or NIH3T3 was seeded in 96-well flat-bottom plate, and the next day IL-26 (10 ng ml^{-1} in PBS) was added to each well. Cells were harvested at each time point, and cell lysates were prepared in RIPA buffer containing Halt Protease and Phosphatase inhibitor mixture, and 10 μg each lysate was resolved by SDS-PAGE in reducing condition and immunoblotted with antiphosphorylated STAT3 (pY-STAT3) recognizing both human and murine Ags, followed (*Figure legend continues*)

Prevention of obliterative bronchiolitis in whole CB transplant mice by Cav-Ig administration

Given the role of CD26 costimulation in IL-26 production and IL-26 regulation of collagen production, we therefore sought to determine whether disruption of CD26 costimulation by a blocking reagent, Cav-Ig, prolonged survival of the recipient mice associated with a reduction in the incidence of obliterative bronchiolitis. Recipients treated with Cav-Ig survived for 7 mo without any clinical findings of GVHD (Fig. 5A, 5B). Meanwhile, the survival rate of recipient mice treated with control Ig was significantly reduced (Fig. 5A), with clinical signs/symptoms of GVHD (Fig. 5B). Human cells were engrafted similarly in both groups, as shown in Supplemental Fig. 3A, 3B. Histologic findings of the lung showed the development of obliterative bronchiolitis in control Ig, while having normal appearances in Cav-Ig recipient mice, with none having positive pathology scores (Fig. 5C, 5D). These effects of Cav-Ig were also observed in other GVHD-target organs such as the skin and liver (Supplemental Fig. 3C). Moreover, IL-26$^+$CD26$^+$ CD4 T cells in the lung and serum levels of human IL-26 and soluble CD26/DPP4 were significantly decreased in Cav-Ig–administered recipients than in control Ig (Fig. 5E, 5F). Furthermore, collagen contents in the lung were reduced in Cav-Ig–administered recipients (Fig. 5G, 5H). Taken together, the above results support the notion that Cav-Ig administration prevents the development of pulmonary GVHD in whole CB transplant mice by decreasing the number of IL-26$^+$CD26$^+$CD4 T cells.

Effect of Cav-Ig administration after onset of GVHD

Because pulmonary GVHD progresses in an indolent manner over weeks and months, patients often are affected by the clinical findings prior to being diagnosed with cGVHD (50). We therefore sought to determine whether blockade of caveolin-1/CD26 interaction effectively suppresses obliterative bronchiolitis development following the appearance of clinical signs/symptoms. For this purpose, treatment began on day +29 following the appearance of an increase in GVHD scores, indicating the early stages of cGVHD development. Recipients treated with Cav-Ig survived for 7 mo with remission of GVHD symptoms (Fig. 6A, 6B). Meanwhile, the survival rate of recipients treated with control Ig was significantly decreased (Fig. 6A), with progression of clinical signs/symptoms of GVHD (Fig. 6B). Human cells were engrafted similarly in both groups (Supplemental Fig. 4A, 4B). In contrast to progressive obliterative bronchiolitis of control Ig-treated recipients, peribronchial inflammation shown at 5 wk posttransplantation was attenuated at 10 wk posttransplantation in Cav-Ig–treated recipients (Fig. 6C). Correspondingly, the pathologic scores of control Ig-treated recipients were significantly increased at 10 wk, as compared with those at 5 wk (Fig. 6D). Meanwhile, the pathologic scores of Cav-Ig–treated recipients were significantly reduced at 10 wk, as compared with those at 5 wk (Fig. 6D), and were clearly decreased as compared with those of control Ig-treated recipients (Fig. 6D). These effects of Cav-Ig administration were observed in the skin and liver (Supplemental Fig. 4C–F). Moreover, levels of human IFN-γ^+ and IL-26$^+$CD26$^+$CD4 T cells in the lung of control Ig-treated recipients were significantly increased at 10 wk, as compared with those at 5 wk (* of Fig. 6E). In contrast, levels of human IFN-γ^+ and IL-26$^+$CD26$^+$CD4 T cells in the lung of Cav-Ig–treated recipients were significantly reduced at 10 wk, as compared with those at 5 wk (** of Fig. 6E), and were clearly decreased as compared with those of control Ig-treated recipients (*** of Fig. 6E). Furthermore, total collagen contents in the lung were significantly lower in Cav-Ig–treated recipients than control Ig-treated recipients (Fig. 6F). Taken together, these data suggest that Cav-Ig administration not only prevents the development of cGVHD, but also provides a novel therapeutic approach for the early stages of cGVHD by regulating levels of IL-26$^+$CD26$^+$CD4 T cells.

Treatment with Cav-Ig preserves GVL capability in recipient mice

Because GVHD and GVL effects are highly linked immune reactions (51), we evaluated the potential influence of Cav-Ig treatment on GVL effect. For this purpose, cohorts of Cav-Ig–– or control Ig-treated recipient mice of whole CB transplant were irradiated at sublethal doses and then injected i.v. with luciferase-transfected A20 (A20-luc) cells 1 d prior to whole CB transplantation to allow for dissemination of tumor cells. The next day following transplantation, treatment with Cav-Ig or control Ig thrice per week began on day +1 until day +28. Mice inoculated with A20 cells alone all died of tumor progression within 6 wk (Fig. 7A, 7B). Recipients treated with control Ig exhibited clinical evidence of GVHD such as weight loss and ruffled fur and died of GVHD without tumor progression in 13 wk (Fig. 7A, 7B). In contrast, recipient mice treated with Cav-Ig displayed significantly prolonged survival (Fig. 7A) without involvement of A20-luc cells (Fig. 7B). To better characterize the potency of the GVL effect, we repeated these studies with injection of A20-luc cells on day +28 after whole CB transplantation to allow for acquisition of immunosuppression by Cav-Ig treatment. Mice inoculated with A20 cells alone all died of tumor progression within 2 wk after tumor inoculation (Fig. 7C, 7D). Recipient mice treated with control Ig

by stripping and reprobing with anti-STAT3 pAb (total STAT3) recognizing both human and murine Ags. Representative data are shown from three independent experiments with similar results. (**D**) Collagen production of NHLF (**Di**) or NIH3T3 (**Dii**) cells stimulated with exogenous IL-26 in the presence or absence of neutralizing anti–IL-20RA pAb or rabbit Ig (contl. pAb). Data are shown as mean ± SEM, resulting from three independent experiments with triplicates. The amount of secreted soluble collagen increased with increasing level of exogenous IL-26 in a dose-dependent manner (*$p < 0.0001$ versus corresponding control solvent), and production of collagen was inhibited by the presence of neutralizing anti–IL-20RA pAb (**$p < 0.0001$ versus corresponding contl. pAb). (**E**) H&E, Azan-Mallory staining, and anti–IL-26 immunohistochemical staining of sequential sections of the lung from NOG mice at 4 wk after transplantation of BM and splenocytes isolated from parental B6 (B6 WT), 190-*IFNG* BAC Tg (190-IFNG Tg), or ΔCNS-77 Tg mice. The lung of recipients of 190-IFNG Tg mice showed obliterative bronchiolitis with collagen deposition and IL-26$^+$ cell infiltration, whereas recipients of B6 WT or ΔCNS-77 Tg mice showed peribronchial and septal infiltration without collagen deposition or IL-26$^+$ cells. Representative histology is shown from three independent experiments (for each, $n = 6$). Original magnification ×100. Scale bars, 100 μm. (**F**) Recipient mice were sacrificed at 4 wk posttransplantation, and the lungs were removed. Collagen contents in the lung were quantified by Sircol Collagen Assay. The mean number (±SEM) of total collagen contents (μg) per wet lung tissue weight (mg) was determined from three independent experiments (for each, $n = 10$). Increased collagen contents were clearly observed in recipients of 190-IFNG Tg mice, compared with those in recipients of B6 WT or ΔCNS-77 Tg mice. Each dot indicates individual value, and horizontal bars indicate mean value. (**G**) Whole CB transplant mice were administered anti–IL-26 Ab or control Ab (each 50 μg/dose) i.p. thrice per week, beginning at day +21 after transplantation until day +32. Recipient mice were sacrificed at 5 wk posttransplantation, and the lungs were removed. Collagen contents in the lung were quantified by Sircol Collagen Assay. The mean number (±SEM) of total collagen contents (μg) per wet lung tissue weight (mg) was determined from two independent experiments (for each, $n = 5$). Decreased collagen contents were clearly observed in the recipients of anti–IL-26 Ab. Each dot indicates individual value, and horizontal bars indicate mean value.

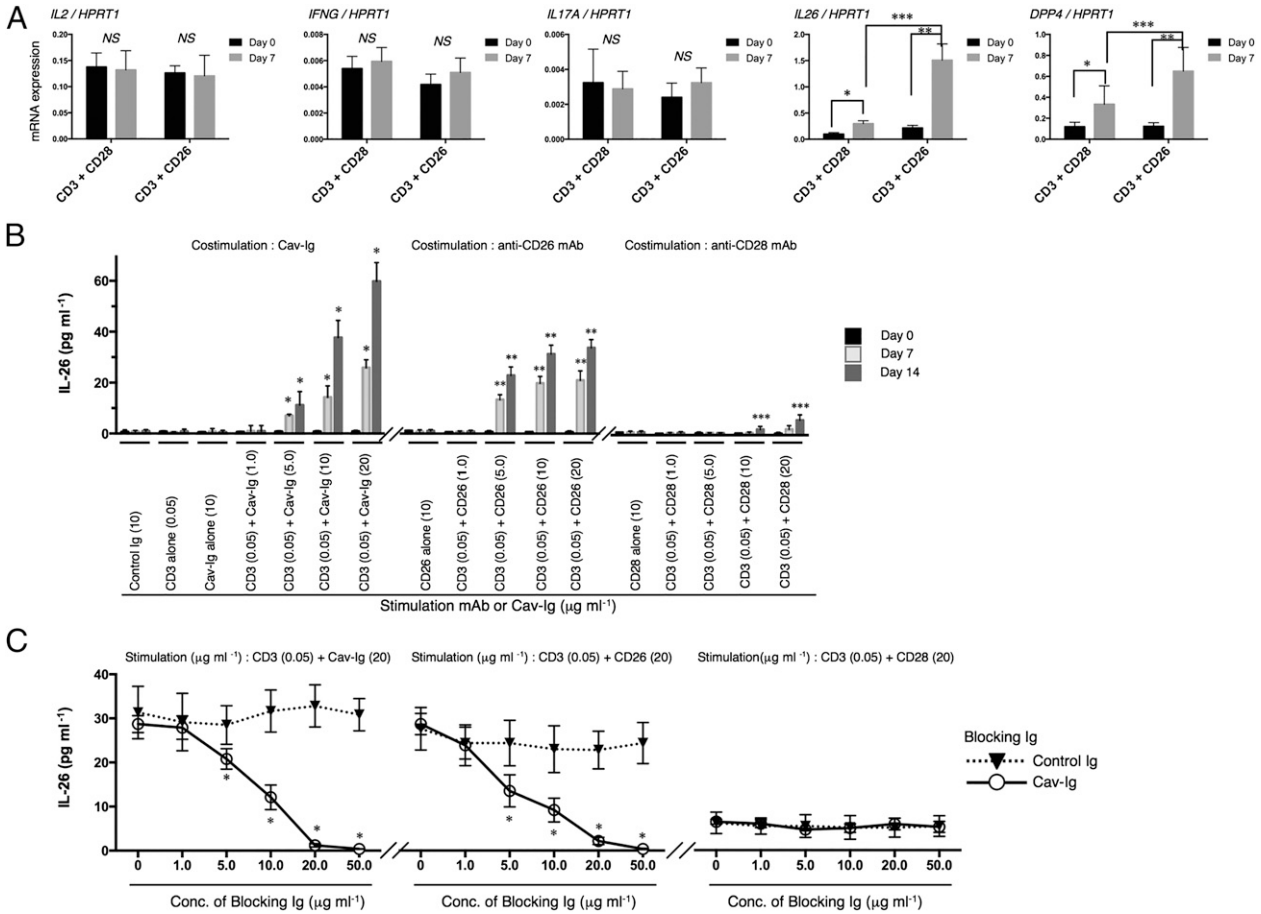

FIGURE 4. CD26 costimulation enhances IL-26 production in HuCB CD4 T cells, and blockade by the CD26 ligand caveolin-1 reduces production of IL-26. (**A**) HuCB CD4 T cells were stimulated with immobilized anti-CD3 (0.05 μg ml^{-1}) plus anti-CD28 (10 μg ml^{-1}) or anti-CD26 (10 μg ml^{-1}) mAbs. After 7 d of stimulation, mRNA levels of human *IL2*, *IFNG*, *IL17A*, *IL26*, and *DPP4* were quantified by real-time RT-PCR. Each expression was normalized to HPRT1. Data are shown as mean ± SEM, resulting from three independent experiments with triplicates. *$p < 0.05$, **·***$p < 0.0001$. (**B**) HuCB CD4 T cells were stimulated with plate-bound anti-CD3, anti-CD28, anti-CD26 mAbs, or Cav-Ig immobilized at the indicated concentration. The supernatants were harvested 7 or 14 d after stimulation, and levels of human IL-26 were quantified. Data are shown as mean ± SEM, resulting from three independent experiments with triplicates (*·***$p < 0.0001$ or ***$p < 0.05$ versus corresponding samples at day 0). (**C**) HuCB CD4 T cells were treated with blocking Cav-Ig (solid line) or control Ig (dotted line) at the indicated concentration. After 1 h of incubation with blocking Cav-Ig or control Ig, cells were stimulated with immobilized anti-CD3 (0.05 μg ml^{-1}) plus Cav-Ig (20 μg ml^{-1}), anti-CD28 (20 μg ml^{-1}), or anti-CD26 (20 μg ml^{-1}) mAbs. After 7 d of stimulation, the supernatants were harvested and levels of human IL-26 were quantified. Data are shown as mean ± SEM, resulting from three independent experiments with triplicates. *$p < 0.0001$ versus corresponding control Ig.

demonstrated clinical evidence of GVHD such as weight loss and ruffled fur and died of GVHD without tumor progression within 13 wk after transplantation (Fig. 7C, 7D). In contrast, recipients treated with Cav-Ig exhibited significantly prolonged survival (Fig. 7C) without involvement of A20-luc cells (Fig. 7D). Collectively, these results demonstrate that Cav-Ig treatment of recipient mice of whole CB transplant was effective in reducing the symptoms of cGVHD without a concomitant loss of the GVL effect.

Discussion

In the current study, we demonstrated that obliterative bronchiolitis developed in NOG mice transplanted with HuCB (whole CB transplant). Utilizing this humanized mouse model, we found that donor-derived CD4 T cells predominantly infiltrated in the lung of obliterative bronchiolitis, and that IL-26 as well as IFN-γ levels were enhanced significantly in the infiltrating human CD26^{+}CD4 T cells.

Originally discovered in *Herpesvirus saimiri*–transformed T cells (52), IL-26 is now classified as belonging to the IL-10 family of cytokines (42). IL-26 is a secreted protein produced by T, NK cells, or synoviocytes (53, 54), and binding of IL-26 to a distinct cell surface receptor consisting of IL-20RA and IL-10RB results in functional activation via STAT3 phosphorylation (26). IL-26 gene expression or protein production has been analyzed in patients with RA, inflammatory bowel diseases, and hepatitis C virus infection (54–58). However, the effect of IL-26 on the pathophysiology of cGVHD has not yet been determined. Moreover, there has been little information available regarding the biological functions of IL-26 using animal models due to the absence of the IL-26 gene in mouse (41, 47). In this study, we described a novel effect of IL-26 on fibroproliferation in transplant-related obliterative bronchiolitis, using a humanized pulmonary cGVHD murine model. Moreover, we demonstrated that human IL-26, not IFN-γ, induced collagen deposition in obliterative bronchiolitis of murine allogeneic transplantation model utilizing 190-*IFNG* Tg and ΔCNS-77 Tg mice. In both 190-*IFNG* Tg and ΔCNS-77 Tg mice, production of IFN-γ by T or NK cells is equivalent in both tissue culture studies and analysis of basal levels in various tissues, including spleen, lymph node, and colon (28). In contrast, expression of IL-26 is observed in Th1- or Th17-polarizing CD4 cells of 190-*IFNG* Tg mice, whereas it is

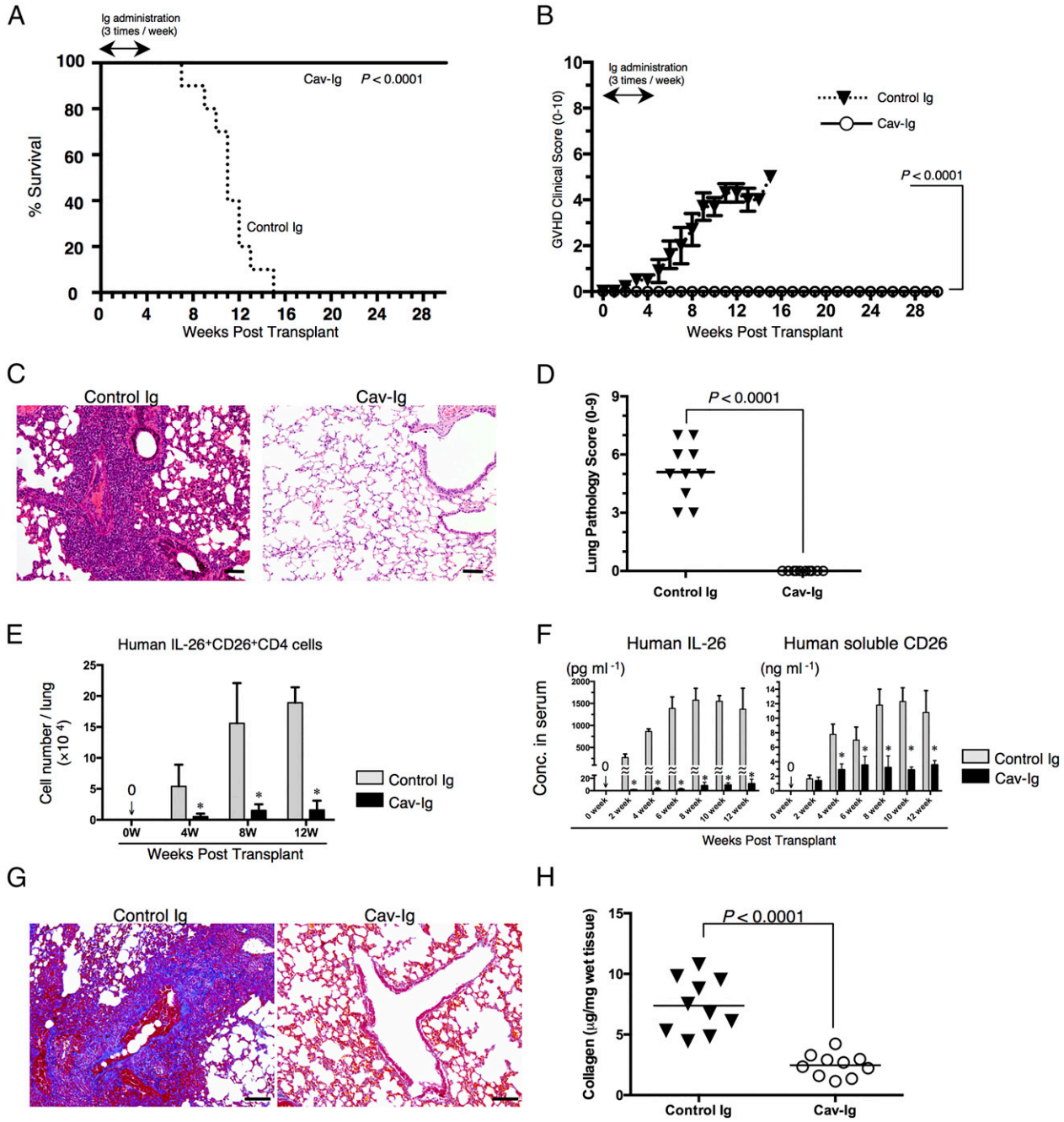

FIGURE 5. Administration of Cav-Ig prevents obliterative bronchiolitis by reducing level of IL-26$^+$CD26$^+$CD4 cells and collagen deposition. Sublethally irradiated NOG mice were transplanted with 1×10^7 MNCs isolated from HuCB. Cav-Ig or control Ig (each 100 μg/dose) was administered i.p. thrice per week, beginning at day +1 after transplantation until day +28. (**A**) Overall survival and (**B**) clinical GVHD score (mean ± SEM). Data are cumulative results from three independent experiments (for each, $n = 10$). (**C**) H&E staining of the lung of recipients administered with control Ig or Cav-Ig group (6 wk posttransplantation). Representative histology is shown from three independent experiments (for each, $n = 10$). Original magnification ×100. Scale bars, 100 μm. (**D**) Pathologic damage in the lung of recipients administered with Cav-Ig or control Ig was examined at 6 wk posttransplantation, using a semiquantitative scoring system. Each dot indicates individual value, and horizontal bars indicate mean value. (**E**) Absolute cell number of human IL-26$^+$CD26$^+$CD4 cells in the lung of recipients of Cav-Ig or control Ig group. Data are cumulative results from three independent experiments (for each, $n = 10$ in Cav-Ig group, and $n = 10$ at 0–4 wk, $n = 9$ at 8 wk, and $n = 2$ at 12 wk in control Ig group). *$p < 0.0001$ versus corresponding control Ig group. (**F**) Sera of recipients of Cav-Ig or control Ig group were collected at the indicated week posttransplantation, and serum levels of human IL-26 and soluble CD26/DPP4 were quantified. Data are cumulative results from three independent experiments (for each, $n = 10$ in Cav-Ig group, and $n = 10$ at 0–6 wk, $n = 9$ at 8 wk, $n = 7$ at 10 wk, and $n = 2$ at 12 wk in control Ig group). *$p < 0.0001$ versus corresponding control Ig group. (**G**) Collagen deposition was determined in the lung tissues of recipients of Cav-Ig or control Ig group (6 wk posttransplantation) with an Azan-Mallory staining. Representative histology is shown from three independent experiments (for each, $n = 6$). Original magnification ×100. Scale bars, 100 μm. (**H**) Collagen contents in the lung of recipients of Cav-Ig or control Ig group (6 wk posttransplantation) were quantified by Sircol Collagen Assay. The mean number (±SEM) of total collagen contents (μg) per wet lung tissue weight (mg) was determined from three independent experiments (for each, $n = 10$). Decreased collagen contents were clearly observed in recipients of Cav-Ig group. Each dot indicates individual value, and horizontal bars indicate mean value.

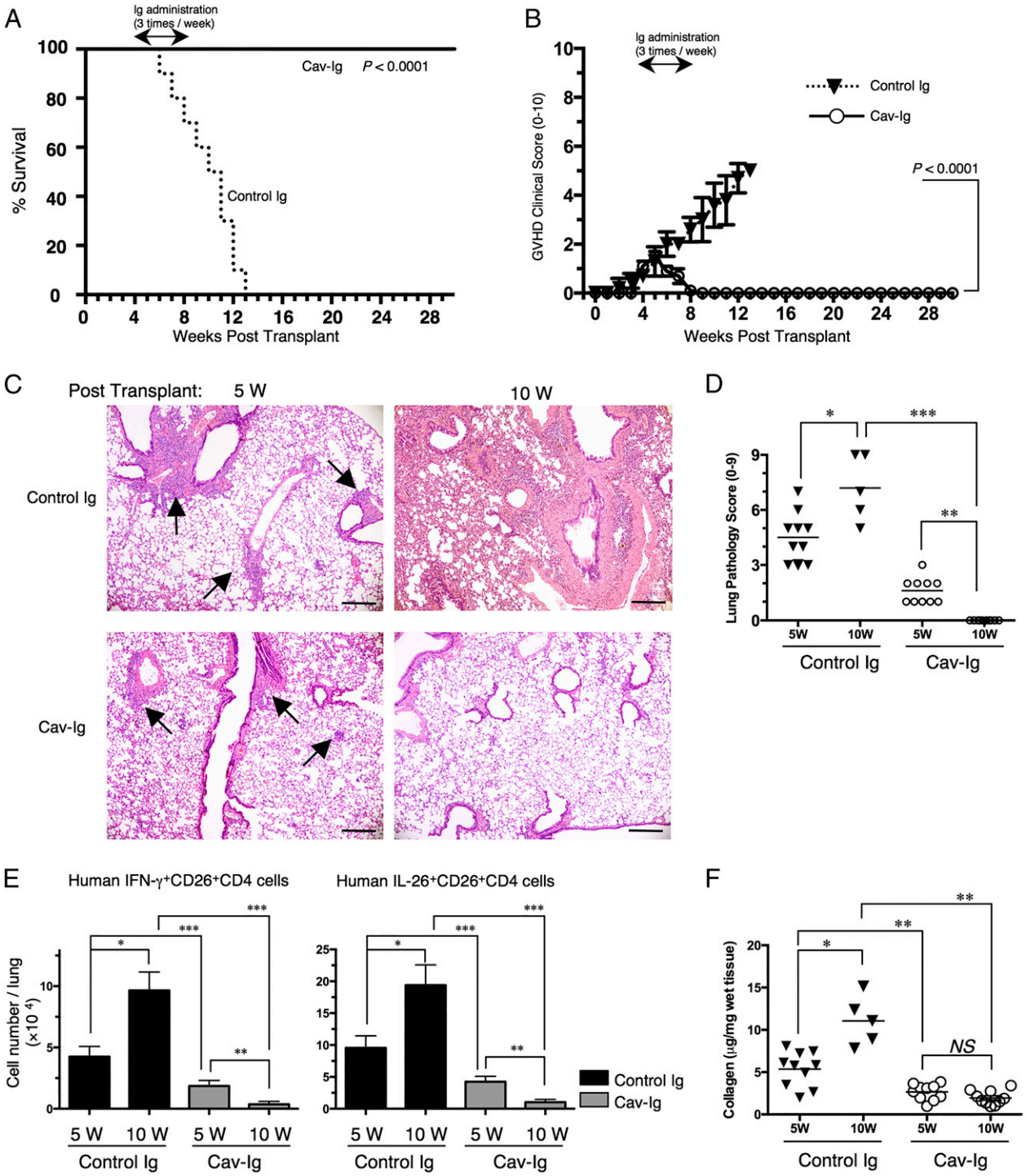

FIGURE 6. Administration of Cav-Ig during early GVHD development impedes lethal GVHD by reducing level of IL-26$^+$CD26$^+$CD4 cells and collagen deposition in the lung. Sublethally irradiated NOG mice were transplanted with 1×10^7 MNCs isolated from HuCB. Cav-Ig or control Ig (each 100 μg/dose) was administered i.p. thrice per week, beginning at day +29 after transplantation until day +56. (**A**) Overall survival and (**B**) clinical GVHD score (mean ± SEM). Data are cumulative results from three independent experiments (for each, $n = 10$). (**C**) H&E staining of the lung tissues of control Ig group and Cav-Ig group at 5 or 10 wk posttransplantation. Representative histology is shown from three independent experiments (for each, $n = 10$ in Cav-Ig group, and $n = 10$ at 5 wk and $n = 5$ at 10 wk in control Ig group). Arrows indicate perivascular and peribronchial inflammation of the small airway. Original magnification ×100. Scale bars, 100 μm. (**D**) Pathologic damage in the lung of recipients administered with Cav-Ig or control Ig was examined at 5 and 10 wk posttransplantation using a semiquantitative scoring system. Each dot indicates individual value, and horizontal bars indicate mean value. Data are cumulative results from three independent experiments (for each, $n = 10$ in Cav-Ig group, and $n = 10$ at 5 wk and $n = 5$ at 10 wk in control Ig group). $*p < 0.01$, $**$-$****p < 0.0001$. (**E**) Absolute cell number of human IFN-γ$^+$ or IL-26$^+$CD26$^+$CD4 cells in the lung of recipients of Cav-Ig or control Ig group. Data are cumulative results from three independent experiments (for each, $n = 10$ in Cav-Ig group, and $n = 10$ at 5 wk and $n = 5$ at 10 wk in control Ig group). $*$-$*****p < 0.0001$. (**F**) Collagen contents in the lung of recipients of Cav-Ig or control Ig group (5 and 10 wk posttransplantation) were quantified by Sircol Collagen Assay. The mean number (±SEM) of total collagen contents (μg) per wet lung tissue weight (mg) was determined from three independent experiments (for each, $n = 10$ in Cav-Ig group, and $n = 10$ at 5 wk and $n = 5$ at 10 wk in control Ig group). Each dot indicates individual value, and horizontal bars indicate mean value. $*$-$***p < 0.0001$.

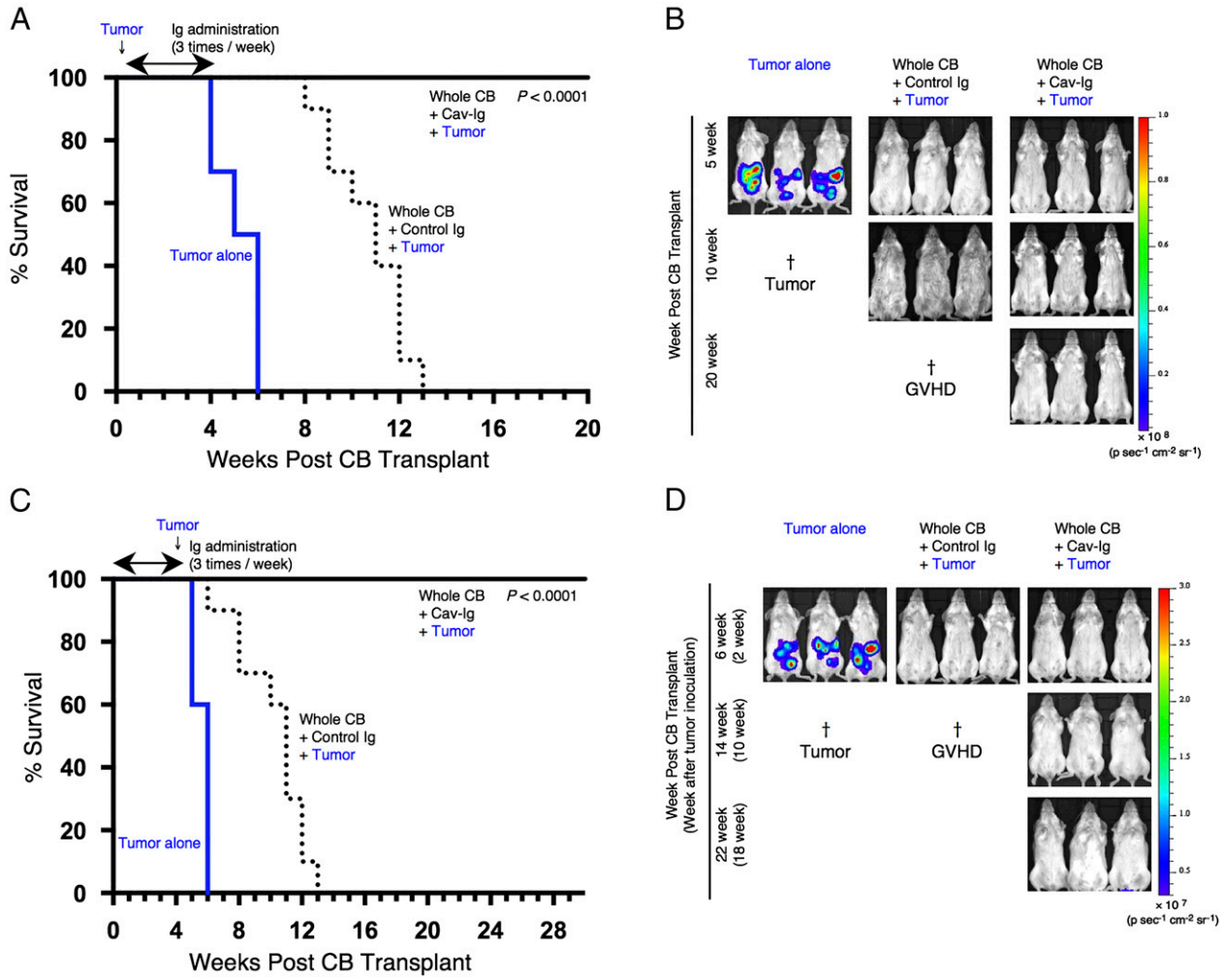

FIGURE 7. Cav-Ig preserves GVL effect. (**A**) NOG mice were irradiated at sublethal dose (200 cGy) and the next day were inoculated with 1×10^4 A20-luc cells via tail vein, and then were transplanted the following day with 1×10^7 MNCs isolated from HuCB. Cav-Ig or control Ig (each 100 μg/dose) was administered i.p. thrice per week, beginning at day +1 after transplantation until day +28. Overall survival is depicted from cumulative results from three independent experiments (for each, $n = 10$). $p < 0.0001$ versus recipients of control Ig by log-rank test. (**B**) In vivo bioluminescence imaging was performed at the indicated time points after treatment, as described in (A). Representative mice are shown. Ruffled fur consistent with skin GVHD is shown in recipients of control Ig group at 10 wk posttransplant (*middle panel*). †Death of all mice in the group of tumor alone or control Ig groups. (**C**) Sublethally irradiated NOG mice were transplanted with MNCs isolated from HuCB. Cav-Ig or control Ig was administered i.p. thrice per week, beginning at day +1 after transplantation until day +28. A total of 1×10^5 A20-luc cells was inoculated via tail vein on day +28 posttransplantation. Overall survival is depicted from cumulative results from three independent experiments (for each, $n = 10$). $p < 0.0001$ versus recipients of control Ig by log-rank test. (**D**) In vivo bioluminescence imaging was performed at the indicated time points after treatment, as described in (C). Representative mice are shown. Slightly ruffled fur consistent with skin GVHD is shown in recipients of control Ig group at 6 wk posttransplant (*middle panel*). †Death of all mice in the group of tumor alone or control Ig groups.

completely abrogated in ΔCNS-77 Tg mice (41). Moreover, IFN-γ^+CD4 T cells infiltrating in the lung of obliterative bronchiolitis exclusively expressed IL-26, whereas IL-17A$^+$CD4 T cells were negative for IL-26. To characterize the role of IL-26$^+$CD26$^+$CD4 T cells in patients with obliterative bronchiolitis, we analyzed the lung specimen of a patient with dyspnea and ground glass opacity detected on the chest X-ray examination on day +95 of alloPBSCT for ALL. Although a limited number of samples was obtained because invasive examinations including lung biopsy are not necessary to diagnose lung cGVHD (4), our data obtained from a human lung sample confirm the findings shown in the above murine model. Collectively, our data imply that IL-26$^+$CD26$^+$ Th1 cells play an important role in the pathogenesis of obliterative bronchiolitis observed in a cGVHD patient as well as in whole CB transplant mice. Regarding its specific receptor, IL-26 primarily binds to IL-20RA, followed by recruitment of IL-10RB (26). Although IL-10RB is broadly expressed on most cell types and tissues, IL-20RA is not expressed in lymphoid organs, but is expressed in the lung as well as skin (59). It is thus conceivable that IL-26–related fibroproliferation occurs in the lung and skin.

It has been reported that allogeneic Th17 cells could induce severe forms of acute GVHD associated with cutaneous and pulmonary pathologic manifestations (60). Moreover, in studies of lung transplant recipients using murine model and human samples, IL-17 was shown to be involved in the pathogenesis of obliterative bronchiolitis associated with chronic rejection (61, 62). In the current study, we demonstrated that levels of *IL17A* and IL-17–producing cells were slightly increased in CD4 T cells infiltrating the obliterative bronchiolitis lung. Although the role of IL-17 in cGVHD is still unclear (63), we could not exclude the possibility that small populations of IL-17$^+$CD4 T cells are involved in

the pathogenesis of obliterative bronchiolitis in cGVHD. In addition, Th17 cells display a great degree of context-dependent plasticity, as they are capable of acquiring functional characteristics of Th1 cells (64). This late plasticity may play a role in the development of obliterative bronchiolitis regulated by $CD26^+CD4$ Th1 cells, and may be associated with the emergence of $IL\text{-}26^+CD26^+$ Th1 cells.

Several causes of obliterative bronchiolitis after alloHSCT have been proposed, including donor-derived T cell–mediated injury, several profibrotic factors, and autoantibody deposition (7). Recent report using a murine model showed that donor-derived B cell activation and maturation with the aid of T follicular helper cells were necessary for cGVHD, and bronchiolitis obliterans syndrome was reversed by the abrogation of IL-21 signaling (65). However, our present model using human donor cells did not demonstrate the presence of B cells in the lung of obliterative bronchiolitis, whereas a substantial B cell population was detected in the recipient PBL. In fact, no direct evidence for a causal relationship for autoantibodies or alloantibodies in the pathogenesis of organ manifestation of cGVHD has been observed in humans (9). Furthermore, cGVHD of the visceral organs seemed to respond poorly to B cell depletion therapy such as rituximab (7, 9). It is speculated that this observed discrepancy is due to differences in the B cell maturation process between mice and humans (11). Despite these limitations of murine or humanized murine models, targeting CD4 T cells to control cGVHD is a reasonable therapeutic approach because T cell help plays a pivotal role in B cell maturation and activation in cGVHD (66).

A related issue concerns the process of B cell development in humanized mice. Previous work has shown that reconstituted human $CD45^+$ cells in other models of humanized mice were overcome by $CD3^+$ T cells within several months of transplantation due to reduced B cell development (40). However, given the fact that HuCB contains ample HSC as well as naive lymphocytes, the use of HuCB as donor cells led to sustained recovery of lymphocytes in the recipient PBL, as had also been reported by other investigators (24, 38, 39, 67). In addition, it has been demonstrated that specific Abs in human B cells generated in the humanized mice transplanted with HSC isolated from HuCB are effectively synthesized (23, 24, 38, 40). A potential concern regarding the applicability of results obtained from our model is the lack of intestinal GVHD. Because recent work demonstrated that neutrophils play an important role in intestinal GVHD (68), one possible explanation for the lack of intestinal GVHD in our model is that achieving effective engraftment of neutrophils in our model is particularly difficult (40). Despite the limitations of cross-species comparisons, our study provides insights into the pathogenesis of clinical pulmonary cGVHD induced by human lymphocytes. Furthermore, data obtained from our study have identified potential novel therapeutic targets in the management of clinical cGVHD.

Because we previously showed an effectiveness of anti-CD26 mAb on an aGVHD model using adult PBL (13), we performed preliminary testing of anti-CD26 mAb effect on recipient mice of whole CB transplant, and found a high incidence of graft failure (data not shown). Our speculation of the reason for this failure is as follows: we previously reported that HuCB CD4 T cells broadly express CD26 (21), and other investigators observed that $CD34^+CD38^{low/-}$ or $CD34^+CD38^+$ hematopoietic stem/progenitor cells in HuCB preferentially express CD26 (69). These findings suggest that treatment with anti-CD26 mAb in a HuCB transplant model may reduce the levels of hematopoietic stem/progenitor and/or CD4 T cells in the graft of HuCB, resulting in increased graft failure. Meanwhile, it has been reported that endogenous CD26 expression on donor cells negatively regulates homing and engraftment (70), and that inhibition of DPP4 enzyme activity enhances engraftment of hematopoietic cells in mice and humans (71, 72). In the current study, we observed no difference of engraftment between Cav-Ig– and control Ig-treated mice. It is conceivable that continuous inhibition of DPP4 enzyme activity was not achieved by the alternate-day schedule of administration of Cav-Ig used in the current study, with the resultant lack of continuous inhibition of related chemokines, cytokines, and CSFs (71).

In addition to issues involving the use of anti-CD26 mAb, it is important to point out that there may be potential adverse events such as off-target effects associated with the proposed use of Cav-Ig therapy. Although caveolin-1 exists in the inner surface of most cell types (49), its N terminus is detected on endothelial cells as well as APCs after activation (73). Therefore, it is possible that Cav-Ig binds to cell surface caveolin-1 and is consumed in such endothelial cells. Other issues relate to the GVL effects. Our data demonstrated that Cav-Ig clearly impeded GVHD in our model with preservation of GVL effects. We speculate that CD26-dependent xenogeneic priming of CD4 T cells is inhibited by Cav-Ig (13, 20), whereas CD28-dependent GVL effects are exerted after engraftment (74). However, studying GVHD and GVL effects that require similar CD4- or CD8-dependent pathways with the use of primary leukemic cells rather than cell lines should help to generate reliable models of GVL. Despite these concerns, our work revealed no abnormal findings in the vessels and organs of Cav-Ig–treated recipient mice with preservation of the GVL effect, hence suggesting a potentially promising novel therapeutic approach for controlling cGVHD.

The administration of Cav-Ig may potentially result in renal damage because CD26 is also expressed in the kidney (44, 45). However, we observed no pathological changes in the kidney in mice treated with Cav-Ig (data not shown). These findings may be partially due to the fact that CD26 in the kidney is mainly expressed in the proximal tubules (75), and that immune complex deposition of complexes consisting of Cav-Ig and membrane-bound CD26 did not occur in the glomeruli to cause renal injury.

In conclusion, our present work demonstrates that caveolin-1 blockade can control pulmonary GVHD by suppressing the immune functions of donor-derived T cells and decreasing IL-26 production. Moreover, $IL\text{-}26^+CD26^+CD4$ T cell infiltration appears to play a significant role in the lung of obliterative bronchiolitis. Although complete suppression of cGVHD with current interventional strategies represents a difficult challenge at the present time, our data demonstrate that control of cGVHD clinical findings can be achieved in a murine experimental system by regulating $IL\text{-}26^+CD26^+$ CD4 T cells with Cav-Ig. Our work also suggests that Cav-Ig treatment may be a novel therapeutic approach for chronic inflammatory diseases, including RA and inflammatory bowel diseases, in which IL-26 plays an important role.

Disclosures

The authors have no financial conflicts of interest.

References

1. Champlin, R. E., N. Schmitz, M. M. Horowitz, B. Chapuis, R. Chopra, J. J. Cornelissen, R. P. Gale, J. M. Goldman, F. R. Loberiza, Jr., B. Hertenstein, et al. 2000. Blood stem cells compared with bone marrow as a source of hematopoietic cells for allogeneic transplantation. *Blood* 95: 3702–3709.
2. Socié, G., and J. Ritz. 2014. Current issues in chronic graft-versus-host disease. *Blood* 124: 374–384.
3. Baird, K., and S. Z. Pavletic. 2006. Chronic graft versus host disease. *Curr. Opin. Hematol.* 13: 426–435.
4. Filipovich, A. H., D. Weisdorf, S. Pavletic, G. Socie, J. R. Wingard, S. J. Lee, P. Martin, J. Chien, D. Przepiorka, D. Couriel, et al. 2005. National Institutes of Health consensus development project on criteria for clinical trials in chronic graft-versus-host disease: I. Diagnosis and staging working group report. *Biol. Blood Marrow Transplant.* 11: 945–956.

5. Bergeron, A., C. Godet, S. Chevret, G. Lorillon, R. Peffault de Latour, T. de Revel, M. Robin, P. Ribaud, G. Socié, and A. Tazi. 2013. Bronchiolitis obliterans syndrome after allogeneic hematopoietic SCT: phenotypes and prognosis. *Bone Marrow Transplant.* 48: 819–824.
6. Chu, Y. W., and R. E. Gress. 2008. Murine models of chronic graft-versus-host disease: insights and unresolved issues. *Biol. Blood Marrow Transplant.* 14: 365–378.
7. Barker, A. F., A. Bergeron, W. N. Rom, and M. I. Hertz. 2014. Obliterative bronchiolitis. *N. Engl. J. Med.* 370: 1820–1828.
8. Reddy, P., K. Johnson, J. P. Uberti, C. Reynolds, S. Silver, L. Ayash, T. M. Braun, and V. Ratanatharathorn. 2006. Nephrotic syndrome associated with chronic graft-versus-host disease after allogeneic hematopoietic stem cell transplantation. *Bone Marrow Transplant.* 38: 351–357.
9. Shimabukuro-Vornhagen, A., M. J. Hallek, R. F. Storb, and M. S. von Bergwelt-Baildon. 2009. The role of B cells in the pathogenesis of graft-versus-host disease. *Blood* 114: 4919–4927.
10. Seok, J., H. S. Warren, A. G. Cuenca, M. N. Mindrinos, H. V. Baker, W. Xu, D. R. Richards, G. P. McDonald-Smith, H. Gao, L. Hennessy, et al. 2013. Genomic responses in mouse models poorly mimic human inflammatory diseases. *Proc. Natl. Acad. Sci. USA* 110: 3507–3512.
11. Benitez, A., A. J. Weldon, L. Tatosyan, V. Velkuru, S. Lee, T. A. Milford, O. L. Francis, S. Hsu, K. Nazeri, C. M. Casiano, et al. 2014. Differences in mouse and human nonmemory B cell pools. *J. Immunol.* 192: 4610–4619.
12. Antin, J. H., B. E. Bierer, B. R. Smith, J. Ferrara, E. C. Guinan, C. Sieff, D. E. Golan, R. M. Macklis, N. J. Tarbell, E. Lynch, et al. 1991. Selective depletion of bone marrow T lymphocytes with anti-CD5 monoclonal antibodies: effective prophylaxis for graft-versus-host disease in patients with hematologic malignancies. *Blood* 78: 2139–2149.
13. Hatano, R., K. Ohnuma, J. Yamamoto, N. H. Dang, T. Yamada, and C. Morimoto. 2013. Prevention of acute graft-versus-host disease by humanized anti-CD26 monoclonal antibody. *Br. J. Haematol.* 162: 263–277.
14. Fox, D. A., R. E. Hussey, K. A. Fitzgerald, O. Acuto, C. Poole, L. Palley, J. F. Daley, S. F. Schlossman, and E. L. Reinherz. 1984. Ta1, a novel 105 KD human T cell activation antigen defined by a monoclonal antibody. *J. Immunol.* 133: 1250–1256.
15. Morimoto, C., and S. F. Schlossman. 1998. The structure and function of CD26 in the T-cell immune response. *Immunol. Rev.* 161: 55–70.
16. Ohnuma, K., N. H. Dang, and C. Morimoto. 2008. Revisiting an old acquaintance: CD26 and its molecular mechanisms in T cell function. *Trends Immunol.* 29: 295–301.
17. Ohnuma, K., O. Hosono, N. H. Dang, and C. Morimoto. 2011. Dipeptidyl peptidase in autoimmune pathophysiology. *Adv. Clin. Chem.* 53: 51–84.
18. Ohnuma, K., Y. Munakata, T. Ishii, S. Iwata, S. Kobayashi, O. Hosono, H. Kawasaki, N. H. Dang, and C. Morimoto. 2001. Soluble CD26/dipeptidyl peptidase IV induces T cell proliferation through CD86 up-regulation on APCs. *J. Immunol.* 167: 6745–6755.
19. Ohnuma, K., T. Yamochi, M. Uchiyama, K. Nishibashi, N. Yoshikawa, N. Shimizu, S. Iwata, H. Tanaka, N. H. Dang, and C. Morimoto. 2004. CD26 up-regulates expression of CD86 on antigen-presenting cells by means of caveolin-1. *Proc. Natl. Acad. Sci. USA* 101: 14186–14191.
20. Ohnuma, K., M. Uchiyama, R. Hatano, W. Takasawa, Y. Endo, N. H. Dang, and C. Morimoto. 2009. Blockade of CD26-mediated T cell costimulation with soluble caveolin-1-Ig fusion protein induces anergy in $CD4^+$T cells. *Biochem. Biophys. Res. Commun.* 386: 327–332.
21. Kobayashi, S., K. Ohnuma, M. Uchiyama, K. Iino, S. Iwata, N. H. Dang, and C. Morimoto. 2004. Association of CD26 with CD45RA outside lipid rafts attenuates cord blood T-cell activation. *Blood* 103: 1002–1010.
22. Sato, K., H. Nagayama, and T. A. Takahashi. 1999. Aberrant CD3- and CD28-mediated signaling events in cord blood T cells are associated with dysfunctional regulation of Fas ligand-mediated cytotoxicity. *J. Immunol.* 162: 4464–4471.
23. Shultz, L. D., M. A. Brehm, J. V. Garcia-Martinez, and D. L. Greiner. 2012. Humanized mice for immune system investigation: progress, promise and challenges. *Nat. Rev. Immunol.* 12: 786–798.
24. Tezuka, K., R. Xun, M. Tei, T. Ueno, M. Tanaka, N. Takenouchi, and J. Fujisawa. 2014. An animal model of adult T-cell leukemia: humanized mice with HTLV-1-specific immunity. *Blood* 123: 346–355.
25. Morimoto, C., Y. Torimoto, G. Levinson, C. E. Rudd, M. Schrieber, N. H. Dang, N. L. Letvin, and S. F. Schlossman. 1989. 1F7, a novel cell surface molecule, involved in helper function of CD4 cells. *J. Immunol.* 143: 3430–3439.
26. Hör, S., H. Pirzer, L. Dumoutier, F. Bauer, S. Wittmann, H. Sticht, J. C. Renauld, R. de Waal Malefyt, and H. Fickenscher. 2004. The T-cell lymphokine interleukin-26 targets epithelial cells through the interleukin-20 receptor 1 and interleukin-10 receptor 2 chains. *J. Biol. Chem.* 279: 33343–33351.
27. Ohnuma, K., M. Uchiyama, T. Yamochi, K. Nishibashi, O. Hosono, N. Takahashi, S. Kina, H. Tanaka, X. Lin, N. H. Dang, and C. Morimoto. 2007. Caveolin-1 triggers T-cell activation via CD26 in association with CARMA1. *J. Biol. Chem.* 282: 10117–10131.
28. Collins, P. L., S. Chang, M. Henderson, M. Soutto, G. M. Davis, A. G. McLoed, M. J. Townsend, L. H. Glimcher, D. P. Mortlock, and T. M. Aune. 2010. Distal regions of the human *IFNG* locus direct cell type-specific expression. *J. Immunol.* 185: 1492–1501.
29. Cooke, K. R., L. Kobzik, T. R. Martin, J. Brewer, J. Delmonte, Jr., J. M. Crawford, and J. L. Ferrara. 1996. An experimental model of idiopathic pneumonia syndrome after bone marrow transplantation: I. The roles of minor H antigens and endotoxin. *Blood* 88: 3230–3239.
30. Anderson, B. E., J. M. McNiff, C. Matte, I. Athanasiadis, W. D. Shlomchik, and M. J. Shlomchik. 2004. Recipient $CD4^+$ T cells that survive irradiation regulate chronic graft-versus-host disease. *Blood* 104: 1565–1573.
31. Kaplan, D. H., B. E. Anderson, J. M. McNiff, D. Jain, M. J. Shlomchik, and W. D. Shlomchik. 2004. Target antigens determine graft-versus-host disease phenotype. *J. Immunol.* 173: 5467–5475.
32. Aoe, K., V. J. Amatya, N. Fujimoto, K. Ohnuma, O. Hosono, A. Hiraki, M. Fujii, T. Yamada, N. H. Dang, Y. Takeshima, et al. 2012. CD26 overexpression is associated with prolonged survival and enhanced chemosensitivity in malignant pleural mesothelioma. *Clin. Cancer Res.* 18: 1447–1456.
33. Hatano, R., K. Ohnuma, J. Yamamoto, N. H. Dang, and C. Morimoto. 2013. CD26-mediated co-stimulation in human $CD8^+$ T cells provokes effector function via pro-inflammatory cytokine production. *Immunology* 138: 165–172.
34. Ohnuma, K., T. Saito, R. Hatano, O. Hosono, S. Iwata, N. H. Dang, H. Ninomiya, and C. Morimoto. 2014. Comparison of two commercial ELISAs against an in-house ELISA for measuring soluble CD26 in human serum. *J. Clin. Lab. Anal.* DOI: 10.1002/jcla.21736.
35. Chen, X., J. Dodge, R. Komorowski, and W. R. Drobyski. 2013. A critical role for the retinoic acid signaling pathway in the pathophysiology of gastrointestinal graft-versus-host disease. *Blood* 121: 3970–3980.
36. Yamamoto, J., K. Ohnuma, R. Hatano, T. Okamoto, E. Komiya, H. Yamazaki, S. Iwata, N. H. Dang, K. Aoe, T. Kishimoto, et al. 2014. Regulation of somatostatin receptor 4-mediated cytostatic effects by CD26 in malignant pleural mesothelioma. *Br. J. Cancer* 110: 2232–2245.
37. Ito, M., H. Hiramatsu, K. Kobayashi, K. Suzue, M. Kawahata, K. Hioki, Y. Ueyama, Y. Koyanagi, K. Sugamura, K. Tsuji, et al. 2002. NOD/SCID/γc^{null} mouse: an excellent recipient mouse model for engraftment of human cells. *Blood* 100: 3175–3182.
38. Matsumura, T., Y. Kametani, K. Ando, Y. Hirano, I. Katano, R. Ito, M. Shiina, H. Tsukamoto, Y. Saito, Y. Tokuda, et al. 2003. Functional $CD5^+$ B cells develop predominantly in the spleen of NOD/SCID/γc^{null} (NOG) mice transplanted either with human umbilical cord blood, bone marrow, or mobilized peripheral blood CD34+ cells. *Exp. Hematol.* 31: 789–797.
39. Yahata, T., K. Ando, Y. Nakamura, Y. Ueyama, K. Shimamura, N. Tamaoki, S. Kato, and T. Hotta. 2002. Functional human T lymphocyte development from cord blood $CD34^+$ cells in nonobese diabetic/Shi-*scid*, IL-2 receptor γ null mice. *J. Immunol.* 169: 204–209.
40. Ito, R., T. Takahashi, I. Katano, and M. Ito. 2012. Current advances in humanized mouse models. *Cell. Mol. Immunol.* 9: 208–214.
41. Collins, P. L., M. A. Henderson, and T. M. Aune. 2012. Lineage-specific adjacent *IFNG* and *IL26* genes share a common distal enhancer element. *Genes Immun.* 13: 481–488.
42. Donnelly, R. P., F. Sheikh, H. Dickensheets, R. Savan, H. A. Young, and M. R. Walter. 2010. Interleukin-26: an IL-10-related cytokine produced by Th17 cells. *Cytokine Growth Factor Rev.* 21: 393–401.
43. Bengsch, B., B. Seigel, T. Flecken, J. Wolanski, H. E. Blum, and R. Thimme. 2012. Human Th17 cells express high levels of enzymatically active dipeptidylpeptidase IV (CD26). *J. Immunol.* 188: 5438–5447.
44. Gorrell, M. D., V. Gysbers, and G. W. McCaughan. 2001. CD26: a multifunctional integral membrane and secreted protein of activated lymphocytes. *Scand. J. Immunol.* 54: 249–264.
45. Wang, Z., C. Grigo, J. Steinbeck, S. von Hörsten, K. Amann, and C. Daniel. 2014. Soluble DPP4 originates in part from bone marrow cells and not from the kidney. *Peptides* 57: 109–117.
46. Yi, T., Y. Chen, L. Wang, G. Du, D. Huang, D. Zhao, H. Johnston, J. Young, I. Todorov, D. T. Umetsu, et al. 2009. Reciprocal differentiation and tissue-specific pathogenesis of Th1, Th2, and Th17 cells in graft-versus-host disease. *Blood* 114: 3101–3112.
47. Fickenscher, H., and H. Pirzer. 2004. Interleukin-26. *Int. Immunopharmacol.* 4: 609–613.
48. Kloosterboer, F. M., S. A. van Luxemburg-Heijs, R. Willemze, and J. H. Falkenburg. 2006. Similar potential to become activated and proliferate but differential kinetics and profiles of cytokine production of umbilical cord blood T cells and adult blood naive and memory T cells. *Hum. Immunol.* 67: 874–883.
49. Engelman, J. A., X. Zhang, F. Galbiati, D. Volonte, F. Sotgia, R. G. Pestell, C. Minetti, P. E. Scherer, T. Okamoto, and M. P. Lisanti. 1998. Molecular genetics of the caveolin gene family: implications for human cancers, diabetes, Alzheimer disease, and muscular dystrophy. *Am. J. Hum. Genet.* 63: 1578–1587.
50. Soiffer, R. 2008. Immune modulation and chronic graft-versus-host disease. *Bone Marrow Transplant.* 42(Suppl. 1): S66–S69.
51. Wu, C. J., and J. Ritz. 2009. Revealing tumor immunity after hematopoietic stem cell transplantation. *Clin. Cancer Res.* 15: 4515–4517.
52. Knappe, A., S. Hör, S. Wittmann, and H. Fickenscher. 2000. Induction of a novel cellular homolog of interleukin-10, AK155, by transformation of T lymphocytes with herpesvirus saimiri. *J. Virol.* 74: 3881–3887.
53. Wilson, N. J., K. Boniface, J. R. Chan, B. S. McKenzie, W. M. Blumenschein, J. D. Mattson, B. Basham, K. Smith, T. Chen, F. Morel, et al. 2007. Development, cytokine profile and function of human interleukin 17-producing helper T cells. *Nat. Immunol.* 8: 950–957.
54. Corvaisier, M., Y. Delneste, H. Jeanvoine, L. Preisser, S. Blanchard, E. Garo, E. Hoppe, B. Barré, M. Audran, B. Bouvard, et al. 2012. IL-26 is overexpressed in rheumatoid arthritis and induces proinflammatory cytokine production and Th17 cell generation. *PLoS Biol.* 10: e1001395.
55. Goris, A., M. G. Marrosu, and K. Vandenbroeck. 2001. Novel polymorphisms in the IL-10 related AK155 gene (chromosome 12q15). *Genes Immun.* 2: 284–286.
56. Vandenbroeck, K., S. Cunningham, A. Goris, I. Alloza, S. Heggarty, C. Graham, A. Bell, and M. Rooney. 2003. Polymorphisms in the interferon-gamma/

interleukin-26 gene region contribute to sex bias in susceptibility to rheumatoid arthritis. *Arthritis Rheum.* 48: 2773–2778.
57. Silverberg, M. S., J. H. Cho, J. D. Rioux, D. P. McGovern, J. Wu, V. Annese, J. P. Achkar, P. Goyette, R. Scott, W. Xu, et al. 2009. Ulcerative colitis-risk loci on chromosomes 1p36 and 12q15 found by genome-wide association study. *Nat. Genet.* 41: 216–220.
58. Miot, C., E. Beaumont, D. Duluc, H. Le Guillou-Guillemette, L. Preisser, E. Garo, S. Blanchard, I. Hubert Fouchard, C. Créminon, P. Lamourette, et al. 2014. IL-26 is overexpressed in chronically HCV-infected patients and enhances TRAIL-mediated cytotoxicity and interferon production by human NK cells. *Gut* DOI: 10.1136/gutjnl-2013-306604.
59. Wolk, K., S. Kunz, K. Asadullah, and R. Sabat. 2002. Cutting edge: immune cells as sources and targets of the IL-10 family members? *J. Immunol.* 168: 5397–5402.
60. Carlson, M. J., M. L. West, J. M. Coghill, A. Panoskaltsis-Mortari, B. R. Blazar, and J. S. Serody. 2009. In vitro-differentiated TH17 cells mediate lethal acute graft-versus-host disease with severe cutaneous and pulmonary pathologic manifestations. *Blood* 113: 1365–1374.
61. Fan, L., H. L. Benson, R. Vittal, E. A. Mickler, R. Presson, A. J. Fisher, O. W. Cummings, K. M. Heidler, M. R. Keller, W. J. Burlingham, and D. S. Wilkes. 2011. Neutralizing IL-17 prevents obliterative bronchiolitis in murine orthotopic lung transplantation. *Am. J. Transplant.* 11: 911–922.
62. Burlingham, W. J., R. B. Love, E. Jankowska-Gan, L. D. Haynes, Q. Xu, J. L. Bobadilla, K. C. Meyer, M. S. Hayney, R. K. Braun, D. S. Greenspan, et al. 2007. IL-17-dependent cellular immunity to collagen type V predisposes to obliterative bronchiolitis in human lung transplants. *J. Clin. Invest.* 117: 3498–3506.
63. Serody, J. S., and G. R. Hill. 2012. The IL-17 differentiation pathway and its role in transplant outcome. *Biol. Blood Marrow Transplant.* 18: S56–S61.
64. Muranski, P., and N. P. Restifo. 2013. Essentials of Th17 cell commitment and plasticity. *Blood* 121: 2402–2414.
65. Flynn, R., J. Du, R. G. Veenstra, D. K. Reichenbach, A. Panoskaltsis-Mortari, P. A. Taylor, G. J. Freeman, J. S. Serody, W. J. Murphy, D. H. Munn, et al. 2014. Increased T follicular helper cells and germinal center B cells are required for cGVHD and bronchiolitis obliterans. *Blood* 123: 3988–3998.
66. Zhang, C., I. Todorov, Z. Zhang, Y. Liu, F. Kandeel, S. Forman, S. Strober, and D. Zeng. 2006. Donor $CD4^+$ T and B cells in transplants induce chronic graft-versus-host disease with autoimmune manifestations. *Blood* 107: 2993–3001.
67. Ishikawa, F., M. Yasukawa, B. Lyons, S. Yoshida, T. Miyamoto, G. Yoshimoto, T. Watanabe, K. Akashi, L. D. Shultz, and M. Harada. 2005. Development of functional human blood and immune systems in NOD/SCID/IL2 receptor γ $chain^{null}$ mice. *Blood* 106: 1565–1573.
68. Schwab, L., L. Goroncy, S. Palaniyandi, S. Gautam, A. Triantafyllopoulou, A. Mocsai, W. Reichardt, F. J. Karlsson, S. V. Radhakrishnan, K. Hanke, et al. 2014. Neutrophil granulocytes recruited upon translocation of intestinal bacteria enhance graft-versus-host disease via tissue damage. *Nat. Med.* 20: 648–654.
69. Campbell, T. B., G. Hangoc, Y. Liu, K. Pollok, and H. E. Broxmeyer. 2007. Inhibition of CD26 in human cord blood $CD34^+$ cells enhances their engraftment of nonobese diabetic/severe combined immunodeficiency mice. *Stem Cells Dev.* 16: 347–354.
70. Christopherson, K. W., II, G. Hangoc, C. R. Mantel, and H. E. Broxmeyer. 2004. Modulation of hematopoietic stem cell homing and engraftment by CD26. *Science* 305: 1000–1003.
71. Broxmeyer, H. E., J. Hoggatt, H. A. O'Leary, C. Mantel, B. R. Chitteti, S. Cooper, S. Messina-Graham, G. Hangoc, S. Farag, S. L. Rohrabaugh, et al. 2012. Dipeptidylpeptidase 4 negatively regulates colony-stimulating factor activity and stress hematopoiesis. *Nat. Med.* 18: 1786–1796.
72. Farag, S. S., S. Srivastava, S. Messina-Graham, J. Schwartz, M. J. Robertson, R. Abonour, K. Cornetta, L. Wood, A. Secrest, R. M. Strother, et al. 2013. In vivo DPP-4 inhibition to enhance engraftment of single-unit cord blood transplants in adults with hematological malignancies. *Stem Cells Dev.* 22: 1007–1015.
73. Ohnuma, K., H. Inoue, M. Uchiyama, T. Yamochi, O. Hosono, N. H. Dang, and C. Morimoto. 2006. T-cell activation via CD26 and caveolin-1 in rheumatoid synovium. *Mod. Rheumatol.* 16: 3–13.
74. Blazar, B. R., P. A. Taylor, M. W. Boyer, A. Panoskaltsis-Mortari, J. P. Allison, and D. A. Vallera. 1997. CD28/B7 interactions are required for sustaining the graft-versus-leukemia effect of delayed post-bone marrow transplantation splenocyte infusion in murine recipients of myeloid or lymphoid leukemia cells. *J. Immunol.* 159: 3460–3473.
75. Hatano, R., T. Yamada, S. Matsuoka, S. Iwata, H. Yamazaki, E. Komiya, T. Okamoto, N. H. Dang, K. Ohnuma, and C. Morimoto. 2014. Establishment of monoclonal anti-human CD26 antibodies suitable for immunostaining of formalin-fixed tissue. *Diagn. Pathol.* 9: 30–42.

Biochemical and Biophysical Research Communications 460 (2015) 1069–1075

Contents lists available at ScienceDirect

Biochemical and Biophysical Research Communications

journal homepage: www.elsevier.com/locate/ybbrc

The role of Cas-L/NEDD9 as a regulator of collagen-induced arthritis in a murine model

Tomoki Katayose [a, 1], Satoshi Iwata [a, 2], Naoki Oyaizu [b], Osamu Hosono [c], Taketo Yamada [d, 3], Nam H. Dang [e], Ryo Hatano [a, 2], Hirotoshi Tanaka [a, c, 4], Kei Ohnuma [c, *], Chikao Morimoto [a, c, 2]

[a] Division of Clinical Immunology, Advanced Clinical Research Center, IMSUT Hospital, The Institute of Medical Science, The University of Tokyo, 4-6-1 Shirokanedai, Minato-ku, Tokyo 108-8639, Japan
[b] Department of Laboratory Medicine, IMSUT Hospital, The Institute of Medical Science, The University of Tokyo, 4-6-1 Shirokanedai, Minato-ku, Tokyo 108-8639, Japan
[c] Department of Rheumatology and Allergy, IMSUT Hospital, The Institute of Medical Science, The University of Tokyo, 4-6-1 Shirokanedai, Minato-ku, Tokyo 108-8639, Japan
[d] Department of Pathology, Keio University School of Medicine, 35 Shinanomachi, Shinjuku-ku, Tokyo, 160-8582, Japan
[e] Division of Hematology/Oncology, University of Florida, 1600 SW Archer Road, Box 100278, Room MSB M410A, Gainesville, FL 32610, USA

ARTICLE INFO

Article history:
Received 7 March 2015
Available online 3 April 2015

Keywords:
Cas-L/NEDD9
Rheumatoid arthritis
Collagen-induced arthritis
IL-10
T cell

ABSTRACT

Cas-L/NEDD9 is a cytoplasmic docking protein downstream of β1 integrin-mediated signaling pathway and is essential for cellular migration and β1 integrin-mediated costimulation of T cells. We previously found that increased number of Cas-L positive leukocytes migrated into the inflamed joints of HTLV-I tax transgenic mice which spontaneously develop polyarthritis, suggesting a role of Cas-L in rheumatoid arthritis (RA) pathophysiology. Our current study expanded these findings on the role of Cas-L/NEDD9 in the development of RA by analyzing the pathophysiological changes in a *Nedd9*$^{-/-}$ mouse collagen-induced arthritis (CIA) model. *Nedd9*$^{-/-}$ mice exhibited a decrease in arthritis severity as compared to *Nedd9*$^{+/+}$ mice. In addition, as being conducted bone marrow transplantation experiments with a CIA model, *Nedd9*$^{-/-}$→*Nedd9*$^{+/+}$ transplant showed a decrease in the incidence and severity score of arthritis, compared to those of *Nedd9*$^{+/+}$→*Nedd9*$^{-/-}$ transplant. For analysis of serum levels of various cytokines, IL-1β, IL-6, IL-17, TNF-α, IFN-γ and anti-collagen antibody were decreased, while IL-4 and IL-10 levels were increased, in *Nedd9*$^{-/-}$ mice as compared to those in *Nedd9*$^{+/+}$ mice. Furthermore, collagen-mediated cellular responses of lymphocytes isolated from spleen or affected lymph nodes of *Nedd9*$^{-/-}$ mice were reduced. Our results strongly suggest that Cas-L/NEDD9 plays a pivotal role in the pathophysiology of CIA, and that Cas-L/NEDD9 may be a potential molecular target for the treatment of RA.
© 2015 Elsevier Inc. All rights reserved.

Abbreviations: BM, bone marrow; BMT, bone marrow transplantation; CII, chicken type II collagen; Cas-L, Crk-associated substrate lymphocyte type; CFA, complete Freund's adjuvant; CIA, collagen-induced arthritis; FCS, fetal calf serum; FN, fibronectin; HTLV-I, human T lymphotropic virus type I; IHC, immunohistochemistry; mAb, monoclonal antibody; LN, lymph node; NEDD9, neural precursor cell–expressed, developmentally downregulated 9; PMA, phorbol 12-myristate 13-acetate; RA, rheumatoid arthritis; TBI, total body irradiation; TCR, T cell receptor.

* Corresponding author. Department of Therapy Development and Innovation for Immune Disorders and Cancers, Graduate School of Medicine, Juntendo University, 2-1-1, Hongo, Bunkyo-ku, Tokyo 113-8421, Japan. Fax: +81 3 3868 2310.
E-mail address: kohnuma@juntendo.ac.jp (K. Ohnuma).
[1] Current affiliation: Department of Internal Medicine, National Hospital Organization Murayama Medical Center, 2-37-1, Gakuen, Musashimurayama, Tokyo 208-0011, Japan.
[2] Department of Therapy Development and Innovation for Immune Disorders and Cancers, Graduate School of Medicine, Juntendo University, 2-1-1, Hongo, Bunkyo-ku, Tokyo 113-8421, Japan.
[3] Department of Pathology Saitama Medical University, Morohongo 38, Moroyama-cho, Iruma-gun, Saitama 350-0459, Japan.
[4] Center for Antibody and Vaccine Therapy, IMSUT Hospital, The Institute of Medical Science, The University of Tokyo, 4-6-1 Shirokanedai, Minato-ku, Tokyo 108-8639, Japan.

http://dx.doi.org/10.1016/j.bbrc.2015.03.156
0006-291X/© 2015 Elsevier Inc. All rights reserved.

1. Introduction

β1 integrins exhibit a variety of biological functions through specific interaction with their ligands including fibronectin (FN) [1]. We initially identified pp105 as the major phosphotyrosine-containing protein in H9 T-cell line stimulated with β1-integrins [2,3]. Sequence analysis of isolated cDNA clone revealed homology with p130 Crk-associated substrate (Cas)/breast cancer anti-estrogen resistance 1 (*BCAR1*) which was identified as a tyrosine-phosphorylated protein in v-Crk and v-Src–transformed fibroblasts [4], thus designating pp105 as Crk-associated substrate lymphocyte type (Cas-L). Cas-L is identical to neural precursor cell–expressed, developmentally down-regulated 9 (NEDD9) [5] and human enhancer of filamentation 1 (HEF1) [6]. Cas-L/NEDD9/HEF1 is an integrin signaling adaptor or docking protein that consists of multiple preserved domains common to Cas family members [7]. Cas-L/NEDD9 is phosphorylated at its tyrosine residues by integrins and other stimuli. Ligation of T- and B-cell antigen receptors caused tyrosine phosphorylation of Cas-L/NEDD9, resulting in the association of Crk, Crk-L, and C3G [8]. Integrin- or integrin/T cell receptor (TCR)-elicited tyrosine phosphorylation of Cas-L/NEDD9 was mediated by focal adhesion kinase (FAK) and Src family tyrosine kinases [9]. Ectopic expression of Cas-L/NEDD9 conferred T cells with enhanced motility on the co-engagement of TCR/CD3 complex and β1-integrins [10,11], suggesting a pivotal role of tyrosine-phosphorylated Cas-L/NEDD9 in TCR- and integrin-mediated cell motility.

We previously investigated the *in vivo* role of Cas-L/NEDD9 in the pathophysiology of rheumatoid arthritis (RA) in a mouse model of RA (using human T lymphotropic virus type I (HTLV-I) *tax* transgenic mice) as well as in RA patients [12]. HTLV-I transgenic mice that carry the env-pX gene developed high incidence of inflammatory arthropathy [13]. Our previous study demonstrated that Cas-L/NEDD9 involvement in the pathogenesis of RA-like disease in *tax* transgenic mice was mediated by its overexpression and hyperphosphorylation, resulting in markedly enhanced lymphocyte motility [12]. Moreover, we described the infiltration of Cas-L/NEDD9–positive, CD3-positive T cells into the affected joint lesion of RA patients [12]. These findings strongly suggest that Cas-L/NEDD9 plays a role in the pathophysiology of RA. However, it is unclear whether Cas-L/NEDD9 has a role in arthritis development in the absence of Tax since Cas-L/NEDD9 associates with Tax in HTLV-I-transformed cells [11]. To further characterize the role of Cas-L/NEDD9 in the pathogenesis of RA, our current work utilized a collagen-induced arthritis (CIA) model in *Nedd9*$^{-/-}$ mice to analyze the relevant clinical signs/symptoms, histopathology, serum levels of anti-collagen antibody and various cytokines, and lymphocytes characteristics.

2. Materials and methods

2.1. Mice

Nedd9$^{-/-}$ mice derived of C57BL/6J (B6) were generously provided by Dr. Seo from the Department of Hematology and Oncology, Graduate School of Medicine, University of Tokyo (Tokyo, Japan) [14]. Mice were used at 8–12 weeks. Animal experiments were conducted following protocols approved by the Animal Care and Use Committees at the Institute of Medical Science, University of Tokyo. All mice were housed in a specific pathogen-free facility in micro-isolator cages. All surgery was performed under sodium pentobarbital anesthesia, and all efforts were made to minimize suffering.

2.2. Induction of CIA and bone marrow transplantation (BMT)

CIA was induced as previously described with minor modifications [15]. Briefly, mice were injected intradermally at the base of tail with 200 μg of chicken type II collagen (CII) (Sigma, USA) in 10 mM acetic acid, emulsified in complete Freund's adjuvant (CFA) (Difco Laboratories, USA). Twenty-one days after the first immunization, the mice were boosted by the same methods. Day of the first immunization was designated as day 0 for CIA induction. Arthritis clinical scores in CIA mice were evaluated as described in previously published literature [16]. For adoptive transfer experiments, after 6hrs of total body irradiation (TBI) at 950 cGy, *Nedd9*$^{+/+}$ or *Nedd9*$^{-/-}$ mice were injected intravenously with 1×10^6 CD34$^+$ bone marrow (BM) cells isolated from *Nedd9*$^{-/-}$ (*Nedd9*$^{-/-}$→*Nedd9*$^{+/+}$) or *Nedd9*$^{+/+}$ (*Nedd9*$^{+/+}$→*Nedd9*$^{-/-}$), respectively. After 28 days and 49 days of transplantation, mice were immunized and evaluated by the same methods as described above.

2.3. Histopathology and immunohistochemistry (IHC)

Specimens of paw joints for histopathology and IHC were prepared by the same method as described in our previous report [12]. Antibodies used in IHC assays were anti-CD3 rabbit monoclonal antibody (mAb) (clone SP7) from Nichirei Bioscience (Japan), anti-mouse CD45R, B220 mAb (clone RA3-6B2) from BD Pharmingen (USA), and anti-Ly-6G/GR1 rat mAb (clone RB6-8C5) from Acris Antibodies (Germany).

2.4. Measurement of cytokines and anti-CII antibody

The collected sera were analyzed for various cytokines using Procarta Cytokine Assay (VERITAS, Tokyo, Japan) with Bio-Plex Suspension Array System (Bio-Rad Laboratories, USA). The serum antibody level to CII was evaluated using Mouse Anti-Chick Type II Collagen IgG Antibody Assay Kit (Chondrex, USA). All samples were run in triplicates.

2.5. Flow cytometry

The following antibodies were from BD Biosciences: Fluorescein isothiocyanate conjugated anti-mouse CD4 rat mAb (clone H129.19), phycoerythrin conjugated anti-mouse CD8α rat mAb (clone 53-6.7), peridinin-chlorophyll-a Protein-Cy5.5 conjugated anti-mouse CD19 rat mAb (clone 1D3), and allophycocyanin conjugated anti-mouse TCRβ hamster mAb (clone H57-597). Analysis was performed on 2-laser FACSCalibur (BD Biosciences) and files were analyzed in FlowJo software (Tree Star, USA).

2.6. In vitro costimulation assay

For assay of proliferative responses to FN, CD4$^+$T cells were purified from splenocytes isolated from *Nedd9*$^{+/+}$ or *Nedd9*$^{-/-}$ mice using mouse CD4$^+$T cell Isolation Kit II (Miltenyi Biotec, Germany). 1×10^5 cells per well were seeded in 96-well flat bottom plate with immobilized 0.5 μg/ml of anti-mouse CD3ε hamster mAb (clone 145-2C11, BD Pharmingen) and/or 1.0 μg/ml of FN (BIOPUR, Switzerland). The cells were cultured for 72hrs, and pulsed with [^{3}H]-thymidine (1μCi/well; Perkin–Elmer, USA) for the last 6hrs. The incorporated radioactivity was measured using a microplate beta counter (Micro Beta Plus; Wallac, USA). For assay of proliferative responses to CII, mononuclear cells were isolated from brachial, axillary, inguinal and popliteal lymph nodes (LNs) of *Nedd9*$^{+/+}$ or *Nedd9*$^{-/-}$ mice after 6 days of CIA immunization. Single suspension cells were prepared from LN lymphocytes using Spleen

Dissociation Kit, mouse (Miltenyi Biotec). 2×10^5 cells per well were cultured in the presence of 100 or 200 μg/ml of CII. Cell proliferation was evaluated by the same [^{3}H]-thymidine uptake assay as described above.

2.7. Statistical analysis

All experiments were performed in triplicates and repeated at least 3 times. Data were analyzed by two-tailed Student's *t* test for two group comparison or by ANOVA test for multiple comparison testing followed by the Tukey–Kramer *post-hoc* test. *P* values ≤ 0.05 were considered statistically significant. The calculations were conducted using SPSS Statistics software (IBM, USA).

3. Results and discussion

3.1. Reduced severity of CIA in Nedd9$^{-/-}$ mice

We first compared clinical signs/symptoms of arthritis between *Nedd9*$^{+/+}$ and *Nedd9*$^{-/-}$ mice following induction of CIA. The incidence of onset of arthritis in *Nedd9*$^{-/-}$ CIA mice was significantly decreased compared to that in *Nedd9*$^{+/+}$ CIA mice (Fig. 1A). Moreover, *Nedd9*$^{-/-}$ CIA mice exhibited decreased arthritis score compared to *Nedd9*$^{+/+}$ CIA mice (Fig. 1B). In addition, the severity and incidence of arthritis in *Nedd9* hetero knockout *Nedd9*$^{+/-}$ CIA mice were in-between those of *Nedd9*$^{+/+}$ and *Nedd9*$^{-/-}$ CIA mice (Fig. 1A and B). These data suggest that expression levels of Cas-L/NEDD9 affect induction of CIA.

To further characterize the clinical picture of the arthritis induced in this mouse model, we analyzed affected joints using planar X-ray examination. In *Nedd9*$^{-/-}$ CIA mice, metatarsal and tarsal bones at day 56 following the first immunization showed no significant changes as compared to findings seen in non-immunized mice (cricles in panels b and c of Fig. 1C), while metatarsal and tarsal joints of *Nedd9*$^{+/+}$ CIA mice exhibited narrowing, deformation and synostosis (circle in panel a of Fig. 1C). For additional analysis of the extent of arthritis, we conducted histopathologic examination using specimens of affected joints obtained at day 56 following the first immunization. As shown in Fig. 1D, *Nedd9*$^{+/+}$ CIA mice showed obvious thinning of articular cartilage and hyperplasia of synovium with infiltration of inflammatory cells (panels a and b), in contrast to the normal structure found in non-immunized mice (panel c). Meanwhile, the affected joint in *Nedd9*$^{-/-}$ CIA mice exhibited few signs of inflammation with slight thinning of articular cartilage and synovitis (panel d of Fig. 1D). To characterize the subsets of inflammatory cells found in the affected joints, we performed IHC using specimens of affected joints obtained at day 56 following the first immunization. In the affected joint of *Nedd9*$^{+/+}$ CIA mice, Ly-6G-positive granulocytes were predominantly found (panel a of Fig. 1E), while CD3-poistive T and B220-positive B cells were at undetectable levels (panels b and c of Fig. 1E). On the other hand, in *Nedd9*$^{-/-}$ CIA mice, inflammatory cells were not detected by IHC in the affected joint (panels d–f of Fig. 1E). Taken together, these results suggest that Cas-L/NEDD9 has an important role in the development of inflammatory arthral changes in CIA.

To define the role of Cas-L/NEDD9 in leukocytes in the development of CIA, we next conducted adoptive transfer experiments. For this purpose, BM cells were harvested from *Nedd9*$^{+/+}$ or *Nedd9*$^{-/-}$ mice, and transplanted into the opposite recipient mice after TBI. Recipients *Nedd9*$^{+/+}$ mice of *Nedd9*$^{-/-}$ BM cells (*Nedd9*$^{-/-}$ → *Nedd9*$^{+/+}$) showed a decrease in the incidence and severity score of arthritis, compared to those seen in recipients *Nedd9*$^{-/-}$ mice of *Nedd9*$^{+/+}$ BM cells (*Nedd9*$^{+/+}$ → *Nedd9*$^{-/-}$) (Fig. 1F and G). Meanwhile, CIA in *Nedd9*$^{+/+}$ → *Nedd9*$^{+/+}$ BMT recipients was induced at a similar level to that seen in *Nedd9*$^{+/+}$ CIA mice as shown in Fig. 1 (data not shown), while CIA was induced in *Nedd9*$^{-/-}$ → *Nedd9*$^{-/-}$ BMT recipients at lower levels than *Nedd9*$^{+/+}$ → *Nedd9*$^{+/+}$ BMT recipients, which were similar to that seen in *Nedd9*$^{-/-}$ CIA mice as shown in Fig. 1 (data not shown). These data strongly suggest that the presence of Cas-L/NEDD9 in leukocytes, but not in joint organs, is associated with the development of CIA, and that the development of CIA is not affected by BMT with TBI.

3.2. Decreased level of splenic lymphocytes in Nedd9$^{-/-}$ CIA mice

Since Cas-L/NEDD9 is involved in lymphocyte function [14,17], we next analyzed the lymphocytes in spleen and LN of *Nedd9*$^{-/-}$ CIA mice. For this purpose, spleen and LN cells were isolated from *Nedd9*$^{+/+}$ and *Nedd9*$^{-/-}$ mice before and after immunization, and we evaluated the cell numbers of each lymphocyte subset of spleen and LN cells. In spleen cells of *Nedd9*$^{-/-}$ mice, decreased levels of CD4$^+$T, CD8$^+$T and CD19$^+$B cells were observed after immunization (Table 1). On the other hand, in spleen cells of *Nedd9*$^{+/+}$ mice, increased level of CD19$^+$B cells was detected, while the levels of CD4$^+$T and CD8$^+$T cells were almost similar before and after immunization (Table 1). Moreover, among the LN lymphocytes of *Nedd9*$^{-/-}$ mice, increased level of CD19$^+$B cells was observed after immunization, while the levels of CD4$^+$T and CD8$^+$T cells were almost similar before and after immunization (Table 1). Among the LN lymphocytes of *Nedd9*$^{+/+}$ mice, level of CD19$^+$B cells was almost similar before and after immunization, and the levels of CD4$^+$T and CD8$^+$T cells were reduced after immunization (Table 1). Collectively, these data suggest that both T and B cells are involved in CIA of *Nedd9*$^{-/-}$ mice.

3.3. Decreased T and B cell functions in Nedd9$^{-/-}$ CIA mice

Given our previous findings that Cas-L/NEDD9 is involved in costimulatory signaling to CD3/TCR pathway associated with engagement of β1 integrins in T cells [2,9,18,19], we next examined T cell responses in *Nedd9*$^{-/-}$ or *Nedd9*$^{+/+}$ CIA mice. For this purpose, *in vitro* costimulation experiments using CD4$^+$T cells purified from spleen were conducted. As shown in Fig. 2A, CD4$^+$T cells from spleen of immunized or non-immunized *Nedd9*$^{-/-}$ mice exhibited decreased cellular proliferation following TCR plus FN (a ligand for β1 integrin) costimulation, compared to those from *Nedd9*$^{+/+}$ mice. Meanwhile, proliferative responses to PMA plus ionomycin were at similar levels of full activation for CD4$^+$T cells from both *Nedd9*$^{+/+}$ and *Nedd9*$^{-/-}$ CIA mice, with or without immunization (Fig. 2A). These data suggest that Cas-L/NEDD9 is involved in T cell activation through TCR and engagement of β1 integrin. To further characterize the role of Cas-L/NEDD9 in cell proliferation, we examined proliferative response of lymphocytes to CII. As shown in Fig. 2B, LN mononuclear cells isolated from *Nedd9*$^{-/-}$ CIA mice exhibited decreased CII-mediated cell proliferation, compared to those from *Nedd9*$^{+/+}$ CIA mice. Meanwhile, proliferative responses to PMA plus ionomycin were at similar levels of full activation in both *Nedd9*$^{+/+}$ and *Nedd9*$^{-/-}$ CIA mice (Fig. 2B).

Migration and adhesion of B cells in *Nedd9*$^{-/-}$ mice have been shown previously to be impaired [14]. To further define the role of Cas-L/NEDD9 on the humoral response in CIA, we analyzed the immunologic response to CII in *Nedd9*$^{-/-}$ CIA mice. For this purpose, serum levels of anti-CII antibody were assayed. As shown in Fig. 2C, serum levels of anti-CII antibody in *Nedd9*$^{-/-}$ CIA mice were significantly decreased as compared to those in *Nedd9*$^{+/+}$ CIA mice, data which are consistent with the findings regarding the incidence and severity of clinical signs/symptoms of arthritis. Taken together, our data strongly suggest that Cas-L/NEDD9 in T cells as well as in B cells plays an important role in the development of arthritis in a CIA model.

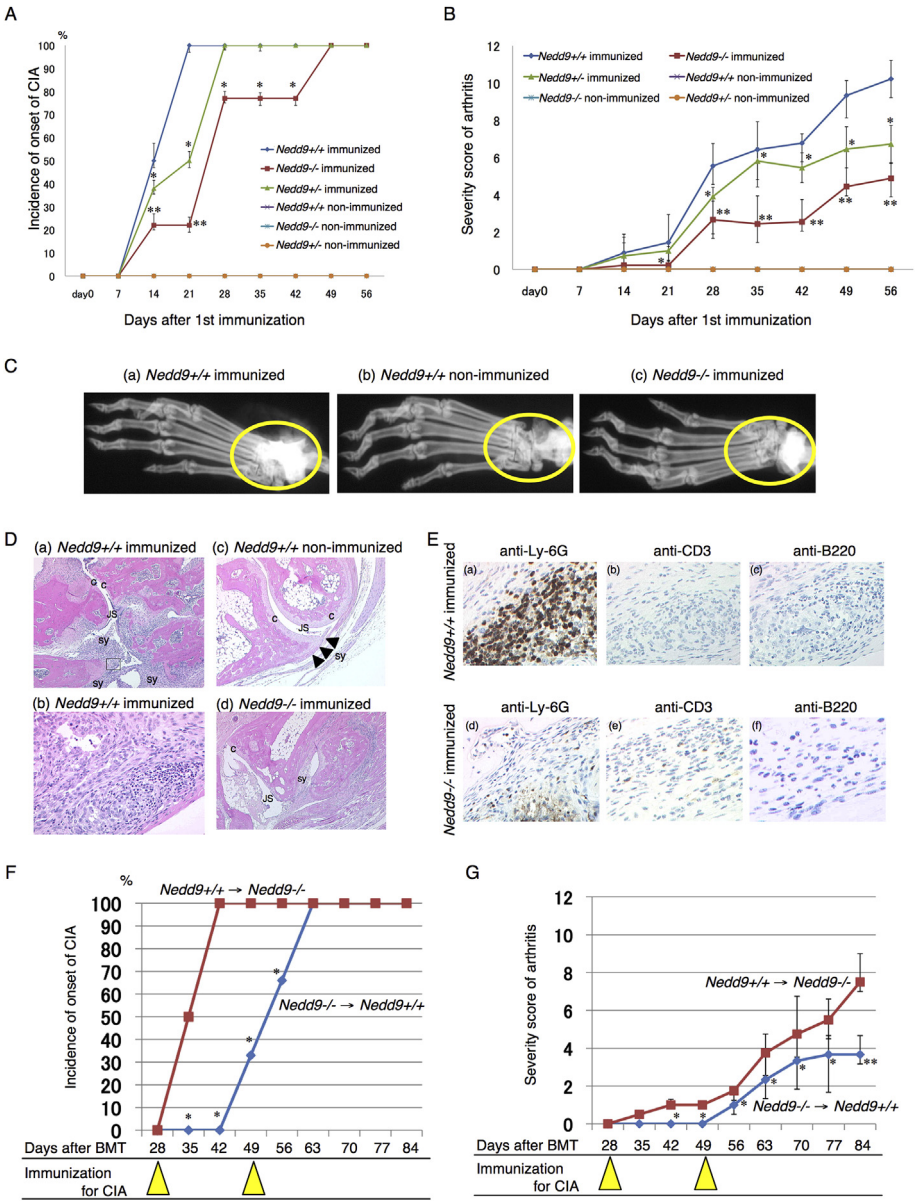

Fig. 1. Reduced incidence and severity of CIA in *Nedd9*$^{-/-}$ mice. A. The incidence of mice developing CIA was calculated as % ratio of mice with severity score ≥1 to total in each cohort (each, n = 9). Incidence of CIA decreased in *Nedd9*$^{-/-}$ cohort, compared to that in *Nedd9*$^{+/+}$ mice. Incidence of CIA in immunized *Nedd9*$^{+/-}$ subset (green line) was in-between that found in *Nedd9*$^{+/+}$ (blue line) and *Nedd9*$^{-/-}$ (red line) cohorts. None of the non-immunized *Nedd9*$^{+/+}$ (purple line), *Nedd9*$^{+/-}$ (orange line) or *Nedd9*$^{-/-}$ (light blue line) mice developed CIA. * indicates $P < 0.05$ *vs.* immunized *Nedd9*$^{+/+}$ CIA cohort, and ** indicates $P < 0.01$ *vs.* immunized *Nedd9*$^{+/+}$ or *Nedd9*$^{+/-}$ CIA cohort. B. The arthritis severity score was evaluated as described in Materials and methods. Severity of CIA decreased in *Nedd9*$^{-/-}$ cohort, compared to that in *Nedd9*$^{+/+}$ mice. Level of arthritis severity score of immunized *Nedd9*$^{+/-}$ CIA cohort (green line) was in-between that of immunized *Nedd9*$^{+/+}$ (blue line) and *Nedd9*$^{-/-}$ (red line) CIA cohorts. None of the non-immunized *Nedd9*$^{+/+}$ (purple line), *Nedd9*$^{+/-}$ (orange line) or *Nedd9*$^{-/-}$ (light blue line) mice developed CIA. *indicates $P < 0.05$ *vs.* immunized *Nedd9*$^{+/+}$ CIA cohort, and ** indicates $P < 0.01$ *vs.* immunized *Nedd9*$^{+/+}$ or *Nedd9*$^{+/-}$ CIA cohort. Data were shown as mean ± standard deviation. C. Representative planar X-ray images of the upper limbs of *Nedd9*$^{+/+}$ mice with or without CIA immunization (panels a or b, respectively), and immunized *Nedd9*$^{-/-}$ CIA mice (panel c) on day 56 after the first immunization. D. H&E staining of the upper limbs of *Nedd9*$^{+/+}$ mice with or without CIA immunization (panels a,b or c, respectively), and immunized *Nedd9*$^{-/-}$ CIA mice (panel d). The specimens were resected on day 56 after the first immunization. Representative histology is shown from 3 independent experiments (each, n = 6). C, JS or Sy denotes articular cartilage, joint space, or synovium, respectively. Panel b is focused in the inset of panel a. Original magnification × 20 for panels a,c,d, and × 100 for panel b. E. Representative immunohistochemical images of the upper limbs of immunized *Nedd9*$^{+/+}$ or *Nedd9*$^{-/-}$ CIA mice. Representative histology is shown from 3 independent experiments (each, n = 6). Original magnification × 100. F. After total body irradiation, *Nedd9*$^{+/+}$ or *Nedd9*$^{-/-}$ mice received BM cells of *Nedd9*$^{-/-}$ (*Nedd9*$^{-/-}$→*Nedd9*$^{+/+}$) or *Nedd9*$^{+/+}$ (*Nedd9*$^{+/+}$→*Nedd9*$^{-/-}$) mice, respectively (each, n = 6). Recipient mice were immunized for CIA after 28 and 49 days of BM transplantation (indicated in yellow triangles). The incidence of mice developing CIA was calculated as % ratio of mice with severity score ≥1 to total in each cohort. Incidence of CIA decreased in *Nedd9*$^{-/-}$→*Nedd9*$^{+/+}$ cohort (blue line), compared to that seen in the *Nedd9*$^{+/+}$→*Nedd9*$^{-/-}$ group (red line). * indicates $P < 0.01$ *vs.* *Nedd9*$^{+/+}$→*Nedd9*$^{-/-}$ cohort. G. Mice were treated by the same method as described in F. The arthritis severity score was evaluated as described in Materials and methods. Severity of CIA decreased in *Nedd9*$^{-/-}$→*Nedd9*$^{+/+}$ cohort (blue line), compared to that seen in the *Nedd9*$^{+/+}$→*Nedd9*$^{-/-}$ group (red line). * or ** indicates $P < 0.05$ or $P < 0.001$ *vs.* *Nedd9*$^{+/+}$→*Nedd9*$^{-/-}$ cohort, respectively. Data were shown as mean ± standard deviation. (For interpretation of the references to colour in this figure legend, the reader is referred to the web version of this article.)

Table 1
Number of $CD19^+$ B, $CD4^+$ and $CD8^+$ T cells in spleen or lymph nodes of *Nedd9*$^{+/+}$ or *Nedd9*$^{-/-}$ mice before and after CIA immunization.

(Organ)	(Subset)	*Nedd9*+/+		*Nedd9*−/−	
		Non-immunized	Immunized	Non-immunized	Immunized
Spleen (× 10^7/ml)	$CD19^+$B cell	2.60 ± 0.9	3.40 ± 1.4*	2.20 ± 0.7	1.20 ± 0.4**
	$CD4^+$T cell	0.90 ± 0.3	1.00 ± 0.4	1.00 ± 0.3	0.50 ± 0.1**
	$CD8^+$T cell	1.20 ± 0.4	1.40 ± 0.6	0.60 ± 0.2	0.35 ± 0.1**
Lymph node (× 10^7/ml)	$CD19^+$B cell	0.17 ± 0.1	0.11 ± 0.0	0.10 ± 0.0	0.40 ± 0.1**
	$CD4^+$T cell	0.35 ± 0.2	0.15 ± 0.0**	0.21 ± 0.1	0.20 ± 0.0
	$CD8^+$T cell	0.34 ± 0.2	0.17 ± 0.0*	0.18 ± 0.1	0.19 ± 0.0

CIA was induced in *Nedd9*$^{+/+}$ or *Nedd9*$^{-/-}$ mice as described in Materials and methods. Spleen and regional lymph nodes of the affected joints were resected on day 56 following the first immunization. Cells were subjected to flow cytometric analysis as shown in Supplemental Figure. Data were shown as mean of absolute cell number ± standard errors. of cumulative results from 3 independent experiments (each, n = 9). * or ** indicates $P < 0.05$ or $P < 0.01$ *vs.* those in each non-immunized cohort, respectively.

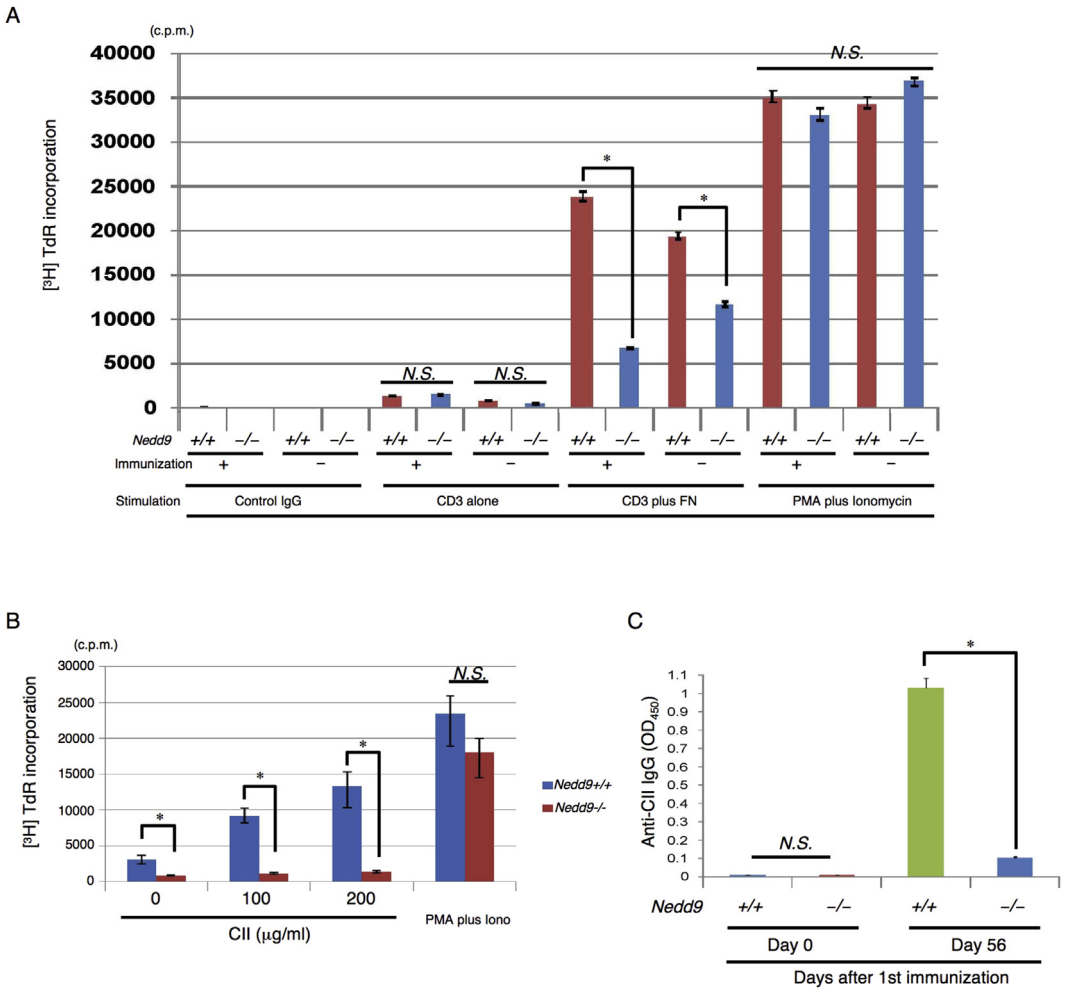

Fig. 2. Decreased proliferation of $CD4^+$T cells and anti-collagen antibody levels in *Nedd9*$^{-/-}$ CIA mice. A. $CD4^+$T cells were purified from spleen cells of *Nedd9*$^{+/+}$ or *Nedd9*$^{-/-}$ mice before and after immunization. Cells were stimulated with plate-bound anti-CD3 monoclonal antibody (mAb) and/or fibronectin (FN) at indicated concentrations, and assayed for cell proliferation by [^{3}H]-thymidine (TdR) incorporation. Data were shown as mean±standard errors (each, n = 6). * indicates $P < 0.001$, and *N.S.*, not significant. B. Lymph node (LN) mononuclear cells were isolated from the regional LNs of *Nedd9*$^{+/+}$ or *Nedd9*$^{-/-}$ mice after immunization. Cells were stimulated with type II collagen (CII) at indicated concentrations, and assayed for cell proliferation by [^{3}H]-thymidine (TdR) incorporation. Cell proliferation by CII stimulation was significantly enhanced in *Nedd9*$^{+/+}$ mice (*). Data were shown as mean±standard errors (each, n = 6). * indicates $P < 0.001$, and *N.S.*, not significant. C. Serum levels of anti-CII IgG antibody in *Nedd9*$^{+/+}$ or *Nedd9*$^{-/-}$ mice on day 0 and day 56 after immunization were measured using ELISA. Data were shown as mean±standard errors with triplicates (each, n = 9). * indicates $P < 0.001$.

3.4. Decrease of proinflammatory cytokines and increase of anti-inflammatory cytokines in Nedd9$^{-/-}$ CIA mice

We previously reported that Cas-L/NEDD9 is involved in TGF-β-related cell regulation [20]. However, it has been unclear whether production of other cytokines is associated with Cas-L/NEDD9. To examine whether Cas-L/NEDD9 has an affect on cytokine production in CIA, we assayed for serum levels of various cytokines in *Nedd9*$^{+/+}$ and *Nedd9*$^{-/-}$ CIA mice. As shown in Fig. 3A, levels of proinflammatory cytokines such as IL-1β (panel a), IL-6 (panel b), IL-17 (panel c), IFN-γ (panel d), and TNF-α (panel e) were significantly decreased in sera of *Nedd9*$^{-/-}$ CIA

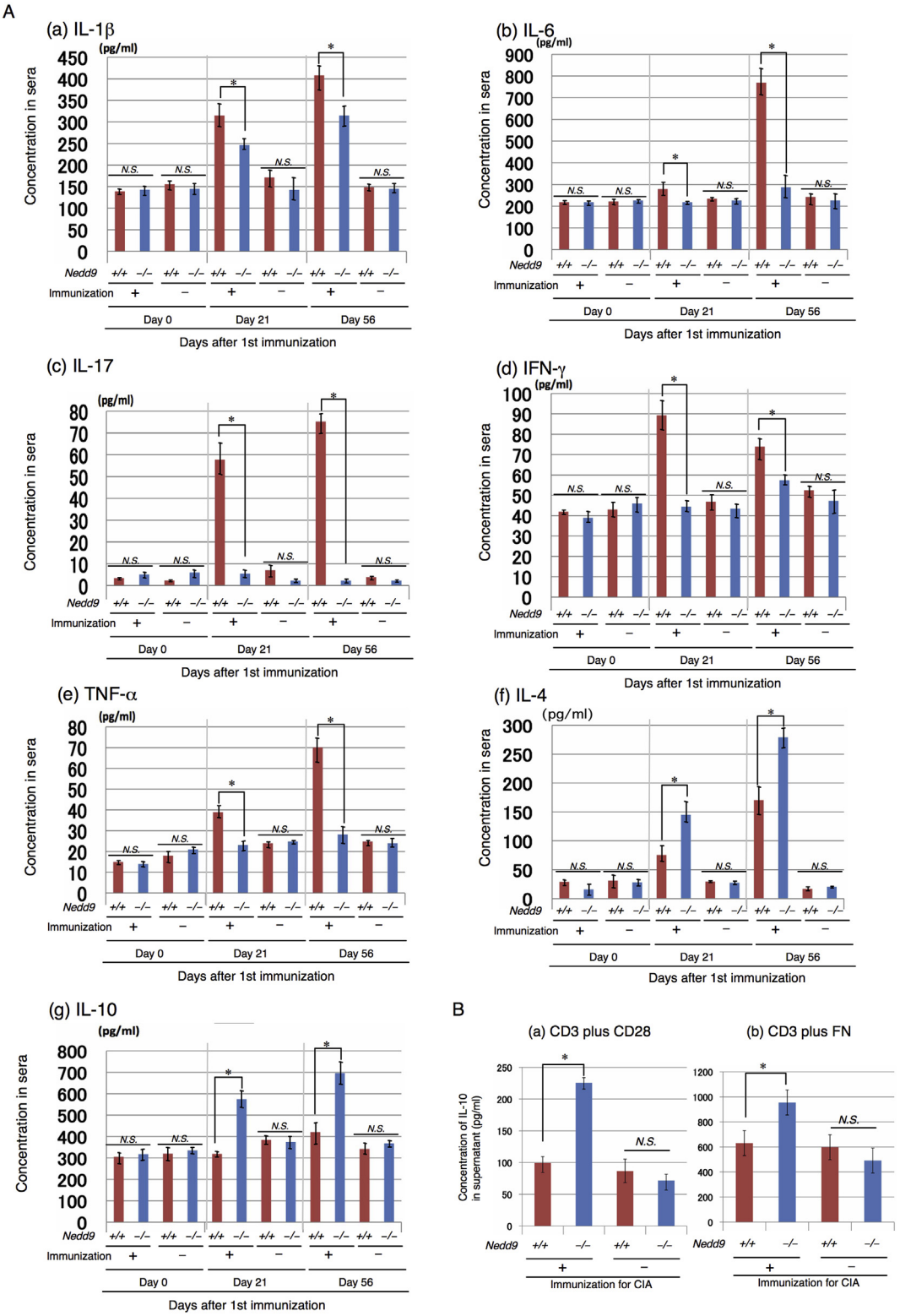

Fig. 3. Increase of IL-10 level in *Nedd9*$^{-/-}$ CIA mice. A. Sera of *Nedd9*$^{+/+}$ or *Nedd9*$^{-/-}$ mice were collected at the indicated day after CIA immunization, and serum levels of IL-1β (panel a), IL-6 (panel b), IL-17 (panel c), IFN-γ (panel d), TNF-α (panel e), IL-4 (panel f) and IL-10 (panel g) were quantified. Data are shown as mean±standard errors of cumulative results from 3 independent experiments (each, n = 9). * indicates $P < 0.001$, and *N.S.*, not significant. B. CD4^{+}T cells were purified from spleen cells of *Nedd9*$^{+/+}$ or *Nedd9*$^{-/-}$ mice before and after immunization. Cells were stimulated with plate-bound anti-CD3 mAb plus anti-CD28 mAb (panel a), or anti-CD3 mAb plus fibronectin (FN). After 72 h, the supernatants were harvested, and subjected to IL-10 assay. Data are shown as mean±standard errors with triplicates (each, n = 6). * indicates $P < 0.001$, and *N.S.*, not significant.

mice as compared to *Nedd9*$^{+/+}$ CIA mice. Meanwhile, levels of anti-inflammatory cytokines such as IL-4 and IL-10 were significantly increased in sera of *Nedd9*$^{-/-}$CIA mice as compared to *Nedd9*$^{+/+}$ CIA mice (panels f and g of Fig. 3A). These data suggest that the decrease in T cell responses seen in *Nedd9*$^{-/-}$ mice is mediated at least partly by increased production of the anti-inflammatory cytokine IL-10.

To further evaluate this possibility, we conducted *in vitro* cytokine production assay using CD4^{+}T cells isolated from *Nedd9*$^{-/-}$ and *Nedd9*$^{+/+}$ CIA mice. As shown in Fig. 3B, production of IL-10 by CD3 plus CD28 costimulation was significantly enhanced in CD4^{+}T cells from *Nedd9*$^{-/-}$ CIA mice, compared to that of non-immunized *Nedd9*$^{-/-}$ or *Nedd9*$^{+/+}$ mice and *Nedd9*$^{+/+}$ CIA mice (panel a). Similarly, production of IL-10 by CD3 plus FN costimulation was significantly enhanced in CD4^{+}T cells from *Nedd9*$^{-/-}$ CIA mice, compared to that of non-immunized *Nedd9*$^{-/-}$ or *Nedd9*$^{+/+}$ mice and *Nedd9*$^{+/+}$ CIA mice (panel b of Fig. 3B). These results suggest that the decreased incidence and severity of CIA seen in *Nedd9*$^{-/-}$ mice are partly associated with an increase in IL-10 production by T cells as well as a decrease in inflammatory T cell responses.

Collectively, our present results strongly suggest that Cas-L/NEDD9 in lymphocytes plays a pivotal role in the pathogenesis of CIA, and that targeting Cas-L/NEDD9 may be an effective novel therapeutic approach for autoimmune diseases including RA.

Conflict of interest

The authors declare no conflict of interest.

Acknowledgments

This study was supported in part by a grant of the Ministry of Education, Science, Sports and Culture, Japan (K.O. and C.M.), a grant of the Ministry of Health, Labour, and Welfare, Japan (C.M.) and a Grant-in-Aid (S1311011) from the Foundation of Strategic Research Projects in Private Universities from the Ministry of Education, Culture, Sports, Science, and Technology, Japan (K.O. and C.M.).

T.K, and S.I. contributed to the conception and design of the study, or acquisition of data, O.N., O.S., R.H., T.Y. and H.T. contributed to analysis and interpretation of data, K.O. and C.M. designed the research, interpreted the data and wrote the paper, N.H.D. interpreted the data, assisted with the paper, and proofread the manuscript. All authors showed final approval of the version to be submitted.

Appendix A. Supplementary data

Supplementary data related to this article can be found at http://dx.doi.org/10.1016/j.bbrc.2015.03.156.

Transparency document

Transparency document related to this article can be found online at http://dx.doi.org/10.1016/j.bbrc.2015.03.156.

References

[1] R.O. Hynes, Integrins: versatility, modulation, and signaling in cell adhesion, Cell 69 (1992) 11–25.
[2] Y. Nojima, D.M. Rothstein, K. Sugita, et al., Ligation of VLA-4 on T cells stimulates tyrosine phosphorylation of a 105-kD protein, J. Exp. Med. 175 (1992) 1045–1053.
[3] M. Minegishi, K. Tachibana, T. Sato, et al., Structure and function of Cas-L, a 105-kD Crk-associated substrate-related protein that is involved in β1 integrin-mediated signaling in lymphocytes, J. Exp. Med. 184 (1996) 1365–1375.
[4] R. Sakai, A. Iwamatsu, N. Hirano, et al., A novel signaling molecule, p130, forms stable complexes in vivo with v-Crk and v-Src in a tyrosine phosphorylation-dependent manner, EMBO J. 13 (1994) 3748–3756.
[5] S. Kumar, Y. Tomooka, M. Noda, Identification of a set of genes with developmentally down-regulated expression in the mouse brain, Biochem. Biophys. Res. Commun. 185 (1992) 1155–1161.
[6] S.F. Law, J. Estojak, B. Wang, et al., Human enhancer of filamentation 1, a novel p130^{cas}-like docking protein, associates with focal adhesion kinase and induces pseudohyphal growth in Saccharomyces cerevisiae, Mol. Cell. Biol. 16 (1996) 3327–3337.
[7] G.M. O'Neill, S. Seo, I.G. Serebriiskii, et al., A new central scaffold for metastasis: parsing HEF1/Cas-L/NEDD9, Cancer Res. 67 (2007) 8975–8979.
[8] Y. Ohashi, K. Tachibana, K. Kamiguchi, et al., T cell receptor-mediated tyrosine phosphorylation of Cas-L, a 105-kDa Crk-associated substrate-related protein, and its association of Crk and C3G, J. Biol. Chem. 273 (1998) 6446–6451.
[9] K. Tachibana, T. Urano, H. Fujita, et al., Tyrosine phosphorylation of Crk-associated substrates by focal adhesion kinase. A putative mechanism for the integrin-mediated tyrosine phosphorylation of Crk-associated substrates, J. Biol. Chem. 272 (1997) 29083–29090.
[10] Y. Ohashi, S. Iwata, K. Kamiguchi, C. Morimoto, Tyrosine phosphorylation of Crk-associated substrate lymphocyte-type is a critical element in TCR- and β1 integrin-induced T lymphocyte migration, J. Immunol. 163 (1999) 3727–3734.
[11] S. Iwata, A. Souta-Kuribara, A. Yamakawa, et al., HTLV-I Tax induces and associates with Crk-associated substrate lymphocyte type (Cas-L), Oncogene 24 (2005) 1262–1271.
[12] R. Miyake-Nishijima, S. Iwata, S. Saijo, et al., Role of Crk-associated substrate lymphocyte type in the pathophysiology of rheumatoid arthritis in tax transgenic mice and in humans, Arthritis Rheum. 48 (2003) 1890–1900.
[13] Y. Iwakura, M. Tosu, E. Yoshida, et al., Induction of inflammatory arthropathy resembling rheumatoid arthritis in mice transgenic for HTLV-I, Science 253 (1991) 1026–1028.
[14] S. Seo, T. Asai, T. Saito, et al., Crk-associated substrate lymphocyte type is required for lymphocyte trafficking and marginal zone B cell maintenance, J. Immunol. 175 (2005) 3492–3501.
[15] E.F. Rosloniec, M. Cremer, A. Kang, L.K. Myers, Collagen-induced arthritis, Chapter 15, Curr. Protoc. Immunol. (2001). Unit 15 15.
[16] D.D. Brand, K.A. Latham, E.F. Rosloniec, Collagen-induced arthritis, Nat. Protoc. 2 (2007) 1269–1275.
[17] S. Iwata, Y. Ohashi, K. Kamiguchi, C. Morimoto, β1-integrin-mediated cell signaling in T lymphocytes, J. Dermatol. Sci. 23 (2000) 75–86.
[18] K. Kamiguchi, K. Tachibana, S. Iwata, et al., Cas-L is required for β1 integrin-mediated costimulation in human T cells, J. Immunol. 163 (1999) 563–568.
[19] T. Matsuyama, A. Yamada, J. Kay, et al., Activation of CD4 cells by fibronectin and anti-CD3 antibody. A synergistic effect mediated by the VLA-5 fibronectin receptor complex, J. Exp. Med. 170 (1989) 1133–1148.
[20] S. Inamoto, S. Iwata, T. Inamoto, et al., Crk-associated substrate lymphocyte type regulates transforming growth factor-β signaling by inhibiting Smad6 and Smad7, Oncogene 26 (2007) 893–904.

Japan College of Rheumatology
MODERN RHEUMATOLOGY

http://informahealthcare.com/mor
ISSN 1439-7595 (print), 1439-7609 (online)

Mod Rheumatol, 2015; 25(4): 562–570
© 2015 Japan College of Rheumatology
DOI: 10.3109/14397595.2014.983262

Taylor & Francis
Taylor & Francis Group

ORIGINAL ARTICLE

Modulation of immunological responses and amelioration of collagen-induced arthritis by the novel roxithromycin derivative 5-I

Noriko Otsuki[1,5], Satoshi Iwata[1,6], Taketo Yamada[2], Osamu Hosono[3], Nam H. Dang[4], Ryo Hatano[1,6], Kei Ohnuma[3,6], and Chikao Morimoto[1,6]

[1]*Division of Clinical Immunology, Advanced Clinical Research Center, The Institute of Medical Science, The University of Tokyo, Minato-ku, Tokyo, Japan,* [2]*Department of Pathology, Keio University School of Medicine, Shinjuku-ku, Tokyo, Japan,* [3]*Department of Rheumatology and Allergy, IMUST Hospital, The Institute of Medical Science, The University of Tokyo, Minato-ku, Tokyo, Japan,* [4]*Division of Hematology/Oncology, University of Florida, Gainesville, FL, USA,* [5]*Division of food additives, National Institute of Health Sciences, Setagaya-ku, Tokyo, Japan, and* [6]*Department of Therapy Development and Innovation for Immune disorders and Cancers, Graduate School of Medicine, Juntendo University, Bunkyo-ku, Tokyo, Japan*

Abstract

Objective. Macrolide antibiotics have immunomodulatory properties that are distinct from their antibacterial functions. We synthesized 5-I, which is a new derivative of RXM with less antimicrobial activity, and evaluated its immunomodulatory effects through both *in vitro* and *in vivo* studies.

Methods. Proliferative response, cytokine production, and expression of mRNA of T cells stimulated with anti-CD3 and anti-CD28 mAbs in the presence or absence of monocytes, cytokine production of monocytes stimulated with lipopolysaccharide, and transendothelial migration of T cells in various concentrations of 5-I were analyzed. The effect of 5-I treatment was also evaluated in a mouse model of collagen-induced arthritis.

Results. 5-I specifically inhibited production of Th1, Th17, and proinflammatory cytokines such as IL-2, IFN-γ, TNF-α, IL-6, and IL-17A. 5-I reduced the expression of *RORC* on $CD4^+$ T cells, which codes for RORγt, the master regulator of Th17, and it also inhibited migration of activated T cells. Importantly, administration of 5-I to mice with collagen-induced arthritis reduced the severity of arthritis, and this effect was also observed when treatment was delayed till after the onset of disease.

Conclusion. Our findings strongly suggest that 5-I may be useful as a potential therapeutic agent for human rheumatoid arthritis.

Keywords

5-I, Collagen-induced arthritis, Monocytes, Rheumatoid arthritis, Roxithromycin, T cells

History

Received 5 August 2014
Accepted 30 October 2014
Published online 20 March 2015

Introduction

Macrolide antibiotics have many biological activities apart from their antibacterial actions. Low-dose and long-term erythromycin treatment was recently shown to be effective in chronic respiratory tract disease, including diffuse panbronchiolitis [1] and bronchial asthma [2], although the mechanism of action of this drug remains unclear. Moreover, macrolide antibiotics have reported activity in other extra-pulmonary diseases and selected biological conditions including rhinosinusitis [2], bone resorption and remodeling [3], inflammatory bowel diseases [4], and psoriasis [5]. The immunomodulatory effects of these agents are thought to result from processes involved in leukocyte activation such as stimulation of phagocytosis, natural killer cell activity, production of superoxide anion and neutrophil chemotaxis [6, 7]. Roxithromycin (RXM), a macrolide antibiotic, has a 14-member macrocyclin ring structure resembling that of erythromycin [8]. RXM is characterized by rapid and complete absorption after oral administration, resulting in high serum concentrations [9]. *In vitro* studies revealed that RXM modifies the function of neutrophils [10] and keratinocytes [11]. RXM also affects lymphocyte functions including proliferation induced by mitogens and purified protein derivative [12], as well as proliferation and cytokine secretion induced by mitogens [13].

We showed previously that RXM inhibited *in vitro* production of proinflammatory cytokines by T cells and macrophages, such as tumor necrosis factor-α (TNF-α) and interleukin 6 (IL-6), as well as suppressing T cell migration [14]. Interestingly, RXM treatment of mice with collagen-induced arthritis reduced the severity of arthritis and serum level of IL-6, along with leukocyte migration into the affected joints and destruction of bones and cartilages [14]. These results indicate that RXM may function both as an immunomodulatory agent and an antibiotic. However, it is of concern that the long-term use of antibiotics such as RXM may potentially induce adverse effects including nausea, QT prolongation, and induction of bacterial resistance. Therefore, components isolated from RXM with immunomodulatory properties may potentially be used for the treatment for autoimmune diseases such as rheumatoid arthritis (RA).

Correspondence to: Dr. Kei Ohnuma, Department of Therapy Development and Innovation for Immune disorders and Cancers, School of Medicine, Juntendo University, 2-1-1, Hongo, Bunkyo-ku, Tokyo 113-8421, Japan. Tel: +81-3-3868-2310. Fax: +81-3-3868-2310. E-mail: kohnuma@juntendo.ac.jp

In the present study, we synthesized a new derivative named 5-I from RXM with less antibiotic property. We then assessed the immunomodulatory activity of 5-I on human peripheral lymphocytes as well as its therapeutic effect on a mouse model of human RA.

Materials and methods

Roxithromycin and its derivative, 5-I

RXM was purchased from Sigma (R4393; St. Louis, MO) and 5-I was supplied from Y's Therapeutics Co., Ltd. (Ebisu, Tokyo, Japan). For all *in vitro* experiments, except for transendothelial migration assay, RXM and 5-I were first dissolved in methyl alcohol and further diluted in the culture medium consisting of RPMI-1640 medium supplemented with L-glutamine and 10% fetal calf serum (FCS; Invitrogen, Carlsbad, CA). For assessment of transendothelial migration, RXM and 5-I dissolved in methyl alcohol were further diluted in the assay medium consisting of RPMI-1640 medium with 0.6% bovine serum albumin (Sigma). For oral administration to mice in *in vivo* studies, RXM and 5-I were directly dissolved in 1% carboxymethylcellulose (CMC; Sigma)-containing saline (0.9% NaCl; Otsuka Pharmaceutical Co., Ltd., Tokyo, Japan) using a ground-glass homogenizer.

Preparation of peripheral blood mononuclear cells (PBMC) and *in vitro* culture

PBMCs were obtained from healthy volunteers. This study was approved by the institutional ethics committee at the Institute of Medical Science, University of Tokyo (No. 20-30-1009) and was conducted according to the principles of the Declaration of Helsinki; each healthy volunteer was provided with a written informed consent. PBMC were isolated by density gradient centrifugation. $CD3^+$ T cells and $CD4^+$ T cells were isolated from PBMC by negative selection using human Pan T cell isolation kit II (Miltenyi Biotec GmbH, Bergisch Gladbach, Germany), and human $CD4^+$ T cell isolation kit (Miltenyi Biotec GmbH), respectively. $CD14^+$ monocytes were isolated from PBMCs by positive selection using human CD14 MicroBeads (Miltenyi Biotec GmbH). The purities of $CD3^+$ T cells, $CD4^+$ T cells, and $CD14^+$ monocytes were greater than 97%, 97%, and 98% by flow cytometry, respectively. PBMC or $CD3^+$ T cells were stimulated (2×10^5 cells/well) with immobilized anti-CD3 (1 μg/ml, OKT3, IgG2a) and soluble anti-CD28 (5 μg/ml, 4B10, IgG1) mAb in the presence or absence of RXM or 5-I at the indicated concentration (5, 10, 20 and 40 μg/ml) in 96 well flat-bottom plates. Supernatants from triplicate cultures were collected after 24 h for assessment of IL-2 and IL-4 production. For assessment of IL-5, IL-6, IL-17A, IFN-γ and TNF-α, the supernatants were collected after 48 h. All cytokines except for IL-17A were measured using BD OptEIA ELISA set (BD Biosciences, San Jose, CA). The production of IL-17A was measured using "Ready-set-go!" ELISA Kits (eBioscience, San Diego, CA). For assay of proliferative responses, PBMCs or purified $CD3^+$ T cells (2×10^5 cells/well) were cultured with or without RXM or 5-I as described above for 72 h. The cells were pulsed with [^{3} H]-thymidine (1 mCi/well; Perkin-Elmer, Waltham, MA) for the last 18 h and harvested on a Micro 96 Cell Harvester (Skatron, Sterling, VA). The incorporated radioactivity was measured using a microplate beta counter (Micro Beta Plus; Wallac, Turku, Finland). For monocyte activation, purified $CD14^+$ monocytes were stimulated with 0.1, 1, 5, or 10 μg/ml of lipopolysaccharide (LPS; Sigma). After 24 h of culture, the supernatants were collected and subjected to ELISA for TNF-α and IL-6.

Determination of minimal inhibitory concentration (MIC)

For MIC testing, gram-positive bacteria, including *Staphylococcus aureus* (*S. aureus*) (ATCC 29213) or *Streptococcus pneumoniae* (*S. pneumoniae*) (ATCC 49619) was incubated in 96-well flat plates in the presence of RXM or 5-I for 24 h. Mueller-Hinton broth (MH broth; BD Difco, Franklin Lakes, NJ) and MH broth supplemented with 5% horse blood were used for *S. aureus*, or *S. pneumoniae*, respectively. The range of antibiotics concentration was set by two-fold serial dilution, specifically, 100, 50, 25, 12.5, 6.25, 3.13, 1.56, 0.78, 0.39, 0.2, 0.1, and 0.05 μg/ml. After 24 h of culture, growth inhibition was confirmed by visual inspection.

Transendothelial-migration assay

Transendothelial migration activity was assessed as described previously [15], with some modifications. Human umbilical vein endothelial cells (HUVEC; from KURABO Industries Ltd., Osaka, Japan) were pre-cultured at 3×10^5 cells/well to make monolayer sheets on fibronectin-coated Transwell Inserts with 3.0 mm pore size (BD Biosciences, San Jose, CA) for 48 h. Purified $CD3^+$ T cells (1×10^6 cells/ml) were stimulated 10 μg/ml of PHA in 24-well plates for 3 days. After 3 days of culture, PHA was washed out and IL-2 (100 units/ml; BD Pharmingen, San Diego, CA) was added, and the cells were cultured for an additional 2 days. At day 5, viable cells were isolated by density gradient centrifugation and stained with 5 mM CMFDA (CellTracker® Green, Molecular Probe, Eugene, OR). The assay medium was added to the culture plates in a final volume of 1200 μl in the lower chamber. Pre-activated and stained $CD3^+$ T cells (1×10^6 cells/ml) were resuspended with the assay medium, and added to each insert in a final volume of 600 μl in the presence or absence of RXM or 5-I for analysis of cell migration. After 24 h of culture, cells that migrated transendothelially into the lower chamber were collected to plastic tubes and stained with 7-amino-actinomycin D (7-AAD, BD Pharmingen) for exclusion of dead cells. $FL1^{high}$ $7\text{-}AAD^{negative}$ cells were counted at specific time limit (204 sec) and flow rate (high) by flow cytometry using FACSCalibur and CellQuest software (BD Biosciences).

Induction of collagen-induced arthritis (CIA), macrolides treatment, and clinical assessments of arthritis

CIA was induced as previously described with minor modifications [16]. Briefly, male DBA/1 J mice (7 week old) were injected intradermally at the base of tail with 100 mg of bovine type II collagen (CII) (Collagen Research Center, Tokyo, Japan) in 0.05 M acetic acid, emulsified in complete Freund's adjuvant (CFA) (Difco, Detroit, MI). Twenty-one days after primary immunization, the mice were boosted in the same way. Day of the second immunization (boost) was designated as day 0. Five non-immunized mice were included as the negative control group. The immunized mice were divided into four groups on the basis of body weight, and treated with the following regimens. Each group of mice was treated with either control saline (1% CMC, 200 μl), 5-I (200, 400 μg/body), or RXM (400 μg/body), intraperitoneally from day 0. The treatment was continued until day 20 every other day. In the experiments involving delayed treatment, 400 μg/body of 5-I was administrated at alternate days from day 4 to day 20. Each group consisted of 10 mice in all experiments. Mice were examined daily for the onset of CIA. The swelling of four paws was graded from 0 to 4 as follows: grade 0, no swelling; grade 1, swelling of finger joints or focal redness; grade 2, mild swelling of wrist or ankle joints; grade 3, severe swelling of the entire paw; grade 4, deformity or ankylosis. Each paw

was graded, and the four scores were totaled so that the maximal score per mouse was 16. Incidence was expressed as the number of paws that showed swelling in the total number of mice examined, body weight was measured on day 0, 7, 14, and 21, and the time of onset was expressed as the mean time when paw swelling was first observed in individual mouse. Animal experiments were conducted following protocols approved by the Animal Care and Use Committees at the Institute of Medical Science, University of Tokyo.

Histological analysis

Mice were euthanized by CO_2 asphyxiation and hind paws were then removed from the mice 3 weeks after the second immunization. The paws were fixed in 10% phosphate-buffered formalin (pH7.4), decalcified in 10% EDTA, and embedded in paraffin. Sections (4 μm) were stained with hematoxylin and eosin.

Quantification of mRNA by real-time RT-PCR

Purified $CD4^+$ T cells were cultured with immobilized anti-CD3 mAb (1 μg/ml) and soluble anti-CD28 mAbs (10 μg/ml) in the presence or absence of RXM or 5-I for 6 h and 10 h. Total cellular RNA from $CD4^+$ T cells (2×10^6) cultured as above were isolated using High Pure RNA Isolation Kit (Roche Diagnostics GmbH, Mannheim, Germany), according to the manufacturer's instructions. The quality and quantity of total RNA were assessed by NanoDrop spectrophotometer (ND-1000, Thermo Fisher Scientific Inc., MA). Complementary DNA (cDNA) was synthesized from 1 μg of total RNA using Transcriptor First Strand cDNA Synthesis Kit (Roche Diagnostics). The expression levels of *HPRT, TNFAIP6, WISP1* and *RORC* were evaluated by real-time RT-PCR using LightCycler® TaqMan® Master (Roche Diagnostics) with specific primers (Supplementary Table 1 available online at http://informahealthcare.com/doi/abs/10.3109/14397595.2014.983262). Reaction condition was 95°C 10 min, 35 cycles of 95°C 30 sec and 60°C 20 sec. TaqMan® probe (Universal Probe Library, Roche Diagnostics) was used to detect specific PCR products. Amplification and detection of TaqMan® probe were performed with LightCycler® ST300 (Roche Diagnostics). The human HPRT gene was used as a housekeeping reference gene to normalize expression levels between the samples.

Statistical analysis

Data were analyzed by two-tailed Student's *t* test for two group comparison or by ANOVA test for multiple comparison testing followed by the Tukey-Kramer *post-hoc* test. *P* values less than or equal to 0.05 were considered statistically significant.

Results

Determination of minimal inhibitory concentration for growth of RXM-susceptible bacteria

The chemical structures of Roxithromycin and its derivative 5-I are outlined in Figure 1A and B, respectively. To ascertain the relative deficiency of antimicrobial activity of 5-I, we determined the MIC for growth of two RXM-susceptible bacterial strains, *S. aureus* and *S. pneumoniae*, for 5-I as compared to RXM. As shown in Figure 1C, the MICs of RXM for *S. aureus* and *S. pneumoniae* were observed at 0.05 μg/ml and 0.78 μg/ml respectively, whereas those of 5-I were observed at 100 μg/ml and 25 μg/ml, respectively. These data hence indicated that 5-I was a defective derivative of RXM in antimicrobial activity, with 5-I antimicrobial activity being approximately 30 to 2,000 fold lower than that of RXM.

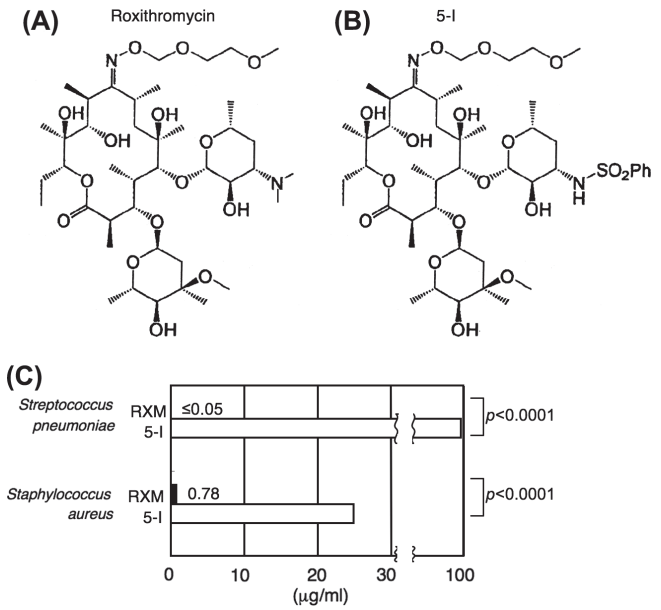

Figure 1. The antibiotic effects of Roxithromycin (RXM) and its new derivative 5-I. (A) The chemical structure of RXM. (B) The chemical structure of 5-I, a new derivative of RXM. (C) *Staphylococcus aureus* or *Streptococcus pneumoniae* were incubated in 96-well flat plates, in the presence of RXM or 5-I for 24 h. After 24 h of incubation, growth inhibition was confirmed by visual inspection. X-axis represents the concentration of RXM or 5-I. One representative set of data from three independent experiments are shown.

Effect of RXM and 5-I on proliferative response and cytokine production

Since we previously demonstrated the inhibitory effect of RXM on the proliferation and cytokine production of purified T cells [14], we therefore examined the effect of 5-I as well as RXM on $CD3^+$ T cells purified from PBMC. Both RXM and 5-I had either no inhibitory effect on the proliferative responses of $CD3^+$ T cells from different donors at concentrations ranging from 5 to 40 μg/ml, with similar results being observed in PBMC which contain monocytes/macrophages as well as T cells (Supplementary Figure 1 available online at http://informahealthcare.com/doi/abs/10.3109/14397595.2014.983262). To characterize the immunomodulatory properties of RXM and 5-I, we next assessed their effect on the production of various cytokines by purified $CD3^+$ T cells alone, and $CD3^+$ T cells plus $CD14^+$ monocytes stimulated with anti-CD3 and anti-CD28 mAb, or $CD14^+$ monocytes stimulated with LPS. Production of IL-2, IL-17A and INF-γ by $CD3^+$ T cells was reduced by the addition of RXM or 5-I (Figure 2A). TNF-α production by $CD3^+$ T cells was slightly reduced by the addition of RXM and 5-I (*panel a* of Figure 2B), while IL-6 production by purified $CD3^+$ T cells was below the level of detection in our *in vitro* system (data not shown). Since the main sources of TNF-α and IL-6 were monocyte/macrophage cells, we next conducted co-culture experiment using $CD3^+$ T cells with $CD14^+$ monocytes at a ratio of 40:1, and assessed the production of TNF-α and IL-6. As shown in Figure 2B, TNF-α (*panel b*) and IL-6 (*panel c*) production was clearly suppressed by the addition of RXM or 5-I. When we examined the production of TNF-α and IL-6 by LPS-stimulated $CD14^+$ monocytes, our data indicated that levels of TNF-α and IL-6 were significantly inhibited (approximately 20%) by the addition of RXM or 5-I (Figure 2C). Since Th2-type $CD4^+$ T cells may play a role in allergic disorders such as allergic rhinitis and bronchial asthma [17], we also examined the effect of RXM and 5-I on Th2-type cytokine production, and found that RXM and 5-I did not inhibit

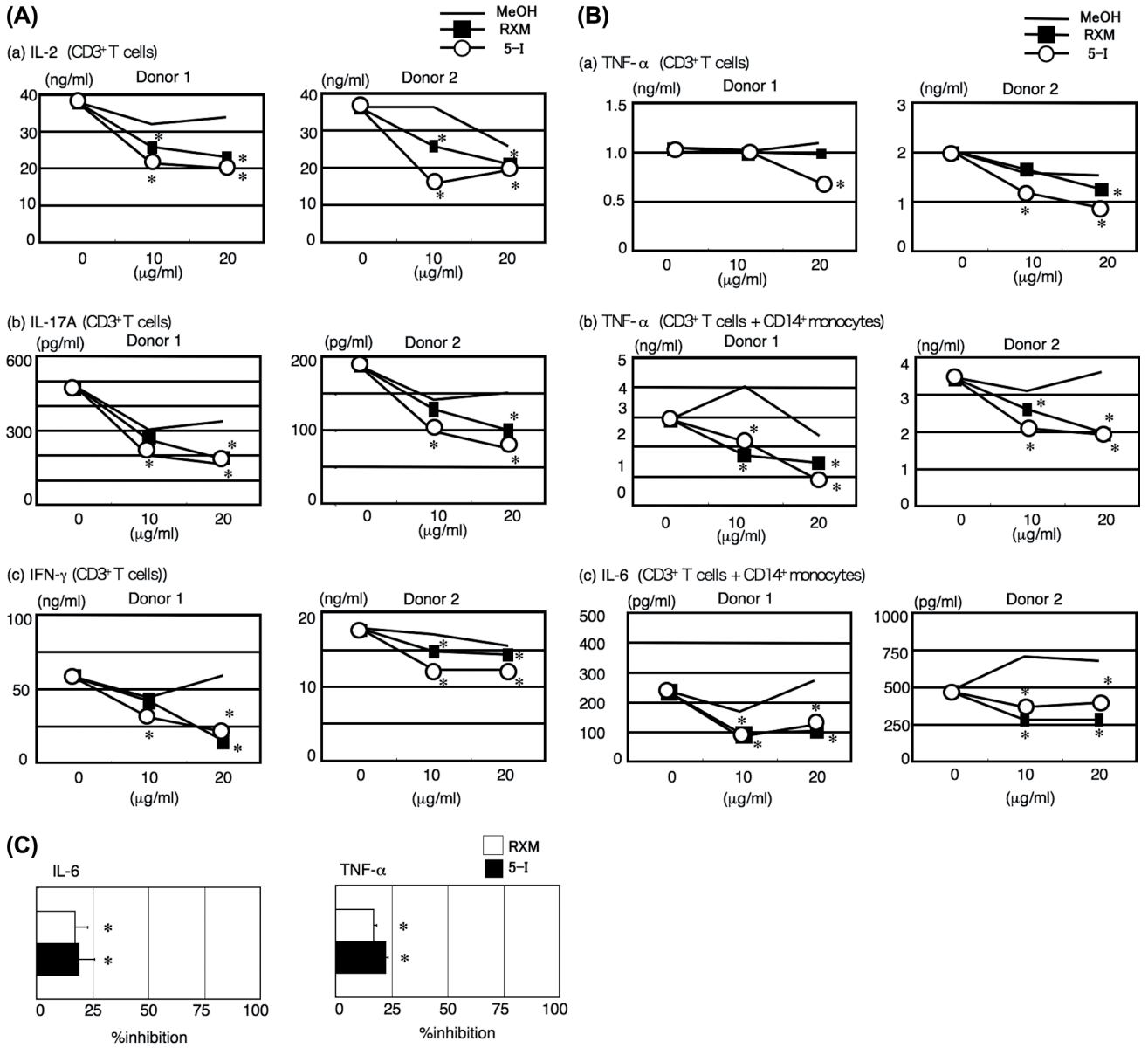

Figure 2. Inhibitory effect of RXM and 5-I on cytokine production by $CD3^+$ T cells and/or $CD14^+$ monocytes. (A) Levels of IL-2 (*panel a*), IL-17A (*panel b*), and IFN-γ (*panel c*) in purified $CD3^+$ T cells (2×10^5 cells) culture supernatants after stimulation with anti-CD3 (1 μg/ml) and anti-CD28 (5 μg/ml) mAbs in the presence or absence of vehicle (Met OH), RXM or 5-I at the indicated concentrations for 24 h (IL-2) and 48 h (IFN-γ and IL-17A) are shown. Results of 2 donors in four independent experiments are shown as representative of 10 different donors, with similar results being obtained. Statistically significant difference compared to the MeOH-treated control is shown ($*p < 0.01$). (B) Level of TNF-α (*panel a*) in $CD3^+$ T cells (2×10^5 cells) alone and level of TNF-α (*panel b*) or IL-6 (*panel c*) in $CD3^+$ T cells (2×10^5 cells) plus $CD14^+$ monocytes (5×10^3 cells) culture supernatants after stimulation by the same method as described in panel (A) for 48 h are shown. Results of 2 donors in four independent experiments are shown as representative of 10 different donors, with similar results being obtained. Statistically significant difference compared to the MeOH-treated control is shown ($*p < 0.01$). (C) Inhibition of TNF-α and IL-6 production in LPS (0.1 μg/ml)-stimulated $CD14^+$ monocyte culture supernatants in the presence of 20 μg/ml of RXM (open column) or 5-I (closed column) are shown. Data are presented as means ± SE of %inhibition to the MeOH-treated control from four experiments using 10 different donors ($*p < 0.001$).

IL-4 or IL-5 production (Supplementary Figures 2A or 2B available online at http://informahealthcare.com/doi/abs/10.3109/14397595.2014.983262, respectively). Given the fact that IL-10 regulates anti-inflammatory responses via the activation of T cells, and exerts inhibitory effects on proinflammatory cytokine production, we also assessed the effect of RXM and 5-I on IL-10 production. As shown in Supplementary Figures 2C available online at http://informahealthcare.com/doi/abs/10.3109/14397595.2014.983262, RXM and 5-I did not affect IL-10 production at any tested dose. Taken together, our results indicated that RXM and 5-I directly regulated T cell function by inhibiting the production of Th1- and Th17-type cytokines such as IL-2, IFN-γ and IL-17A, and regulated monocyte function by suppressing the production of proinflammatory cytokines such as TNF-α and IL-6, without any effect on IL-10 mediated anti-inflammatory pathway. Similar to RXM, 5-I therefore modulated activation of both T cells and monocytes by regulating cytokine production without having direct growth inhibitory effect.

Effect of 5-I on transendothelial migration of activated T cells as compared to RXM

Having demonstrated previously that RXM inhibited the transendothelial migration of activated T cells, we thus examined the effect of 5-I on this biological activity of PHA-activated T lymphocytes. Pre-activated T cells spontaneously migrate from the upper chamber to the lower chamber through the endothelial monolayer, a process termed chemokinesis. As described in Materi-

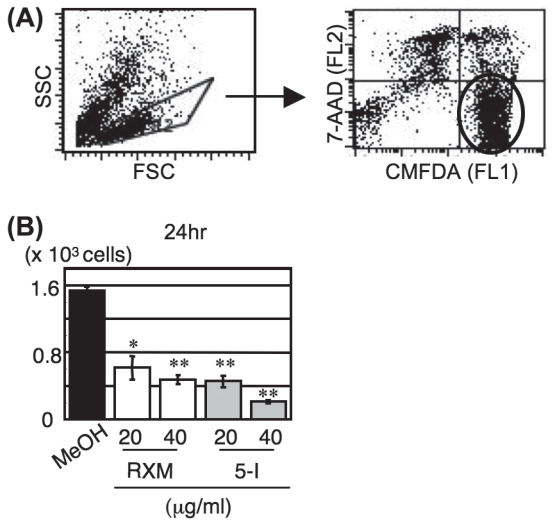

Figure 3. Inhibitory effect of RXM and 5-I on transendothelial migration of PHA-activated T cells. (A) Definition of transendothelially migrated T cells by flow cytometry. T cells pre-stained with CMFDA were acquired by FSC-SSC (gated in the quadrangle area of the left panel) and the migrated live cells were quantified by FL1 positive with 7-AAD negative as viable cells (gated in the circle area of the right panel). (B) The conditions of cell cultures were described as in Materials and Methods. Transendothelially migrated cells were counted by flow cytometry at specific time limit (204 sec) and flow rate (high). Bars show mean of cell numbers ± SE of triplicate cultures. Data were obtained from 10 different donors with four independent experiments. Statistically significant difference from the control vehicle-treated group is shown ($^{*}p < 0.05$, $^{**}p < 0.01$).

als and Methods, migrated viable cells were defined as FL1^{high} 7-AAD^{negative} cells, which could be analyzed through flow cytometry (Figure 3A). As shown in Figure 3B, T cell migration was significantly inhibited by RXM and 5-I at concentrations of 20 μg/ml and 40 μg/ml when these agents were present during the course of the endothelial migration assay. In contrast, when we pretreated HUVEC with various concentrations of RXM and 5-I for 48 h, and HUVEC were then washed and exposed to PHA-stimulated T cells, neither RXM nor 5-I affected the migration of activated T cells through HUVEC even at highest concentration (80 μg/ml) (data not shown). These findings suggested that inhibition of transendothelial migration of activated T cells was exerted by RXM or 5-I effect on T cells, but not on endothelial cells.

Regulation of mRNA expression by RXM and 5-I

To elucidate the cellular mechanisms involved in the immunomodulatory effect of RXM or 5-I on human lymphocyte activation, we examined the changes induced by RXM or 5-I in mRNA expression profiles of purified CD4^{+} T cells stimulated via CD3 and CD28 pathways (RXM, 5-I or vehicle-treated). Since the addition of RXM or 5-I clearly inhibited production of Th1- and Th17-type cytokines, such as IL-2 and IL-17, and proinflammatory cytokines, such as TNF-α and IL-6 (Figure 2), we particularly focused on the change of expression of Th-regulated genes. For this purpose, we conducted real-time RT-PCR analysis of the relevant transcription factors in purified CD4^{+} T cells. T-bet, GATA-3, and RORC are the master regulators of Th1, Th2, and Th17 subset, respectively. As shown in Figure 4A, the expression of *RORC* was reduced within 10 h of RXM or 5-I treatment whereas we could not detect any enhancing or suppressive effect on *TBX21* (T-bet) and *GATA3* mRNA expression (data not shown). To evaluate the early transcriptional events of cytokine genes involved in the polarization of T helper subsets, the expressions of *IL23R* and *TGFBR2* for Th17, *IL13RA1* for Th2, and tumor necrosis factor α-induced protein 6 (*TNFAIP6*) mRNA were analyzed. Although Th1 and Th17-related cytokine genes were not altered (data not shown), the expression of *TNFAIP6* was diminished within 10 h of RXM or 5-I treatment (Figure 4B). Besides those genes affected by the addition of RXM or 5-I, our data indicated a decrease in the level of WNT1-inducible-signaling pathway protein 1 (*WISP1*) (Figure 4C), a pro-mitogenic, pro-survival factor which mediates TNF-α-induced inflammatory responses. These data suggested that RXM and 5-I inhibited the polarization into Th17 cells by suppressing or delaying *RORC* transcription, and decreased inflammatory responses with subsequent TNF-α secretion in the early phase of CD4^{+} T cell activation.

Preventive and therapeutic effects of 5-I on CIA pathophysiology

Expanding on our findings above, we next investigated the potential effect of 5-I on the development of CIA. For this purpose, DBA/1 J mice were immunized twice with bovine CII in CFA to elicit CIA. Four groups of mice were treated intraperitoneally with either 200, 400 μg of 5-I, 400 μg of RXM, or 200 μl of saline as control solvent. Administration of RXM, 5-I, and saline was started at the time of secondary immunization of CII (day 0), and was continued on a schedule of every-other-day treatment up to day 20. As shown in Figure 5A, mice treated with control saline developed severe arthritis. In contrast, administration of 5-I significantly ameliorated the clinical manifestations of arthritis in a dose-dependent manner (Figure 5A), similar to results observed with 400 μg of RXM. The mean body weight of mice within each group was inversely correlated with their arthritis severity (Figure 5B). As summarized in Table 1, treatment with 400 μg of 5-I significantly decreased the mean arthritis score and the percentage of arthritic paw number. In addition, the mean body weight was markedly different from the saline-treated group, although the day of onset was not affected.

To determine whether 5-I therapy would still be effective even after the onset of disease manifestation, we next conducted a study involving delayed treatment of 5-I. Since disease onset typically occurred on day 4, we initiated a treatment regimen similar to our earlier work from day 4 onward, and then evaluated the clinical scores of the tested animals. As shown in Figure 5C,

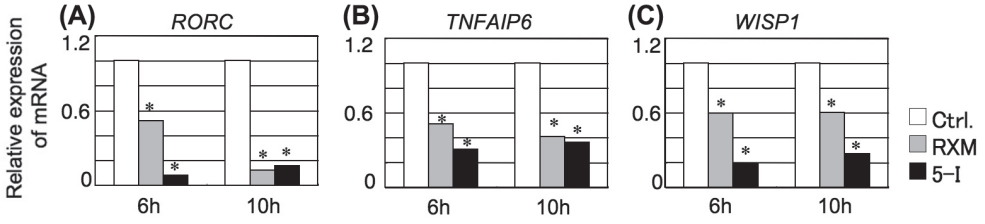

Figure 4. Measurement of gene expression by real-time RT-PCR. Purified CD4^{+} T cells were subjected to CD3/CD28-stimulation in the presence or absence of RXM and 5-I. After 24 h of culture, mRNA was extracted and alterations in gene expression in these cells were evaluated. Real-time PCR analysis for (A) *RORC*, (B) *TNFAIP6*, and (C) *WISP1*. Y-axis indicates relative expression level of indicated genes in the cultured CD4^{+} T cells (the expression level of control cells was set to 1.0). Data shown were representative of 4 independent experiments from 10 donors. Statistically significant difference from control cells is shown ($^{*}p < 0.01$).

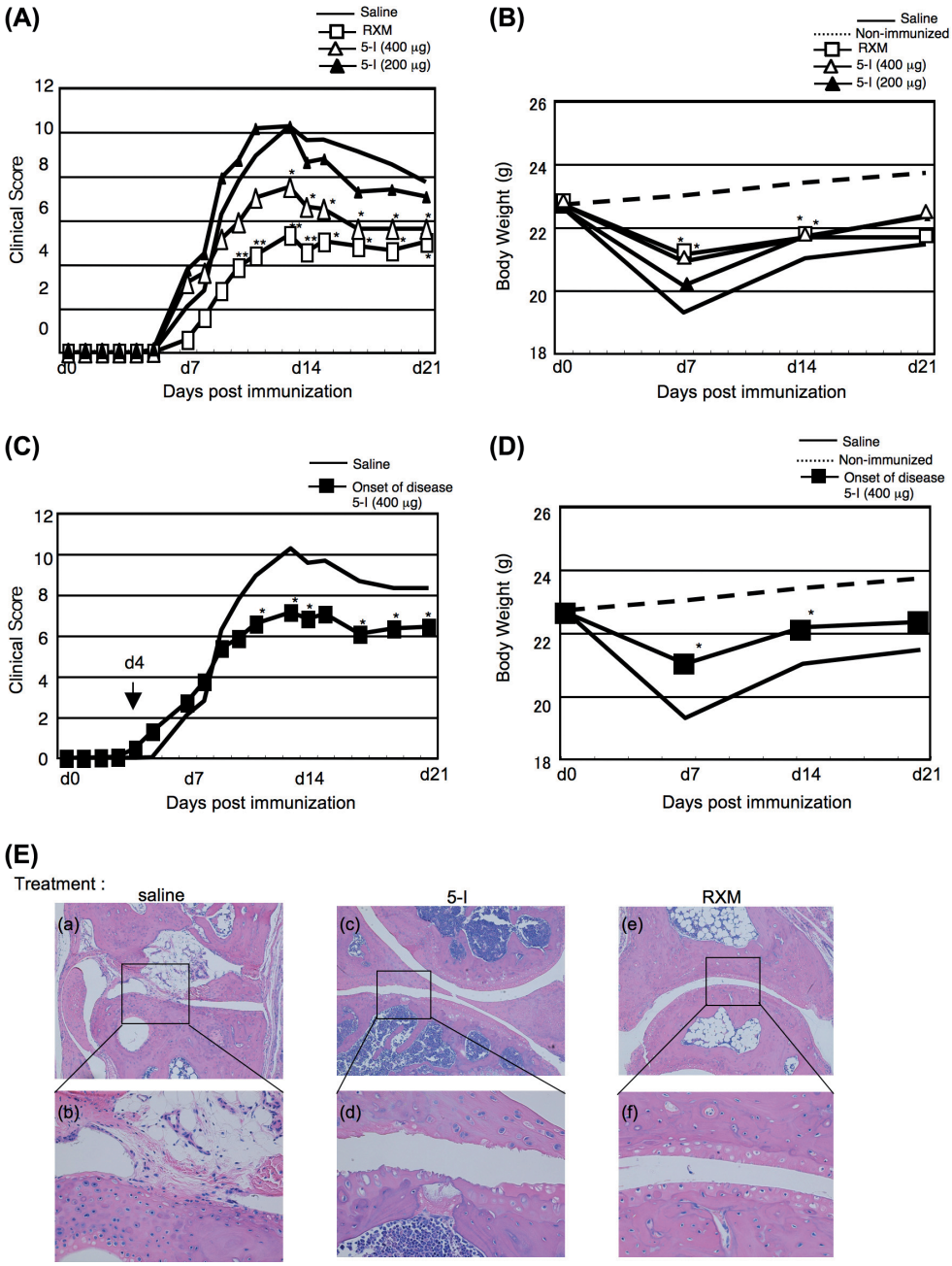

Figure 5. Effect of RXM and 5-I treatment on clinical score, body weight and histopathology of arthritis. Collagen-induced arthritis (CIA) was induced by primary (day − 21) and secondary (day 0) immunization with bovine type II collagen (CII) in complete Freund's adjuvant. (A) Four groups of mice were injected intraperitoneally with either control saline (−), 200 μg of 5-I (▲), 400 μg of 5-I (△), or RXM (□) every other day between day 0 and day 20. Changes of the clinical arthritis score are shown. (B) Body weight change of CIA-mice in A compared with non-immunized mice (–). (C) For studies involving delayed 5-I treatment, two groups of mice were injected intraperitoneally with control saline (−) or 400 μg of 5-I (■) every other day between day 4 and day 20. Changes of the clinical arthritis score are shown. (D) Body weight change of delayed treatment mice, compared with saline-treated mice (−) and non-immunized mice (–). Data were expressed as the mean of ten mice in each group. Data shown were representative of three independent experiments with similar results. Statistically significant difference compared to the control saline-treated group (*$p < 0.05$). (E) Administration of RXM, 5-I, and saline was started on the day of secondary immunization of CII (day 0), and continued on a schedule of every-other-day treatment up to day 20. The mice treated with saline as control solvent developed severe arthritis (*panels a* and *b*). In contrast, administration of 5-I or RXM significantly ameliorated destruction of cartilage and bone (*panels c* and *d*, or *e* and *f*, respectively).

delayed treatment with 5-I was also effective in reducing the clinical arthritis scores. Moreover, as shown in Figure 5D, the mean body weight of the treated group was restored significantly as compared to the saline-treated control group. These results indicated that 5-I therapy started either before or after the onset of disease could reduce the severity of arthritis, suggesting that 5-I-mediated immunomodulatory effects improved the inflammation associated with CIA.

We also performed histological studies of CIA mice. As shown in Figure 5E, mice treated with control saline developed arthritis with pannus formation (*panels a* and *b*). In contrast, RXM administration significantly inhibited destruction of cartilages and bones (*panels c* and *d* of Figure 5E). Although the superficial layers of cartilage were degraded slightly in the 5-I treated mice, bone destruction or pannus formation was not observed (*panels e* and *f* of Figure 5E). These findings suggest that 5-I, as well as RXM, exert immunomodulatory effects *in vivo*.

Finally, we examined serum levels of anti-CII antibody in CIA mice. As shown in Supplementary Figures 3 available online at http://informahealthcare.com/doi/abs/10.3109/14397595.2014.983262, an anti-CII antibody was detected after Day 7 of the second immunization of CII in each cohort, while titers for anti-CII antibody in CIA mice treated with RXAM or 5-I were similar to those of the control group. Taken together with the data of *in vitro* experiments, our observations indicate that 5-I, as well as

Table 1. Effect of 5-I treatment on CIA[a].

	Saline	RXM	5-I
Day of onset	5.3 ± 2.0	7.4 ± 2.0	6.0 ± 0.5
Clinical Score (day 14)	9.6 ± 2.7	4.6 ± 2.8[c]	6.6 ± 3.6[b]
Body weight (grams) (day 7)	19.3 ± 1.8	21.1 g ± 0.7[b]	21.0 g ± 1.3[b]
Arthritic paw (day 14)	90.9%	75.0%	77.5%

[a]CIA was induced as described in Figure 5 and treated with either 400 μg of RXM or 5-I, or control saline, for every other day from day 1 to day 21.

[b,c]Statistically different from the control saline-treated group([b]$p < 0.05$, [c]$p < 0.01$).

RXM, exert immunomodulatory effects resulted from inhibition of proinflammatory cytokines, and strongly suggested that 5-I may be useful as potential therapy for human RA.

Discussion

In this study, we evaluated the immunomodulatory effects of 5-I, a newly synthesized derivative of RXM. We showed that 5-I exhibited only weak antibacterial activity but clearly reduced production of Th1-, Th17-, and proinflammatory cytokines such as IL-6 and TNF-α by activated T cells and monocytes. In addition, 5-I inhibited transendothelial migration of activated T cells, while suppressing transcription of RORγt mRNA from CD3- and CD28-stimulated $CD4^+$ T cells. In addition, and most importantly, 5-I administration ameliorated the clinical manifestations of CIA, with its beneficial effect being similarly seen when given after the onset of CIA-related arthritis symptoms.

Naïve CD4 T cells may differentiate into one of several lineages of Th cells, including Th1, Th2, Th17, and inducible regulatory T cells (iTreg), as defined by their pattern of cytokine production and functions [18], and these T cell subsets play important roles in T cell-dependent immune regulations. The cellular interactions involved in subset differentiation are generally well-defined, with both Th1 and Th2 cells controlling the differentiation of Th17 cells and with Th17 cells inhibiting Th1 and Th2 development [19]. Since RXM and 5-I suppressed *in vitro* production of IL-17, we examined the expression of IL-17-A-related mRNAs using real-time RT-PCR assays. *RORC*, a transcription factor coding-gene for the orphan nuclear receptor, retinoic orphan receptor γ t (RORγt), is uniquely expressed in IL-17A-producing mouse T cells and is required for the *in vitro* and *in vivo* upregulation of this cytokine in T cells [20]. It has been reported recently that RORγt has a central function in the differentiation of human Th17 cells from naïve $CD4^+$ T cells [21]. Therefore, data demonstrating suppression of *RORC* expression by RXM or 5-I supported the *in vitro* results of RXM or 5-I-mediated inhibition of IL-17.

Several studies have identified the critical roles of TGF-β and IL-6 as proximal factors essential for the induction of Th17 development, and IL-23 has been shown to have a functional role subsequent to Th17 commitment, contingent upon the upregulation of the inducible component of the IL-23 receptor [22]. Based on these reports, it is conceivable that RXM or 5-I may modulate the expression of cytokine receptors or transcription factors required for naive $CD4^+$ T cells to differentiate into Th1, Th2, or Th17 subset. We assessed the expression of *IL12RB* and *TBX21* for Th1, *IL13RA* and *GATA3* for Th2, and *IL23R* and *TGFBR2* for Th17. However, no detectable modulation in the expression of mRNAs encoding for these molecules, including *IL23R*, was observed following treatment by RXM or 5-I (data not shown). A potential explanation for this observation may be the fact that the optimal time point following RXM or 5-I treatment to detect changes in specific gene expression has yet to be determined. We also performed gene profiling microarray analysis of purified $CD4^+$ T cells following *in vitro* treatment of RXM or 5-I (data not shown). Although the expression levels of mRNAs encoding numerous genes were altered by the addition of the macrolides, only *TNFAIP6* and *WISP1* mRNAs were consistently down-regulated among all the different donors, as detected by real-time RT-PCR assays. Since TNFAIP6 (also known as TSG-6) and WISP1 (also known as CCN4) have been reported to be involved in inflammatory disorders including RA [23–27], it is conceivable that down–regulation of their expression levels by RXM or 5-I may be potentially beneficial in reducing the joint inflammation seen in conditions such as RA. Other investigators have reported that macrolides inhibit TNF or WNT signaling pathways in inflammation process [25, 28–30]. It is conceivable that 5-I, a derivative of RXM, may have the inhibitory effects on these pathways. Moreover, it will be elucidated in a future study whether 5-I more effectively suppressed *RORC*, *TNFAIP6*, and *WISP1* than RXM.

In both CIA and RA, the inflamed synovium is characterized by elevated level of IL-6, TNF-α, and IL-17 [31–33]. A complex interaction among T cells, monocytes, and fibroblasts in the synovium leads to the development of arthritis. Specifically, activated T cells stimulate monocytes and synoviocytes through direct cell-cell contact and release of cytokines such as IFN-γ and IL-17. These cells in turn may amplify the inflammatory cascade through the release of additional cytokines, such as IL-1 and TNF-α, which then stimulate mesenchymal cells to release IL-6 and other factors [31–33]. Local inflammation is triggering and exacerbating cartilage destruction in the joint, and then promotes bone erosion. At the initial step of the perpetuation of this inflammatory process, the *in vivo* effectiveness of 5-I in preventing CIA development likewise RXM, might be intimately linked to the ability of 5-I to inhibit T cell transendothelial migration and cytokine production by T cells and monocytes *in vitro*.

Various costimulatory pathways, which regulate the production of IL-17, TNF-α, or IL-6, have been implicated in the pathogenesis of RA based on studies of human tissues and animal models [34–37]. Advances in understanding disease pathogenesis have led to the identification of molecular targets for immuno-therapeutic intervention. Therapies inhibiting TNF-α activity in patients with active RA result in rapid and sustained improvement in symptoms and signs of disease [38]. It is also conceivable that patients who fail to respond to therapy with specific TNF-α inhibitors could have IL-17-driven disease. Concurrent or sequential inhibition of TNF-α and IL-17 could enable two different cell types with roles in disease pathogenesis to be simultaneously targeted, such as T cells and macrophages.

Other investigators reported that the regulatory mechanism of arthritis involved dysfunction of CII-reactive Th17 cell differentiation by overexpression of T-bet [39]. While titers for anti-CII antibody in CIA mice treated with RXAM or 5-I were similar to those of the control group, we could not exclude the possibility that 5-I or RXM exerts an effect on autoreactive lymphocytes, and this possibility will be investigated in a future study involving human cells as well as CIA mice.

Pharmacokinetics data on RXM provided by a pharmaceutical company indicated that the mean peak plasma concentration was 6.6 μg/ml and the AUC was 96 μg.h/ml following the administration of a single oral dose of RXM 150 mg to healthy young adults [40]. At steady state following doses of 150 mg twice daily, the mean peak plasma concentration was 9.3 μg/ml and the AUC was 71 μg.h/ml [40]. This information would suggest that the doses of RXM used in this study correspond to the potential physiological ranges. Although pharmacokinetics data on 5-I are not yet available, it is estimated that dosages for 5-I are comparable to those for RXM, based on similar molecular profiles. Therefore, it is conceivable that the concentration ranges of RXM or 5-I used in this study are appropriate physiologically.

In conclusion, 5-I is a potent immunomodulatory macrolide that ameliorates CIA through anti-inflammatory actions and suppression of Th1, Th17, and proinflammatory cytokines such as TNF-α and IL-6. Since 5-I therapy is also effective as delayed treatment following the clinical onset of disease, our results strongly suggest that it may have a role in the clinical setting as an effective therapeutic agent. Since RXM has been used successfully for bronchial asthma, inflammatory bowel disease, and RA, 5-I may also be useful for treating diseases with Th17 having a significant role in disease pathophysiology, such as multiple sclerosis [41], psoriasis [42], and Crohn's disease [43].

Acknowledgement

This study was supported in part by a grant of the Ministry of Education, Science, Sports and Culture, Japan (K.O. and C.M.), a grant of the Ministry of Health, Labour, and Welfare, Japan (C.M.) and a Grant-in-Aid (E2628 and S1311011) from the Foundation of Strategic Research Projects in Private Universities from the Ministry of Education, Culture, Sports, Science, and Technology, Japan (K.O. and C.M.).

Authorship contributions

Contributions: N.O., S.I. and R.H. performed the experiments, interpreted the data, O.H. assisted with the paper, K.O. and C.M. designed the research, interpreted the data and wrote the paper, N.H.D. interpreted the data, assisted with the paper, and proofread the manuscript, and T.Y. performed the experiments, analyzed pathological results, interpreted the data and assisted with the paper.

Conflict of interest

None.

References

1. Kudoh S, Keicho N. Diffuse panbronchiolitis. Semin Respir Criti Care Med. 2003;24(5):607–18.
2. Gotfried MH. Macrolides for the treatment of chronic sinusitis, asthma, and COPD. Chest. 2004;125(2 Suppl):52S–60S.
3. Park CS, Park YS, Park YJ, Cho JH, Kang JM, Kim SY. The inhibitory effects of macrolide antibiotics on bone remodeling in chronic rhinosinusitis. Otolaryngology–head and neck surgery. 2007;137(2):274–9.
4. Inoue S, Nakase H, Matsuura M, Ueno S, Uza N, Kitamura H, et al. Open label trial of clarithromycin therapy in Japanese patients with Crohn's disease. J Gastroenterol Hepatol. 2007;22(7):984–8.
5. Polat M, Lenk N, Yalcin B, Gur G, Tamer E, Artuz F, Alli N. Efficacy of erythromycin for psoriasis vulgaris. Clin Exp Dermatol. 2007;32(3):295–7.
6. Fraschini F, Scaglione F, Ferrara F, Marelli O, Braga PC, Teodori F. Evaluation of the immunostimulating activity of erythromycin in man. Chemotherapy. 1986;32(3):286–90.
7. Anderson R. Erythromycin and roxithromycin potentiate human neutrophil locomotion *in vitro* by inhibition of leukoattractant-activated superoxide generation and autooxidation. J Infect Dis. 1989;159(5):966–73.
8. Chantot JF, Bryskier A, Gasc JC. Antibacterial activity of roxithromycin: a laboratory evaluation. J Antibiot (Tokyo). 1986;39(5):660–8.
9. Young RA, Gonzalez JP, Sorkin EM. Roxithromycin. A review of its antibacterial activity, pharmacokinetic properties and clinical efficacy. Drugs. 1989;37(1):8–41.
10. Noma T, Hayashi M, Yoshizawa I, Aoki K, Shikishima Y, Kawano Y. A comparative investigation of the restorative effects of roxithromycin on neutrophil activities. Int J Immunopharmacol. 1998;20(11): 615–24.
11. Wakita H, Tokura Y, Furukawa F, Takigawa M. The macrolide antibiotic, roxithromycin suppresses IFN-γ-mediated immunological functions of cultured normal human keratinocytes. Biol Pharm Bull. 1996;19(2):224–7.
12. Konno S, Adachi M, Asano K, Okamoto K, Takahashi T. Inhibition of human T-lymphocyte activation by macrolide antibiotic, roxithromycin. Life Sci. 1992;51(24):PL231–6.
13. Yoshimura T, Kurita C, Yamazaki F, Shindo J, Morishima I, Machida K, et al. Effects of roxithromycin on proliferation of peripheral blood mononuclear cells and production of lipopolysaccharide-induced cytokines. Biol Pharm Bull. 1995;18(6):876–81.
14. Urasaki Y, Nori M, Iwata S, Sasaki T, Hosono O, Kawasaki H, et al. Roxithromycin specifically inhibits development of collagen induced arthritis and production of proinflammatory cytokines by human T cells and macrophages. J Rheumatol 2005;32:1765–74.
15. Iwata S, Yamaguchi N, Munakata Y, Ikushima H, Lee JF, Hosono O, et al. CD26/dipeptidyl peptidase IV differentially regulates the chemotaxis of T cells and monocytes toward RANTES: possible mechanism for the switch from innate to acquired immune response. Int Immunol 1999;11:417–26.
16. Rosloniec EF, Cremer M, Kang A, Myers LK. Collagen-induced arthritis. In: Coligan JE, Kruisbeek AM, Margulies AH, Shevach EM, Strober W, eds. Current Protocols in Immunology.
17. Endo Y, Hirahara K, Yagi R, Tumes DJ, Nakayama T. Pathogenic memory type Th2 cells in allergic inflammation. Trends Immunol. 2014;35(2):69–78.
18. Christie D, Zhu J. Transcriptional Regulatory Networks for CD4 T Cell Differentiation. Curr Top Microbiol Immunol. 2014;381:125–72.
19. Korn T, Bettelli E, Oukka M, Kuchroo VK. IL-17 and Th17 Cells. Annu Rev Immunol. 2009;27:485–517.
20. Ivanov, II, McKenzie BS, Zhou L, Tadokoro CE, Lepelley A, Lafaille JJ, et al. The orphan nuclear receptor RORγt directs the differentiation program of proinflammatory IL-17$^+$ T helper cells. Cell. 2006;126(6):1121–33.
21. Manel N, Unutmaz D, Littman DR. The differentiation of human T_H-17 cells requires transforming growth factor-β and induction of the nuclear receptor RORγt. Nat Immunol. 2008;9(6):641–9.
22. Bettelli E, Oukka M, Kuchroo VK. T_H-17 cells in the circle of immunity and autoimmunity. Nat Immunol. 2007;8(4):345–50.
23. Glant TT, Kamath RV, Bardos T, Gal I, Szanto S, Murad YM, et al. Cartilage-specific constitutive expression of TSG-6 protein (product of tumor necrosis factor alpha-stimulated gene 6) provides a chondroprotective, but not antiinflammatory, effect in antigen-induced arthritis. Arthritis Rheum. 2002;46(8):2207–18.
24. Bayliss MT, Howat SL, Dudhia J, Murphy JM, Barry FP, Edwards JC, Day AJ. Up-regulation and differential expression of the hyaluronan-binding protein TSG-6 in cartilage and synovium in rheumatoid arthritis and osteoarthritis. Osteoarthritis Cartilage. 2001;9(1):42–8.
25. Milner CM, Day AJ. TSG-6: a multifunctional protein associated with inflammation. J Cell Sci. 2003;116(Pt 10):1863–73.
26. Venkatachalam K, Venkatesan B, Valente AJ, Melby PC, Nandish S, Reusch JE, et al. WISP1, a pro-mitogenic, pro-survival factor, mediates tumor necrosis factor-alpha (TNF-α)-stimulated cardiac fibroblast proliferation but inhibits TNF-α-induced cardiomyocyte death. J Biol Chem. 2009;284(21):14414–27.
27. Mori H, Nishida K, Ozaki T, Inoue H, Setsu K, Tsujigiwa H, et al. Expression of WISP-1 (ccn4), WISP-2 (ccn5) and WISP-3 (ccn6) in rheumatoid arthritis synovium evaluated by DNA microarrays. J Hard Tissue Biol. 2006;15(3):89–95.
28. Takahashi H, Hashimoto Y, Ishida-Yamamoto A, Iizuka H. Roxithromycin suppresses involucrin expression by modulation of activator protein-1 and nuclear factor-κB activities of keratinocytes. J Dermatol Sci. 2005;39(3):175–82.
29. Asano K, Tryka E, Cho JS, Keicho N. Macrolide therapy in chronic inflammatory diseases. Mediators Inflamm. 2012;2012:692352.
30. Du Q, Geller DA. Cross-Regulation Between Wnt and NF-κB Signaling Pathways. For Immunopathol Dis Therap 2010;1(3):155–81.
31. Aarvak T, Chabaud M, Miossec P, Natvig JB. IL-17 is produced by some proinflammatory Th1/Th0 cells but not by Th2 cells. J Immunol. 1999;162(3):1246–51.
32. Chabaud M, Durand JM, Buchs N, Fossiez F, Page G, Frappart L, Miossec P. Human interleukin-17: A T cell-derived proinflammatory cytokine produced by the rheumatoid synovium. Arthritis Rheum. 1999;42(5):963–70.
33. Marinova-Mutafchieva L, Williams RO, Mason LJ, Mauri C, Feldmann M, Maini RN. Dynamics of proinflammatory cytokine expression in the joints of mice with collagen-induced arthritis (CIA). Clin Exp Immunol. 1997;107(3):507–12.
34. Durie FH, Fava RA, Foy TM, Aruffo A, Ledbetter JA, Noelle RJ. Prevention of collagen-induced arthritis with an antibody to gp39, the ligand for CD40. Science. 1993;261(5126):1328–30.
35. Iwai H, Kozono Y, Hirose S, Akiba H, Yagita H, Okumura K, et al. Amelioration of collagen-induced arthritis by blockade of inducible costimulator-B7 homologous protein costimulation. J Immunol. 2002;169(8):4332–9.
36. Webb LM, Walmsley MJ, Feldmann M. Prevention and amelioration of collagen-induced arthritis by blockade of the CD28 co-stimulatory pathway: requirement for both B7–1 and B7–2. Eur J Immunol. 1996;26(10):2320–8.
37. Yoshioka T, Nakajima A, Akiba H, Ishiwata T, Asano G, Yoshino S, et al. Contribution of OX40/OX40 ligand interaction to the pathogenesis of rheumatoid arthritis. Eur J Immunol. 2000;30(10):2815–23.
38. Lipsky PE, van der Heijde DM, St Clair EW, Furst DE, Breedveld FC, Kalden JR, et al. Infliximab and methotrexate in the treatment of rheumatoid arthritis. Anti-Tumor Necrosis Factor Trial in Rheumatoid Arthritis with Concomitant Therapy Study Group. New Engl J Med. 2000;343(22):1594–602.

39. Kondo Y, Iizuka M, Wakamatsu E, Yao Z, Tahara M, Tsuboi H, et al. Overexpression of T-bet gene regulates murine autoimmune arthritis. Arthritis Rheum. 2012;64(1):162–72.
40. Product Information, RULIDE® & RULIDE® D. http://www.sanofi.com.au/products/aus_pi_rulide.pdf; 2012.
41. Kebir H, Kreymborg K, Ifergan I, Dodelet-Devillers A, Cayrol R, Bernard M, et al. Human T_H17 lymphocytes promote blood-brain barrier disruption and central nervous system inflammation. Nat Med. 2007;13(10):1173–5.
42. Zaba LC, Cardinale I, Gilleaudeau P, Sullivan-Whalen M, Suarez-Farinas M, Fuentes-Duculan J, et al. Amelioration of epidermal hyperplasia by TNF inhibition is associated with reduced Th17 responses. J Exp Med. 2007;204(13):3183–94.
43. Yen D, Cheung J, Scheerens H, Poulet F, McClanahan T, McKenzie B, et al. IL-23 is essential for T cell-mediated colitis and promotes inflammation via IL-17 and IL-6. J Clin Invest. 2006;116(5):1310–6.

Supplementary material available online

Supplementary Table 1 and Figures 1 – 3.

Journal of Clinical Laboratory Analysis 29: 106–111 (2015)

Comparison of Two Commercial ELISAs against an In-House ELISA for Measuring Soluble CD26 in Human Serum

Kei Ohnuma,[1]* Tatsuhiko Saito,[2] Ryou Hatano,[1] Osamu Hosono,[3] Satoshi Iwata,[1] Nam H. Dang,[4] Hiroki Ninomiya,[5] and Chikao Morimoto[1]

[1]Department of Therapy Development and Innovation for Immune Disorders and Cancers, Graduate School of Medicine, Juntendo University, Hongo, Bunkyo-ku, Tokyo, Japan

[2]Department of Diabetes and Metabolism Internal Medicine, Kobari General Hospital, Yokouchi, Noda City, Chiba, Japan

[3]Department of Rheumatology and Allergy, Research Hospital, Institute of Medical Science, University of Tokyo, Shrokanedai, Minato-ku, Tokyo, Japan

[4]Division of Hematology/Oncology, University of Florida, Gainesville, Florida,

[5]Kobari General Hospital, Yokouchi, Noda City, Chiba, Japan

Background: CD26 is a T-cell costimulatory molecule with dipeptidyl peptidase IV (DPPIV) activity in its extracellular region. The relevance of sCD26 levels and disease activity has been reported in rheumatic or infectious disease. For certain metabolic and endocrine conditions, DPPIV inhibitors were recently developed as a new class of antidiabetic drugs that act by inhibiting DPPIV, the enzyme that inactivates incretin hormone. Higher levels of sCD26 in diabetic patients have been shown to be associated with a poor clinical response to DPPIV inhibitors, with sCD26/DPPIV being an adipokine that may impair insulin sensitivity. With the increasing use of serum sCD26 and DPPIV enzyme activity as biomarkers with potential clinical implications, accurate measurements of serum sCD26 levels and DPPIV enzyme activity are needed. *Methods:* We compare two commercially widely available and an in-house enzyme-linked immunosorbent assays (ELISAs) for measurement of serum sCD26 in healthy or diabetic human sera. *Results:* The significant discrepancies among the results obtained from commercially available and the in-house sCD26 assays were found. We also observed that a linear correlation between serum sCD26 level and DPPIV enzyme activity exists with the in-house ELISA, while the commercial ELISAs demonstrate a lack of consistency between serum sCD26 level and DPPIV enzyme activity. *Conclusion:* These data strongly suggest that new commercial assays for sCD26 plasma levels need detailed evaluation and validation with samples from clinically well-characterized patients, and results obtained from these newer assays should be compared to those obtained from well-established in-house assays such as our assay or other validated sCD26 ELISA assays. J. Clin. Lab. Anal. 29:106–111, 2015. © 2014 Wiley Periodicals, Inc.

Key words: CD26; dipeptidyl peptidase IV; T cell costimulation

INTRODUCTION

CD26 is a 110 kDa surface glycoprotein with dipeptidyl peptidase IV (DPPIV, EC 3.4.14.5) activity, being a serine protease that cleaves dipeptides from the N-terminus of peptides at the penultimate position (1). CD26 is also associated with T-cell signal transduction processes as a costimulatory molecule, as well as being a marker of T-cell activation (2). We have previously reported that effector CD26-mediated costimulatory activity is exerted via its DPPIV enzyme activity (2, 3). More recently, we have shown that serum-soluble CD26 (sCD26) and DPPIV enzyme activity are inversely correlated with disease activity of patients with systemic lupus erythematosus (4).

Grant sponsor: The Ministry of Education, Science, Sports and Culture, Ministry of Health, Labour, and Welfare, Japan.

*Correspondence to: Kei Ohnuma, Department of Therapy Development and Innovation for Immune Disorders and Cancers, Graduate School of Medicine, Juntendo University, 2-1-1, Hongo, Bunkyo-ku, Tokyo 113-8421, Japan. E-mail: kohnuma@juntendo.ac.jp

Received 7 May 2013; Accepted 12 December 2013
DOI 10.1002/jcla.21736
Published online in Wiley Online Library (wileyonlinelibrary.com).

© 2014 Wiley Periodicals, Inc.

Other investigators have reported that serum sCD26 level was lower in rheumatoid arthritis (RA) patients than in healthy control or in patients with osteoarthritis (OA) (5, 6). sCD26 lacks transmembrane and cytolasmic domains (the sequence starting at the 39th amino acid position of the full-length of CD26) (7), although its molecular weight is similar to that of the full-length transmembrane CD26 since it exists as a homodimer in serum/plasma and is heavily glycosylated between the 48 and 324th amino acid positions (8). Meanwhile, DPPIV enzyme activity has been widely studied in metabolic and endocrine disorders, and DPPIV inhibitors have been developed as a new class of antidiabetic drugs that act by inhibiting DPPIV, the enzyme that inactivates incretin hormone (9). For instance, higher serum level of sCD26 was reported to be associated with a worse response to sitagliptin in patients with type 2 diabetes (T2DM) controlled inadequately by metformin and/or sulfonylurea therapy (10). Moreover, other investigators have reported that sCD26/DPPIV is one of the adipokines that may impair insulin sensitivity (11). The potentially important role played by CD26/DPPIV in the clinical setting has led to rising interest in the quantification of serum sCD26 level and DPPIV enzyme activity over the past decade. This is also reflected in the number of publications on this topic and in the recent worldwide availability of commercial CD26 enzyme-linked immunosorbent assays (ELISAs), which can help researchers working in this area avoid the time-consuming process of in-house assay development and maintenance. However, it is our belief that these new commercial assays should be proven to deliver accurate, reliable, and reproducible data prior to usage for analysis of valuable patient-derived samples, even if the assay is certified by the manufacturer. In addition, DPPIV enzymatic activity has been correlated with sCD26 concentration (12), with the enzymatic activity of DPPIV being determined with the use of either chromogenic or fluorogenic substrates. Meanwhile, commercially available DPPIV activity assay kits have been shown to provide comparable results (13). On the other hand, comparative studies of different assay kits for sCD26 quantification have not yet been rigorously performed using human samples. The aim of this study is therefore to compare two commercially worldwide available sCD26 ELISA assays and our own in-house ELISA for detecting both sCD26 level and specific DPPIV enzyme activity.

MATERIALS AND METHODS

Serum Collections and Storage

Peripheral blood samples were collected from healthy adult volunteers and T2DM patients (regularly seen and treated at the Kobari General Hospital), using BD Vacutainer blood collection tube SSTII (BD, Franklin Lakes, NJ). Serum was obtained from 5 ml whole blood by centrifugation at 1,500 × *g* at 4°C for 10 min, and stored at −80°C in 500 μl aliquots. Human study protocols were approved by the Ethics Committees at the Kobari General Hospital (Authorization Number 10) and Juntendo University (Authorization Number 2012192). Informed consent was obtained from all patients. Patients' gender and age were matched between normal and T2DM groups. All studies on human subjects were conducted according to the principles set out in the Declaration of Helsinki.

ELISA Procedure

Serum samples were removed from the −80°C freezer and quickly thawed in a water bath at 37°C. All samples were centrifuged 3,000 × *g* for 5 min to discard debris, and were then assayed in duplicate. Two commercial ELISA kits (Human sCD26 Platinum ELISA Kit, or Human DPPIV/CD26 Quantikine ELISA Kit) were purchased from eBioscience (Vienna, Austria), or R&D Systems, Inc. (Minneapolis, MN), respectively. Measurement of sCD26 level was performed according to the manufacturers' instructions. An in-house sandwich ELISA for sCD26 was established in our laboratory (14). Briefly, Maxisorp ELISAimmunoplates (Nunc, Roskilde, Denmark) were coated with 100 μl of 10 μg/ml anti-CD26 monoclonal antibody (mAb) (clone: 5F8, mouse IgG_1) in 0.05 M carbonate/bicarbonate buffer, pH 9.6, by incubating overnight at 4°C. Remaining binding sites were blocked with 200 μl of 25% StartingBlock Blocking Buffer (Thermo Scientific, South Logan, UT) for 2 h at room temperature. Plates were then incubated with 100 μl of serum appropriately diluted with 0.01 M phosphate buffered saline (PBS) containing 0.05% Tween 20 at 4°C overnight. Bound sCD26 molecules were detected by incubating with 100 μl of biotin conjugated anti-CD26 mAb (clone: 9C11, mouse IgG_1) followed by ExtrAvidin-alkaline phosphatase (Sigma-Aldrich, St. Louis, MO). The plates were developed with 1 mg/ml *p*-nitrophenyl phosphate in 10 mM diethanolamine buffer, pH 9.6, containing 0.5 mM $MgCl_2$. Color development was monitored at 405 nm on an iMark Microplate Reader (Bio-Rad Laboratories, Hercules, CA). Absorbance data were analyzed using Microplate Manager 6 Software (Bio-Rad Laboratories). In parallel with sCD26 protein concentration, DPPIV enzyme activity of bound sCD26 to 5F8 was detected by incubation with glycylproline *p*-nitroanilide (Gly-Pro-p-NA, 1 mg/ml in PBS; Sigma-Aldrich). Color development was measured at 405 nm. These results were standardized by a standard curve for *p*-nitroaniline (Sigma-Aldrich). Recombinant CD26/DPPIV (R&D Systems, Inc.) for a standard curve was used as the identical reagent in all three assays. 5F8

TABLE 1. Details of ELISA Assays as Specified by ELISA Manufactures and In-House Protocols

	R&D Quantikine	eBioscience	In-house
Kit format	12 by 8-well strips (flat-bottom)	12 by 8-well strips (flat-bottom)	96-well plate (flat-bottom)
Capture antibody	Rat mAb (no further information)	mAb (no further information)	Mouse mAb (5F8), house-made
Sample dilution and preparation	100-fold dilution	Five-fold dilution	20-fold dilution
Volume/ELISA-well	150 μl	100 μl	100 μl
Dilution buffer	Buffered protein base with blue dye and preservative	No information	0.05% Tween 20-PBS
Sample incubation temperature	Room temperature	Room temperature	4°C
Sample incubation period	2 h	3 h	Overnight
Wash buffer	Buffered surfactant with preservative	1% Tween 20-PBS	0.05% Tween 20-PBS
Detection antibody	HRP conjugated pAb	Biotinylated mAb	Biotinylated mouse mAb (9C11)
Conjugate/substrate	Direct conjugation to detection pAb/TMB	Streptavidin-HRP/TMB	ExtrAvidin-ALP/PNPP
Optical density values (nm)	450	450	405
Standard[a]	Recombinant human DPPIV	Recombinant human DPPIV	Recombinant human DPPIV
Dynamic range (of Standard curve)	0.00031–0.020 (μg/ml)	0.0156–0.5 (μg/ml)	0.005–3.0 (μg/ml)
Data reduction	Log concentration of serial diluted standard against OD values	Log concentration of serial diluted standard against OD values	Log concentration of serial diluted standard against OD values
Precision (intra/interassay)	4–7.3%/8.2–9.1% (precision supplied by manufacturer)	0.8–13.7%/3.3–14.7% (precision supplied by manufacturer)	0.8–14.3%/4.1–15.9%

ALP, alkaline phosphatase; HRP, horseradish peroxidase; PBS, phosphate buffered saline; PNPP, *p*-nitrophenyl phosphate; TMB, tetramethylbenzidine.

[a]Recombinant human DPPIV is composed of the 34–766th amino acids of human CD26/DPPIV, with a C-terminal 6xHis tag, produced with the use of mouse myeloma cells NS0. This human DPPIV is highly glycosylated and shows 115 kDa in reducing sodium dodecyl sulfate-polyacrylamide gel electrophoresis, and presents as a homodimer in nonreducing condition.

was produced by immunizing BALB/cJ mice with a phytohemagglutinin-stimulated T cell line derived from the New World primate species *Aotus trivirgatus* (15). 9C11 was produced by immunizing mice with murine pre-B 300–19 cell line of human CD26 transfectant (16). Selected details for the three sCD26 assays including assay precisions are summarized in Table 1.

Intra-assay and Interassay Variations

To analyze for intra-assay variation, three replicates of three different samples were run in one assay. To analyze for interassay variation, three different samples were run in three independent assays. The intra-assay or interassay variations were calculated using the following formula:

$$(\text{SD of assay results})/(\text{mean of assay results}) \times 100(\%).$$

Statistical Analysis

The values measured are shown as mean ± standard deviation (SD). The differences between groups were analyzed by one-way repeated measures ANOVA. 95% CIs were calculated and P values ≤ 0.05 were considered statistically significant. Correlation was calculated as Pearson product-moment correlation coefficient. Statistical analysis was performed using Microsoft Excel 2011 (Microsoft Corp., Redmond, WA) or GraphPad PRISM version 6 (GraphPad Software Inc., La Jolla, CA).

RESULTS AND DISCUSSION

As shown in Figure 1A, serum sCD26 concentrations of healthy adults ($n = 12$) measured by the two commercial kits and the in-house assay differed in all samples by approximately fourfold (0.34 ± 0.14 μg/ml or 0.36 ± 0.15 μg/ml vs. 1.20 ± 0.31 μg/ml). The values measured by our in-house assay were significantly higher than those by the R&D Quantikine assay ($P < 0.0001$ [95% CI, 0.65–1.03]), or eBioscience Platinum assay ($P < 0.0001$ [95% CI, 0.63–1.02]) (Fig. 1A). It has been reported that DPPIV enzymatic activity has been correlated with the concentration of sCD26 using the normal human sera (12). We therefore evaluated for potential correlation between DPPIV enzymatic activity and sCD26 level in the serum samples described above. For this purpose, we performed our in-house capture assay method using anti-human CD26 mAb as a capture antibody for detecting DPPIV specific

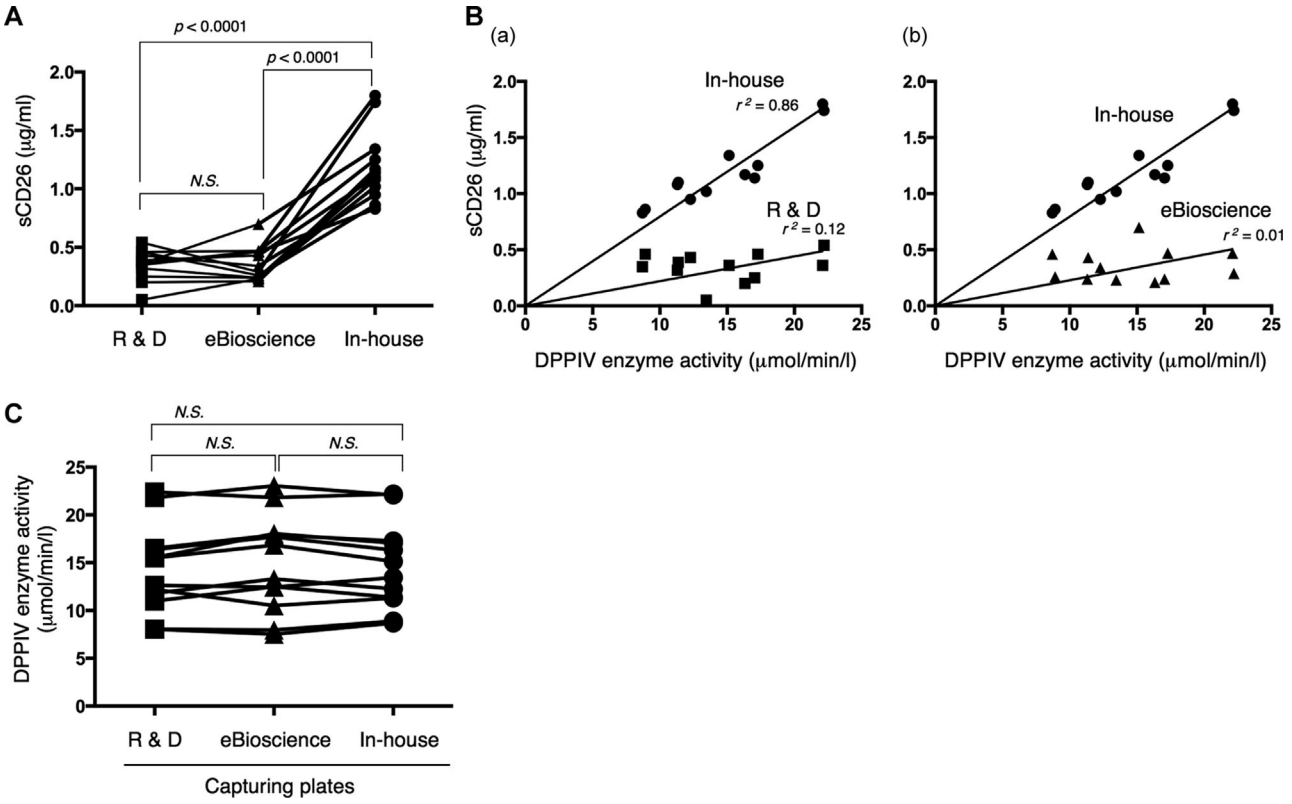

Fig. 1. Comparison of 12 normal serum samples, tested with three different ELISA assays for sCD26. (A) sCD26 levels in serum samples of 12 healthy adults were measured using the R&D Quantikine (solid squares), eBioscience Platinum (solid triangles), or in-house ELISA assays (solid circles). Each dot indicates individual value. Data of same samples are connected with horizontal lines. (B) Correlation between levels of sCD26 and DPPIV enzyme activity in serum samples of 12 healthy adults. (a) Comparison between in-house and the R&D Quantikine ELISA assays. (b) Comparison between in-house and the eBioscience Platinum ELISA assays. DPPIV enzyme activity was measured using our in-house capture method as described in Materials and Methods. (C) DPPIV enzyme activity in serum samples of 12 healthy adults was measured using the R&D Quantikine (solid squares), eBioscience Platinum (solid triangles), or in-house ELISA plates (solid circles). The samples were prepared and applied to each plate by the same method as the in-house method. DPPIV enzyme activity was measured using our in-house capture method as described in Materials and Methods. Data of same samples are connected with horizontal lines. *N.S.* denotes not significant.

to sCD26. It is conceivable that 5F8 is used for capturing sCD26 without affecting DPPIV enzyme activity in the plate since the epitope of human CD26 recognized by 5F8 is in the extracellular region of the truncated human CD26 containing the N-terminal residues 1–449th lacking DPPIV enzyme activity (16). Moreover, 5–10% of DPPIV activity in normal plasma/serum has been reported to be associated with other DPPIV-like peptidases such as DASH (DPPIV activity and/or structure homologues) proteins (17). Therefore, it is also possible to correlate the DPPIV activity with sCD26 level by capturing sCD26 molecules from the samples. As shown in Figure 1B, levels of sCD26 measured by our in-house assay clearly correlated with DPPIV enzyme activity ($r^2 = 0.86$; slope, 0.08 ± 0.002) (solid circles in panels a or b), while levels of sCD26 measured by the R&D Quantikine (solid squares in panel a) or eBioscience Platinum assays (solid triangles in panel b) did not correlate with DPPIV enzyme activity ($r^2 = 0.12$; slope, 0.02 ± 0.003, or $r^2 = 0.01$; slope, 0.02 ± 0.003, respectively). To exclude the possibility that the incubation period of samples may influence the results, assays for sCD26 using the R&D Quantikine or eBioscience Platinum kits were conducted in which the sample incubation period in the capture step was extended to overnight at 4°C, which was the same method as in our in-house sCD26 assay. However, the obtained values were not influenced by extending the incubation period in the capture step (data not shown). Moreover, it was important to determine whether the values for DPPIV enzyme activity measured by the in-house plate were equal to those obtained from the commercial plates. To address this point, we evaluated captured DPPIV enzyme activity on the plates coated with the capture antibody in the R&D Quantikine or eBioscience Platinum kits. As shown in Figure 1C, the values of the captured DPPIV enzyme activity were similar for each assay. These results suggest that the ability to capture sCD26 is similar among the two commercial and our in-house plates, and

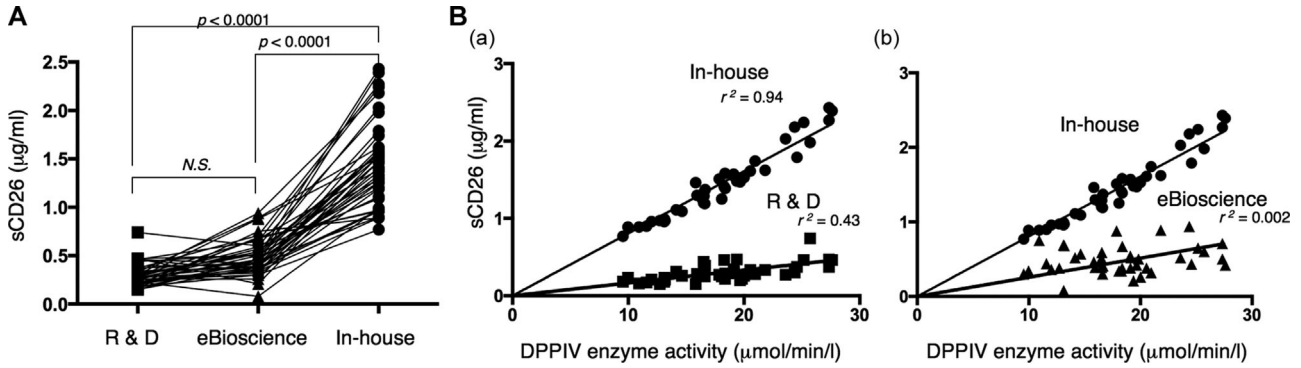

Fig. 2. Comparison of 50 serum samples of patients with T2DM, tested with three different ELISA assays for sCD26. (A) sCD26 levels in serum samples of 50 T2DM adults were measured using the R&D Quantikine (solid squares), eBioscience Platinum (solid triangles), or in-house ELISA assays (solid circles). Each dot indicates individual value. Data of same samples are connected with horizontal lines. *N.S.* denotes not significant. (B) Correlation between levels of sCD26 and DPPIV enzyme activity in serum samples of 50 T2DM patients. (a) Comparison between in-house and the R&D Quantikine ELISA assays. (b) Comparison between in-house and the eBioscience Platinum ELISA assays. DPPIV enzyme activity was measured using our in-house capture method as described in Materials and Methods.

that the observed variability among the assays may be due to differences in the sCD26 detection process.

We next determined serum levels of sCD26 in T2DM patients who were not being treated with DPPIV inhibitor therapy ($n = 50$). As shown in Figure 2A, serum sCD26 concentrations of T2DM patients measured by the two commercial and our in-house assays differed in all samples by approximately four- to fivefold (0.30 ± 0.12 μg/ml or 0.40 ± 0.10 μg/ml vs. 1.45 ± 0.34 μg/ml). The two commercial assays measured samples of T2DM patients in the range of 0.15–0.74 μg/ml or 0.19–0.74 μg/ml (Fig. 2A), values that were compatible with the previously reported range of serum sCD26 concentrations of T2DM patients, using commercial assays (10, 18). As observed in healthy samples (Fig. 1A), the values measured by our in-house assay were significantly higher than those by the R&D Quantikine assay ($P < 0.0001$ [95% CI, 1.04–1.27]) or eBioscience Platinum assay ($P < 0.0001$ [95% CI, 0.91–1.19]) (Fig. 2A). Moreover, levels of sCD26 measured by our in-house assay clearly correlated with DPPIV enzyme activity ($r^2 = 0.94$; slope, 0.08 ± 0.001) (solid circles in panels a or b of Fig. 2B), while levels of sCD26 measured by the R&D Quantikine (solid squares in panel a of Fig. 2B) or eBioscience Platinum (solid triangles in panel b of Fig. 2B) assays did not correlate with DPPIV enzyme activity ($r^2 = 0.43$; slope, 0.02 ± 0.001, or $r^2 = 0.002$; slope, 0.02 ± 0.001, respectively). These data indicated that serum sCD26 concentration in human samples may be underestimated by the commercially available sCD26 assay, and that poor linearity between DPPIV enzyme activity and sCD26 level may misinterpret the clinical relevance of this molecule.

A critical issue for ELISAs is that the standard curve is stably plotted among different assays. In the present assays, we used commercially available recombinant human DPPIV derived from the same lot as the standard compound for all three ELISAs (Table 1), and obtained almost identical standard curves among various assays (data not shown). Therefore, the differences seen in sCD26 levels between the two commercial and our in-house ELISAs were likely not to be due to differences in the quality of the standard. To exclude the possibility that the clones of the capture antibody may influence the results, the in-house DPPIV enzyme activity assay was conducted with 1F7 as a capture antibody, a different epitope from 5F8. However, the obtained values were not influenced by the different epitope capture antibody (data not shown), suggesting higher validity of the in-house DPPIV enzyme activity assay. Moreover, it is theoretically possible that single nucleotide polymorphisms (SNPs) may affect the reactivity of the sandwich antibody sets of the commercial kits. One nonsynonymous coding region SNP Arg492Lys (G-≥A, exon 18) was reported, although its frequency or functional significance has not yet been determined (19). Since information regarding the clones of the capture and detection antibodies or the concentrations of these antibodies used in the commercial assays is not publicly available, the exact reasons for the observed inconsistencies seen with the commercial assays evaluated in this article are not clear. The epitopes of the anti-human CD26 mAbs used in our in-house assay are distinct from each other (16), that is, 5F8 or 9C11 recognizes 359–449th or 740–766th amino acids of human CD26, respectively. Moreover, these epitopes are also distinct from that of the humanized anti-CD26 mAb, which was developed in our laboratory for clinical uses, such as in the potential treatment of malignant methothelioma, or graft-versus-host disease (20, 21). Therefore, our in-house sCD26 assay can

be used to detect sCD26 or DPPIV enzyme activity as biomarkers of patients who are subjected to humanized anti-CD26 mAb therapy.

CONCLUSIONS

Given emerging data indicating the importance of serum levels of sCD26 in certain clinical settings, there is an urgent need for precise measurement and correlation of values obtained from different assays. In light of the discrepancies noted with results obtained from commercially available sCD26 assays in the current study, it seems unlikely that the established associations between sCD26 plasma levels and diseases such as T2DM, RA, OA, chronic infection, or malignant diseases can be reliably reproduced by the commercial assays (1, 10, 17). On the other hand, in view of the linearity observed between sCD26 level and DPPIV enzyme activity, our in-house assay appears to be superior to the commercial assays as a means to evaluate sCD26/DPPIV as clinically relevant biomarkers. The current study strongly suggests that new commercial assays for sCD26 plasma levels need detailed evaluation and validation with samples from clinically well-characterized patients, and results obtained from these newer assays should be compared to those obtained from well-established in-house assays such as our assay or other validated sCD26 ELISA assays.

ACKNOWLEDGEMENTS

The authors thank Ms. Aya Miwa for excellent assistance with measurement of sCD26 and DPPIV enzyme activity.

CONFLICT OF INTEREST

The authors declare no competing financial interests associated with this article.

REFERENCES

1. Ohnuma K, Takahashi N, Yamochi T, Hosono O, Dang NH, Morimoto C. Role of CD26/dipeptidyl peptidase IV in human T cell activation and function. Front Biosci 2008;13:2299–2310.
2. Morimoto C, Schlossman SF. The structure and function of CD26 in the T-cell immune response. Immunol Rev 1998;161:55–70.
3. Tanaka T, Kameoka J, Yaron A, Schlossman SF, Morimoto C. The costimulatory activity of the CD26 antigen requires dipeptidyl peptidase IV enzymatic activity. Proc Natl Acad Sci USA 1993;90:4586–4590.
4. Kobayashi H, Hosono O, Mimori T, et al. Reduction of serum soluble CD26/dipeptidyl peptidase IV enzyme activity and its correlation with disease activity in systemic lupus erythematosus. J Rheumatol 2002;29:1858–1866.
5. Cuchacovich M, Gatica H, Pizzo SV, Gonzalez-Gronow M. Characterization of human serum dipeptidyl peptidase IV (CD26) and analysis of its autoantibodies in patients with rheumatoid arthritis and other autoimmune diseases. Clin Exp Rheumatol 2001;19:673–680.
6. Sedo A, Duke-Cohan J, Balaziova E, Sedova L. Dipeptidyl peptidase IV activity and/or structure homologs: Contributing factors in the pathogenesis of rheumatoid arthritis? Arthritis Res Ther 2005;7:253–269.
7. Iwaki-Egawa S, Watanabe Y, Kikuya Y, Fujimoto Y. Dipeptidyl peptidase IV from human serum: Purification, characterization, and N-terminal amino acid sequence. J Biochem 1998;124:428–433.
8. Durinx C, Lambeir AM, Bosmans E, et al. Molecular characterization of dipeptidyl peptidase activity in serum: Soluble CD26/dipeptidyl peptidase IV is responsible for the release of X-Pro dipeptides. Eur J Biochem 2000;267:5608–5613.
9. Drucker DJ, Nauck MA. The incretin system: Glucagon-like peptide-1 receptor agonists and dipeptidyl peptidase-4 inhibitors in type 2 diabetes. Lancet 2006;368:1696–1705.
10. Aso Y, Ozeki N, Terasawa T, et al. Serum level of soluble CD26/dipeptidyl peptidase-4 (DPP-4) predicts the response to sitagliptin, a DPP-4 inhibitor, in patients with type 2 diabetes controlled inadequately by metformin and/or sulfonylurea. Transl Res 2011;159:25–31.
11. Lamers D, Famulla S, Wronkowitz N, et al. Dipeptidyl peptidase 4 is a novel adipokine potentially linking obesity to the metabolic syndrome. Diabetes 2011;60:1917–1925.
12. Andrieu T, Thibault V, Malet I, et al. Similar increased serum dipeptidyl peptidase IV activity in chronic hepatitis C and other viral infections. J Clin Virol 2003;27:59–68.
13. Matheeussen V, Lambeir AM, Jungraithmayr W, et al. Method comparison of dipeptidyl peptidase IV activity assays and their application in biological samples containing reversible inhibitors. Clin Chim Acta 2012;413:456–462.
14. Hosono O, Homma T, Kobayashi H, et al. Decreased dipeptidyl peptidase IV enzyme activity of plasma soluble CD26 and its inverse correlation with HIV-1 RNA in HIV-1 infected individuals. Clin Immunol 1999;91:283–295.
15. Torimoto Y, Dang NH, Tanaka T, Prado C, Schlossman SF, Morimoto C. Biochemical characterization of CD26 (dipeptidyl peptidase IV): Functional comparison of distinct epitopes recognized by various anti-CD26 monoclonal antibodies. Mol Immunol 1992;29:183–192.
16. Dong RP, Tachibana K, Hegen M, et al. Correlation of the epitopes defined by anti-CD26 mAbs and CD26 function. Mol Immunol 1998;35:13–21.
17. Sedo A, Malik R. Dipeptidyl peptidase IV-like molecules: Homologous proteins or homologous activities? Biochim Biophys Acta 2001;1550:107–116.
18. Lee SA, Kim YR, Yang EJ, et al. CD26/DPP4 levels in peripheral blood and T cells in patients with type 2 diabetes mellitus. J Clin Endocrinol Metab 2013;98:2553–2561.
19. Ohnuma K, Morimoto C. DPP4 (dipeptidyl-peptidase 4). Atlas Genet Cytogenet Oncol Haematol 2012;17:301–312.
20. Inamoto T, Yamada T, Ohnuma K, et al. Humanized anti-CD26 monoclonal antibody as a treatment for malignant mesothelioma tumors. Clin Cancer Res 2007;13:4191–4200.
21. Hatano R, Ohnuma K, Yamamoto J, Dang NH, Yamada T, Morimoto C. Prevention of acute graft-versus-host disease by humanized anti-CD26 monoclonal antibody. Br J Haematol 2013;162:263–277.

CD26-Mediated Induction of EGR2 and IL-10 as Potential Regulatory Mechanism for CD26 Costimulatory Pathway

Ryo Hatano,*,† Kei Ohnuma,* Haruna Otsuka,* Eriko Komiya,* Izumi Taki,* Satoshi Iwata,* Nam H. Dang,‡ Ko Okumura,† and Chikao Morimoto*

CD26 is associated with T cell signal transduction processes as a costimulatory molecule, and CD26$^+$ T cells have been suggested to be involved in the pathophysiology of diverse autoimmune diseases. Although the cellular and molecular mechanisms involved in CD26-mediated T cell activation have been extensively evaluated by our group and others, potential negative feedback mechanisms to regulate CD26-mediated activation still remain to be elucidated. In the present study, we examine the expression of inhibitory molecules induced via CD26-mediated costimulation. We show that coengagement of CD3 and CD26 induces preferential production of IL-10 in human CD4$^+$ T cells, mediated through NFAT and Raf-MEK-ERK pathways. A high level of early growth response 2 (EGR2) is also induced following CD26 costimulation, possibly via NFAT and AP-1–mediated signaling, and knockdown of EGR2 leads to decreased IL-10 production. Furthermore, CD3/CD26-stimulated CD4$^+$ T cells clearly suppress proliferative activity and effector cytokine production of bystander T cells in an IL-10–dependent manner. Taken together, our data suggest that robust CD26 costimulatory signaling induces preferential expression of EGR2 and IL-10 as a potential mechanism for regulating CD26-mediated activation. ***The Journal of Immunology*****, 2015, 194: 960–972.**

CD26 is a 110-kDa type II membrane-bound glycoprotein with dipeptidyl peptidase IV (DPPIV) activity in its extracellular domain (1–3). CD26 is associated with T cell signal transduction processes as a costimulatory molecule, as well as being a marker of T cell activation (4, 5). Whereas CD26 expression is increased following activation of resting T cells, CD4$^+$ CD26^{high} T cells respond maximally to recall Ags such as tetanus toxoid (6). Moreover, crosslinking of CD26 and CD3 with solid-phase immobilized mAbs can induce T cell costimulation and IL-2 production by CD26$^+$ T cells. Furthermore, high CD26 cell surface expression in CD4$^+$ T cells is correlated with the production of Th1 and Th17-type cytokines and high migratory activity (4, 7). In fact, patients with autoimmune diseases, such as multiple sclerosis (MS), Grave's disease, and rheumatoid arthritis, have been found to have increased numbers of CD4$^+$CD26$^+$ T cells in inflamed tissues as well as in their peripheral blood, with enhancement of CD26 expression correlating with the autoimmune disease severity (8–10). We have recently found that cytotoxic activity of CD8$^+$ T cells is also regulated via CD26-mediated costimulation, and that CD26$^+$ T cells are deeply involved in the pathophysiology of acute graft-versus-host disease (11, 12). These findings imply that CD26$^+$ T cells play an important role in the inflammatory process and subsequent tissue damage in such diseases.

Activation of T cells through costimulatory signals is essential for an effective Ag-specific immune response, whereas the suppressive control of excessive immune responses is also critical for maintaining self tolerance and preventing autoimmunity. CD28 is a representative T cell costimulatory molecule, required for optimal production of cytokines and proliferation, and CD28-deficient mice have markedly reduced responses to exogenous Ags (13, 14). Alternatively, CTLA-4 functions as a potent negative regulator of the T cell response, and CTLA-4–deficient mice develop massive lymphadenopathy, autoimmunity, and early death (15, 16). Both CD28 and CTLA-4 are members of the Ig supergene family and are able to bind CD80 and CD86 expressed on APCs. CTLA-4 is not expressed on naive T cells, but it is induced after activation. CTLA-4 interacts with CD80 and CD86 with a 50- to 100-fold higher binding avidity than CD28, leading to interference of CD28 signaling (17). In addition to the ligand competition, the cytoplasmic domain of CTLA-4 associates with phosphatases SHP2 and PP2A to negatively regulate T cell activation, and it also inhibits the formation of lipid rafts (18). We have identified caveolin-1 on APCs as a functional ligand for CD26, and the ligation of CD26 with caveolin-1 recruits a complex consisting of CD26, CARMA1, Bcl10, MALT1, and IκB kinase to lipid rafts, leading to NF-κB activation (19, 20). CD26 possesses DPPIV enzyme activity, able to cleave dipeptides from polypeptides with N-terminal penultimate proline or alanine. Molecules displaying DPPIV-like enzymatic activity and/or structural similarity to the DPPIV/CD26 have been grouped to a family of "dipeptidyl pep-

*Department of Therapy Development and Innovation for Immune Disorders and Cancers, Graduate School of Medicine, Juntendo University, Tokyo 113-8421, Japan; †Atopy (Allergy) Research Center, Juntendo University Graduate School of Medicine, Tokyo 113-8421, Japan; and ‡Division of Hematology/Oncology, University of Florida, Gainesville, FL 32610

Received for publication August 28, 2014. Accepted for publication November 19, 2014.

This work was supported by a grant-in-aid from the Ministry of Education, Culture, Sports, Science and Technology, Japan (to K. Ohnuma and C.M.) and the Ministry of Health, Labor and Welfare, Japan (to C.M.), as well as Foundation of Strategic Research Projects in Private Universities Grant-in-Aid S1311011 from the Ministry of Education, Culture, Sports, Science and Technology, Japan (to C.M.). This work was also supported by Japan Society for the Promotion of Science KAKENHI Grant 26860760 (to R.H.) and Japan Society for the Promotion of Science Research Fellowships for Young Scientists (to R.H.).

Address correspondence and reprint requests to Dr. Chikao Morimoto, Department of Therapy Development and Innovation for Immune Disorders and Cancers, Graduate School of Medicine, Juntendo University, 2-1-1, Hongo, Bunkyo-ku, Tokyo 113-8421, Japan. E-mail address: morimoto@ims.u-tokyo.ac.jp

The online version of this article contains supplemental material.

Abbreviations used in this article: Cav-Ig, fusion protein of the N-terminal domain of human caveolin-1 and human IgG1 Fc; CD26 sup, supernatant of CD3/CD26-stimulated T cells; CD28 sup, supernatant of CD3/CD28-stimulated T cells; CyA, cyclosporin A; DPPIV, dipeptidyl peptidase IV; EGR2, early growth response 2; IRF4, IFN regulatory factor 4; LAG3, lymphocyte-activation gene 3; LAP, latency-associated protein; MFI, mean fluorescence intensity; MS, multiple sclerosis; siRNA, small interfering RNA; Treg, regulatory T cell; Tr1, type 1 regulatory T cell.

Copyright © 2015 by The American Association of Immunologists, Inc. 0022-1767/15/$25.00

www.jimmunol.org/cgi/doi/10.4049/jimmunol.1402143

tidase IV activity and/or structure homologs (DASH)," including enzymatically active members such as fibroblast activation protein-α, quiescent cell proline dipeptidase/DPP-II/DPP7, DPP8, DPP9, and enzymatically inactive members such as DPP6 and DPP10 (21). However, a DASH family member that functions as a negative regulator of CD26-caveolin-1–mediated T cell activation has not yet been reported.

Active suppression by regulatory T cells (Tregs) is essential for the control of autoreactive cells. Tregs suppress immune responses through either direct cell–cell interactions or the release of inhibitory cytokines. $CD4^+CD25^{high}$ Tregs expressing FOXP3, a master regulatory gene for the suppressive activity, suppress immune cells mainly through soluble or membrane-bound TGF-β (22). Recently, IL-35 has been reported as a new inhibitory cytokine preferentially expressed by mouse $Foxp3^+$ Tregs, and it is required for their maximal suppressive activity (23). IL-35 is a member of the IL-12 heterodimeric cytokine family, composed of EBV-induced 3 and p35 (also known as IL-12α). Type 1 Tregs (Tr1s) are characterized by high-level production of IL-10 with regulatory activity (24). Lymphocyte-activation gene 3 (LAG3) and early growth response 2 (EGR2) have been recently reported as markers of Tr1-like cells (25). LAG3 binds to MHC class II molecules with higher affinity than CD4, leading to transduction of inhibitory signals for both T cells and APCs (26, 27). EGR2 is an essential transcription factor that regulates the T cell anergy program by directly upregulating diacylglycerol kinase α, and it also plays an important role in the induction of LAG3 and IL-10 expression (28).

Although the signaling events involved in CD26-mediated T cell activation or the cellular functions of CD26-expressing T cells have been studied extensively by our group and others, the potential negative feedback mechanism of CD26-mediated costimulation still remains to be elucidated. The present study focuses on the expression of inhibitory molecules induced in $CD4^+$ T cells following CD26 costimulation and the signaling pathways involved in this biological process.

Materials and Methods

Preparation of human T cells

Human PBMCs were collected from healthy adult volunteers after the documented informed consent and Institutional Review Board approval were obtained. This study has been performed according to the principles set out in the Declaration of Helsinki. For purification, the MACS cell separation system (Miltenyi Biotec, Bergisch Gladbach, Germany) and MACS human $CD4^+$ T cell isolation kit (Miltenyi Biotec) were used. Purity of $CD4^+$ T cells was ≥97% as confirmed by FACSCalibur (BD Biosciences, San Jose, CA).

Abs and reagents

For T cell stimulation, anti-CD3 mAb (OKT3), anti-CD28 mAb (4B10), anti-CD26 mAb (1F7), and the fusion protein of the N-terminal domain of human caveolin-1 and human IgG1 Fc (Cav-Ig) developed in our laboratory were used (20). The following human-specific Abs were used for flow cytometry: FITC-labeled anti-LAG3 mAb (clone 17B4) and FITC-labeled mouse IgG1, κ isotype control (clone MOPC-21) were purchased from Enzo Life Sciences (Farmingdale, NY). PE-labeled anti–CTLA-4 mAb (clone L3D10) and PE-labeled mouse IgG_1, κ isotype control (clone MOPC-21) were purchased from BioLegend (San Diego, CA). PE-labeled anti–IL-10 mAb (clone JES3-9D7) and PE-labeled rat IgG1, κ isotype control (clone eBRG1) were purchased from eBioscience (San Diego, CA). PerCP-labeled anti–latency-associated protein (LAP) mAb (clone 27232) and PerCP-labeled mouse IgG1 isotype control (clone 11711) were purchased from R&D Systems (Minneapolis, MN). Alexa Fluor 647–labeled anti–IFN-γ mAb (clone B27), Alexa Fluor 647–labeled anti-FOXP3 mAb (clone 259D/C7), and Alexa Fluor 647–labeled mouse IgG1, κ isotype control (clone MOPC-21) were purchased from BD Biosciences. Alexa Fluor 647–labeled anti-CD26 mAb (clone 19) recently developed in our laboratory was used for the detection of CD26 even in the presence of another anti-CD26 mAb, 1F7 (29). For Western blot analysis, mouse anti-NFAT1 mAb (clone 639402), goat anti-NFAT2 polyclonal Ab, and rabbit anti–p-ERK1 (pT202/pY204)/ERK2 (pT185/pY187) polyclonal Ab were purchased from R&D Systems. Mouse anti–TATA-binding protein mAb (clone mAbcam 51841) and rabbit anti-EGR2 mAb (clone EPR4004) were purchased from Abcam (Cambridge, U.K.). Mouse anti–β-actin mAb (clone AC-15) was purchased from Sigma-Aldrich (St. Louis, MO). HRP-conjugated sheep anti-mouse IgG and donkey anti-rabbit IgG were purchased from GE Healthcare (Buckinghamshire, U.K.), and HRP-conjugated donkey anti-goat IgG was purchased from Santa Cruz Biotechnology (Santa Cruz, CA). For neutralizing IL-10, anti–human IL-10 mAb (clone JES3-9D7), anti–human IL-10R mAb (clone 3F9), rat IgG1, κ isotype control (clone RTK2071), and rat IgG2a, κ isotype control (clone RTK2758) were purchased from BioLegend. Recombinant human IL-10 and the NFAT inhibitor cyclosporin A (CyA) were purchased from Sigma-Aldrich. The MEK1/2 inhibitor U0126 and the NF-κB activation inhibitor quinazoline were purchased from Merck Millipore (Billerica, MA).

Preparation of culture supernatant and measurement of cytokines

Purified $CD4^+$ T cells (1×10^5) were cultured in serum-free AIM-V medium (Invitrogen, Carlsbad, CA) in 96-well flat-bottom plates (Costar; Corning, Corning, NY), with stimulatory mAbs or Cav-Ig being bound in the wells beforehand at the following concentrations: 0.5 μg/ml OKT3 and/or 2, 5, 10, 20, or 50 μg/ml 4B10 or 1F7 or Cav-Ig. Cells were cultured in 5% CO_2 and 100% humidified incubator at 37°C for 48, 72, 96, or 120 h. After incubation, supernatants were collected and cytokine concentrations were examined using ELISA. BD OptEIA kits for human IL-2, IL-4, IL-5, IL-10, TNF-α, IFN-γ, or TGF-β1 were purchased from BD Biosciences, and the Ready-SET-Go! kits for human IL-17A or IL-21 were purchased from eBioscience. The absorbance at 450/570 nm was measured in a microplate reader (Bio-Rad, Hercules, CA), and data were analyzed with Microplate Manager 6 software (Bio-Rad).

Flow cytometry

Purified $CD4^+$ T cells (1×10^5) were incubated with plate-bound OKT3 (0.5 μg/ml) and/or 2, 5, 10, 20, or 50 μg/ml of 4B10 or 1F7 in 96-well flat bottom plates for 96 h, and cells were then collected and prepared for the analysis of cell surface expression of CTLA-4, LAG3, and LAP. Acquisition was performed using FACSCalibur, and data were analyzed with FlowJo software (Tree Star, Ashland, OR). For the analysis of intracellular FOXP3 and LAG3, a human FOXP3 buffer set (BD Biosciences) was used. For the staining of intracellular cytokines, cells were treated with GolgiStop (monensin) (BD Biosciences) for the last 5 h of culture in the presence or absence of 50 ng/ml PMA (Sigma-Aldrich) plus 1 μg/ml ionomycin (Merck Millipore) and then stained using BD Cytofix/Cytoperm Plus fixation/permeabilization kit (BD Biosciences) according to the manufacturer's instructions.

Preparation of lysates and Western blotting

To analyze nuclear expression of ERK or NFAT, purified $CD4^+$ T cells (1.5×10^6 cells/well, three wells per sample) were incubated with plate-bound OKT3 (0.5 μg/ml) and/or 4B10 (50 μg/ml) or 1F7 (50 μg/ml) in 24-well flat-bottom plates (Costar) for 0.5, 1, or 2 h. After incubation, cells were collected and nuclear extracts were prepared using EpiQuik nuclear extraction kit (Epigentek, Farmingdale, NY) supplemented with 2% protease inhibitor mixture (Sigma-Aldrich) and 1× PhosSTOP (Roche Diagnostics, Tokyo, Japan). For the analysis of EGR2 expression, purified $CD4^+$ T cells (1.5×10^6 cells/well) were stimulated in the above conditions for 24 or 48 h. After incubation, cells were collected and whole-cell lysates were prepared using RIPA buffer. Each sample was resolved by SDS-PAGE in reducing condition. SDS-PAGE and Western blot analysis were conducted as described previously (30). The images were taken using luminescent image analyzer LAS 4000 (GE Healthcare), and data were analyzed with image reader LAS 4000 and Multi Gauge software (GE Healthcare).

T cell proliferation assay

Purified $CD4^+$ T cells (1×10^5) were incubated with plate-bound OKT3 (0.5 μg/ml) and/or 4B10 or 1F7 in 96-well flat-bottom plates for 96 h in the presence or absence of signal inhibitor or culture supernatant. To evaluate T cell proliferation, a cell proliferation ELISA, BrdU Kit (Roche Diagnostics) was used. BrdU was added to each well for the last 2 h of incubation, and proliferation was assessed by measuring BrdU incorporation by ELISA. The absorbance at 450/655 nm was measured in a microplate reader, and data were analyzed with Microplate Manager 6 software. T cell proliferation was also assessed by using Cell Counting

Kit-8 (Dojindo, Kumamoto, Japan). 2-(2-Methoxy-4-nitrophenyl)-3-(4-nitrophenyl)-5-(2,4-disulfophenyl)-2H tetrazolium monosodium salt (WST-8) was added to each well at a concentration of 1/10 volume for the last 3 h, and the absorbance at 450/595 nm was measured. For the analysis of the number of cell divisions, a Vybrant CFDA SE cell tracer kit (Molecular Probes, Carlsbad, CA) was used. Purified $CD4^+$ T cells labeled with 2 μmol/l CFSE were incubated for 96 h with plate-bound stimulatory mAbs as described above, and cells were then harvested and analyzed by FACSCalibur.

Small interfering RNA against human EGR2

We selected two target sequences from nucleotides +1802 to 1820 (sense1) and +1890 to 1908 (sense2) downstream of the start codon of human EGR2 mRNA: sense1 small interfering RNA (siRNA), 5′-GAGUUGAUCUAAGACGUUUdTdT-3′, and sense2 siRNA, 5′-CACUUUAUGGCUUGGGACUdTdT-3′. siRNAs against EGR2 were purchased from Sigma-Aldrich, and negative control siRNA (oligonucleotide sequences are not disclosed) was purchased from Qiagen (Valencia, CA). Fifty picomoles siRNA duplexes were transfected into 5×10^5 purified $CD4^+$ T cells by using HVJ-E vector (GenomONE-Si; Ishihara Sangyo Kaisha, Osaka, Japan) according to the manufacturer's instructions (19, 20).

Quantitative real-time RT-PCR assay

Purified $CD4^+$ T cells or siRNA transfected $CD4^+$ T cells (5×10^5) were incubated with plate-bound OKT3 (0.5 μg/ml) and/or 4B10 or 1F7 or Cav-Ig in 24-well flat-bottom plates for 6, 12, 24, 48, or 72 h in the presence or absence of signal inhibitor or culture supernatant. After incubation, cells were collected and total RNA was extracted by the use of an RNeasy Micro kit according to the manufacturer's instructions (Qiagen). cDNA was produced by using a PrimeScript II first strand cDNA synthesis kit (TaKaRa Bio, Shiga, Japan) with oligo(dT) primers. Quantification of mRNA was performed using the 7500 real-time PCR System and SYBR Select Master Mix (Applied Biosystems, Foster City, CA). The obtained data were analyzed with 7500 System SDS software (Applied Biosystems), being normalized to hypoxanthine phosphoribosyltransferase expression. Sequences of primers used in quantitative real-time RT-PCR analysis are shown in Supplemental Table I.

Statistical analysis

Data were analyzed by the paired Student *t* test (two-tailed) for two group comparison, or by the ANOVA test for multiple comparison testing. The assay was performed in triplicate wells, and data are presented as mean ± SD of triplicate samples of the representative experiment, or mean ± SE of triplicate samples of independent experiments. Significance was analyzed using MS Excel (Microsoft) and p values < 0.01 were considered significant and are indicated in the corresponding figures and figure legends.

Results

CD26-mediated costimulation induces the development of $CD4^+$ T cells to a Tr1-like phenotype with high IL-10 production

To explore the negative feedback mechanism associated with CD26-mediated costimulation, we first examined the cytokine production profile of $CD4^+$ T cells, focusing particularly on the production of immunosuppressive cytokines such as TGF-β and IL-10. To characterize the specific phenotype associated with CD26 costimulation, we compared the level of cytokine production following costimulation with either CD26 or CD28, a representative T cell costimulatory pathway. As shown in Fig. 1A, only a small amount of cytokines was produced following stimulation with anti-CD3 mAb alone (gray lines), whereas both anti-CD3 plus anti-CD26 and anti-CD3 plus anti-CD28 costimulation greatly enhanced cytokine production (red or blue lines). Production of IL-10 by $CD4^+$ T cells was preferentially increased following CD26-mediated costimulation compared with CD28-mediated costimulation over the tested time intervals (Fig. 1Aa). IL-21 production was also greatly enhanced in the late phase of CD26 costimulation (Fig. 1Ab). Alternatively, production of IL-2, IL-5, or TNF-α was much lower following CD26 costimulation than CD28 costimulation (Fig. 1Af–h). In contrast, no difference in the production of IL-17A, IFN-γ, or IL-4 was observed following CD26- or CD28-mediated costimulation (Fig. 1Ac–e). Real-time RT-PCR analysis was then conducted to confirm the above results. As shown in Fig. 1B, IL-10 and IL-21 mRNA expression levels were higher after 24 h of CD26 costimulation than CD28 costimulation. Meanwhile, the amount of TGF-β1 was below the detection limit (0.125 ng/ml), and mRNA expression level of IL-35 subunits (EBV-induced 3 and p35) was not elevated following CD26- or CD28-mediated costimulation (data not shown). These data indicate that CD26 and CD28 costimulation of $CD4^+$ T cells results in different profiles of cytokine production, with IL-10 production being preferentially enhanced following CD26 costimulation.

To further characterize the biological process involved in IL-10 production following CD26 costimulation, we evaluated the effect of a wide range of concentrations of anti-CD26 and anti-CD28 mAbs. Additionally, to assess whether caveolin-1, a physiological ligand of CD26, can induce IL-10, we activated $CD4^+$ T cells with anti-CD3 mAb and Cav-Ig as described in *Materials and Methods*. As shown in Fig. 2Aa, CD26-mediated costimulation by both anti-CD3 plus anti-CD26 and anti-CD3 plus Cav-Ig greatly enhanced IL-10 production compared with CD28-mediated costimulation. It is noteworthy that the enhancement in CD26-mediated IL-10 production via either anti-CD26 mAb or Cav-Ig was dose-dependent, whereas IL-10 production decreased with increasing doses of anti-CD28 mAb (Fig. 2Aa). IL-17A production following CD26-mediated costimulation was similar to that observed following CD28-mediated costimulation (Fig. 2Ab). Although the amount of IL-2 produced by $CD4^+$ T cells following CD26 costimulation was 1–10 ng/ml and significantly higher than anti-CD3 mAb alone, it was consistently lower than that induced by CD28 costimulation (Fig. 2Ac, Supplemental Fig. 1A). T cell proliferation in response to CD26 costimulation was significantly decreased in the presence of neutralizing anti–IL-2 mAb, indicating that a relatively small amount of IL-2 induced by CD26 costimulation was sufficiently functional for enhancing T cell proliferation (Supplemental Fig. 1B). For further confirmation, we analyzed the intracellular expression of IL-10 in $CD4^+$ T cells through flow cytometry. Because inhibition of protein transport by monensin or brefeldin A is essential for intracellular cytokine staining, we analyzed IL-10 expression in T cells stimulated by anti-CD3 plus a high dose (50 μg/ml) of anti-CD26 or anti-CD28 with monensin for the last 5 h of culture. As shown in Fig. 2B, IL-10 and IFN-γ were equally induced in $CD4^+$ T cells following CD26 costimulation (Fig. 2Bb), whereas CD28 costimulation induced only IFN-γ but hardly induced IL-10 (Fig. 2Ba). Note that only ~2% of $CD4^+$ T cells expressed IL-10 following CD26 costimulation, but this induction was significant and was consistently seen in all the repeated experiments. In contrast with IFN-γ level, which was clearly detected by restimulation with PMA plus ionomycin, detection of the IL-10 level was relatively difficult because restimulation with PMA plus ionomycin hardly affected the percentage of IL-10–expressing cells following either CD26- or CD28-mediated costimulation (the results with similar stimulatory condition are shown in Fig. 6B). Previous work by Jonuleit et al. (31) investigating IL-10 expression also demonstrated a relatively low level of IL-10 expression when human peripheral blood $CD4^+$ T cells from healthy volunteers were primed and restimulated with allogeneic dendritic cells. We also noted that another anti-human IL-10 mAb from BD Biosciences gave similar results (data not shown). To define whether IL-10–expressing $CD4^+$ T cells following CD26-mediated costimulation expressed CD26, we stained cell surface CD26 and intracellular IL-10. For this purpose, as described in *Materials and Methods*, we used an anti-human CD26 mAb recognizing a different epitope from the one recognized by

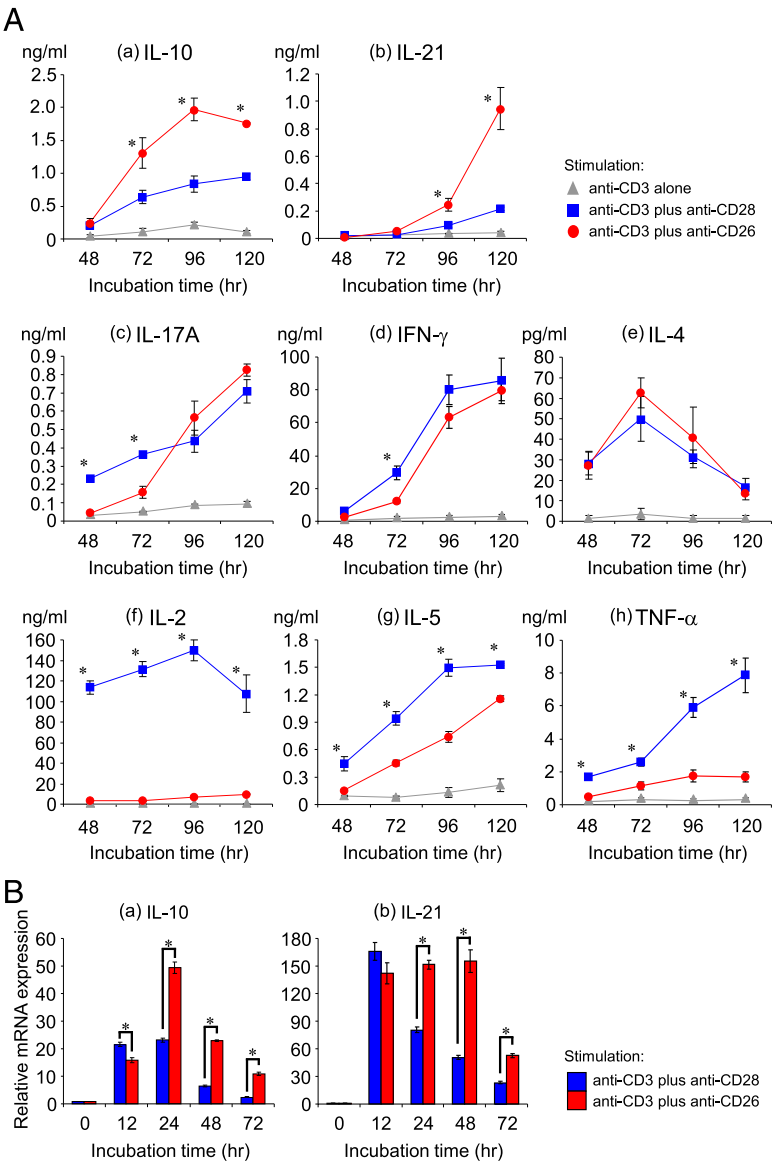

FIGURE 1. CD26-mediated costimulation of $CD4^+$ T cells induces greater levels of IL-10 and IL-21 than does CD28-mediated costimulation. Freshly purified $CD4^+$ T cells were stimulated with anti-CD3 mAb alone, anti-CD3 plus anti-CD28 mAbs (5 μg/ml), or anti-CD3 plus anti-CD26 mAbs (5 μg/ml) for the indicated times. (**A**) Concentrations of IL-10 (**a**), IL-21 (**b**), IL-17A (**c**), IFN-γ (**d**), IL-4 (**e**), IL-2 (**f**), IL-5 (**g**), and TNF-α (**h**) were examined by ELISA. (**B**) mRNA expression of IL-10 (**a**) and IL-21 (**b**) was quantified by real-time RT-PCR. Each expression was normalized to HPRT1, and relative expression levels compared with resting $CD4^+$ T cells (0 h) were shown. Representative data of seven (A) and three (B) independent donors are shown as mean ± SD of triplicate samples, comparing values in anti-CD3 plus anti-CD26 to those in anti-CD3 plus anti-CD28 (*$p < 0.01$), and similar results were obtained in each experiment.

the immobilized anti-CD26 mAb, 1F7, used for CD26 costimulation. As shown in Fig. 2Bc, all of the IL-10–expressing $CD4^+$ T cells were shown to express CD26. Taken together, these results indicate that CD26-mediated costimulation in $CD4^+CD26^+$ T cells preferentially induces IL-10, and this effect increases with enhancing intensity of CD26-mediated signaling.

We next examined the expression of selected molecules with well-characterized immunosuppressive functions by flow cytometry, including the cell surface expression of CTLA-4 and LAP complexed with TGF-β1, and the intracellular expression of transcription factor FOXP3. Because LAG3 has been reported to be continuously recycled and rapidly translocated to the plasma membrane in response to antigenic stimulation (32), we analyzed both the cell surface and intracellular expression of LAG3. As shown in Fig. 3, both the cell surface and intracellular expression of LAG3 was clearly enhanced with increasing doses of anti-CD26 mAb, and CD26-induced enhancement of LAG3 was more pronounced than the effect of CD28-mediated costimulation (Fig. 3Aa). Alternatively, both CD26- and CD28-mediated costimulation enhanced the expression of CTLA-4 and FOXP3, with no significant difference being detected between these two costimulatory pathways (Fig. 3Ac, d). In contrast with CD28 costimulation, LAP was hardly induced following CD26 costimulation (Fig. 3Ab). Although the mean fluorescence intensity (MFI) results of LAP, CTLA-4, or FOXP3 correlated with those of percentage of cells expressing LAP, CTLA-4, or FOXP3 shown in Fig. 3A, the values of MFI, especially for LAP and FOXP3, were low and the difference between CD26- and CD28-mediated costimulation was minimal (data not shown). Alternatively, as shown in Fig. 3B, all of the $CD4^+$ T cells expressed LAG3 following CD26 or CD28 costimulation, and no difference was observed in the percentage of LAG3-expressing cells, whereas the expression intensity of LAG3 after CD26-mediated costimulation was higher than after CD28-mediated costimulation. LAG3 also serves as a marker of IL-10–producing Tregs (25), suggesting that signaling events via CD26 may induce the development of $CD4^+$ T cells to a Tr1-like phenotype.

NFAT and Raf-MEK-ERK signalings are indispensable for CD26-mediated T cell activation

We next examined the signaling events associated with CD26-mediated enhancement in IL-10 production in $CD4^+$ T cells. Although cytokine receptor signaling through JAK-STAT plays a crucial role in T cell differentiation into specific effector subsets or Tregs, the initial signaling events for inducing cytokine production in T cells are associated with the TCR signaling pathway. Therefore, we first examined the effect of signal inhibitors against

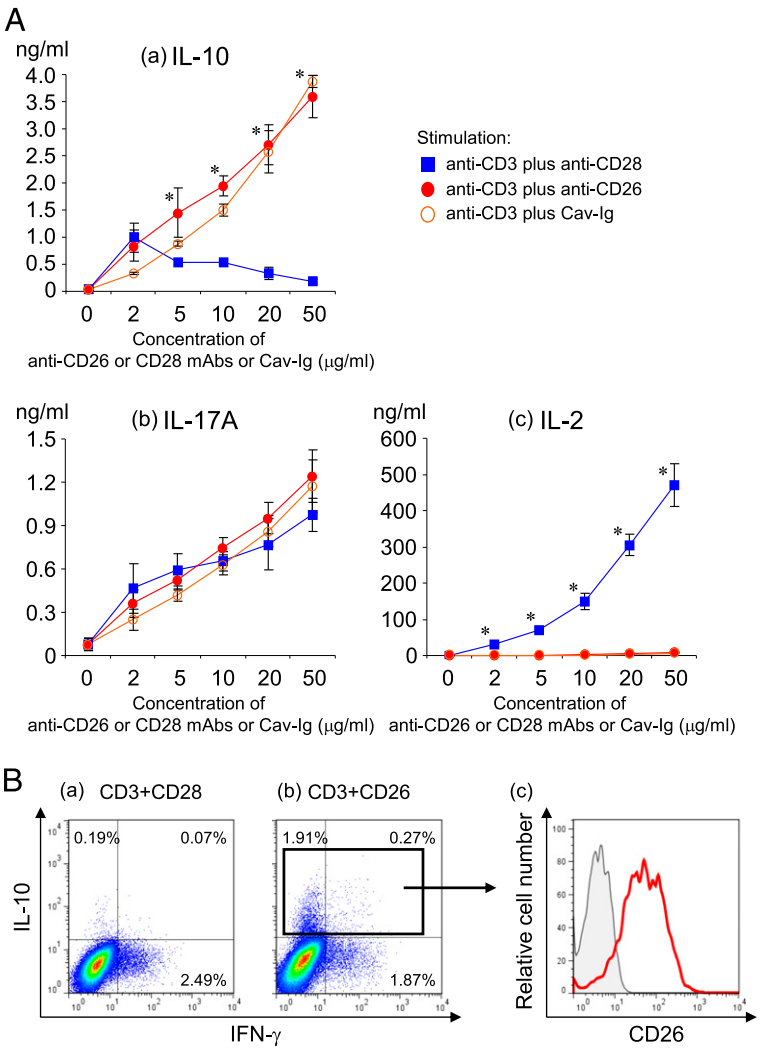

FIGURE 2. CD26-mediated costimulation of $CD4^+$ T cells greatly enhances IL-10 in a stimulation intensity–dependent manner. (**A**) Freshly purified $CD4^+$ T cells were stimulated with anti-CD3 mAb alone, anti-CD3 plus anti-CD28 mAbs, anti-CD3 plus anti-CD26 mAbs, or anti-CD3 mAb plus Cav-Ig at the indicated concentrations for 96 h. Concentrations of IL-10 (A**a**), IL-17A (A**b**), and IL-2 (A**c**) were examined by ELISA. Representative data of five independent donors are shown as mean ± SD of triplicate samples, comparing values in anti-CD3 plus anti-CD26 or anti-CD3 plus Cav-Ig to those in anti-CD3 plus anti-CD28 (*$p < 0.01$), and similar results were obtained in each experiment. (**B**) Freshly purified $CD4^+$ T cells were stimulated with anti-CD3 plus anti-CD28 mAbs (50 μg/ml) (**a**) or anti-CD3 plus anti-CD26 mAbs (50 μg/ml) (**b** and **c**) for 72 h. Cells were treated with monensin in the absence of PMA plus ionomycin restimulation for the last 5 h of culture, and cell surface CD26, intracellular IFN-γ, and IL-10 were detected by flow cytometry. (Ba and b) Two-dimensional dot plot of IFN-γ or IL-10 staining gated for $CD4^+$ T cells is shown. (Bc) Following gating for $CD4^+IL\text{-}10^+$ population as indicated in (Bb), the expression of CD26 was analyzed. The data are shown as histogram of CD26 intensity, and the gray area in the histogram show the data on the isotype control. A representative plot or histogram of four independent donors is shown, and similar results were obtained in each experiment.

NFAT, AP-1, or NF-κB, essential transcription factors for T cell activation located at the terminal end of TCR signaling. We first assessed T cell proliferation by measuring BrdU incorporation by ELISA, which is generally accepted to be equivalent to the [^{3}H]thymidine incorporation assay. As shown in Fig. 4A, the NFAT inhibitor CyA and the MEK1/2 inhibitor U0126 markedly inhibited the proliferative activity of $CD4^+$ T cells following CD26 or CD28 costimulation. Of note, T cells activated with anti-CD3 and anti-CD26 were much more sensitive to these inhibitors as compared with CD28 costimulation, and a high dose of CyA and U0126 suppressed the proliferation of T cells to the same level of proliferative activity as anti-CD3 alone (Fig. 4A). Additionally, we conducted a T cell proliferation assay by using tetrazolium salt, and results similar to those obtained with the BrdU incorporation assay were observed (Fig. 4B). As shown in Fig. 4C, the effects of NFAT and MEK1/2 inhibitors on IL-10 production were very similar to those on T cell proliferation. Whereas the NF-κB inhibitor quinazoline also suppressed T cell proliferation and IL-10 production in a dose-dependent manner, its effect on $CD4^+$ T cells following CD26 costimulation was less apparent as compared with NFAT and MEK1/2 inhibitors (Fig. 4A–C). These three inhibitors had similar effects on IL-17A and IFN-γ production as they did with IL-10 production (data not shown). These results indicate that both NFAT- and Raf-MEK-ERK–related signals are indispensable for CD26-mediated T cell activation, and they suggest that the intensity or persistence of these two signal pathways in $CD4^+$ T cells are different between CD26 and CD28 costimulation.

To further define the difference between CD26- and CD28-mediated costimulatory signaling pathways, we next examined the amount of NFAT and p-ERK1/2 translocated to the nucleus of $CD4^+$ T cells following CD26 or CD28 costimulation. The NFAT family consists of five members (NFAT1–5), and only NFAT5 is regulated by osmotic stress, not by calcium–calcineurin signaling (33). Because NFAT3 is reported to be absent in T cells, we analyzed the expression of NFAT1, NFAT2, and NFAT4. As shown in Fig. 4D, stimulation with both anti-CD3 plus anti-CD28 and anti-CD3 plus anti-CD26 resulted in increased nuclear levels of p-ERK1/2 and NFAT2 compared with anti-CD3 alone. Nuclear levels of p-ERK1/2 peaked at 30 min and then gradually decreased following CD28-mediated costimulation, whereas accumulation of NFAT2 in the nucleus reached a maximum after 2 h of CD28 costimulation. Alternatively, CD26-mediated costimulation resulted in greater enhancement of nuclear level of NFAT2 compared with CD28 costimulation, whereas the maximum level of p-ERK1/2 following CD26-mediated costimulation was lower than that seen with CD28 costimulation, but the effect of CD26 costimulation on p-ERK1/2 persisted until 2 h after stimulation. In contrast, no difference in nuclear level of NFAT1 was observed following CD26 or CD28 costimulation. As shown in Fig. 4D, when each sample was immunoblotted with anti-NFAT2, two bands were detected in molecular mass regions at ~110,000 and

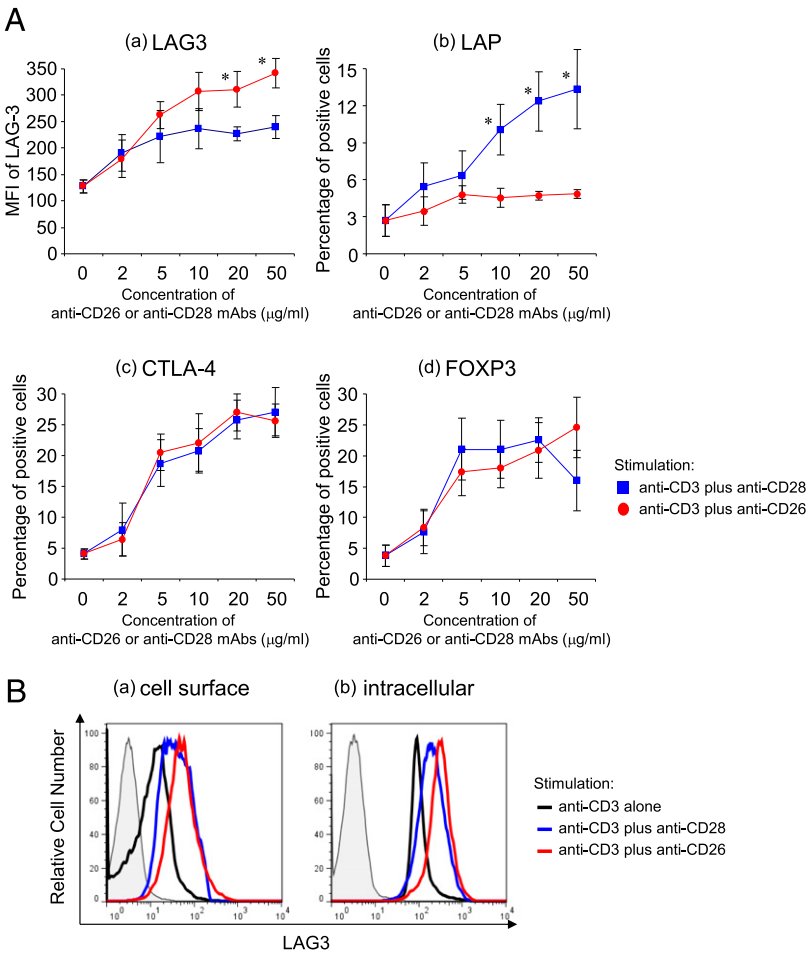

FIGURE 3. CD26-mediated costimulation of $CD4^+$ T cells induces greater LAG3 expression than does CD28-mediated costimulation. (**A**) Freshly purified $CD4^+$ T cells were stimulated with anti-CD3 mAb alone, anti-CD3 plus anti-CD28 mAbs, or anti-CD3 plus anti-CD26 mAbs at the indicated concentrations for 96 h. Cell surface LAP (A**b**), CTLA-4 (A**c**), intracellular LAG3 (A**a**), and FOXP3 (A**d**) gated for $CD4^+$ T cells were detected by flow cytometry. Data are shown as mean ± SE of MFI (Aa) or percentage positive cells (Ab–d) from five independent donors, comparing values in anti-CD3 plus anti-CD26 to those in anti-CD3 plus anti-CD28 (*$p < 0.01$), and similar results were obtained in each experiment. (**B**) Freshly purified $CD4^+$ T cells were stimulated with anti-CD3 mAb alone, anti-CD3 plus anti-CD28 mAbs (50 μg/ml), or anti-CD3 plus anti-CD26 mAbs (50 μg/ml) for 96 h. After stimulation, cell surface (a) or intracellular (b) expression of LAG3 gated for $CD4^+$ T cells was analyzed by flow cytometry. Data are shown as histogram of LAG3 and are representative of five independent donors. The gray areas in each histogram show the data of isotype control.

130,000 Da. The band with the higher molecular mass is thought to represent the constitutively expressed NFAT2 isoform, and the one with the lower molecular mass probably represents the inducible NFAT2 isoform (33). In contrast with NFAT4, which was only slightly expressed both in the cytoplasm and the nucleus of peripheral blood $CD4^+$ T cells (data not shown), the protein level of NFAT2 was abundant and clearly increased in response to CD26 or CD28 costimulation compared with NFAT1, suggesting that among the NFAT family, NFAT2 plays a crucial role in regulating human $CD4^+$ T cell activation. NFAT protein is known to synergistically interact with many transcription factors, including AP-1, which is the main transcriptional partner of NFAT during T cell activation. Alternatively, in the absence of AP-1, NFAT directs transcription of a specific program of gene expression that may be responsible for blocking TCR signaling (33). Taken together, these results strongly suggest that persistent NFAT–AP-1 cooperation is responsible for CD26-mediated T cell activation, leading to a specific pattern of gene expression different from CD28-mediated costimulation.

Increased EGR2 expression following CD26-mediated costimulation is associated with preferential IL-10 production

The findings above suggest that persistent NFAT–AP-1 activation following CD26-mediated costimulation is associated with enhanced IL-10 production. The molecular mechanisms involved in the process of IL-10 transcription in T cells have been well characterized, with the involvement of many transcription factors having been reported previously. c-Maf and IFN regulatory factor 4 (IRF4) directly transactivate IL-10 gene expression through binding to the IL-10 promoter (34, 35), whereas Blimp-1 positioned downstream of EGR2, GATA-3, and E4BP4 (also known as NFIL3) enhances IL-10 expression epigenetically by acetylating or methylating histones to change the chromatin structure at the IL-10 locus (36–38). We hypothesized that preferential IL-10 production of $CD4^+$ T cells following CD26-mediated costimulation was associated with the induction of such transcription factors. To validate the above assumption, we conducted a real-time RT-PCR assay to analyze the expression levels of the transcription factors discussed above following CD26 or CD28 costimulation. As shown in Fig. 5Aa, CD26 costimulation resulted in greater enhancement of EGR2 expression in $CD4^+$ T cells during the tested time intervals as compared with CD28 costimulation. Alternatively, both CD26 and CD28 costimulation markedly increased the expression of IRF4 compared with unstimulated T cells, but no difference was observed between these two costimulatory pathways (Fig. 5Ab). In contrast, both CD26 and CD28 costimulation of T cells led to a decrease in c-Maf or Blimp-1 expression (Fig. 5Ac, d), as well as a decline in expression levels of GATA-3 and E4BP4 (data not shown), indicating that EGR2 expression was preferentially induced following CD26-mediated costimulation. Western blot analysis was then conducted to confirm the above results. As shown in Fig. 5B, the protein level of EGR2 was higher after 24 or 48 h of CD26 costimulation than CD28 costimulation. Because it has been reported that EGR2 transcription is regulated by NFAT (39), we next examined the potential involvement of NFAT in the induction of EGR2 expression following CD26 costimulation. As shown in Fig. 5C, stimulation with both anti-CD3 plus anti-CD26 and anti-CD3 plus Cav-Ig clearly enhanced EGR2 expression compared with CD28 costimulation, a process that was partially inhibited by the NFAT

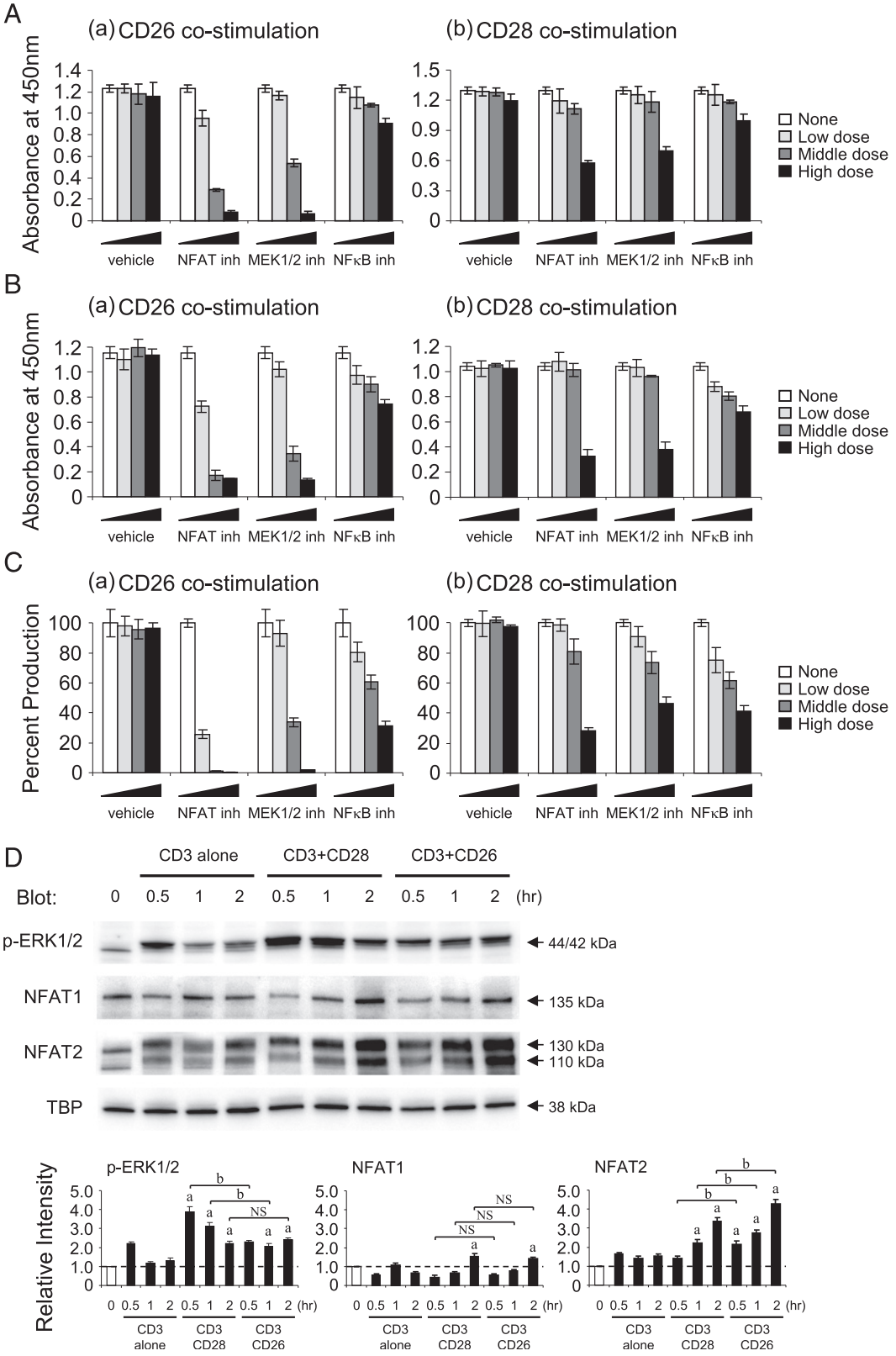

FIGURE 4. NFAT and Raf-MEK-ERK signaling events are indispensable for CD26-mediated CD4$^+$ T cell activation. (**A**–**C**) Freshly purified CD4$^+$ T cells were stimulated with anti-CD3 plus anti-CD26 mAbs (25 μg/ml) (**a**) or anti-CD3 plus anti-CD28 mAbs (25 μg/ml) (**b**) for 96 h in the presence of increasing doses of vehicle (DMSO, 0.0025, 0.0075, 0.025%), NFAT inhibitor (CyA, 0.01, 0.1, 1 μM), MEK1/2 inhibitor (U0126, 0.5, 1.5, 5 μM), or NF-κB inhibitor (quinazoline, 0.1, 0.5, 2.5 μM). (A) BrdU was added for the last 2 h of culture, and proliferation was assessed by measuring BrdU incorporation by ELISA. (B) Tetrazolium was added for the last 3 h of culture, and the absorbance at 450 nm was measured. (C) Concentration of IL-10 was examined by ELISA. Representative data of two (A) and four (B and C) independent donors are shown as mean ± SD of triplicate samples, and similar results were obtained in each experiment. (**D**) Freshly purified CD4$^+$ T cells were stimulated with anti-CD3 mAb alone, anti-CD3 plus anti-CD28 mAbs (50 μg/ml), or anti-CD3 plus anti-CD26 mAbs (50 μg/ml) for the indicated times. Nuclear extracts were separated by SDS-PAGE (each at 5 μg), and p-ERK1/2, NFAT1, or NFAT2 were detected by immunoblotting. The same blots were stripped and reprobed with Abs specific (*Figure legend continues*)

inhibitor alone and completely abrogated by the combination of the NFAT and MEK1/2 inhibitors. Furthermore, to determine whether EGR2 expression was associated with IL-10 production, we conducted knockdown experiments using siRNA against EGR2 in primary $CD4^+$ T cells. Expression level of EGR2 in T cells following CD26 costimulation was determined by real-time RT-PCR in the presence of control siRNA or two different sequences of EGR2-siRNA. As shown in Fig. 5Da, b, EGR2-siRNA treatment reduced EGR2 expression by ~50% as compared with control siRNA, which was associated with a significant decrease in IL-10 production by $CD4^+$ T cells. Because similar results were also obtained with a different siRNA sense2 designed to target a separate EGR2 site, data obtained with EGR2-siRNA sense1 as described in *Materials and Methods* are shown. Because it has been shown that EGR2-deficient $CD4^+$ T cells in mice produced high levels of IFN-γ and IL-17 following TCR stimulation (40), we therefore examined the effect of EGR2 knockdown on IL-17A and IFN-γ production by human $CD4^+$ T cells. As shown in Fig. 5Dc, d, production of both cytokines was vigorously enhanced by EGR2-siRNA compared with control siRNA. These results rule out the possibility that the decrease in IL-10 production seen with EGR2-siRNA treatment was due to the nonspecific off-target effects of siRNA. Taken together, these observations strongly suggest that CD26-mediated costimulation of $CD4^+$ T cells results in enhanced NFAT/AP-1–dependent EGR2 expression, which is associated with the preferential production of IL-10.

Supernatants of CD3/CD26-stimulated $CD4^+$ T cells suppress activation of bystander T cells in an IL-10–dependent manner

To address the functional significance of enhanced IL-10 production by $CD4^+$ T cells following CD26-mediated costimulation, we prepared culture supernatant of $CD4^+$ T cells stimulated with anti-CD3 plus a high dose (50 μg/ml) of anti-CD26 or anti-CD28 as a control and then examined whether the supernatant of CD3/CD26-stimulated T cells (CD26 sup) suppressed activation of bystander T cells. We confirmed that higher levels of IL-10 and lower levels of IL-2 were contained in CD26 sup as compared with the supernatant of CD3/CD28-stimulated T cells (CD28 sup), as shown in Fig. 2A. As shown in Fig. 6Aa, b, addition of CD26 sup to freshly purified $CD4^+$ T cells incubated under stimulatory condition with anti-CD3 plus anti-CD26 for 24 h resulted in a significant reduction in expression levels of both IL-2 and IFN-γ as compared with AIM-V medium, and this inhibitory effect was abrogated by the addition of anti–IL-10 plus anti–IL-10R. In contrast, IL-10 expression in $CD4^+$ T cells was significantly enhanced by CD26 sup, and this enhancing effect was almost completely reversed by anti–IL-10 plus anti–IL-10R (Fig. 6Ac). These results indicate that IL-10 contained in the CD26 sup suppresses the expression of effector cytokines such as IL-2 and IFN-γ but upregulated the expression of IL-10. Alternatively, treatment with CD28 sup markedly upregulated IL-2 expression, suggesting the presence in CD28 sup of soluble factors such as IL-2 that enhance the process of T cell activation (Fig. 6Aa). In contrast, addition of anti–IL-10 plus anti–IL-10R in the presence of CD28 sup increased the expression of IFN-γ but decreased IL-10 expression, suggesting that the relatively small amount of IL-10 in the CD28 sup was sufficient to regulate $CD4^+$ T cell cytokine production (Fig. 6Ab, c). To analyze the effect of CD26 sup on the proportion of IL-10 or effector cytokine-expressing cells, we next performed intracellular staining of IL-10 and IFN-γ in $CD4^+$ T cells. As shown in Fig. 6Ba, d, stimulation of freshly purified $CD4^+$ T cells with anti-CD3 plus anti-CD26 in the presence of CD26 sup for 3 d resulted in a decrease in the relative percentage of IFN-γ–expressing cells (from 18.5 to 11.1%) as compared with AIM-V medium, whereas the proportion of IL-10–expressing cells was hardly affected by CD26 sup. The effect of CD26 sup on the proportion of IFN-γ–expressing cells was reversed by anti–IL-10 plus anti–IL-10R (Fig. 6Be). Alternatively, addition of CD28 sup to $CD4^+$ T cells did not change the proportion of IFN-γ–expressing cells, but CD28 sup treatment in the presence of anti–IL-10 and anti–IL-10R led to an increase in the level of IFN-γ^+ cells (Fig. 6Bb, c), suggesting that the CD28 sup contained both activating and inhibitory factors such as IL-10. These findings strongly suggest that CD26 sup preferentially suppresses the proliferation of effector cytokine–expressing cells in an IL-10–dependent manner.

We next analyzed the effect of CD26 sup on T cell proliferation. As shown in Fig. 7A, CD26 sup clearly inhibited the proliferative activity of freshly purified $CD4^+$ T cells following CD26 costimulation. Although CD28 sup also slightly suppressed the proliferation of T cells following CD26 costimulation, the suppressive effect of CD26 sup was much more pronounced compared with CD28 sup. Interestingly, the suppressive effect on T cells following CD26 costimulation was more evident compared with T cells following CD28 costimulation (Fig. 7A). To further evaluate this observed difference, we conducted the same T cell proliferation assay in the presence of rIL-10. As shown in Supplemental Fig. 2A and 2B, T cells stimulated with anti-CD3 plus anti-CD26 were much more sensitive to the inhibitory effect of IL-10 as compared with CD28 costimulation, and the difference between CD26 and CD28 costimulation was markedly evident in cytokine production compared with proliferative activity. We further analyzed the expression of IL-10R on $CD4^+$ T cells following CD26- or CD28-mediated costimulation but observed no difference in the expression intensity of IL-10R between these two costimulatory approaches (Supplemental Fig. 2C). To characterize in more detail the effect of CD26 sup on T cell proliferation, we analyzed the cell division process of CFSE-labeled $CD4^+$ T cells by flow cytometry. As shown in Fig. 7Ba, b, d, e, CD26 sup exhibited a very potent suppressive effect on the proliferation of T cells stimulated with anti-CD3 plus anti-CD26 compared with CD28 sup, and this effect was partially reversed by addition of anti–IL-10 plus anti–IL-10R. It is noteworthy that 10 ng/ml rIL-10, a higher concentration than that found in CD26 sup, clearly suppressed T cell proliferation, but this effect was not more potent than CD26 sup (Fig. 7Bd, f). Alternatively, CD26 sup only slightly inhibited the proliferation of T cells stimulated with anti-CD3 plus anti-CD28, and these CD3/CD28-stimulated $CD4^+$ T cells were much less sensitive to the inhibitory effect of IL-10 as compared with CD3/CD26-stimulated T cells (Fig. 7Cc, d). These results correlated strongly with the proliferative activity shown in Fig. 7A. Taken together, these data strongly suggest that soluble factors secreted from $CD4^+$ T cells following CD26-mediated costimulation profoundly suppress bystander T cell proliferation, with IL-10 having a synergistic effect on the suppressive activity of these soluble factors.

for TATA-binding protein (TBP) as a loading control. Band intensity of p-ERK1/2, NFAT1, or NFAT2 was normalized to TBP, and relative intensity compared with resting $CD4^+$ T cells (0 h) is indicated in the *bottom panel*. Data are shown as mean ± SE of relative intensity from three independent donors, comparing values in anti-CD3 plus anti-CD28 or anti-CD3 plus anti-CD26 to those in anti-CD3 alone at the same stimulation period ($^a p < 0.01$), and anti-CD3 plus anti-CD26 to those in anti-CD3 plus anti-CD28 at the same stimulation period ($^b p < 0.01$).

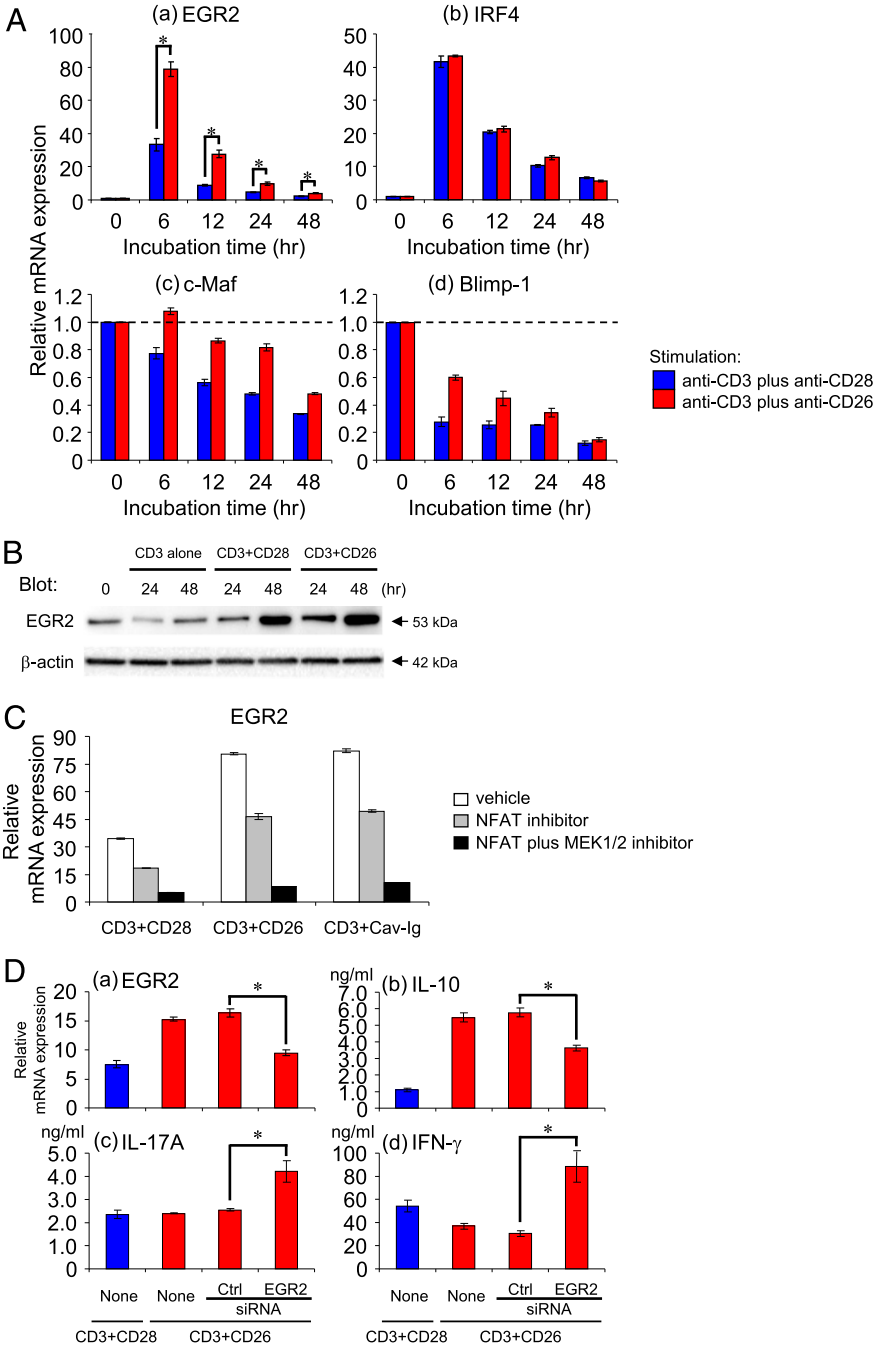

FIGURE 5. EGR2 expression strongly induced via CD26-mediated costimulation is associated with IL-10 production. (**A** and **B**) Freshly purified CD4$^+$ T cells were stimulated with anti-CD3 alone, anti-CD3 plus anti-CD28 mAbs (25 μg/ml), or anti-CD3 plus anti-CD26 mAbs (25 μg/ml) for the indicated times. (A) mRNA expression of EGR2 (**a**), IRF4 (**b**), c-Maf (**c**), and Blimp-1 (**d**) was quantified by real-time RT-PCR. Each expression was normalized to HPRT1, and relative expression levels compared with resting CD4$^+$ T cells (0 h) are shown. Representative data of four independent donors are shown as mean ± SD of triplicate samples, comparing values in anti-CD3 plus anti-CD26 to those in anti-CD3 plus anti-CD28 (*$p < 0.01$). (B) Whole-cell lysates were separated by SDS-PAGE (each 10 μg), and EGR2 was detected by immunoblotting. The same blots were stripped and reprobed with Abs specific for β-actin as a loading control. Data shown are representative of two independent experiments with similar results. (**C**) Freshly purified CD4$^+$ T cells were stimulated with anti-CD3 plus anti-CD28 mAbs (25 μg/ml), anti-CD3 plus anti-CD26 mAbs (25 μg/ml), or anti-CD3 mAb plus Cav-Ig (25 μg/ml) for 6 h in the presence of vehicle (DMSO, 0.025%), NFAT inhibitor (CyA, 1 μM), or NFAT inhibitor plus MEK1/2 inhibitor (U0126, 5 μM). mRNA expression of EGR2 was quantified by real-time RT-PCR, and the relative expression level is shown as in (A). Representative data of three independent donors are shown as mean ± SD of triplicate samples. (**D**) Freshly purified CD4$^+$ T cells were transfected with siRNA against EGR2 or control siRNA (Ctrl) and stimulated with anti-CD3 plus anti-CD28 mAbs (25 μg/ml) or anti-CD3 plus anti-CD26 mAbs (25 μg/ml) for 24 h (**a**) or 96 h (**b**–**d**). (Da) mRNA level of EGR2 is shown as in (A). (Db–d) Concentrations of IL-10 (b), IL-17A (c), and IFN-γ (d) were examined by ELISA. Representative data of four independent donors are shown as mean ± SD of triplicate samples, comparing values with EGR2 siRNA to those with control siRNA (*$p < 0.01$), and similar results were obtained in each experiment.

Discussion

In the present study, we show that coengagement of CD3 and CD26 induces the development of CD4$^+$ T cells to a Tr1-like phenotype with a high level of IL-10 production and LAG3 expression. CD26 costimulation also induces a high level of EGR2 associated with preferential IL-10 production, possibly via NFAT- and AP-1–mediated signaling. Furthermore, supernatants of these CD3/CD26-stimulated CD4$^+$ T cells clearly suppress the proliferative activity and effector cytokine production of bystander T cells in an IL-10–dependent manner.

Because the maintenance of peripheral tolerance by Tregs is critical to the potential development of autoimmunity, there is considerable interest in elucidating the molecular mechanisms for inducing the differentiation of CD4$^+$ T cells into specific Treg subsets. Although the mechanisms of Treg induction through exogenous cytokine stimulation have been extensively studied, such as TGF-β for Foxp3$^+$ Tregs or IL-27 for Tr1 cells (41), costimulatory signals for the induction of Tregs have not been fully understood. ICOS and CD46 have been reported as costimulatory signals inducing Tr1-type cells (42, 43). ICOS costimulation regulates c-Maf expression possibly through the enhancement of NFAT2 signal (44). CD46 costimulation induces interaction of the cytoplasmic tail of CD46 (CYT-1-BC1) with SPAK, leading to sustained phosphorylation of ERK1/2 (45). The importance of sustained phosphorylation of ERK1/2 has also been reported for the development of IL-10–producing Th1 cells (46). However, sustained phosphorylation of ERK1/2 alone is not sufficient to explain the preferential IL-10 production, and transcription factors such as c-Maf, IRF4, Blimp-1, GATA-3, and E4BP4 (NFIL3) may be associated with the transcription of IL-10 (34–38). Our present study indicates that EGR2 expression is enhanced in CD4$^+$ T cells following CD26-mediated costimulation (Fig. 5A, B), and EGR2

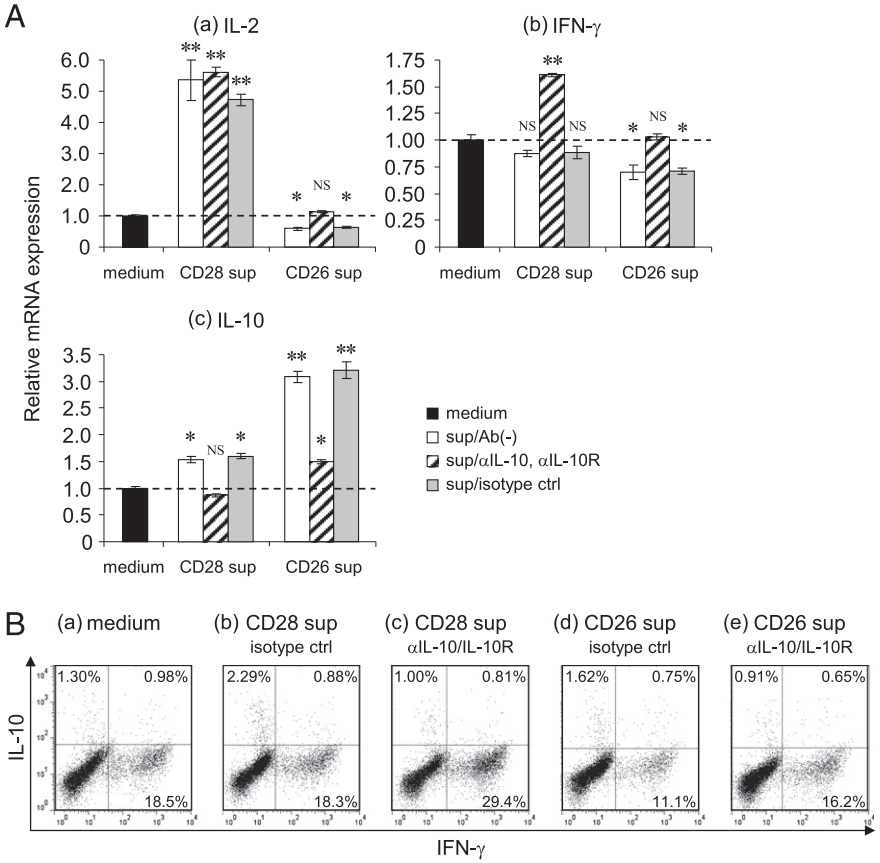

FIGURE 6. Supernatants of CD3/CD26-activated CD4$^+$ T cells suppress effector function of bystander T cells while augmenting IL-10 expression in an IL-10–dependent manner. Culture supernatants of CD4$^+$ T cells stimulated with anti-CD3 plus anti-CD28 mAbs (50 μg/ml) or anti-CD3 plus anti-CD26 mAbs (50 μg/ml) for 72 h were collected, and freshly purified CD4$^+$ T cells were stimulated with anti-CD3 plus anti-CD26 mAbs (5 μg/ml) in the presence of the supernatant (CD28 sup or CD26 sup) or AIM-V medium as a control. Prior to the onset of culture, the combination of anti-human IL-10 mAb and anti-human IL-10 receptor mAb (αIL10/IL10R) or isotype control mAbs (isotype ctrl) were added to the culture wells to give a final concentration of 20 μg/ml each. (**A**) After 24 h of incubation, cells were harvested and mRNA expression of IL-2 (**a**), IFN-γ (**b**), or IL-10 (**c**) was quantified by real-time RT-PCR. Each expression was normalized to HPRT1, and relative expression levels compared with the sample of control medium are shown. Representative data of three independent donors are shown as mean ± SD of triplicate samples, comparing values in each sample to that in control medium. *$p < 0.01$, **$p < 0.0001$. (**B**) On day 3, cells were restimulated with PMA plus ionomycin in the presence of monensin for the last 5 h of culture, and the intracellular expression of IFN-γ and IL-10 was detected by flow cytometry. Two-dimensional dot plot of IFN-γ or IL-10 staining gated for CD4$^+$ T cells is shown as a representative plot of three independent donors, and similar results were obtained in each experiment.

knockdown in CD4$^+$ T cells decreases IL-10 while markedly enhancing IL-17A and IFN-γ production (Fig. 5D). These observations strongly suggest that the induction of EGR2 expression is associated with the preferential production of IL-10 after CD26 costimulation. In mice, it has been recently reported that a high level of EGR2 expression is induced by IL-27/IL-27R–STAT3 signaling, and Blimp-1 induced by EGR2 is important for IL-10 production in CD4$^+$ T cells (47). In contrast with the marked upregulation of EGR2 following CD26-mediated costimulation, the expression level of Blimp-1 is not enhanced as compared with unstimulated T cells, although the decrease is more apparent in T cells following CD28 costimulation (Fig. 5A). To characterize more precisely the molecular mechanisms involved in IL-10 induction following CD26-mediated costimulation, the role of Blimp-1 or c-Maf needs to be better defined. NFAT is considered to be a regulator of EGR2 expression in T cells (39). Our present work shows that EGR2 is highly induced via CD26 costimulatory signal, and its expression is partially decreased by the NFAT inhibitor CyA and completely abrogated by the combination of CyA and the MEK1/2 inhibitor U0126 (Fig. 5C). These results strongly suggest that not only NFAT but also Raf-MEK-ERK signaling is involved in the induction of EGR2 expression. The association of ERK1/2 signaling in the induction of EGR2 expression has been recently reported in osteoprogenitors or breast adipose fibroblasts (48, 49), suggesting that the ERK signaling pathway is also associated with the transcription of EGR2 in T cells.

The importance of the anti-inflammatory effects of IL-10 has been confirmed in IL-10–deficient mice. IL-10–deficient mice develop spontaneous colitis at an early age, indicating that IL-10 is essential for intestinal homeostasis (50). IL-10–deficient mice also exhibit severe neuroinflammation with loss of recovery in experimental autoimmune encephalomyelitis (51). Furthermore, the generation of Tr1 cells from peripheral CD4$^+$ T cells has been shown to be greatly impaired in MS patients in comparison with healthy controls (52). Therefore, Tr1-mediated immunotherapy may be a potentially effective approach for the treatment of many autoimmune disorders, including inflammatory bowel disease or MS. Several groups have attempted to generate large numbers of Tr1 in vitro for clinical applications, and IL-27 is being considered currently to be an essential factor for the generation of Tr1 cells (53). In addition to IL-27, costimulatory signals through ICOS or CD46 play an important role in the generation or expansion of Tr1 cells. Our present study raises the possibility that CD26 is a novel costimulatory molecule inducing preferential IL-10 production in

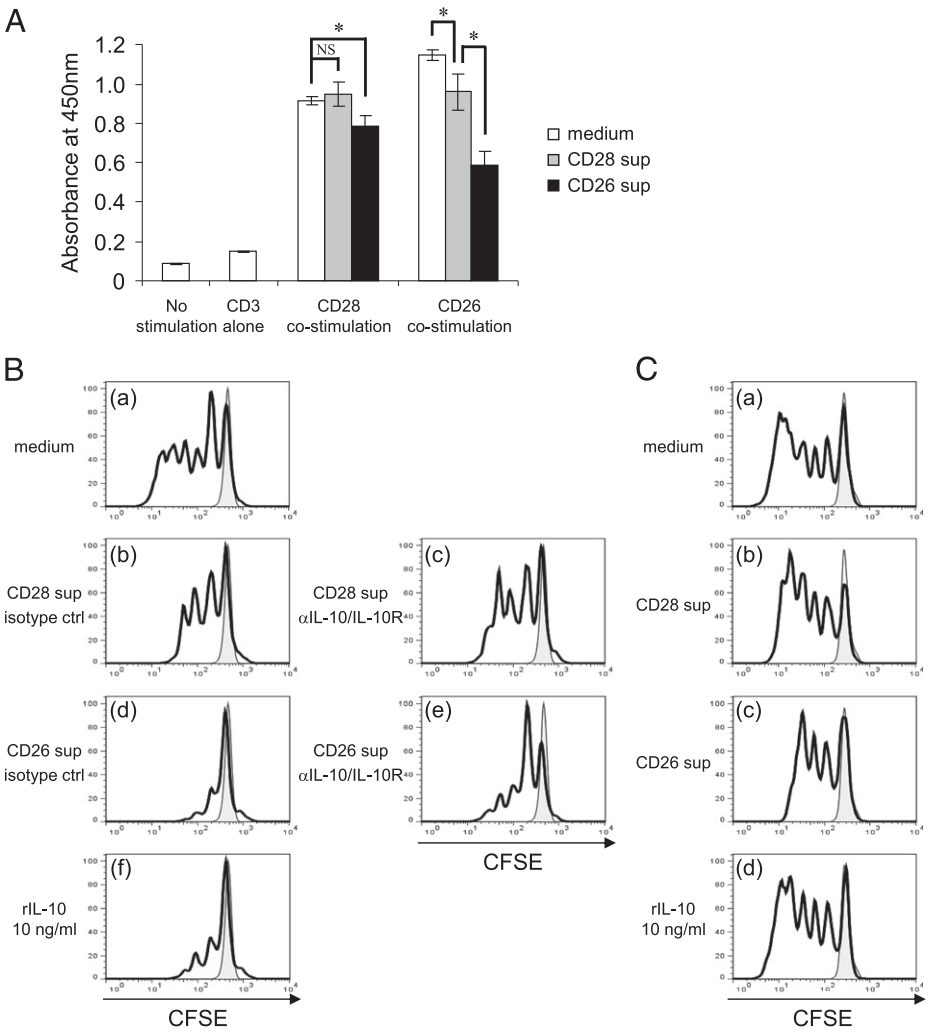

FIGURE 7. Supernatants of CD3/CD26-activated $CD4^+$ T cells significantly suppress the proliferation of bystander T cells through partial dependence on IL-10. Culture supernatants were prepared by the same method as shown in Fig. 6. (**A**) Freshly purified $CD4^+$ T cells were stimulated with anti-CD3 mAb alone, anti-CD3 plus anti-CD28 mAbs (5 μg/ml), or anti-CD3 plus anti-CD26 mAbs (5 μg/ml) for 96 h in the presence of the supernatant (CD28 sup or CD26 sup) or AIM-V medium as a control. Tetrazolium was added for the last 3 h of culture, and the absorbance at 450 nm was measured. Representative data of five independent donors are shown as mean ± SD of triplicate samples, comparing values with culture supernatants to those with control medium ($*p < 0.01$). (**B**) CFSE-labeled freshly purified $CD4^+$ T cells were stimulated with anti-CD3 plus anti-CD26 mAbs (5 μg/ml) in the presence of the supernatant [CD28 sup (**b** and **c**) or CD26 sup (**d** and **e**)] or recombinant human IL-10 (rIL-10, 10 ng/ml) (**f**) or AIM-V medium (**a**) as a control. Prior to the onset of culture, the combination of anti-human IL-10 mAb and anti-human IL-10 receptor mAb (αIL-10/IL-10R) (Bc and e) or isotype control mAbs (isotype ctrl) (Bb and d) were added to the culture wells to give a final concentration of 20 μg/ml each. (**C**) CFSE-labeled freshly purified $CD4^+$ T cells were stimulated with anti-CD3 plus anti-CD28 mAbs (5 μg/ml) in the presence of the supernatant [CD28 sup (**b**) or CD26 sup (**c**)] or recombinant human IL-10 (rIL-10, 10 ng/ml) (**d**) or AIM-V medium (**a**) as a control. After 96 h of incubation, cells were harvested and analyzed by flow cytometry. The data are shown as histograms of CFSE intensity gated for $CD4^+$ T cells and are representative of three independent donors, and similar results were obtained in each experiment. The gray areas in each histogram show the data of T cells cultured for 96 h without any stimulation.

$CD4^+$ T cells. Because CD26, ICOS, and CD46 belong to different families and their downstream signaling events are considered to be different, the combination of these costimulatory pathways may have additive effects on the induction of Tr1 cells. For this purpose, identification of the T cell subsets producing a high level of IL-10 following CD26 costimulation is needed. Because the $CD4^+$ T cells used in this study contained all the T cell subsets such as naive, Th1, Th2, Th17, follicular helper T, or Treg, we conducted costimulation assays following purification of $CD4^+$ naive, memory, or Treg subsets. Although the absolute amount of IL-10 produced by $CD45RO^+$ memory T cells was higher than $CD45RA^+$ naive T cells, both naive and memory $CD4^+$ T cells costimulated through CD26 produced greater levels of IL-10 compared with CD28 costimulation (Supplemental Fig. 3). In contrast, purified $CD4^+CD25^{high}CD127^{low}FOXP3^+$ cells apparently produced a low level of IL-10 following CD26 costimulation compared with other populations of $CD4^+$ T cells (Supplemental Fig. 3). These observations indicate that naturally occurring $CD4^+CD25^{high}CD127^{low}FOXP3^+$ cells are not the source of IL-10 production, and they suggest that the subpopulation included in memory $CD4^+$ T cells is the main source of IL-10, whereas naive $CD4^+$ T cells also produce IL-10 in response to CD26 costimulation. Additionally, in vivo studies focusing on the suppressive activity of this population of in vitro–differentiated $CD4^+$ T cells, or the stability or plasticity of this IL-10–producing phenotype, need to be considered in future work.

CD28 is a representative T cell costimulatory pathway, and the negative feedback mechanism through CTLA-4 is associated with this pathway as a means of controlling excessive T cell activation. CD26 also functions as a costimulatory molecule in human T cells,

and $CD26^+$ T cells have been suggested to be involved in the pathophysiology of various immune disorders such as MS, rheumatoid arthritis, and graft-versus-host disease (8, 10, 12). Our present study shows that stimulation through TCR and high-intensity interaction of caveolin-1–CD26-mediated signaling induces the development of $CD4^+$ T cells to a Tr1-like phenotype. Caveolin-1 is a ubiquitously expressed ligand of CD26 in many cell types such as epithelial cells, endothelial cells, fibroblasts, macrophages, and neutrophils. We have previously shown that caveolin-1 was detected on the cell surface of monocytes 12–24 h after Ag uptake, and that CD26 and caveolin-1 colocalized at the T cell/monocyte contact site (19). Moreover, caveolin-1 expression is regulated by NF-κB, and stimulation with LPS or TNF-α increases the expression of caveolin-1 mRNA and protein (54), suggesting that expression of caveolin-1 may be increased on cells accumulated at sites of inflammation, leading to the transduction of intensive CD26-mediated signaling in $CD26^+$ T cells. Taken together, our data strongly suggest that $CD4^+$ T cells receiving robust caveolin-1–CD26-mediated signaling at the inflammatory site produce a high level of IL-10 and potentially other inhibitory factors to curtail the inflammatory process. Because striking defects in the induction of Tr1 cells through CD46 costimulation have been reported in patients with MS (52), it is conceivable that negative feedback mechanisms for regulating excessive CD26-mediated activation may be impaired in patients with autoimmune diseases, and further research is required to evaluate this hypothesis.

The cytoplasmic domain of CD28 has several common motifs that bind to signaling molecules such as PI3K, growth factor receptor–bound protein 2, or IL-2–inducible T cell kinase, whereas the cytoplasmic tail of CD26 consists of only 6 aa without any conserved kinase or protein-binding motifs (18). We have previously shown that CD26 localizes into lipid rafts, and stimulation with anti-CD3 plus anti-CD26 promotes aggregation of lipid rafts, leading to colocalization of CD45 to TCR signaling molecules such as $p56^{Lck}$, ZAP-70, or TCRζ (30). Our present data strongly suggest that persistent NFAT–AP-1 cooperation is responsible for CD26-mediated T cell activation, and sustained activation of NFAT and ERK1/2 is possibly due to the aggregation of signaling molecules in lipid rafts following CD26-mediated costimulation. Furthermore, we have previously shown that DPPIV enzyme activity is partially involved in the costimulatory activity of CD26 through studies using wild-type CD26 ($DPPIV^+$) or mutant CD26 ($DPPIV^-$)–transfected Jurkat T cell lines (55). Other groups reported that the synthetic competitive DPPIV inhibitor Lys[$Z(NO_2)$] significantly suppressed the proliferation and production of IL-2, IL-10, and IFN-γ in PWM-stimulated human T cells (56). They showed that these DPPIV inhibitors markedly increased the secretion of latent TGF-β1 by PWM-stimulated T cells, resulting in suppression of T cell activation. To further characterize the role of DPPIV enzyme activity in T cell activation, we are now examining the effect of the clinically used DPPIV specific inhibitor sitagliptin. Our preliminary data indicate that sitagliptin strongly suppresses the proliferative activity and production of cytokines including IL-10 of human $CD4^+$ T cells following CD26-mediated costimulation compared with CD28-mediated costimulation (data not shown), with the precise molecular mechanisms involved in this process being currently investigated.

In conclusion, intensive CD26 costimulatory signaling induces the development of $CD4^+$ T cells to a Tr1-like phenotype with a high level of IL-10 production, possibly for regulating potentially excessive CD26-mediated activation. Whether this possible negative feedback mechanism of CD26 costimulation is normally maintained or impaired in patients with autoimmune diseases is the subject of future investigations.

Disclosures

The authors have no financial conflicts of interest.

References

1. Fox, D. A., R. E. Hussey, K. A. Fitzgerald, O. Acuto, C. Poole, L. Palley, J. F. Daley, S. F. Schlossman, and E. L. Reinherz. 1984. Ta1, a novel 105 KD human T cell activation antigen defined by a monoclonal antibody. *J. Immunol.* 133: 1250–1256.
2. Nanus, D. M., D. Engelstein, G. A. Gastl, L. Gluck, M. J. Vidal, M. Morrison, C. L. Finstad, N. H. Bander, and A. P. Albino. 1993. Molecular cloning of the human kidney differentiation antigen gp160: human aminopeptidase A. *Proc. Natl. Acad. Sci. USA* 90: 7069–7073.
3. Tanaka, T., D. Camerini, B. Seed, Y. Torimoto, N. H. Dang, J. Kameoka, H. N. Dahlberg, S. F. Schlossman, and C. Morimoto. 1992. Cloning and functional expression of the T cell activation antigen CD26. *J. Immunol.* 149: 481–486.
4. Morimoto, C., and S. F. Schlossman. 1998. The structure and function of CD26 in the T-cell immune response. *Immunol. Rev.* 161: 55–70.
5. Ohnuma, K., N. H. Dang, and C. Morimoto. 2008. Revisiting an old acquaintance: CD26 and its molecular mechanisms in T cell function. *Trends Immunol.* 29: 295–301.
6. Morimoto, C., Y. Torimoto, G. Levinson, C. E. Rudd, M. Schrieber, N. H. Dang, N. L. Letvin, and S. F. Schlossman. 1989. 1F7, a novel cell surface molecule, involved in helper function of CD4 cells. *J. Immunol.* 143: 3430–3439.
7. Bengsch, B., B. Seigel, T. Flecken, J. Wolanski, H. E. Blum, and R. Thimme. 2012. Human Th17 cells express high levels of enzymatically active dipeptidylpeptidase IV (CD26). *J. Immunol.* 188: 5438–5447.
8. Krakauer, M., P. S. Sorensen, and F. Sellebjerg. 2006. $CD4^+$ memory T cells with high CD26 surface expression are enriched for Th1 markers and correlate with clinical severity of multiple sclerosis. *J. Neuroimmunol.* 181: 157–164.
9. Eguchi, K., Y. Ueki, C. Shimomura, T. Otsubo, H. Nakao, K. Migita, A. Kawakami, M. Matsunaga, H. Tezuka, N. Ishikawa, et al. 1989. Increment in the $Ta1^+$ cells in the peripheral blood and thyroid tissue of patients with Graves' disease. *J. Immunol.* 142: 4233–4240.
10. Ohnuma, K., H. Inoue, M. Uchiyama, T. Yamochi, O. Hosono, N. H. Dang, and C. Morimoto. 2006. T-cell activation via CD26 and caveolin-1 in rheumatoid synovium. *Mod. Rheumatol.* 16: 3–13.
11. Hatano, R., K. Ohnuma, J. Yamamoto, N. H. Dang, and C. Morimoto. 2013. CD26-mediated co-stimulation in human $CD8^+$ T cells provokes effector function via pro-inflammatory cytokine production. *Immunology* 138: 165–172.
12. Hatano, R., K. Ohnuma, J. Yamamoto, N. H. Dang, T. Yamada, and C. Morimoto. 2013. Prevention of acute graft-versus-host disease by humanized anti-CD26 monoclonal antibody. *Br. J. Haematol.* 162: 263–277.
13. Bluestone, J. A. 1995. New perspectives of CD28-B7-mediated T cell costimulation. *Immunity* 2: 555–559.
14. Shahinian, A., K. Pfeffer, K. P. Lee, T. M. Kündig, K. Kishihara, A. Wakeham, K. Kawai, P. S. Ohashi, C. B. Thompson, and T. W. Mak. 1993. Differential T cell costimulatory requirements in CD28-deficient mice. *Science* 261: 609–612.
15. Tivol, E. A., F. Borriello, A. N. Schweitzer, W. P. Lynch, J. A. Bluestone, and A. H. Sharpe. 1995. Loss of CTLA-4 leads to massive lymphoproliferation and fatal multiorgan tissue destruction, revealing a critical negative regulatory role of CTLA-4. *Immunity* 3: 541–547.
16. Waterhouse, P., J. M. Penninger, E. Timms, A. Wakeham, A. Shahinian, K. P. Lee, C. B. Thompson, H. Griesser, and T. W. Mak. 1995. Lymphoproliferative disorders with early lethality in mice deficient in Ctla-4. *Science* 270: 985–988.
17. Stamper, C. C., Y. Zhang, J. F. Tobin, D. V. Erbe, S. Ikemizu, S. J. Davis, M. L. Stahl, J. Seehra, W. S. Somers, and L. Mosyak. 2001. Crystal structure of the B7-1/CTLA-4 complex that inhibits human immune responses. *Nature* 410: 608–611.
18. Rudd, C. E., and H. Schneider. 2003. Unifying concepts in CD28, ICOS and CTLA4 co-receptor signalling. *Nat. Rev. Immunol.* 3: 544–556.
19. Ohnuma, K., T. Yamochi, M. Uchiyama, K. Nishibashi, N. Yoshikawa, N. Shimizu, S. Iwata, H. Tanaka, N. H. Dang, and C. Morimoto. 2004. CD26 up-regulates expression of CD86 on antigen-presenting cells by means of caveolin-1. *Proc. Natl. Acad. Sci. USA* 101: 14186–14191.
20. Ohnuma, K., M. Uchiyama, T. Yamochi, K. Nishibashi, O. Hosono, N. Takahashi, S. Kina, H. Tanaka, X. Lin, N. H. Dang, and C. Morimoto. 2007. Caveolin-1 triggers T-cell activation via CD26 in association with CARMA1. *J. Biol. Chem.* 282: 10117–10131.
21. Stremenová, J., V. Mares, V. Lisá, M. Hilser, E. Krepela, Z. Vanicková, M. Syrucek, O. Soula, and A. Sedo. 2010. Expression of dipeptidyl peptidase-IV activity and/or structure homologs in human meningiomas. *Int. J. Oncol.* 36: 351–358.
22. Nakamura, K., A. Kitani, and W. Strober. 2001. Cell contact-dependent immunosuppression by $CD4^+CD25^+$ regulatory T cells is mediated by cell surface-bound transforming growth factor β. *J. Exp. Med.* 194: 629–644.
23. Collison, L. W., C. J. Workman, T. T. Kuo, K. Boyd, Y. Wang, K. M. Vignali, R. Cross, D. Sehy, R. S. Blumberg, and D. A. Vignali. 2007. The inhibitory cytokine IL-35 contributes to regulatory T-cell function. *Nature* 450: 566–569.
24. Groux, H., A. O'Garra, M. Bigler, M. Rouleau, S. Antonenko, J. E. de Vries, and M. G. Roncarolo. 1997. A $CD4^+$ T-cell subset inhibits antigen-specific T-cell responses and prevents colitis. *Nature* 389: 737–742.
25. Okamura, T., K. Fujio, M. Shibuya, S. Sumitomo, H. Shoda, S. Sakaguchi, and K. Yamamoto. 2009. $CD4^+CD25^-LAG3^+$ regulatory T cells controlled by the transcription factor Egr-2. *Proc. Natl. Acad. Sci. USA* 106: 13974–13979.

26. Huard, B., P. Prigent, F. Pagès, D. Bruniquel, and F. Triebel. 1996. T cell major histocompatibility complex class II molecules down-regulate $CD4^+$ T cell clone responses following LAG-3 binding. *Eur. J. Immunol.* 26: 1180–1186.
27. Maçon-Lemaître, L., and F. Triebel. 2005. The negative regulatory function of the lymphocyte-activation gene-3 co-receptor (CD223) on human T cells. *Immunology* 115: 170–178.
28. Zheng, Y., Y. Zha, G. Driessens, F. Locke, and T. F. Gajewski. 2012. Transcriptional regulator early growth response gene 2 (Egr2) is required for T cell anergy in vitro and in vivo. *J. Exp. Med.* 209: 2157–2163.
29. Hatano, R., T. Yamada, S. Matsuoka, S. Iwata, H. Yamazaki, E. Komiya, T. Okamoto, N. H. Dang, K. Ohnuma, and C. Morimoto. 2014. Establishment of monoclonal anti-human CD26 antibodies suitable for immunostaining of formalin-fixed tissue. *Diagn. Pathol.* 9: 30.
30. Ishii, T., K. Ohnuma, A. Murakami, N. Takasawa, S. Kobayashi, N. H. Dang, S. F. Schlossman, and C. Morimoto. 2001. CD26-mediated signaling for T cell activation occurs in lipid rafts through its association with CD45RO. *Proc. Natl. Acad. Sci. USA* 98: 12138–12143.
31. Jonuleit, H., E. Schmitt, M. Stassen, A. Tuettenberg, J. Knop, and A. H. Enk. 2001. Identification and functional characterization of human $CD4^+CD25^+$ T cells with regulatory properties isolated from peripheral blood. *J. Exp. Med.* 193: 1285–1294.
32. Okamura, T., K. Fujio, S. Sumitomo, and K. Yamamoto. 2012. Roles of LAG3 and EGR2 in regulatory T cells. *Ann. Rheum. Dis.* 71(Suppl. 2): i96–i100.
33. Macian, F. 2005. NFAT proteins: key regulators of T-cell development and function. *Nat. Rev. Immunol.* 5: 472–484.
34. Xu, J., Y. Yang, G. Qiu, G. Lal, Z. Wu, D. E. Levy, J. C. Ochando, J. S. Bromberg, and Y. Ding. 2009. c-Maf regulates IL-10 expression during Th17 polarization. *J. Immunol.* 182: 6226–6236.
35. Ahyi, A. N., H. C. Chang, A. L. Dent, S. L. Nutt, and M. H. Kaplan. 2009. IFN regulatory factor 4 regulates the expression of a subset of Th2 cytokines. *J. Immunol.* 183: 1598–1606.
36. Cretney, E., A. Xin, W. Shi, M. Minnich, F. Masson, M. Miasari, G. T. Belz, G. K. Smyth, M. Busslinger, S. L. Nutt, and A. Kallies. 2011. The transcription factors Blimp-1 and IRF4 jointly control the differentiation and function of effector regulatory T cells. *Nat. Immunol.* 12: 304–311.
37. Shoemaker, J., M. Saraiva, and A. O'Garra. 2006. GATA-3 directly remodels the IL-10 locus independently of IL-4 in $CD4^+$ T cells. *J. Immunol.* 176: 3470–3479.
38. Motomura, Y., H. Kitamura, A. Hijikata, Y. Matsunaga, K. Matsumoto, H. Inoue, K. Atarashi, S. Hori, H. Watarai, J. Zhu, et al. 2011. The transcription factor E4BP4 regulates the production of IL-10 and IL-13 in $CD4^+$ T cells. *Nat. Immunol.* 12: 450–459.
39. Safford, M., S. Collins, M. A. Lutz, A. Allen, C. T. Huang, J. Kowalski, A. Blackford, M. R. Horton, C. Drake, R. H. Schwartz, and J. D. Powell. 2005. Egr-2 and Egr-3 are negative regulators of T cell activation. *Nat. Immunol.* 6: 472–480.
40. Zhu, B., A. L. Symonds, J. E. Martin, D. Kioussis, D. C. Wraith, S. Li, and P. Wang. 2008. Early growth response gene 2 (Egr-2) controls the self-tolerance of T cells and prevents the development of lupuslike autoimmune disease. *J. Exp. Med.* 205: 2295–2307.
41. Sabat, R., G. Grütz, K. Warszawska, S. Kirsch, E. Witte, K. Wolk, and J. Geginat. 2010. Biology of interleukin-10. *Cytokine Growth Factor Rev.* 21: 331–344.
42. Hutloff, A., A. M. Dittrich, K. C. Beier, B. Eljaschewitsch, R. Kraft, I. Anagnostopoulos, and R. A. Kroczek. 1999. ICOS is an inducible T-cell co-stimulator structurally and functionally related to CD28. *Nature* 397: 263–266.
43. Kemper, C., A. C. Chan, J. M. Green, K. A. Brett, K. M. Murphy, and J. P. Atkinson. 2003. Activation of human $CD4^+$ cells with CD3 and CD46 induces a T-regulatory cell 1 phenotype. *Nature* 421: 388–392.
44. Nurieva, R. I., J. Duong, H. Kishikawa, U. Dianzani, J. M. Rojo, Ic. Ho, R. A. Flavell, and C. Dong. 2003. Transcriptional regulation of th2 differentiation by inducible costimulator. *Immunity* 18: 801–811.
45. Cardone, J., G. Le Friec, P. Vantourout, A. Roberts, A. Fuchs, I. Jackson, T. Suddason, G. Lord, J. P. Atkinson, A. Cope, et al. 2010. Complement regulator CD46 temporally regulates cytokine production by conventional and unconventional T cells. *Nat. Immunol.* 11: 862–871.
46. Saraiva, M., J. R. Christensen, M. Veldhoen, T. L. Murphy, K. M. Murphy, and A. O'Garra. 2009. Interleukin-10 production by Th1 cells requires interleukin-12-induced STAT4 transcription factor and ERK MAP kinase activation by high antigen dose. *Immunity* 31: 209–219.
47. Iwasaki, Y., K. Fujio, T. Okamura, A. Yanai, S. Sumitomo, H. Shoda, T. Tamura, H. Yoshida, P. Charnay, and K. Yamamoto. 2013. Egr-2 transcription factor is required for Blimp-1-mediated IL-10 production in IL-27-stimulated $CD4^+$ T cells. *Eur. J. Immunol.* 43: 1063–1073.
48. Chandra, A., S. Lan, J. Zhu, V. A. Siclari, and L. Qin. 2013. Epidermal growth factor receptor (EGFR) signaling promotes proliferation and survival in osteoprogenitors by increasing early growth response 2 (EGR2) expression. *J. Biol. Chem.* 288: 20488–20498.
49. To, S. Q., K. C. Knower, and C. D. Clyne. 2013. NFκB and MAPK signalling pathways mediate TNFα-induced early growth response gene transcription leading to aromatase expression. *Biochem. Biophys. Res. Commun.* 433: 96–101.
50. Kühn, R., J. Löhler, D. Rennick, K. Rajewsky, and W. Müller. 1993. Interleukin-10-deficient mice develop chronic enterocolitis. *Cell* 75: 263–274.
51. Bettelli, E., M. P. Das, E. D. Howard, H. L. Weiner, R. A. Sobel, and V. K. Kuchroo. 1998. IL-10 is critical in the regulation of autoimmune encephalomyelitis as demonstrated by studies of IL-10- and IL-4-deficient and transgenic mice. *J. Immunol.* 161: 3299–3306.
52. Astier, A. L., G. Meiffren, S. Freeman, and D. A. Hafler. 2006. Alterations in CD46-mediated Tr1 regulatory T cells in patients with multiple sclerosis. *J. Clin. Invest.* 116: 3252–3257.
53. Vasanthakumar, A., and A. Kallies. 2013. IL-27 paves different roads to Tr1. *Eur. J. Immunol.* 43: 882–885.
54. Tiruppathi, C., J. Shimizu, K. Miyawaki-Shimizu, S. M. Vogel, A. M. Bair, R. D. Minshall, D. Predescu, and A. B. Malik. 2008. Role of NF-κB-dependent caveolin-1 expression in the mechanism of increased endothelial permeability induced by lipopolysaccharide. *J. Biol. Chem.* 283: 4210–4218.
55. Tanaka, T., J. Kameoka, A. Yaron, S. F. Schlossman, and C. Morimoto. 1993. The costimulatory activity of the CD26 antigen requires dipeptidyl peptidase IV enzymatic activity. *Proc. Natl. Acad. Sci. USA* 90: 4586–4590.
56. Reinhold, D., U. Bank, F. Bühling, U. Lendeckel, J. Faust, K. Neubert, and S. Ansorge. 1997. Inhibitors of dipeptidyl peptidase IV induce secretion of transforming growth factor-β_1 in PWM-stimulated PBMC and T cells. *Immunology* 91: 354–360.

nature medicine

Hair follicle–derived IL-7 and IL-15 mediate skin-resident memory T cell homeostasis and lymphoma

Takeya Adachi[1], Tetsuro Kobayashi[1,2], Eiji Sugihara[3], Taketo Yamada[4,7], Koichi Ikuta[5], Stefania Pittaluga[6], Hideyuki Saya[3], Masayuki Amagai[1] & Keisuke Nagao[1,2]

The skin harbors a variety of resident leukocyte subsets that must be tightly regulated to maintain immune homeostasis. Hair follicles are unique structures in the skin that contribute to skin dendritic cell homeostasis through chemokine production. We demonstrate that CD4$^+$ and CD8$^+$ skin-resident memory T cells (T_{RM} cells), which are responsible for long-term skin immunity, reside predominantly within the hair follicle epithelium of the unperturbed epidermis. T_{RM} cell tropism for the epidermis and follicles is herein termed epidermotropism. Hair follicle expression of IL-15 was required for CD8$^+$ T_{RM} cells, and IL-7 for CD8$^+$ and CD4$^+$ T_{RM} cells, to exert epidermotropism. A lack of either cytokine in the skin led to impaired hapten-induced contact hypersensitivity responses. In a model of cutaneous T cell lymphoma, epidermotropic CD4$^+$ T_{RM} lymphoma cell localization depended on the presence of hair follicle–derived IL-7. These findings implicate hair follicle–derived cytokines as regulators of malignant and non-malignant T_{RM} cell tissue residence, and they suggest that the cytokines may be targeted therapeutically in inflammatory skin diseases and lymphoma.

Hair follicles are unique structures in the mammalian skin that provide a niche for keratinocyte and melanocyte stem cells[1,2]. Various leukocyte subsets localize to hair follicles[3]. We recently demonstrated that hair follicles recruit skin dendritic cells to sites of minor trauma[4]. Keratinocytes in the hair follicle infundibulum and isthmus produce the chemokines CCL2 and CCL20, recruiting myeloid cells after experiencing physical perturbation. A subset of keratinocytes in the suprabasal layer of the follicular bulge region express another chemokine, CCL8, which prevents local Langerhans cell (LC) accumulation, a mechanism that may protect bulge stem cells from excessive leukocyte infiltration[4]. These data establish that hair follicles actively promote immune homeostasis.

T cells that reside in peripheral tissues have been described in recent years, and their importance is now well established[5–9]. Skin-resident T_{RM} cells display an effector memory phenotype, and are generated after immunological insults such as viral infection[6,8]. In the context of infection, CD4$^+$ memory T cells accumulate primarily in the dermis, whereas CD8$^+$ T_{RM} cells accumulate within the epidermis[7]. Both T cell subsets exhibited tropism to the hair follicles[7]. Skin T_{RM} cells express CD69 and CD103 (ref. 10). CD69 suppresses sphingosine-1-phosphate receptor 1 expression, which prevents T cells from emigrating from lymphoid organs or other tissues into circulation[11,12]. CD103-mediated retention of T cells in the skin probably occurs by adhesion to E-cadherin[13]. The non-migratory nature of CD8$^+$ T_{RM} cells has been established in parabiotic mice[8], and CD4$^+$ T_{RM} cells in human skin have been engrafted onto immunodeficient mice[14].

Infiltration of T cells into the epidermis is a prominent feature in both inflammatory and neoplastic human diseases, including graft-versus-host disease, drug eruptions and cutaneous T cell lymphoma (CTCL). In fixed drug eruption, CD8$^+$ T cells attack the epidermis to cause keratinocyte cell death in the presence of the drug(s)[15]. After clinical resolution, CD8$^+$ T cells with a memory phenotype persist within the epidermis[15,16]. The majority of CTCL is caused by CD4$^+$ lymphoma cells[17]. In the classic form—mycosis fungoides—lymphoma cells with a T_{RM} cell phenotype infiltrate the epidermis, including the follicular epithelium[18,19], and they slowly accumulate and proliferate to form tumors. Such epidermis- and follicle-infiltrating T cells are termed epidermotropic T cells[20].

Given the importance of T_{RM} cells in conferring long-term immunological memory[6,8] and regulatory functions that maintain immunological homeostasis[13,21,22], elucidation of mechanisms that support long-term persistence in the skin may provide insight into T cell homeostasis in health and disease. Here we demonstrate that the epidermotropism of T_{RM} cells is supported by the hair follicle–derived cytokines IL-7 and IL-15.

RESULTS

CD4$^+$ and CD8$^+$ T cells in steady-state epidermis

To characterize T_{RM} cells in the epidermis, we prepared vertical sections of frozen skin samples taken from unmanipulated adult C57BL/6J mice, and then visualized CD4$^+$ and CD8$^+$ T cells

[1]Department of Dermatology, Keio University School of Medicine, Tokyo, Japan. [2]Dermatology Branch, Center for Cancer Research, National Cancer Institute, National Institutes of Health, Bethesda, Maryland, USA. [3]Division of Gene Regulation, Institute for Advanced Medical Research, Keio University School of Medicine, Tokyo, Japan. [4]Department of Pathology, Keio University School of Medicine, Tokyo, Japan. [5]Laboratory of Biological Protection, Department of Biological Responses, Institute for Virus Research, Kyoto University, Kyoto, Japan. [6]Laboratory of Pathology, Center for Cancer Research, National Cancer Institute, National Institutes of Health, Bethesda, Maryland, USA. [7]Present address: Department of Pathology, Saitama Medical University School of Medicine, Saitama, Japan. Correspondence should be addressed to K.N. (keisuke.nagao@nih.gov).

Received 2 July; accepted 2 September; published online 19 October 2015; doi:10.1038/nm.3962

using immunofluorescence microscopy. We routinely observed small numbers of both CD4$^+$ and CD8$^+$ T cells in the follicular epithelium (**Fig. 1a**). Visualization of the basement membrane using integrin α_6 staining confirmed that both CD4$^+$ and CD8$^+$ T cells resided within the follicular epithelium (**Supplementary Fig. 1a**). Staining epidermal sheets revealed that CD8$^+$ T cells were present both in hair follicles and in the interfollicular epidermis, whereas CD4$^+$ T cells were localized exclusively around hair follicles (**Supplementary Fig. 1b**). In flow cytometry analysis of epidermal cell suspensions, exclusion of LCs and dendritic epidermal T cells enabled the identification of small numbers of CD4$^+$ and CD8$^+$ T cells, consistent with the immunofluorescence microscopy results (**Fig. 1b**). The number of CD4$^+$ T cells in the epidermis was comparable to that in the dermis (**Fig. 1c**). CD8$^+$ T cells were found exclusively in epidermal cell suspensions (**Fig. 1c**)[7]. Contamination of the epidermal preparation with dermal leukocytes and vice versa seemed unlikely (**Supplementary Fig. 1c,d**).

Phenotypic analysis suggests that most of these CD4$^+$ and CD8$^+$ T cells are effector memory T cells, as assessed by their cell surface expression of CD44 and CD62L, and they are resident cells, as suggested by CD103 and CD69 co-expression (**Fig. 1d**). CD4$^+$ T cells in the epidermis expressed slightly lower levels of CD103 than did those in the dermis (**Fig. 1e**). Furthermore, the epidermis contained fewer CD4$^+$ FoxP3$^+$ regulatory T_{RM} cells than did the dermis (**Fig. 1f**), suggesting that the organization of CD4$^+$ T_{RM} cells in the two skin compartments may be differentially regulated. Hereafter, memory T cells that reside in the epidermis and the follicles will be referred to as epidermotropic T_{RM} cells, not to indicate their entity as a distinct T cell subset, but solely to describe their localization in the skin.

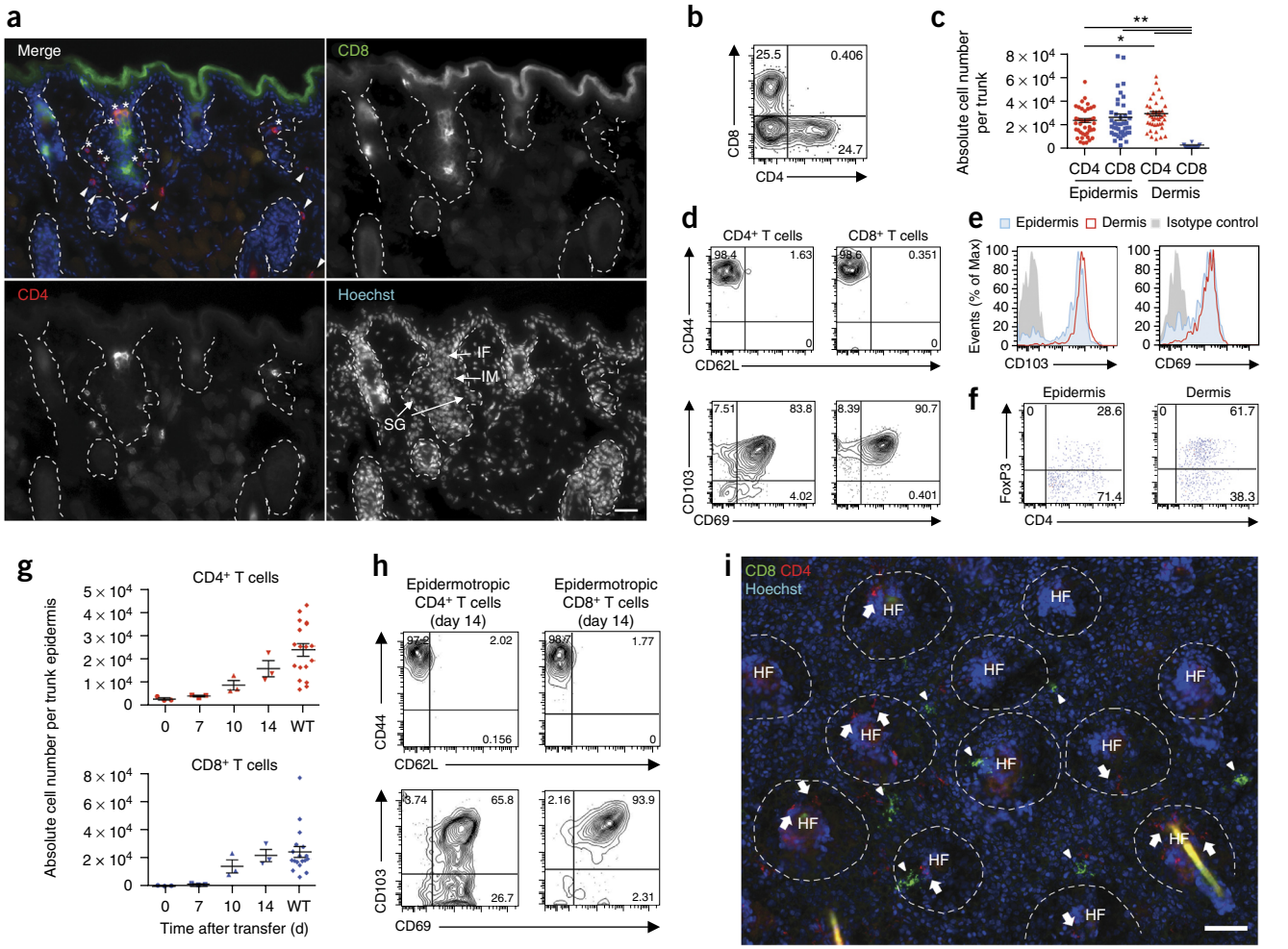

Figure 1 Epidermotropic CD4$^+$ and CD8$^+$ T_{RM} cells associate with hair follicles. (**a**) Skin sections from wild-type (WT) mice, stained as indicated. Dotted lines delineate hair follicles. Asterisks and arrowheads depict CD4$^+$ T cells in epidermis and dermis, respectively. Scale bar, 50 µm. IF: infundibulum, IM: isthmus, SG: sebaceous glands. (**b**) Flow cytometry analysis of CD45$^+$CD3$^+$MHCII (class II MHC)$^-$TCR (T cell receptor) γδ$^-$ epidermal cells from WT mice. Numbers represent frequencies (%) of gated subsets among the analyzed population. (**c**) T cell numbers in the epidermis and dermis. $^*P < 0.05$, $^{**}P < 0.01$ (unpaired two-tailed Student's *t*-test). (**d**) CD44 and CD62L, and CD103 and CD69 expression on T cells in the epidermis. (**e**) CD103 and CD69 expression levels on CD4$^+$ T cells in the epidermis (blue) and dermis (red) with isotype controls (gray). (**f**) Frequency of CD4$^+$FoxP3$^+$ T_{reg} cells in the epidermis and dermis. (**g**) Number of donor T cells in *Rag2*$^{-/-}$ recipient epidermis monitored by flow cytometry at the indicated dates after adoptive transfer of WT splenocytes. (**h**) Epidermotropic T cells from **g** were analyzed using flow cytometry as in **d**, 14 d after transfer. (**i**) Epidermal sheets of a mouse from **g**, day 14 after transfer, were stained as indicated. Dashed lines delineate hair follicles (HF), arrows and arrowheads indicate CD4$^+$ and CD8$^+$ T cells, respectively. Scale bar, 100 µm. Data are from one experiment representative of three independent experiments with three mice per group (**a**,**b**,**d**–**i**), or from ten independent experiments with a total of 42 mice (**c**). Each symbol represents an individual mouse; horizontal lines depict the mean; error bars indicate s.e.m. (**c**,**g**).

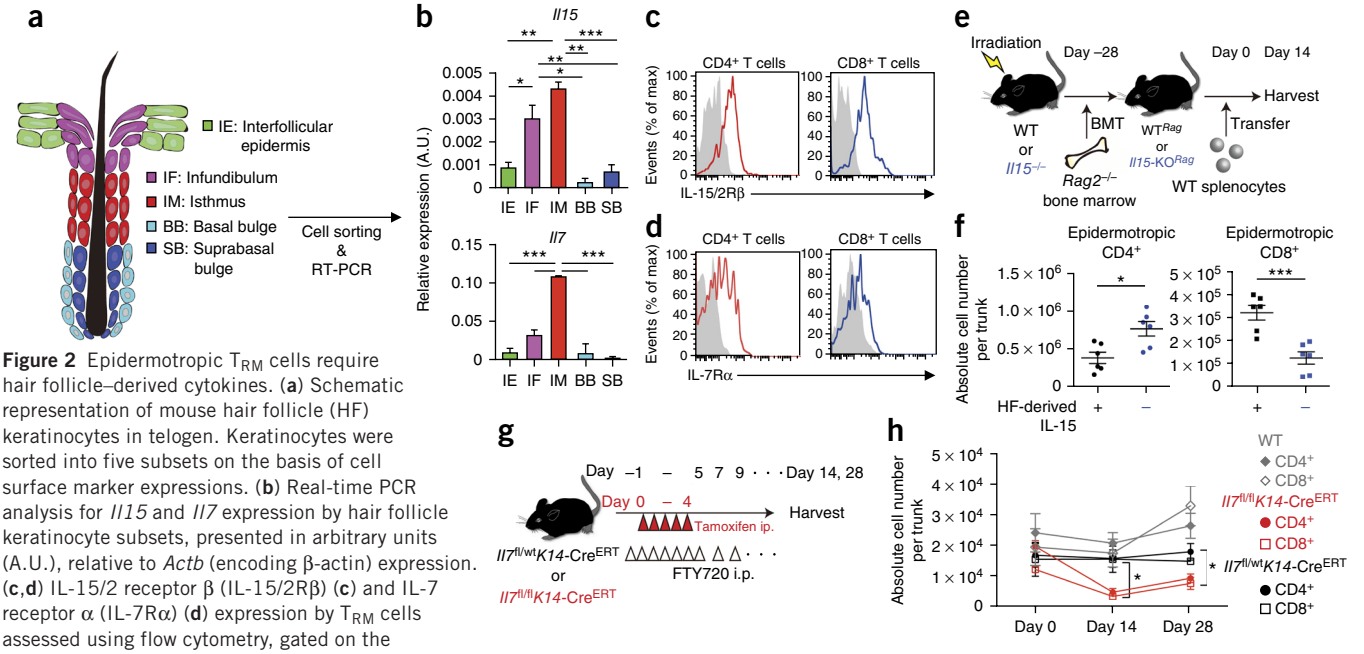

Figure 2 Epidermotropic T_{RM} cells require hair follicle–derived cytokines. (**a**) Schematic representation of mouse hair follicle (HF) keratinocytes in telogen. Keratinocytes were sorted into five subsets on the basis of cell surface marker expressions. (**b**) Real-time PCR analysis for *Il15* and *Il7* expression by hair follicle keratinocyte subsets, presented in arbitrary units (A.U.), relative to *Actb* (encoding β-actin) expression. (**c**,**d**) IL-15/2 receptor β (IL-15/2Rβ) (**c**) and IL-7 receptor α (IL-7Rα) (**d**) expression by T_{RM} cells assessed using flow cytometry, gated on the $CD45^+CD3^+MHCII^-TCR\gamma\delta^-$ population ($n = 3$). (**e**) Experimental scheme for the analysis of T_{RM} cell dependence on hair follicle–derived IL-15. Wild-type (WT) or *Il15*$^{-/-}$ mice were reconstituted with *Rag2*$^{-/-}$ bone marrow (WT^{Rag} or *Il15*-KO^{Rag}), and were adoptively transferred with WT splenocytes. BMT: bone marrow transplantation. (**f**) Epidermotropic T_{RM} cell numbers in recipient WT^{Rag} or *Il15*-KO^{Rag} mice ($n = 6$). Symbols represent individual mice. (**g**) Experimental scheme for analyzing T_{RM} cell dependence on hair follicle–derived IL-7. Indicated mice were treated with tamoxifen intraperitoneally (i.p.) on days 0–4. FTY720 was injected i.p. from day –1 for 7 consecutive days and every other day thereafter, until the time of tissue harvest. (**h**) Epidermotropic T_{RM} cell numbers after tamoxifen-induced ablation of hair follicle IL-7 ($n = 3$). Data are representative of three (**b–d**) or two (**f**,**h**) independent experiments. $^*P < 0.05$, $^{**}P < 0.01$, $^{***}P < 0.001$ (unpaired two-tailed Student's *t*-test). Horizontal lines depict the mean, and error bars indicate s.e.m. in all graphs.

T_{RM} cells associate with hair follicles during epidermal entry

T_{RM} cells are generated during skin infection and accumulate not only at sites of primary inoculation, but also at distant sites[8,23]. To model this distribution of T_{RM} cells, we adoptively transferred wild-type (WT) splenocytes into *Rag2*$^{-/-}$ mice, which lack lymphocytes. After being transferred into a lymphopenic environment, donor T cells undergo homeostatic proliferation, and we hypothesized that such T cells might distribute to peripheral tissues such as the epidermis and skin. Indeed, $CD4^+$ and $CD8^+$ T cells appeared in the epidermis of *Rag2*$^{-/-}$ recipients 10 d after transfer, and by day 14, their numbers had reached levels detectable in WT mice (**Fig. 1g**). Donor T cells displayed effector memory and resident cell phenotypes (**Fig. 1h**), and thus represent epidermotropic T_{RM} cells.

Visualization of $CD4^+$ and $CD8^+$ T_{RM} cells during active epidermal repopulation revealed close association with hair follicles (**Fig. 1i**). $CD4^+$ T_{RM} cells initially appeared within the dermis, accumulated around hair follicles in frozen sections on day 7 after transfer, and then distributed within the epidermis and dermis thereafter (**Supplementary Fig. 1e**). In contrast to $CD4^+$ T_{RM} cells, $CD8^+$ T_{RM} cells appeared directly within the interfollicular epidermis, and then accumulated around the hair follicles (**Supplementary Fig. 1e,f**). Thus, the anatomical modes of entry for $CD4^+$ and $CD8^+$ T_{RM} cells seem to be distinct.

Hair follicle keratinocytes express *Il15* and *Il7*

IL-15 and IL-7 are important cytokines that enable the generation and maintenance of memory T cells[24,25]. Our previous study[4] revealed that hair follicle keratinocyte subsets exhibit distinct chemokine expression profiles. To determine whether hair follicle keratinocytes expressed mRNA encoding IL-15 and IL-7, we sorted epidermal keratinocytes into those from the interfollicular epidermis, infundibulum, isthmus, basal layer bulge or suprabasal layer bulge[4] (**Fig. 2a**). Similarly to previously described patterns of chemokine expression[4], real-time PCR analysis revealed that both *Il15* and *Il7* mRNA were predominantly expressed by keratinocytes in the infundibulum and isthmus (**Fig. 2b**). Because most of the mouse pelage hair follicles are in telogen, we studied the vibrissae to determine whether cytokines were expressed during anagen. The transient portions of anagen hair follicles did not express *Il7*, but the bulb expressed low levels of *Il15* (**Supplementary Fig. 2a**). We also analyzed cytokine mRNA expression in major leukocyte subsets in the epidermis and found that LCs, but not dendritic epidermal T cells, expressed *Il15* (**Supplementary Fig. 2b**). Both leukocyte subsets lacked *Il7* expression (data not shown).

Epidermotropic T_{RM} cells require hair follicle–derived cytokines

Analysis of $CD4^+$ and $CD8^+$ T_{RM} cells using flow cytometry revealed that both T cell subsets expressed IL-15/2Rβ and IL-7Rα (**Fig. 2c,d**). Given the unavailability of an animal model enabling conditional ablation of IL-15, we generated bone marrow (BM) chimeric mice to determine whether epidermotropic T_{RM} cells were influenced by hair follicle–derived cytokines. Reconstitution of WT or *Il15*$^{-/-}$ mice with BM from *Rag2*$^{-/-}$ mice led to the generation of lymphopenic mice that either expressed (WT^{Rag}) or lacked (*Il15*-knockout(KO)^{Rag}) IL-15 in peripheral tissues, including the skin (**Fig. 2e**). We then transferred WT splenocytes into these BM chimeric mice and analyzed the numbers of epidermotropic T_{RM} cells at day 14 after the transfer (**Fig. 2e**). The numbers of epidermotropic $CD4^+$ T_{RM} cells had slightly increased in recipient *Il15*-KO^{Rag} mice, whereas epidermotropic $CD8^+$ T_{RM} numbers had been reduced (**Fig. 2f**). The numbers of $CD4^+$ and

CD8$^+$ T cells in the spleen were comparable in recipient *Il15*-KO^{Rag} and WT^{Rag} mice (**Supplementary Fig. 2c**), indicating that the difference in the numbers of epidermotropic CD8$^+$ T_{RM} cells was due to the loss of IL-15 in the skin. The numbers of epidermotropic CD8$^+$ T_{RM} cells were tenfold higher than those of unmanipulated WT mice. Upregulation of IL-15 mRNA expression in keratinocytes in lethally irradiated mice may have contributed to the enhanced population of CD8$^+$ T_{RM} cells in the epidermis (**Supplementary Fig. 2d**).

Because LCs also expressed *Il15* mRNA, we studied the effect of LC depletion on epidermotropic T_{RM} cells using two different models. Neither constitutive loss nor depletion of LCs affected the numbers of epidermotropic T_{RM} cells (**Supplementary Fig. 3a–c**). Thus, hair follicle–derived IL-15 is crucial for the maintenance of epidermotropic CD8$^+$ T_{RM} cells.

A different approach was taken to evaluate the contribution of hair follicle–derived IL-7, because T cells failed to undergo homeostatic proliferation when transferred into *Il7*-KO^{Rag} mice (data not shown). We crossed *K14*-Cre^{ERT} mice[26] with *Il7*-floxed mice to generate mice in which ablation of IL-7 in the epidermis could be specifically induced in the skin of adult mice by administering tamoxifen injections (**Supplementary Fig. 2e**). Because of the potential for a continuous influx of newly generated T_{RM} cells, which could alter total cell numbers during and after IL-7 ablation, we treated mice with FTY720, a sphingosine-1-phosphate receptor 1 inhibitor that inhibits lymphocyte egress from lymph nodes, thereby preventing the influx of endogenous T_{RM} cells into the epidermis (**Fig. 2g**). Epidermal ablation of IL-7 reduced the numbers of both CD4$^+$ and CD8$^+$ T_{RM} cells 14 d after the loss of IL-7, an effect that persisted for at least 28 d (**Fig. 2h**). The numbers of splenic T cells remained unaffected by the loss of IL-7 in the skin (**Supplementary Fig. 2f**). Therefore, hair follicle–derived IL-7 is required for both CD4$^+$ and CD8$^+$ T_{RM} cells to persist in the epidermis.

Impaired contact hypersensitivity responses in the absence of IL-7 and IL-15

Impaired anatomical localization of T_{RM} cells during the steady state in the absence of hair follicle–derived IL-15 and IL-7 might affect subsequent immune responses in the skin. To address this, we induced contact hypersensitivity (CHS) with a hapten in mice that lacked hair follicle–derived cytokines. To analyze the effect of IL-15 deficiency in the context of CD8$^+$ T_{RM} cells, we generated WT^{Rag} and *Il15*-KO^{Rag} mice using BM transplantation (**Fig. 2e**). These BM chimeric mice were injected with CD8$^+$ T cells obtained from skin-draining lymph nodes of 1-fluoro-2,4-dinitrobenzene (DNFB)-sensitized mice (**Fig. 3a**). Transferred CD8$^+$ T cells are expected to undergo homeostatic proliferation and distribute to peripheral tissues, including the skin, in WT^{Rag}, but not in *Il15*-KO^{Rag} mice (**Figs. 1g** and **2f**). Recipient mice were then challenged with DNFB, and ear-swelling responses were monitored. Both ear swelling and lymphocytic infiltration were reduced in the absence of tissue-derived IL-15 (**Fig. 3b**,**c**).

The roles of hair follicle–derived IL-7 and T_{RM} cells were assessed in the context of CD4$^+$ T cell–mediated CHS. To generate lymphopenic mice that constitutively lack IL-7 in the epidermis, *K5*-Cre mice and *Il7*-floxed mice[27] were each crossed to the *Rag2*$^{-/-}$ background (*Il7*$^{fl/fl}$*K5*-Cre × *Rag2*$^{-/-}$ mice). CD4$^+$ T cells isolated from skin-draining lymph nodes of DNFB-sensitized WT mice were transferred into *Il7*$^{fl/fl}$*K5*-Cre × *Rag2*$^{-/-}$ mice or control *Rag2*$^{-/-}$ mice. Recipient mice were challenged with DNFB 14 d after transfer, and ear-swelling responses were assessed (**Fig. 3d**). Ear swelling and

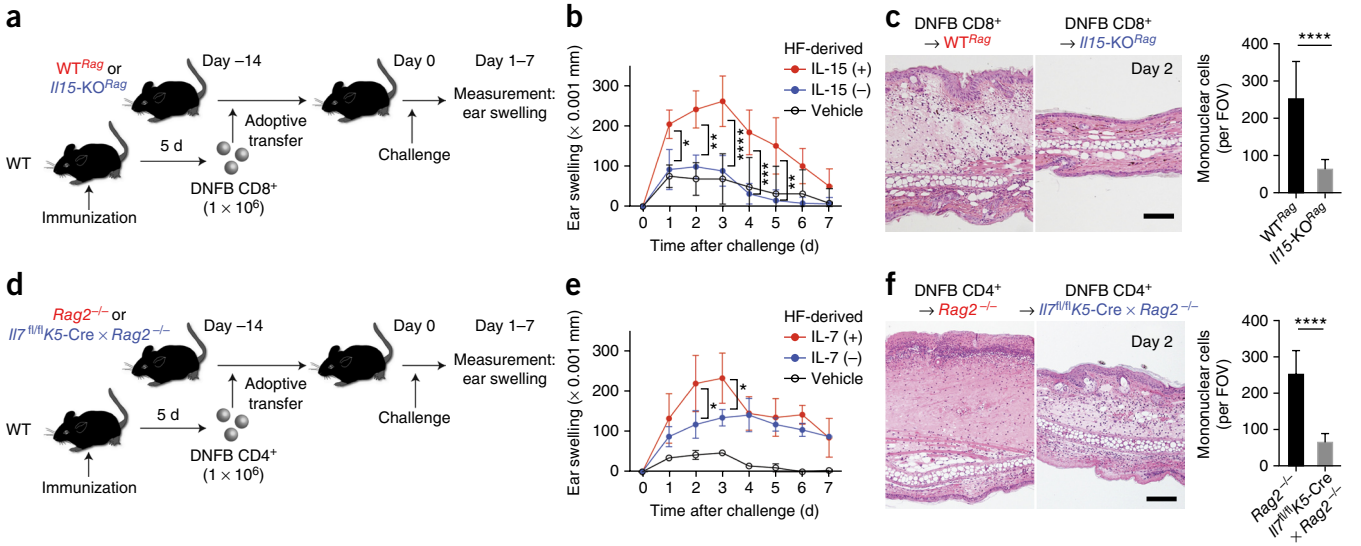

Figure 3 Impaired CHS responses in the absence of hair follicle–derived cytokines. (**a**) Experimental scheme for the analysis of CD8$^+$ T_{RM} cell–mediated CHS in the absence of peripheral tissue (hair follicle)-derived IL-15. CD8$^+$ T cells from DNFB (DNFB CD8$^+$) or vehicle-immunized (vehicle CD8$^+$) WT mice were transferred into indicated lymphopenic mice. 14 d later, recipients were challenged with DNFB on their ears, and ear-swelling responses were measured. (**b**) Ear thickness (Δmm) of DNFB CD8$^+$-transferred WT^{Rag} (red), *Il15*-KO^{Rag} (blue) and vehicle CD8$^+$-transferred WT^{Rag} (black) ($n = 3$). (**c**) H&E staining of ear sections from indicated mice, day 2 after challenge and quantification of skin-infiltrating mononuclear cells. (**d**) Experimental scheme for analyzing CD4$^+$ T_{RM} cell–mediated CHS in the absence of hair follicle–derived IL-7. DNFB CD4$^+$ or vehicle CD4$^+$ were adoptively transferred into indicated lymphopenic mice. (**e**) Ear thickness (Δmm) of DNFB CD4$^+$-transferred *Rag2*$^{-/-}$ (red), *Il7*$^{fl/fl}$*K5*-Cre × *Rag2*$^{-/-}$ (blue) or vehicle CD4$^+$-transferred *Rag2*$^{-/-}$ (black) ($n = 3$). (**f**) H&E staining of ear sections from indicated mice, day 2 after challenge and quantification of skin-infiltrating mononuclear cells. Data are from one experiment, representative of two independent experiments with three mice per group in each (**b**,**c**,**e**,**f**). Cell counts represent pools of three fields of view per section (original magnification: 100×) from three mice per group (**c**,**f**). Scale bars, 100 μm (**c**,**f**). $^*P < 0.05$, $^{**}P < 0.01$, $^{***}P < 0.001$, $^{****}P < 0.0001$ (two-way ANOVA). Error bars are s.e.m.

lymphocytic infiltration were both reduced in *Il7*$^{fl/fl}$*K5*-Cre × *Rag2*$^{-/-}$ mice on days 2 and 3 after the challenge (**Fig. 3e,f**). This transient effect might reflect the generation and influx of newly generated recipient T_{RM} cells after DNFB challenge.

A CD4+ T cell lymphoma model with skin involvement

Epidermotropism of T cells is a histological hallmark in human CTCL. In particular, lymphoma cells in mycosis fungoides exhibit a T_{RM} cell phenotype[18,19,28]. *IL7* expression is increased in CTCL skin[29]. Whether lymphoma cells also require hair follicle–derived cytokines remains unclear. Thus, we extended our T_{RM} cell repopulation model in *Rag2*$^{-/-}$ mice by generating a novel lymphoma model.

Mutations in, or upregulation of, the oncogene *MYC*[30,31], as well as mutations in the tumor-suppressor gene *INK4A/ARF* (officially known as *CDKN2A*), have been implicated[17,30] in human lymphoma and CTCL. *Cdkn2a*$^{-/-}$ mice are prone to tumor development, including T cell lymphoma[32,33]. *Cdkn2a*$^{-/-}$ progenitor B cells transduced with *Myc* generate B cell lymphoma[34]. Taking advantage of these previous findings, we isolated CD4+ T cells from *Cdkn2a*$^{-/-}$ mice and retrovirally transduced them with *Myc* (**Fig. 4a**). Approximately 50% of T cells were transduced, as determined by GFP expression (*Myc*$^{+}$*Cdkn2a*$^{-/-}$ CD4+ T cells) (**Fig. 4b**). Recipient *Rag2*$^{-/-}$ mice developed erythroderma (redness and fine scaling of the entire skin surface) approximately 3 weeks after the transfer of *Myc*$^{+}$*Cdkn2a*$^{-/-}$ CD4+ T cells (**Fig. 4c**). Flow cytometry analysis revealed increased numbers of epidermotropic CD4+ T cells in *Rag2*$^{-/-}$ mice that had been transferred with *Myc*$^{+}$*Cdkn2a*$^{-/-}$ CD4+ T cells as compared to those transferred with WT CD4+ T cells (**Fig. 4d**). The majority of epidermotropic CD4+ T cells in *Myc*$^{+}$*Cdkn2a*$^{-/-}$ CD4+ T cell–transferred mice expressed *Myc*-GFP (**Fig. 4e**) with increased IL-7Rα expression (**Fig. 4e**).

Histology revealed epidermotropism of lymphocytes with large, atypical nuclei, recapitulating that of human CTCL (**Fig. 4f**)[17]. Consistently, flow cytometry analysis revealed that *Myc*$^{+}$*Cdkn2a*$^{-/-}$ CD4+ T cells were enlarged in size (**Fig. 4g**). Infiltrating lymphocytes expressed K_i-67, demonstrating that they were proliferative (**Fig. 4h**). Epidermotropic CD4+ T cells were of the T_{RM} cell phenotype (**Fig. 4i**), and they accumulated around the hair follicles (**Fig. 4f,j**). Collectively, *Myc*$^{+}$*Cdkn2a*$^{-/-}$ CD4+ T cells that had been transferred into *Rag2*$^{-/-}$ mice infiltrated the skin and epidermis, exhibiting histologic features of human CTCL. These mice also exhibited lymphoma in the lymph nodes and spleen, and they died within 10 weeks after transfer (**Supplementary Fig. 4**), thereby also recapitulating an aspect of Sezary's syndrome, a leukemic subtype of CTCL[30].

Epidermotropism in CTCL depends on IL-7

To determine whether CD4+ lymphoma cells also relied on hair follicle–derived IL-7, we transferred *Myc*$^{+}$*Cdkn2a*$^{-/-}$ CD4+ T cells into *Rag2*$^{-/-}$ or *Il7*$^{fl/fl}$*K5*-Cre × *Rag2*$^{-/-}$ mice (**Fig. 5a**). In contrast to *Rag2*$^{-/-}$ mice, *Il7*$^{fl/fl}$*K5*-Cre × *Rag2*$^{-/-}$ mice did not develop erythroderma (**Fig. 5b**). Furthermore, the absolute numbers of epidermotropic lymphoma cells were reduced in the absence of hair follicle–derived IL-7 (**Fig. 5c**), whereas significant differences were not observed in the lymph nodes and spleen (**Fig. 5d**). Histologic analysis of control *Rag2*$^{-/-}$ mice revealed abundant epidermotropic

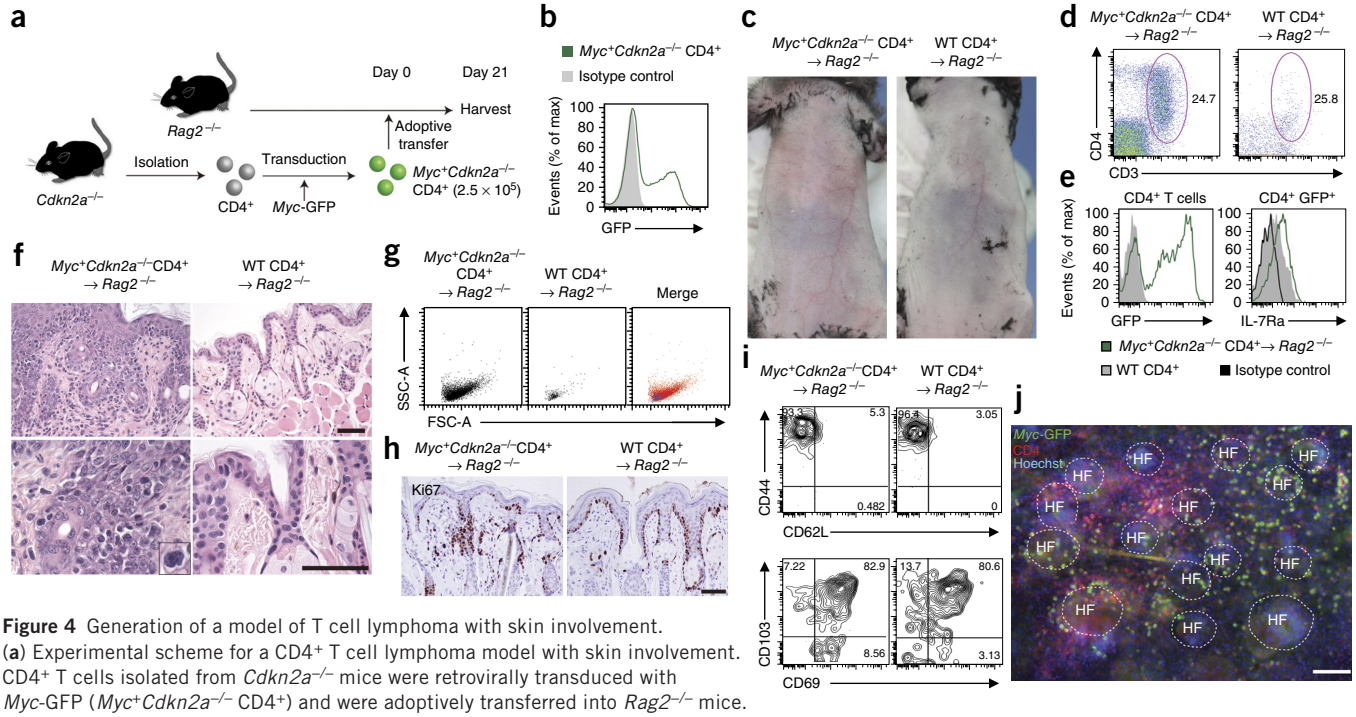

Figure 4 Generation of a model of T cell lymphoma with skin involvement. (**a**) Experimental scheme for a CD4+ T cell lymphoma model with skin involvement. CD4+ T cells isolated from *Cdkn2a*$^{-/-}$ mice were retrovirally transduced with *Myc*-GFP (*Myc*$^{+}$*Cdkn2a*$^{-/-}$ CD4+) and were adoptively transferred into *Rag2*$^{-/-}$ mice. (**b**) Flow cytometry analysis of *Myc*-GFP expression on *Myc*$^{+}$*Cdkn2a*$^{-/-}$ CD4+ T cells before transfer. (**c**) Skin phenotype of *Myc*$^{+}$*Cdkn2a*$^{-/-}$ CD4+-transferred (left) or wild-type (WT) CD4+-transferred *Rag2*$^{-/-}$ mice (right). (**d**) Flow cytometry analysis of CD3+CD4+ epidermotropic cells in recipient mice, as indicated by the purple gate. CD45+MHCII−TCRγδ− cells are shown. (**e**) Expression of GFP and IL-7Rα on cells within the purple gate in **d**. (**f**) H&E staining of skin sections from indicated mice. (**g**) Forward scatter (FSC) and side scatter (SSC) profiles of cells within the purple gate in **d**. (**h**) immunohistochemical staining for K_i-67. (**i**) CD44 versus CD62L, and CD103 versus CD69 expression on CD45+MHCII−TCRγδ− CD3+CD4+GFP+ cells (left panels) or CD45+MHCII−TCRγδ− CD3+CD4+ cells (right panels). (**j**) Immunofluorescence microscopy of epidermal sheets, visualized for *Myc*-GFP, CD4 and Hoechst. Dashed lines delineate the hair follicles (HF). Scale bar, 100 μm (**f**,**h**,**j**). All data are from one experiment representative of three independent experiments with three mice per group in each.

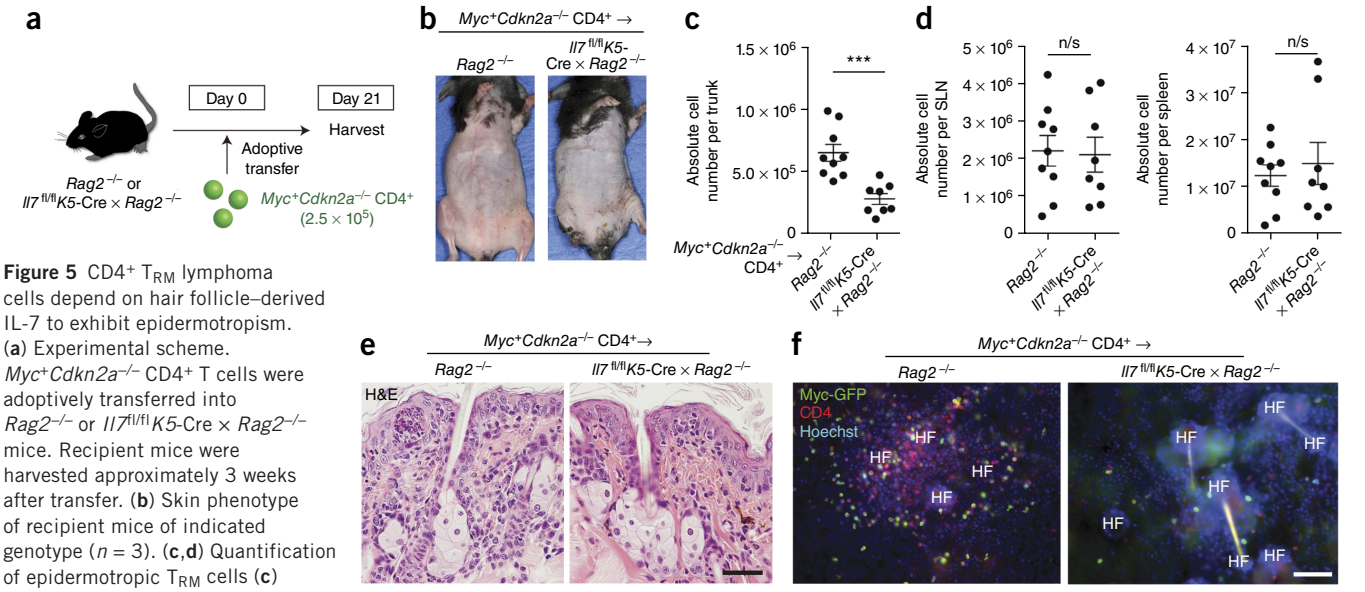

Figure 5 CD4$^+$ T_{RM} lymphoma cells depend on hair follicle–derived IL-7 to exhibit epidermotropism. (**a**) Experimental scheme. *Myc*$^+$*Cdkn2a*$^{-/-}$ CD4$^+$ T cells were adoptively transferred into *Rag2*$^{-/-}$ or *Il7*$^{fl/fl}$*K5*-Cre × *Rag2*$^{-/-}$ mice. Recipient mice were harvested approximately 3 weeks after transfer. (**b**) Skin phenotype of recipient mice of indicated genotype ($n = 3$). (**c**,**d**) Quantification of epidermotropic T_{RM} cells (**c**) or T cells in skin-draining LNs (SLN) and spleen (**d**), assessed on day 21 after adoptive transfer ($n = 9$ for *Rag2*$^{-/-}$ or $n = 8$ for *Il7*$^{fl/fl}$*K5*-Cre × Rag2$^{-/-}$ mice). $^{***}P < 0.001$ (unpaired two-tailed Student's *t*-test). Each symbol represents an individual mouse; horizontal lines depict the mean; error bars indicate s.e.m. (**c**,**d**). (**e**) Histology of skin sections from indicated mice, stained for H&E. (**f**) Immunofluorescence microscopy of ear epidermal sheets of indicated mice, visualized for *Myc*-GFP, CD4 and Hoechst, assessed on day 21 after adoptive transfer ($n = 3$). HF: hair follicles. Scale bars, 100 μm (**e**,**f**). Data are from one experiment representative of three independent experiments with two to three mice per group in each (**b**,**e**,**f**) or an accumulation of three independent experiments (**c**,**d**).

lymphocytes with epidermal thickening, but histological changes were minimal in *Il7*$^{fl/fl}$*K5*-Cre × *Rag2*$^{-/-}$ mice (**Fig. 5e**). Visualization of CD4$^+$ T cells in epidermal sheets confirmed these findings (**Fig. 5f**). Thus, epidermotropic CD4$^+$ T_{RM} cells continued to require hair follicle–derived IL-7 after neoplastic transformation.

In CTCL, IL-7 is upregulated in human hair follicles

To examine whether our findings could be extended to humans, we studied human hair follicles. Whereas hair follicles in the trunk skin of mice and humans are mostly found in telogen, the majority of those in human scalp are in anagen. The terminus end is called the bulb, and the portion between the bulb and the stem cell–containing bulge is referred to as the suprabulb (**Fig. 6a** and **Supplementary Fig. 5**). We dissected hair follicles from normal human scalp to isolate the interfollicular epidermis, infundibulum, bulge, suprabulb and bulb, and we obtained RNA from each of these sites (**Fig. 6a**)[4]. We then performed real-time PCR for *IL15* and *IL7*. *IL15* was predominantly expressed by hair follicle keratinocytes in the

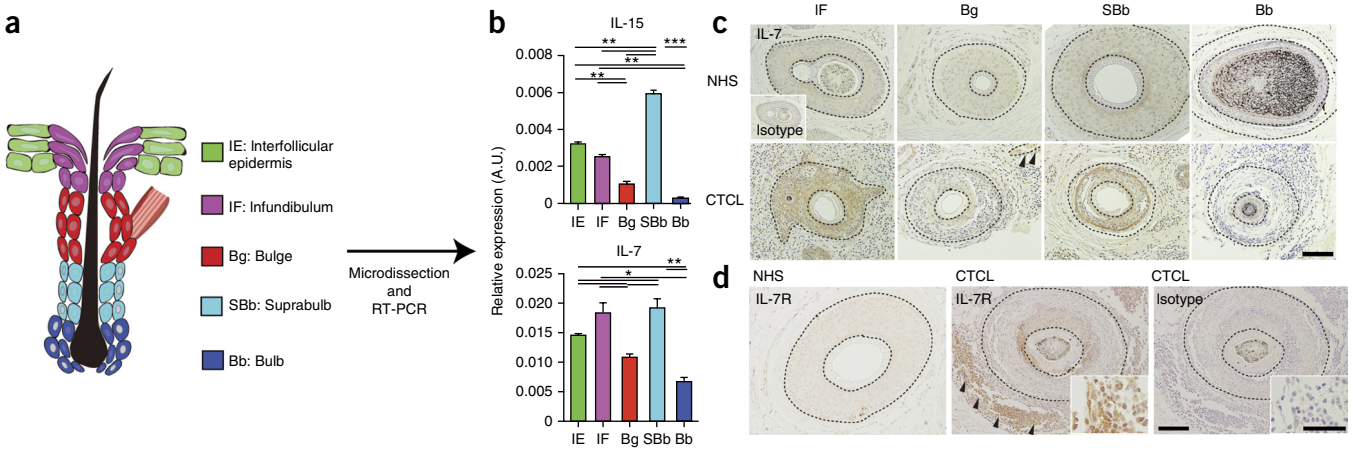

Figure 6 IL-7 and IL-15 expression in human hair follicles from normal scalp and cutaneous T cell lymphoma. (**a**) Schematic representation of human hair follicle keratinocytes. (**b**) Real-time PCR analysis for *IL15* and *IL7* expression at distinct sites in the hair follicle. $^{*}P < 0.05$, $^{**}P < 0.01$, $^{***}P < 0.001$ (unpaired two-tailed Student's *t*-test). Horizontal lines depict the mean, and error bars indicate s.e.m. (**c**) Immunohistochemistry of normal scalp sections from humans (NHS) ($n = 3$ samples from three subjects) and from subjects with CTCL ($n = 6$ samples from three subjects), stained with an IL-7–specific antibody or with an isotype control. Scale bar, 100 μm. Arrowheads indicate arrector pili muscle (reflecting the bulge region). (**d**) Immunohistochemistry of scalp sections from patients with CTCL, stained with an IL-7R–specific antibody or with an isotype control ($n = 6$ samples from three subjects). Scale bar, 100 μm in low-power field, 50 μm in high-power field. Dashed lines delineate hair follicles. Arrowheads indicate IL-7R–positive lymphoma cells. Data are from one experiment representative of three (**b**,**c**) or two (**d**) independent experiments.

suprabulb, and *IL7* expression was highest in the infundibulum and suprabulb (**Fig. 6b**).

We additionally evaluated IL-7 expression in hair follicles from both normal human scalp and lesional scalp skin of patients with CTCL. Faint immunohistochemical staining for IL-7 was detected in normal human hair follicles. IL-7 expression was apparent in a CTCL-affected subject, in which the staining was detected in the infundibulum and the suprabulbar area (**Fig. 6c**), consistent with the real-time PCR data from normal human scalp. In other patients, IL-7 staining was increased not only in hair follicle keratinocytes, but also in keratinocytes in the interfollicular epidermis (**Supplementary Fig. 6**).

Consistent with our observations in mice, IL-7R expression by T cells was increased in lesional CTCL epidermis in comparison to that on T cells in normal human scalp skin (**Fig. 6d** and **Supplementary Fig. 5**). IL-7R expression in lesional keratinocytes in CTCL seems to be increased relative to keratinocytes in normal scalp skin, although the significance of this has yet to be determined.

DISCUSSION

Epidermotropism of T_{RM} cells, both non-malignant and malignant, is regulated by the hair follicle–derived cytokines IL-7 and IL-15. Previous studies[6–8] have focused on T_{RM} cell biology in the context of viral infections. We studied the requirement of epidermotropic T_{RM} cells during the steady state by using non-malignant and malignant models. The lack of hair follicle–derived cytokines led to the failure of both $CD4^+$ and $CD8^+$ T_{RM} cells to persist in skin. Impaired CHS responses in the absence of hair follicle–derived cytokines highlight the importance of homeostatic organization of T_{RM} cells before inflammation.

The requirement of IL-7 and IL-15 for the generation and maintenance of memory T cells is well established[24,25], but the fate of T_{RM} cells in peripheral tissues that are deprived of these cytokines remains unclear. In particular, whether the cells undergo cell death or migration deserves further attention in the context of lymphoma.

The tropism that $CD4^+$ T_{RM} cells exhibit to the hair follicles demonstrated in this study is compatible with and complementary to a previous report[7] in which approximately 30% of virus-specific $CD4^+$ memory T cells were found to associate with the hair follicles after herpes simplex virus skin infection. To date, T_{RM} cells in the skin have mainly been characterized in the context of $CD8^+$ T cells. Although $CD4^+$ memory T cells may well be comparable to $CD8^+$ T_{RM} cells as skin residents on the basis of surface marker expression and past reports[13,22], thorough studies on $CD4^+$ memory T cells as bona fide T_{RM} cells have yet to be performed. Our observation that epidermal and dermal T_{RM} cells have subtle differences in CD103 expression, in conjunction with the higher observed ratio of $CD4^+$ $FoxP3^+$ T_{RM} cells in the dermis, suggests that $CD4^+$ T_{RM} cells in these skin compartments might be regulated through distinct mechanisms.

In conclusion, we have demonstrated the importance of hair follicle–derived IL-7 and IL-15 in T_{RM} cell homeostasis in the epidermis, which represents an attractive therapeutic target in inflammatory skin diseases and malignant lymphoma, and which may also be relevant in other peripheral tissues.

METHODS

Methods and any associated references are available in the online version of the paper.

Note: Any Supplementary Information and Source Data files are available in the online version of the paper.

ACKNOWLEDGMENTS

We thank M. Ohyama for helpful discussion on human hair follicles; N. Sakai, K. Eguchi and S. Sato (Keio University School of Medicine) for their technical assistance; H. Kong (National Institutes of Health) for their discussions on human CTCL; Y. Madokoro (Keio University School of Medicine) for human CTCL immunohistochemical staining; T. Kitamura (University of Tokyo) for providing the retroviral vector pMXs-IG and Plat-E cells; J. Takeda (Osaka University) for providing *K5*-Cre mice; D.H. Kaplan (University of Minnesota) for providing Langerin-DTA mice; and B.E. Clausen (Johannes Gutenberg University of Mainz) for providing Langerin-DTR mice. This work was supported by the Japan Society for the Promotion of Science, The Kanae Foundation for the Promotion of Medical Science, the Japanese Society for Investigative Dermatology's (JSID's) Fellowship Shiseido Award and the NIH NCI Intramural Research Programs.

AUTHOR CONTRIBUTIONS

T.A. and K.N. conceived of and designed all experiments. Experiments were performed by T.A. with the assistance of T.K.; E.S. and H.S. provided *Cdkn2a*$^{-/-}$ mice and assisted with retroviral transduction; T.Y. assisted with immunohistochemical staining; K.I. provided *Il7*-floxed mice; S.P. provided human CTCL samples; M.A. discussed the data and provided administrative support; K.N. guided the project; and T.A. and K.N. wrote the manuscript.

COMPETING FINANCIAL INTERESTS

The authors declare no competing financial interests.

Reprints and permissions information is available online at http://www.nature.com/reprints/index.html.

1. Cotsarelis, G., Sun, T.T. & Lavker, R.M. Label-retaining cells reside in the bulge area of pilosebaceous unit: implications for follicular stem cells, hair cycle, and skin carcinogenesis. *Cell* **61**, 1329–1337 (1990).
2. Nishimura, E.K. *et al.* Dominant role of the niche in melanocyte stem-cell fate determination. *Nature* **416**, 854–860 (2002).
3. Christoph, T. *et al.* The human hair follicle immune system: cellular composition and immune privilege. *Br. J. Dermatol.* **142**, 862–873 (2000).
4. Nagao, K. *et al.* Stress-induced production of chemokines by hair follicles regulates the trafficking of dendritic cells in skin. *Nat. Immunol.* **13**, 744–752 (2012).
5. Clark, R.A. *et al.* The vast majority of CLA^+ T cells are resident in normal skin. *J. Immunol.* **176**, 4431–4439 (2006).
6. Gebhardt, T. *et al.* Memory T cells in nonlymphoid tissue that provide enhanced local immunity during infection with herpes simplex virus. *Nat. Immunol.* **10**, 524–530 (2009).
7. Gebhardt, T. *et al.* Different patterns of peripheral migration by memory $CD4^+$ and $CD8^+$ T cells. *Nature* **477**, 216–219 (2011).
8. Jiang, X. *et al.* Skin infection generates non-migratory memory $CD8^+$ T(RM) cells providing global skin immunity. *Nature* **483**, 227–231 (2012).
9. Wakim, L.M., Waithman, J., van Rooijen, N., Heath, W.R. & Carbone, F.R. Dendritic cell-induced memory T cell activation in nonlymphoid tissues. *Science* **319**, 198–202 (2008).
10. Mackay, L.K. *et al.* The developmental pathway for $CD103^+CD8^+$ tissue-resident memory T cells of skin. *Nat. Immunol.* **14**, 1294–1301 (2013).
11. Shiow, L.R. *et al.* CD69 acts downstream of interferon-α/β to inhibit S1P1 and lymphocyte egress from lymphoid organs. *Nature* **440**, 540–544 (2006).
12. Bromley, S.K., Yan, S., Tomura, M., Kanagawa, O. & Luster, A.D. Recirculating memory T cells are a unique subset of $CD4^+$ T cells with a distinct phenotype and migratory pattern. *J. Immunol.* **190**, 970–976 (2013).
13. Suffia, I., Reckling, S.K., Salay, G. & Belkaid, Y. A role for CD103 in the retention of $CD4^+CD25^+$ T_{reg} and control of *Leishmania major* infection. *J. Immunol.* **174**, 5444–5455 (2005).
14. Sanchez Rodriguez, R. *et al.* Memory regulatory T cells reside in human skin. *J. Clin. Invest.* **124**, 1027–1036 (2014).
15. Shiohara, T. & Moriya, N. Epidermal T cells: their functional role and disease relevance for dermatologists. *J. Invest. Dermatol.* **109**, 271–275 (1997).
16. Mizukawa, Y. *et al.* Direct evidence for interferon-γ production by effector-memory-type intraepidermal T cells residing at an effector site of immunopathology in fixed drug eruption. *Am. J. Pathol.* **161**, 1337–1347 (2002).
17. Hwang, S.T., Janik, J.E., Jaffe, E.S. & Wilson, W.H. Mycosis fungoides and Sezary syndrome. *Lancet* **371**, 945–957 (2008).
18. Campbell, J.J., Clark, R.A., Watanabe, R. & Kupper, T.S. Sezary syndrome and mycosis fungoides arise from distinct T-cell subsets: a biologic rationale for their distinct clinical behaviors. *Blood* **116**, 767–771 (2010).
19. Clark, R.A. *et al.* Skin effector memory T cells do not recirculate and provide immune protection in alemtuzumab-treated CTCL patients. *Sci. Transl. Med.* **4**, 117ra7 (2012).
20. Edelson, R.L. Cutaneous T cell lymphoma: mycosis fungoides, Sezary syndrome, and other variants. *J. Am. Acad. Dermatol.* **2**, 89–106 (1980).
21. Seneschal, J., Clark, R.A., Gehad, A., Baecher-Allan, C.M. & Kupper, T.S. Human epidermal Langerhans cells maintain immune homeostasis in skin by activating skin resident regulatory T cells. *Immunity* **36**, 873–884 (2012).
22. Sanchez Rodriguez, R. *et al.* Memory regulatory T cells reside in human skin. *J. Clin. Invest.* **124**, 1027–1036 (2014).

23. Ariotti, S. *et al.* T cell memory. Skin-resident memory CD8+ T cells trigger a state of tissue-wide pathogen alert. *Science* **346**, 101–105 (2014).
24. Lanzavecchia, A. & Sallusto, F. Understanding the generation and function of memory T cell subsets. *Curr. Opin. Immunol.* **17**, 326–332 (2005).
25. van Leeuwen, E.M., Sprent, J. & Surh, C.D. Generation and maintenance of memory CD4+ T cells. *Curr. Opin. Immunol.* **21**, 167–172 (2009).
26. Vasioukhin, V., Degenstein, L., Wise, B. & Fuchs, E. The magical touch: genome targeting in epidermal stem cells induced by tamoxifen application to mouse skin. *Proc. Natl. Acad. Sci. USA* **96**, 8551–8556 (1999).
27. Liang, B. *et al.* Role of hepatocyte-derived IL-7 in maintenance of intrahepatic NKT cells and T cells and development of B cells in fetal liver. *J. Immunol.* **189**, 4444–4450 (2012).
28. Dorfman, D.M. & Shahsafaei, A. CD69 expression correlates with expression of other markers of Th1 T cell differentiation in peripheral T cell lymphomas. *Hum. Pathol.* **33**, 330–334 (2002).
29. Yamanaka, K. *et al.* Skin-derived interleukin-7 contributes to the proliferation of lymphocytes in cutaneous T-cell lymphoma. *Blood* **107**, 2440–2445 (2006).
30. Espinet, B. & Salgado, R. Mycosis fungoides and Sezary syndrome. *Methods Mol. Biol.* **973**, 175–188 (2013).
31. Kanavaros, P. *et al.* Mycosis fungoides: expression of C-myc p62 p53, bcl-2 and PCNA proteins and absence of association with Epstein-Barr virus. *Pathol. Res. Pract.* **190**, 767–774 (1994).
32. Kamijo, T., Bodner, S., van de Kamp, E., Randle, D.H. & Sherr, C.J. Tumor spectrum in *ARF*-deficient mice. *Cancer Res.* **59**, 2217–2222 (1999).
33. Serrano, M. *et al.* Role of the *INK4a* locus in tumor suppression and cell mortality. *Cell* **85**, 27–37 (1996).
34. Sugihara, E. *et al.* Ink4a and Arf are crucial factors in the determination of the cell of origin and the therapeutic sensitivity of Myc-induced mouse lymphoid tumor. *Oncogene* **31**, 2849–2861 (2012).

JDA Japanese Dermatological Association
THE JOURNAL OF DERMATOLOGY
doi: 10.1111/1346-8138.12829
Journal of Dermatology 2015; **42**: 511–514

CONCISE COMMUNICATION

Recurrent gastrointestinal perforation in a patient with Ehlers–Danlos syndrome due to tenascin-X deficiency

Tomo SAKIYAMA,[1,2] Akiharu KUBO,[2] Takashi SASAKI,[2,3] Taketo YAMADA,[4,5] Nobushige YABE,[6] Ken-ichi MATSUMOTO,[7] Yuko FUTEI[1]

[1]Division of Dermatology, Ogikubo Hospital, [2]Department of Dermatology, Keio University School of Medicine, [3]KOSÉ Endowed Program for Skin Care and Allergy Prevention, Keio University School of Medicine, [4]Department of Pathology, Keio University School of Medicine, Tokyo, [5]Department of Pathology, Saitama Medical University, Saitama, [6]Division of Surgery, Ogikubo Hospital, Tokyo, [7]Department of Biosignaling and Radioisotope Experiment, Interdisciplinary Center for Science Research, Organization for Research, Shimane University, Shimane, Japan

ABSTRACT

Ehlers–Danlos syndrome (EDS) is a clinically and genetically heterogeneous disorder. Using a customized targeted exome-sequencing system we identified nonsense mutations in *TNXB* in a patient who had recurrent gastrointestinal perforation due to tissue fragility. This case highlights the utility of targeted exome sequencing for the diagnosis of congenital diseases showing genetic heterogeneity, and the importance of attention to gastrointestinal perforation in patients with tenascin-X deficient type EDS.

Key words: customized targeted exome sequencing, Ehlers–Danlos syndrome, gastrointestinal perforation, next-generation sequencer, tenascin-X.

INTRODUCTION

Ehlers–Danlos syndrome (EDS) is a heritable connective-tissue disorder characterized by skin hyperextensibility, joint hypermobility and tissue fragility. EDS is classified into six major types and other minor forms according to clinical features and causative gene mutations. A total of 22 types and 15 causative genes have been reported.[1] EDS due to tenascin-X (TNX) deficiency is a rare variant of EDS. TNX-deficient EDS was first reported by Burch *et al.* in 1997,[2] and only 18 cases have been reported to date. TNX, encoded by *TNXB* located on chromosome 6p, is a glycoprotein that is widely distributed in the extracellular matrix of tissues throughout the body, especially in muscle.[3] TNX plays a role in collagen fibrillogenesis and regulation of type VI collagen synthesis.[4] Herein, we report the first Asian patient diagnosed with TNX-deficient EDS. She had a history of recurrent gastrointestinal perforation, and two novel nonsense mutations in *TNXB* were detected by customized targeted exome sequencing for genodermatoses.

CASE REPORT

A 45-year-old woman was initially referred to the dermatology department of our hospital with a history suggestive of EDS. She had had skin hyperextensibility, easy bruising, scoliosis and recurrent subluxations since childhood. She underwent multiple surgical procedures for subluxations of her hip joints. In her 20s, recurrent periodontitis and abdominal pain were recognized. Episodes of both spontaneous and secondary gastrointestinal ileus and perforations were repeatedly observed commencing in her 40s with diverticular perforation of the sigmoid colon, followed by incarcerated hernia at the drain tube insertion site and ileus after stoma closure. At 45 years of age, the patient experienced a spontaneous ileus followed by duodenal perforation (likely due to ileus tube insertion). An ovarian cyst was observed at 41 years of age. There was no apparent delay in wound healing of her skin or intestine, although both were very fragile. In her 40s, she had felt numbness in her fingers, neck pain and reduced grip strength. The family history was uncertain because her parents had already died, but no symptoms of joint hypermobility or skin hyperextensibility had been recognized. Her elder sister (II-3 in Fig. 1a) had mild skin hyperelasticity, mild joint hypermobility and pes planus. Her niece (III-2 in Fig. 1a) had mild skin hyperelasticity and her nephew (III-1 in Fig. 1a) had pes planus.

On examination, her face was slack-skinned with prominent eyes and a thin nose (Fig. 1b). Periodontitis was observed (Fig. 1b). Her hyperextensive skin was thin, translucent, soft and velvety. Although she had mild joint hypermobility, her Beighton score was 3 of 9 (a 9-point scale to define joint hypermobility, with cut-off points for generalized joint hypermobility of ≥4/9 for men and ≥5/9 for women). She had pes planus, piezogenic papules on her feet and deformity due to

Correspondence: Akiharu Kubo, M.D., Ph.D., Department of Dermatology, Keio University School of Medicine, 35 Shinanomachi, Shinjuku-ku, Tokyo 160-8582, Japan. Email: akiharu@a5.keio.jp
Received 3 December 2014; accepted 26 January 2015.

© 2015 Japanese Dermatological Association

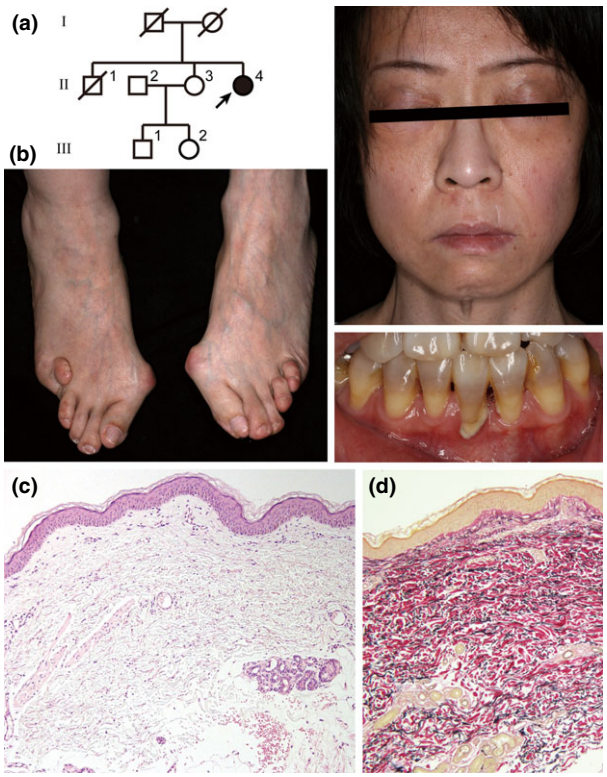

Figure 1. (a) Patient pedigree. (b) The patient's face was slack-skinned with prominent eyes and a thin nose. She had periodontitis, pes planus and deformity due to subluxation of the right little toe. (c) Hematoxylin–eosin stain of the patient's skin (original magnification ×100). (d) Elastica van Gieson stain of skin (×100).

subluxation of the right little toe (Fig. 1b). There was non-atrophic broad scar formation on her knees and elbows. Ophthalmologic examination showed conjunctivochalasis in both eyes. Computed tomography (CT) scan and echocardiography revealed no cardiovascular abnormality. She was incapable of opening a bottle cap due to numbness in her thumbs and reduced grip strength (right, 10.0 kg; left, 6.8 kg). Electromyogram and nerve conduction studies from her upper extremities showed bilateral median, left musculocutaneous and mild left radial sensory neuropathy. Skin biopsy from her left upper arm showed thin and loosely assembled collagen bundles, especially apparent around the sweat glands (Fig. 1c). There was marked hemorrhage around blood vessels in the dermis (Fig. 1c). Fragmented and curly elastin fibers were confirmed by elastica van Gieson staining as previously described (Fig. 1d).[5]

We developed a custom panel for mutation screening of approximately 450 genes of genodermatoses using the SureDesign program and Haloplex target enrichment system (Agilent Technologies, Santa Clara, CA, USA). The custom panel included 13 EDS-associated genes (Fig. 2a) with the exclusion of two of these (*B3GALT6* and *DSE*)[1] that were identified after the panel was established. Next-generation sequencing analysis was performed using the panel according to the supplier's protocol, and two novel nonsense mutations in *TNXB*, c.2539C>T (p.R847*) and c.3574C>T (p.Q1192*) were identified. No disease-associated mutations were identified in the other 12 genes tested (Fig. 2a). The nonsense mutations in *TNXB* were confirmed by Sanger DNA sequencing (Fig. 2b). We further confirmed complete absence of TNX protein in the patient's serum and skin. Immunoblot analysis of the patient's serum using rabbit polyclonal anti-tenascin-X antibody (α-hu30),[6] detected with IRDye 680-conjugated donkey anti-rabbit immunoglobulin (Ig)G (LI-COR Biosciences, Lincoln, NE, USA) using an Odyssey infrared imaging system (LI-COR) demonstrated the complete absence of soluble 75- and 140-kDa forms of TNX protein (Fig. 3a).[7] Immunostaining with an anti-TNX antibody (AF6999 polyclonal sheep IgG; R&D Systems, Minneapolis, MN, USA) detected by means of rabbit anti-sheep Ig conjugated with horseradish peroxidase (DAKO, Glostrup, Denmark), VECTOR SG Kit (Vector Laboratories, Burlingame, CA, USA) and 3,3′-diaminobenzidine-tetrachloride (DAB; Dojindo Laboratories, Kumamoto, Japan) revealed that skin sections were negative for TNX expression (Fig. 3b). Together with the results of genetic testing, the patient was diagnosed with TNX-deficient type EDS due to probable compound heterozygosity of the two novel nonsense mutations in *TNXB*.

DISCUSSION

Tenascin-X-deficient type EDS is clinically characterized by hyperextensibility, joint hypermobility, easy bruising, normal wound healing and lack of atrophic scar formation. Neuromuscular complaints are seen in several types of EDS, and axonal sensorimotor polyneuropathy is predominant in the TNX-deficient type.[8] Patients can also suffer from luxation, valvular heart disease, pes planus and piezogenic papules on the feet. Based on clinical features alone, it is difficult to distinguish TNX-deficient type EDS from other types of EDS, and especially from classical EDS exhibiting a mild clinical phenotype. Therefore, genetic testing is important for diagnosis of the EDS type.

The genetic heterozygosity of EDS and the large size of several of the causative genes (including *TNXB*) make it difficult to routinely diagnose EDS genetically. Targeted exome sequencing has enabled comprehensive screening of causative mutations in a set of selected genes associated with disease. We developed a custom panel for next-generation sequencing to screen mutations in approximately 450 causative genes for genodermatoses. With this system, 13 causative genes for EDS and EDS-related diseases (including *TNXB*) were sequenced comprehensively (Fig. 2a), enabling identification of the two novel nonsense mutations of *TNXB* rapidly and at low cost. Targeted exome sequencing is considered very useful for the diagnosis of genodermatoses that show genetic and clinical heterogeneity, such as EDS, epidermolysis bullosa, ichthyosiform erythroderma and palmoplantar keratoderma.

© 2015 Japanese Dermatological Association

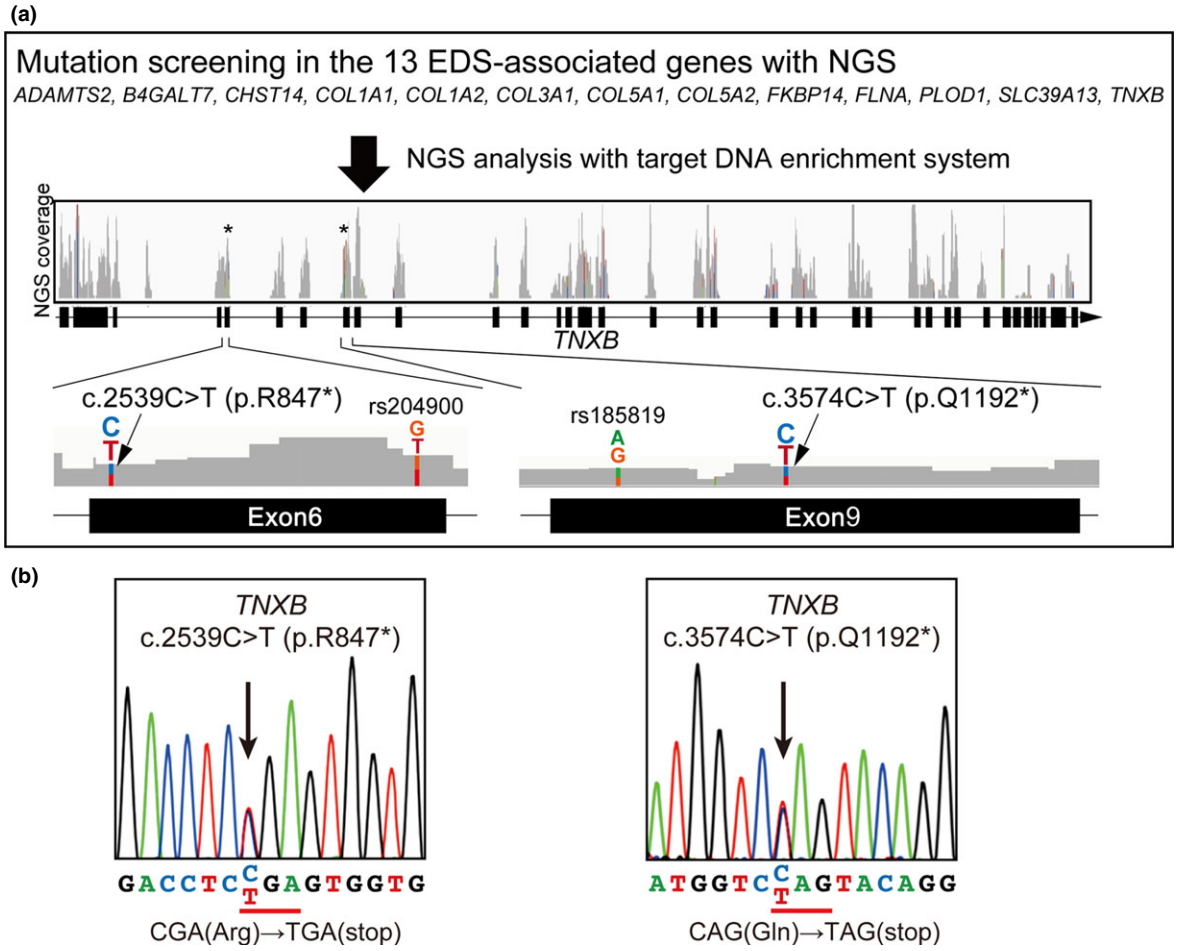

Figure 2. (a) Targeted exome sequencing analysis with next-generation sequencing (NGS) of 13 Ehlers–Danlos syndrome (EDS)-associated genes, including *TNXB*. Single nucleotide polymorphisms including two nonsense mutations were identified. (b) Sanger DNA sequencing analysis of *TNXB* revealed p.R847* and p.Q1192* nonsense mutations.

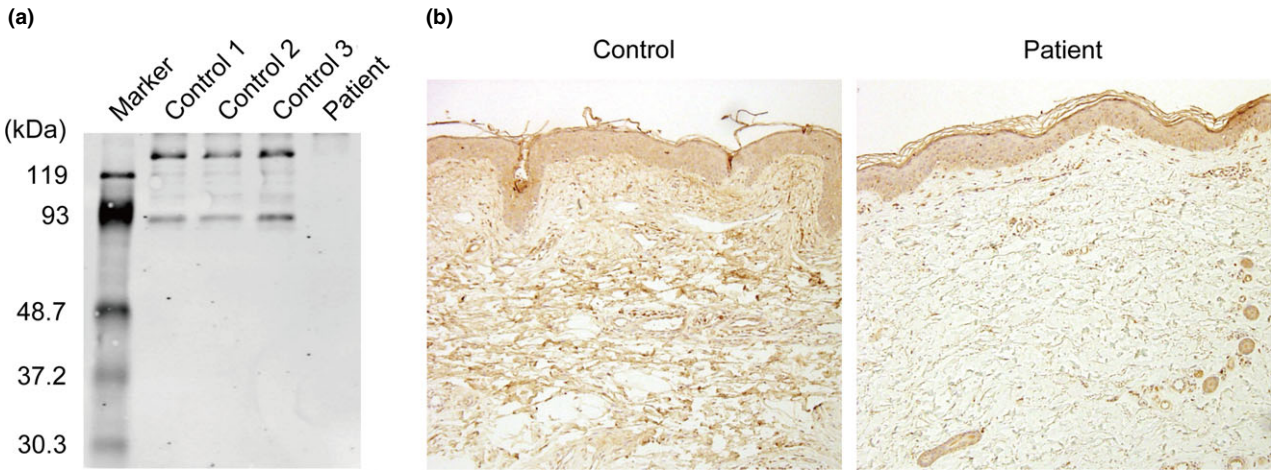

Figure 3. (a) Western blot of the patient's serum revealed complete deficiency of both the 140- and 75-kDa species of serum tenascin-X (TNX). (b) TNX immunostaining of the patient's skin and that of a control individual (original magnification ×100).

© 2015 Japanese Dermatological Association

Recurrent gastrointestinal perforation and fragility of the intestinal tract were distinctive features in this patient. The intestinal specimen obtained during the surgery for duodenum perforation showed very loose interstitium. Of the six major types of EDS, vascular type EDS patients are known to have the highest risk of gastrointestinal complications, namely, spontaneous and/or iatrogenic rupture of the sigmoid colon.[9] Upon review of the published work, we found that five of 19 patients of TNX-deficient type EDS (including this case) had gastrointestinal involvement (three hernias,[10,11] three diverticuloses,[10] two bowel perforations,[10] one recurrent rectal prolapse[10] and one gastrointestinal bleeding[12]). Mutations in *TNXB* were identified in three of the five patients, and no apparent genotype–phenotype correlation was observed compared with other patients.[11,12] The high incidence of gastrointestinal involvement in TNX-deficient type EDS patients indicates the importance of attention to invasive procedures and treatment of gastrointestinal disorders, not only in vascular type EDS but also in TNX-deficient type EDS.

TNXB haploinsufficiency is observed prevalently in heterozygous females with *TNXB* deficiency showing generalized joint hypermobility.[13] Examination of 20 heterozygous family members revealed that nine of 14 females and zero of six males exhibited generalized joint hypermobility similar to hypermobility type EDS.[13] *TNXB* haploinsufficiency is dominantly inherited and appears to produce clinical findings primarily in females, consistent with clinical descriptions of hypermobility type EDS. In our case, the proband's sister and her daughter revealed mild skin hyperelasticity. However, as no genetic tests were performed whether they were heterozygous for TNX deficiency remains unknown.

In conclusion, we report the first Asian case of TNX deficiency, diagnosed by customized targeted exome sequencing. This case indicates the importance of attention to gastrointestinal perforation due to tissue fragility in TNX-deficient type EDS patients.

ACKNOWLEDGMENT: This work was supported in parts by grants from the Ministry of Health, Labour and Welfare of Japan.

CONFLICT OF INTEREST: None declared.

REFERENCES

1 Online Mendelian Inheritance in Man (130000, 130010, 130020, 130050, 130060, 130070, 130080, 130090, 225310, 225320, 225400, 225410, 300537, 305200, 601776, 615539, 606408, 608763, 612350, 614557, 615349). [cited 4 Sept 2014.] Availabe from URL: http://www.ncbi.nlm.nih.gov/omim
2 Burch GH, Gong Y, Liu W *et al.* Tenascin-X deficiency is associated with Ehlers-Danlos syndrome. *Nat Genet* 1997; **17**: 104–108.
3 Matsumoto K, Saga Y, Ikemura T *et al.* The distribution of tenascin-X is distinct and often reciprocal to that of tenascin-C. *J Cell Biol* 1994; **125**: 483–493.
4 Minamitani T, Ariga H, Matsumoto K. Deficiency of tenascin-X causes a decrease in the level of expression of type VI collagen. *Exp Cell Res* 2004; **297**: 49–60.
5 Zweers MC, van Vlijmen-Willems IM, van Kuppevelt TH *et al.* Deficiency of tenascin-X causes abnormalities in dermal elastic fiber morphology. *J Invest Dermatol* 2004; **122**: 885–891.
6 Satoh K, Tsukamoto M, Shindoh M *et al.* Increased expression of tenascin-X in thoracic and abdominal aortic aneurysm tissues. *Biol Pharm Bull* 2010; **33**: 1898–1902.
7 Egging DF, Peeters ACTM, Grebenchtchikov N *et al.* Identification and characterization of multiple species of tenascin-X in human serum. *FEBS J* 2007; **274**: 1280–1289.
8 Voermans NC, Van Alfen N, Pillen S *et al.* Neuromuscular involvement in various types of Ehlers-Danlos syndrome. *Ann Neurol* 2009; **65**: 687–697.
9 Burcharth J, Rosenberg J. Gastrointestinal surgery and related complications in patients with Ehlers-Danlos syndrome: a systematic review. *Dig Surg* 2012; **29**: 349–357.
10 Lindor NM, Bristow J. Tenascin-X deficiency in autosomal recessive Ehlers-Danlos syndrome. *Am J Med Genet A* 2005; **135**: 75–80.
11 Penisson-Besnier I, Allamand V, Beurrier P *et al.* Compound heterozygous mutations of the TNXB gene cause primary myopathy. *Neuromuscul Disord* 2013; **23**: 664–669.
12 Schalkwijk J, Zweers MC, Steijlen PM *et al.* A recessive form of the Ehlers-Danlos syndrome caused by tenascin-X deficiency. *N Engl J Med* 2001; **345**: 1167–1175.
13 Zweers MC, Bristow J, Steijlen PM *et al.* Haploinsufficiency of TNXB is associated with hypermobility type of Ehlers-Danlos syndrome. *Am J Hum Genet* 2003; **73**: 214–217.

© 2015 Japanese Dermatological Association

PLOS ONE

RESEARCH ARTICLE

A Novel Phthalimide Derivative, TC11, Has Preclinical Effects on High-Risk Myeloma Cells and Osteoclasts

Maiko Matsushita[1], Yoshie Ozaki[1], Yuka Hasegawa[1], Fukiko Terada[1], Noriko Tabata[2], Hirokazu Shiheido[2], Hiroshi Yanagawa[2], Tsukasa Oikawa[3], Koichi Matsuo[3], Wenlin Du[4], Taketo Yamada[4], Masashi Hozumi[1], Daiju Ichikawa[1], Yutaka Hattori[1]*

1 Clinical Physiology and Therapeutics, Faculty of Pharmacy, Keio University, Tokyo, Japan, **2** Department of Biosciences and Informatics, Faculty of Science and Technology, Keio University, Yokohama, Japan, **3** Cell and Tissue Biology, School of Medicine, Keio University, Tokyo, Japan, **4** Department of Pathology, School of Medicine, Keio University, Tokyo, Japan

* hattori-yt@pha.keio.ac.jp

CrossMark
click for updates

OPEN ACCESS

Citation: Matsushita M, Ozaki Y, Hasegawa Y, Terada F, Tabata N, Shiheido H, et al. (2015) A Novel Phthalimide Derivative, TC11, Has Preclinical Effects on High-Risk Myeloma Cells and Osteoclasts. PLoS ONE 10(1): e0116135. doi:10.1371/journal.pone.0116135

Academic Editor: Dominique Heymann, Faculté de médecine de Nantes, FRANCE

Received: April 18, 2014

Accepted: November 24, 2014

Published: January 24, 2015

Copyright: © 2015 Matsushita et al. This is an open access article distributed under the terms of the Creative Commons Attribution License, which permits unrestricted use, distribution, and reproduction in any medium, provided the original author and source are credited.

Data Availability Statement: All relevant data are within the paper.

Funding: This work was supported in part by a Grant-in-Aid for Scientific Research (Y. Hattori, MM) and a grant from the Private University Strategic Research Base Development Program (Y. Hattori) of MEXT (the Ministry of Education, Culture, Sports, Science and Technology) of Japan, Keio Gijuku Academic development Funds (Y. Hattori) and Japan Leukemia Research Fund (Y. Hattori, MM). The funders had no role in study design, data collection and

Abstract

Despite the recent advances in the treatment of multiple myeloma (MM), MM patients with high-risk cytogenetic changes such as t(4;14) translocation or deletion of chromosome 17 still have extremely poor prognoses. With the goal of helping these high-risk MM patients, we previously developed a novel phthalimide derivative, TC11. Here we report the further characterization of TC11 including anti-myeloma effects *in vitro* and *in vivo*, a pharmacokinetic study in mice, and anti-osteoclastogenic activity. Intraperitoneal injections of TC11 significantly delayed the growth of subcutaneous tumors in human myeloma-bearing SCID mice. Immunohistochemical analyses showed that TC11 induced apoptosis of MM cells *in vivo*. In the pharmacokinetic analyses, the C_{max} was 2.1 μM at 1 h after the injection of TC11, with 1.2 h as the half-life. TC11 significantly inhibited the differentiation and function of tartrate-resistant acid phosphatase (TRAP)-positive multinucleated osteoclasts in mouse osteoclast cultures using M-CSF and RANKL. We also revealed that TC11 induced the apoptosis of myeloma cells accompanied by α-tubulin fragmentation. In addition, TC11 and lenalidomide, another phthalimide derivative, directly bound to nucleophosmin 1 (NPM1), whose role in MM is unknown. Thus, through multiple molecular interactions, TC11 is a potentially effective drug for high-risk MM patients with bone lesions. The present results suggest the possibility of the further development of novel thalidomide derivatives by drug designing.

Introduction

Multiple myeloma (MM) is a neoplasm of plasma cells that is accompanied by various clinical manifestations including lytic bone lesions, hypercalcemia, renal dysfunction, immunodeficiency, and anemia [1, 2]. Despite recent advances in the use of newly developed drugs

analysis, decision to publish, or preparartion of the manuscript.

Competing Interests: The authors have declared that no competing interests exist.

including immune-modulatory drugs (IMiDs) such as thalidomide, lenalidomide, and pomalidomide and proteasome inhibitors such as bortezomib, carfilzomib, and MLN9708, MM is still an incurable disease [3–7]. In particular, MM patients harboring 17p deletion, t(14;16), t(14;20), or t(4;14) are classified as a high-risk group and have shown significantly shorter survival [8–10]. For example, it is reported that even lenalidomide plus dexamethasone or bortezomib could not substantially improve the survival of refractory patients with del 17p [11, 12]. With the goal of helping prolong the survival of these high-risk MM patients, we screened 29 synthetic phthalimide derivatives and found a novel compound, 2-(2,6-diisopropylphenyl)-5-amino-1*H*-isoindole-1,3-dione (TC11), which induced the apoptosis of KMS34 cells with t(4;14) and del17p13 [13].

Bone lytic lesions, which are seen in 80%–90% of MM patients, have clinical manifestations that include pain, pathologic fractures, spinal cord compression, and hypercalcemia, thus providing a negative impact on the quality of life of MM patients [1]. In the clinical setting, bisphosphonate, radiotherapy, and surgery are used to treat bone disease. Bisphosphonate can significantly reduce skeletal-related events in MM patients [14], but side effects such as renal impairment and osteonecrosis of the jaw are seen in some patients [15, 16]. The development of novel agents to effectively treat bone lesions without severe side effects is thus necessary.

In the present study, we evaluate the anti-myeloma effects of TC11 *in vitro* and *in vivo*, and we investigated the effects of TC11 on the differentiation of osteoclasts to determine whether this new drug could be effective for treating high-risk MM patients with bone lesions. We also examined nucleophosmin-1 (NPM1) as a molecule that binds directly to phthalimide, and the results raised the possibility that α-tubulin is involved in the anti-myeloma effect of TC11.

Materials and Methods

Cell lines

Human myeloma cell lines KMS11, KMS 26, KMS28, and KMS34 were established by Dr. T. Otsuki (Kawasaki Medical School, Kurashiki, Japan) from Japanese patients [17, 18] and these cell lines were kindly provided by him. MUM24 was established from a patient with thalidomide-resistant MM [19]. These cell lines were maintained in RPMI1640 medium (Sigma-Aldrich, St. Louis, MO) containing 10% fetal bovine serum (FBS). The human macrophage cell line RAW264.7 was purchased from American Type Culture Collection (Rockville, MD) and cultured in DMEM medium (Sigma-Aldrich) containing 10% FBS (Hyclone Laboratories, Logan, UT).

Reagents

We synthesizedTC11 [2-(2,6-diisopropylphenyl)-5-amino-1*H*-isoindole-1,3-dione] from phthalic acid anhydride with a nitro group and amines, followed by catalytic hydrogenation under a nitrogen atmosphere. The benzene ring moiety of TC11 is different from those of thalidomide and lenalidomide (Fig. 1A). Dexamethasone sodium phosphate (MSD K.K., Tokyo) was used for *in vitro* proliferation assay.

Patients' samples

Bone marrow samples were obtained from patients with MM treated in Keio University Hospital. Mononuclear cells were isolated by Ficoll density gradient centrifugation and cryopreserved in a liquid nitrogen tank until further use. All samples contained more than 30% myeloma cells. This study was approved by the ethics committee of the Keio University School of

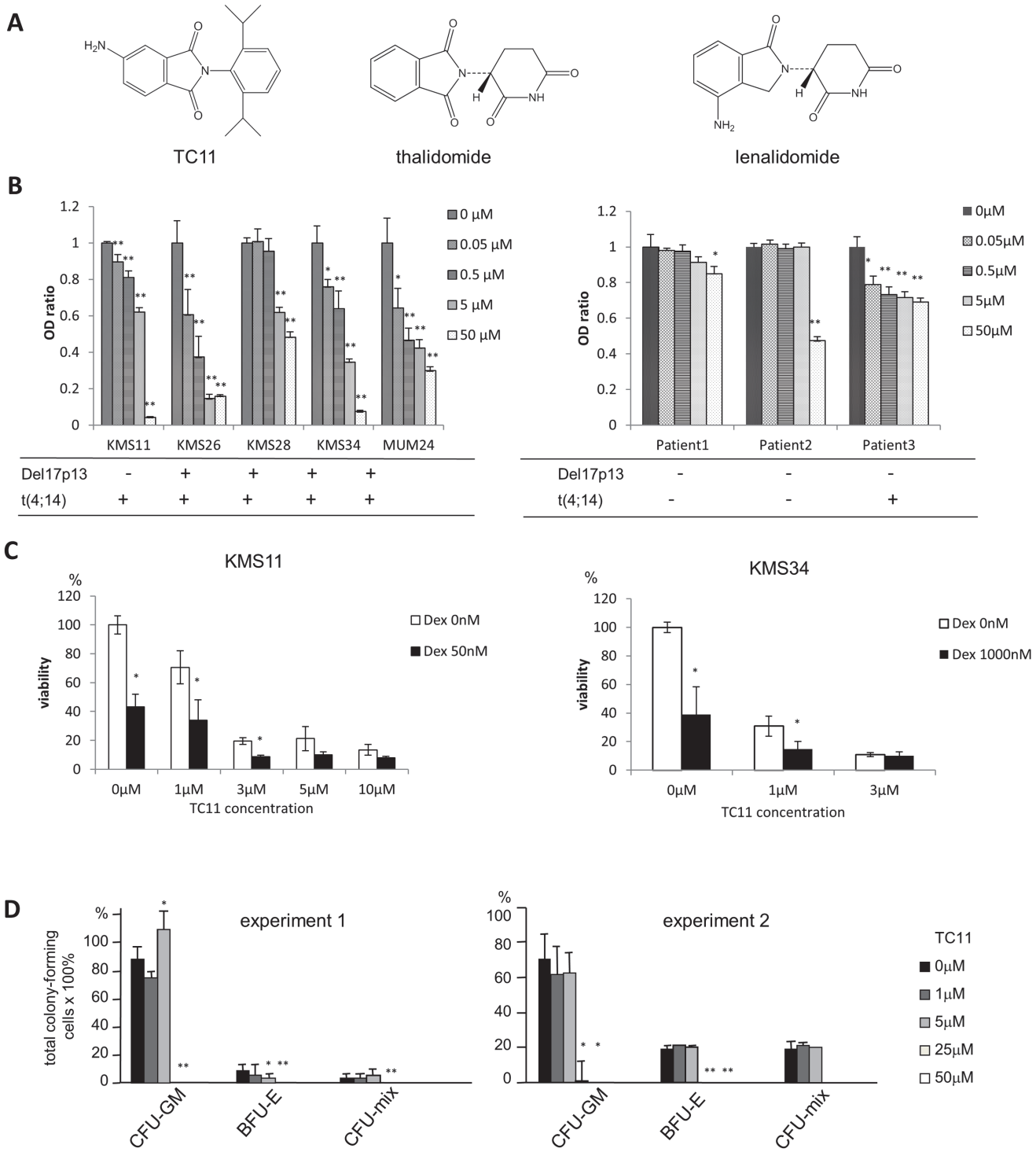

Figure 1. TC11 inhibited the growth of MM cell lines. (A) The chemical structures of TC11, thalidomide, and lenalidomide. (B) The dose-dependent inhibition of MM cells by TC11. Cell lines KMS11, KMS26, KMS28, KMS34, MUM24 with del 17p13 and/or t(4;14) were cultured for 48 h with the indicated dose of TC11, followed by an assessment of cell viability using MTT assays. Mononuclear cells separated from bone marrow samples of three MM patients were also treated with TC11 and examined by MTT assay. (C) Synergistic effects of TC11 with dexamethasone were examined by MTT assay. Bars indicate means±SD. *$p<0.05$ (Student's *t*-test). (D) The effect of TC11 on the number of hematopoietic progenitor cells was examined by colony assay. Mice bone

marrow cells were plated in 1.2% methylcellulose medium containing 20 ng/mL mIL-3, 10 ng/mL mIL-6, 20 ng/mL mSCF and 1 U/mL hEPO in the presence or absence of TC11. The numbers of colony-forming cells were counted after 14 days. Bars indicate means±SD. *$p<0.05$, **$p<0.01$ (Student's *t*-test).

doi:10.1371/journal.pone.0116135.g001

Medicine (99–7 and 15–21) and Faculty of Pharmacy (G110107–1). Written informed consent was obtained from all patients.

Cell viability assay

MM cells (2×10^4 cells per well) were seeded in 96-well plates and incubated with various concentrations of TC11 (0–50 μM) at 37°C for 48 h. The number of viable cells was assessed by MTT dye absorbance (Roche Diagnostics, Indianapolis, IN) according to the manufacturer's instructions.

Colony-forming cell assay

To evaluate the hematological toxicity of TC11, 4×10^4 cells/mL of bone marrow cells from 13-wk-old male ICR mice were cultured in methylcellulose medium (Stem Cell Technologies, Vancouver, BC) containing FBS, 2-mercaptoethanol, 20 ng/mL mouse stem cell factor (mSCF), 20 ng/mL mouse interleukin 3 (mIL-3), 10 ng/mL mouse interleukin-6 (mIL-6), and 1 U/mL human erythropoietin (hEPO) (kindly provided by Kyowa Hakko Kirin Co., Tokyo) in the presence or absence of TC11. On day 14, various types of colony-forming cells were counted.

In vivo tumor growth assay

All of the animal experiments were approved by the Ethics Committee for Animal Experiments at Keio University Faculty of Pharmacy (Approval no.09118-(0), 09118-(1)). The *in vivo* tumor-inhibitory activity assay was performed as described with several modifications [18]. Briefly, 3×10^7 KMS34 or KMS11 cells were subcutaneously inoculated into 5-wk-old male ICR/SCID mice (Clea Japan, Tokyo) and plasmacytoma developed in 4–7 wks. In addition, twenty mg/kg of TC11 dissolved in 10% DMSO (Sigma-Aldrich)-1% Tween80 at the concentration of 2.5 mg/mL or only 10% DMSO-1% Tween80 as a control was injected intraperitoneally twice every 3 days for 15 days (n = 7). The tumor volume was calculated according to the following formula as described [18]: width × length^2 × 0.52.

Histopathologic examination

The histopathologic analysis was performed as described with several modifications [18]. When the subcutaneous tumors reached 50 mm^3, the intraperitoneal injections of TC11 was started. After 14 days of observation, the mice were sacrificed and the isolated tumors were fixed with 10% formalin and embedded in paraffin. Sliced sections were stained with hematoxylin and eosin (H. E.). Anti-human cleaved PARP (Asp214) polyclonal antibody (Cell Signaling Technology Japan, Tokyo), anti-cleaved caspase-3 (Asp175) polyclonal antibody (Cell Signaling Technology Japan) and anti-human Ki-67 monoclonal antibody (clone MIB-1) (Dako Japan, Tokyo) were used for immunohistochemistry.

Pharmacokinetics study

To evaluate the pharmacokinetics of TC11, we obtained peripheral blood with a heparinized needle from the tail veins of 5-wk-old male ICR mice at 0.5, 1, 1.5, 4, 8, 12, and 24 h after an injection of a low dose (20 mg/kg) or a high dose (100 mg/kg) of TC11. Blood samples were

centrifuged immediately at 3400*g* for 15 min at 4°C. The plasma fraction was transferred to a polypropylene tube and stored at −80°C until the assay. The plasma samples were thawed and diluted with 10% ethanol in phosphate-buffered saline (PBS). A stock solution of TC11 was prepared in ethanol at 1 mg/mL. A series of standard solutions at designated concentrations were prepared by diluting the stock solution with ethanol. All of the samples were analyzed by high-pressure liquid chromatography (HPLC; a Jasco HPLC system, Jasco, Tokyo). The C18 column (Sep-Pak; Waters Associates, Milford, MA) was used. The mobile phases were acetonitrile and 25 mM ammonium acetate (60:40).

Osteoclast differentiation assay

We prepared murine osteoclasts from bone marrow cells as described [20]. In brief, cells obtained from the bone marrow of 5-wk-old male ICR mice were cultured in α-MEM containing 10% FBS with macrophage-colony stimulating factor (M-CSF; R&D Systems, Minneapolis, MN) (10 ng/mL). After 3 days of culture, we removed the floating cells and used the attached cells including bone marrow-derived macrophages (BMMs) as osteoclast precursors. To generate osteoclasts, BMMs were further cultured with M-CSF (10 ng/mL) and receptor activator of nuclear factor κB ligand (RANKL; R&D Systems) (10 ng/mL). After an additional 3–6 days of culture, the cells were fixed and stained for tartrate-resistant acid phosphatase (TRAP) as described [20]. TRAP-positive multinucleated cells containing more than three nuclei were considered $TRAP^+$ multinuclear osteoclasts ($TRAP^+$ MNCs).

Pit formation assay

RAW 264.7 cells were incubated for 5–8 days with RANKL (10 ng/mL). After maturation into osteoclasts, the cells were seeded on BioCoat Osteologic multi-test slides (BD Falcon, BD Biosciences, San Jose, CA). Various concentrations of TC11, thalidomide (Wako, Osaka, Japan), bortezomib (Toronto Research Chemicals Inc., ON, Canada), and osteoprotegerin (OPG; R&D Systems) were added every 2 days for 7 days. Finally Von Kossa stain was conducted to visualize resorption pits. The resorption pits were observed by fluorescence microscopy (BZ-9000, Keyence, Tokyo). The pit area was quantified using Image J software (NIH).

Immunocytochemistry

KMS34 cells were treated with 5 μM TC11 for 4 h and attached to a slide using CYTOSPIN4 (Thermo Fisher Scientific, Rockford, IL), then fixed with 2% paraformaldehyde and permeabilized with 0.5% Triton X followed by blocking with 1% bovine serum albumin (BSA) in PBS. The sample was stained with antibody against α-tubulin (Sigma-Aldrich) followed by FITC-conjugated anti-mouse IgG (Takara Bio, Shiga, Japan), and then observed by fluorescence microscopy (BZ-9000).

Surface plasmon resonance (SPR) analysis

We determined the binding kinetics by a surface plasmon resonance (SPR) analysis with the Biacore 3000 system (GE Healthcare, Buckinghamshire, UK). All experiments were performed at 25°C using TBS buffer (25 mM Tris-HCl, pH 7.4, 137 mM NaCl, 3 mM KCl). Recombinant NPM1 was expressed in *E. coli* and purified. The NPM1 obtained (1.84 μM, 100 μL) was immobilized onto the sensor chip NTA (GE Healthcare). The measurements were performed under conditions of 662 resonance units of the ligand and at a flow rate of 30 μL/min. To determine the dissociation constants, we injected three different concentrations of TC11 and lenalidomide (Santa Cruz Biotechnology, Santa Cruz, CA). The injection periods for association and

dissociation were 60 and 300 s, respectively. The binding data were analyzed with 1:1 binding with the mass transfer model in the BIA evaluation software ver. 4.1 (Biacore).

Statistical analysis

The significance of differences was determined using Student's *t*-test. The level of significance was specified as $p<0.05$.

Results

TC11 inhibited the growth of MM cells with chromosomal abnormalities *in vitro*

We examined whether TC11 could inhibit the growth of four different MM cell lines harboring del 17p and/or t(4;14) in addition to previously reported KMS34 cells [13]. We also analyzed TC11's effect on the bone marrow cells obtained from three MM patients. In an MTT assay, TC11 inhibited the proliferation of the KMS11, KMS26, KMS28, and MUM24 cells as well as the proliferation of all of the bone marrow cells from the MM patients, in a dose-dependent manner (Fig. 1B). TC11 was effective both for high risk and standard risk myeloma cells. As shown in Fig. 1C, dexamethasone (Dex) potentiated TC11 anti-myeloma effect of TC11 in KMS 11 as well as KMS34 cells.

Suppression of the growth of normal hematopoietic cells by TC11

To evaluate the effect of TC11 on normal hematopoiesis, we conducted a colony formation assay using bone marrow cells from ICR mice (Fig. 1D). 1–5 μM of TC11 (IC50 values of most MM cell lines were 3–5 μM) did not suppress the production of the total colonies of normal hematopoietic cells. 25 μM or higher concentrations of TC11 almost completely inhibited the colony formation. TC11 did not inhibit the production of colony-forming unit-granulocyte macrophage (CFU-GM), even though the number of burst-forming unit-erythroid (BFU-E) was decreased by the addition of a 5 μM of TC11 ($p<0.05$) (Fig. 1D).

TC11 inhibited the growth of MM cells in the xenograft mouse model through the induction of apoptosis *in vivo*

We evaluated the anti-myeloma effect of TC11 *in vivo* in the KMS34-bearing xenograft model. KMS34 tumor xenografts (~50 mm^3) were treated with intraperitoneal injections of 20 mg/kg TC11 twice every 3 days for 2 wks, followed by a time-course analysis of the tumor volumes for 15 days. Fig. 2A shows that the tumor growth was significantly suppressed by the TC11 injections compared to the control ($p<0.01$). The average weight of the tumors of the TC11-treated mice on day 14 was 153.94 mg, whereas that of the control mice was 314.14 mg ($p<0.01$) (Fig. 2C). In addition, neither weight loss nor organ damage in lung, kidney or liver was observed macroscopically after the administration of TC11 (data not shown). Higher dose of TC11 (100 mg/kg) was injected to the xenograft model derived from another myeloma cell line, KMS11. As shown in Fig. 2D, TC11 significantly delayed the tumor growth. In one xenograft model, the tumor had almost disappeared after injection of TC11. During treatment of higher dose of TC11, significant body weight loss was not observed in TC11-treated mice.

The hematoxylin-eosin (H.E.) staining of KMS34 and KMS11-derived tumor tissues revealed elevated numbers of cells with aggregated chromatin in the TC11-treated mice compared to the untreated mice (Fig. 2B and 2E). Immunohistochemical analyses showed that cleaved PARP and cleaved caspase 3 were intensely stained in TC11-treated KMS11 tumors, especially in the cell death area (Fig. 2E). Ki-67 antigen, which is preferentially expressed during

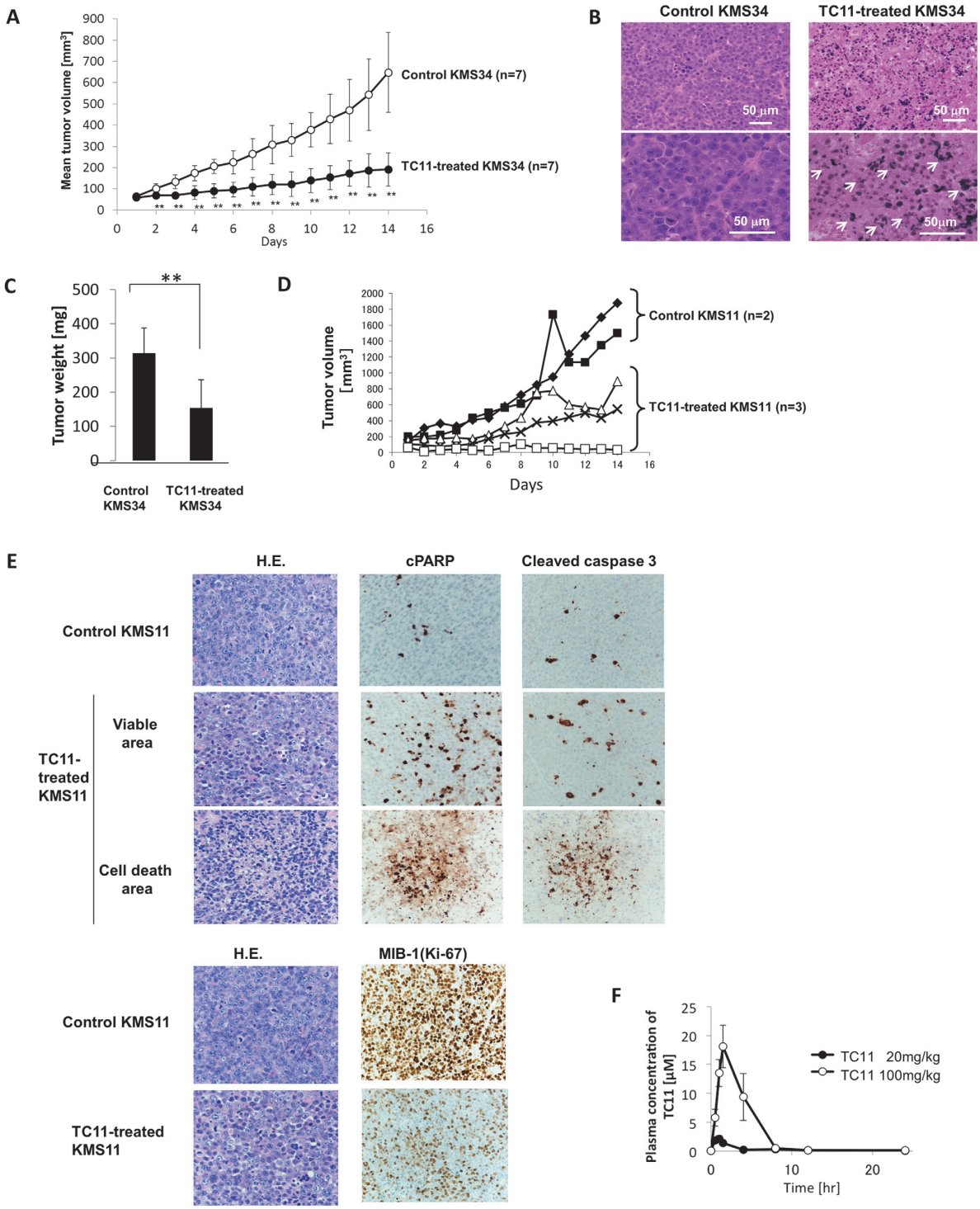

Figure 2. *In vivo* growth inhibition of myeloma cells by intraperitoneal injections of TC11. A total of 3×10^7 KMS34 or KMS11 cells were inoculated subcutaneously into ICR/SCID mice. When the tumors reached 50 mm^3 (day 0), TC11 (20 mg/kg or 100 mg/kg) or vehicle was administered intraperitoneally twice every 3 days for 2 wks. (A) Growth of KMS34-derived subcutaneous plasmacytomas was examined (n = 7). (B) Sections of dissected KMS34-derived tumors were stained with hematoxylin and eosin. The arrows indicate nuclear fragmentation of TC11-treated cells. (C) The weights of KMS34-derived tumors dissected from the KMS34-innoculated mice were measured on day 14. Bars: means ±SD.**$p<0.01$ (Students *t*-test). (D) Growth of KMS11-derived

subcutaneous plasmacytomas was examined. (E) Pathological examination of KMS11-derived tumors was shown. Immunohistochemical staining of the KMS11-derived tumors were also shown. (F) Pharmacokinetics of TC11. Plasma concentrations of TC11 in mice after a single injection of 20 mg/kg or 100 mg/kg of TC11 determined by HPLC.

doi:10.1371/journal.pone.0116135.g002

all active phases of the cell cycle but is absent in resting cells, was less weakly stained in TC11-treated tumors (Fig. 2E). These results suggested that TC11 exhibited anti-tumor activity *in vivo* through the inhibition of cell proliferation and the induction of apoptosis of myeloma cells.

Pharmacokinetics of TC11 in the mouse model

For the pharmacokinetic study, we examined the plasma concentrations of TC11 in mice after a single injection of 20 mg/kg or 100 mg/kg of TC11 using HPLC (Fig. 2F). The maximum concentration (C_{max}) was 2.1 μM, which was observed at 1 hr after the injection (T_{max}). The plasma concentration of TC11 gradually decreased to 0.25 μM at 4 h and to 0.04 μM at 24 h. The elimination half-life (T1/2) was estimated to be 1.2 h. When a higher dose of TC11 (100 mg/kg) was injected, the C_{max} was 18.1 μM and the T_{max} was 1.5 h; the plasma concentration was 0.45 μM at 8 h and 0.16 μM at 24 h. The T1/2 was estimated to be 2.6 h.

TC11 inhibited the differentiation of osteoclasts and bone resorption

The hyperactivity of osteoclasts is considered one of the causes of lytic bone lesions, suggesting that the control of osteoclast activity could be a key to treating bone lesions in MM patients. We therefore examined the effects of TC11 on the differentiation and function of osteoclasts using mouse bone marrow primary cell culture. We analyzed M-CSF and RANKL-treated osteoclasts by TRAP staining after treatment with various concentrations of TC11 (0.01μM–5 μM) (Fig. 3A). The number of TRAP-positive multinuclear cells was significantly lower in the cells treated with more than 0.5 μM of TC11 (Fig. 3B). In contrast, 10 μM of thalidomide or 1 nM of bortezomib did not affect the number of TRAP-positive cells.

We next examined TC11's effect on the bone resorption activity of TC11 in a pit formation assay (Fig. 3C). After the treatment of RAW264.7 cells with TC11 (3 μM, 5 μM), the bone resorption area was reduced in a dose-dependent manner (Fig. 3D). Treatment with thalidomide (10 μM) or bortezomib (1 nM) did not change the resorption area compared to the control.

TC11 induced the fragmentation of α-tubulin

Because we previously found that TC11 binds to α-tubulin, we examined the tubulin formation in KMS34 cells after TC11 treatment. The immunohistochemical analysis showed that TC11-treated cells exhibited elevated levels of α-tubulin fragmentation (Fig. 4A). The percentage of cells with tubulin fragmentation was 6.5% in the cells treated with TC11, which is significantly higher compared to the 0.8% in the untreated cells (Fig. 4B).

Binding between NPM and TC11 or lenalidomide

We previously identified NPM1 as one of the TC11-binding proteins, by mRNA display. In our previous observation, TC11 bound to the NH2-terminal 183-amino-acid (aa) region of monomeric NPM1. In the present study, we assessed the binding capacity of both TC11 and lenalidomide to the full length of NPM1. The SPR analysis showed that not only TC11 but also lenalidomide could bind to NPM1 (Fig. 5A,B). The K_D values of TC11 and lenalidomide were 6.23×10^{-8}M and 7.66×10^{-7}M, respectively.

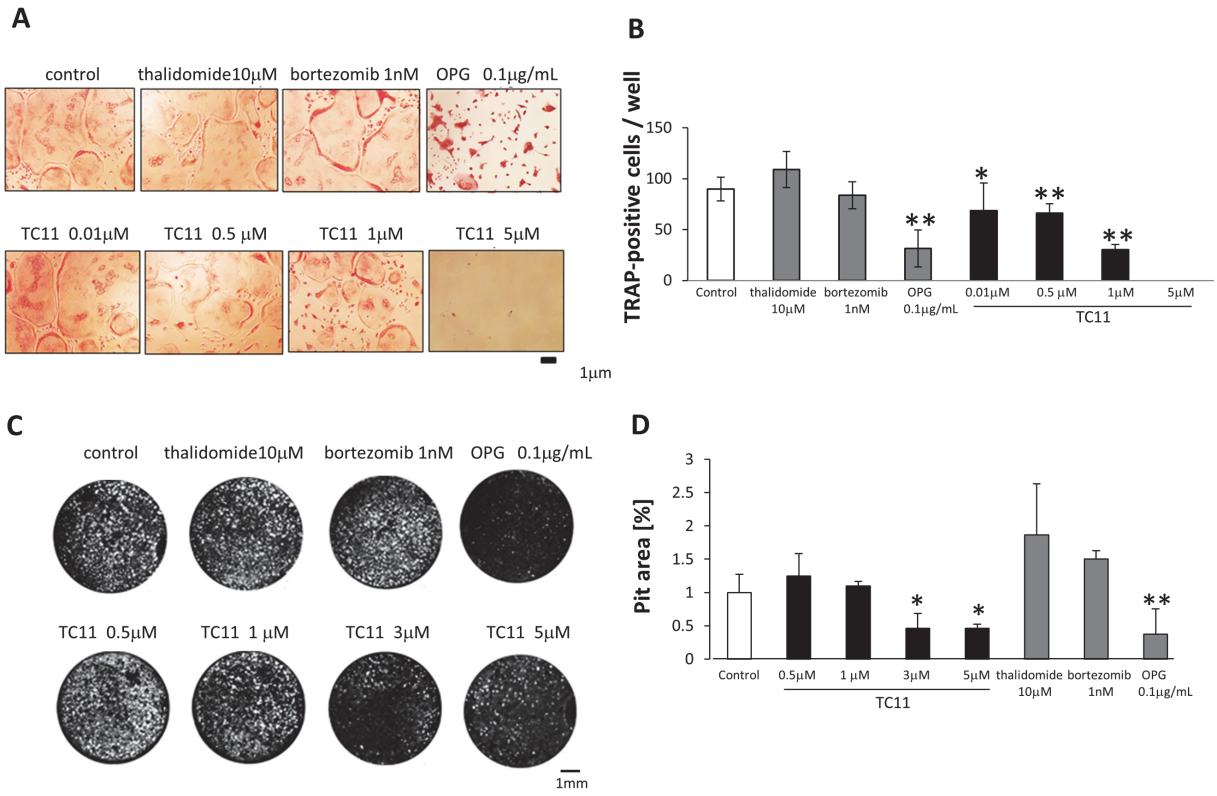

Figure 3. TC11 inhibited both the maturation and function of bone marrow-derived osteoclasts. Mice bone marrow cells were cultured with M-CSF (10 ng/mL) for 3 days, then further cultured with M-CSF (10 ng/mL) and RANKL (10 ng/mL). After an additional 3–6 days of culture with the indicated concentration of TC11, thalidomide, bortezomib, or DMSO, the cells were fixed and stained for TRAP as described in the Materials and Methods section. TRAP-positive multinucleated cells containing more than three nuclei were considered $TRAP^+$ multinuclear osteoclasts. (A) The number and size of $TRAP^+$ multinuclear osteoclasts were decreased by treatment with 0.5–1μM of TC11. (B) The number of $TRAP^+$ multinuclear osteoclasts in each well of a 96-well plate was counted. Bars: means±SD. *$p<0.05$, **$p<0.01$ (Student's *t*-test). (C) RAW 264.7 cells were incubated for 5–8 days with RANKL (10 ng/mL) and seeded on multi-test slides. The indicated concentrations of TC11, thalidomide, bortezomib, or OPG were added every 2 days for 7 days, followed by Von Kossa staining. The resorption pits were observed by fluorescence microscopy and the number of the pits was quantified using Image J software. (B) Bone resorption is indicated by white spots (pit). Bone resorption was suppressed by treatment with 3–5 μM of TC11. (D) The pit area was measured by ImageJ software. The pit area of the DMSO-treated wells was used as the control (= 1). Data shown are representative of three independent experiments. Bars: means±SD. *$p<0.05$, **$p<0.01$ (Student's *t*-test)

doi:10.1371/journal.pone.0116135.g003

Discussion

MM remains difficult to treat and cure, and MM patients with high-risk cytogenetic changes in particular have shown very poor prognosis when treated with existing drugs. To overcome this unmet clinical need, in previous work we screened phthalimide derivatives and identified TC11 as a novel candidate drug for MM. TC11 is different from other IMiDs in chemical structure, lacking glutarimide moiety. That is, TC11 is a phthalimide derivative containing a benzene ring instead of a glutarimide structure (Fig. 1A). In the present study, we observed that TC11 inhibited the growth of MM cell lines, even though some of the myeloma cells harbored high-risk chromosomal abnormalities such as del17, or t(4;14). In addition, growth inhibition of bone marrow cells obtained from the relapsed MM patients was also examined. TC11 more or less inhibited proliferation of myeloma cells obtained from all the patients. Patient #3 showed t(4;14), and patient #2 had extramedullary disease in the liver. Even though these two patients were high-risk cases, TC11 regulated proliferation of the tumor cells (Fig. 1B). Moreover, the growth of total colony-forming cells was not suppressed by the treatment with 1–5

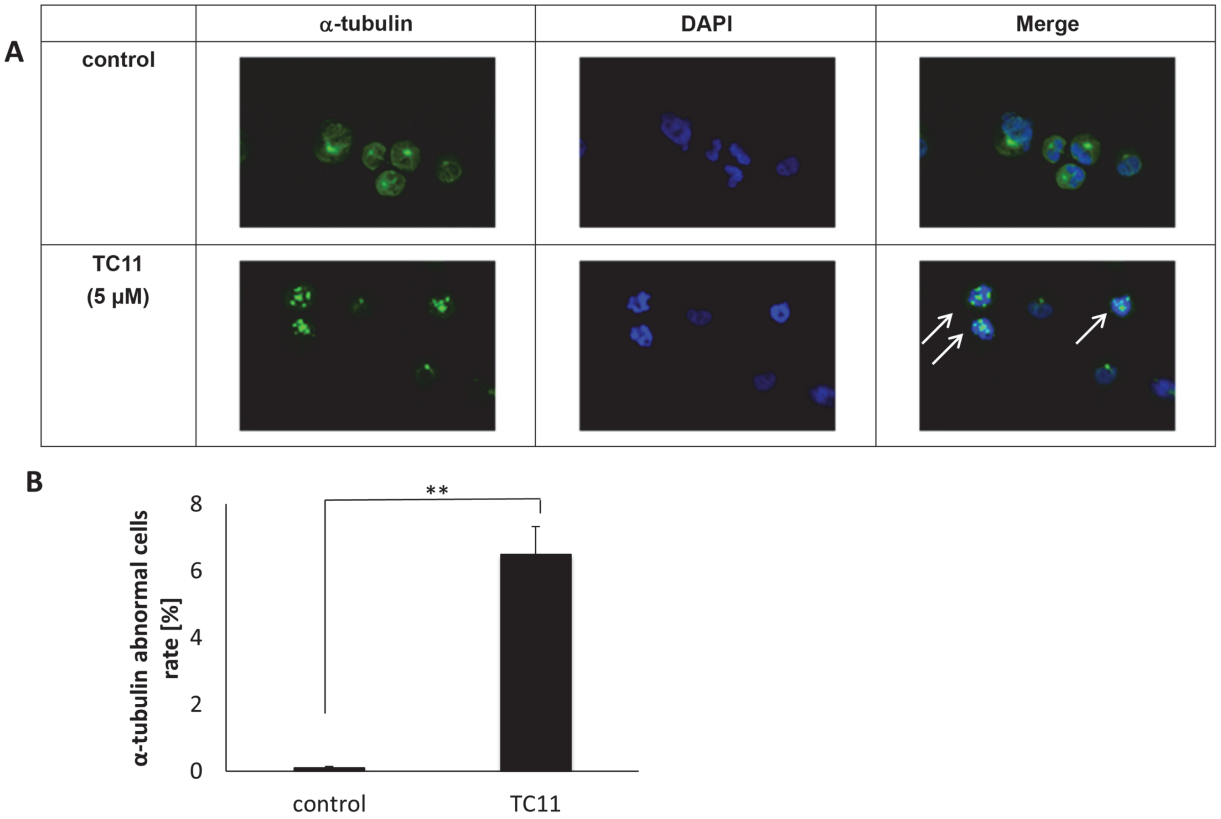

Figure 4. TC11 altered the α-tubulin formation of myeloma cells. KMS34 was treated with 5μM TC11 for 4 hours and attached to a slide by cytospin. The sample was fixed and stained with antibody against α-tubulin followed by FITC-conjugated anti-mouse IgG (green). Nucleus was stained with DAPI (blue). A, Representative mitotic cells with or without TC11 treatment. B, The percentage of cells with fragmented α-tubulin in 2500 cells was calculated independently in 9 areas. **P<0.01 (Student *t*-test). A and B indicate representative data from 3 experiments.

doi:10.1371/journal.pone.0116135.g004

μM of TC11 even though TC11 significantly inhibited the growth of all MM cell lines in such concentrations, suggesting low hematological toxicity. It is speculated that myeloma cells may proliferate more dependently on TC11-associated molecules such as NPM1. Further study is needed to discriminate the molecular function of TC11 on myeloma cells from that on normal hematopoietic cells.

We also confirmed an *in vivo* anti-myeloma effect of TC11 by using intraperitoneal injections of TC11 to KMS34 and KMS11-bearing ICR/SCID mice. The tumor growth in these mice was significantly delayed by the administration of 20 mg/kg or higher dose of TC11. The histopathological examination revealed apoptosis of MM cells, which is consistent with our previous study showing that TC11 induces apoptosis through the activation of caspase 3, 8 and 9 *in vitro* [13]. In addition, no systemic side effects including weight loss occurred.

Our pharmacokinetics study indicated that TC11 was completely eliminated from the plasma at 4 h after the injection of a low dose (20 mg/kg) of TC11 and at 8 h after the injection of a high dose (100 mg/kg) of TC11. These data suggest that TC11 would not accumulate in patients by the administration of TC11 twice at a 3-day interval. To obtain stronger anti-tumor effects, it might be necessary to develop a new drug-delivery system or change the schedule of drug administration.

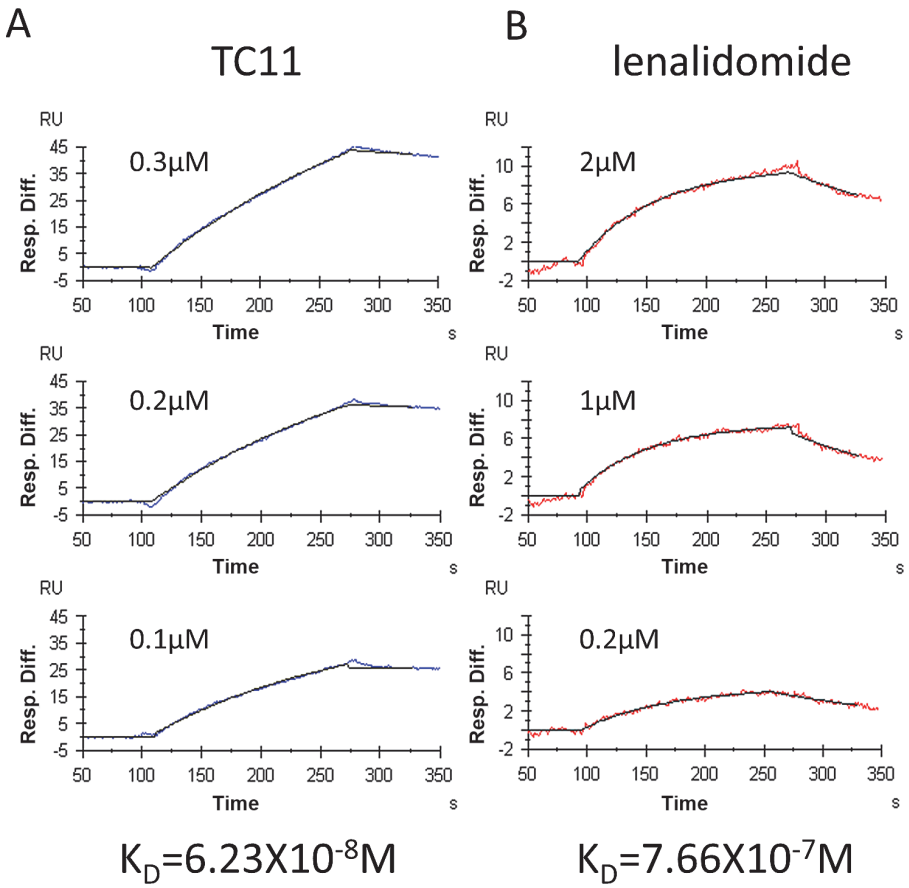

Figure 5. NPM1 interacts with TC11 and lenalidomide. Recombinant NPM1 was expressed in *E. coli* and purified. The NPM1 obtained was immobilized onto the sensor chip NTA followed by an SPR analysis. Panels A and B show representative biosensorgrams of TC11 and lenalidomide, respectively.

doi:10.1371/journal.pone.0116135.g005

Lytic bone disease in MM is thought to be associated with both enhanced activity of osteoclasts and impaired function of osteoblasts. It was reported that bortezomib could cause an increase in bone formation by activating osteoblastic function, which leads to the improvement of osteolytic lesions [21]. Here, we found that TC11 inhibited both the maturation and function of osteoclasts. Osteoclasts are differentiated from hematopoietic stem cells through stimulation with M-CSF and RANKL. Under normal conditions, the balance between bone formation and bone resorption is well-controlled.

However, MM cells produce macrophage inflammatory protein-1 (MIP-1), which stimulates osteoclasts to express receptor activator of nuclear factor-κB (RANK). RANK interacts with RANKL on stromal cells or osteoblasts. This interaction leads to the activation of nuclear factor-kappa B (NF- κB) and nuclear factor of activated T cell c1 (NFATc1) via an activation of AP-1 [22]. In our M-CSF and RANKL-stimulated mouse bone marrow model, we observed that the differentiation of osteoclasts was significantly suppressed by at least 0.5 μM TC11. We also found that the function of osteoclasts was reduced by 3 μM TC11. These anti-osteoclastic effects might be characteristic of TC11, because these effects were not seen in the cells treated with thalidomide nor bortezomib. We also found that this effect was not due simply to the induction of apoptosis of the bone marrow cells, but rather occurred by a direct inhibition of

osteoclast maturation, since apoptosis of osteoclasts was not observed after treatment with 3 μM TC11 (data not shown). It would be worthwhile to investigate the effects of TC11 on the expression of osteoclast-related genes such as AP-1.

To clarify the mechanism of TC11's anti-myeloma effect, we investigated the effects of TC11 on NPM1, since we have found that NPM1 is one of the binding targets of TC11 by an mRNA display (i.e., the IVV method) [13]. In the present study, the results obtained by the SPR analysis indicated that TC11 binds to the full length of NPM1, with the K_D value of 6.23×10^{-8} M. However, the pharmacological significance of the binding of TC11 to NPM1 has not been elucidated.

NPM1 is a nuclear phosphoprotein which plays a variety of roles in cancer cells by affecting DNA repair, centrosome duplication, and molecular chaperoning [23–25]. NPM1 is also important in hematopoiesis by controlling the cell cycle of hematopoietic progenitor cells [26]. In addition, mutation of NPM1 is found in one-third of acute myelogenous leukemia (AML) patients, which changes the localization of NPM1 from the nucleus to the cytoplasm [27–29].

Little is known about the role of NPM1 in MM patients. To our knowledge, there is only one report on NPM and MM, showing an overexpression of NPM1 in hyperdiploid MM cells [30]. All of the MM cell lines we used in the present study expressed NPM1 proteins, but NPM1 gene mutation was not observed in these MM cell lines, and TC11 did not cause an accumulation of NPM1 in the cytoplasm of KMS34 as seen in leukemic cells (data not shown).

Another possibility explaining the role of NPM1 in TC11's effects is that TC11 blocks the oligomerization of NPM1, since the binding site of TC11 contains the oligomerization domain of NPM1. NPM1 normally exists in oligomer form [31]. Therefore, TC11 might affect myeloma cells by blocking the oligomerization of NPM1 and inhibiting its various functions. Qi et al. showed that the inhibition of the oligomerization of NPM1 by a small-molecule inhibitor, NSC348884, induces the apoptosis of cancer cells through the activation of p53 [32]. Balusu et al. reported that NSC348884 could induce the apoptosis of AML cell lines [33].

It is also possible that TC11 impairs centrosomal disruption by binding to NPM1, because NPM1 has been reported to be indispensable to normal centrosomal duplication [34]. The NPM1 gene is located on chromosome 5q35, which is occasionally deleted in myelodysplastic syndrome ($5q^-$MDS) [35]. Considering our observation that lenalidomide could also bind to NPM1, the contribution of these interactions to the anti-tumor effects should be further investigated.

We then analyzed the effects of TC11 on α-tubulin's structure, since we identified α-tubulin as another TC11-binding protein using the IVV method in our previous work [13]. Alpha-tubulin is a component of microtubules that is important for cell division and cellular transport. Drugs that alter the formation of microtubules, such as vinca alkaloids, have been used in cancer therapy. However, the target sites and effects of these drugs on microtubules are different [36, 37]. In the case of TC11, we observed abnormal α-tubulin fragmentation in TC11-treated KMS34 cells (Fig. 4), which suggests that the apoptosis induced by TC11 might be triggered by an abnormal formation of microtubules. In the previous report, knockdown of NPM1 gene induced centrosomal disruption followed by activation of caspase-9 and significant reduction in cell viability [12]. Therefore, it is speculated that the principal actions of TC11 on myeloma cells are centrosomal disruption and abnormal microtubule assembly by binding to NPM1 and α-tubulin, respectively. Consequently, TC11-treated myeloma cells fall into mitotic catastrophe because NPM1 and tubulin families are key molecules for cell division. After these series of actions initiated by TC11-treatment, those cells caused apoptosis. As a next step to clarify exact signaling pathway after binding of TC11 to NPM1, we are trying to knock-down of NPM1 gene in myeloma cells and examine the effects of TC11 on oligomerization and phosphorylation of NPM1 in myeloma cells.

Cereblon (CRBN: cerebral protein with ion protease), a component of the E3 ubiquitin ligase complex, has been identified as a target of thalidomide-mediated teratogenicity [38, 39]. It was shown that not only thalidomide but also lenalidomide and pomalidomide bind to CRBN, attenuating the proliferation of myeloma cells through several pathways such as the down-regulation of autoubiquitination of CRBN [40–41]. However, our experiments using the IVV method failed to screen CRBN as a TC11-binding protein. The difference might be explained by the structure of TC11, because CRBN was reported to bind to a glutarimide moiety of lenalidomide or pomalidomide, which was not included in TC11. On the other hand, NPM1 may bind to the phthalimide moiety which is a common component of TC11 and other IMiDs, since our data showed both TC11 and lenalidomide could bind to NPM1.

Thus, TC11 exerts its anti-myeloma effect via molecular interactions which do not involve CRBN. In addition, TC11 does not form racemate and is expected to lack teratogenicity. The results of our present study suggest that new phthalimide derivatives other than thalidomide, lenalidomide and pomalidomide could be developed by drug designing for the treatment of MM.

In conclusion, we have demonstrated that TC11, a novel phthalimide derivative, has anti-tumor activity against MM cells with high-risk genetic abnormality including del 17p and t (4;14), *in vitro* and *in vivo*. This novel compound also down-regulates the differentiation and function of osteoclasts. Our data provide a strong preclinical rationale for TC11 as a safe and effective drug for the treatment of high-risk MM patients with bone disease. The actions of this drug relating to α-tubulin and NPM1 remain to be further investigated.

Acknowledgments

We thank Dr. Takemi Otsuki for gift of multiple myeloma cell lines.

Author Contributions

Conceived and designed the experiments: HY TO KM TY Y. Hattori. Performed the experiments: YO Y. Hasegawa FT NT HY TO WD TY MH Y. Hattori. Analyzed the data: MM YO Y. Hasegawa FT NT HS HY TO KM WD TY DI Y. Hattori. Wrote the paper: MM HY TO KM DI Y. Hattori.

References

1. Rajkumar SV (2013) Multiple myeloma: 2013 update on diagnosis, risk-stratification, and management. Am J Hematol. 88(3): 226–235. doi: 10.1002/ajh.23390
2. Bird JM, Owen RG, D'Sa S, Snowden JA, Pratt G, et al. (2011) Guidelines for the diagnosis and management of multiple myeloma 2011. Br J Haematol. 154(1): 32–75. doi: 10.1111/j.1365-2141.2011.08573.x PMID: 21569004
3. Terpos E, Kanellias N, Christoulas D, Kastritis E, Dimopoulos MA (2013) Pomalidomide: a novel drug to treat relapsed and refractory multiple myeloma. Onco Targets Ther. 6: 531–538. doi: 10.2147/OTT.S34498 PMID: 23690693
4. McCurdy AR, Lacy MQ (2013) Pomalidomide and its clinical potential for relapsed or refractory multiple myeloma: an update for the hematologist. Ther Adv Hematol. 4(3): 211–216. doi: 10.1177/2040620713480155 PMID: 23730498
5. Siegel DS (2012) Relapsed/Refractory multiple myeloma: defining refractory disease and identifying strategies to overcome resistance. Semin Hematol. 49 Suppl 1: S3–15. doi: 10.1053/j.seminhematol.2012.05.005 PMID: 22727390
6. Lacy MQ (2011) New immunomodulatory drugs in myeloma. Curr Hematol Malig Rep. 6(2): 120–125. doi: 10.1007/s11899-011-0077-y PMID: 21327565
7. Pan B, Lentzsch S (2012) The application and biology of immunomodulatory drugs (IMiDs) in cancer. Pharmacol Ther. 136(1): 56–68. doi: 10.1016/j.pharmthera.2012.07.004 PMID: 22796518

8. Bergsagel PL, Mateos MV, Gutierrez NC, Rajkumar SV, San Miguel JF (2013) Improving overall survival and overcoming adverse prognosis in the treatment of cytogenetically high-risk multiple myeloma. Blood. 121(6): 884–892. doi: 10.1182/blood-2012-05-432203 PMID: 23165477
9. Avet-Loiseau H, Attal M, Campion L, Caillot D, Hulin C, et al. (2012) Long-term analysis of the IFM 99 trials for myeloma: cytogenetic abnormalities [t(4;14), del(17p), 1q gains] play a major role in defining long-term survival. J Clin Oncol. 30(16): 1949–1952. doi: 10.1200/JCO.2011.36.5726 PMID: 22547600
10. Sawyer JR (2011) The prognostic significance of cytogenetics and molecular profiling in multiple myeloma. Cancer Genet. 204(1): 3–12. doi: 10.1016/j.cancergencyto.2010.11.002 PMID: 21356186
11. Mateos MV, Gutierrez NC, Martin-Ramos ML, Paiva B, Montalban MA, et al. (2011) Outcome according to cytogenetic abnormalities and DNA ploidy in myeloma patients receiving short induction with weekly bortezomib followed by maintenance. Blood. 118(17): 4547–4553. doi: 10.1182/blood-2011-04-345801 PMID: 21900193
12. Chang H, Jiang A, Qi C, Trieu Y, Chen C, et al. (2010) Impact of genomic aberrations including chromosome 1 abnormalities on the outcome of patients with relapsed or refractory multiple myeloma treated with lenalidomide and dexamethasone. Leuk Lymphoma. 51(11):2084–2091. doi: 10.3109/10428194.2010.524325 PMID: 20929319
13. Shiheido H, Terada F, Tabata N, Hayakawa I, Matsumura N, et al. (2012) A phthalimide derivative that inhibits centrosomal clustering is effective on multiple myeloma. PLoS One. 7(6):e38878. doi: 10.1371/journal.pone.0038878 PMID: 22761710
14. Chesi M, Bergsagel PL (2013) Molecular pathogenesis of multiple myeloma: basic and clinical updates. Int J Hematol. 97(3): 313–323. doi: 10.1007/s12185-013-1291-2 PMID: 23456262
15. Modi ND, Lentzsch S (2012) Bisphosphonates as antimyeloma drugs. Leukemia. 26(4): 589–594. doi: 10.1038/leu.2011.282 PMID: 22005788
16. Raje N, Roodman GD (2011) Advances in the biology and treatment of bone disease in multiple myeloma. Clin Cancer Res. 17(6):1278–1286. doi: 10.1158/1078-0432.CCR-10-1804 PMID: 21411443
17. Namba M, Ohtsuki T, Mori M, Togawa A, Wada H, et al. (1989) Establishment of five human myeloma cell lines. In Vitro Cell Dev Biol. 25(8): 723–729. doi: 10.1007/BF02623725 PMID: 2768132
18. Du W, Hattori Y, Yamada T, Matsumoto K, Nakamura T, et al. (2007) NK4, an antagonist of hepatocyte growth factor (HGF), inhibits growth of multiple myeloma cells: molecular targeting of angiogenic growth factor. Blood. 109(7): 3042–3049. PMID: 17179234
19. Hattori Y, Du W, Yamada T, Ichikawa D, Matsunami S, et al. (2013) A myeloma cell line established from a patient refractory to thalidomide therapy revealed high-risk cytogenetic abnormalities and produced vascular endothelial growth factor. Blood Cancer J. 3:e115. doi: 10.1038/bcj.2013.13 PMID: 23686003
20. Oikawa T, Oyama M, Kozuka-Hata H, Uehara S, Udagawa N, et al. (2012) Tks5-dependent formation of circumferential podosomes/invadopodia mediates cell-cell fusion. J Cell Biol. 197(4): 553–568. doi: 10.1083/jcb.201111116 PMID: 22584907
21. Zangari M, Terpos E, Zhan F, Tricot G (2012) Impact of bortezomib on bone health in myeloma: a review of current evidence. Cancer Treat Rev. 38(8):968–980. doi: 10.1016/j.ctrv.2011.12.007 PMID: 22226939
22. Matsuo K, Galson DL, Zhao C, Peng L, Laplace C, et al. (2004) Nuclear factor of activated T-cells (NFAT) rescues osteoclastogenesis in precursors lacking c-Fos. J Biol Chem. 279(25): 26475–26480. doi: 10.1074/jbc.M313973200 PMID: 15073183
23. Lindstrom MS (2011) NPM1/B23: A Multifunctional Chaperone in Ribosome Biogenesis and Chromatin Remodeling. Biochem Res Int.:195–209.
24. Colombo E, Alcalay M, Pelicci PG (2011) Nucleophosmin and its complex network: a possible therapeutic target in hematological diseases. Oncogene. 30(23): 2595–2609. doi: 10.1038/onc.2010.646 PMID: 21278791
25. Grisendi S, Mecucci C, Falini B, Pandolfi PP (2006) Nucleophosmin and cancer. Nat Rev Cancer. 6(7): 493–505. doi: 10.1038/nrc1885 PMID: 16794633
26. Li J, Sejas DP, Rani R, Koretsky T, Bagby GC, et al. (2006) Nucleophosmin regulates cell cycle progression and stress response in hematopoietic stem/progenitor cells. J Biol Chem. 281 (24):16536–16545. doi: 10.1074/jbc.M601386200 PMID: 16608843
27. Estey EH (2013) Acute myeloid leukemia: 2013 update on risk-stratification and management. Am J Hematol. 88(4): 318–327. doi: 10.1002/ajh.23404 PMID: 23526416
28. Falini B, Gionfriddo I, Cecchetti F, Ballanti S, Pettirossi V, et al. (2011) Acute myeloid leukemia with mutated nucleophosmin (NPM1): any hope for a targeted therapy? Blood Rev. 25(6):247–254. doi: 10.1016/j.blre.2011.06.001 PMID: 21724308

29. Falini B, Bolli N, Liso A, Martelli MP, Mannucci R, et al. (2009) Altered nucleophosmin transport in acute myeloid leukaemia with mutated NPM1: molecular basis and clinical implications.Leukemia. 23(10): 1731–1743. doi: 10.1038/leu.2009.124 PMID: 19516275

30. Weinhold N, Moreaux J, Raab MS, Hose D, Hielscher T, et al. (2010) NPM1 is overexpressed in hyperdiploid multiple myeloma due to a gain of chromosome 5 but is not delocalized to the cytoplasm. Genes Chromosomes Cancer. 49(4): 333–341. PMID: 20073075

31. Lee HH, Kim HS, Kang JY, Lee BI, Ha JY, et al. (2007) Crystal structure of human nucleophosmin-core reveals plasticity of the pentamer-pentamer interface.Proteins. 69(3): 672–678. doi: 10.1002/prot.21504 PMID: 17879352

32. Qi W, Shakalya K, Stejskal A, Goldman A, Beeck S, et al. (2008) NSC348884, a nucleophosmin inhibitor disrupts oligomer formation and induces apoptosis in human cancer cells.Oncogene. 27(30): 4210–4220. doi: 10.1038/onc.2008.54 PMID: 18345031

33. Balusu R, Fiskus W, Rao R, Chong DG, Nalluri S, et al. (2011) Targeting levels or oligomerization of nucleophosmin 1 induces differentiation and loss of survival of human AML cells with mutant NPM1. Blood. 118(11): 3096–3106. doi: 10.1182/blood-2010-09-309674 PMID: 21719597

34. Okuda M, Horn HF, Tarapore P, Tokuyama Y, Smulian AG, et al. (2000) Nucleophosmin/B23 is a target of CDK2/cyclin E in centrosome duplication. Cell. 103(1): 127–140. doi: 10.1016/S0092-8674(00)00093-3 PMID: 11051553

35. Ebert BL (2011) Molecular dissection of the 5q deletion in myelodysplastic syndrome. Semin Oncol. 38 (5): 621–626. doi: 10.1053/j.seminoncol.2011.04.010 PMID: 21943668

36. Spagnuolo PA, Hu J, Hurren R, Wang X, Gronda M, et al. (2010) The antihelmintic flubendazole inhibits microtubule function through a mechanism distinct from Vinca alkaloids and displays preclinical activity in leukemia and myeloma. Blood. 115(23):4824–4833. doi: 10.1182/blood-2009-09-243055 PMID: 20348394

37. Perez EA (2009) Microtubule inhibitors: Differentiating tubulin-inhibiting agents based on mechanisms of action, clinical activity, and resistance. Mol Cancer Ther. 8(8): 2086–2095. doi: 10.1158/1535-7163.MCT-09-0366 PMID: 19671735

38. Ito T, Ando H, Handa H (2011) Teratogenic effects of thalidomide: molecular mechanisms. Cell Mol Life Sci. 68(9):1569–1579. doi: 10.1007/s00018-010-0619-9 PMID: 21207098

39. Ito T, Ando H, Suzuki T, Ogura T, Hotta K, et al. (2010) Identification of a primary target of thalidomide teratogenicity. Science. 327(5971):1345–1350. doi: 10.1126/science.1177319 PMID: 20223979

40. Lopez-Girona A, Mendy D, Ito T, Miller K, Gandhi AK, et al. (2012) Cereblon is a direct protein target for immunomodulatory and antiproliferative activities of lenalidomide and pomalidomide. Leukemia. 26(11):2326–2335. doi: 10.1038/leu.2012.119 PMID: 22552008

41. Zhu YX, Braggio E, Shi CX, Bruins LA, Schmidt JE, et al. (2011) Cereblon expression is required for the antimyeloma activity of lenalidomide and pomalidomide. Blood. 118(18):4771–4779. doi: 10.1182/blood-2011-05-356063 PMID: 21860026

Acta Med. Okayama, 2015
Vol. 69, No. 5, pp. 261–266
Copyright©2015 by Okayama University Medical School.

Acta Medica Okayama
http://escholarship.lib.okayama-u.ac.jp/amo/

Original Article

Pilot Analysis of Asbestos-induced Diffuse Pleural Thickening with Respiratory Compromise

Daisuke Nojima[a,f], Nobukazu Fujimoto[b]*, Katsuya Kato[c], Yasuko Fuchimoto[d], Katsuyuki Kiura[e], Takumi Kishimoto[f], and Mitsune Tanimoto[a]

[a]Department of Hematology, Oncology and Respiratory Medicine, Okayama University Graduate School of Medicine, Dentistry and Pharmaceutical Sciences, Departments of [c]Radiology and [e]Allergy and Respiratory Medicine (Thoracic Oncology), Okayama University Hospital, Okayama 700–8558, Japan, Department of [b]Medical Oncology, [d]Respiratory Medicine, and [f]Internal Medicine, Okayama Rosai Hospital, Okayama 702–8055, Japan

We investigated the clinical features of asbestos-induced diffuse pleural thickening (DPT) with severe respiratory compromise. We conducted a retrospective study of consecutive subjects with asbestos-induced DPT. Medical data such as initial symptoms, radiological findings, respiratory function test results, and clinical course were collected and analyzed. There were 24 patients between 2003 and 2012. All were men, and the median age at the development of DPT was 74 years. The top occupational category associated with asbestos exposure was dockyard workers. The median duration of asbestos exposure was 35.0 years, and the median latency from first exposure to the onset of DPT was 49.0 years. There were no significant differences in respiratory function test results between the higher and lower Brinkman index groups or between unilateral and bilateral DPT. Thirteen patients had a history of benign asbestos pleural effusion (BAPE), and the median duration from pleural fluid accumulation to DPT with severe respiratory compromise was 28.4 months. DPT with severe respiratory compromise can develop after a long latency following occupational asbestos exposure and a history of BAPE.

Key words: asbestos, pleural thickening, MRC dyspnea scale, respiratory function test, costophrenic angle

Asbestos-related health problems remain a major public health concern. Asbestos-related pleural diseases include malignant pleural mesothelioma (MPM), benign asbestos pleural effusion (BAPE), and diffuse pleural thickening (DPT) [1]; cases of these diseases will continue to be seen in the next several decades due to past industrial asbestos use. Asbestos-induced DPT is considered to be a consequence of asbestos-induced inflammation of the visceral pleura, which leads to adhesion to the parietal pleura. However, the actual pathogenesis is still unknown and the radiological definition of DPT is ambiguous. McLoud *et al.* described DPT on chest X-rays as a smooth, uninterrupted pleural density extending over at least one-quarter of the chest wall, with or without involvement of the costophrenic angle (CPA) [2]. Yates *et al.* also proposed a definition of DPT based on dimensional criteria, in which DPT is characterized by pleural thickening of ≥ 5 mm that extends over more than one-quarter of the chest wall, with or without obliteration of the CPA [3].

Received January 29, 2015; accepted April 20, 2015.
*Corresponding author. Phone:+81–86–262–0131; Fax:+81–86–262–3391
E-mail:nobufujimot@gmail.com (N. Fujimoto)

Conflict of Interest Disclosures: No potential conflict of interest relevant to this article was reported.

Several studies have examined the characteristics of DPT [2, 4–7]. A major limitation of these earlier studies is that their definitions of DPT varied; as such, some studies may have included patients with pleural plaques, BAPE, and MPM, mainly due to the difficulty of confirming a diagnosis of DPT based on chest X-ray without computed tomography (CT) images.

DPT often induces significant impairment of lung function [8]. In Japan, patients with DPT are provided worker's compensation or given financial relief by the Act on Asbestos Health Damage Relief if they present severe respiratory compromise. We recently retrospectively analyzed the clinical features and radiological findings of DPT, and we reported that some of the radiological findings, such as the involvement of CPA and pleural thickness and the craniocaudal and horizontal extension of pleural thickening (as determined by chest CT) were correlated with impaired respiratory function in patients with DPT [9]. There are few reports concerning the features of DPT in patients with severe respiratory compromise, however.

The objectives of the present retrospective analysis, which was conducted in a single region of Japan, were to clarify the clinical features of DPT patients with severe respiratory compromise, including the clinical course. We focused on the association between BAPE and DPT. We also investigated clinical issues associated with the diagnosis, evaluation, and handling of compensation for DPT.

Materials and Methods

Subjects. The consecutive subjects diagnosed as having asbestos-induced DPT in Okayama Rosai Hospital (Okayama, Japan) between 2003 and 2012 were identified. The inclusion criteria were a history of occupational asbestos exposure, pleural thickening >5 mm on chest X-ray extending for more than one-half of the lateral thoracic wall (LTW) in patients with unilateral DPT or more than one-quarter of the LTW in patients with bilateral DPT, and impaired respiratory function (defined below). The subjects had to have been followed up for at least 6 months after the diagnosis of DPT. Medical data from these patients were collected and analyzed retrospectively. The medical information included age, gender, initial symptoms, modified Medical Research Council (mMRC) dyspnea grade, smoking history, radiological findings, respiratory function test results, and the clinical course. Former smoker was defined as those quitted smoking for more than 6 months. Information about the history of asbestos exposure was also collected. In some patients who changed to local hospitals or clinics, we made inquiries about their information at outcome at the relevant medical institutions.

This study was done according to Ethical Guidelines for Epidemiological Research issued by the Japanese Ministry of Education, Culture, Sports, Science and Technology and the Japanese Ministry of Health, Labour and Welfare. This study was approved by the ethics committee of the Japan Labour Health and Welfare Organization and the institutional review board of Okayama Rosai Hospital.

Respiratory function test. Respiratory function tests were performed in clinical settings based on the guidelines set forth in the Official Statement of the American Thoracic Society [10]. The data obtained included the percentage of vital capacity (%VC) and the forced expiratory volume percentage in 1 sec (FEV1). Blood gas data such as PaO_2 (the partial pressure of O_2 in arterial blood) and $PaCO_2$ (the partial pressure of carbon dioxide in arterial blood) were also extracted. The data obtained closest in time to when the chest CT was performed were used for the analyses. Impaired respiratory function was defined as (1) %VC $<60\%$ or (2) %VC 60–80%, FEV1 $\leq$ 70%, and FEV1/forced vital capacity (FVC) $<50\%$ or PaO_2 on arterial blood gas test ≤ 60 Torr.

Statistical analysis. Comparisons between groups were performed using a nonparametric analysis with the Wilcoxon rank-sum test. The latency period of DPT was calculated as the time between the first exposure to asbestos and the onset of DPT. In the patients with a history of BAPE, the period from the detection of pleural effusion to the onset of DPT and the development of severe respiratory impairment were calculated. Correlations were examined in a regression analysis. The software package used for the statistical analyses was JMP 10.0.2 (SAS Institute, Cary, NC, USA).

Results

Patient characteristics. A total of 24 patients were analyzed retrospectively. The patients' demo-

graphic details are listed in Table 1. All of the patients were men, and the median age at the diagnosis of DPT was 74 years. More than 90% of the patients smoked, and the Brinkman index was ≥ 600 in 14 (58.3%) of the patients. Fifteen patients had visited a clinic or a hospital with symptoms, 5 had an abnormal shadow on a chest X-ray at a medical checkup, and 4 were diagnosed with DPT while receiving medical treatment for other diseases. The mMRC dyspnea grade at the diagnosis of DPT was 1 in 3 patients, 2 in 15 patients, 3 in 3 patients, and 4 in 3 patients.

Occupational asbestos exposure history. Occupational categories associated with asbestos exposure are listed in Table 2 and included dockyard, construction, and heating trade work and more. The median (range) duration of asbestos exposure was 35.0 (3.0–50.0) years. The median (range) latency period since the first exposure to the onset of DPT was 49.0 (37.0–64.0) years.

Radiological findings. Unilateral DPT was found in the thorax in 6 cases and bilateral DPT was found in 18 cases at the time of diagnosis. In the 6 cases with unilateral DPT, DPT was found in the right thorax in 4 cases and in the left thorax in 2 cases. Radiographic findings associated with DPT are listed in Table 3. All of the cases showed CPA involvement on chest X-ray. Pleural plaques were detected in most of the patients. Pulmonary asbestosis was diagnosed in 3 (12.5%) cases, and the profusion rate according to the International Labour Organization criteria [11] was 1 in 2 cases and 3 in one case. Rounded atelectasis was detected in 18 (75.0%) cases on chest CT. Crow's feet signs, defined as fibrous strands with accompanying circumscribed pleural thickening, was detected in all cases on chest CT.

Respiratory function test. The median (range) value of %VC was 51.4% (31.2–70.7%); the %VC was < 60% in 22 (91.7%) patients. The median (range) value for FEV1 was 82.9% (47.7–100%). Eighteen (75.0%) patients showed restrictive ventilatory impairment, and 6 (25.0%) showed combined restrictive and obstructive ventilatory impairment. Blood gas data were available in 23 cases, and the median (range) values for PaO_2 and $PaCO_2$ were 78.9 (53–86) Torr and 43.3 (35.8–56.5) Torr, respectively.

We then examined the association between respiratory function and smoking history. First, we compared %VC and FEV1 between lower (< 600) and higher (≥ 600) Brinkman index groups ($n = 10$ and 14, respectively). Never-smokers were included in lower Brinkman index group. The median values for %VC in the lower (< 600) and higher (≥ 600) Brinkman index groups were 50.9% and 51.4%, respectively. The median values for FEV1 in the lower (< 600) and higher (≥ 600) Brinkman index groups were 71.7% and 85.4%, respectively. There

Table 1 Demographics of the study population ($n = 24$)

Characteristics		No. of patients (%)
Median age (range)		74 (63–92) years
Gender	Male	24 (100.0%)
Smoking	Never	6 (25.0%)
	Former	16 (66.7%)
	Present	2 (8.3%)
Initial symptom	Cough	14 (56.0%)
	Chest pain	3 (12.0%)
	Sputum	1 (4.0%)
mMRC* grade	0/1/2/3/4	0/3/15/3/3

*modified Medical Research Council.

Table 2 Occupational category of asbestos exposure ($n = 24$)

Occupation	No. of patients
Dockyards	7
Construction	4
Heating trade	3
Demolition work	2
Asbestos product industry	2
Furnace installation	1
Electric work	1
Painting	1
Plumbing	1
Welding	1
Shipman	1

Table 3 Radiographic findings associated with DPT

Findings	No. of patients (%)
Asbestosis	3 (12.5%)
Pleural plaques (X-ray)	14 (58.3%)
Pleural plaque (CT*)	22 (91.7%)
Rounded atelectasis	18 (75.0%)
Crow's feet sign	24 (100.0%)
Costophrenic angle involvement	24 (100.0%)

*Computed tomography. DPT: diffuse pleural thickening.

were no significant differences in %VC ($p = 0.5780$) and FEV1 ($p = 0.5387$) between the 2 Brinkman index groups (Fig. 1). We also compared the %VC and FEV1 values between lower (< 400) and higher (≥ 400) Brinkman index groups ($n = 6$ and 18, respectively). The median values for %VC in the lower (< 400) and higher (≥ 400) Brinkman index groups were 56.3% and 50.1%, respectively. The median values for FEV1 in the lower (< 400) and higher (≥ 400) Brinkman index groups were 68.1% and 86.4%, respectively. There were no significant differences in %VC ($p = 0.5709$) and FEV1 ($p = 0.0773$) between these 2 Brinkman index groups.

We next examined the association between respiratory function and unilateral or bilateral DPT. The median values for %VC in the unilateral ($n = 6$) and bilateral ($n = 18$) DPT cases were 53.3% and 51.4%, respectively. The median values for FEV1 in the unilateral and bilateral DPT cases were 67.7% and 84.4%, respectively. There were no significant differences in %VC ($p = 0.7642$) or FEV1 ($p = 0.3014$) between the cases of unilateral and bilateral DPT.

We compared respiratory function between 2 groups: those with longer asbestos exposure (≥ 30 years: $n = 16$) and those with shorter asbestos exposure (< 30 years: $n = 8$). The median VC values in the longer- and shorter-exposure groups were 48.4% and 54.2%, respectively. The median FEV1 values in the longer- and shorter-exposure groups were 76.4% (41.3–70.7%) and 85.4%, respectively. The longer-exposure group showed more impaired respiratory function, although the difference was not significant ($p = 0.3123$ for %VC and $p = 0.4813$ for FEV1).

Clinical course of DPT. Thirteen patients had a medical history of BAPE that preceded the diagnosis of DPT. The date of the accumulation of pleural effusion was identified based on their medical records, except in one case. The median (range) duration from the accumulation of pleural effusion to the development of DPT was 28.4 (8.9–255.3) months. The median duration from the accumulation of pleural effusion to the development of impaired respiratory function was 35.1 (2.8–255.3) months. We examined the correlation between the duration from the fluid accumulation to the onset of DPT and the duration of asbestos exposure using a regression analysis, but there was no significant correlation (r = 0.09). In 2 of the 6 cases with unilateral DPT, the DPT had progressed to the other side of the thorax in 3.2 and 18.7 months, respectively. At the time of the analysis, 15 patients were alive and 9 patients had died. Of the 9 patients who had died, 4 died of respiratory failure, and 1 died of lung cancer. The other 4 patients died of unknown causes. There was no patient who developed MPM.

Discussion

We retrospectively analyzed the characteristic features of asbestos-induced DPT. We focused in particular on DPT cases with severe respiratory compromise. The criteria that we applied are those used for worker's compensation and the Act on Asbestos Health Damage Relief in Japan. The top

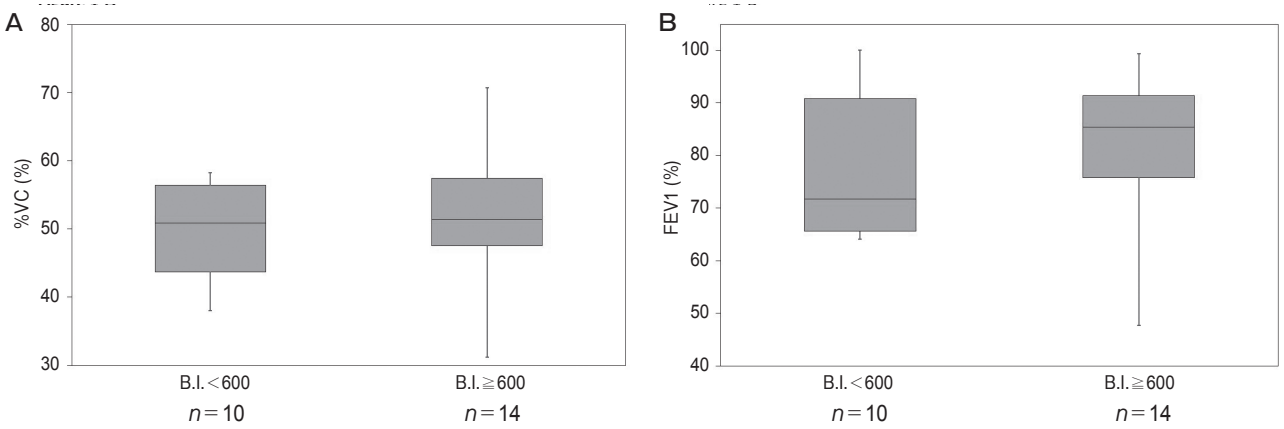

Fig. 1 Comparison of the percentage of vital capacity (%VC) (A) and the forced expiratory volume percentage in 1 sec (FEV1) (B), between the groups with lower and higher Brinkman index values.

occupational category in which the patients had been exposed to asbestos was dockyard workers, as there is a dockyard facility in the suburbs of the Okayama area. The median duration of asbestos exposure was 35 years, and the median latency period for the development of DPT from the first asbestos exposure was 49.0 years. These results are similar to those of our previous study [9] and those from other groups [7, 12]. The results of the present study confirm that DPT can develop after long latency periods following occupational asbestos exposure.

Making a diagnosis of DPT is challenging. In the present study, we defined DPT as pleural thickening of > 5 mm on a posteroanterior chest X-ray, extending for more than one-half of the LTW in the patients with unilateral DPT, or over more than one-quarter of the LTW in the patients with bilateral DPT. These definitions were made based on dimensional criteria [3], because these are the criteria that are applied when making a diagnosis for the certification of worker's compensation or the Act on Asbestos Health Damage Relief in Japan. However, these criteria are based on chest X-rays and are ambiguous and subjective.

Ameille *et al.* reported that obliteration of the CPA was a far more reliable sign than dimensional criteria in the characterization of DPT [13]. Accordingly, the revised International Labor Office (ILO) Classification of Radiographs of Pneumoconiosis provided clearer criteria, in which involvement of the CPA had to be demonstrated for DPT [11]. We recently reported that the involvement of the CPA was negatively correlated with %VC [9]. This finding supports the use of CPA involvement not only for making a diagnosis of DPT, but also for assessing the severity of DPT. There is still room for discussion regarding the most relevant radiological diagnostic criteria for DPT.

Our present findings demonstrated that breathlessness, cough, and chest pain were the most frequent symptoms of DPT; this finding was similar to that of Yates *et al.* [3]. Moreover, 75.0% of the patients showed restrictive ventilatory impairment, and 25.0% of the patients showed combined ventilatory impairment. The characteristic features of DPT with respect to respiratory function testing are a restrictive ventilator defect, decreased compliance, a reduction in total lung capacity, and impairment of gas transfer [8]. We suggest that the obstructive ventilatory impairment demonstrated in some of the patients in our study may be due to a history of smoking, although we could find no clear association between respiratory function and smoking history.

Unilateral DPT has been reported to cause less severe ventilatory impairment than bilateral DPT [8]. However, there were no differences in ventilatory impairment between the patients with unilateral or bilateral DPT in the present study and in our previous study [9]. However, caution should be used when drawing conclusions from these results, since the sample size was small. In the present study, FEV1 in unilateral DPT was lower than that in bilateral DPT. In fact, among 6 cases with unilateral DPT, there were 3 cases with mild pulmonary emphysema, 1 case with asbestosis, and 1 case with pulmonary emphysema and bronchial asthma. We consider that these concomitant diseases contributed to lower FEV1 in unilateral DPT.

Severe respiratory compromise is the key factor for approval for worker's compensation, and thus the most appropriate method for assessing respiratory impairment associated with DPT should be investigated further.

In the present study, we focused on the sequence of DPT and BAPE (also known as asbestos pleuritis). Epler *et al.* advocated the following diagnostic criteria for BAPE: (1) previous asbestos exposure, (2) determination of pleural effusion by chest X-ray or thoracentesis, and (3) absence of other causes of effusion [4]. We examined the patients' history of pleural fluid accumulation based on the medical information available and their subsequent clinical courses. We found that 54.2% of the 24 DPT cases had a history of pleural fluid accumulation, and they subsequently developed DPT at a median of 28.4 months. In addition, these patients developed severe respiratory compromise at a median of 35.1 months following the episode of pleural fluid accumulation. In a previous report, 40% of DPT cases were preceded by the development of pleural effusion [7]. However, in the present study, there were some cases in which it was difficult to determine the radiological change from BAPE to DPT, especially in patients with BAPE in the organizing stage. Diagnostic criteria for differentiating between BAPE in the organizing stage and DPT would be of critical importance with respect to

worker's compensation in Japan.

Our present findings demonstrated that the main cause of death was respiratory failure. Karjalainen *et al.* reported that asbestos-induced benign pleural disease raised the risk of MPM, but the risk of lung cancer was only slightly elevated [14]. In our study, only one of the 24 patients died of lung cancer and there were no patients with MPM. Associations between DPT and MPM or lung cancer should be clarified in a large-scale, long-term study.

In conclusion, our results indicate that DPT can develop after a long latency period following occupational asbestos exposure and a history of BAPE. Radiological diagnostic criteria that are suitable for practical use and appropriate methods for assessing respiratory impairment due to DPT should be established. Clinical, pathological, and temporal alterations that occur in the transition from BAPE to DPT should be clarified, and the association between DPT and MPM or lung cancer should be examined in large-scale, long-term prospective studies.

Acknowledgments. This study was supported by the Japanese Ministry of the Environment. This study is a part of the research and development and dissemination projects related to 9 fields of occupational injuries and illnesses of the Japan Labour Health and Welfare Organization.

References

1. American Thoracic Society: Diagnosis and initial management of nonmalignant diseases related to asbestos. Am J Respir Crit Care Med (2004) 170: 691–715.
2. McLoud TC, Woods BO, Carrington CB, Epler GR and Gaensler EA: Diffuse pleural thickening in an asbestos-exposed population: prevalence and causes. AJR Am J Roentgenol (1985) 144: 9–18.
3. Yates DH, Browne K, Stidolph PN and Neville E: Asbestos-related bilateral diffuse pleural thickening: natural history of radiographic and lung function abnormalities. Am J Respir Crit Care Med (1996) 153: 301–306.
4. Epler GR, McLoud TC and Gaensler EA: Prevalence and incidence of benign asbestos pleural effusion in a working population. JAMA (1982) 247: 617–622.
5. Hillerdal G and Ozesmi M: Benign asbestos pleural effusion: 73 exudates in 60 patients. Eur J Respir Dis (1987) 71: 113–121.
6. de Klerk NH, Cookson WO, Musk AW, Armstrong BK and Glancy JJ: Natural history of pleural thickening after exposure to crocidolite. Br J Ind Med (1989) 46: 461–467.
7. Jeebun V and Stenton SC: The presentation and natural history of asbestos-induced diffuse pleural thickening. Occup Med (Lond) (2012) 62: 266–268.
8. Rudd RM: New developments in asbestos-related pleural disease. Thorax (1996) 51: 210–216.
9. Fujimoto N, Kato K, Usami I, Sakai F, Tokuyama T, Hayashi S, Miyamoto K and Kishimoto T: Asbestos-related diffuse pleural thickening. Respiration (2014) 88: 277–284.
10. American Thoracic Society: Standardization of Spirometry, 1994 Update. Am J Respir Crit Care Med (1995) 152: 1107–1136.
11. International Labour Office: Guidelines for the use of the ILO International Classification of Radiographs of Pneumoconioses. Revised edition 2011. (2011) Geneva, International Labour Office.
12. Kee ST, Gamsu G and Blanc P: Causes of pulmonary impairment in asbestos-exposed individuals with diffuse pleural thickening. Am J Respir Crit Care Med (1996) 154: 789–793.
13. Ameille J, Matrat M, Paris C, Joly N, Raffaelli C, Brochard P, Iwatsubo Y, Pairon JC and Letourneux M: Asbestos-related pleural diseases: dimensional criteria are not appropriate to differentiate diffuse pleural thickening from pleural plaques. Am J Ind Med (2004) 45: 289–296.
14. Karjalainen A, Pukkala E, Kauppinen T and Partanen T: Incidence of cancer among Finnish patients with asbestos-related pulmonary or pleural fibrosis. Cancer Causes Control (1999) 10: 51–57.

Lung Cancer 90 (2015) 111–117

Contents lists available at ScienceDirect

Lung Cancer

journal homepage: www.elsevier.com/locate/lungcan

Prognostic significance of the lymphocyte-to-monocyte ratio in patients with malignant pleural mesothelioma☆

Tomoko Yamagishi[a], Nobukazu Fujimoto[b,*], Hideyuki Nishi[c], Yosuke Miyamoto[a], Naofumi Hara[a], Michiko Asano[a], Yasuko Fuchimoto[a], Sae Wada[a], Kenichi Kitamura[a], Shinji Ozaki[a], Takumi Kishimoto[d]

[a] Department of Respiratory Medicine,Okayama Rosai Hospital, Okayama, Japan
[b] Department of Medical Oncology, Okayama Rosai Hospital, Okayama, Japan
[c] Department of Surgery, Okayama Rosai Hospital, Okayama, Japan
[d] Department of Internal Medicine, Okayama Rosai Hospital, Okayama, Japan

ARTICLE INFO

Article history:
Received 4 April 2015
Received in revised form 2 July 2015
Accepted 27 July 2015

Keywords:
Asbestos
Lymphocyte-to-monocyte ratio
Malignant pleural mesothelioma
Prognostic score

ABSTRACT

Objectives: Chronic inflammation plays a key role in the pathogenesis of malignant pleural mesothelioma (MPM) as a result of asbestos exposure. Several inflammation-based prognostic scores including the lymphocyte-to-monocyte ratio (LMR), Glasgow Prognostic Score (GPS), neutrophil-to-lymphocyte ratio (NLR), and platelet-to-lymphocyte ratio (PLR) reportedly predict survival in many malignancies, while the role of LMR in MPM remains unclear. The aim of this study was to evaluate the clinical value of LMR and to compare the prognostic value of these inflammation-based scores in predicting overall survival (OS) in MPM.

Materials and methods: One hundred and fifty patients with histologically proven MPM were included in this retrospective study. Kaplan–Meier curves and multivariate Cox-regression analyses were calculated for OS. The area under the receiver operating characteristics curve (AUC) was calculated to compare the discriminatory ability of each scoring system.

Results: An elevated LMR was significantly associated with prolonged OS. Patients with LMR <2.74 had significantly poor survival compared with LMR ≥2.74 (median, 5.0 versus 14.0 months; $p = 0.000$). The LMR consistently had a higher AUC value at 6 months (0.722), 12 months (0.712), and 24 months (0.670), compared with other scores. Multivariate analysis showed that the LMR was independently associated with OS.

Conclusions: The LMR is an independent prognostic marker for OS in patients with MPM and is superior to other inflammation-based prognostic scores with respect to prognostic ability.

© 2015 Elsevier Ireland Ltd. All rights reserved.

1. Introduction

Malignant pleural mesothelioma (MPM) is a rare but aggressive primary pleural malignancy that is associated with asbestos exposure [1]. Its prognosis remains poor, as most patients present with unresectable disease at diagnosis or are deemed inoperable owing to age or medical comorbidities. Although several treatment options have been delivered to patients with MPM, the median survival time is approximately 12 months [2]. Despite a very poor prognosis, some selected patients live with the disease for a considerable period of time; median survival is 12.8–46.9 months when treated using a multimodality therapy that contains either (1) neoadjuvant chemotherapy and surgery with or without radiation therapy, or (2) adjuvant chemotherapy [3].

The best-known clinical prognostic scoring systems for MPM have originated from the European Organization for Research and Treatment of Cancer (EORTC) [4] and the Cancer and Leukemia Group B (CALGB) [5], and take into account a combination of biological and clinical factors. However, these scoring systems are not routinely used in MPM prognosis because they are time-consuming to perform.

It is well known that systemic inflammatory response plays an important role in cancer progression [6]. Although the mechanisms

☆ This study is supported by "the research and development and the dissemination projects related to the 9 fields of occupational injuries and illnesses" of the Japan Labour Health and Welfare Organization.

* Corresponding author at: Department of Medical Oncology, Okayama Rosai Hospital, 1-10-25 Chikkomidorimachi, Okayama 7028055, Japan. Fax: +81 86 2623391.
E-mail address: nobufujimot@gmail.com (N. Fujimoto).

http://dx.doi.org/10.1016/j.lungcan.2015.07.014
0169-5002/© 2015 Elsevier Ireland Ltd. All rights reserved.

of carcinogenesis in MPM are incompletely understood, chronic inflammation is critically involved in the pathogenesis of MPM as a result of asbestos exposure. In addition to its involvement in the pathogenesis of cancer-related cachexia, systemic inflammation can predict clinically meaningful outcomes, such as overall survival (OS) and response to systemic treatment [7]. Several studies have shown that inflammation-based prognostic scores that include a combination of serum C-reactive protein (CRP) and albumin (ALB) (e.g., the Glasgow Prognostic Score [GPS] and modified GPS [mGPS]), a combination of neutrophil and lymphocyte counts (e.g., the neutrophil-to-lymphocyte ratio, NLR), and a combination of platelet (PLT) and lymphocyte counts (e.g., the platelet-to-lymphocyte ratio, PLR) are associated with survival in patients with various cancers, including MPM [8,9]. Lymphocytes act as tumor suppressors by inducing cytotoxic cell death and inhibiting tumor cell proliferation and migration [10]. The important role of monocytes and macrophages in cancer, including thoracic malignancies, has recently been uncovered [11]. More recently, some studies demonstrated that lymphocyte-to-monocyte ratio (LMR) is associated with prognosis in several cancers, including hematological malignancy [12] and some solid tumors. However, to the best of our knowledge, there is no evidence determining the association between LMR and the survival of MPM patients.

The aim of this study was to assess the prognostic role of inflammation-based prognostic scores such as the GPS, mGPS, NLR, PLR, and LMR in patients with MPM.

2. Materials and methods

2.1. Patient population

The study included 150 consecutive patients with histologically proven MPM between July 1993 and October 2014, at Okayama Rosai Hospital. No patients showed obvious clinical evidence of infection or other inflammatory conditions such as rheumatoid arthritis at the diagnosis of MPM. Baseline prognostic clinical and laboratory variables were collected retrospectively from patients' medical records. These included age, gender, histological subtype, stage, and Eastern Cooperative Oncology Group (ECOG) performance status (PS). Staging was determined according to the International Mesothelioma Interest Group (IMIG) staging system [13], based on enhanced CT of whole body, magnetic resonance imaging of the brain, and bone scintigraphy. Positron-emission tomography was available since 2012 and substituted to bone scintigraphy in 20 cases.

This study followed REMARK guidelines [14] and was conducted according to The Ethical Guidelines for Epidemiological Research by Japanese Ministry of Education, Culture, Sports, Science and Technology, and the Ministry of Health, Labour and Welfare. This study was approved by the Japan Labour, Health and Welfare Organization and the institutional review boards of Okayama Rosai Hospital. Patient confidentiality was strictly maintained.

2.2. Inflammation-based prognostic scores and other variables

Blood samples were obtained at the time of diagnosis of MPM for measurement of white blood cell count (WBC), absolute neutrophil count (ANC), absolute lymphocyte count (ALC), absolute monocyte count (AMC), PLT, CRP, and ALB. The LMR was defined as the ALC divided by the AMC. The NLR was calculated by dividing the ANC by the ALC; we applied a cutoff value of ≤ 5 versus >5 in accordance with the first report of NLR in MPM [15]. The same calculation was applied to derive the PLR; the cutoff for positivity was 150 [16].

The GPS was calculated as described in previous studies [17]. Briefly, patients with both elevated CRP (>1.0 mg/dL) and low ALB (<3.5 g/dL) were allocated a score of 2. Patients in whom only one of these biochemical abnormalities was present were allocated a score of 1. Patients in whom neither abnormality was present were allocated a score of 0. Regarding mGPS, patients with both elevated CRP (>1.0 mg/dL) and low ALB (<3.5 g/dL) were allocated a score of 2, patients in whom only CRP was elevated (>1.0 mg/dL) were allocated a score of 1, and those with normal CRP were allocated a score of 0 [18]. The EORTC Prognostic Score (EPS) was devised to subcategorize patients into low-risk or high-risk groups based on age, gender, histology, probability of diagnosis, and leukocyte count [4]. The CALGB score incorporates the presence of non-epithelial histology, weight loss, or chest pain; high platelet (PLT) and WBC; low hemoglobin; high serum lactate dehydrogenase; advanced age; and PS [5]. The CALGB groups were combined into three prognostic groups (e.g., groups 1/2, 3/4, or 5/6), because of the small numbers in the even numbered groups [19].

2.3. Statistical analysis

Receiver operating characteristic (ROC) curve analysis was performed to select the most appropriate cut-off point for LMR, AMC, and ALC to predict poor prognosis in patients with MPM. The score with the maximum sensitivity and specificity was selected as the best cut-off value. Survival outcomes were dichotomized by survival (alive versus death) in the ROC analysis. The relationships between the LMR and clinico-pathological features were evaluated using the chi-squared test. The primary objective of this study was to assess the association of inflammation-based scores and OS, which was defined as the time from diagnosis until death from any cause. OS was obtained by using Kaplan–Meier methods, and between-group differences were compared using the log-rank test. Univariate and multivariate analyses were performed regarding the potential prognostic factors using the Cox proportional hazard model. A stepwise backward procedure was used to derive a final model of the variables. Age (<70 versus $\geq$70 years), gender (male versus female), ECOG PS ($\leq$1 versus >1), histological subtype (epithelioid versus non-epithelioid), IMIG stage (I/II versus III/IV), EPS (high-risk versus low-risk), CALGB scoring system (group 1/2 versus group 3/4 versus group 5/6), surgical intervention (yes versus no), baseline WBC ($\leq 8.3 \times 10^9$/L versus $>8.3 \times 10^9$/L) and PLT ($\leq 400 \times 10^9$/L versus $>400 \times 10^9$/L), ALB ($\geq$3.5 g/dL versus <3.5 g/dL), and difference in hemoglobin (<10 g/L versus $\geq$10 g/L) entered the calculations. An ROC curve was also generated and the area under the curve (AUC) was calculated to evaluate the discriminatory ability of each scoring system. A two-tailed p-value <0.05 was considered statistically significant. All statistical analysis was performed using STATA software (version 12.1; StataCorp, College Station, Texas).

3. Results

3.1. Patient characteristics

The patient and tumor characteristics at baseline are shown in Table 1. Median age at the time of diagnosis was 70 (range: 38–92) years. The majority of study participants were male (93.3%) and had a diagnosis of stage III/IV (64.0%). Surgery was performed in 44 (29.3%) patients including 38 extrapleural pneumonectomy, 3 pleural decortication, and 3 tumor excision. Systemic chemotherapy and radiotherapy were delivered as initial treatment to 86 (57.3%) and 3 (2.0%) patients, respectively. The remaining 17 (11.3%) patients received best supportive care. The median follow-up duration was 11 (range: 1.0–150.0) months. At the time of analysis, 116 (77.3%) patients had died, and the median OS was 13.0 [95% confidence interval (CI), 10.0–16.0] months.

Table 1
Patient characteristics ($n = 150$).

	No. of patients	%
Median age at diagnosis (range)	70 (38–92)	
Gender		
Male	140	93.3
Female	10	6.7
ECOG PS		
≤1	129	86.0
>1	21	14.0
Histological subtype		
Epithelioid	97	64.7
Non-epithelioid	53	36.3
IMIG stage at diagnosis		
I/II	54	36.0
III/IV	96	64.0
Treatment modalities		
Surgery (including multimodal treatment)	44	29.3
Systemic chemotherapy only	86	57.3
Radiotherapy only	3	2.0
Best supportive care only	17	11.3
CALGB group		
1–2	49	32.7
3–4	68	45.3
5–6	33	22.0
EORTC prognostic score		
Low risk	91	60.7
High risk	59	39.3
Platelet counts, mean ± SD ($\times 10^9$/L)	299.5 ± 102.1	
≤400	130	86.7
>400	20	13.3
Hemoglobin difference (g/L)		
<10	18	12.0
≥10	132	88.0
Albumin (g/dL)		
≥3.5	76	50.7
<3.5	74	49.3
White cell count, mean ± SD ($\times 10^9$/L)	8.32 ± 5.25	
≤8.3	102	68.0
>8.3	48	32.0
Neutrophil count, mean ± SD ($\times 10^9$/L)	6.01 ± 5.00	
Lymphocyte count, mean ± SD ($\times 10^9$/L)	1.50 ± 0.57	
Monocyte count, mean ± SD ($\times 10^9$/L)	0.57 ± 0.42	
Neutrophil-to-lymphocyte ratio, mean ± SD	5.63 ± 10.99	
≤5	112	74.7
>5	38	25.3
Platelet-to-lymphocyte ratio, mean ± SD	228.40 ± 114.18	
<150	44	29.3
≥150	106	70.7
Lymphocyte-to-monocyte ratio, mean ± SD	3.36 ± 2.26	
≥2.74	109	72.7
<2.74	41	27.3
The Glasgow Prognostic Score		
0	45	30.0
1	37	24.7
2	68	45.3
The modified Glasgow Prognostic Score		
0	51	34.0
1	31	20.7
2	68	45.3

ECOG: Eastern Cooperative Oncology Group; PS: performance status; IMIG: International Mesothelioma Interest Group; CALGB: Cancer and Leukemia Group B; EORTC, EORTC: European Organisation for Research and Treatment of Cancer.

3.2. The cutoff value for ALC, AMC, and LMR at diagnosis for survival analysis

The mean (±SD) lymphocyte count was 1.50 (±0.57) × 10^9/L, and the mean monocyte count was 0.57(±0.42) × 10^9/L. The mean (±SD) LMR level was 3.36 (±2.26). Applying ROC analysis, the optimal LMR cut-off was 2.74 (AUC, 0.736; 95% CI, 0.647–0.824) for OS. All patients were categorized as either high-LMR (≥2.74) or low-LMR (<2.74). Overall, there were 41 (27.3%) patients with LMR <2.74 and 109 (72.7%) patients with LMR ≥2.74. Similarly, AMC of 0.28 × 10^9/L (AUC, 0.741; 95% CI, 0.648–0.834) and ALC of 1.73 × 10^9/L (AUC, 0.532; 95% CI, 0.408–0.656) were selected as the optimal cut-off values.

3.3. Prognostic factor analysis for OS

Univariate analysis variables that predicted poor OS included male gender ($p = 0.022$), PS > 1 ($p = 0.001$), non-epithelioid histologic subtype ($p = 0.000$), stages III–IV ($p = 0.000$), no surgical intervention ($p = 0.000$), baseline WBC >8.30 × 10^9/L ($p = 0.038$), baseline ALB <3.5 g/L ($p = 0.031$), high CALGB ($p = 0.010$), high-risk EPS ($p = 0.014$, Fig. 1A), NLR >5 ($p = 0.002$, Fig. 1B), PLR >150 ($p = 0.014$, Fig. 1C), LMR <2.74 ($p = 0.000$, Fig. 1D), high GPS ($p = 0.006$), high mGPS ($p = 0.014$), AMC ≥0.28 × 10^9/L ($p = 0.011$, Fig. 1E), and ALC <1.73 × 10^9/L ($p = 0.009$, Fig. 1F). Multivariate analysis revealed PS > 1 (hazard ratio [HR], 1.84; 95% CI, 1.07–3.16; $p = 0.027$), non-epithelioid histologic subtype (HR, 2.24; 95% CI, 1.51–3.33; $p = 0.000$), stage III/IV (HR, 1.70; 95% CI, 1.08–2.69; $p = 0.022$), no surgical intervention (HR, 2.41; 95% CI, 1.43–4.04; $p = 0.001$), LMR <2.74 (HR, 2.34; 95% CI, 1.58–3.47; $p = 0.000$) as independent prognostic factors of OS (Table 3).

ROC curves were constructed for survival status at 6, 12, and 24 months of follow-up, and the areas under the ROC curves were compared to assess the discrimination ability of each inflammation scoring system. The LMR consistently had higher AUC value at 6 months (0.772), 12 months (0.712), and 24 months (0.670) in comparison with other inflammation-based prognostic scores (Fig. 2).

An elevated LMR was significantly associated with prolonged OS. Patients with an LMR of <2.74 exhibited a median OS of 5.0 (95% CI, 4.0–10.0) months, while patients with an LMR ≥2.74 had a median OS of 14.0 (95% CI, 13.0–23.0) months ($p = 0.000$). Subgroup analyses were performed regarding histological subtype (epithelioid versus non-epithelioid), stage (I/II versus III/IV), and surgical intervention (yes versus no). In univariate analysis, the prognostic value of LMR was significant in patients with epithelioid subtype (HR, 2.76; 95% CI, 1.61–4.71; $p = 0.000$), patients with non-epithelioid subtype (HR, 3.38; 95% CI, 1.67–6.87; $p = 0.001$), and patients designated stage I/II (HR, 2.85; 95% CI, 1.21–6.71; $p = 0.016$) or stage III/IV (HR, 2.71; 95% CI, 1.69–4.35; $p = 0.000$). In addition, the predictive value of LMR was significantly stratified by surgical intervention (HR, 2.90; 95% CI, 1.20–6.98; $p = 0.017$) and by no surgical intervention (HR, 3.15; 95% CI, 1.98–5.05; $p = 0.000$). Kaplan–Meier curves revealed that decreased LMR (<2.74) about these factors was significantly associated with decreased OS (Fig. 3).

This study demonstrated that the LMR was associated with ECOG PS ($p = 0.001$), histological subtype ($p = 0.035$), stage ($p = 0.010$), surgical intervention ($p = 0.043$), CALGB ($p = 0.022$), EPS ($p = 0.001$), and baseline ALC ($p = 0.000$) and AMC ($p = 0.000$) (Table 2).

4. Discussion

In the present study, we demonstrated that elevated LMR, an inflammation-based prognostic score, was a favorable prognosis factor for OS in MPM. To the best of our knowledge, this study is the first to demonstrate that the LMR is an independent marker of prognosis in patients with MPM and features prognostic ability superior to that of the NLR, PLR, GPS, and mGPS.

Accumulating studies have demonstrated a strong link between systemic inflammatory responses (including neutrophils, lymphocytes, and monocytes) and cancer, and those responses have been

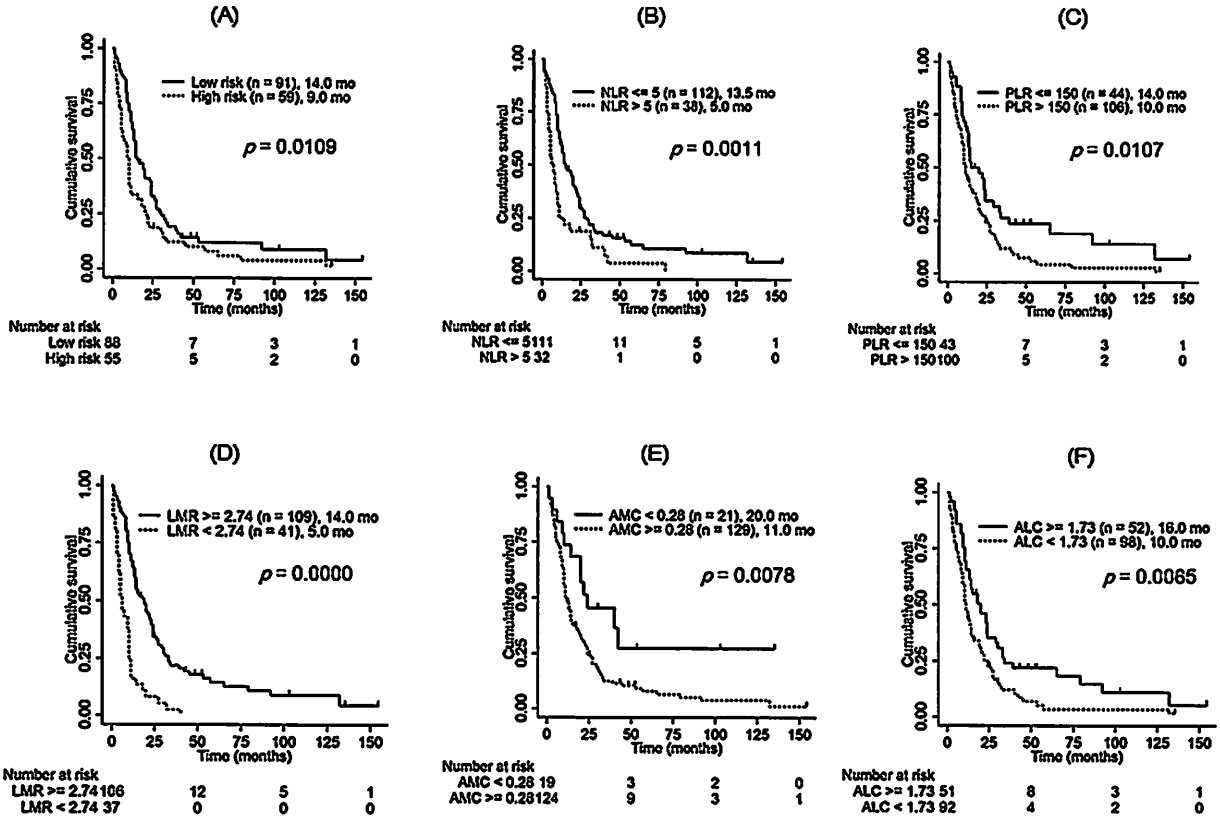

Fig. 1. Kaplan–Meier survival curves for patients affected by malignant pleural mesothelioma, stratified by European Organisation for Research and Treatment of Cancer prognostic score (A), neutrophil-to-lymphocyte ratio (NLR) (B), platelet-to-lymphocyte ratio (PLR) (C), lymphocyte-to-monocyte ratio (LMR) (D), absolute monocyte count (AMC) (E), and absolute lymphocyte count (ALC) (F).

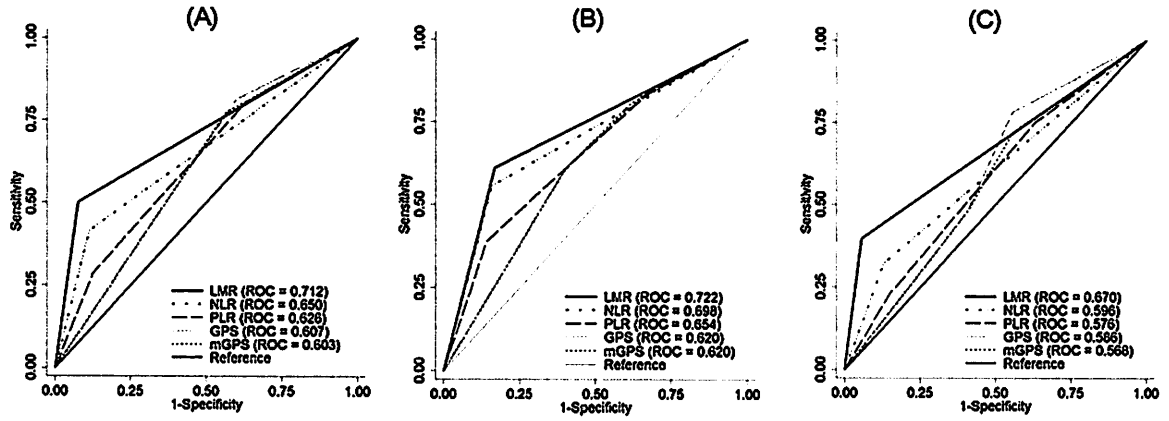

Fig. 2. Comparison of the areas under the receiver operating characteristic curves, for outcome prediction between the inflammation-based prognostic scores at (A) 6 months, (B) 12 months, and (C) 24 months in patients with malignant pleural mesothelioma. LMR, lymphocyte-to-monocyte ratio; NLR, neutrophil-to-lymphocyte ratio; PLR, platelet-to-lymphocyte ratio; GPS, Glasgow Prognostic Score; mGPS, modified Glasgow Prognostic Score.

significantly associated with clinical outcomes in cancer patients [20,21]. Among some inflammation-based scores, GPS is the most extensively validated [22]. However, recent years have seen a wealth of information about the prognostic value of ALC and AMC, together with their ratio, LMR.

Lymphocytes are components of the host immunity; they are important in the destruction of residual tumor cells and related micrometastases [23], and infiltrating lymphocytes can activate an effective antitumor cellular immune response [24]. Over the last few decades, a vast amount of evidence has highlighted the importance of monocytes and macrophages in cancer. Macrophages are derived from circulating monocytes and myeloid progenitor cells when entering tissues. Macrophages in tumors, which are usually referred to as tumor-associated macrophages (TAM), promote tumor cell invasion, migration, tumor-associated angiogenesis [25], and the suppression of antitumor immune reactions [26]. The role of TAMs in tumor biology and their prognostic value in various cancers, including thoracic malignancies, has become a major topic of interest [11]. The peripheral monocytes may reflect an increased production of tissue macrophage as a surrogate marker of high tumor burden. Burt et al. reported that higher numbers of circulating monocytes are associated with poor survival in all patients with MPM and higher densities of tumor-infiltrating macrophages are associated with poor survival in patients with the non-epithelioid

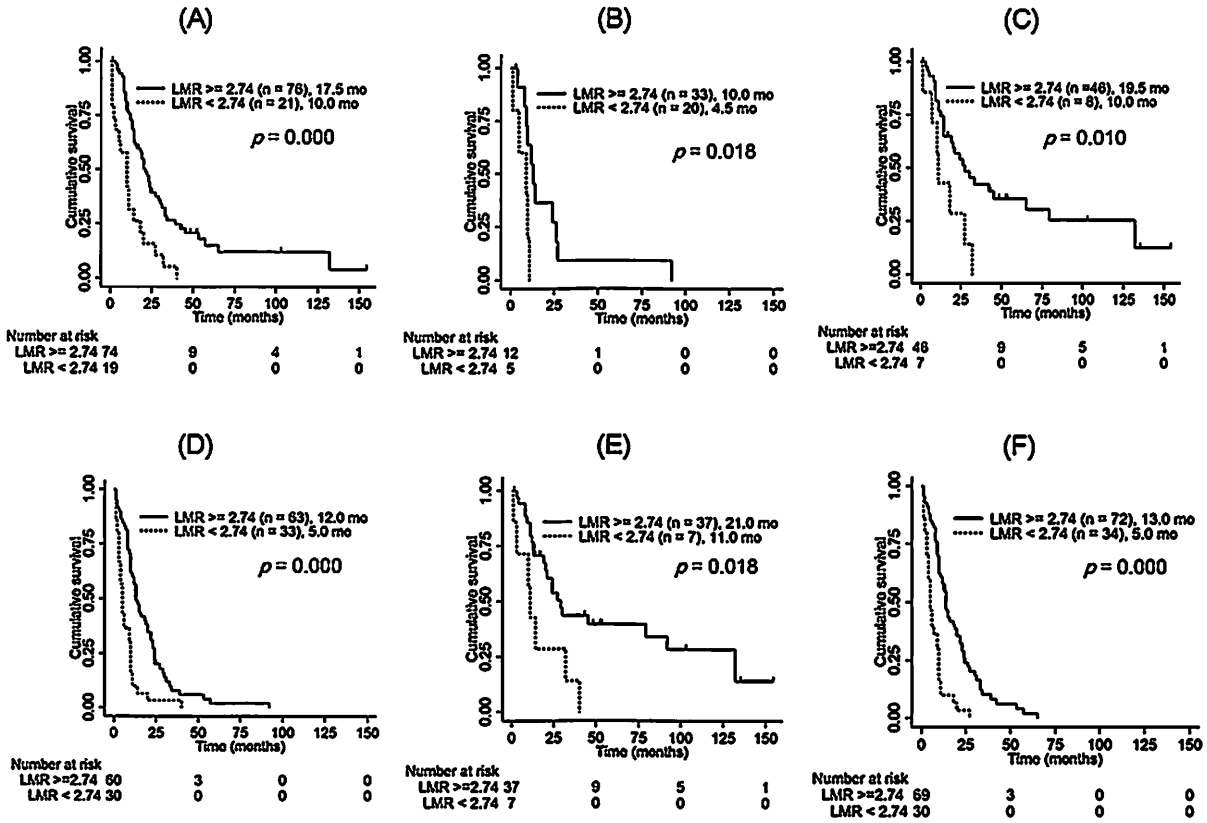

Fig. 3. Kaplan–Meier survival curves, stratified by lymphocyte-to-monocyte ratio (LMR) in patients with epithelioid subtype (A), with non-epithelioid subtype (B), with stage I/II disease (C), with stage III/IV disease (D), with surgical intervention (E), and without surgical intervention (F).

Table 2
Association of LMR with baseline clinical characteristics.

Variable	LMR ≥ 2.74 *N* = 109 (%)	LMR < 2.74 *N* = 41 (%)	*p*
Age, years			0.828
<70	51 (47)	20 (49)	
≥70	58 (53)	21 (51)	
Gender			0.352
Male	103 (95)	37 (90)	
Female	6 (5)	4 (10)	
ECOG PS			0.001
≤1	100 (92)	29 (70)	
>1	9 (8)	12 (30)	
Histological subtype			0.035
Epithelioid	76 (70)	21 (51)	
Non-epithelioid	33 (30)	20 (49)	
IMIG stage			0.010
I/II	46 (42)	8 (20)	
III/IV	63 (58)	33 (80)	
Surgery			0.043
Yes	72 (66)	34 (83)	
No	37 (34)	7 (17)	
CALGB group			0.022
1–2	40 (37)	9 (22)	
3–4	51 (47)	17 (41)	
5–6	18 (16)	15 (37)	
EORTC prognostic score			0.001
Low risk	75 (69)	16 (39)	
High risk	34 (31)	25 (61)	
Lymphocyte count, mean ± SD ($\times 10^9$/L)	1.63 ± 0.54	1.13 ± 0.48	0.000
Monocyte count, mean ± SD ($\times 10^9$/L)	0.44 ± 0.17	0.93 ± 0.62	0.000

LMR: lymphocyte-to-monocyte ratio; ECOG: Eastern Cooperative Oncology Group; PS: performance status; IMIG: International Mesothelioma Interest Group; CALGB: Cancer and Leukemia Group B; EORTC: European Organisation for Research and Treatment of Cancer.

subtype [27]. These findings might explain how decreasing LMR confers a negative prognosis in cancer patients.

Historically, the prognostic value of LMR was investigated mainly in hematological malignancies [12,28], and data were sparse in the context of solid tumors. In recent years, LMR has also been documented as an independent predictor of survival in a variety of patients with solid tumors, including colorectal tumor [29], breast cancer [30], lung cancer [31,32], pancreatic cancer [33], bladder cancer [34], and nasopharyngeal carcinoma [35]. However, until now, LMR data has not been reported in patients with MPM.

MPM is strongly associated with exposure to airborne asbestos fibers. Inhaled asbestos fibers present in the lung cause circulating macrophages to infiltrate the pleural space, where they attempt to phagocytose the inhaled foreign bodies [36]. As the macrophages are unable to eliminate the asbestos fibers, a state of chronic inflammation occurs, during which the secretion of free radicals causes genotoxic damage, which in turn facilitates the transformation of normal mesothelial cells to malignant mesothelioma [37].

In the present study, we initially evaluated the usefulness of LMR for predicting OS in patients with MPM. This study demonstrated that the ALC ($\geq 1.73 \times 10^9$/L) was a favorable prognosis factor and the AMC ($\geq 0.28 \times 10^9$/L) was an inferior prognostic factor for MPM patients. Multivariate analysis showed that LMR, ECOG PS, histological subtype, stage, and surgical intervention were significantly associated with OS. Moreover, AUC analysis has shown that the LMR was superior to other inflammation-based prognostic scores regarding predictive accuracy. In our study cohort, an elevated LMR (≥2.74) was significantly associated with increased OS. Similar results were observed in Hodgkin's lymphoma [38], diffuse large B-cell lymphoma [28], and nasopharyngeal carcinoma [35]. We also focused on the relationship between LMR and prognosis according to subtype. Our results showed that decreased

Table 3
Analysis of prognostic factors regarding overall survival.

Variable	OS (univariate analysis)		OS (multivariate analysis)	
	Hazard ratio (95% CI)	p	Hazard ratio (95% CI)	p
Age (<70/≥70 years)	1.00 (0.69–1.43)	0.993	NI	
Gender (male/female)	2.36 (1.13–4.93)	0.022	NI	
ECOG PS (≤1/>1)	2.39 (1.44–3.98)	0.001	1.84 (1.07–3.16)	0.027
Histological subtype (epithelioid/non-epithelioid)	1.95 (1.34–2.84)	0	2.24 (1.51–3.33)	0
IMIG stage (I/II vs. III/IV)	2.73 (1.81–4.12)	0	1.70 (1.08–2.69)	0.022
Surgery (yes/no)	0.35 (0.22–0.55)	0	2.41 (1.43–4.04)	0.001
Hemoglobin difference (g/L) (<10/≥10)	1.33 (0.76–2.33)	0.31	NI	
White cell count ($\times 10^9$/L) (≤8.30/>8.30)	1.49 (1.02–2.17)	0.038	NI	
Platelet count ($\times 10^9$/L) (≤400/>400)	1.17 (0.72–1.90)	0.517	NI	
Albumin (g/dL) (≥3.5/<3.5)	1.48 (1.03–2.12)	0.031	NI	
CALGB group (1–2/3–4/5–6)	1.43 (1.09–1.89)	0.01	NI	
EPS (low risk/high risk)	1.57 (1.09–2.26)	0.014	NI	
NLR (≤5/>5)	1.93 (1.28–2.92)	0.002	NI	
PLR (≤150/>150)	1.65 (1.10–2.47)	0.014	NI	
LMR (≥2.74/<2.74)	3.10 (2.07–4.66)	0	2.34 (1.58–3.47)	0
GPS (0/1/2)	1.32 (1.08–1.63)	0.006	NI	
mGPS (0/1/2)	1.28 (1.05–1.56)	0.014	NI	
AMC ($\times 10^9$/L) (<0.28/≥0.28)	2.16 (1.19–3.93)	0.011	NI	
ALC ($\times 10^9$/L) (≥1.73/<1.73)	1.66 (1.13–2.44)	0.009	NI	

ECOG: Eastern Cooperative Oncology Group; PS: performance status; IMIG: International Mesothelioma Interest Group; CALGB: Cancer and Leukemia Group B; EPS: European Organisation for Research and Treatment of Cancer prognostic score; NLR: neutrophil-to-lymphocyte ratio; PLR: platelet-to-lymphocyte ratio; LMR: lymphocyte-to-monocyte ratio; GPS: Glasgow Prognostic Score; mGPS: modified Glasgow Prognostic Score; AMC: absolute monocyte count; ALC: absolute lymphocyte count; NI: Not included.

LMR was significantly associated with poor prognosis for patients with the epithelioid subtype, as well as for those with the non-epithelioid subtype. In addition, the predictive value of LMR was also significant in patients with stage I/II and stage III/IV disease, and in patients with or without surgical intervention. Some studies reported that the inflammation-based prognostic scores are associated with responses to treatment (e.g., chemotherapy and radiotherapy) and perioperative outcomes (e.g., post-operative mortality and complications) [17,21]. Additional work is required to define the clinical utility of LMR within the individual therapeutic process.

Although the roles of monocytes and macrophage in tumor biology and their prognostic value in cancer have become major topics of interest, and much recent research has been dedicated to targeting these cells, there is currently no available clinical therapy to target these cells in patients with MPM. Conventional treatment strategies have met with limited success for patients with MPM. The combination strategy, which targets cancer cells directly, as well as macrophages and monocytes, may present a potentially new therapeutic approach [39]. Additional research is warranted regarding the use of immune-modulatory therapies to treat this malignancy.

One potential limitation of this study is that this is a retrospective and single-centre study. In addition, the study did not assess potential confounding factors (e.g., local or systemic infection, ischemia, acute coronary syndrome, metabolic syndrome, diabetes mellitus, and renal or hepatic dysfunction) that might affect the lymphocyte and monocyte counts. A large-scale prospective validation study is needed to confirm the results.

5. Conclusion

Our study is the first to demonstrate that the LMR is an independent marker of prognosis in patients with MPM and is superior to the other inflammation-based scores regarding prognostic ability. LMR is easily assessed using a simple complete blood count test, and is both technically and financially feasible to predict patients' clinical outcomes in routine practice. The identification of simple and valuable prognostic markers for MPM will enable clinicians to select patients who are most likely to benefit from intensive therapy, and avoid subjecting unsuitable candidates to futile treatment.

Conflict of interest

The authors declare that they have no competing interests.

Acknowledgements

The authors thank Dr. Nobuaki Ochi, Kawasaki Medical School, Okayama, Japan, for expert advice regarding statistical analyses.

This study is a part of "the research and development and the dissemination projects related to the 9 fields of occupational injuries and illnesses" of the Japan Labour Health and Welfare Organization. This sponsor had no involvement in the study design, collection, analysis and interpretation of the data, writing of the manuscript, or decision to submit the manuscript for publication.

References

[1] K. Gemba, N. Fujimoto, K. Kato, K. Aoe, Y. Takeshima, K. Inai, et al., National survey of malignant mesothelioma and asbestos exposure in Japan, Cancer Sci. 103 (2012) 483–490.
[2] C. Cao, D. Tian, J. Park, J. Allan, K.A. Pataky, T.D. Yan, A systematic review and meta-analysis of surgical treatments for malignant pleural mesothelioma, Lung Cancer 83 (2014) 240–245.
[3] C. Cao, D. Tian, C. Manganas, P. Matthews, T.D. Yan, Systematic review of trimodality therapy for patients with malignant pleural mesothelioma, Ann. Cardiothorac. Surg. 1 (2012) 428–437.
[4] D.A. Fennell, A. Parmar, J. Shamash, M.T. Evans, M.T. Sheaff, R. Sylvester, et al., Statistical validation of the EORTC prognostic model for malignant pleural mesothelioma based on three consecutive phase II trials, J. Clin. Oncol. 23 (2005) 184–189.
[5] J.E. Herndon, M.R. Green, A.P. Chahinian, J.M. Corson, Y. Suzuki, N.J. Vogelzang, Factors predictive of survival among 337 patients with mesothelioma treated between 1984 and 1994 by the Cancer and Leukemia Group B, Chest 113 (1998) 723–731.
[6] A. Mantovani, P. Allavena, A. Sica, F. Balkwill, Cancer-related inflammation, Nature 454 (2008) 436–444.
[7] A. Linton, N. van Zandwijk, G. Reid, S. Clarke, C. Cao, S. Kao, Inflammation in malignant mesothelioma—friend or foe? Ann. Cardiothorac. Surg. 1 (2012) 516–522.
[8] D. Bugada, M. Allegri, P. Lavand'homme, M. De Kock, G. Fanelli, Inflammation-based scores: a new method for patient-targeted strategies and improved perioperative outcome in cancer patients, Biomed. Res. Int. 2014 (2014) 142425.
[9] D.J. Pinato, F.A. Mauri, R. Ramakrishnan, L. Wahab, T. Lloyd, R. Sharma, Inflammation-based prognostic indices in malignant pleural mesothelioma, J. Thorac. Oncol. 7 (2012) 587–594.
[10] L.M. Coussens, Z. Werb, Inflammation and cancer, Nature 420 (2002) 806–867.

[11] L.A. Lievense, K. Bezemer, J.G. Aerts, J.P. Hegmans, Tumor-associated macrophages in thoracic malignancies, Lung Cancer 80 (2013) 256–262.
[12] L.F. Porrata, D.J. Inwards, S.M. Ansell, I.N. Micallef, P.B. Johnston, W.J. Hogan, et al., Day 100 peripheral blood absolute lymphocyte/monocyte ratio and survival in classical Hodgkin's lymphoma postautologous peripheral blood hematopoietic stem cell transplantation, Bone Marrow Res. (2013) 658371, http://dx.doi.org/10.1155/2013/658371
[13] V.W. Rusch, A proposed new international TNM staging system for malignant pleural mesothelioma. From the International Mesothelioma Interest Group, Chest 108 (1995) 1122–1128.
[14] L.M. McShane, D.G. Altman, W. Sauerbrei, S.E. Taube, M. Gion, G.M. Clark, Reporting recommendations for tumor marker prognostic studies, J. Clin. Oncol. 23 (2005) 9067–9072.
[15] S.C. Kao, N. Pavlakis, R. Harvie, J.L. Vardy, M.J. Boyer, Z. van, N. andwijk, et al., High blood neutrophil-to-lymphocyte ratio is an indicator of poor prognosis in malignant mesothelioma patients undergoing systemic therapy, Clin. Cancer Res. 16 (2010) 5805–5813.
[16] Ji-Feng Feng, Ying Huang, Qi-Xun Chen, Preoperative platelet lymphocyte ratio (PLR) is superior to neutrophil lymphocyte ratio (NLR) as a predictive factor in patients with esophageal squamous cell carcinoma, World J. Surg. Oncol. 12 (2014) 58.
[17] D.C. McMillan, The systemic inflammation-based Glasgow Prognostic Score: a decade of experience in patients with cancer, Cancer Treat. Rev. 39 (2013) 534–540.
[18] M.J. Proctor, D.S. Morrison, D. Talwar, S.M. Balmer, D.S. O'Reilly, A.K. Foulis, et al., An inflammation-based prognostic score (mGPS) predicts cancer survival independent of tumour site: a Glasgow Inflammation Outcome Study, Br. J. Cancer 104 (2011) 726–734.
[19] J. Edwards, K. Abrams, J. Leverment, T. Spyt, D. Waller, K. O'Byrne, Prognostic factors for malignant mesothelioma in 142 patients: validation of CALGB and EORTC prognostic scoring systems, Thorax 55 (2000) 731–735.
[20] A. Kinoshita, H. Onoda, N. Imai, A. Iwaku, M. Oishi, N. Fushiya, et al., Comparison of the prognostic value of inflammation-based prognostic scores in patients with hepatocellular carcinoma, Br. J. Cancer 107 (2012) 988–993.
[21] D. Bugada, M. Allegri, P. Lavand'homme, M. De Kock, G. Fanelli, Inflammation-based scores: a new method for patient-targeted strategies and improved perioperative outcome in cancer patients, Biomed. Res. Int. (2014) 142425, http://dx.doi.org/10.1155/2014/142425
[22] M.J. Proctor, D.S. Morrison, D. Talwar, S.M. Balmer, D.S. O'Reilly, A.K. Foulis, et al., An inflammation-based prognostic score (mGPS) predicts cancer survival independent of tumour site: a Glasgow Inflammation Outcome Study, Br. J. Cancer 104 (2011) 726–734.
[23] P. Fogar, C. Sperti, D. Basso, M.C. Sanzari, E. Greco, C. Davoli, et al., Decreased total lymphocyte counts in pancreatic cancer: an index of adverse outcome, Pancreas 32 (2006) 22–28.
[24] H. Rabinowich, R. Cohen, I. Bruderman, Z. Steiner, A. Klajman, Functional analysis of mononuclear cells infiltrating into tumors: lysis of autologous human tumor cells by cultured infiltrating lymphocytes, Cancer Res. 47 (1987) 173–177.
[25] J.W. Pollard, Tumour-educated macrophages promote tumour progression and metastasis, Nat. Rev. Cancer 4 (2004) 71–78.
[26] D.I. Gabrilovich, S. Nagaraj, Myeloid-derived suppressor cells as regulators of the immune system, Nat. Rev. Immunol. 9 (2009) 162–174.
[27] B.M. Burt, S.J. Rodig, T.R. Tilleman, A.W. Elbardissi, R. Bueno, D.J. Sugarbaker, Circulating and tumor-infiltrating myeloid cells predict survival in human pleural mesothelioma, Cancer 117 (2011) 5234–5244.
[28] Z.M. Li, J.J. Huang, Y. Xia, J. Sun, Y. Huang, Y. Wang, et al., Blood lymphocyte-to-monocyte ratio identifies high-risk patients in diffuse large B-cell lymphoma treated with R-CHOP, PLoS One 7 (2012) e41658, http://dx.doi.org/10.1371/journal.pone.0041658
[29] M. Stotz, M. Pichler, G. Absenger, J. Szkandera, F. Arminger, R. Schaberl-Moser, et al., The preoperative lymphocyte to monocyte ratio predicts clinical outcome in patients with stage III colon cancer, Br. J. Cancer 110 (2014) 435–440.
[30] X.J. Ni, X.L. Zhang, Q.W. Ou-Yang, G.W. Qian, L. Wang, S. Chen, et al., An elevated peripheral blood lymphocyte-to-monocyte ratio predicts favorable response and prognosis in locally advanced breast cancer following neoadjuvant chemotherapy, PLoS One 9 (2014) e111886, http://dx.doi.org/10.1371/journal.pone.0111886
[31] P. Hu, H. Shen, G. Wang, P. Zhang, Q. Liu, J. Du, Prognostic significance of systemic inflammation-based lymphocyte- monocyte ratio in patients with lung cancer: based on a large cohort study, PLoS One 9 (2014) e108062, http://dx.doi.org/10.1371/journal.pone.0108062
[32] G.N. Lin, J.W. Peng, J.J. Xiao, D.Y. Liu, Z.J. Xia, Prognostic impact of circulating monocytes and lymphocyte-to-monocyte ratio on previously untreated metastatic non-small cell lung cancer patients receiving platinum-based doublet, Med. Oncol. 31 (2014) 70.
[33] Y. Fujiwara, T. Misawa, H. Shiba, Y. Shirai, R. Iwase, K. Haruki, et al., Postoperative peripheral absolute blood lymphocyte-to-monocyte ratio predicts therapeutic outcome after pancreatic resection in patients with pancreatic adenocarcinoma, Anticancer Res. 34 (2014) 5133–5138.
[34] S. Temraz, D. Mukherji, Z.A. Farhat, R. Nasr, M. Charafeddine, M. Shahait, et al., Preoperative lymphocyte-to-monocyte ratio predicts clinical outcome in patients undergoing radical cystectomy for transitional cell carcinoma of the bladder: a retrospective analysis, BMC Urol. 14 (2014) 76.
[35] J. Li, R. Jiang, W.S. Liu, Q. Liu, M. Xu, Q.S. Feng, et al., A large cohort study reveals the association of elevated peripheral blood lymphocyte-to-monocyte ratio with favorable prognosis in nasopharyngeal carcinoma, PLoS One 8 (2013) e83069, http://dx.doi.org/10.1371/journal.pone.0083069
[36] B.T. Mossman, A. Churg, Mechanisms in the pathogenesis of asbestosis and silicosis, Am. J. Respir. Crit. Care Med. 157 (1998) 1666–1680.
[37] A.J. Bograd, K. Suzuki, E. Vertes, C. Colovos, E.A. Morales, M. Sadelain, et al., Immune responses and immunotherapeutic interventions in malignant pleural mesothelioma, Cancer Immunol. Immunother. 60 (2011) 1509–1527.
[38] L.F. Porrata, K. Ristow, J.P. Colgan, T.M. Habermann, T.E. Witzig, D.J. Inwards, et al., Peripheral blood lymphocyte/monocyte ratio at diagnosis and survival in classical Hodgkin's lymphoma, Haematologica 97 (2012) 262–269.
[39] M.A. Lameijer, J. Tang, M. Nahrendorf, R.H. Beelen, W.J. Mulder, Monocytes and macrophages as nanomedicinal targets for improved diagnosis and treatment of disease, Expert Rev. Mol. Diagn. 13 (2013) 567–580.

DNA copy number gains in malignant pleural mesothelioma

MASASHI FURUKAWA[1], SHINICHI TOYOOKA[1,2], TATSURO HAYASHI[1,3], HIROMASA YAMAMOTO[1,3], NOBUKAZU FUJIMOTO[4], JUNICHI SOH[1], SHINSUKE HASHIDA[1,2], KAZUHIKO SHIEN[1,2], HIROAKI ASANO[1], KEISUKE AOE[5], KAZUNORI OKABE[3], HARVEY I. PASS[6], KAZUNORI TSUKUDA[1], TAKUMI KISHIMOTO[4] and SHINICHIRO MIYOSHI[1]

Departments of [1]Thoracic, Breast and Endocrinological Surgery, and [2]Clinical Genomic Medicine, Okayama University Graduate School of Medicine, Dentistry and Pharmaceutical Sciences, Okayama, Okayama 700-8558; [3]Department of Thoracic Surgery, National Hospital Organization Yamaguchi-Ube Medical Center, Ube, Yamaguchi 755-0241; [4]Department of Internal Medicine, Okayama Rosai Hospital, Okayama, Okayama 702-8055; [5]Department of Medical Oncology, National Hospital Organization Yamaguchi-Ube Medical Center, Ube, Yamaguchi 755-0241, Japan; [6]Division of Thoracic Surgery, Department of Cardiothoracic Surgery, New York University Langone Medical Center, NY 10016, USA

Received October 15, 2014; Accepted July 30, 2015

DOI: 10.3892/ol.2015.3652

Abstract. Malignant pleural mesothelioma (MPM) is a highly aggressive tumor with an extremely poor prognosis. The incidence of MPM is increasing as a result of widespread exposure to asbestos. The molecular pathogenesis of MPM remains unclear. The present study analyzed the frequency of various genomic copy number gains (CNGs) in MPM using reverse transcription-quantitative polymerase chain reaction. A total of 83 primary MPMs and 53 primary lung adenocarcinomas were analyzed to compare the CNGs of *EGFR*, *KRAS*, *MET*, *FGFR1* and *SOX2*. In MPM, the CNGs of *EGFR*, *KRAS*, *MET*, *FGFR1* and *SOX2* were detected in 12 (14.5%), 8 (9.6%), 5 (6.0%), 4 (4.8%) and 1 (1.2%) of the samples, respectively. In lung adenocarcinomas, the CNGs of *EGFR*, *KRAS*, *MET*, *FGFR1* and *SOX2* were detected in 21 (39.6%), 12 (22.6%), 5 (9.4%), 10 (18.9%) and 0 (0.0%) of the samples, respectively. The CNGs of *EGFR*, *KRAS* and *FGFR1* were significantly less frequent in the MPMs compared with the lung adenocarcinomas (P=0.0018, 0.048 and 0.018, respectively). Overall, the MPMs exhibited these CNGs less frequently compared with the lung adenocarcinomas (P=0.0002). The differences in CNGs between the two tumor types suggested that they are genetically different.

Correspondence to: Professor Shinichi Toyooka, Department of Clinical Genomic Medicine, Okayama University Graduate School of Medicine, Dentistry and Pharmaceutical Sciences, 2-5-1 Shikata, Kita, Okayama, Okayama 700-8558, Japan
E-mail: toyooka@md.okayama-u.ac.jp

Key words: malignant pleural mesothelioma, lung adenocarcinoma, copy number, reverse transcription-quantitative polymerase chain reaction

Introduction

Malignant pleural mesothelioma (MPM) is a tumor derived from the mesothelial cells lining the pleural spaces. MPM has highly invasive and aggressive clinical characteristics. Approximately 80% of MPM patients have a history of occupational asbestos exposure, which is considered to be a risk factor for the development of the disease (1). The molecular pathogenesis of MPM is not well understood. The most common mutations in MPMs are losses in 9p21, 1p36, 14q32 and 22q12, and gains in 5p, 7p and 8q24, which have been detected by comparative genomic hybridization analysis (2,3). Homozygous deletion of the 9p21 locus encoding two critical cyclin-dependent kinase inhibitors, $p16^{INK4a}$ and $p15^{INK4b}$, have been reported in up to 80% of MPMs, and this mutation may be of diagnostic utility (4,5). The tumor suppressor neurofibromin 2 is encoded by the *NF2* gene, located on chromosome 22q12. Mutations in *NF2* are found in ~40% of MPMs, and heterozygous loss of *NF2* is identified in ~74% of MPMs (6,7). Mutations are rare in the *TP53* and *RAS* genes, which are frequently present in epithelial solid tumors (8,9). Epigenetic alterations, such as DNA methylation, have been found in MPMs, which have a different profile compared with lung cancer (10-12). MPMs, particularly of the epithelioid subtype, may be hard to differentiate from adenocarcinoma arising in the lung periphery, and epidemiological evidence indicates that asbestos and smoking are shared risk factors for these diseases (2,13,14). Currently, the differential diagnosis of MM is based on a range of morphological analyses, including a combination of histological and immunohistochemical staining, and electron microscopy (13,15,16).

Cytogenetic studies have been performed on MPMs and adenocarcinomas arising in the lung periphery, however, no chromosomal aberrations specific to either of the tumor types have been identified (2,14).

Reverse transcription-quantitative polymerase chain reaction (RT-qPCR) is a method for evaluating DNA copy number

changes, including losses, gains and amplifications of DNA sequences (17-19). Copy number gains (CNGs) of *EGFR* and *KRAS* have been observed in lung cancer, particularly in adenocarcinoma (18,20). Furthermore, CNGs of *FGFR1* and *SOX2* have been observed in lung cancer, particularly in squamous cell carcinoma (21-25). c-Met was recently reported to be activated in MPM by overexpression or mutations in *MET* (26), and *MET* amplification is a known cause of resistance to *EGFR*-tyrosine kinase inhibitor (TKI) treatment in lung cancer (27). RT-qPCR was used in the present study on 83 primary MPM and 53 primary lung adenocarcinomas to compare the CNGs of *EGFR*, *KRAS*, *MET, FGFR1* and *SOX2*.

Materials and methods

Tumor samples. Surgically resected specimens of 53 lung adenocarcinomas and 83 MPMs (57 epithelioid, 8 sarcomatoid, 15 biphasic, 2 desmoplastic and 1 lymphohistiocytic) were obtained. All the lung adenocarcinomas and 11 of the MPM samples were obtained from Okayama University Hospital (Okayama, Japan). Another 18 MPMs were obtained from Yamaguchi-Ube Medical Center (Ube, Japan), 2 were obtained from Okayama Rosai Hospital (Okayama, Japan) and the remaining 52 were obtained from Karmanos Cancer Center (Detroit, MI, USA). All Japanese samples were collected between March 2002 and September 2011, and all samples from the USA were collected >10 years ago. Resected tumors were stored at -80˚C until DNA extraction. Permission from the Institutional Review Board and informed consent were obtained at each collection site.

DNA extraction. Genomic DNA was obtained from primary tumors by standard phenol:chloroform (1:1) extraction, followed by ethanol precipitation, or using a DNeasy Tissue kit (Qiagen, Inc., Valencia, CA, USA).

RT-qPCR for copy number evaluation. CNGs of *EGFR*, *KRAS, MET, FGFR1* and *SOX2* genes were determined by RT-qPCR assays using Power SYBR® Green PCR Master Mix (Thermo Fisher Scientific, Waltham, MA, USA), as previously described (18,19). Briefly, samples of 1 μl were analyzed per assay using with StepOne Plus Real-Time PCR System (Themo Fisher Scientific). PCR conditions were initial denaturation at 95˚C for 10 min followed by 40 cycles of amplification at 95˚C for 15 sec and 60˚C for 60 sec. The samples were analyzed in triplicate using StepOne Plus RT PCR software (version 2.0; Themo Fisher Scientific) and the *LINE1* gene was used as a reference gene for all copy number analyses, as this is the most abundant autonomous retrotransposon in the human genome, constituting 17%. Each amplification reaction was checked for the absence of non-specific PCR products by performing a melting curve analysis. The copy number calculation was conducted using the comparative cycle threshold (Ct) method following validation of the PCR reaction efficiency of *EGFR, KRAS, MET, FGFR1, SOX2* and *LINE1*. The PCR primer sequences for *EGFR, KRAS, MET* and *LINE1* primers have previously been described (17-19). The PCR primer sequences for *FGFR1* and *SOX2* were designed by Primer 3 plus software and by modification of the sequences. The PCR primer sequences were as follows: *FGFR1* forward, 5'-AGC CAC CAC ATG GCA TAC TT-3' and reverse, 5'-GGT GAC AAG GCT CCA CAT CT-3'; and *SOX2* forward, 5'-CGT CAC ATG GAT GGT TGT CT-3' and reverse, 5'-GCC GCC GAT GAT TGT TAT TA-3'. The relative copy number of each sample was determined by comparing the ratio of the target gene to *LINE1* in each sample with the ratio of these genes in normal human genomic DNA (EMD Biosciences, Darmstadt, Germany) prepared from a mixture of human blood cells from 6-8 donors, as a diploid control. Our previous study defined a copy number of ≥4 as a gene gain in cell lines (17,18). However, considering the contamination by non-malignant cells in primary samples (estimated mean per tumor, 50% tumor cells and 50% non-malignant cells), the cut-off value of 3 copy numbers rather than 4 was used for primary tumors in this study (17).

Detection of EGFR mutations. The *EGFR* mutational status was determined using a PCR-based length polymorphism and restriction fragment length polymorphism assay, as previously described (28). Briefly, the common deletions of exon 19 were distinguished from the wild-type based on PCR product length polymorphisms using 12% polyacrylamide gel electrophoresis (PAGE) and ethidium bromide staining. For the exon 21 L858R mutation, *Sau*96I digestion, which specifically digests the mutant type, was performed prior to 12% PAGE.

Statistical analyses. Differences between the two groups were assessed using the χ^2 test or Fisher's exact test as required. All data were analyzed using JMP software version 9.0.0 (SAS Institute Inc., Cary, NC, USA). For all analyses, $P<0.05$ was considered to indicate a statistically significant difference.

Results

CNGs in MPMs and lung adenocarcinomas. In the 83 MPM samples, the CNGs of *EGFR*, *KRAS, MET, FGFR1* and *SOX2* were detected in 12 (14.5%), 8 (9.6%), 5 (6.0%), 4 (4.8%), and 1 (1.2%) of the samples, respectively. In the epithelioid subtype of MPM (n=57), the CNGs of *EGFR*, *KRAS*, *MET*, *FGFR1* and *SOX2* were detected in 7 (12.3%), 5 (8.8%), 3 (5.3%), 4 (7.0%) and 0 (0.0%) of the samples, respectively. In the other subtypes of MPMs (n=26), the CNGs of *EGFR*, *KRAS*, *MET*, FGFR and *SOX2* were detected in 5 (19.2%), 3 (11.5%), 2 (7.7%), 0 (0%) and 1 (3.8%) of the samples, respectively. In the 53 lung adenocarcinomas, the CNGs of *EGFR*, *KRAS*, *MET*, *FGFR1* and *SOX2* were detected in 21 (39.6%), 12 (22.6%), 5 (9.4%), 10 (18.9%) and 0 (0.0%) of the samples, respectively (Table I; Fig. 1). Three cases of MPMs were demonstrated to have numerous CNGs of *EGFR* (269, 62 and 14, respectively). The CNGs of *EGFR*, *KRAS* and *FGFR1* were significantly less frequent in the MPMs compared with the lung adenocarcinomas (P=0.0018, 0.048 and 0.018, respectively). In the epithelioid subtype of MPMs, the CNGs of *EGFR* were significantly less frequent than those in the lung adenocarcinomas (P=0.0018), and in other subtypes of MPMs, the CNGs of *FGFR1* were significantly less frequent compared with those of the lung adenocarcinomas (P=0.026). In the MPMs, an absence and presence of CNGs were observed in 64 (77.1%) and 19 (22.9%) of the 83 cases, respectively. In the epithelioid MPMs, absent/present CNGs were observed in 47 (82.5%) and 10 (17.5%) of the 57 cases, respectively. In the other subtypes of

Table I. CNGs of *EGFR*, *KRAS*, *MET*, *FGFR1* and *SOX2* in MPMs and lung adenocarcinomas.

	MPMs (n=83)							
	All (n=83)		Epithelioid subtype (n=57)		Other subtypes (n=26)		Lung adenocarcinoma (n=53)	
Genes	No.	%	No.	%	No.	%	No.	%
EGFR	12[a]	14.5	7[a]	12.3	5	19.2	21	39.6
KRAS	8[b]	9.6	5	8.8	3	11.5	12	22.6
MET	5	6.0	3	5.3	2	7.7	5	9.4
FGFR1	4[b]	4.8	4	7.0	0[b]	0.0	10	18.9
SOX2	1	1.2	0	0.0	1	3.8	0	0.0

CNGs of *FGFR1* and *KRAS* were significantly less frequent in MPMs compared with lung adenocarcinomas. In epithelioid MPMs, CNGs of *EGFR* were found to be significantly less frequent compared with lung adenocarcinomas. In other types of MPMs, CNGs of *FGFR1* were found to be significantly less frequent compared with lung adenocarcinomas ([a]P<0.05; [b]P<0.01). CNGs, copy number gains; MPMs, malignant pleural mesotheliomas.

Table II. Frequency of the absence or presence of CNGs in MPMs and lung adenocarcinomas.

	Absence of CNGs		Presence of CNGs	
Cancer type	No.	%	No.	%
Malignant pleural mesothelioma (n=83)[a]	64[a]	77.1	19	22.9
Epithelioid subtype (n=57)[a]	47[a]	82.5	10	17.5
Other subtypes (n=26)	17	65.4	9	34.6
Lung adenocarcinoma (n=53)	24	45.3	29	54.7

Frequency of none of CNGs in MPMs and epithelioid MPMs was significantly higher compared with lung adenocarcinomas ([a]P<0.01). CNGs, copy number gains; MPM, malignant pleural mesothelioma.

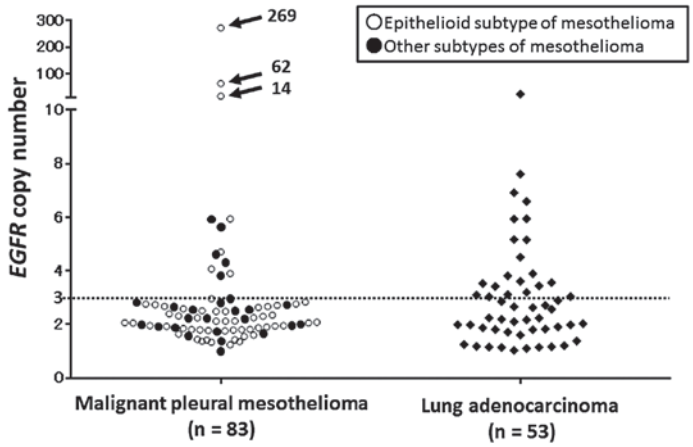

Figure 1. *EGFR* gene copy number, determined by reverse transcription-quantitative polymerase chain reaction in malignant pleural mesotheliomas (MPMs) and lung adenocarcinomas. Copy numbers >3 were considered as copy number gain (CNG). Three cases of MPMs were shown to have high CNGs of *EGFR* (269, 62 and 14, respectively).

the MPMs, the absence and presence of CNGs were observed in 17 (65.4%) and 9 (34.6%) of the 26 cases, respectively. In the lung adenocarcinomas, the absence and presence of CNGs were observed in 24 (45.3%) and 29 (54.7%) of the 53 cases, respectively (Table II). The MPMs and the epithelioid subtypes of the MPMs had less frequent CNGs than the lung adenocarcinomas (P=0.0002 and P=0.0001, respectively).

EGFR mutations. No *EGFR* mutation was detected in the 83 MPMs. In the lung adenocarcinomas, *EGFR* mutations

were detected in 21 (39.6%) cases; 14 cases exhibited an exon 19 deletion and 7 cases exhibited an exon 21 mutation (L858R).

Discussion

The main finding of the present study is that the pattern of DNA CNGs of MPM is different from that in lung adenocarcinoma. MPMs exhibited less CNGs of the genes examined in compared with the lung adenocarcinomas. The epithelioid subtype of MPM, which is often difficult to distinguish from lung adenocarcinoma, similarly exhibited these CNGs less frequently compared with the lung adenocarcinomas. To the best of our knowledge, only a limited number of studies have previously analyzed the presence and frequency of *EGFR* CNGs in MPMs (2,29-32), and no studies have focused on CNGs of *KRAS*, *MET*, *FGFR1* or *SOX2* in MPM. A large number of samples (n=83) were screened in the present study, whereas the previous studies were based on smaller sample sizes and may have underestimated the true frequency of such CNGs.

Although CNGs of *SOX2* were seldom observed in the MPMs and lung adenocarcinomas, the CNGs of the remaining four genes were detected in the MPM samples to a certain extent. The fact that the CNGs of four genes in the MPMs were less frequent in comparison to the lung adenocarcinomas suggested that CNG may not be a pivotal mechanism for the activation of oncogenes in MPMs, and that different mechanisms may be of greater importance. It has been previously reported that *EGFR* is overexpressed in 60-70% of MPM tissue specimens; however, it is not overexpressed in the normal mesothelium (29,33). Furthermore, exposure to asbestos fibers is known to cause *EGFR* aggregation (34). In the present study, *EGFR,* located at 7p12-p13, was the most frequent gene to exhibit CNGs (12 out of 83 MPMs and 20 out of 53 lung adenocarcinomas). Bjorkqvist *et al* (2) reported similar results, such as gains of genetic material in 5p, 6p and 7p between MPMs and lung adenocarcinomas. The study detected a gain in 7p in 7 out of 34 MPMs and 11 out of 30 lung adenocarcinomas (2). MPMs rarely harbor *EGFR* mutations (31,35-37). There were no *EGFR* mutations detected in MPMs in the present study, as expected. Upon analysis, three cases of MPMs exhibited high *EGFR* gene amplification (CNG>10), and these cases were all epithelioid MPMs, which was consistent with the previous studies by Okuda *et al* (29) and Enomoto *et al* (31). It remains unclear whether high-level amplification of *EGFR* is more prominent in MPMs compared with lung adenocarcinomas, although the frequency of CNGs for *EGFR* is lower in MPMs compared with lung adenocarcinomas. In MPMs with *EGFR* amplification, the inhibition of *EGFR* pathways should exert an antitumor effect. In lung cancer, the results of two randomized phase III trials that compared a placebo to erlotinib or gefitinib treatment indicated that *EGFR* copy number detected by fluorescence *in situ* hybridization was the best predictor of survival (38). Patients with colorectal cancer who responded to anti-*EGFR* treatment with cetuximab or panitumumab exhibited an increased *EGFR* copy number (39). Although two phase II studies of single-agent EGFR-TKI therapy to treat MPMs failed to demonstrate their clinical efficacy, in the gefitinib trial, 2 of 43 MPM patients responded to gefitinib (40,41). These data suggest that a small proportion of patients (with *EGFR* gene amplification) may be candidates for anti-*EGFR* treatment (29).

In conclusion, the present study detected novel CNGs in genes other than *EGFR*. MPM samples exhibited these CNGs less frequently compared with lung adenocarcinomas. The differences in DNA CNG between the two tumor types suggested that they are genetically different.

Acknowledgements

The authors would like to thank Ms. Fumiko Isobe for providing excellent technical support. The study received Grant-in-Aids for the 13 fields of occupational injuries and illnesses of the Japan Labor Health and Welfare Organization.

References

1. Spirtas R, Heineman EF, Bernstein L, Beebe GW, Keehn RJ, Stark A, Harlow BL and Benichou J: Malignant mesothelioma: Attributable risk of asbestos exposure. Occup Environ Med 51: 804-811, 1994.
2. Björkqvist AM, Tammilehto L, Nordling S, Nurminen M, Anttila S, Mattson K and Knuutila S: Comparison of DNA copy number changes in malignant mesothelioma, adenocarcinoma and large-cell anaplastic carcinoma of the lung. Br J Cancer 77: 260-269, 1998.
3. Taniguchi T, Karnan S, Fukui T, Yokoyama T, Tagawa H, Yokoi K, Ueda Y, Mitsudomi T, Horio Y, Hida T, *et al*: Genomic profiling of malignant pleural mesothelioma with array-based comparative genomic hybridization shows frequent non-random chromosomal alteration regions including JUN amplification on 1p32. Cancer Sci 98: 438-446, 2007.
4. Chiosea S, Krasinskas A, Cagle PT, Mitchell KA, Zander DS and Dacic S: Diagnostic importance of 9p21 homozygous deletion in malignant mesotheliomas. Mod Pathol 21: 742-747, 2008.
5. Toyooka S, Kishimoto T and Date H: Advances in the molecular biology of malignant mesothelioma. Acta Med Okayama 62: 1-7, 2008.
6. Fleury-Feith J, Lecomte C, Renier A, Matrat M, Kheuang L, Abramowski V, Levy F, Janin A, Giovannini M and Jaurand MC: Hemizygosity of Nf2 is associated with increased susceptibility to asbestos-induced peritoneal tumours. Oncogene 22: 3799-3805, 2003.
7. Nemoto H, Tate G, Kishimoto K, Saito M, Shirahata A, Umemoto T, Matsubara T, Goto T, Mizukami H, Kigawa G, *et al*: Heterozygous loss of NF2 is an early molecular alteration in well-differentiated papillary mesothelioma of the peritoneum. Cancer Genet 205: 594-598, 2012.
8. Metcalf RA, Welsh JA, Bennett WP, *et al*: p53 and Kirsten-ras mutations in human mesothelioma cell lines. Cancer Res 52: 2610-2615, 1992.
9. Papp T, Schipper H, Pemsel H, *et al*: Mutational analysis of N-ras, p53, p16INK4a, p14ARF and CDK4 genes in primary human malignant mesotheliomas. Int J Oncol 18: 425-433, 2001.
10. Toyooka S, Pass HI, Shivapurkar N, Fukuyama Y, *et al*: Aberrant methylation and simian virus 40 tag sequences in malignant mesothelioma. Cancer Res 61: 5727-5730, 2001.
11. Kobayashi N, Toyooka S, Yanai H, *et al*: Frequent p16 inactivation by homozygous deletion or methylation is associated with a poor prognosis in Japanese patients with pleural mesothelioma. Lung Cancer 62: 120-125, 2008.
12. Goto Y, Shinjo K, Kondo Y, *et al*: Epigenetic profiles distinguish malignant pleural mesothelioma from lung adenocarcinoma. Cancer Res 69: 9073-9082, 2009.
13. Addis B and Roche H: Problems in mesothelioma diagnosis. Histopathology 54: 55-68, 2009.
14. Gee GV, Koestler DC, Christensen BC, *et al*: Downregulated microRNAs in the differential diagnosis of malignant pleural mesothelioma. Int J Cancer 127: 2859-2869, 2010.
15. Betta PG, Magnani C, Bensi T, Trincheri NF and Orecchia S: Immunohistochemistry and molecular diagnostics of pleural malignant mesothelioma. Arch Pathol Lab Med 136: 253-261, 2012.

16. Husain AN, Colby T, Ordonez N, Krausz T, Attanoos R, Beasley MB, Borczuk AC, Butnor K, Cagle PT, Chirieac LR, *et al*; International Mesothelioma Interest Group: Guidelines for pathologic diagnosis of malignant mesothelioma: 2012 update of the consensus statement from the International Mesothelioma Interest Group. Arch Pathol Lab Med 137: 647-667, 2013.
17. Yamamoto H, Shigematsu H, Nomura M, Lockwood WW, Sato M, Okumura N, Soh J, Suzuki M, Wistuba II, Fong KM, *et al*: PIK3CA mutations and copy number gains in human lung cancers. Cancer Res 68: 6913-6921, 2008.
18. Soh J, Okumura N, Lockwood WW, Yamamoto H, Shigematsu H, Zhang W, Chari R, Shames DS, Tang X, MacAulay C, *et al*: Oncogene mutations, copy number gains and mutant allele specific imbalance (MASI) frequently occur together in tumor cells. PLoS One 4: e7464, 2009.
19. Kubo T, Yamamoto H, Lockwood WW, Valencia I, Soh J, Peyton M, Jida M, Otani H, Fujii T, Ouchida M, *et al*: *MET* gene amplification or *EGFR* mutation activate *MET* in lung cancers untreated with *EGFR* tyrosine kinase inhibitors. Int J Cancer 124: 1778-1784, 2009.
20. Sasaki H, Hikosaka Y, Kawano O, Moriyama S, Yano M and Fujii Y: Evaluation of Kras gene mutation and copy number gain in non-small cell lung cancer. J Thorac Oncol 6: 15-20, 2011.
21. Zhao X, Weir BA, LaFramboise T, Lin M, Beroukhim R, Garraway L, Beheshti J, Lee JC, Naoki K, Richards WG, *et al*: Homozygous deletions and chromosome amplifications in human lung carcinomas revealed by single-nucleotide polymorphism array analysis. Cancer Res 65: 5561-5570, 2005.
22. Yuan P, Kadara H, Behrens C, Tang X, Woods D, Solis LM, Huang J, Spinola M, Dong W, Yin G, *et al*: Sex-determining region Y-Box 2 (*SOX2*) is a potential cell-lineage gene highly expressed in the pathogenesis of squamous cell carcinomas of the lung. PLoS One 5: e9112, 2010.
23. Kohler LH, Mireskandari M, Knösel T, Altendorf-Hofmann A, Kunze A, Schmidt A, Presselt N, Chen Y and Petersen I: *FGFR1* expression and gene copy numbers in human lung cancer. Virchows Arch 461: 49-57, 2012.
24. Heist RS, Mino-Kenudson M, Sequist LV, Tammireddy S, Morrissey L, Christiani DC, Engelman JA and Iafrate AJ: *FGFR1* amplification in squamous cell carcinoma of the lung. J Thorac Oncol 7: 1775-1780, 2012.
25. Sasaki H, Yokota K, Hikosaka Y, Moriyama S, Yano M and Fujii Y: Increased *SOX2* copy number in lung squamous cell carcinomas. Exp Ther Med 3: 44-48, 2012.
26. Jagadeeswaran R, Ma PC, Seiwert TY, Jagadeeswaran S, Zumba O, Nallasura V, Ahmed S, Filiberti R, Paganuzzi M, Puntoni R, *et al*: Functional analysis of c-met hepatocyte growth factor pathway in malignant pleural mesothelioma. Cancer Res 66: 352-361, 2006.
27. Engelman JA, Zejnullahu K, Mitsudomi T, Song Y, Hyland C, Park JO, Lindeman N, Gale CM, Zhao X, Christensen J, *et al*: *MET* amplification leads to gefitinib resistance in lung cancer by activating ERBB3 signaling. Science 316: 1039-1043, 2007.
28. Asano H, Toyooka S, Tokumo M, Ichimura K, Aoe K, Ito S, Tsukuda K, Ouchida M, Aoe M, Katayama H, *et al*: Detection of *EGFR* gene mutation in lung cancer by mutant-enriched polymerase chain reaction assay. Clin Cancer Res 12: 43-48, 2006.
29. Okuda K, Sasaki H, Kawano O, Yukiue H, Yokoyama T, Yano M and Fujii Y: Epidermal growth factor receptor gene mutation, amplification and protein expression in malignant pleural mesothelioma. J Cancer Res Clin Oncol 134: 1105-1111, 2008.
30. Rena O, Boldorini LR, Gaudino E and Casadio C: Epidermal growth factor receptor overexpression in malignant pleural mesothelioma: Prognostic correlations. J Surg Oncol 104: 701-705, 2011.
31. Enomoto Y, Kasai T, Takeda M, Takano M, Morita K, Kadota E, Iizuka N, Maruyama H, Haratake J, Kojima Y, *et al*: A comparison of epidermal growth factor receptor expression in malignant peritoneal and pleural mesothelioma. Pathol Int 62: 226-231, 2012.
32. Takeda M, Kasai T, Enomoto Y, Takano M, Morita K, Kadota E, Iizuka N, Maruyama H and Nonomura A: Genomic gains and losses in malignant mesothelioma demonstrated by FISH analysis of paraffin-embedded tissues. J Clin Pathol 65: 77-82, 2012.
33. Destro A, Ceresoli GL, Falleni M, Zucali PA, Morenghi E, Bianchi P, Pellegrini C, Cordani N, Vaira V, Alloisio M, *et al*: *EGFR* overexpression in malignant pleural mesothelioma. An immunohistochemical and molecular study with clinico-pathological correlations. Lung Cancer 51: 207-215, 2006.
34. Pache JC, Janssen YM, Walsh ES, Quinlan TR, Zanella CL, Low RB, Taatjes DJ and Mossman BT: Increased epidermal growth factor-receptor protein in a human mesothelial cell line in response to long asbestos fibers. Am J Pathol 152: 333-340, 1998.
35. Cortese JF, Gowda AL, Wali A, Eliason JF, Pass HI and Everson RB: Common *EGFR* mutations conferring sensitivity to gefitinib in lung adenocarcinoma are not prevalent in human malignant mesothelioma. Int J Cancer 118: 521-522, 2006.
36. Velcheti V, Kasai Y, Viswanathan AK, Ritter J and Govindan R: Absence of mutations in the epidermal growth factor receptor (*EGFR*) kinase domain in patients with mesothelioma. J Thorac Oncol 4: 559, 2009.
37. Mezzapelle R, Miglio U, Rena O, Paganotti A, Allegrini S, Antona J, Molinari F, Frattini M, Monga G, Alabiso O, *et al*: Mutation analysis of the *EGFR* gene and downstream signalling pathway in histologic samples of malignant pleural mesothelioma. Br J Cancer 108: 1743-1749, 2013.
38. Tsao MS, Sakurada A, Cutz JC, Zhu CQ, Kamel-Reid S, Squire J, Lorimer I, Zhang T, Liu N, Daneshmand M, *et al*: Erlotinib in lung cancer - molecular and clinical predictors of outcome. N Engl J Med 353: 133-144, 2005.
39. Moroni M, Veronese S, Benvenuti S, Marrapese G, Sartore-Bianchi A, Di Nicolantonio F, Gambacorta M, Siena S and Bardelli A: Gene copy number for epidermal growth factor receptor (*EGFR*) and clinical response to anti*EGFR* treatment in colorectal cancer: a cohort study. Lancet Oncol 6: 279-286, 2005.
40. Govindan R, Kratzke RA, Herndon JE, Niehans GA, Vollmer R, Watson D, Green MR and Kindler HL; Cancer and Leukemia Group B (CALGB 30101): Gefitinib in patients with malignant mesothelioma: A phase II study by the Cancer and Leukemia Group B. Clin Cancer Res 11: 2300-2304, 2005.
41. Garland LL, Rankin C, Gandara DR, Rivkin SE, Scott KM, Nagle RB, Klein-Szanto AJ, Testa JR, Altomare DA and Borden EC: Phase II study of erlotinib in patients with malignant pleural mesothelioma: A Southwest Oncology Group Study. J Clin Oncol 25: 2406-2413, 2007.

Hindawi Publishing Corporation
Pulmonary Medicine
Volume 2015, Article ID 416179, 6 pages
http://dx.doi.org/10.1155/2015/416179

Research Article

Clinical Investigation of Benign Asbestos Pleural Effusion

Nobukazu Fujimoto,[1] Kenichi Gemba,[2,3] Keisuke Aoe,[4] Katsuya Kato,[5,6] Takako Yokoyama,[7] Ikuji Usami,[7] Kazuo Onishi,[8] Keiichi Mizuhashi,[9] Toshikazu Yusa,[10] and Takumi Kishimoto[11]

[1] *Department of Medical Oncology, Okayama Rosai Hospital, 1-10-25 Chikkomidorimachi, Okayama 7028055, Japan*
[2] *Department of Respiratory Medicine, Okayama Rosai Hospital, 1-10-25 Chikkomidorimachi, Okayama 7028055, Japan*
[3] *Department of Respiratory Medicine, Chugoku Chuo Hospital, Fukuyama 7200001, Japan*
[4] *Department of Medical Oncology, Yamaguchi-Ube Medical Center, 685 Higashikiwa, Ube 7550241, Japan*
[5] *Department of Radiology, Okayama University Hospital, 2-5-1 Shikatacho, Okayama 7008558, Japan*
[6] *Department of Diagnostic Radiology 2, Kawasaki Medical School, Okayama 7008505, Japan*
[7] *Department of Respiratory Medicine, Asahi Rosai Hospital, 61 Hirakochokita, Owariasahi 4880875, Japan*
[8] *Department of Respiratory Medicine, Kobe Rosai Hospital, 4-1-23 Kagoikedori, Chuoku, Kobe 6510053, Japan*
[9] *Department of Respiratory Medicine, Toyama Rosai Hospital, 992 Rokuromaru, Uozu 9370042, Japan*
[10] *Department of Thoracic Surgery, Chiba Rosai Hospital, 2-16 Tatsumidaihigashi, Ichihara 2900003, Japan*
[11] *Department of Internal Medicine, Okayama Rosai Hospital, 1-10-25 Chikkomidorimachi, Okayama 7028055, Japan*

Correspondence should be addressed to Nobukazu Fujimoto; nfuji@okayamah.rofuku.go.jp

Received 17 August 2015; Revised 29 October 2015; Accepted 9 November 2015

Academic Editor: Denis Caillaud

Copyright © 2015 Nobukazu Fujimoto et al. This is an open access article distributed under the Creative Commons Attribution License, which permits unrestricted use, distribution, and reproduction in any medium, provided the original work is properly cited.

There is no detailed information about benign asbestos pleural effusion (BAPE). The aim of the study was to clarify the clinical features of BAPE. The criteria of enrolled patients were as follows: (1) history of asbestos exposure; (2) presence of pleural effusion determined by chest X-ray, CT, and thoracentesis; and (3) the absence of other causes of effusion. Clinical information was retrospectively analysed and the radiological images were reviewed. There were 110 BAPE patients between 1991 and 2012. All were males and the median age at diagnosis was 74 years. The median duration of asbestos exposure and period of latency for disease onset of BAPE were 31 and 48 years, respectively. Mean values of hyaluronic acid, adenosine deaminase, and carcinoembryonic antigen in the pleural fluid were 39,840 ng/mL, 23.9 IU/L, and 1.8 ng/mL, respectively. Pleural plaques were detected in 98 cases (89.1%). Asbestosis was present in 6 (5.5%) cases, rounded atelectasis was detected in 41 (37.3%) cases, and diffuse pleural thickening (DPT) was detected in 30 (27.3%) cases. One case developed lung cancer (LC) before and after BAPE. None of the cases developed malignant pleural mesothelioma (MPM) during the follow-up.

1. Introduction

Asbestos-related pathological changes of the pleura include pleural plaques, malignant pleural mesothelioma (MPM), diffuse pleural thickening (DPT), and benign asbestos pleural effusion (BAPE). BAPE is a nonmalignant pleural disease initially described in 1964 [1]. It is also termed asbestos pleuritis. Once a patient is diagnosed with BAPE, he or she is compensated by workers' compensation in Japan. Epler et al. [2] advocated diagnostic criteria for BAPE, which include (1) previous asbestos exposure, (2) determination of pleural effusion by chest X-ray or thoracentesis, and (3) the absence of other causes of effusion. They also stated that follow-up assessments for at least 3 years were essential to confirm the diagnosis and to exclude the development of malignant diseases such as MPM or lung carcinomatous pleuritis. Later, Hillerdal and Ozesmi [3] described that a 1-year follow-up would be sufficient based on a detailed exploration including computed tomographic (CT) scanning. Most of the previous studies included small numbers of

patients and were undertaken in the 1980s, so no detailed information is available about the disease.

In the current study, we retrospectively analysed the clinical features of BAPE in patients in Japan. The aim of the study was to clarify the clinical features of BAPE and to suggest more practical diagnostic standard for the disease.

2. Patients and Methods

2.1. Subjects. Enrolled patients were referred to Rosai Hospital and affiliated hospitals in Japan for an examination for pleural effusion and were finally diagnosed with BAPE. The criteria of enrolled patients were as follows: (1) previous history of asbestos exposure obtained by an in-person questionnaire or interview; (2) presence of pleural effusion determined by chest X-ray, CT, and thoracentesis; and (3) the absence of other causes of effusion. The pleural fluid was collected by thoracentesis or thoracoscopy, and information on cell classification, cytological analysis, and the biochemical examination was extracted from the medical records. Hyaluronic acid (HA), adenosine deaminase (ADA), and carcinoembryonic antigen (CEA) were included among the clinical laboratory tests. The HA concentration was determined using a latex agglutination turbidimetric immunoassay. ADA was measured using an enzymatic technique. CEA was measured using a chemiluminescent immunoassay.

2.2. Data Collection and Analysis. Clinical and demographic information was obtained from the medical records at each facility. The information included age, gender, smoking status, initial symptoms, and results of laboratory testing of the pleural effusion. The work histories, those of the family members, and residential histories were investigated to assess the patient's history of asbestos exposure.

The radiological images were sent to Okayama Rosai Hospital for review. Characteristic radiological findings associated with asbestos exposure were assessed as the presence of pleural effusion, asbestosis, rounded atelectasis, pleural plaques, and DPT. Asbestosis was classified on chest X-rays according to perfusion rate (PR) based on the International Labour Organization (ILO) criteria [4]. DPT was defined as pleural thickening of more than 5 mm on chest X-rays, extending for more than half of the lateral thoracic wall (LTW) in cases of unilateral DPT or more than quarter of the LTW in cases of bilateral DPT [5]. The presence of pleural effusion, rounded atelectasis, and pleural plaques was assessed on chest CT.

Survival data were determined from the day pleural effusion was detected to the day of death or last follow-up and analysed using the Kaplan-Meier method with SPSS 11.0 software (SPSS, Inc., Chicago, IL, USA).

This study was done according to the Ethical Guidelines for Epidemiological Research by the Japanese Ministry of Education, Culture, Sports, Science, and Technology and the Ministry of Health, Labour, and Welfare. This study was approved by Japan Labour Health and Welfare Organization and the institutional review boards of each institution. Patient confidentiality was strictly maintained. This study was carried out according to the principles set out in the Declaration of Helsinki.

Table 1: Patient characteristics.

Age (n = 110)	
Median (range)	74 (36–90)
Gender (n = 110)	
Male/female	110/0
Smoking history (n = 63)	
Ever/current	56
Never	7
Symptoms (n = 65, multiple answers)	
Dyspnea	34
Cough	15
Chest pain	13
Fever	3
Palpitation	2
Sputum	1
Wheezing	1
Back pain	1
Weight loss	1
Fatigue	1

3. Results

3.1. Patient Characteristics. One hundred ten patients from 9 institutions fulfilled the enrolled criteria based on the descriptions in their medical records and review of the radiographs between 1991 and 2012. Characteristics of the patients are shown in Table 1. Smoking history was obtained in 63 cases including 56 ever/current smokers and 7 never smokers, with the median (range) pack-years of 34.5 (0–112). Pleural effusion was found in 56 cases in the right, 25 in the left, and 27 in both thoracis. Sixty-five patients visited the clinic for subjective symptoms, and pleural effusion was detected at the regular medical check-up in 35 cases without any symptoms. Pleural effusion was detected during the treatment of other diseases in another 15 cases. Thoracentesis was performed in all patients to collect pleural fluid. Thoracoscopic exploration was done in 78 patients to exclude carcinomatous pleuritis or MPM and to confirm the diagnosis of BAPE.

3.2. Asbestos Exposure History. A history of asbestos exposure was reported by 109 patients, with one patient whose detailed information of asbestos exposure was not obtained. Among the 109 patients, 108 patients had a history of occupational asbestos exposure and one patient had a history of environmental asbestos exposure. The occupational categories associated with asbestos exposure are shown in Table 2. The median (range) age of the first exposure to asbestos was 21.5 (14–58) years. The median (range) duration of asbestos exposure was 31 (0.75–50) years and the median (range) period of latency for disease onset of BAPE was 48 (17–76) years.

Table 2: Occupational category related to asbestos exposure.

Shipbuilding	25
Construction	20
Chemical facility	10
Asbestos products manufacturing	8
Electrical work	8
Plumbing	7
Asbestos transportation	5
Moisturizing work	4
Asbestos spraying	3
Steel production	3
Demolition work	2
Automobile manufacturing	2
Heat insulation	2
Firebrick manufacturing	2
Glasswork	1
Metallic product manufacture	1
Furnace installation	1
Coating industry	1
Shipman	1
Others	2
Total	108

3.3. Characteristics of the Pleural Effusion. Information regarding the pleural effusion was obtained in 104 cases. The gross impression of the pleural fluid was bloody in 75 cases, light yellow in 27, and light brown and dark red in 1 case each. The effusions were exudative in all cases. A cellular classification of the fluid was obtained in 57 cases and the median proportions of lymphocytes, macrophages, neutrophils, and eosinophils were 77.7%, 9.7%, 8.0%, and 8.0%, respectively. The HA concentration was determined in 106 cases and the mean (standard deviation) concentration was 39,840 (40,228) ng/mL. Mean (standard deviation) values of ADA and CEA were 23.9 (24.9) IU/L and 1.8 (1.3) ng/mL, respectively.

3.4. Concomitant Asbestos-Related Findings. As shown in Table 3, pleural plaques were detected in 98 cases (89.1%), among which 76 cases were calcified. Asbestosis was present in 6 cases, rounded atelectasis was detected in 41 cases (37.3%), and DPT was detected in 30 cases (27.3%). One of the cases developed lung cancer (LC) before and after diagnosis of BAPE. The patient had undergone right upper lobectomy for LC two years before his BAPE diagnosis and left partial lobectomy for another LC two years after his BAPE diagnosis.

3.5. Clinical Course. In most of the cases, thoracentesis and/or thoracotomy were done to collect the fluid and drain the pleural effusion. Oral steroids were prescribed in 5 cases and one of them demonstrated temporal decrease of the effusion. Survival data was obtained in 70 cases from Okayama Rosai Hospital. As shown in Figure 1, median overall survival was 104.2 months (95% confidence interval (CI), 67.3–141.0 months) after a median observation period of 73.0 months (95% CI, 16.2–268.2 months). There were 17 dead cases out of 70 cases at the analysis. The causes of death were determined in 11 cases including 7 respiratory failure cases and each 1 of renal failure, suicide, septic shock due to urinary tract infection, and death of old age. There were 9 cases that developed DPT out of the 17 cases, including the 7 dead cases of respiratory failure. At the time of the analysis, none of the cases had developed MPM.

Table 3: Concomitant asbestos-related radiological findings.

Findings		*n*	%
Pleural plaques		98	89.1
Calcified		76	
Asbestosis		6	5.7
PR[†]	1	3	
	2	2	
	3	1	
Rounded atelectasis		41	37.3
DPT[‡]		30	27.3

[†]Perfusion rate, [‡]diffuse pleural thickening.

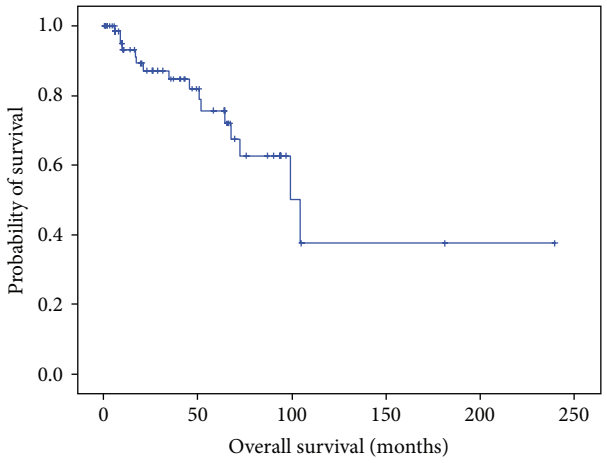

Figure 1: Overall survival of patients with benign asbestos-related pleural effusions at Okayama Rosai Hospital.

4. Discussion

In the current study, we examined the clinical features of BAPE and demonstrated that BAPE developed after long-term asbestos exposure. In a previous report, BAPE occurred 15–20 years after exposure and was more common in younger patients aged 21–40 years [6]. In another report, the interval between asbestos exposure and presentation of BAPE varied between 5 and more than 30 years, and early onset was correlated with higher asbestos exposure [7]. Wagner reported that BAPEs were usually unilateral, and the most common manifestation of asbestos-related pleural disease occurred 10 to 20 years after exposure [8]. A limitation of these earlier studies is that the diagnosis criteria of BAPE were ambiguous in the studies. The median latency period between asbestos exposure and BAPE development in the current study was

Table 4: Proposed diagnostic criteria of benign asbestos pleural effusion.

Diagnostic criteria
(1) Asbestos exposure history.
(2) Exudative effusion.
(3) Exclusion of other pleuritides such as lung cancer, MPM[†], and tuberculous pleuritis by radiological examination and pleural biopsy via thoracoscopy.
Additional diagnostic information
(1) In cases thoracoscopy could not be undergone, the diagnosis should be discussed based on the bacteriological examination and biochemical markers below.
(a) Elevated carcinoembryonic antigen (>5 ng/mL) suggests carcinomatous pleuritis.
(b) Elevated adenosine deaminase (>35 IU/L) suggests tuberculous pleuritis.
(c) Elevated hyaluronic acid (>100,000 ng/dL) suggests MPM.
(2) In cases with some concomitant medical problem such as autoimmune diseases, the activity of the disease should be carefully evaluated.

[†]Malignant pleural mesothelioma.

48 years, which was similar to that observed for MPM (41 years), LC (47 years), and asbestos-induced DPT (46 years) in our previous reports [4, 9, 10]. We consider that BAPE develops after a long latency period in those with a history of asbestos exposure. There is one point, however, that most of the patients of BAPE in the current study have associated with other asbestos-related lesions such as rounded atelectasis and/or diffuse pleural thickening. It is possible that BAPE might have been developed earlier in these cases, and this could be an explanation of the longer latency of BAPE than previously published. The current study suggests that BAPE can develop after moderate-to-high levels of exposure to asbestos, because the occupational category of the subjects in the current study included those of relatively high levels of asbestos exposure such as asbestos product manufacturing, construction, and shipbuilding, although the correlation between the exposure amount and development of BAPE is unclear. The subjects in the current study included substantial portion of those with smoking history. To our knowledge, the correlation between BAPE and smoking history has not been reported.

The diagnosis of BAPE should be based on a history of asbestos exposure and an exclusion of other causes of effusion such as tuberculous pleuritis, bacterial pleuritis, collagen diseases, heart failure, and malignant conditions such as MPM and LC. In our analysis, the gross impression of the pleural fluid was bloody in 72% of the cases, and cellular classification of the fluid demonstrated lymphocyte dominancy. These results are similar to those of a previous report showing that the effusion was exudative and could be hemorrhagic, as well as predominantly eosinophilic [11].

In cases of LC, tumor cells are detected in the fluid in more than 60% of cases [12]. In cases with MPM, tumor cells can be detected in the pleural fluid, but the detection rate has been reported as less than 30% [13]. Tuberculosis pleuritis or bacterial pleuritis could be diagnosed by staining for acid-fast bacteria, polymerase chain reaction detection, or bacterial culture, although the detection rate is usually low. These analyses may not always determine the diagnosis but should be undergone to exclude MPM, LC, and tuberculosis or bacterial pleuritis and to make the diagnosis of BAPE.

In addition, we analysed some markers such as HA concentration, ADA, and CEA. Recently, we reported the clinical usefulness of HA for the differential diagnosis of MPM and BAPE [14]. In cases with tuberculosis pleuritis, elevated values of ADA could help in the diagnosis [15]. However, elevated ADA may not be limited to tuberculous pleuritis, as it is also present in LC or MPM [16]. In cases with elevated CEA values, carcinomatous pleuritis is strongly suggested [17]. These markers should be determined to exclude these conditions and to confirm a diagnosis of BAPE. However, the differential diagnosis of MPM and BAPE is especially difficult, even when based on these markers. Especially in cases with exudative pleural effusions, thoracoscopic exploration and pleural biopsy should be performed to exclude MPM and confirm the diagnosis of BAPE [18].

Based on the findings in the current study and previous reports, we propose more practical diagnostic standard for the diagnosis of BAPE including (1) asbestos exposure history, (2) exudative effusion, and (3) exclusion of other pleuritides such as LC, MPM, and tuberculous pleuritis by radiological examination and pleural biopsy via thoracoscopy. Additional diagnostic information is as follows: (1) in cases thoracoscopy could not be undergone, the diagnosis should be discussed based on the bacteriological examination and biochemical markers such as CEA, ADA, and HA; in cases with elevated CEA (>5 ng/mL), ADA (>35 IU/L), or HA (>100,000 ng/dL), carcinomatous pleuritis, tuberculous pleuritis, or MPM is more likely, respectively; and (2) in cases with some concomitant medical problem such as autoimmune diseases, the activity of the disease should be carefully evaluated, because autoimmune diseases such as systemic lupus erythematosus or rheumatoid arthritis could involve the pleura and cause pleural effusion (Table 4).

"Benign" is meant to refer to a nonmalignant process, but these effusions can be associated with significant morbidity [19]. The effusion generally takes a long time to resolve. It may resolve spontaneously or be followed by DPT, which causes extrapulmonary restriction and may thereby ultimately become disabling. Previous studies reported that a considerable number of patients with BAPE subsequently developed DPT [2, 3]. Actually, in our previous study, half

the patients with asbestos-induced DPT had a history of BAPE [4]. Furthermore, in the current study one patient developed LC before and after being diagnosed with BAPE. The risks of developing MPM or LC in patients with BAPE are increased compared with those of the general population because of their past history of asbestos exposure. Particular attention should be paid to the management of patients with BAPE.

There are a few limitations to the current study. First, this was a retrospective study. Second, pathological analyses including immunohistochemistry were not reviewed. In addition, there are recent reports that increased uptake of fluorodeoxyglucose (FDG) by positron emission tomography (PET) may be a useful marker to distinguish MPM from benign pleural disease [20, 21]. In addition, recent reports revealed that biomarkers such as soluble mesothelin-related peptides (SMRP) are selectively elevated in patients with MPM [22, 23]. A clinical study to evaluate the utility of PET and/or SMRP for the differentiation between MPM and BAPE is warranted.

5. Conclusions

BAPE develops after a long latency period after past asbestos exposure. The diagnosis of BAPE should be based on the exclusion of other pleural diseases. A thorough evaluation, including diagnostic thoracentesis and cytological and bacterial analysis, must be performed. Clinical markers such as HA, ADA, and CEA might help with the differential diagnosis. However, thoracoscopic exploration and pleural biopsy should be performed to confirm a diagnosis of BAPE.

Disclosure

This study is a part of "the research and development and the dissemination projects related to the 9 fields of occupational injuries and illnesses" of Japan Labour Health and Welfare Organization. This organization had no involvement in the study design, collection, analysis, and interpretation of the data, writing of the paper, or decision to submit the paper for publication.

Conflict of Interests

The authors declare that there is no conflict of interests in their submitted paper.

References

[1] H. B. Eisenstadt, "Asbestos pleurisy," *Diseases of the Chest*, vol. 46, pp. 78–81, 1964.

[2] G. R. Epler, T. C. McLoud, and E. A. Gaensler, "Prevalence and incidence of benign asbestos pleural effusion in a working population," *The Journal of the American Medical Association*, vol. 247, no. 5, pp. 617–622, 1982.

[3] G. Hillerdal and M. Ozesmi, "Benign asbestos pleural effusion: 73 exudates in 60 patients," *European Journal of Respiratory Diseases*, vol. 71, no. 2, pp. 113–121, 1987.

[4] N. Fujimoto, K. Kato, I. Usami et al., "Asbestos-related diffuse pleural thickening," *Respiration*, vol. 88, no. 4, pp. 277–284, 2014.

[5] American Thoracic Society, "Medical Section of the American Lung Association: the diagnosis of nonmalignant diseases related to asbestos," *American Review of Respiratory Disease*, vol. 134, pp. 363–368, 1986.

[6] P. Ernst and J. Zejda, "Pleural and airway diseases associated with mineral fibers," in *Mineral Fibers and Health*, D. Lidderll and K. Miller, Eds., pp. 121–134, CRC, Boca Raton, Fla, USA, 1991.

[7] B. W. S. Robinson and A. W. Musk, "Benign asbestos pleural effusion: diagnosis and course," *Thorax*, vol. 36, no. 12, pp. 896–900, 1981.

[8] G. R. Wagner, "Asbestosis and silicosis," *The Lancet*, vol. 349, no. 9061, pp. 1311–1315, 1997.

[9] T. Kishimoto, K. Gemba, N. Fujimoto et al., "Clinical study on mesothelioma in Japan: relevance to occupational asbestos exposure," *American Journal of Industrial Medicine*, vol. 53, no. 11, pp. 1081–1087, 2010.

[10] T. Kishimoto, K. Gemba, N. Fujimoto et al., "Clinical study of asbestos-related lung cancer in Japan with special reference to occupational history," *Cancer Science*, vol. 101, no. 5, pp. 1194–1198, 2010.

[11] A. J. Ghio and V. L. Roggli, "Diagnosis and initial management of nonmalignant diseases related to asbestos," *American Journal of Respiratory and Critical Care Medicine*, vol. 170, no. 6, pp. 691–715, 2004.

[12] K. B. Sriram, V. Relan, B. E. Clarke et al., "Diagnostic molecular biomarkers for malignant pleural effusions," *Future Oncology*, vol. 7, no. 6, pp. 737–752, 2011.

[13] A. Medford and N. Maskell, "Pleural effusion," *Postgraduate Medical Journal*, vol. 81, no. 961, pp. 702–710, 2005.

[14] N. Fujimoto, K. Gemba, M. Asano et al., "Hyaluronic acid in the pleural fluid of patients with malignant pleural mesothelioma," *Respiratory Investigation*, vol. 51, no. 2, pp. 92–97, 2013.

[15] A. Gopi, S. M. Madhavan, S. K. Sharma, and S. A. Sahn, "Diagnosis and treatment of tuberculous pleural effusion in 2006," *Chest*, vol. 131, no. 3, pp. 880–889, 2007.

[16] Y. Ogata, K. Aoe, A. Hiraki et al., "Is adenosine deaminase in pleural fluid a useful marker for differentiating tuberculosis from lung cancer or mesothelioma in Japan, a country with intermediate incidence of tuberculosis?" *Acta Medica Okayama*, vol. 65, no. 4, pp. 259–263, 2011.

[17] H.-Z. Shi, Q.-L. Liang, J. Jiang, X.-J. Qin, and H.-B. Yang, "Diagnostic value of carcinoembryonic antigen in malignant pleural effusion: a meta-analysis," *Respirology*, vol. 13, no. 4, pp. 518–527, 2008.

[18] A. Scherpereel, P. Astoul, P. Baas et al., "Guidelines of the European Respiratory Society and the European Society of Thoracic Surgeons for the management of malignant pleural mesothelioma," *European Respiratory Journal*, vol. 35, no. 3, pp. 479–495, 2010.

[19] R. Myers, "Asbestos-related pleural disease," *Current Opinion in Pulmonary Medicine*, vol. 18, no. 4, pp. 377–381, 2012.

[20] F. Bénard, D. Sterman, R. J. Smith, L. R. Kaiser, S. M. Albelda, and A. Alavi, "Metabolic imaging of malignant pleural mesothelioma with fluorodeoxyglucose positron emission tomography," *Chest*, vol. 114, no. 3, pp. 713–722, 1998.

[21] H. Yildirim, M. Metintas, E. Entok et al., "Clinical value of fluorodeoxyglucose-positron emission tomography/computed tomography in differentiation of malignant mesothelioma from

asbestos-related benign pleural disease: an observational pilot study," *Journal of Thoracic Oncology*, vol. 4, no. 12, pp. 1480–1484, 2009.

[22] A. Scherpereel, B. Grigoriu, M. Conti et al., "Soluble mesothelin-related peptides in the diagnosis of malignant pleural mesothelioma," *American Journal of Respiratory and Critical Care Medicine*, vol. 173, no. 10, pp. 1155–1160, 2006.

[23] N. Fujimoto, K. Gemba, M. Asano et al., "Soluble mesothelin-related protein in pleural effusion from patients with malignant pleural mesothelioma," *Experimental and Therapeutic Medicine*, vol. 1, no. 2, pp. 313–317, 2010.

Author's personal copy

Clin Exp Metastasis
DOI 10.1007/s10585-015-9772-8

RESEARCH PAPER

Brain metastases in malignant pleural mesothelioma

Tomoko Yamagishi[1] · Nobukazu Fujimoto[2] · Yosuke Miyamoto[1] · Michiko Asano[1] · Yasuko Fuchimoto[1] · Sae Wada[1] · Kenichi Kitamura[1] · Shinji Ozaki[1] · Hideyuki Nishi[3] · Takumi Kishimoto[4]

Received: 1 September 2015 / Accepted: 25 November 2015
© Springer Science+Business Media Dordrecht 2015

Abstract The brain is a rare site of metastasis in malignant pleural mesothelioma (MPM), and its clinical features and prognosis remain unclear. The aim of this study was to investigate the incidence, prognosis, and risk factors for brain metastases (BM) in MPM patients. Between July 1993 and October 2014, 150 patients with histologically proven MPM were included in this retrospective study. The cumulative incidence of BM was estimated with the Kaplan–Meier method, and differences between groups were analyzed by the log-rank test. Multivariate logistic regression analysis was applied to assess risk factors for BM. The median follow-up time was 11 months (range 0–154.0 months). A total of eight patients (5.3 %) developed BM during the course of their illness. Multivariate analysis identified age <65 years (odds ratio [OR] = 5.83, $p = 0.038$) and International Mesothelioma Interest Group stage IV (OR = 1.69, $p = 0.040$) as independent factors related to increased risk of developing BM. The 1-and 2-year cumulative rates of BM were 4.0 % (95 % confidence intervals [CI] 1.4–8.5 %) and 5.3 % (95 % CI 2.3–10.2 %), respectively. Our study showed that the overall survival (OS) of patients with BM was worse than that of patients without BM (median OS 6.5 vs. 11.0 months, $p = 0.037$). The prognosis for BM in MPM patients is poor. Clinicians should perform careful screening for BM, especially in patients with risk factors.

Keywords Asbestos · Malignant pleural mesothelioma · Brain metastases · Central nervous system · Brain

Abbreviations

MPM	Malignant pleural mesothelioma
BM	Brain metastasis
ECOG	Eastern Cooperative Oncology Group
PS	Performance status
IMIG	International Mesothelioma Interest Group
EPS	European Organization for Research and Treatment of Cancer Prognostic Score
CALGB	Cancer and Leukemia Group B
MRI	Magnetic resonance imaging
CT	Computed tomography
OS	Overall survival

Introduction

Malignant pleural mesothelioma (MPM) is a rare but aggressive primary pleural neoplasm that is associated with asbestos exposure [1]. Its prognosis remains poor, as most patients have unresectable disease at the time of diagnosis. Although several treatment options are available to patients with MPM, the median survival time is approximately 12 months [2].

Brain metastasis (BM) is the most common type of intracerebral neoplasm and occurs in 10–30 % of adult

✉ Nobukazu Fujimoto
nobufujimot@gmail.com

[1] Department of Respiratory Medicine, Okayama Rosai Hospital, Okayama, Japan

[2] Department of Medical Oncology, Okayama Rosai Hospital, 1-10-25 Chikkomidorimachi, Minamiku, Okayama 702-8055, Japan

[3] Department of Surgery, Okayama Rosai Hospital, Okayama, Japan

[4] Department of Internal Medicine, Okayama Rosai Hospital, Okayama, Japan

Published online: 30 November 2015

Author's personal copy

patients with systemic cancer [3]. The incidence of BM may be increasing, because of improved imaging techniques to detect BM and more effective systemic treatment that can prolong the tumor-bearing period of time, permitting the cancer to disseminate to the brain. Lung cancer, breast cancer, and malignant melanoma are the neoplasms most frequentlyassociated with BM [4].

MPM typically spreads by local invasion or extension. Distant metastasis may occur; however, BM is quite rare and the majority of reported cases were identified by postmortem examination. The incidence of BM was reported to be only 3 % of MPM patients [5]. To date, there have been few reports on BM in patients with MPM. Recently, Chari et al. a case report and review of the literature on the topic [6], however, its clinical features and prognosis remain unclear. The aim of this single-institution retrospective study was to evaluate the incidence, risk factors, and survival outcome associated with BM inpatients with MPM.

Materials and methods

Patient population

The study included 150 consecutive patients with histologically proven MPM who were seen between July 1993 and October 2014 at Okayama Rosai Hospital, Japan. Baseline demographic and clinicopathological variables were collected retrospectively from patients' medical records. These included age at initial diagnosis, gender, histological subtype, clinical stage, and baseline Eastern Cooperative Oncology Group (ECOG) performance status (PS).Clinical staging was determined according to the International Mesothelioma Interest Group (IMIG) staging system [7]. The European Organization for Research and Treatment of Cancer Prognostic Score (EPS) was used to subcategorize patients into low- or high-risk groups based on age, gender, histology, probability of diagnosis, and leukocyte count [8]. We also used the Cancer and Leukemia Group B (CALGB) score, which incorporates the presence of nonepithelial histology, weight loss, chest pain, high platelets and WBC, low hemoglobin, high serum lactate dehydrogenase, advanced age, and PS [9]. The patients were divided based on their CALGB score into three groups (i.e., groups 1/2, 3/4, or 5/6), because of the small numbers in the even-numbered groups [10].

Diagnosis of BM in MPM was based on magnetic resonance imaging (MRI) or contrast-enhanced computed tomography (CT) scans. Routine brain imaging was performed at the diagnosis but not during the follow-up period, unless BM was suspected. Leptomeningeal metastases were not included in the actuarial incidence of BM in this study.

This study was approved by the Japan Labour, Health and Welfare Organization and the institutional review board of Okayama Rosai Hospital. Patient confidentiality was strictly maintained.

Statistical analysis

A comparison of patient characteristics at diagnosis was performed by Fisher's exact test or Student's t test, as appropriate. Overall survival (OS) was calculated from the date of initial diagnosis to the date of last follow-up or death from any cause. OS was obtained by using Kaplan–Meier methods, and between-group differences were compared with the log-rank test. To determine risk factors associated with the development of BM, univariate and multivariate logistic regression models with a stepwise selection procedure were generated. A two-tailed p value of <0.05 was considered statistically significant. All statistical analysis was performed with STATA software (version 12.1; StataCorp, College Station, TX, USA).

Results

Patient characteristics

The median follow-up time for the 150 study participants was 11.0 months (range 0–154.0 months). Eight of the patients developed BM: three at diagnosis of MPM and five during the clinical course of MPM. Thus, the crude incidence rate of BM was 2.0 % (95 % confidence interval [CI] 0.4–5.7 %) at diagnosis and 5.3 % (95 % CI 2.3–10.2 %) overall. The median time from initial diagnosis to development of BM was 4.5 months (range 0–24.0 months); the 1-and 2-year cumulative rates for BM were 4.0 % (95 % CI 1.4–8.5 %) and 5.3 % (95 % CI 2.3–10.2 %), respectively.

In the cohort of patients with BM ($n = 8$), the median (±SD) age was 61.3 (±6.3) years and all patients were men. The majority of the histological types were epithelioid (62.5 %) followed by sarcomatous (37.5 %). Three patients (37.5 %) had stage III disease, and five patients (62.5 %) had stage IV disease. Four patients (50 %) had symptoms of BM, such as ataxia ($n = 2$), headache ($n = 1$), and sensitivity disorders ($n = 1$). BM were in various locations including 5 in parietal lobe (62.5 %), 3 in frontal lobe (37.5 %), and each 2 in temporal lobe (25.0 %) and the cerebellum (25.0 %). The size of BM was 2 cm or less in all cases. At the time of detection of BM, four

Author's personal copy

Table 1 Patients with brain metastases

Age/ gender	Histology	IMIG stage	Treatment for primary tumor	Interval to BM (months)	Metastatic site	Presence of other metastases	Treatment for BM	Clinical response to treatment for BM	Survival post BM (months)	OS (months)
64/M	Epithelioid	T3N0M0, stage III	Chemotherapy	24.0	Multiple	Lung, adrenals, lymph node	WBRT	No	3.0	27.0
70/M	Epithelioid	T3N0M1, stage IV	Chemotherapy	0.0	Right parietal lobe	–	Chemotherapy	No	2.0	2.0
63/M	Sarcomatous	T3N1M0, stage III	Surgery	2.0	Cerebellum	Lung, adrenals, liver, muscle, lymph node	Chemotherapy	No	1.0	3.0
54/M	Epithelioid	T2N0M1, stage IV	Chemotherapy	7.0	Multiple	Adrenals, bone	WBRT	No	1.0	8.0
64/M	Sarcomatous	T3N0M1, stage IV	Best supportive care	0.0	Multiple	Bone	WBRT	No	5.0	5.0
64/M	Epithelioid	T4N2M0, stage IV	Chemotherapy	15.0	Multiple	–	SRT + chemotherapy	Yes	5.0	20.0
49/M	Epithelioid	T3N0M0, stage III	Chemotherapy	7.0	Right frontal lobe	Adrenals, liver	SRT	No	5.0	12.0
66/M	Sarcomatous	T2N0M1, stage IV	Chemotherapy	0.0	Right parietal lobe	–	SRT	No	4.0	4.0

BM brain metastases, *OS* overall survival, *IMIG* International Mesothelioma Interest Group, *WBRT* whole brain radiation therapy, *SRT* stereotactic radiotherapy

patients (50 %) had developed other distant metastases, including adrenal gland ($n = 3$), lung ($n = 2$), lymph node ($n = 2$), liver ($n = 2$), muscle/soft tissue ($n = 1$), and bone ($n = 1$). The patients' baseline characteristics and therapies are presented in Table 1.

The clinicopathological characteristics of the patients with BM were compared with those of patients without BM (non-BM) (Table 2). Age at diagnosis was younger in BM than in non-BM patients ($p = 0.034$), and there were more patients with pleural effusion at initial diagnosis in BM compared to non-BM patients ($p = 0.044$). There was no difference between the two groups with respect to histological subtype.

Treatment and survival

Of the three patients who presented BM at initial diagnosis, one patient underwent whole brain radiotherapy and one underwent radiosurgery. The remaining patient had asymptomatic BM and received systemic chemotherapy. Of the four patients who developed BM after initial systemic chemotherapy, two were treated with whole brain radiotherapy and two underwent radiosurgery. The final patient developed asymptomatic BM during the observation period after initial surgery and received systemic chemotherapy.

The median OS of the non-BM and BM groups was 11.0 months (range 0–154.0 months) and 6.5 months (range 2.0–27.0 months), respectively ($p = 0.037$) (Fig. 1). All patients died of progressive disease, with a median survival of 3.5 months (range 1.0–5.0 months) after the development of BM.

Risk factors

Univariate analysis revealed that age <65 years (odds ratio [OR] 6.06, 95 % CI 1.17–31.19, $p = 0.031$), absence of pleural effusion (OR 4.56; 95 % CI 1.03–20.01, $p = 0.044$), and IMIG stage IV (OR 1.72, 95 % CI 1.05–2.81, $p = 0.031$) were potential risk factors for BM. In the multivariate analysis, age < 65 years (OR 5.83; 95 % CI 1.10–30.73, $p = 0.038$) and IMIG stage IV (OR 1.69 95 % CI 1.02–2.80, $p = 0.040$) remained associated with a high risk of BM (Table 3).Based on the results of multivariate analysis, we analyzed the effect of these two factors on the incidence of BM. For patients age ≥65 years and stage I–III, age <65 years and stage I–III, age ≥65 years and stage IV, and age <65 years and stage IV, the cumulative incidence rates of BM were 0, 8.1, 8.3, and 18.7 %, respectively ($p = 0.003$, Fisher's exact test) (Fig. 2).

Author's personal copy

Table 2 Patient characteristics

Characteristic	Brain metastases ($n = 8$)	No brain metastases ($n = 142$)	p value
Median age, years (range)	61.3 ± 6.7	68.9 ± 9.9	0.034
Men	8 (100 %)	132 (93 %)	0.568
ECOG PS > 2	2 (25 %)	19 (13 %)	0.311
Pleural effusion at diagnosis			0.044
Yes	3 (38 %)	104 (73 %)	
No	5 (62 %)	38 (27 %)	
Histological subtype			0.584
Epithelioid subtype	5 (63 %)	92 (65 %)	
Nonepithelioid subtype	3 (37 %)	50 (35 %)	
Calretinin			0.07
Positive	5 (63 %)	121 (85 %)	
Negative	2 (25 %)	9 (6 %)	
Missing	1 (12 %)	12 (8 %)	
IMIG stage			0.051
I–II	0 (0 %)	54 (38 %)	
III–IV	8 (100 %)	88 (62 %)	
EORTC prognostic score			0.712
High risk	4 (50 %)	87 (61 %)	
Low risk	4 (50 %)	55 (39 %)	
CALGB score			0.076
1–2	0 (0 %)	49 (35 %)	
3–4	5 (63 %)	63 (44 %)	
5–6	3 (37 %)	30 (21 %)	
Treatment modality			0.630
Surgery	1 (12 %)	43 (30 %)	
Systemic chemotherapy alone	6 (75 %)	80 (56 %)	
Radiotherapy	0 (0 %)	3 (2 %)	
Best supportive care	1 (13 %)	16 (11 %)	

ECOG Eastern Cooperative Oncology Group, *PS* performance status, *IMIG* International Mesothelioma Interest Group, *CALGB* Cancer and Leukemia Group B, *EORTC* European Organisation for Research and Treatment of Cancer

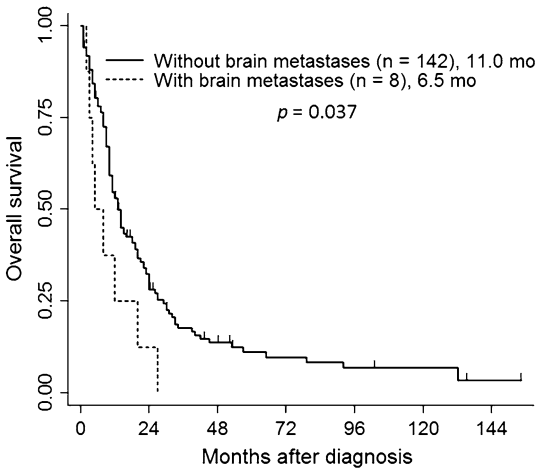

Fig. 1 Overall survival in malignant pleural mesothelioma patients with and without brain metastases

Discussion

MPM is an uncommon tumor of the thorax; typically, there is pernicious local invasion and extension into the pleural space and surrounding organs. The brain is a rare site for metastasis from MPM, and the majority of reported cases were identified in postmortem studies. To the best of our knowledge, this is the first report to have focused on the incidence, risk factors, and survival outcome associated with BM in patients with MPM.

In our patient cohort, eight out of 150 patients (5.3 %) developed BM. Falconieri et al. reviewed 171 cases of MPM at postmortem examination and discovered that 54 % of patients had distant metastases. The most frequently involved organs were the liver (55.9 %), adrenal glands (31.1 %), kidney (30.1 %), and contralateral lung (26.8 %). Intracranial (brain and meningeal) metastases

Author's personal copy

Table 3 Cox regression model for factors associated with incidence of brain metastases

Variable	Univariate		Multivariate	
	Odds ratio (95 % Cl)	*p* value	Odds ratio (95 % CI)	*p* value
Age at initial diagnosis				
≥65 years	1		1	
<65 years	6.06 (1.17–31.19)	0.031	5.83 (1.10–30.73)	0.038
ECOG PS				
≤1	1		NI	
>1	2.15 (0.40–11.48)	0.367		
Pleural effusion at diagnosis				
Yes	1		NI	
No	4.56 (1.03–20.01)	0.044		
Histological subtype				
Epithelioid	1		NI	
Nonepithelioid	1.10 (0.25–4.81)	0.895		
Calretinin				
Positive	1		NI	
Negative	5.02 (0.85–29.62)	0.075		
IMIG stage				
I–III	1		1	
IV	1.72 (1.05–2.81)	0.031	1.69 (1.02–2.80)	0.040
Surgery				
Yes	1		NI	
No	0.32 (0.03–2.75)	0.305		
CALGB score				
1–3	1		NI	
4–6	2.22 (0.53–9.31)	0.273		
EORTC prognostic score				
Low risk	1		NI	
High risk	1.58 (0.37–6.58)	0.529		

ECOG Eastern Cooperative Oncology Group, *PS* performance status, *IMIG* International Mesothelioma Interest Group; *CALGB* Cancer and Leukemia Group B, *EORTC* European Organisation for Research and Treatment of Cancer; *NI* not included

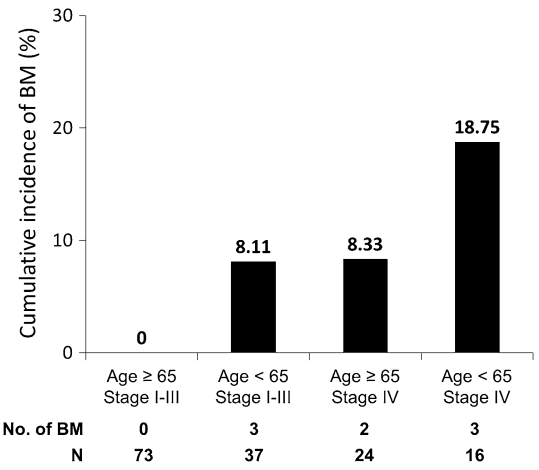

Fig. 2 Cumulative incidence of brain metastases in malignant pleural mesothelioma patients characterized by identified risk factors. *BM* brain metastases

were found in only 3 % of cases [5]. Furthermore, pooling analysis of seven postmortem studies consisting of 655 patients revealed that the rate of intracranial metastases from malignant mesothelioma (including those of pleural, pericardial, and tunica vaginalis testis origin) was 2.7 % [11]. Our study demonstrated that the incidence of BM was approximately 5 %, which is higher than that in previous studies. The previous studies were limited to autopsy cases, and not all MPM patients were included. We believe that the true incidence of BM may be higher.

In our study, multivariate analysis showed that age <65 years and IMIG stage IV were independently associated with BM. An increased risk for BM in younger patients was reported in several studies on other malignancies [12–15]; however, the reason why younger patients are at a higher risk of BM is not well understood. Further

Author's personal copy

investigations are needed to determine the biological factors associated with BM in younger patients.

Among the clinicopathological features of MPM, histological subtype is one of the most important factors influencing survival and sarcomatous histology has the worst prognosis [16]. Miller et al. showed that the sarcomatous subtype predominates in patients with BM [11]; however, another study observed that the rate of extra thoracic dissemination does not differ among histology subtypes [17]. Our findings also demonstrated that histology was not a risk factor for BM.

The current study showed that outcomes for BM were equally poor regardless of treatment modalities. Surgery, stereotactic therapies, and systemic chemotherapy may play a role in selected situations; however, rapid recurrence after surgical excision [18] or after regression in response to systemic chemotherapy [19] has been reported. Clarification regarding the most appropriate treatment strategy for BM is urgently needed. The next best policy would be to identify patients with MPM who are at greater risk of developing BM. Based on our results, it may be reasonable to perform brain imaging on MPM patients with risk factors such as age <65 years and IMIG stage IV, even in the absence of neurological signs and symptoms.

There are a few limitations to the current study. First, this was a retrospective single-institution study. Second, due to the relatively small number of patients and events, statistical analysis was limited. Another limitation is that most BM were detected based on patients' symptoms. Therefore, asymptomatic BM may have been missed.

In conclusion, the prognosis for MPM patients with BM is poor. The incidence of MPM is predicted to reach a peak between 2015 and 2025 [20], and the development of BM has a severe effect on patients' quality of life and survival. Clinicians should perform careful screening for BM, especially in patients with risk factors.

Acknowledgments This study was supported by "The research and development and the dissemination projects related to the 9 fields of occupational injuries and illnesses" of the Japan Labour Health and Welfare Organization and by grants-in-aid from the Ministry of Health, Labor and Welfare, Japan (150401-02).

Compliance with ethical standards

Conflict of interest The authors declare that they have no conflict of interests.

Ethical approval All procedures performed in studies involving human participants were in accordance with the ethical standards of the institutional and/or national research committee and with the 1964 Helsinki declaration and its later amendments or comparable ethical standards. For this type of study (retrospective), formal consent is not required.

References

1. Gemba K, Fujimoto N, Kato K, Aoe K, Takeshima Y, Inai K, Kishimoto T (2012) National survey of malignant mesothelioma and asbestos exposure in Japan. Cancer Sci 103:483–490
2. Cao C, Tian D, Park J, Allan J, Pataky KA, Yan TD (2014) A systematic review and meta-analysis of surgical treatments for malignant pleural mesothelioma. Lung Cancer 83:240–245
3. Wen P, Black P, Loeffler J (2001) Metastatic brain cancer. In: DeVita V, Hellman S, Rosenberg S (eds) Cancer: principles and practice of oncology, 6th edn. Lippincott, Williams & Wilkins, Philadelphia, pp 2655–2670
4. Nayak L, Lee EQ, Wen PY (2012) Epidemiology of brain metastases. Curr Oncol Rep 14:48–54
5. Falconieri G, Grandi G, DiBonito L, Bonifacio-Gori D, Giarelli L (1991) Intracranial metastases from malignant pleural mesothelioma. Report of three autopsy cases and review of the literature. Arch Pathol Lab Med 115:591–595
6. Chari A, Kolias AG, Allinson K, Santarius T (2015) Cerebral metastasis of a malignant pleural mesothelioma: a case report and review of the literature. Cureus 7:e241. doi:10.7759/cureus.241
7. Rusch VW (1995) A proposed new international TNM staging system for malignant pleural mesothelioma. From the International Mesothelioma Interest Group. Chest 108:1122–1128
8. Fennell DA, Parmar A, Shamash J, Evans MT, Sheaff MT, Sylvester R, Dhaliwal K, Gower N, Steele J, Rudd R (2005) Statistical validation of the EORTC prognostic model for malignant pleural mesothelioma based on three consecutive phase II trials. J Clin Oncol 23:184–189
9. Herndon JE, Green MR, Chahinian AP, Corson JM, Suzuki Y, Vogelzang NJ (1998) Factors predictive of survival among 337 patients with mesothelioma treated between 1984 and 1994 by the Cancer and Leukemia Group B. Chest 113:723–731
10. Edwards J, Abrams K, Leverment J, Spyt T, Waller D, O'Byrne K (2000) Prognostic factors for malignant mesothelioma in 142 patients: validation of CALGB and EORTC prognostic scoring systems. Thorax 55:731–735
11. Miller AC, Miettinen M, Schrump DS, Hassan R (2014) Malignant mesothelioma and central nervous system metastases. Report of two cases, pooled analysis, and systematic review. Ann Am Thorac Soc 11:1075–1081
12. Hubbs JL, Boyd JA, Hollis D, Chino JP, Saynak M, Kelsey CR (2010) Factors associated with the development of brain metastases: analysis of 975 patients with early stage nonsmall cell lung cancer. Cancer 116:5038–5046. doi:10.1002/cncr.25254
13. Hsiao SH, Chung CL, Chou YT, Lee HL, Lin SE, Liu HE (2013) Identification of subgroup patients with stage IIIB/IV non-small cell lung cancer at higher risk for brain metastases. Lung Cancer 82:319–323. doi:10.1016/j.lungcan.2013.08.004
14. Warren LE, Guo H, Regan MM, Nakhlis F, Yeh ED, Jacene HA, Hirshfield-Bartek J, Overmoyer BA, Bellon JR (2015) Inflammatory breast cancer and development of brain metastases: risk factors and outcomes. Breast Cancer Res Treat 151:225–232. doi:10.1007/s10549-015-3381-8
15. Frankel TL, Bamboat ZM, Ariyan C, Coit D, Sabel MS, Brady MS (2014) Predicting the development of brain metastases in patients with local/regional melanoma. J Surg Oncol 109:770–774. doi:10.1002/jso.23574
16. Mansfield AS, Symanowski JT, Peikert T (2014) Systematic review of response rates of sarcomatoid malignant pleural mesotheliomas in clinical trials. Lung Cancer 133–136. doi: 10.1016/j.lungcan.2014.08.017
17. Finn RS, Brims FJ, Gandhi A, Olsen N, Musk AW, Maskell NA, Lee YC (2012) Postmortem findings of malignant pleural

Author's personal copy

mesothelioma: a two-center study of 318 patients. Chest 142: 1267–1273
18. Ishikawa T, Wanifuchi H, Abe K, Kato K, Watanabe A, Okada Y (2010) Brain metastasis in malignant pleural mesothelioma presenting as intratumoral hemorrhage. Neurol Med Chir (Tokyo) 50:1027–1030
19. Colleoni M, Liessi G, Avventi C, Pancheri F, Sgarbossa G, Vicario G, Manente P (1996) Response to chemotherapy of brain metastases from malignant pleural mesothelioma. Tumori 82:456–458
20. Hooper CE, Morley AJ, Virgo P, Harvey JE, Kahan B, Maskell NA (2013) A prospective trial evaluating the role of mesothelin in undiagnosed pleural effusions. Eur Respir J 41:18–24

Cancer Treatment Communications (2015) 4, 1–5

Available online at www.sciencedirect.com

SciVerse ScienceDirect

www.elsevier.com/locate/ctrc

Lymphohistiocytoid mesothelioma with a response to cisplatin plus pemetrexed: A case report

Yosuke Miyamoto[a], Nobukazu Fujimoto[b,*], Michiko Asano[a], Takamasa Nakasuka[a], Naofumi Hara[a], Tomoko Yamagishi[a], Yasuko Fuchimoto[a], Sae Wada[a], Kenichi Kitamura[a], Shinji Ozaki[a], Takumi Kishimoto[c]

[a]*Department of Respiratory Medicine, Okayama Rosai Hospital, 1-10-25 Chikkomidorimachi, Okayama 7028055, Japan*
[b]*Department of Medical Oncology, Okayama Rosai Hospital, 1-10-25 Chikkomidorimachi, Okayama 7028055, Japan*
[c]*Department of Internal Medicine, Okayama Rosai Hospital, 1-10-25 Chikkomidorimachi, Okayama 7028055, Japan*

Received 24 November 2014; received in revised form 4 February 2015; accepted 28 February 2015

KEYWORDS
Malignant pleural mesothelioma;
Lymphohistiocytoid mesothelioma;
Asbestos;
Systemic chemotherapy;
Pemetrexed

Abstract
We report the case of a patient with lymphohistiocytoid mesothelioma (LHM) with a response to systemic chemotherapy consisting of cisplatin and pemetrexed. A 72-year-old man was referred to our hospital because of abnormal shadows seen on chest X-rays. He had been exposed to asbestos at shipyards for 3 years. Computed tomography (CT) images of the chest showed multiple masses on the parietal pleura, diaphragm, and the interlobar pleura of the right. CT-guided percutaneous needle biopsy was performed and the biopsy specimen demonstrated fibrous thickening of the pleura with abundant lymphocyte infiltration. Immunohistochemical analyses revealed that the cells were positive for calretinin, WT-1, and CAM5.2, and negative for CEA, TTF-1, CK5/6, AE1/AE3, desmin, CD3, CD20, CD30, and CD68. Based on these findings, the diagnosis was confirmed as LHM. Systemic chemotherapy consisting of cisplatin (75 mg/m^2) and pemetrexed (500 mg/m^2) was delivered. After 6 courses of chemotherapy, multiple tumors had remarkably regressed, and the patient remains on maintenance treatment with pemetrexed. There are few reports of chemotherapy for LHM. The combination of cisplatin and pemetrexed could be a good treatment option for LHM.
© 2015 Elsevier Ltd. This is an open access article under the CC BY-NC-ND license (http://creativecommons.org/licenses/by-nc-nd/4.0/).

*Corresponding author. Tel.: +81 86 2620131; fax: +81 86 2623391.
E-mail address: nobufujimot@gmail.com (N. Fujimoto).

http://dx.doi.org/10.1016/j.ctrc.2015.02.003
2213-0896/© 2015 Elsevier Ltd. This is an open access article under the CC BY-NC-ND license (http://creativecommons.org/licenses/by-nc-nd/4.0/).

1. Introduction

Malignant pleural mesothelioma (MPM) is an aggressive malignancy arising from the mesothelial cells lining the pleura [1] and is generally associated with a history of asbestos exposure [2]. Lymphohistiocytoid mesothelioma (LHM) is a rare subtype of MPM and there are few reports on the efficacy of systemic chemotherapy for this subtype. We report the case of a patient with LHM who had a response to systemic chemotherapy consisting of cisplatin and pemetrexed.

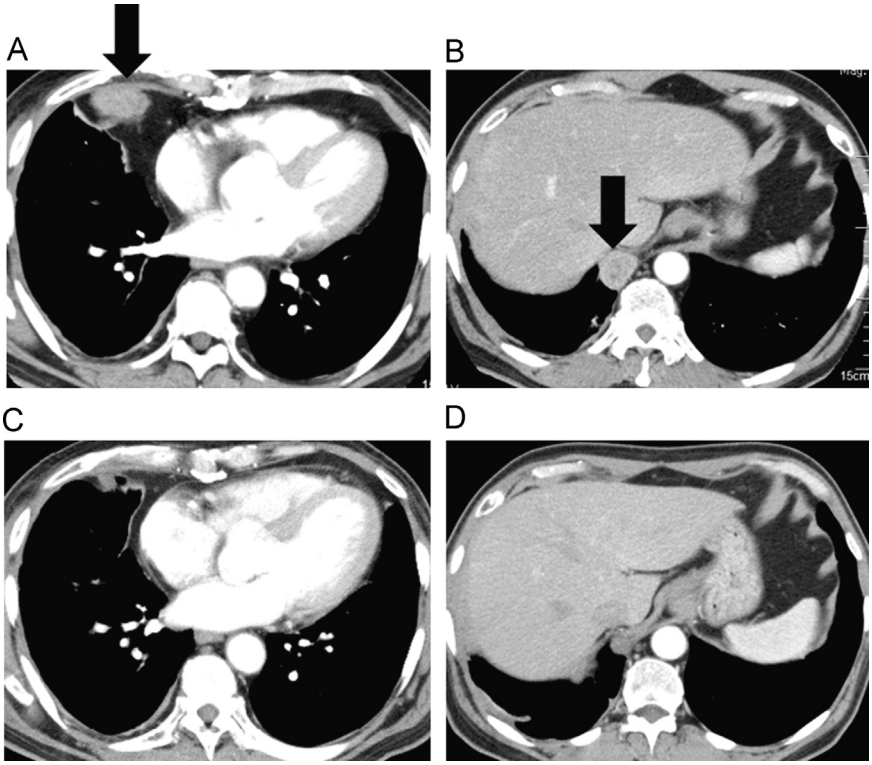

Figure 1 Computed tomography images at diagnosis (A, B) and after the 6 cycles of systemic chemotherapy consisting of cisplatin and pemetrexed (C, D). Black arrows indicate the tumors on the pleura.

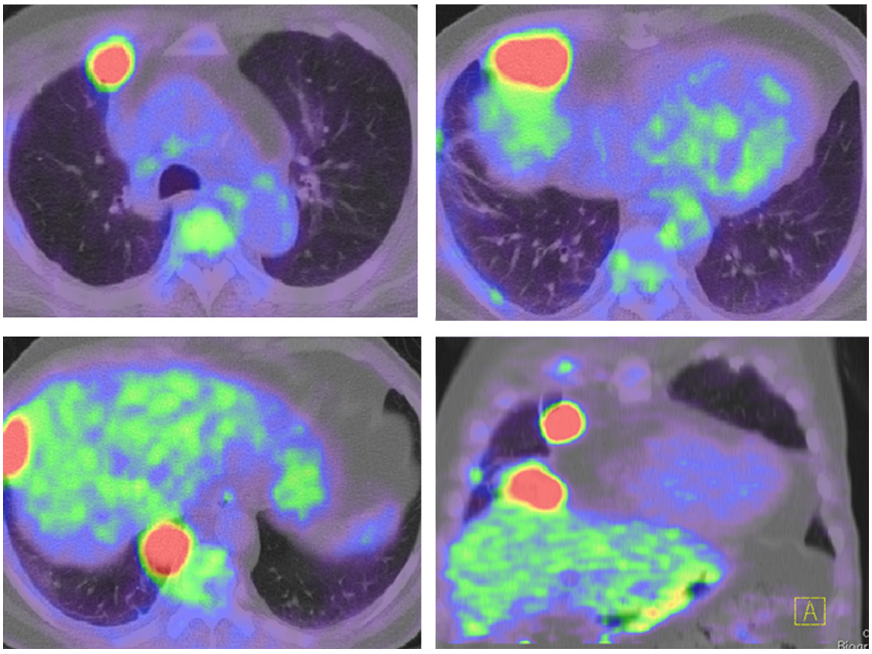

Figure 2 Whole-body fluorine-18 2-fluoro-2-deoxy-D-glucose (FDG) positron emission tomography and CT images demonstrating abnormal FDG uptake (shown in red) in multiple masses on the pleura.

2. Case report

A 72-year-old man was referred to our hospital because of abnormal shadows seen on his chest X-ray determined at a regular medical checkup. He had a history of appendicitis and been diagnosed with type II diabetes mellitus. He had smoked between the ages of 18 and 35 years, and as a teenager had been exposed to asbestos at shipyards for 3 years. His physical examination revealed nothing specific and no superficial lymph nodes were palpable. Blood tests revealed a slight elevation in C-reactive protein and glucose levels. There were no increases in tumor markers. A chest X-ray revealed permeability decay in the right lower lung field, and computed tomography (CT) images of the chest showed multiple masses on the parietal pleura, diaphragm, and the interlobar pleura of the right (Figure 1A and B). Multiple masses on the pleura showed a contrast effect from the early stage of the arterial phase on enhanced CT images. Anterior mediastinal and gastric cardia lymphadenopathy were also detected and suspected to be lymph node metastases. Whole-body fluorine-18 2-fluoro-2-deoxy-D-glucose (FDG) positron emission tomography and CT revealed abnormal FDG uptake in multiple masses and enlarged lymph nodes (Figure 2). CT-guided percutaneous needle biopsy was performed and the biopsy specimen demonstrated fibrous thickening of the pleura with an abundant lymphocyte infiltration (Figure 3). Among them were scattered polygonal cells with a nucleus containing clear oval nucleoli. Immunohistochemical analyses revealed that the cells were positive for calretinin, WT-1, and CAM5.2, and negative for CEA, TTF-1, CK5/6, AE1/AE3, desmin, CD3, CD20, CD30, and CD68 (Figure 4). Based on these findings, the diagnosis was confirmed as LHM. The patient's disease was diagnosed as stage IV (T1bN2M1) based on the International Mesothelioma Study Group staging system [3].

Systemic chemotherapy consisting of cisplatin (75 mg/m^2) and pemetrexed (500 mg/m^2) was delivered. After 6 courses of the chemotherapy, multiple tumors had remarkably regressed (Figure 1C and D). Mediastinal and intraperitoneal lymph nodes were also significantly diminished. The patient has been on maintenance treatment with pemetrexed and his disease remains stable.

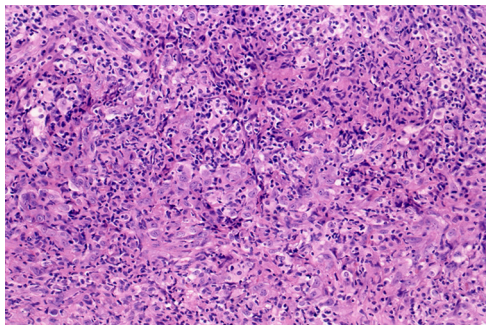

Figure 3 Percutaneous needle biopsy specimen demonstrating fibrous thickening of the pleura with abundant lymphocyte infiltration.

3. Discussion

We report a case of LHM, which is a rare variant of MPM, in a patient who had a remarkable response to systemic chemotherapy consisting of cisplatin and pemetrexed. LHM was first identified in 1988 by Henderson et al. and characterized as having neoplastic cells with a histiocytoid appearance that are surrounded by a marked lymphocytic infiltration. LHM comprises less than 1% of mesotheliomas [4] and was categorized previously as a sarcomatous subtype of MPM [5]. However, in a recent report Galateau-Salle

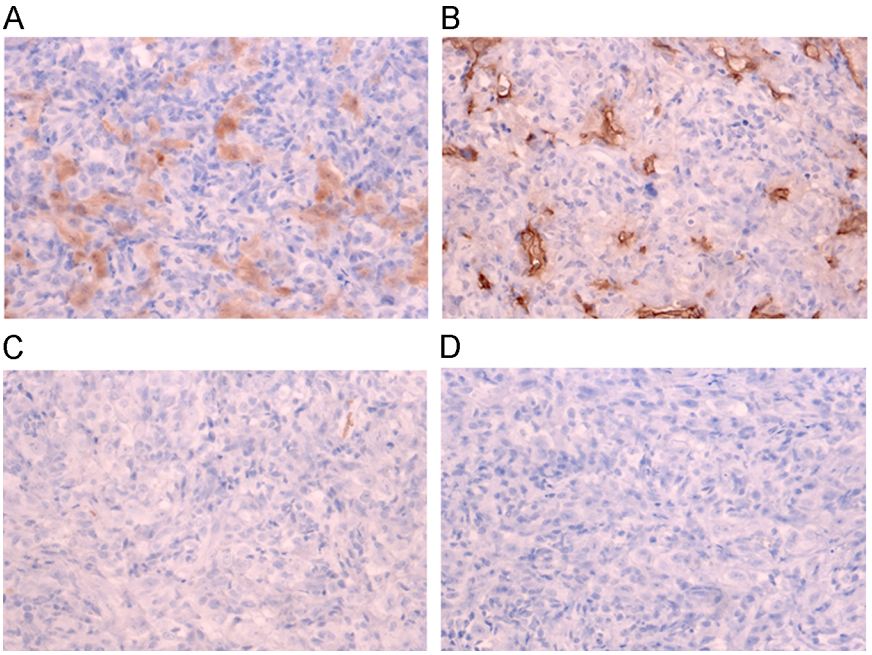

Figure 4 Immunohistochemical analyses of the biopsy specimen revealed that the cells were positive for (A) calretinin and (B) D2-40 and negative for (C) CEA and (D) TTF-1.

Table 1 Literature review of reported cases of lymphohistiocytoid mesothelioma.

Author	Year	Age/ sex	Asbestos exposure	Surgery	Radiotherapy	Chemotherapy	Pleurodesis	Survival (months)
Khalidi et al. [8]	2000	60/M	Unlikely	−	+	−	−	72
Khalidi et al. [8]	2000	74/F	Unknown	N.D.	N.D.	N.D.	N.D.	10
Khalidi et al. [8]	2000	67/M	Unlikely	N.D.	N.D.	N.D.	N.D.	3
Gallateau S et al. [6]	2007	56/F	Probably	−	+	−	+	12
Gallateau S et al. [6]	2007	78/M	Probably	−	−	−	+	3
Gallateau S et al. [6]	2007	62/M	Possibly	Pleurectomy	+	−	−	5
Gallateau S et al. [6]	2007	59/M	Probably	Pleurectomy	−	+	−	4
Gallateau S et al. [6]	2007	78/M	Unlikely	Palliative surgery	+	−	+	8
Gallateau S et al. [6]	2007	71/M	Unlikely	Palliative surgery	+	−	+	40
Gallateau S et al. [6]	2007	80/F	Probably	−	+	−	+	8
Gallateau S et al. [6]	2007	66/M	Probably	−	+	+	+	11
Gallateau S et al. [6]	2007	78/F	Unlikely	Palliative surgery	−	−	−	8
Gallateau S et al. [6]	2007	75/F	Unlikely	N.D.	N.D.	N.D.	N.D.	11
Gallateau S et al. [6]	2007	77/F	Unlikely	−	+	−	+	4
Gallateau S et al. [6]	2007	65/M	Probably	−	−	−	−	37
Gallateau S et al. [6]	2007	74/F	Unlikely	−	−	+	−	25
Gallateau S et al. [6]	2007	67/M	Possibly	Pleurectomy	−	−	−	32
Gallateau S et al. [6]	2007	58/M	Probably	Palliative surgery	+	+	−	7
Gallateau S et al. [6]	2007	82/M	Unknown	−	−	+	−	8
Gallateau S et al. [6]	2007	76/M	Probably	−	+	−	+	11
Gallateau S et al. [6]	2007	68/M	Probably	−	−	+	−	20
Gallateau S et al. [6]	2007	70/M	Probably	−	−	+	−	11
Gallateau S et al. [6]	2007	77/F	Probably	−	−	−	+	6
Gallateau S et al. [6]	2007	50/M	Possibly	−	−	−	+	
Gallateau S et al. [6]	2007	63/F	Probably	Palliative surgery	−	+	+	8
Kawai et al. [4]	2010	59/F	Unknown	Thoracotomy	N.D.	N.D.	N.D.	12
Kawai et al. [4]	2010	52/M	Unknown	Thoracotomy	N.D.	N.D.	N.D.	36
Kawai et al. [4]	2010	61/M	Unknown	−	N.D.	N.D.	N.D.	3
Kawai et al. [4]	2010	63/M	Probably	Extrapleural pneumonectomy	N.D.	N.D.	N.D.	19(alive)
Present case	2015	72/M	Probably	−	−	+	−	14(alive)

N.D.; not described.

et al. suggested that the survival of LHM was more similar to that of the epithelioid or biphasic subtype of MPM [6]. Whether LHM should be categorized as an epithelioid or sarcomatous subtype of MPM is still controversial.

Concerning chemotherapy for MPM, the combination of pemetrexed and cisplatin has shown significantly prolonged survival compared with cisplatin alone in a phase III study [7]. However, it was not clear whether or not LHM cases were included in the study. In fact, there are few reports of chemotherapy for LHM. We reviewed the reported cases of LHM particularly concerning the delivered treatment modalities in Table 1. These previous reports mainly discussed the pathological differentiation and there were few description of treatment. There were 8 cases those were delivered systemic chemotherapy, but the treatment regimen or the tumor responses to those chemotherapy was not described. To our knowledge, the current case might be the first case with a significant response to the treatment regimen. Cisplatin plus pemetrexed could therefore be a good treatment option for LHM.

In conclusion, we present a case of LHM, a rare variant of MPM, in a patient with a significant response to systemic chemotherapy.

Conflict of interest statement

All authors have no conflict of interest to be declared.

Acknowledgments

This study is a part of “the research and development and the dissemination projects related to the 13 fields of occupational injuries and illnesses” of the Japan Labour Health and Welfare Organization (Grant no. 14030101). This sponsor had no involvement in the study design, collection, analysis and interpretation of the data, writing of the manuscript, or decision to submit the manuscript for publication.

References

[1] R. Ismail-Khan, L.A. Robinson, C.C. Williams Jr., C.R. Garrett, G. Bepler, G.R. Simon, Malignant pleural mesothelioma: a comprehensive review, Cancer Control 13 (2006) 255–263.
[2] K. Gemba, N. Fujimoto, K. Kato, K. Aoe, Y. Takeshima, K. Inai, et al., National survey of malignant mesothelioma and asbestos exposure in Japan, Cancer Sci. 103 (2012) 483–490.
[3] V.W. Rusch, A proposed new international TNM staging system for malignant pleural mesothelioma. From the International Mesothelioma Interest Group, Chest 108 (1995) 1122–1128.
[4] T. Kawai, S. Hiroi, K. Nakanishi, K. Takagawa, R. Haba, K. Hayashi, et al., Lymphohistiocytoid mesothelioma of the pleura, Pathol. Int. 60 (2010) 566–574.
[5] D.W. Henderson, H.D. Attwood, T.J. Constance, K.B. Shilkin, R.H. Steele, Lymphohistiocytoid mesothelioma: a rare lymphomatoid variant of predominantly sarcomatoid mesothelioma, Ultrastruct. Pathol. 12 (1988) 367–384.
[6] F. Galateau-Salle, R. Attanoos, A.R. Gibbs, L. Burke, P. Astoul, P. Rolland, et al., Lymphohistiocytoid variant of malignant mesothelioma of the pleura: a series of 22 cases, Am. J. Surg. Pathol. 31 (2007) 711–716.
[7] N.J. Vogelzang, J.J. Rusthoven, J. Symanowski, C. Denham, E. Kaukel, P. Ruffie, et al., Phase III study of pemetrexed in combination with cisplatin versus cisplatin alone in patients with malignant pleural mesothelioma, J. Clin. Oncol. 21 (2003) 2636–2644.
[8] H.S. Khalidi, L.J. Medeiros, H. Battifora, Lymphohistiocytoid mesothelioma. An often misdiagnosed variant of sarcomatoid malignant mesothelioma, Am. J. Clin. Pathol. 113 (2000) 649–654.

Official Case Reports Journal of the Asian Pacific Society of Respirology
Respirology Case Reports
OPEN ACCESS
APSR

Endobronchial T-cell lymphoma in a patient with chronic pyothorax

Shinsaku Matsumoto[1], Nobukazu Fujimoto[2], Yasuko Fuchimoto[3], Michiko Asano[3], Tomofumi Yano[1] & Takumi Kishimoto[1]

[1]Department of Internal Medicine, Okayama Rosai Hospital, Okayama, Japan.
[2]Medical Oncology, Okayama Rosai Hospital, Okayama, Japan.
[3]Respiratory Medicine, Okayama Rosai Hospital, Okayama, Japan.

Keywords
Bronchoscopy, endobronchial tumor, pulmonary lymphoma, pyothorax, T-cell lymphoma.

Correspondence
Nobukazu Fujimoto, Department of Medical Oncology, Okayama Rosai Hospital, 1-10-25 Chikkomidorimachi, Okayama 7028055, Japan. E-mail: nobufujimot@gmail.com

Received: 18 March 2015; Revised: 30 March 2015; Accepted: 02 April 2015.

doi: 10.1002/rcr2.103

Abstract

We report a very rare case of primary endobronchial peripheral T-cell lymphoma (PTCL) not otherwise specified (NOS), which presented as an endobronchial tumor obstructing the main airway. An 81-year-old man was referred to our hospital for a 1-month history of productive cough and wheeze. Computed tomography revealed chronic pyothorax with calcified foci in the right lung and a mass inside the bronchus intermedius. Flexible bronchoscopy identified an endobronchial tumor obstructing the bronchus intermedius. The biopsy specimen showed an infiltration composed predominantly of small atypical lymphocytes. Immunohistochemical analyses demonstrated that the proliferating cells were positive for CD3, CD4, and CD5 and negative for CD8 and CD20. Pathological tests confirmed that the case was PTCL-NOS. PTCL-NOS should be considered in the differential diagnosis of endobronchial tumors.

Introduction

Peripheral T-cell lymphoma (PTCL) is one of the subtypes of T-cell lymphoma (TCL); it comprises a heterogeneous group of nodal and extranodal mature TCLs. Among the PTCLs, a subset is specifically defined as PTCL not otherwise specified (PTCL-NOS). PTCL-NOS do not correspond to any of the known T-cell entities. Primary pulmonary lymphoma (PPL) is a distinct entity that arises de novo in lung tissue [1]. We report an extremely rare case of primary endobronchial PTCL-NOS that presented as a tumor obstructing the main airway.

Case Report

An 81-year-old Japanese man was referred to our hospital for a 1-month history of productive cough and wheeze. He was a smoker (approximately 56 packs per year) and had a medical history of pulmonary tuberculosis at the age of 17 years. He had been diagnosed with chronic pyothorax and treated with intravenous injection of antibiotics 1 year prior to being seen at our facility. Upon examination, his body temperature was 37.2°C and a physical examination revealed wheeze and reduced air entry in the right mid-lung. No superficial lymph nodes were palpated. Blood assays revealed leukocytosis (12,500 leukocytes per microliter) and normal lactate dehydrogenase values (223 IU/L). Carcinoembryonic antigen and soluble interleukin-2 receptor values were slightly elevated to 5.8 ng/mL and 575 U/mL, respectively. A chest X-ray showed hypolucency of the right middle lung field, which suggested fluid accumulation. Computed tomography (CT) revealed chronic pyothorax with calcified foci in the right-hand portion of the right lung and a mass inside the bronchus intermedius (Fig. 1A). No mediastinal lymphadenopathy was detected. Flexible bronchoscopy

© 2015 The Authors. *Respirology Case Reports* published by John Wiley & Sons Ltd on behalf of The Asian Pacific Society of Respirology.
This is an open access article under the terms of the Creative Commons Attribution-NonCommercial-NoDerivs License, which permits use and distribution in any medium, provided the original work is properly cited, the use is non-commercial and no modifications or adaptations are made.

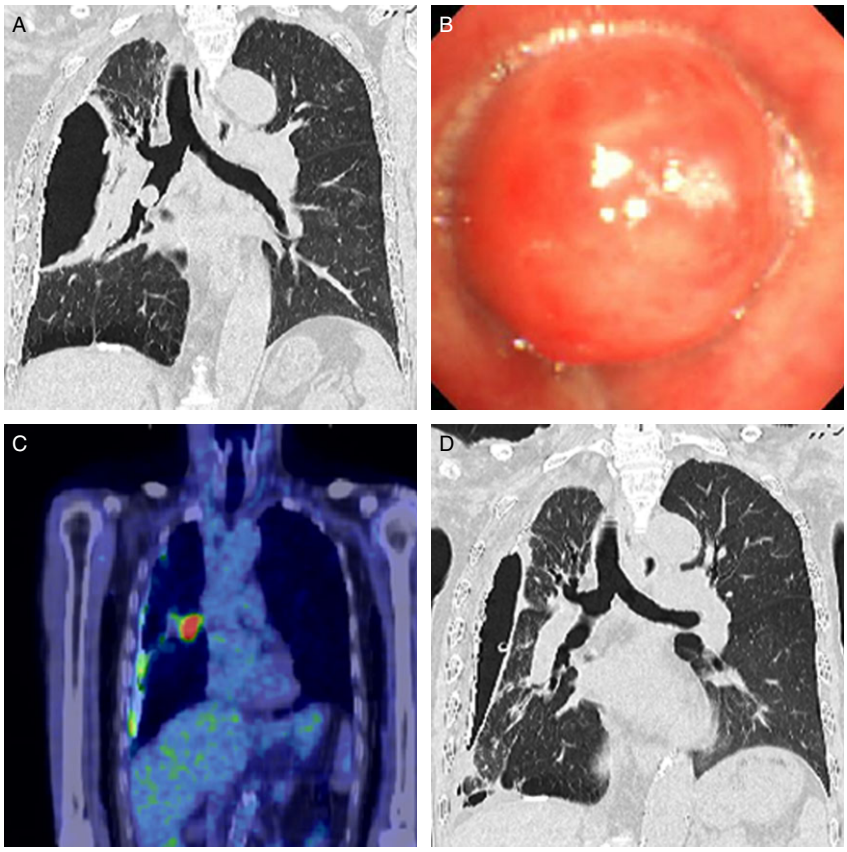

Figure 1. Imaging findings of the case. (A) Computed tomography (CT) revealed chronic pyothorax with calcified foci on the right and a mass inside the bronchus intermedius. (B) Flexible bronchoscopy identified an endobronchial tumor obstructing the bronchus intermedius. (C) Positron emission tomography with [18F] fluoro-2-deoxyglucose and CT revealed uptake at the endobronchial tumor. (D) CT after the chemotherapy demonstrated that the endobronchial tumor markedly diminished.

identified an endobronchial tumor obstructing the bronchus intermedius (Fig. 1B). The biopsy specimen showed an infiltration composed predominantly of small atypical lymphocytes (Fig. 2A). Immunohistochemical analyses demonstrated that the proliferating cells were positive for CD3 (Fig. 2B), CD4, CD5 (Fig. 2C), and CD7 and negative for CD8 (Fig. 2D), CD20 (Fig. 2E), and CD30. The Ki-67 labeling index was low. Based on these findings, we diagnosed the tumor as PTCL-NOS. Positron emission tomography (PET) with [18F] fluoro-2-deoxyglucose and CT revealed uptake at the endobronchial tumor, with a maximum standardized uptake value of 20.6 (Fig. 1C). There was no evidence of abnormal uptake at the pyothorax, mediastinal lymph node, or other extrathoracic organs. His disease was considered stage IE, and the patient was treated with systemic chemotherapy (pirarubicin, cyclophosphamide, vincristine, and prednisone). After the first course of the chemotherapy, the endobronchial tumor markedly diminished on chest CT (Fig. 1D) and bronchoscopy. However, because of complication with refractory pyothorax, fenestration surgery was undertaken in a definitive fashion. Systemic chemotherapy was not delivered thereafter; however, the patient is free of recurrence 1 year after diagnosis.

Discussion

PPL is defined as lymphomas that affect the lungs (parenchyma, bronchi, and/or trachea) with no evidence of extrapulmonary extension in 3-month follow-up [2]. It is a rare condition that comprises only 3–4% of extranodal non-Hodgkin lymphomas (NHL), less than 1% of all NHLs [2], and 0.5–1% of primary pulmonary malignancies [3]. The majority of the reported cases have been of the B-cell type, so-called mucosa-associated or bronchus-associated lymphoid tissue lymphomas [4]. The current patient presented with a solitary endobronchial tumor, which is an extremely rare manifestation of PPL. Solomonov et al. reported that in a series of 441 patients with newly diagnosed NHL over a 7-year period, eight patients presented

© 2015 The Authors. *Respirology Case Reports* published by John Wiley & Sons Ltd on behalf of The Asian Pacific Society of Respirology

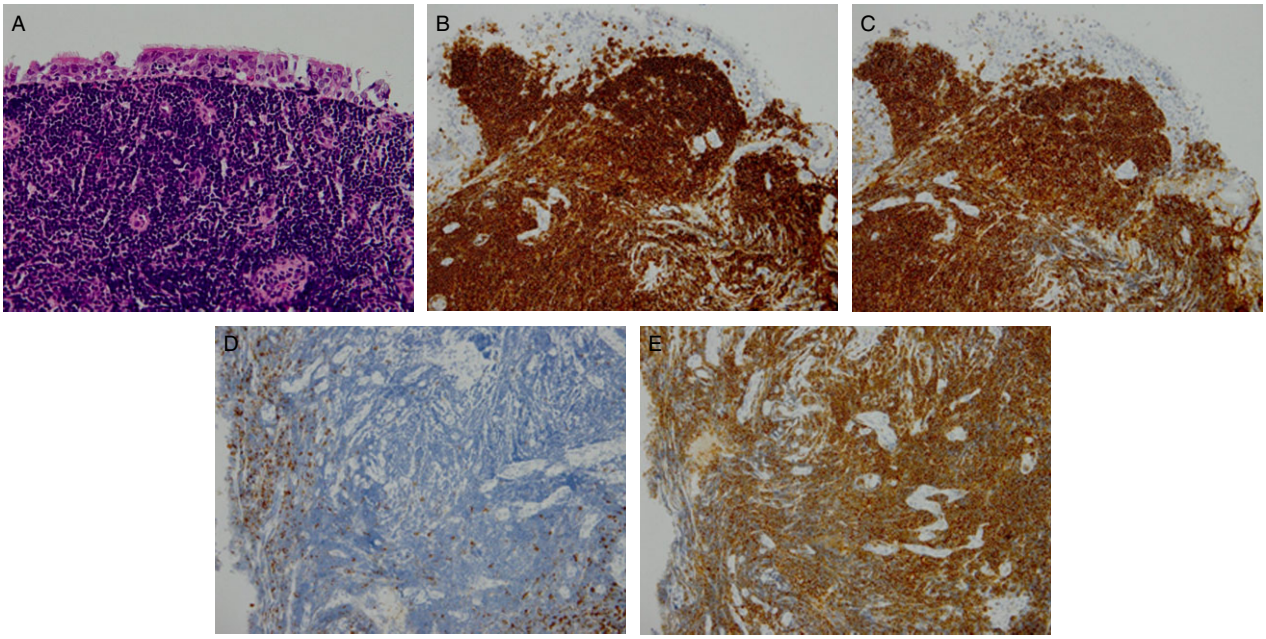

Figure 2. Biopsy specimen showed an infiltration comprised predominantly of small atypical lymphocytes (hematoxylin-eosin, 40×) (A). Immunohistochemical analyses demonstrated that the proliferating cells were positive for CD3 (B) and CD5 (C), and negative for CD8 (D) and CD20 (E).

with a primary endobronchial B-cell lymphoma [1]. To our knowledge, this is the first report of PTCL-NOS presenting as a primary endobronchial tumor. PTCL-NOS is a diagnosis made based on the results of a tissue biopsy that demonstrates evidence of a TCL that does not meet the criteria for other subtypes of TCL including anaplastic large-cell lymphoma, angioimmunoblastic TCL, extranodal NK/TCL, nasal type, subcutaneous panniculitis-like TCL, enteropathy-associated TCL, and hepatosplenic TCL. The differential diagnosis is based on histologic examination and immunophenotype evaluation such as immunohistochemical panel (CD20, CD3, CD10, BCL6, Ki-67, CD5, CD30, CD2, CD4, CD8, CD7, CD56, CD57, CD21, CD23, ALK) or cell surface marker analysis by flow cytometry (kappa/lambda, CD45, CD3, CD5, CD19, CD10, CD20, CD30, CD4, CD8, CD7, CD2), and in difficult or equivocal cases, polymerase chain reaction-based assay for molecular detection of a clonal T-cell receptor rearrangement. The limitation of the current case was that the pathological diagnosis was based on small specimen through flexible bronchoscopy, so not all these markers were examined. However, we are confident of the diagnosis based on multiple immunohistochemical analyses.

The current case was complicated by chronic pyothorax. Pyothorax-associated lymphoma is a category in which a lymphoproliferative disorder develops in the pleural cavity after a long-standing history of pyothorax; it represents an entity distinct from other malignant lymphomas [5]. In our case, PET/CT revealed a hypermetabolic mass at the endobronchial tumor, but there was no abnormal uptake at the pyothorax. Endoscopic examination showed a smooth-surfaced, round tumor with a stalk; these features do not correspond to an outer parietal invasion. However, the coronal CT showed dense scar-like tissue between the wall of pyothorax and bronchus intermedius. These findings might suggest the relationship between the lymphoma and pyothorax. We think that the chronic inflammation could have contributed to the development of the disease.

In conclusion, we have reported upon what is, to the best of our knowledge, the first case of PTCL-NOS, which was confined to the bronchus. PTCL-NOS should be considered in the differential diagnosis of endobronchial tumor.

Disclosure Statements

No conflict of interest declared.

Appropriate written informed consent was obtained for publication of this case report and accompanying images.

Acknowledgments

We thank Drs. Kyotaro Ohno, Yasuharu Sato, and Prof. Tadashi Yoshino, Department of Pathology, Okayama University Graduate School of Medicine, Dentistry and Pharmaceutical Sciences, for detailed pathological analyses.

© 2015 The Authors. *Respirology Case Reports* published by John Wiley & Sons Ltd on behalf of The Asian Pacific Society of Respirology

References

1. Solomonov A, Zuckerman T, Goralnik L, et al. 2008. Non-Hodgkin's lymphoma presenting as an endobronchial tumor: report of eight cases and literature review. Am. J. Hematol. 83:416–419.
2. Chilosi M, Zinzani PL, and Poletti V. 2005. Lymphoproliferative lung disorders. Semin. Respir. Crit. Care Med. 26:490–501.
3. Cadranel J, Wislez M, and Antoine M. 2002. Primary pulmonary lymphoma. Eur. Respir. J. 20:750–762.
4. Cordier JF, Chailleux E, Lauque D, et al. 1993. Primary pulmonary lymphomas. A clinical study of 70 cases in nonimmunocompromised patients. Chest 103: 201–208.
5. Aozasa K, Takakuwa T, and Nakatsuka S. 2005. Pyothorax-associated lymphoma: a lymphoma developing in chronic inflammation. Adv. Anat. Pathol. 12:324–331.

© 2015 The Authors. *Respirology Case Reports* published by John Wiley & Sons Ltd on behalf of The Asian Pacific Society of Respirology

Respiratory Medicine Case Reports 16 (2015) 95–96

Contents lists available at ScienceDirect

Respiratory Medicine Case Reports

journal homepage: www.elsevier.com/locate/rmcr

Case report

Foreign body granuloma mimicking recurrence of malignant pleural mesothelioma

Takamasa Nakasuka [a], Nobukazu Fujimoto [b, *], Naofumi Hara [a], Yosuke Miyamoto [a], Tomoko Yamagishi [a], Michiko Asano [a], Hideyuki Nishi [c], Takumi Kishimoto [d]

[a] Department of Respiratory Medicine, Okayama Rosai Hospital, 1-10-25 Chikkomidorimachi, Okayama 7028055, Japan
[b] Department of Medical Oncology, Okayama Rosai Hospital, 1-10-25 Chikkomidorimachi, Okayama 7028055, Japan
[c] Department of Surgery, Okayama Rosai Hospital, 1-10-25 Chikkomidorimachi, Okayama 7028055, Japan
[d] Department of Internal Medicine, Okayama Rosai Hospital, 1-10-25 Chikkomidorimachi, Okayama 7028055, Japan

ARTICLE INFO

Article history:
Received 17 August 2015
Received in revised form
30 August 2015
Accepted 1 September 2015

Keywords:
Asbestos
Foreign body granuloma
Mesothelioma
Pleura
Pneumonectomy

ABSTRACT

A 72-year-old man visited our hospital due to right pleural effusion. He had worked as a welder at a shipbuilding company and had been exposed to asbestos. Cytological examination and thoracoscopic pleural biopsy yielded a diagnosis of epithelial malignant pleural mesothelioma (MPM); extrapleural pneumonectomy (EPP) was performed. Two years later, he became aware of right-back swelling that became a fist-sized mass over 2 months. Microscopy of a tissue specimen revealed no malignant cells, but did indicate foreign body granuloma. Subcutaneous lesions that develop after EPP do not necessarily result from the recurrence of MPM, but could have benign etiologies.

© 2015 The Authors. Published by Elsevier Ltd. This is an open access article under the CC BY-NC-ND license (http://creativecommons.org/licenses/by-nc-nd/4.0/).

1. Introduction

Malignant pleural mesothelioma (MPM) is an aggressive malignancy arising from the mesothelial cells lining the pleura and is generally associated with a history of asbestos exposure [1]. The clinical benefits of radical surgery for MPM remain controversial. Extrapleural pneumonectomy (EPP) has been performed for patients with earlier disease and good physical condition, but the disease often recurs at wide intervals. Here we report a case of foreign body granuloma (FBG) that mimicked a postoperative recurrence of MPM.

2. Case report

A 72-year-old man visited our hospital for examination of right pleural effusion. He had worked as a welder at a shipbuilding company and had been exposed to asbestos for 43 years. His pleural effusion had been detected at a medical checkup for subjects with an occupational history of past asbestos exposure. Cytological examination of the effusion revealed the aggregated atypical mesothelial cells with nuclear enlargement and nucleus irregularity. Immunohistochemical analyses demonstrated that these cells were positive for calretinin, CAM5.2, CK5/6, AE1/AE3, WT-1, and EMA, and negative for CEA and TTF-1. These findings gave the diagnosis of epithelial subtype of MPM, and thoracoscopic pleural biopsy confirmed the diagnosis. EPP was performed; the pericardium and the diaphragm were also removed because the tumor had invaded the diaphragm. The pericardium and the diaphragm were reconstructed with Gore-Tex® mesh (1 mm in thickness, 20 cm × 15 cm, and 2 mm in thickness, 24 cm × 15 cm, respectively). The disease was categorized as T2N0M0, stage II, based on the staging system of the International Mesothelioma Study Group [2]; adjuvant chemotherapy consisting of carboplatin and pemetrexed was delivered. Talc was not used to treat the effusion during the course.

Two years later, the patient became aware that his right back was swelling. This swelling became a fist-sized mass over 2 months. Computed tomography (CT) of the chest visualized a tumor of soft-tissue density that expanded from the right pleural cavity into the subcutaneous tissue (Fig. 1A). Fluorine-18 2-fluoro-2-deoxy-D-glucose (18F-FDG) positron emission tomography (PET)-CT

Abbreviations: MPM, malignant pleural mesothelioma; EPP, extrapleural pneumonectomy; FBG, foreign body granuloma; CT, computed tomography; 18-F-FDG, fuorine-18 2-fluoro-2-deoxy-D-glucose; PET, positron emission tomography.

* Corresponding author.
E-mail address: nobufujimot@gmail.com (N. Fujimoto).

http://dx.doi.org/10.1016/j.rmcr.2015.09.002
2213-0071/© 2015 The Authors. Published by Elsevier Ltd. This is an open access article under the CC BY-NC-ND license (http://creativecommons.org/licenses/by-nc-nd/4.0/).

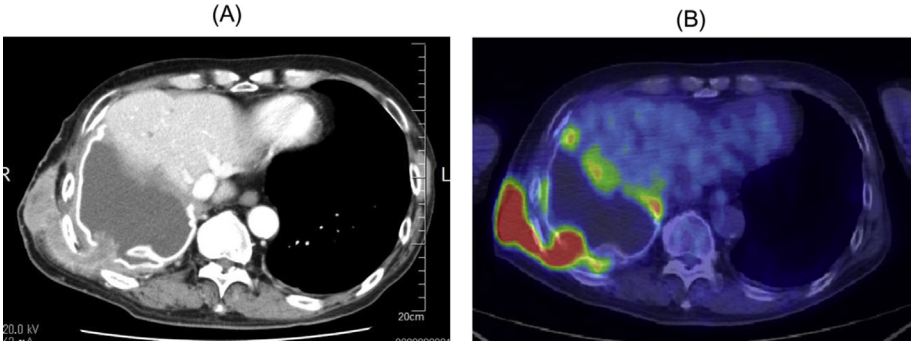

Fig. 1. Subcutaneous tumor on the right back of the patient. (A) CT of the chest revealed a tumor of soft-tissue density that expanded from the right pleural cavity into the subcutaneous tissue. (B) 18F-FDG PET-CT showed accumulation of 18F-FDG in the mass.

revealed an accumulation of 18F-FDG in the mass and along the pleura (Fig. 1B). It was near the chest tube site after the EPP. We suspected a recurrence of MPM, so we performed percutaneous needle biopsy. Microscopy of the tissue specimen showed no malignant cells; rather, we observed granulomas accompanied by giant cells, histiocytes, and inflammatory cells (Fig. 2). Immuno histochemical analyses revealed that these cells were negative for calretinin, CK AE1/3, or CAM5.2. Because the possibility of recurrence of MPM could not be ruled out with small specimen of needle biopsy, a tumorectomy was carried out. The tumor involved the Gore-Tex® mesh, so the mesh was removed with the tumor. Subsequent microscopy confirmed the diagnosis of FBG without evidence of MPM recurrence.

3. Discussion

A standard treatment for MPM has not yet been established. Patients exhibiting earlier stages of this disease have undergone EPP. However, a significant proportion of patients experience local recurrence as the first site of disease recurrence [3]. When patients who have undergone EPP display subcutaneous tumors, it is logical to suspect a recurrence of MPM.

FBG is a tumor-like mass or nodule of granulation tissue, with actively growing fibroblasts and capillary buds, consisting of a collection of modified macrophages resembling epithelial cells, surrounded by a rim of mononuclear cells, chiefly lymphocytes, and sometimes a center of giant multinucleate cells. It is due to a chronic inflammatory process associated with infectious disease or invasion by a foreign body such as surgical materials or pieces of stone or wood from a trauma. In the current case, we suspected that the causative foreign material was the Gore-Tex® mesh that was used to reconstruct the patient's diaphragm. It is quite rare that Gore-Tex mesh induced inflammatory reactions, however, in the current case, the Gore-Tex mash was involved in the tumor, so we considered that the granuloma was originated in the mesh.

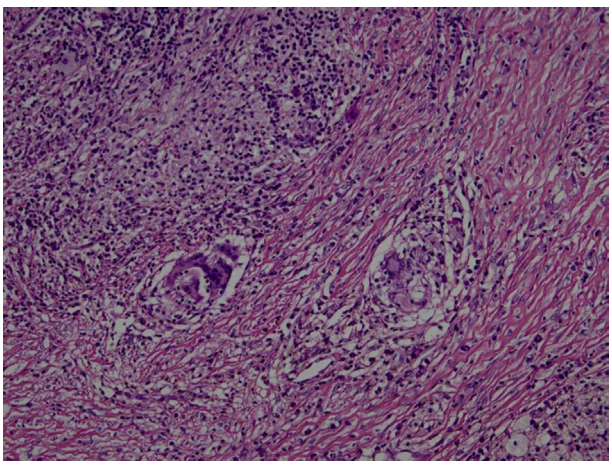

Fig. 2. Microscopy of the tissue specimen revealed a FBG accompanied by foreign-body giant cells, histiocytes, and inflammatory cells (×10).

Clinical diagnosis of FBG is challenging; it is difficult to identify FBG through physiological findings and CT. PET-CT is often applied to detect malignant lesions, but inflammatory lesions or granulomas (including FBG) would also accumulate 18F-FDG [4], rendering it difficult to diagnose FBG by imaging alone. The diagnosis should be confirmed through other means, such as percutaneous biopsy or surgery.

To our knowledge, this is the second report of FBG mimicking the recurrence of MPM; Shrestha et al. recently reported cases with pseudo-tumors that mimicked indwelling pleural catheter-tract metastases of MPM [5]. These cases remind physicians that subcutaneous lesions that develop after EPP do not necessarily result from the recurrence of MPM, but could have benign etiologies. Diagnostic procedures should be considered in such cases.

Conflict of interest

I declare on behalf of my co-authors and myself that we do not have any conflict of interest to declare.

Sources of funding

This study was supported by Research and Development and the Dissemination of Projects Related to the Nine Fields of Occupational Injuries and Illnesses of the Japan Labour Health and Welfare Organization. This work is also supported by grants-in-aid from the Ministry of Health, Labor and Welfare, Japan. These study sponsors had no involvement in study design, writing of the manuscript, the collection of data, and decision to submit the manuscript.

References

[1] K. Gemba, N. Fujimoto, K. Kato, K. Aoe, Y. Takeshima, K. Inai, et al., National survey of malignant mesothelioma and asbestos exposure in Japan, Cancer Sci. 103 (2012) 483–490.
[2] V.W. Rusch, A proposed new international TNM staging system for malignant pleural mesothelioma. From the International Mesothelioma Interest Group, Chest 108 (1995) 1122–1128.
[3] A.S. Tsao, I. Wistuba, J.A. Roth, H.L. Kindler, Malignant pleural mesothelioma, J. Clin. Oncol. 27 (2009) 2081–2090.
[4] M. Hara, Y. Shibamoto, T. Tamaki, M. Nishio, A. Iida, N. Shiraki, The intermediate level of FDG-PET accumulation among various kinds of pulmonary and mediastinal diseases, Radiology 197 (Suppl.) (2003).
[5] R.L. Shrestha, B.A. Wood, Y.C. Lee, Pseudo-tumor mimicking indwelling pleural catheter tract metastasis in mesothelioma, J. Bronchol. Interv. Pulmonol. 21 (2014) 350–352.

The Rapid Appearance and Disappearance of Dendriform Pulmonary Ossification after Diffuse Alveolar Hemorrhage

Tomoko Yamagishi[1], Nobukazu Fujimoto[2], Yosuke Miyamoto[1], Naofumi Hara[1], Michiko Asano[1], Yasuko Fuchimoto[1], Sae Wada[1], Kenichi Kitamura[1], Shinji Ozaki[1], Hideyuki Nishi[3], and Takumi Kishimoto[4]

[1]Department of Respiratory Medicine, [2]Department of Medical Oncology, [3]Department of Surgery, and [4]Department of Internal Medicine, Okayama Rosai Hospital, Okayama, Japan

ORCID ID: 0000-0002-4516-0433 (N.F.).

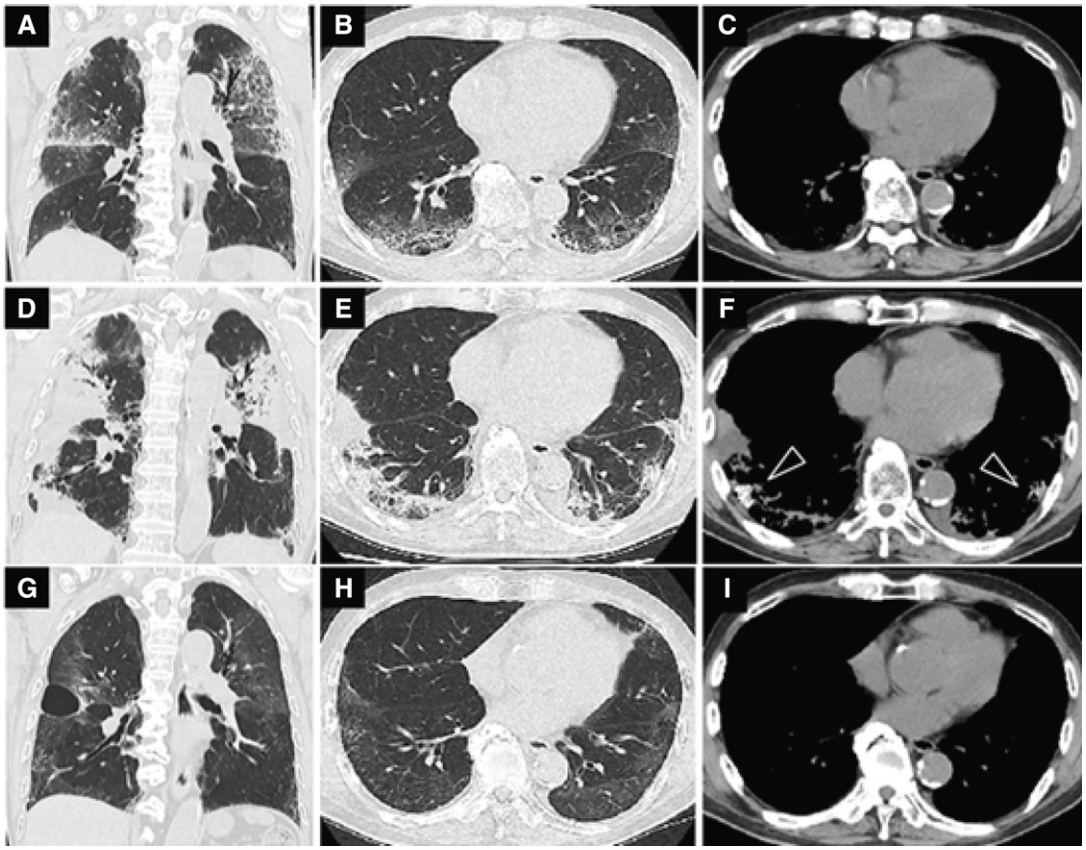

Figure 1. Coronal and axial chest computed tomography images of a 63-year-old man on admission showed diffuse bilateral ground-glass attenuation (*A* and *B*) without evidence of ossification (*C*). Chest computed tomography images 2 weeks after admission showed widespread areas of ground-glass attenuation and consolidation (*D* and *E*) with disseminated pulmonary ossification (*arrowheads*) in the subpleural zone (*F*). One month after administration of steroid therapy, bilateral consolidation and pulmonary ossification were dramatically decreased (*G–I*).

A 63-year-old man with a history of atrial fibrillation that had been treated with apixaban was admitted to our hospital for dyspnea and hemoptysis. Chest computed tomography showed diffuse bilateral ground-glass attenuation (Figures 1A–1C). Bronchoalveolar lavage fluid was bloody and contained hemosiderin-laden macrophages, suggesting apixaban-induced alveolar hemorrhage. Two weeks after cessation of the drug, acute respiratory failure occurred. Repeated chest computed tomography showed worsening

The authors are supported by the Ministry of Health, Labor and Welfare of Japan.

Am J Respir Crit Care Med Vol 193, Iss 3, pp 333–334, Feb 1, 2016
Copyright © 2016 by the American Thoracic Society
Originally published online as DOI: 10.1164/rccm.201506-1199IM on September 25, 2015
Internet address: www.atsjournals.org

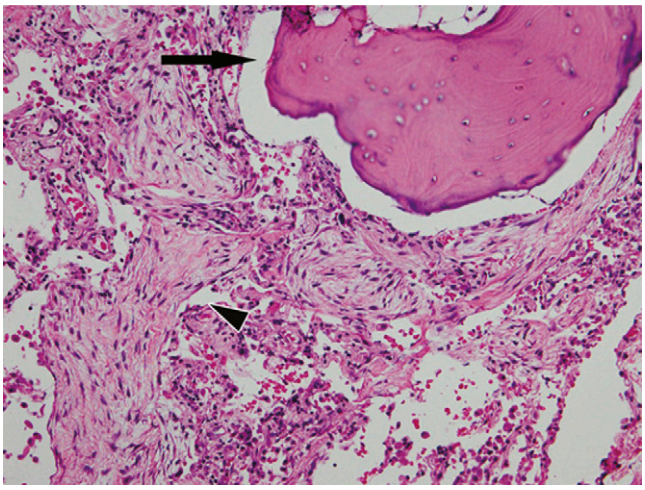

Figure 2. A surgical lung biopsy specimen shows dendriform mature bone formation within an area of scarring and widened alveolar septa (*arrow*). The background alveolar spaces are filled with numerous fibroblastic plugs (*arrowhead*) (hematoxylin and eosin, ×200).

bilateral airspace opacities with patchy diffuse sub-pleural pulmonary ossification (Figures 1D–1F). Surgical lung biopsy specimens revealed organizing pneumonia and branching bone within the fibrous stroma and alveolar spaces, typical of dendriform pulmonary ossification (DPO) (Figure 2). Daily prednisolone (1.0 mg/kg) was admin-istered, and the bilateral consolidation and pulmonary ossification had markedly de-creased 1 month later (Figures 1G–1I).

DPO is a rare condition, defined by the finding of branching lung in the air spaces of the distal lung. Patients are generally asymptomatic, and the condition is usually discovered after postmortem examination (1). Its pathogenesis is unclear, but DPO can occur after lung injuries such as pulmonary fibrosis and alveolar hemorrhage (2). There are no reports of DPO responding to steroids, and effective treatment for DPO has not yet been established (3, 4). However, this case suggests remission is possible with corticosteroid medications. ■

Author disclosures are available with the text of this article at www.atsjournals.org.

References

1. Peros-Golubicić T, Tekavec-Trkanjec J. Diffuse pulmonary ossification: an unusual interstitial lung disease. *Curr Opin Pulm Med* 2008;14:488–492.
2. Chan ED, Morales DV, Welsh CH, McDermott MT, Schwarz MI. Calcium deposition with or without bone formation in the lung. *Am J Respir Crit Care Med* 2002;165:1654–1669.
3. Martinez JB, Ramos SG. Dendriform pulmonary ossification. *Lancet* 2013;382:e22.
4. Mathai SK, Schwarz MI, Ellis JH Jr. Extensive diffuse pulmonary ossification after acute respiratory distress syndrome. *Am J Respir Crit Care Med* 2013;187:890.

Respiratory Medicine Case Reports 16 (2015) 169–171

Contents lists available at ScienceDirect

Respiratory Medicine Case Reports

journal homepage: www.elsevier.com/locate/rmcr

Case report

Lymphoproliferative disorder in pleural effusion in a subject with past asbestos exposure

Naofumi Hara [a], Nobukazu Fujimoto [b, *], Yosuke Miyamoto [a], Tomoko Yamagishi [a], Michiko Asano [a], Yasuko Fuchimoto [a], Sae Wada [a], Shinji Ozaki [a], Takumi Kishimoto [c]

[a] Department of Respiratory Medicine, Okayama Rosai Hospital, Okayama, Japan
[b] Department of Medical Oncology, Okayama Rosai Hospital, Okayama, Japan
[c] Department of Internal Medicine, Okayama Rosai Hospital, Okayama, Japan

ARTICLE INFO

Article history:
Received 14 October 2015
Received in revised form
2 November 2015
Accepted 8 November 2015

Keywords:
Asbestos
Lymphoma
Mesothelioma
Pleural effusion
Thoracoscopy

ABSTRACT

Primary effusion lymphoma (PEL) is a subtype of non-Hodgkin lymphoma that presents as serous effusions without detectable masses or organomegaly. Here we report a case of PEL-like lymphoma in a patient with past asbestos exposure. A 65-year-old man was referred to our hospital due to dyspnea upon exertion. He had been exposed to asbestos for three years in the construction industry. Chest X-ray and CT images demonstrated left pleural effusion. Cytological analysis of the pleural effusion revealed large atypical lymphocytes with distinct nuclear bodies and high nucleus-to-cytoplasm ratio. Immunohistochemical analyses showed that the cells were $CD20^{+}$, $CD3^{-}$, $CD5^{-}$, and $CD10^{-}$. These findings led to a diagnosis of diffuse large B-cell lymphoma. PEL or PEL-like lymphoma should be considered a potential cause of pleural effusion in subjects with past asbestos exposure.

© 2015 The Authors. Published by Elsevier Ltd. This is an open access article under the CC BY-NC-ND license (http://creativecommons.org/licenses/by-nc-nd/4.0/).

1. Introduction

Primary effusion lymphoma (PEL) is a subtype of non-Hodgkin lymphoma that presents as serous effusions without detectable masses or organomegaly. PEL usually occurs in the setting of immunodeficiency and is associated with human herpesvirus (HHV) - 8. Here we report a case of PEL-like lymphoma in a subject with a history of asbestos exposure.

2. Case report

A 65-year-old man was referred to our hospital due to dyspnea upon exertion. He was an occasional smoker and had been exposed to asbestos from 18 to 20 years old while employed in the construction industry, cutting asbestos-containing building material. Chest X-ray showed left pleural effusion (Fig. 1A), and computed tomographic (CT) images revealed left pleural effusion and calcified pleural plaques without pleural tumor (Fig. 1B). Thoracoscopic exploration revealed red–brown pleural effusion and plaques, but no tumor was detected on the pleura. Culture of the pleural effusion was negative, and cytological examination revealed a cellular distribution of 1.0% macrophages, 1.5% neutrophils, and 97.5% lymphocytes. Other examinations of the fluid showed nonspecific findings. Pleural biopsy showed no evidence of malignancy.

During follow-up, the patient repeatedly exhibited accumulation of left pleural effusion, which was treated each time with thoracentesis. Four years after the first admission, analysis of pleural effusion from the fourth thoracentesis revealed large atypical lymphocytes with distinct nuclear bodies and a high nucleus-to-cytoplasm ratio (Fig. 2). Malignant lymphoma was suspected and thoracoscopic pleural biopsy was performed again, and the biopsy specimen from the fibrin tissues attached to the parietal pleura showed several groups of small round atypical lymphocytes. All of acid-fast bacteria stain, PCR analysis of tuberculosis, and culture for acid fast bacillus were negative. A culture test for standard plate count bacteria was also negative. Immunohistochemical analyses revealed that these cells were $CD20^{+}$ (Fig. 3), $CD3^{-}$, $CD5^{-}$, and $CD10^{-}$. Based on these findings, the diagnosis was confirmed as diffuse large B-cell lymphoma (DLBCL). Contrast-enhanced CT imaging of whole body (neck to pelvis) revealed no lymphadenopathy or tumor. Serological tests for hepatitis-C virus, human T-cell lymphoma virus-1, and Epstein–Barr virus were negative, as was the

Abbreviations: PEL, primary effusion lymphoma; HHV, human herpesvirus; CT, computed tomography; DLBCL, diffuse large B-cell lymphoma.

* Corresponding author. Department of Medical Oncology, Okayama Rosai Hospital, 1-10-25 Chikkomidorimachi, Okayama 7028055, Japan.
E-mail address: nobufujimot@gmail.com (N. Fujimoto).

http://dx.doi.org/10.1016/j.rmcr.2015.11.002
2213-0071/© 2015 The Authors. Published by Elsevier Ltd. This is an open access article under the CC BY-NC-ND license (http://creativecommons.org/licenses/by-nc-nd/4.0/).

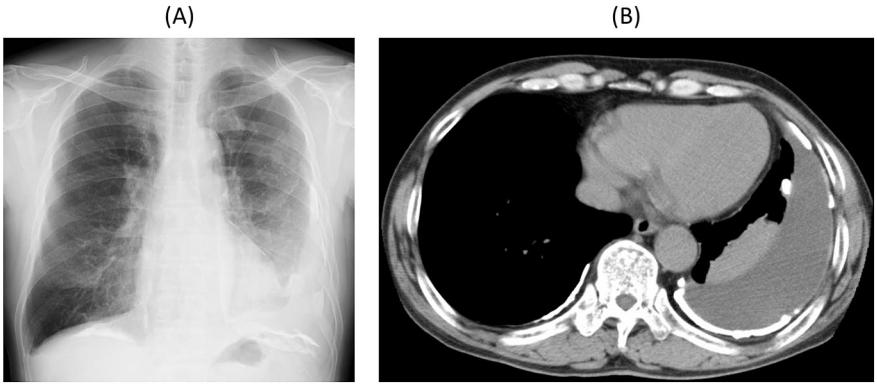

Fig. 1. Left pleural effusion and calcified pleural plaques visible on chest X-ray (A) and computed tomographic (B) images.

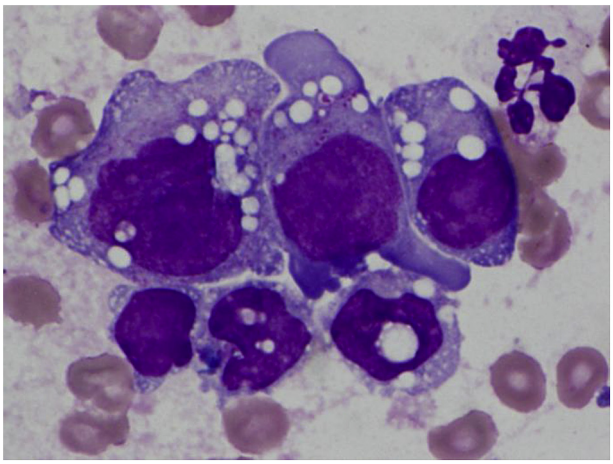

Fig. 2. Cytological analysis of pleural effusion revealed large atypical lymphocytes with distinct nuclear body and high nucleus-to-cytoplasm ratio (×40).

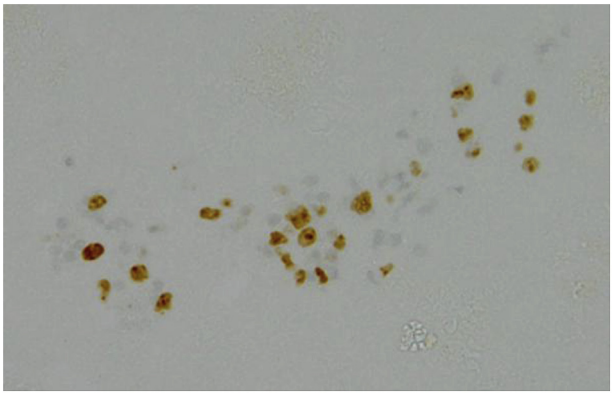

Fig. 3. Immunohistochemical analyses revealed that the cells were $CD20^{+}$ (×10).

immunohistochemical analysis for HHV8. The patient has been followed-up, and has shown no disease progression for 3 years.

3. Discussion

The 2001 World Health Organization classification defines PEL as a disease entity representing a part of diffuse large B-cell lymphoma [1]. PEL is commonly associated with HHV8 infection [2]; however, PEL-like disease processes have recently been reported in HHV8-negative patients. Those cases are considered a rare disease entity called HHV8-unrelated PEL-like lymphoma [3]. Advanced age [4] remains the only known risk factor for PEL-like lymphoma, and the pathogenic mechanisms remain unclear. It has been reported that patients with HHV8-unrelated PEL-like lymphoma show better outcomes than patients with PEL [5].

In our present case, the patient was elderly and had a past occupational history of asbestos exposure, but showed no immunological deterioration. To our knowledge, this is the first report of PEL-like lymphoma in a subject with past asbestos exposure. While no association has been established between lymphoproliferative disorder and asbestos exposure, it is possible that asbestos-induced chronic inflammation, in addition to advanced age, may have triggered lymphoproliferative disorder in the current case, though we cannot deny the possibility that the disease developed independently, considering relative short term of asbestos exposure.

In conclusion, here we report a rare manifestation of PEL-like lymphoma from a subject with past asbestos exposure. Subjects with past asbestos exposure sometimes develop pleural effusion, and suspected diagnoses include malignant pleural mesothelioma, lung cancer, benign asbestos pleural effusion, or tuberculous pleuritis. Our present case suggests that PEL or PEL-like lymphoma should also be considered as a potential cause of pleural effusion in subjects with past asbestos exposure.

Conflict of interest

I declare on behalf of my co-authors and myself that we do not have any conflict of interest to declare.

Source of funding

This study was supported by Research and Development and the Dissemination of Projects Related to the Nine Fields of Occupational Injuries and Illnesses of the Japan Labour Health and Welfare Organization. This work is also supported by grants-in-aid from the Ministry of Health, Labor and Welfare (grant number: 150401-02), Japan. These study sponsors had no involvement in study design, writing of the manuscript, the collection of data, and decision to submit the manuscript.

References

[1] P.M. Banks, R.A. Warnke, Primary effusion lymphoma, in: E.S. Jaffe, N.L. Harris, H. Stein, J.W. Verdiman (Eds.), World Health Organization Classification of Tumours. Pathology and Genetics of Tumours of Haematopietic and Lymphoid Tissues, IARC Press, Lyon, 2001.
[2] D.S. Karcher, S. Alkan, Human herpesvirus-8-associated body cavity-based lymphoma in human immunodeficiency virus-infected patients: a unique B-

cell neoplasm, Hum. Pathol. 28 (1997) 801–808.
[3] A. Carbone, A. Gloghini, PEL and HHV8-unrelated effusion lymphomas: classification and diagnosis, Cancer 114 (2008) 225–227.
[4] F. Mohammad, M.N. Siddique, F. Siddiqui, M. Popalzai, M. Asgari, M. Odaimi, A unique case of malignant pleuropericardial effusion: HHV-8-unrelated PEL-like lymphoma-a case report and review of the literature, Case Rep. Oncol. Med. (2014) 436821.
[5] Y. Kobayashi, Y. Kamitsuji, J. Kuroda, S. Tsunoda, N. Uoshima, S. Kimura, et al., Comparison of human herpes virus 8 related primary effusion lymphoma with human herpes virus 8 unrelated primary effusion lymphoma-like lymphoma on the basis of HIV: report of 2 cases and review of 212 cases in the literature, Acta Haematol. 117 (2007) 132–144.

厚生労働省
労災疾病臨床研究事業費補助金

悪性中皮腫に対するヒト化抗CD26抗体を基盤とする安全かつ有効な新規併用療法の確立

平成27年度　総括・分担研究報告書

平成 28 年 3 月 31 日発行

発行：研究代表者　森本　幾夫
〒113-8421　東京都文京区本郷 2-1-1
順天堂大学大学院医学研究科　免疫病・がん先端治療学講座
TEL：03-3868-2310